LATE NEOPROTEROZOIC EPITHERMAL-STYLE AU MINERALIZATION OF THE BURIN PENINSULA, NEWFOUNDLAND: U-Pb GEOCHRONOLOGY AND DEPOSIT CHARACTERISTICS

by

© Sarah Anne Ferguson, B.Sc. (Hons)

A thesis submitted to the

School of Graduate Studies

in partial fulfillment of the requirements for the degree of

Master of Science

Department of Earth Science

Memorial University of Newfoundland

October, 2017

St. John's, Newfoundland and Labrador

ABSTRACT

The Burin Peninsula lies within the western portion of the Avalon Zone in Newfoundland. The Avalon Zone constitutes the eastern extent of the northern Appalachian orogen and includes extensive late Neoproterozoic magmatic arc-related volcanic, plutonic and epiclastic sedimentary rocks. The stratigraphy of the Burin Peninsula region is primarily composed of the Marystown, Musgravetown and Long Harbour Groups, all of which are host to high- and/or low-sulphidation epithermal precious metal mineralization, including the Hickey's Pond, Tower, Stewart (and Forty Creek), Heritage, Big Easy and Long Harbour prospects. A 580-573 Ma plutonic suite, now recognized as the source to extensive hydrothermal activity in the region, runs along the length of the peninsula, intruding roughly coeval volcaniclastic rocks of the Marystown Group.

New U-Pb (CA-TIMS) ages for volcanic host rocks within the Marystown Group constrain the timing of high-sulphidation mineralization to a maximum age of 584 ± 3 Ma at Hickey's Pond and 576.7 ± 2.5 Ma ('Caribou Tuff') at Stewart. A previous host rock age of 572.5 ± 1.5 Ma at Hickey's Pond is re-interpreted as a hydrothermal zircon age, which provides a more explicit age for the high-sulphidation mineralization at the prospect. New U/Pb zircon ages for the Marystown Group stratigraphy of the Stewart prospect also include 575.2 ± 2.1 Ma ('Stewart Tuff'), 575.9 ± 2 Ma and 575.6 ± 1.7 Ma for other volcanic rocks, and 576.0 ± 2.7 Ma for the 'Bat Zone' granite (part of the 'Burin Knee Intrusive Suite'). In conjunction with field observations, these ages confirm a northwest younging direction within the local Marystown Group stratigraphy at Stewart. The tightly overlapping ages also further link the 580-573 Ma regional plutonism to the volcaniclastic stratigraphy and to the regional high-sulphidation mineralization. A new age of 573.3 ± 2.7 Ma for rhyolite from the Musgravetown Group, proximal to the low-sulphidation Big Easy prospect, demonstrates contemporaneity with the Marystown Group. The Musgravetown Group and Marystown Group are also of similar lithogeochemical affinity, and are presumed to represent different facies within a single, contemporaneous volcanic arc environment, undergoing active subduction between 585 and 570 Ma. The Long Harbour Group is younger than, and compositionally distinct

from the Marystown and Musgravetown Groups. A new age for the flow-banded rhyolite of the Belle Bay Formation, host to low-sulphidation epithermal mineralization at the Long Harbour prospect, constrains the timing of the mineralization to a maximum age of 566.5 ± 1.9 Ma. The stratigraphy of the Long Harbour Group is characteristically alkaline and associated with late arc-extension. Thus, the low-sulphidation deposits in the Burin Peninsula region are related to at least two discrete volcano-plutonic sequences. A sample of epiclastic sediment from the Grandy's Pond Arenite Belt yielded a preliminary youngest detrital zircon age of 566.2 ± 4.4 Ma, which corresponds to the age of Long Harbour volcanism. The belt is predominantly derived from the erosion of volcanic rocks of the Marystown Group based on their similar geochemical signatures, but also contains additional detritus from the younger Long Harbour Group, possibly in the form of ash during active volcanism.

SEM-EDX analysis was used to assess the deportment of precious metal mineralization in both high- and low-sulphidation epithermal prospects. At Hickey's Pond, the most auriferous high-sulphidation prospect, gold occurs as part of the hypogene assemblage as native gold and calaverite ($AuTe_2$), and in the late supergene/weathering assemblage as fischesserite (Ag_3AuSe_2). At the low-sulphidation Long Harbour prospect, gold occurs as native gold and electrum, and silver occurs in the form of various Ag-tellurides. Forty Creek, of possible intermediate-sulphidation origin and located proximal to the regionally-developed high-sulphidation epithermal systems, contains gold and silver in the form of various precious-metal tellurides including petzite (Ag_3AuTe_2) and sylvanite ($(Ag,Au)Te_2$).

Sulphur isotope microanalyses of pyrite, chalcopyrite and galena from the high-sulphidation Hickey's Pond, Tower, and Stewart prospects, together yield a single population displaying a normal distribution, and $\delta^{34}S$ values ranging from -6.8 to +5.9‰ with an average of -0.6‰, consistent with a magmatic sulphur source for these deposits. Sulphur isotope measurements at Forty Creek have an average $\delta^{34}S$ of -7.8‰, significantly lighter than the high-sulphidation deposits, and indicative of a sulphur source perhaps influenced by biogenically derived sulphur from metasediments, and not purely the result of magmatic input.

ACKNOWLEDGEMENTS

First and foremost I would like to thank my supervisor, Dr. Graham Layne for his ongoing guidance, encouragement and enthusiasm throughout this process, as well as my supervisory committee member, Dr. Greg Dunning for his geochronological expertise and insights.

I would like to extend a special thank you to Greg Sparkes (Geological Survey of Newfoundland and Labrador), a key collaborator in this project, whose knowledge and continual guidance (from mentoring me during initial field work, to supplying supplemental geochemical and field data, to providing edits, to answering my many, many geological inquiries) has been invaluable.

I would like to thank Dr. Tom Setterfield of TerraX Minerals and Peter Dimmell, formerly of Silver Spruce Resources, for their assistance and enthusiasm in establishing this research project, and for their guidance and input throughout. In addition, Vic French and Greg Woodland of Puddle Pond Resources provided property tours and field support, and contributed valuable insight during initial field work on the Heritage prospect.

I would also like to thank Dr. George Jenner for providing advice and helpful edits pertaining to lithogeochemistry. Additional people at Memorial University that I would like to acknowledge for their much appreciated help include: Dylan Goudie and David Grant (SEM-EDX laboratory), Glenn Piercey (SIMS laboratory), and Pam King and Amanda Langille (sample crushing, processing and preparation, and CL imaging for geochronology).

Finally, I would like to thank my parents, Steve and Judy, for their unconditional love and support, my friends for being so kind and understanding, and listening to my many woes, and my best friend, Frank, for always brightening my day, and keeping me company in the field and during long days in the office.

This project was funded by the Research and Development Corporation of Newfoundland and Labrador (RDC) GeoEXPLORE program with support from Silver Spruce Resources and TerraX Minerals. Valuable additional financial and logistical support was provided by the Geological Survey of Newfoundland and Labrador for field and laboratory work.

TABLE OF CONTENTS

LIST OF TABLES

LIST OF FIGURES

LIST OF PLATES

LIST OF ABBREVIATIONS

Minerals

acn=acanthite
adl=adularia
Ag=native silver
alb=albite
alt=altaite
alun=alunite
ang=anglesite
apy=arsenopyrite
Au=native gold
Bi=native bismuth
bn=bornite
boh=bohdanowiczite
brt=barite
cal=calcite
cc=chalcocite
chd-=chenguodaite
chl=chlorite
cin=cinnabar
cld=coloradoite
clh=clausthalite
clv=calaverite
cov=covellite
cpx=clinopyroxene
cpy=chalcopyrite
crv=cervelleite
el=electrum
en=enargite
ep=epidote
fsc=fischesserite
fsp=feldspar
gn=galena
gph=granophyric texture
grd=grundmannite
hem=hematite
hes=hessite
ilm=ilmenite
klm=klockmannite
ksp=potassium feldspar
lz=lazulite
mag=magnetite
mo=molybdenite
ms=muscovite
nm=naumannite
par=paragonite
pth=perthitic texture
phg=phengite
plag=plagioclase
ptz=petzite
py=pyrite
prph=pyrophyllite
qtz=quartz
rtl=rutile
scor=scorodite
Se=native selenium
ser=sericite
slv=sylvanite
spec=specularite
sph=sphalerite
stph=stephanite
sv=svanbergite
Te=native tellurium
tit=titanite
tm=tiemannite
tn=tennantite
toz=topaz
tsu=tsumoite
umg=umangite
wdh=woodhouseite
wtc=wittichenite
xn=xenotime
zr=zircon

Rock Units

BKIS=Burin Knee Intrusive Suite
GPAB=Grandy's Pond Arenite Belt
SCIS=Swift Current Intrusive Suite

Analytical

BSE=back scatter electron
CA-TIMS=chemical abrasion-thermal ionization mass spectrometry
CL=cathodoluminescence
EDX=energy dispersive X-ray spectrometry
PPL=plane polarized light
SEM=scanning electron microscopy
SIMS=secondary ion mass spectrometry
VIRS=visible infrared reflectance spectroscopy
XPL=cross polarized light

Other

HFSE=high field strength elements
HREE=heavy-group rare-earth elements
HS=high-sulphidation
IS=intermediate-sulphidation
LS=low-sulphidation
LREE=light-group rare-earth elements

LIST OF APPENDICES

CHAPTER 1: INTRODUCTION

1.1 Synopsis

The study area for this thesis is located in southeastern Newfoundland. It covers the entire length of the Burin Peninsula, extending northwards to Clarenville and westward to include the western shore of Fortune Bay (*Figure 1-1)*. Geologically, the peninsula comprises part of the western margin of the Avalon Zone, which makes up the eastern extent of the northern Appalachian orogen (Williams, 1979). This lithotectonic zone formed in an extensional arc setting along the margin of Gondwana during the Neoproterozoic (O'Brien et al., 1996; Nance et al., 2002). Avalon Zone geology is defined by extensive arc-related volcanic, clastic-sedimentary, and plutonic rocks, overlain by late-Neoproterozoic to early-Ordovician fine-grained siliciclastic sediments (O'Brien et al., 1996). The rocks are variably deformed and are of a low metamorphic grade, locally exhibiting greenschist facies assemblages

Both high- and low-sulphidation precious metal bearing epithermal systems have been identified throughout the Burin Peninsula, hosted within the Neoproterozoic volcanic-arc-related stratigraphy. In addition, the potential for related porphyry gold (-copper) mineralization has also been recognized. Although all three of these deposit types may be genetically consanguineous within specific intrusion-driven hydrothermal systems, this does not necessarily imply that all of these occurrences are uniformly contemporaneous.

Given that epithermal systems typically form coevally with their volcanic (or epiclastic) host rocks, it can be presumed that the accompanying gold-mineralization is Neoproterozoic in age as well. The preservation of epithermal systems of this age is highly unusual in global terms, as their shallow depth of formation typically makes them very susceptible to erosion. Furthermore, the Burin Peninsula prospects are actually part of a much larger gold-mineralized epithermal belt of peri-Gondwanan arc affinity, spanning the length of the eastern Appalachians from the eastern edge of the Avalon Zone in Newfoundland, south through to the Carolina Slate Belt (O'Brien et al., 1998).

Therefore, a greater understanding of these deposits in the region of study will not only help to refine exploration targets for gold mineralization on the Burin Peninsula, but potentially throughout eastern Appalachia.

1.2 Location and Access

The study area is approximately 200km long and 50km wide and is located within Zone 21 of the UTM Grid. The area encompasses the length of the Burin Peninsula northwards to Clarenville, located off the Trans-Canada Highway, and extends westward to include the western shore of Fortune Bay (*Figure 1-1*).

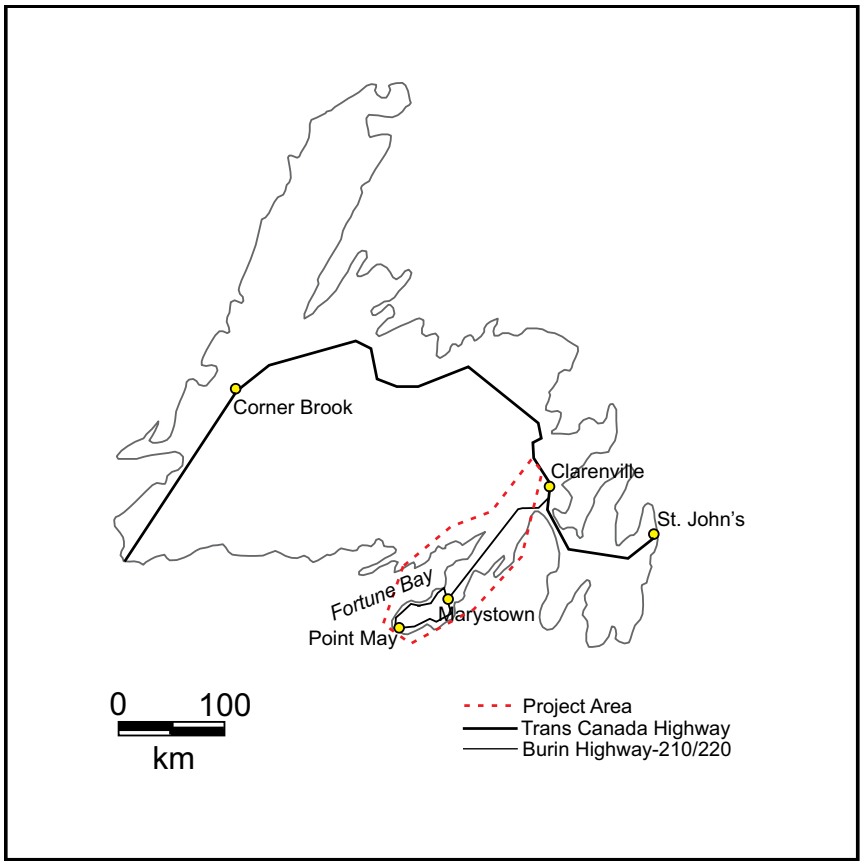

***Figure 1-1**: Map of Newfoundland showing major cities, the Trans-Canada Highway, and the project area, centred along the Burin Peninsula (outlined by dashed red line).*

The Burin Peninsula Highway (Hwy. 210, Hwy. 220), runs south from the Trans-Canada highway at Goobies, and provides access to most of the peninsula. The Monkstown Road (Route 214) is a gravel road running southeast from Highway 210 towards the western shore of Placentia Bay providing access to a portion of the study

area. The Burin Peninsula Trailway, developed from 2008 onwards, is a series of interconnected ATV trails, which extends more than 100km, and provides ATV access to the central portion of the peninsula, and part of the study area, west of route 210. Field work on the western shore of Fortune Bay, and the northeast portion of the Burin Peninsula was conducted with helicopter assistance.

1.3 Purpose and Scope

The Burin Peninsula is host to a variety of precious metal bearing epithermal-style systems. The main objective of this study was to examine the spatial and temporal correlations of these deposits on a regional scale, based on geochronological constraints and the observed characteristics of the individual prospects.

U-Pb geochronology was used to: 1) bracket the epithermal mineralization ages, 2) further link late Neoproterozoic plutonism (considered to be, at the very least, a heat source to the epithermal systems) with the volcanic host rocks, and 3) understand in greater detail the stratigraphy of the extensive Marystown Group, host to the majority of the prospects. A regional lithogeochemical study was also completed to complement this work.

The intent of this project was also to document the mineralogy of the alteration and ore assemblages at the various prospects in greater detail, to further characterize these deposits within the epithermal realm, and to decipher what might make some showings more prospective than others. This was done using scanning electron microscopy (SEM) with energy dispersive X-ray spectrometry (EDX), petrography, and visible infra-red reflectance spectroscopy (VIRS). A preliminary sulphur isotope analysis was also conducted on select high-sulphidation prospects to further characterize them and to compare their isotopic signatures.

1.4 Overview of Epithermal Gold Systems

A brief overview of epithermal gold deposits is presented here, including the general setting, deposit subtypes, fluid characteristics, and common deposit attributes. A

more detailed description of high- and low-sulphidation epithermal systems can be found in *Chapter 5* and *6*, respectively, including a more explicit discussion of ore genesis models. Unless otherwise noted, the majority of this summary has been extracted from the comprehensive reviews of epithermal systems presented by White and Hedenquist (1995), Hedenquist et al. (2000) and Sillitoe and Hedenquist (2003), and references therein. A condensed summary of the definitive deposit characteristics discussed below can be found in *Table 1-1*.

Epithermal gold deposits are defined as hydrothermal deposits formed at shallow depths (generally <1km) from surface, and at relatively low temperatures (<300°C). These deposits are precious metal dominated (Au±Ag), but can also contain appreciable amounts of base metals such as Cu, Pb, or Zn. They are associated with convergent plate margins, most commonly forming coevally with arc magmatism during subduction, and during post-subduction extension. Their formation at shallow depths plays an important role in ore genesis, with boiling possible due to decompression, and temperature and chemical gradients consequent to fluid mixing. This results in significant changes in the pH and oxidation state of fluids, and the subsequent precipitation of gold. Given their shallow depth of formation and therefore, susceptibility to erosion, they are typically preserved in terranes that are Cretaceous or younger. Exceptions to this are relatively uncommon, but include the Neoproterozoic Hope Brook deposit in southwestern Newfoundland (Dubé et al., 1995), and the Enasen deposit of Paleoproterozoic age in central Sweden (Hallberg, 1994).

Important examples also include the Brewer, Haile and Ridgeway deposits in South Carolina (Zwaschka and Scheetz, 1995; Maddry and Kilbey, 1995; Gillon et al., 1995), which are reviewed in more detail below.

Epithermal deposits can be usefully divided into two main types: high-sulphidation and low-sulphidation. This particular terminology was first introduced by Hedenquist (1987), and is currently the most widely accepted nomenclature for these deposits. The classification is based on the sulphidation state, essentially the range in T-

fS_2 space indicated by the hypogene sulphide assemblage (Barton and Skinner, 1967; Barton, 1970; Einaudi et al., 2003; Sillitoe and Hedenquist, 2003). In older literature, the high-and low-sulphidation subtypes are also commonly referred to as quartz-alunite-kaolinite (or acid sulphate) and adularia-sericite, respectively, in reference to their most characteristic alteration assemblages (Heald et al., 1987).

In more recent years, a third subdivision, "intermediate-sulphidation", has been introduced, which reflects an ore assemblage indicative of a sulphidation-state intermediate to that of the two original end members (Hedenquist et al., 2000). Although it is sometimes usefully considered as a sub-class of the low-sulphidation type, this sub-type will not be discussed at great length in the chapters that follow.

The high- and low-sulphidation end members form from contrasting fluid chemistries, primarily a result of the degree to which the fluids have equilibrated with their host rocks prior to ore deposition (Giggenbach, 1992). High-sulphidation deposits typically occur during active subduction, roughly simultaneous with related calc-alkaline arc volcanism. They are situated proximal to an underlying oxidized magma source, their primary surficial expressions being high-temperature, acidic fumaroles (*Figure 1-2*). Exsolved magmatic fluids are transported directly to the near surface, usually facilitated by a structural control, without any significant water-rock interactions at depth. The result is a highly acidic, moderately saline, oxidized fluid, derived primarily from magmatic input, with only minor meteoric water influence. The shallowly emplaced degassing oxidized source intrusions, which are both spatially and genetically, closely linked to high-sulphidation deposits, can also result in proximal porphyry-style mineralization at depth (*Figure 1-2*). Many examples of contemporaneous porphyry and high-sulphidation deposits have been documented (Sillitoe, 1999).

Low-sulphidation deposits tend to form during late- or post-subduction related extension, or even rifting, in bimodal volcanic suites. Generally, they do not display a direct spatial affiliation with underlying intrusions as clearly as their high-sulphidation counterparts do - occurring as much as 5-6 km away from a magmatic source (*Figure 1-*

2). Exsolved magmatic fluids combine with meteoric waters and undergo significant water-rock interactions at depth during a prolonged ascent, allowing for equilibration with the host rocks. The resulting fluid is near-neutral, weakly saline, and reduced, with a composition dominated by meteoric water; the original magmatic input now only a minor constituent. These systems commonly generate hot springs as a surficial signature.

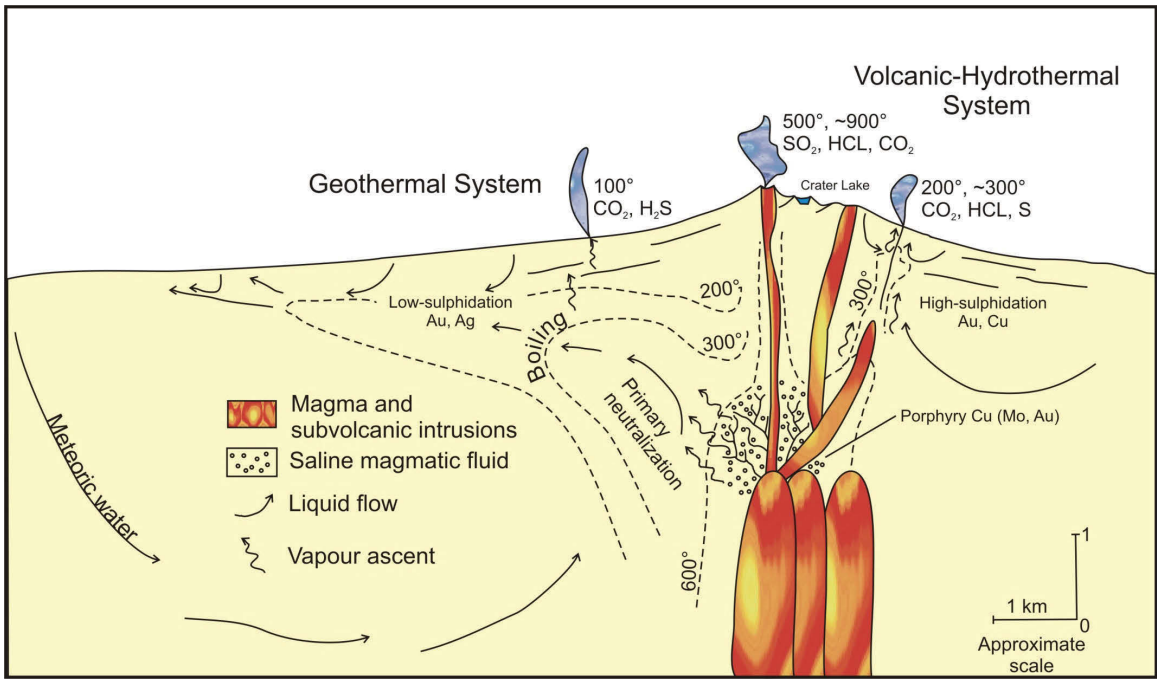

Figure 1-2*: Schematic illustrating the environments in which high-sulphidation (volcanic-hydrothermal) and low-sulphidation (geothermal) deposits form, and their spatial relationship to the main parent intrusion driving the systems. Within this environment, the parent intrusion also commonly spawns porphyry-style mineralization at depth. Fluid and vapour flow paths and basic mixing and physiochemical gradients are also shown (From Hedenquist and Lowenstern, 1994).*

High- and low-sulphidation deposits display distinct alteration and ore mineral assemblages, and ore mineral textures.

High-suphidation deposits exhibit strong alteration zoning, with a characteristic vuggy residual silica core, grading outwards to an advanced argillic alteration assemblage of quartz-alunite±pyrophyllite-dickite/kaolinite, followed by an argillic assemblage of illite-smectite, which is surrounded by more distal, and less diagnostic, phyllic and propylitic alterations. Mineralization occurs as disseminated, or replacement style ore, but

veining and brecciation is also common. Characteristic ore minerals include enargite, pyrite, luzonite, famatinite, covellite, tennantite and tetrahedrite (Einaudi et al., 2003).

Low-sulphidation deposits are more spatially confined, with the occurrence of most alteration and ore minerals restricted to the boundaries of cavity filling veins and breccias. Alteration minerals include quartz, adularia, and chalcedony, typically forming as crustiform and colloform banding in veins, with calcite as blades in zones of boiling. Commonly occurring sulphides include pyrite, arsenopyrite, chalcopyrite, and pyrrhotite (Einaudi et al., 2003).

Deposit Type	Host Rocks	Hydrothermal Alteration	Ore Style	Ore Related Textures	Enriched Metals	Tellurides/ Selenides	Precious Metal Ore	Other Sulphides/Ore
PORPHYRY	felsic-intermediate porphyritic intrusives and lesser volcaniclastics	quartz-K-feldspar-biotite, quartz-sericite/white mica, quartz-kaolinite, epidote-chlorite	vein and fracture fill, within stockwork veining, disseminated	veining, stockwork veining, alteration zoning	Cu, Au, Mo, Ag, Zn, Pb, As, Sb, Sn, Te	Tellurides	native Au, Au-tellurides	chalcopyrite, pyrite, bornite, enargite, chalcocite, molybdenite, sphalerite, galena, tetrahedrite
HIGH-SULPHIDATION	Subaerial, intermediate volcanics/ volcaniclastics	vuggy silica, quartz-alunite (APS) +/- dickite-pyrophyllite, illite-smectite, sericite/white mica, barite	disseminated, replacement style, breccia and vein fill	massive and vuggy silica, veining, breccias, alteration zoning	Au, Ag, Cu, Bi, As, Sb, Te, Sn, Mo, Pb	Tellurides (rare selenides)	Electrum, native Au, acanthite, Au-tellurides	pyrite, enargite, luzonite-famatinite, tetrahedrite-tennantite, covellite, bornite, chalcocite, diginite, chalcopyrite
INTERMEDIATE-SULPHIDATION	Andesite-rhyolite	quartz, illite, sericite/white mica, Mn-carbonates	vein fill, within breccias and stockworks	veining, crustiform and comb texture quartz	Ag, Au, Zn, Pb, Cu	Tellurides (rare selenides)	Ag-sulfosalts, acanthite, native Au	chalcopyrite, sphalerite, tennantite-tetrahedrite, pyrite, galena
LOW-SULPHIDATION	bimodal basalt-rhyolite, volcanics, volcaniclastics, and sedimentary rocks	quartz, chalcedony, adularia, calcite, illite-smectite	vein fill with sharp boundaries, within stockworks and breccias	veining with crustiform/ colloform banding, breccia, comb texture quartz, blading, sillica sinter	Ag, Au, As, Sb, Se, Zn, Hg, Pb	Selenides (rare tellurides, but abundant when associated with alkaline magmatism)	Electrum, native Au, Au/Ag-selenides, acanthite, (Au-tellurides)	pyrite, arsenopyrite, chalcopyrite, pyrrhotite, sphalerite, galena

Table 1-1*: Characteristics of porphyry and epithermal (high-, intermediate-, and low-sulphidation) deposits. Epithermal deposits have been summarized from White and Hedenquist (1995), Hedenquist et al. (2000), Cooke and Simmons (2000), Sillitoe and Hedenquist (2003), and Einaudi et al. (2003). Porphyry deposits summarized from Berger et al. (2008). (APS=aluminum phosphate-sulfate minerals).*

1.5 Overview and Brief Tectonic History of Avalonia, and Other Neoproterozoic, Peri-Gondwanan Terranes of the Appalachian Orogen Associated with Epithermal Gold Mineralization

1.5.1 Avalon Zone, Avalon Terrane, Avalonia: An Explanation of Terminology

The Canadian extent of the Appalachian Orogen was first described in detail, and subdivided into zones, based on tectonostratigraphic criteria, by Williams (1979). Five zones were defined, representing the ancient Laurentian margin (Humber Zone), remnants of the Iapetus Ocean (Dunnage and Gander Zones), and the ancient Gondwanan margin (Avalon and Meguma Zones) (*Figure 1-3)*.

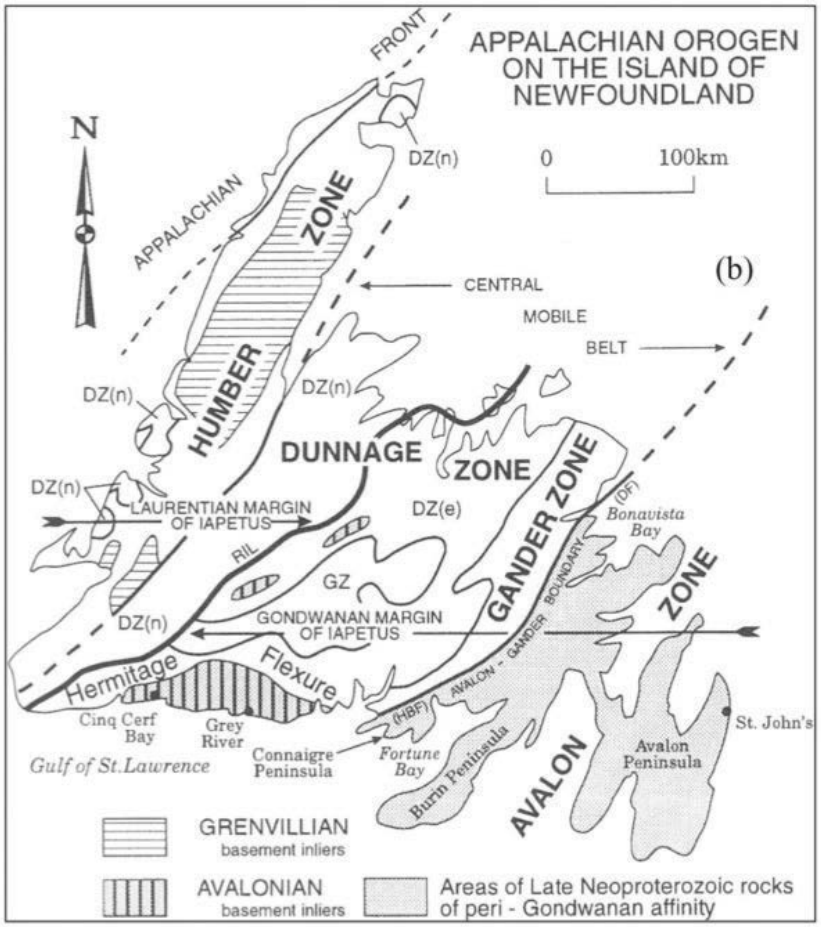

Figure 1-3*: Tectonic subdivision of the Appalachian orogeny on the island of Newfoundland. In this subdivision, the region known as the Hermitage Flexure, to the South, is included as part of the Avalon Zone. This region was correlated based on the identification of basement rocks with similar affinity to Avalon Pre-Cambrian geology (Dunning and O'Brien, 1989) (from O'Brien et al., 1996). DZ(e)=Dunnge Zone (Exploits subzone), DZ(n)=Dunnage Zone (Notre Dame subzone), GZ=Gander Zone, HBF=Hermitage Bay Fault, DF=Dover Fault, RIL=Red Indian Line.*

The Avalon Zone encompassed eastern Newfoundland, Cape Breton Island, northern Nova Scotia, and eastern New Brunswick. However, Williams (1979) noted the presence of analogous rocks to the south, along the coast of New England and throughout the extensive Carolina Slate Belt of the Southern Appalachians. Not long after, a new tectonic division was implemented, coined the Avalon Terrane, which encompassed all of the aforementioned localities, spanning the entire length of the Appalachian belt from north to south (Williams and Hatcher, 1983; *Figure 1-4*). A small westward extension of the northern Avalon margin in Newfoundland was later included, after a large basement block, on the southern shore of the island and west of the Avalon-Gander margin, was recognized to be of Pre-Cambrian, Avalonian geological affinity. This region, known as the Hermitage Flexure Zone, became correlated with the Avalon Zone (Dunning and O'Brien, 1989; *Figures 1-3, 1-4*). This composite Avalon Terrane, correlating northern Avalon geology with rocks of the southern Carolina Slate Belt, was widely accepted for many years and adopted by many authors (e.g., O'Brien et al., 1998; Nance et al., 2002; Murphy and Nance, 2002).

In more recent years it has been recognized, that fairly significant variations do exist in the tectonic histories of the northern and southern portions of the previously defined Avalon Terrane, and that this extensive domain could be constructively subdivided. Hibbard et al. (2006, 2007, 2010) set forth new precedents, in which the peri-Gondwanan portion of the Appalachians is broken up into four separate tectonic elements (Carolinia, Ganderia, Avalonia, and Meguma), each of which represent the remnants of individual peri-Gondwanan microcontinents (*Figure 1-4*). Avalonia is fault bounded and extends through the eastern coasts of Newfoundland and Cape Breton Island, northern Nova Scotia, southeastern New Brunswick, and along the coast of New England. Avalonia does not include the western extension of the Hermitage Flexure Zone, which is instead assigned to Ganderia. This concept has been well received and is currently the widely accepted standard. Despite these recent broad-scale changes, the older Avalon Zone terminology, and configuration including the Hermitage Flexure Zone, is what is still most commonly used for work focused in Newfoundland. Both annotations,

Avalonia and Avalon Zone, are used in the following text, which is why this clarification was included. Avalonia will be used when describing broader scale tectonics, and Avalon Zone, when exclusively discussing the geology of Newfoundland.

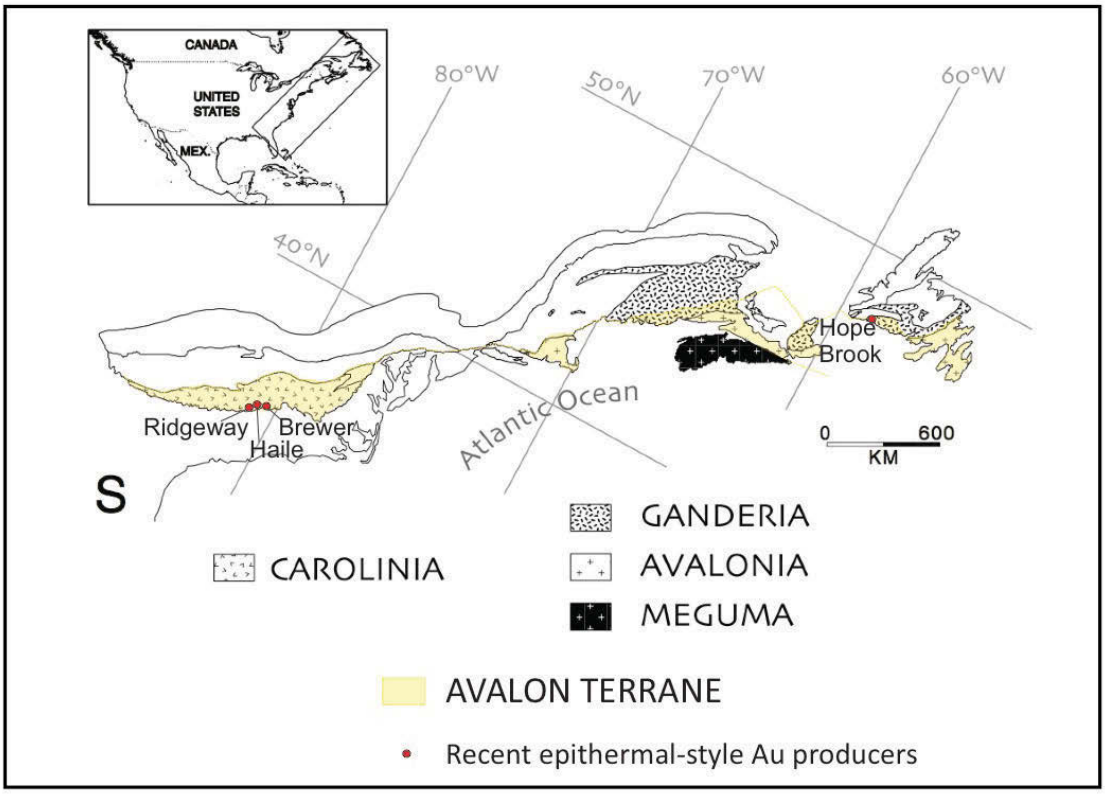

Figure 1-4*: Map displaying the current, most widely accepted subdivision of the lithotectonic elements comprising the peri-Gondwanan portion of the Appalachians, based on the criterion established by Hibbard et al. (2006, 2007, 2010). The separate elements are Carolinia, Ganderia, Avalonia, and Meguma, each representing the remnants of individual peri-Gondwanan microcontinents. Highlighted in yellow, is the more traditional 'Avalon terrane' (Williams and Hatcher, 1983; Hatcher et al., 1990), which encompasses Avalonia, most of Carolinia, and the southern tip of Ganderia in Newfoundland (Dunning and O'Brien, 1989), extending throughout the full extent of the Appalachian belt. Highlighted in red are the locations of the most prosperous epithermal gold deposits to date, occurring within the extensive Avalon terrane, all of which were in production until the 1990s (Modified from Hibbard et al., 2007a).*

1.5.2 Tectonic History of Avalonia with Comparisons to Carolinia

The peri-Gondwanan blocks (Carolinia, Ganderia, Avalonia, Meguma) of the Appalachian orogen, formed along the northern margin of Gondwana in the Neoproterozoic and early Paleozoic (Hibbard et al., 2007a; *Figure 1-5A*). They each progressively separated from Gondwana during the early Paleozoic, opening up the Rheic

Ocean in their wake, and closing the Iapetus Ocean in front of them (e.g., Murphy et al., 2006; Nance et al., 2010). In the same sequence as their departures, they each eventually accreted to the margin of Laurentia between middle Ordovician and Devonian time (Hibbard et al., 2010; *Figure 1-5B*).

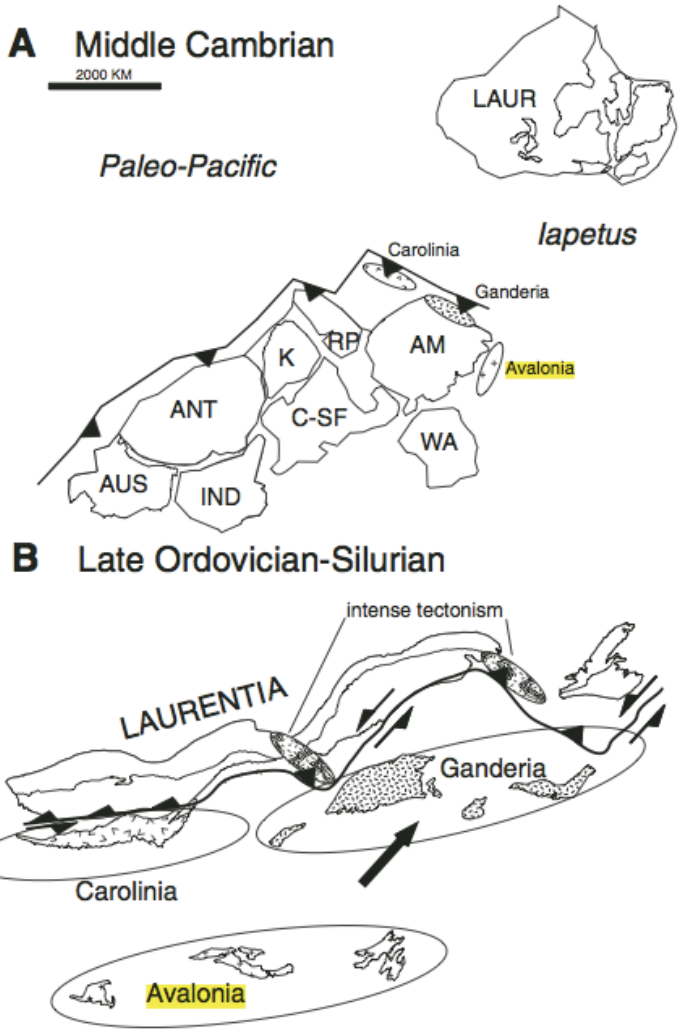

***Figure 1-5**: Hypothesized paleogeographic reconstructions for Carolinia, Ganderia, and Avalonia during, A) the Middle Cambrian and, B) the Late Ordovician-Silurian. AM-Amazonia, ANT-Antarctica, AUS-Australia, C-SF-Congo-Sao Francisco, IND-India, K-Kalahari, LAUR-Laurentia, RP-Rio de la Plata, WA-West Africa (from Hibbard et al., 2007a).*

In greater detail, the origins of Avalonia lie in Neoproterozoic time, associated with the formation (~1.1 Ga) and subsequent breakup (~750 Ma) of the supercontinent Rodinia (Pisarevsky et al., 2003). There is no known direct exposure of Avalonian basement (or proto-Avalonia). However, Sm-Nd isotopic data consistently indicate the presence of a juvenile ca. 1 Ga. basement (e.g., Nance and Murphy, 1996; Hibbard et al., 2007a; Murphy et al., 2008b), interpreted to have formed as a series of primitive island

arcs in the ocean surrounding Rodinia during its amalgamation (Murphy et al., 2000). The breakup of Rodinia initiated renewed subduction in the surrounding ocean, resulting in an early phase of Avalonian arc volcanism from ~760-660 Ma (Murphy et al., 2000, Nance et al., 2002; Murphy et al., 2008b). This early phase of arc volcanism occurred, for the most part, in a contractional tectonic environment (O'Brien et al., 1996).

Continued subduction eventually led to the accretion of Avalonia to the northern margin of Gondwana, by approximately 650 Ma (Murphy et al., 2000; Nance et al., 2002; Murphy et al., 2008a). The stratigraphy resulting from this period of early magmatism is complex, with different volcanic-sedimentary-plutonic assemblages of different ages, and volcanic hiatuses, variably preserved in different parts of Avalonia (van Staal and Barr, 2012). A similarly aged, but more confined period of arc volcanism is also recorded for Carolinia between about 685 and 670 Ma (Hibbard et al., 2007a).

Sometime between 650 and 550 Ma, the Iapetus Ocean began to open, separating Laurentia from West Gondwana. Meanwhile to the north, subduction beneath Gondwana was occurring, resulting in peak arc volcanism over Avalonia from ~635-570 Ma (e.g., Nance et al., 1991; O'Brien et al., 1996; Nance et al., 2002). Nance et al. (2002) proposed that subduction beneath Avalonia occurred obliquely, causing extensional stress in the crust. Similarly, peak arc volcanism was also occurring in Carolinia in an ocean setting between about 630 and 610 Ma due to subduction along the margin of Gondwana (Samson et al 1995; Wortman et al. 2000; Pollock et al., 2010; Pollock et al., 2012).

The cessation of arc magmatism over Avalonia around 570 Ma, is marked geologically by a shift to bimodal, within-plate magmatism, and continental clastic sedimentation along major faults, indicative of extensional basin development (e.g., Smith and Hiscott, 1984; O'Brien et al., 1996; Calon, 2001). This is interpreted to be a result of the development of an intracontinental wrench fault system that initiated as early as ca. 590 Ma, but not becoming well established until ca. 570 Ma and which persisted until ca. 540 Ma (Murphy et al., 1999; Nance et al., 2002). This termination of arc volcanism and transition to a transform regime is considered to be the result of both the

initial oblique subduction angle, and the collision of a spreading ridge at the subduction zone, analogous to the development of the San Andreas transform fault system of North America (*Figure 1-6*).

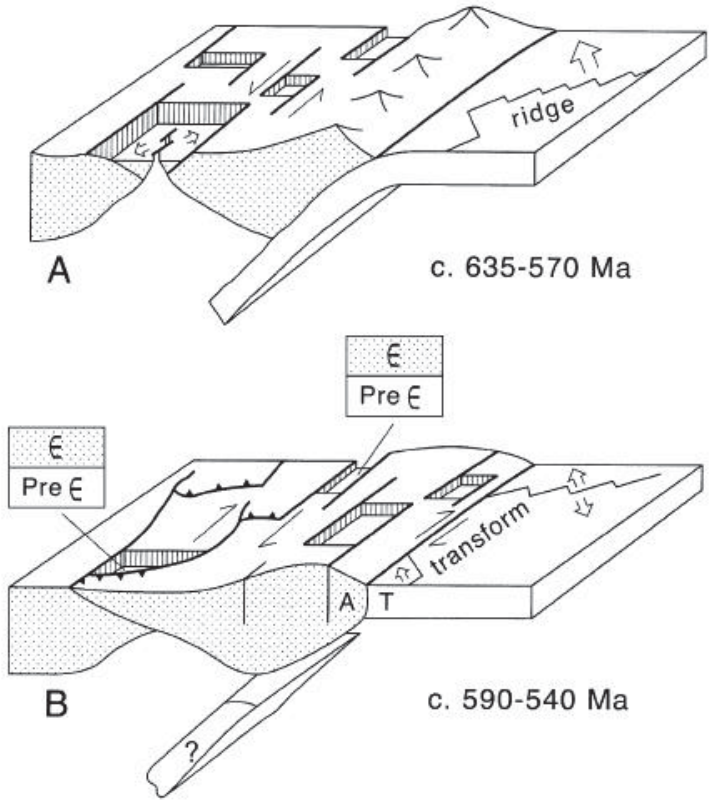

***Figure 1-6**: A) Oblique subduction during peak Avalonian arc volcanism from 635-570Ma causing extensional stress in the crust, and subsequent formation of arc-back-arc extensional basins. B) Continued subduction leading to collision of spreading ridge causing dextral transform faulting, the development of new extensional basins, and local thrust faulting (From Nance et al. 2002).*

-

Following transform faulting, Avalonia, for the most part, remained a stable platform from latest Neoproterozoic to the Silurian, represented by a thick, shallow marine, clastic sedimentary sequence (e.g., O'Brien et al. 1996). Separation of Avalonia from the Gondwana margin occurred during this interval, in the early Ordovician, an interpretation supported by faunal, paleomagnetic, U-Pb detrital zircon, and local geological data, including minor bimodal rift volcanics of this age (e.g., van Staal et al., 1998; Fortey and Cocks, 2003; Pollock et al., 2009). The accretion of Avalonia to the Laurentian margin, via subduction beneath Ganderia situated at the leading edge of Laurentia at this time (*Figure 1-5B*), is marked by the onset of syn-late collision-related plutonism and deformation, occurring within earlier subduction-related arc volcanics. This event is referred to as the Acadian orogeny, which occurred during the late Silurian

and early Devonian (e.g., Dunning et al., 1990; Dallmeyer and Nance, 1994; Zagorevski et al., 2007; vanStaal et al., 2009).

In contrast to the post 570 Ma evolution of Avalonia, Carolinia underwent continued mature arc magmatism along the Gondwana margin, with related intra-arc sedimentation, into the Cambrian, from ca. 560 to at least ca. 532 Ma (Hibbard et al., 2002; Pollock et al., 2012). This final stage of arc volcanism is interpreted as an island arc-back-arc rift system, with the later stages of rifting associated with the departure of Carolinia from Gondwana (Pollock and Hibbard, 2010). Mutiple lines of evidence suggest that accretion to Laurentia occurred between late Ordovician and early Silurian in the Cherokee orogeny (e.g., Dorsch et al., 1994; Ayuso et al., 1997; Hibbard et al., 2010).

1.5.3 The Widespread Occurrence of Epithermal Gold Mineralization in NeoProterozoic aged Peri-Gondwanan Magmatic Arc Terranes

Carolinia and Avalonia have traditionally been correlated based, most notably, on their geological similarities. Both have stratigraphies indicative of corresponding periods of Neoproterozoic arc volcanism along the margin of Gondwana, both are overlain by a clastic sedimentary sequence, and both have corresponding positions along the eastern margin of the orogen (Williams and Hatcher, 1983). However, another important correlative feature of these terranes, is the presence of significant epithermal gold mineralization along the entire length of this region of eastern Appalachia (e.g., O'Brien et al., 1998). As previously mentioned, the preservation of these systems in rocks of this age is not typical due to their shallow depth of formation. Therefore, finding them preserved with such continuity on such a large geographic scale is even more impressive. Therefore, despite the recognition that Carolinia and Avalonia are in fact distinct sub-terranes with somewhat divergent tectonic histories, as outlined above, their origins as epithermal gold generating-volcanic arcs along the margin of Gondwana remains relevant in considering gold metallogeny.

The most productive gold deposits to date are of high-sulphidation epithermal style. The former Hope Brook mine in southwestern Newfoundland, and the Brewer mine

in the Carolina Slate Belt, have both been unequivocally classified as high-sulphidation style, exhibiting extensive advanced argillic alteration zones containing pyrophyllite and andalusite, with alunite also characteristic at Hope Brook (Dubé et al., 1995, Foley and Ayuso, 2012). Also in the Carolina Slate Belt are the Haile and Ridgeway mines. Significant deformation and metamorphism in the Carolina Slate Belt makes classification of these deposits a bit more elusive. Both deposits were originally considered to be of high-sulphidation affinity, but recent studies argue that they are more likely low-sulphidation style (Foley and Ayuso, 2012). All of the aforementioned mines were operational well into the 1990s, and the Haile mine began renewed production in December, 2016. They are all hosted in, and presumed syngenetic with, volcanic rocks of late Neoproterozoic to earliest Paleozoic age (Feiss et al., 1993, Dubé et al., 1995), the same time interval observed for gold mineralization on the Burin Peninsula (*Table 1-2*).

Deposit	Tonnage (million tons)	Grade (g/t)	Style	Age of Mineralization
HOPE BROOK	**11.2** [1]	**4.54**	**High-Sulphidation**	•**578-574Ma** (U-Pb zircon of host rock and cross-cutting dyke) [5]
BREWER	**5.6** [2]	**1.2**	**High-Sulphidation**	•**550Ma** (U-Pb zircon of host rock) [6]
HAILE	**15.3** [3]	**3.1**	**Low-Sulphidation/ Epithermal**	•**553Ma** (U-Pb zircon of host rock) [6] •**554Ma** (Re-Os on molybdenite) [7]
RIDGEWAY	**56** [4]	**1.1**	**Low-Sulphidation/ Epithermal**	•**556Ma** (U-Pb zircon of host rock) [6] •**552Ma, 558Ma** (Re-Os on molybdenite) [7]

Table 1-2*: Gold deposits of the Avalon Terrane. 1. McKenzie (1986); 2. Zwaschka and Scheetz (1995); 3. Maddry and Kilbey (1995); 4. Gillon et al. (1995); 5. Dubé et al. (1995); 6. Ayuso et al. (2005); 7. Stein et al. (1996). (modified from O'Brien et al., 1998).*

The Hope Brook deposit occurs in southwestern Newfoundland in the Cinq Cerf Bay region, ~240 km west of the Burin Peninsula (*Figure 1-4*). It is typically described as lying within the western extension of the Avalon Zone of Newfoundland (e.g., Dube et al., 1995, O'Brien et al., 1998), however, in accordance with newer interpretations, considered to lie within the nominal margins of Ganderia. It is hosted by a sedimentary, and lesser volcanic, sequence that has been intruded by multiple phases of predominantly felsic intrusives (Roti Intrusive Suite). The host rocks have ages between 583 and 563 Ma, and the gold mineralization and alteration is tightly constrained to between 578 and 574 Ma by U-Pb geochronology of mineralized and un-mineralized dykes (Dube et al., 1995). The deposit sits within an extensive 3 km by 400 m wide hydrothermal advanced argillic alteration zone, with two stages of silica alteration present. Ore is predominantly hosted in the later stage, massive grey silica alteration contained within a wide alteration envelope of buff silica.

The Brewer deposit, within the Carolina Slate Belt (*Figure 1-4*), is hosted in felsic volcanic and volcaniclastic rocks, and breccias associated with a subvolcanic quartz porphyry, dated at 550 Ma (Ayuso et al., 2005). The alteration zone includes andalusite, topaz, and pyrophyllite, with sulfides forming in structurally controlled massive veins and as sulfide breccias (Foley and Ayuso, 2012).

The low-sulphidation Haile and Ridgeway deposits are located south of the Brewer deposit, in the Carolina Slate Belt (*Figure 1-4*). They are hosted in felsic volcaniclastics and associated sediments, including laminated siltstones, which are interpreted to have been deposited in a marine volcanic-arc basinal setting (Foley and Ayuso, 2012). The volcanic host rocks at Haile have been dated at 553 Ma, and at Ridgeway, 556 Ma (Ayuso et al., 2005). Gold is associated with quartz and pyrite, which form as colloform stringers, layers, and replacements (Foley and Ayuso, 2012). Mineralization is accompanied by an alteration assemblage of sericite, illite-smectite, adularia and kaolinite (Foley et al., 2000).

All three of the significant Carolina Slate Belt deposits (Brewer, Haile, Ridgeway)

lie along a transition from predominantly volcanic-volcaniclastic rocks of the Persimmon Fork Formation to volcanic-epiclastic rocks of the overlying Albermarle (Richtex) Formation. The Haile deposit, in particular, is localized directly adjacent to this boundary (Ayuso et al., 2005). This stratigraphic transition is therefore regarded as an important parameter for the prospectivity of epithermal gold mineralization in the region

1.6 Geology of the Avalon Zone in Newfoundland

The Avalon Zone within Newfoundland is comprised of a series of fault-bounded Neoproterozoic arc-related volcanic-sedimentary belts and associated plutonic rocks, covered by an early Paleozoic platformal, shale-dominated sedimentary sequence (e.g., O'Brien et al., 1996; van Staal and Barr, 2012). Preserved in the stratigraphy of the Avalon Zone of Newfoundland is a narrative of the tectonic history of Avalonia as outlined above. The major events include: 1) early arc volcanism and accretion to Gondwana (ca. 760-660 Ma); 2) peak arc volcanism (ca. 635-570 Ma; 3) development of an extensional transform fault system (ca. 570-550 Ma); 4) transition to a stable platform through the Cambrian; 5) Ordovician separation from Gondwana; 6) Silurian-Devonian accretion to Laurentia.

Early 760-660 Ma arc volcanism

Rocks from the early 760-660 Ma phase of arc magmatism are variably preserved across Avalonia and within Newfoundland itself, and lack much chronological continuity. The oldest known magmatic event in Avalonia, is represented by the ca. 760 Ma Burin Group, which occurs along the southeastern edge of the Burin Peninsula in Newfoundland (Krogh et al., 1988; Murphy et al., 2008b; *Figure 1-7*). The Burin Group is a fault-bounded sequence of greenschist-facies submarine mafic rocks, which includes pillow basalt, mafic breccia, tuff and related sediments (Strong et al., 1978a, 1978b; Strong, 1979). This sequence is intruded by a mafic intrusive complex, dated at 763±3 Ma (Krogh et al., 1988). Most of the volcanic and plutonic rocks of the Burin Group are tholeiitic in composition (Strong et al., 1978a), and interpreted to represent immature oceanic island arcs (Taylor, 1978; Strong and Dostal, 1980; O'Brien et al., 1996) that

formed in the ocean surrounding Rodinia, in response to the initiation of its breakup (Murphy et al., 2008b). On the eastern Avalon Peninsula, along the southern shore of Conception Bay, vestiges of ca. 730 Ma arc volcanism are preserved in what is known as the Hawke Hills Tuff, preserved within the core of the Holyrood Horst (O'Brien et al., 2001; *Figure 1-8*). The unit is comprised of subaerial felsic to mafic volcanics, which includes a felsic tuff bed, dated at 729±7 Ma (Israel, 1998), making it the oldest phase of felsic volcanism recognized within Avalonia (O'Brien et al., 2001).

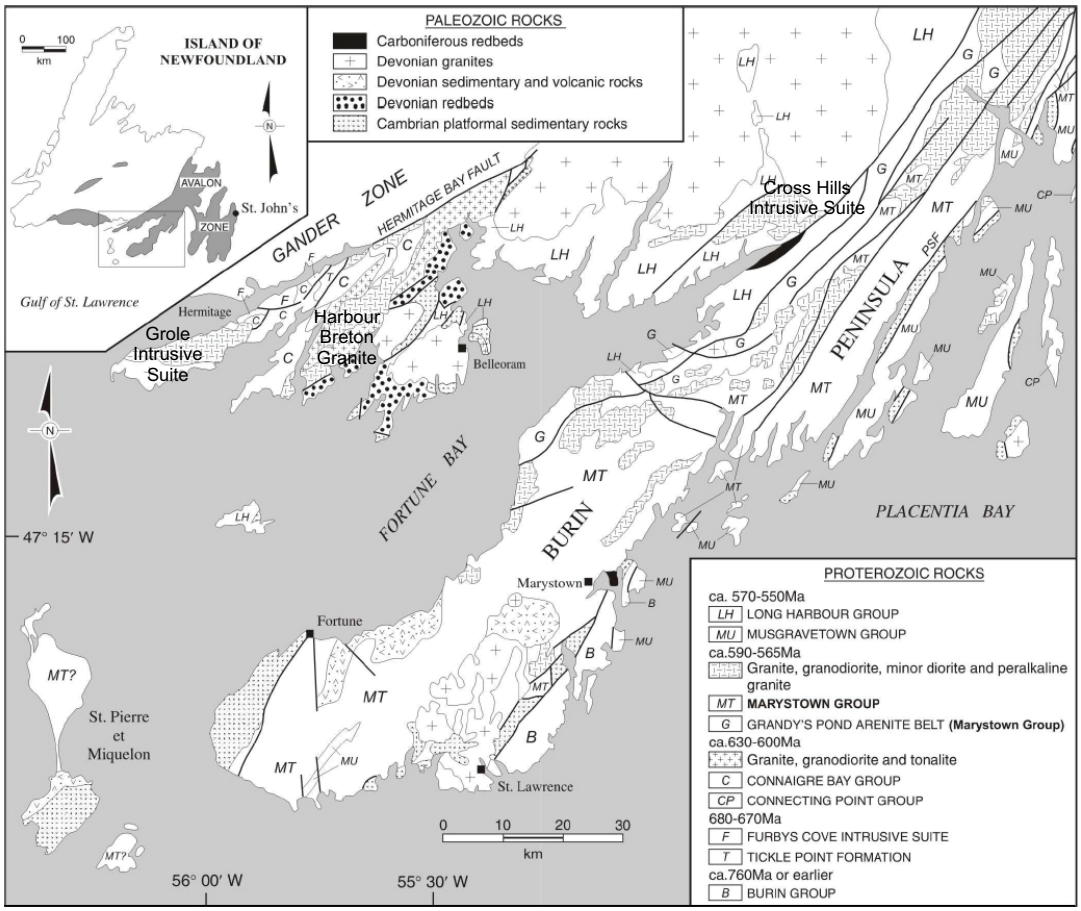

Figure 1-7*: Generalized geological map of the Burin and Connaigre Peninsulas (southwestern Avalon Zone) with the Grole, and Cross Hills Intrusive Suites, and Harbour Breton Granite (referred to in the text) labeled. The ca. 760 Ma Burin Group (B) is shown on the southeastern margin of the Burin Peninsula (Modified from O'Brien et al., 1999; 1996). TF=Terrenceville fault; WHF=White Horse fault.*

On the Connaigre Peninsula in southern Newfoundland, ca. 685-670 Ma early arc volcanism is indicated by the presence of the Tickle Point Formation; a suite of predominantly rhyolitic, calc-alkaline flows and pyroclastics (O'Brien et al., 1992, 1995;

Figure 1-7). Rhyolites from this unit have yielded U/Pb zircon ages of 682±3 (O'Brien et al., 1994; Tucker, 1991, unpublished data) and 682.8±1.6 Ma (Swinden and Hunt, 1991). The Tickle Point Formation is intruded by the bimodal, Furby's Cove Intrusive Suite (O'Brien et al., 1992), dated at 673±3 Ma within a granitic phase of the complex (O'Brien et al., 1994; Tucker, 1991, unpublished data). These 685-670 Ma rocks host mylonitic shear zones and local amphibolite grade metamorphism, which are both absent from the overlying cover rocks, which are younger than 635 Ma (O'Brien et al., 1996). This gives a minimum age for the deformation, which is thought to represent the orogenic event of the accretion of Avalonia to the northern margin of Gondwana ca. 650 Ma (Murphy et al., 2000; Nance et al., 2002; Murphy et al., 2008a).

After an apparent hiatus, the main phase of Avalonian arc volcanism was initiated ca. 635 Ma as a result of subduction beneath the margin of Gondwana, with extensive arc-, and continental extension-related magmatism and sedimentation, which continued to occur until ca. 550 Ma (e.g., O'Brien et al., 1996; Nance et al., 2002; Hibbard et al., 2007a). This coarse interval can be broken up (with some stratigraphic overlap) into three sub-intervals; 635-590 Ma, 590-570 Ma, and 570-550 Ma, which are each distinctly represented in the geological record of Newfoundland.

Early 635-590 Ma peak arc volcanism

The earliest period (635-590 Ma) of peak arc volcanism is characterized by extensive volcanism and plutonism, as well as related marine sedimentation, in arc and arc-adjacent basin settings (King, 1990; Sears, 1990; Dec et al., 1992; O'Brien et al., 1990, 1994). The volcanic lithologies are diverse, ranging from submarine to subaerial, basalt through to rhyolite (e.g., Strong et al., 1978a; O'Driscoll and Strong, 1979; O'Brien et al., 1995). Geochemical signatures are also variable, including calc-alkaline to tholeiitic rocks to island arc (arc-rift) tholeiites (Hussey 1979; O'Brien et al. 1990; Sears, 1990). From west to east, these rocks include the Connaigre Bay, Love Cove, and Harbour Main groups, most of which are intruded by, roughly coeval, lithologically similar, calc-alkaline plutonic complexes (O'Driscoll and Strong, 1979; O'Brien et al.,

1996). Thick successions of marine siliciclastic rocks are also locally associated with the volcanic rocks of this age, forming in arc-adjacent basins (Dec et al., 1992).

The volcano-sedimentary Connaigre Bay Group (*Figure 1-7*), contains a 626±3 Ma rhyolite near its base (Tucker unpublished data; O'Brien et al., 1994), and is intruded by the Simmons Brook Intrusive Suite – a calc-alkaline plutonic complex (Williams, 1971; O'Brien et al., 1992), which includes a 621±3 Ma granodiorite (Tucker unpublished data; O'Brien et al., 1994). On the Avalon Peninsula, rocks of this age are represented by the subaerial volcanics of the Harbour Main Group, and the co-magmatic, calc-alkaline plutonic rocks of the Holyrood Intrusive Suite, which make up the core of the Holyrood Horst (McCartney, 1967; King, 1988a, 1990; Hayes and O'Driscoll, 1989, 1990; O'Brien and O'Driscoll, 1996; O'Brien et al. 1997; *Figure 1-8*). The main granitic phase and type example of the Holyrood Intrusive Suite has been dated at ca. 620 Ma (e.g., Krogh et al., 1988, Sparkes et al., 2005). Felsic volcanic rocks associated with this same period of magmatism and assigned to the Harbour Main Group, include 622±2 Ma hydrothermally altered volcanics found between the towns of Harbour Main and Avondale, and the 606±3 Ma Peak Tuff (Krogh et al., 1988; O'Brien et al., 2001).

The last representation of pre-590 Ma arc volcanism can be found in the northwest Avalon Zone within the Love Cove Group - a submarine volcano-sedimentary sequence containing a rhyolite unit with an age of 620±2 Ma (O'Brien et al., 1989; *Figure 1-9*). This predominantly volcanic sequence is overlain by, and partially intercalated with the overlying sediment dominated Connecting Point Group (O'Brien and Knight, 1988; Normore, 2012; *Figures 1-9, 1-7*). This is perhaps the best example of arc-related marine sedimentation, and combined with upper portions of the Love Cove Group, makes up a 4-5km thick sequence of clastic marine sediments and interlayered tuffs, interpreted to have formed in arc-adjacent basins (Dec et al., 1992). One tuff bed, located mid-succession, yielded a zircon age of 610±1 Ma (Dunning, unpublished data, in Dec et al., 1992). Another example of marine sedimentation during this time is the 621+5/-4 Ma and younger (Israel, 1998) turbidites locally preserved within the Holyrood Horst, and typically assigned to the Conception Group.

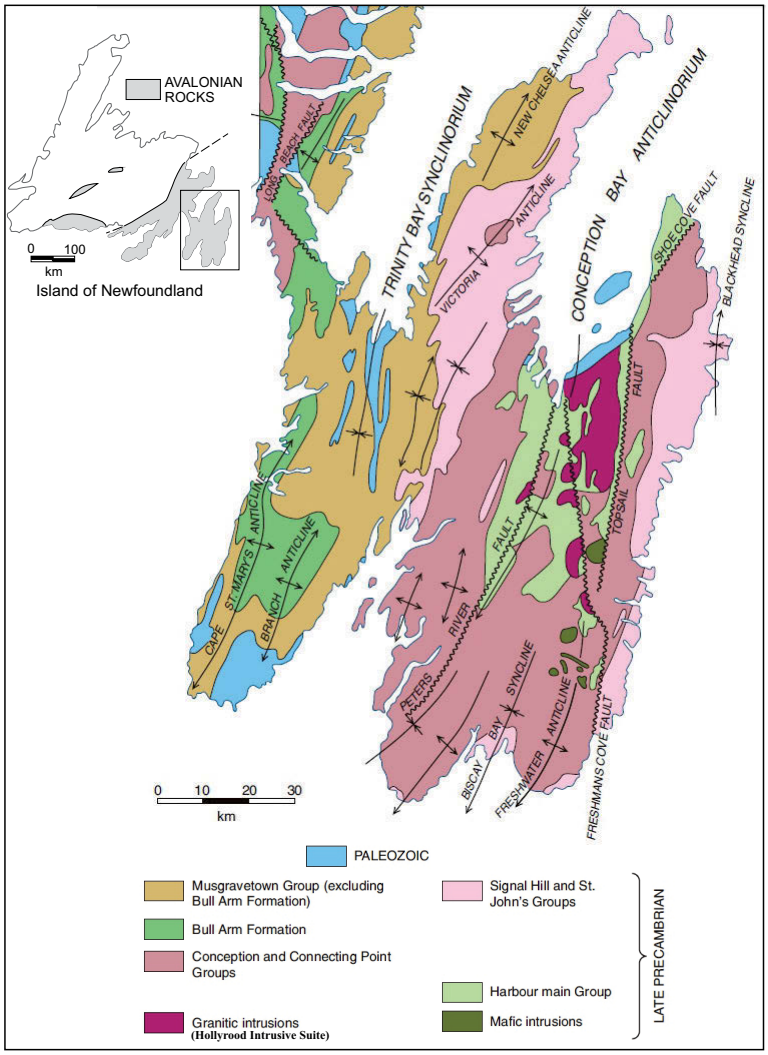

***Figure 1-8**: Simplified geological map of the Avalon Peninsula (eastern Avalon Zone). The Holyrood Horst is situated between the Topsail and Peters River faults (Modified from King, 1988b; inset modified from Sparkes and Dunning, 2014; O'Brien et al., 1998).*

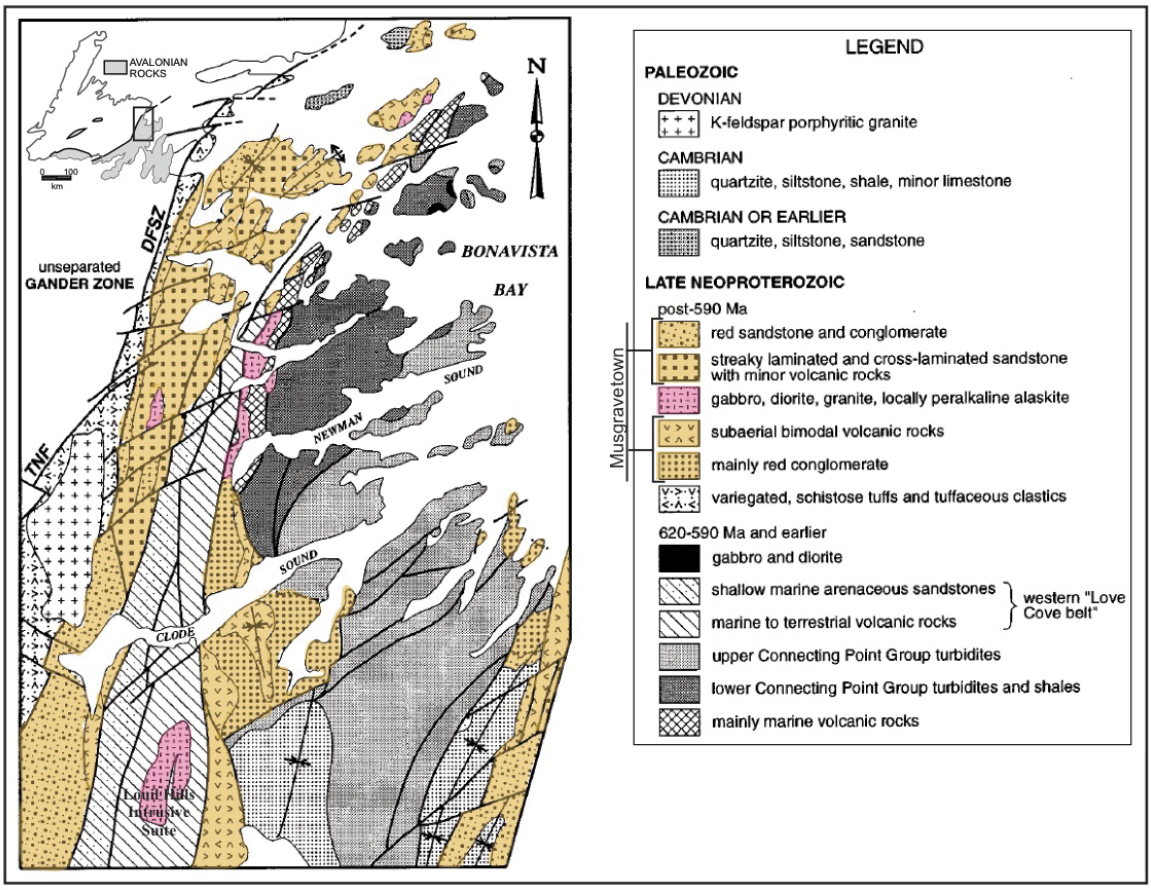

Figure 1-9*: Geological map of the northwestern Avalon Zone around Bonavista Bay, with the Musgravetown Group highlighted, and the Louil Hills Intrusive Suite labeled (Modified from O'Brien et al., 1996; inset modified from Sparkes and Dunning, 2014; O'Brien et al., 1998). DFSZ=Dover Fault Shear Zone; TNF=Terra Nova fault.*

Late 590-570 Ma peak arc volcanism

The next geologically distinct period (590-570 Ma) is characterized by extensive arc-related volcanism and plutonism, and is best represented by the rocks of the Marystown Group (Strong et al., 1978a,b), which make up the majority of the Burin Peninsula region (*Figure 1-7*). The ca. 590-570 Ma Marystown Group is composed of subaerial, calc-alkaline and tholeiitic, predominantly volcaniclastic rocks, ranging in composition from basalt to rhyolite (e.g., Hussey, 1979; O'Brien et al., 1999). Marystown volcanics have been dated by various authors, most commonly yielding ages between 580 and 570 Ma. Krogh et al. (1988) reported an age of 608+20/-7 Ma in an ash flow tuff. However, this archived sample was reassessed by Sparkes and Dunning (2014), who determined an age of 574.4±2.5 Ma – an age more congruous with the range

of other reported ages for the Marystown Group. The Marystown Group volcanics are intruded by a series of high-level, coeval plutons, including the 577±3 Ma Swift Current Granite (Tucker, unpublished data, O'Brien et al., 1998).

Similarly aged arc-volcanism can also be traced to the east, where subaerial, mainly felsic volcanic rocks of the Manuels Volcanic Suite (considered part of the Harbour Main Group) have been dated at 584±1 Ma (Sparkes et al., 2005; *Figure 1-8*). Overlying this suite is a succession of mafic volcanics, and shallow marine sedimentary rocks of the Wych Hazel Pond Complex (O'Brien et al., 2001), with a lower age limit of 582±1.5 Ma, as determined in a tuff bed at the base of the sequence (Sparkes et al., 2005).

570-550 Ma continental extension and transform faulting

The final period of Avalonian magmatism (570-550Ma) has been interpreted to mark the cessation of arc volcanism, and transition to an extensional transform fault system (Nance et al., 2002). This is represented geologically in Newfoundland by a shift to more bimodal, within-plate magmatism, and continental clastic sedimentation, commonly along major faults (e.g., Smith and Hiscott, 1984; O'Brien et al., 1996; Calon, 2001). Volcanic and sedimentary rocks of this affinity can be found in the Long Harbour Group (overlying the Marystown Group) and the Musgravetown Group, flanking the Marystown Group along its eastern margin and also occurring as a continuous belt north towards Bonavista Bay. The Long Harbour Group is dominated by subaerial felsic volcanics of alkaline to peralkaline affinity, and shallow-marine siliciclastics, but also includes upper bimodal volcanic horizons, and is capped by red beds, interpreted as pull apart basins (O'Brien et al., 1996; *Figure 1-7*). Rhyolites at the base and top of the succession have been dated at 568±5 Ma and 552±3 Ma, respectively (O'Brien et al 1995; Tucker and McKerrow, 1995; Tucker unpublished data). The Musgravetown Group, lying unconformably on the Connecting Point Group, is predominantly composed of an overall shoaling-upward sequence of marine to terrestrial epiclastic-sedimentary rocks, but also includes minor subaerial, bimodal volcanics (O'Brien et al., 1996; O'Brien et al., 1999; *Figures 1-9, 1-8, 1-7*). Rhyolite from the base of the Rocky Harbour Formation,

which occurs in the upper portion of the overall Musgravetown Group succession, has been dated at 570 +5/-3 Ma (O'Brien et al., 1989; Dunning, unpublished data; O'Brien and King, 2004).

Multiple examples of plutonic rocks of this age are also present. Locally intruding the Long Harbour Group is the mafic dominated, alkaline to peralkaline Cross Hills Intrusive Suite, with a preliminary age of 547 +3/-6 Ma (Tuach, 1991; O'Brien et al., 1996; *Figure 1-7*). Unlike most of the plutonism occurring across the Avalon Zone, most examples of plutonism during this time are not directly associated spatially with abundant volcanic rocks of the same age. On the Connaigre Peninsula the ca. 570 Ma Harbour Breton Granite, and the Grole and Hardy's Cove Intrusive Suites intrude into the much older Connaigre Bay Group and Tickle Point Formation (O'Brien et al., 1994; O'Brien et al., 1995; Dunning, unpublished data 1994; Tucker, unpublished data; *Figure 1-7*). The intrusive suites display a range in composition from gabbro to granodiorite and are roughly coeval with the earliest volcanism at the base of the Long Harbour Group (O'Brien et al., 1995). To the north towards Bonavista Bay, the 572+3/-2 Ma Louil Hills Intrusive Suite (O'Brien et al., 1989; Dunning, unpublished data, 1989; O'Brien et al., 1996) intrudes into older rocks of the Love Cove and Connecting Point Groups (*Figure 1-9*). This alkaline-peralkaline suite is interpreted to be coeval with the alkaline volcanism associated with the adjacent Musgravetown Group (O'Brien et al., 1989).

Latest Neoproterozoic-Cambrian stable platform

Latest Neoproterozoic through to Cambrian time is defined by the presence of platformal sedimentary cover sequences, which cap the extensive arc volcanics, and occur across the Avalon Zone. Minor facies variations occur from west to east in these early Paleozoic rocks, typically with deeper, shale-rich platform sediments exposed to the west, and shallower successions occurring towards the east (O'Brien et al., 1996). In the western Avalon Zone, terminal Proterozoic, alluvial sedimentation, initially in pull-apart basins, marked by the red beds of the upper Long Harbour Group, transition conformably into Cambrian near shore and open shelf marine sedimentation, forming a fossiliferous

siliciclastic platformal cover sequence (e.g., Smith and Hiscott, 1984; O'Brien et al., 1996; *Figure 1-7*). Similarly, the upper part of the Musgravetown Group is dominated by sediments, which also record a general transition from a subaerial to a shallow marine setting (O'Brien and Knight, 1988; *Figure 1-9*). To the east, the Harbour Main Group on the Avalon Peninsula is overlain by the Conception, St. John's, and Signal Hill Groups, which record a transition from deep-water turbidites (Conception), to deltaic sandstones (St. John's), and finally fluvial and alluvial facies sediments (Signal Hill) (King, 1990; *Figure 1-8*). A maximum age for the latter two has been defined at 565±3 Ma (Dunning 1988 unpublished data; Benus, in King 1988a) by a tuff bed immediately above a Neoproterozoic Ediacaran-fossil-bearing bed, near the top of the Conception Group (Williams and King, 1979).

Ordovician rifting from Gondwana

The separation of Avalonia from Gondwana is interpreted to have occurred in early Ordovician based on multiple lines of evidence (e.g., van Staal et al., 1998; Fortey and Cocks, 2003; Hamilton and Murphy, 2004). Geologically, this transition is represented in Newfoundland by the presence of a transgressive arenitic cover sequence found in the early Ordovician quartzites of the Bell Island Group, which unconformably overlies the Cambrian platformal sequence (Pollock et al., 2009).

Late Silurian-early Devonian accretion to Laurentia

Finally, all of the Proterozoic volcanics and early Paleozoic cover rocks underwent deformation and metamorphism while accreting to Laurentia during the Acadian orogeny in the Silurian-early Devonian (van Staal, 2007; van Staal et al., 2009). Deformation intensity increases across the Avalon Zone from east to west, towards the Dover and Hermitage Bay Faults, which mark the tectonic contact between Avalonia and Ganderia (Blackwood and Kennedy, 1975; Kennedy et al., 1982). Regional greenschist-grade metamorphism, and Devonian granitic plutonism also become increasingly evident, approaching this western contact (Dallmeyer et al., 1983; O'Brien et al., 1996; van Staal et al., 2009).

1.6.1 Other Epithermal Gold Occurrences within the Avalon Zone, Newfoundland

In addition to the aforementioned Hope Brook Mine in southwestern Newfoundland, and the Burin Peninsula epithermal occurrences that are the focus of this study (discussed in greater detail below), epithermal gold mineralization also occurs on the eastern Avalon Peninsula, where epithermal alteration and gold mineralization can be traced along a 15 km-long belt that follows the eastern margin of the Holyrood Horst (Manuels-Grog Pond belt; *Figure 1-10*). Here, felsic volcanics of the Manuels Volcanic Suite host both high- and low-sulphidation epithermal style systems. The high-sulphidation occurrences include Mine Hill, Trout Pond, Dog Pond, and Oval Pit Mine. Although they are all devoid of significant gold mineralization, they do contain substantial zones of advanced argillic alteration consisting of pyrophyllite and diaspore. Host rocks at the Oval Pit Mine have been dated at ~584Ma (Sparkes et al., 2005). The low-sulphidation occurrences include the Bergs and Steep Nap prospects, which are located within 1 km of the Oval Pit mine, and contain veining, hydrothermal brecciation, and relatively anomalous gold values. Host rocks at the Bergs Prospect have been dated at 582Ma (Sparkes et al., 2005).

Most of the epithermal occurrences currently identified within the Avalon Zone of Newfoundland are hosted by subaerial felsic volcanic rocks, which formed between 590 and 550 Ma (Sparkes and Dunning, 2014). These volcanic host rocks are interbedded with marine, deltaic, and fluviatile siliciclastic sedimentary sequences, and similar to the deposits of the Carolina Slate Belt, are often also overlain by these sedimentary rocks. For the epithermal occurrences of the eastern Avalon Zone, Sparkes et al. (2005) demonstrated the importance of the deposition of these overlying sediments for the subsequent preservation of the underlying epithermal systems, through the process of rapid burial.

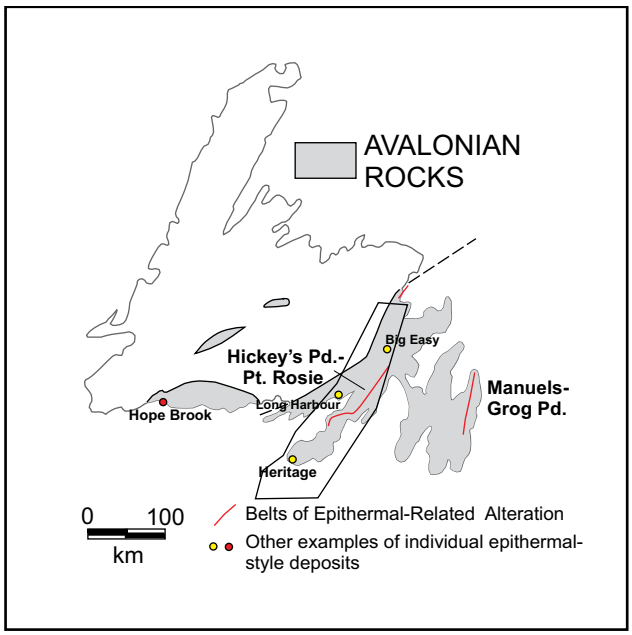

***Figure 1-10**: Epithermal alteration belts and other Au-occurrences within the Avalon Zone of Newfoundland, with the Burin Peninsula region outlined. Yellow and red dots represent low-sulphidation and high-sulphidation style mineralization, respectively (modified from Sparkes and Dunning, 2014; O'Brien et al., 1998).*

1.7 Geology of the Burin Peninsula

Building upon the general regional stratigraphic picture, this section focuses strictly on the geology of the Burin Peninsula, including immediately adjacent, stratigraphically related regions to the north and west, which make up the study area. The three most widespread stratigraphic groups in the area are the Marystown, Musgravetown, and Long Harbour Groups, all of which are host to epithermal-style gold mineralization

The Burin Peninsula region, making up the western portion of the Avalon Zone in Newfoundland, is characterized by wide-spread, late-Neoproterozoic magmatic arc activity, the majority of which occurred between ca. 590 and 550 Ma (e.g., Krogh et al., 1988; O'Brien et al., 1995; 1996; Sparkes and Dunning, 2014). Volcanism was associated with arc, arc-adjacent, or continental extensional settings, occurring partly simultaneous to the development and infilling of marine, deltaic, and terrestrial siliciclastic sedimentary basins (O'Brien et al., 1998, O'Brien et al., 1999).

The majority of the Burin Peninsula is comprised of the ca. 590-570 Ma Marystown Group, which makes up the core of a broad-scale north-northeast trending

anticlinorium (Strong et al., 1978b; O'Brien et al., 1999; *Fig 1-11*). The Marystown Group is composed of greenschist-facies subaerial flows and pyroclastics, ranging in composition from basalt through to rhyolite, all of variable calc-alkaline and tholeiitic affinity (Hussey, 1979; O'Brien et al., 1990; 1996; 1999). Although these lithologies would be typical products of caldera-forming eruptions, individual caldera centres or the associated structures, have not yet been defined by detailed mapping. The western margin of the Marystown Group is made up of clastic and epiclastic sediments of the Grandy's Pond Arenite Belt, which separate the Marystown volcanics from the bimodal volcanics of the Long Harbour Group to the west. The Marystown Group has been intruded by a series of high-level, coeval plutons consisting of hornblende-biotite granite, granodiorite, diorite and gabbro (O'Brien et al., 1999). On the northern half of the peninsula, these form a semi-continuous, north-northeast-trending plutonic belt, which includes the 577±3 Ma Swift Current Granite in the north (Tucker, unpublished data, O'Brien et al., 1998), and the 575.5±1 Ma 'Burin Knee Granite' (Sparkes and Dunning, 2014) to the south (*Figure 1-11*).

Flanking the Marystown Group along its eastern margin, and also occurring as a continuous belt north of the Burin Peninsula towards Bonavista Bay, is the ca. 570 Ma Musgravetown Group (O'Brien et al., 1989; *Fig 1-11*). This group is primarily composed of fluviatile and shallow marine epiclastic sedimentary rocks, but also includes lesser subaerial, bimodal volcanics. The sequence displays an overall transition from subaerial to shallow marine deposition (O'Brien et al., 1996; 1999).

Overlying the Marystown Group to the west and north is the ca. 570-550 Ma Long Harbour Group (*Figure 1-11*). The Long Harbour Group is dominated by subaerial felsic volcanics of alkaline to peralkaline affinity, with lesser bimodal horizons and siliciclastic sedimentary rocks. The Long Harbour Group can be further subdivided into a lower volcanic sequence (Belle Bay Formation), a middle clastic sedimentary unit (Anderson's Cove Formation), an upper volcanic sequence (Mooring Cove Formation), and an upper clastic sedimentary sequence (Recontre Formation) (Williams, 1971; O'Brien et al., 1995).

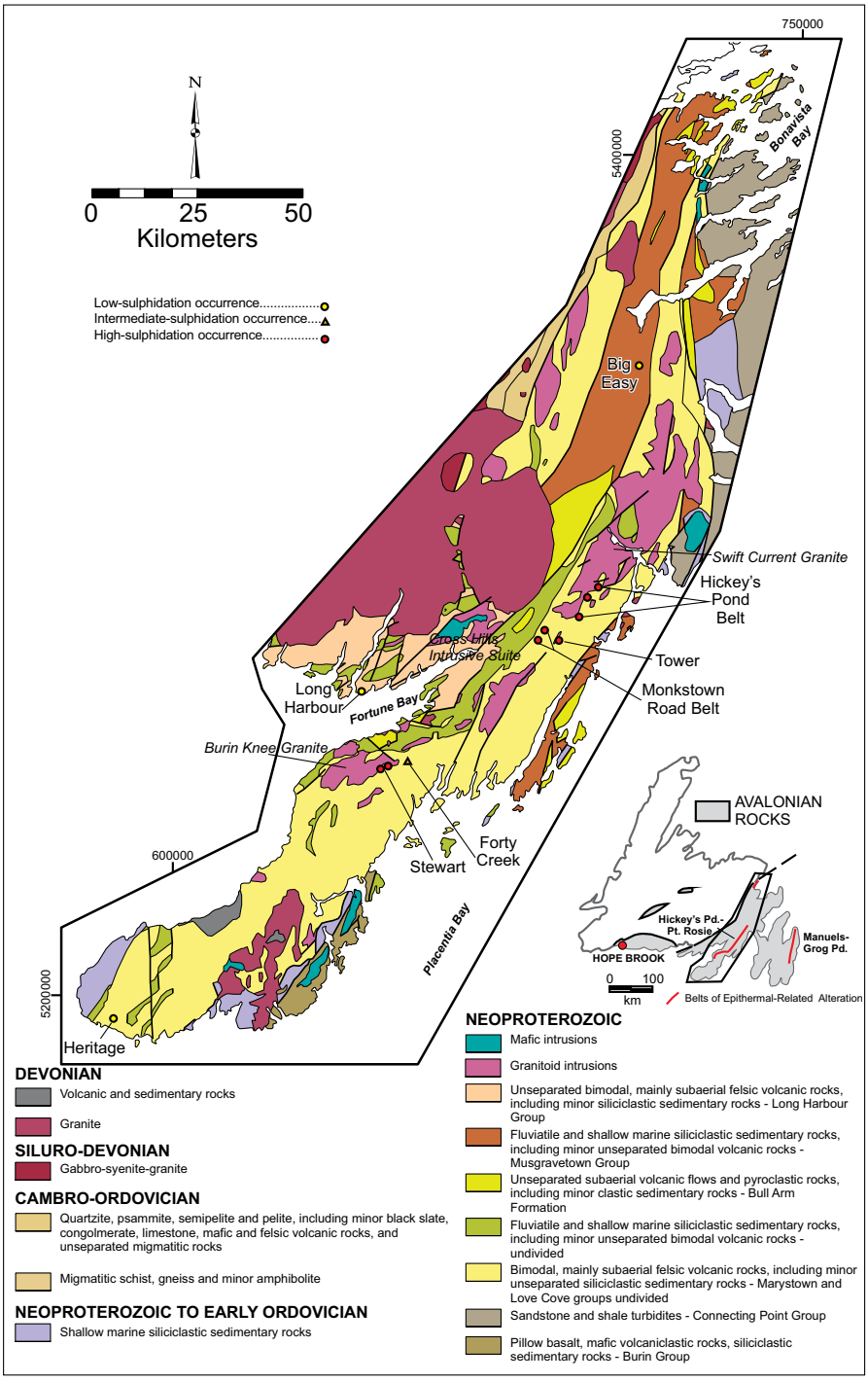

Figure 1-11*: Regional geology map of the western Avalon Zone of Newfoundland, with key epithermal prospects highlighted (modified from Sparkes and Dunning, 2014; O'Brien et al., 1998; coordinates are listed in NAD 27, Zone 21)*

All three of these Neoproterozoic aged groups are host to the epithermal-style gold mineralization present in the study region (e.g., Huard and O'Driscoll, 1985, 1986; O'Brien et al., 1998, 1999; Sparkes, 2012; Sparkes and Dunning, 2014; *Fig 1-11*).

1.7.1 Epithermal Gold Occurrences on the Burin Peninsula and a Summary of Previous Work

Examples of both high- and low-sulphidation, epithermal-style gold mineralization, are present throughout the Burin Peninsula, and – for the purpose of this study – the extended area as far north as Thorburn Lake-Clarenville.

The high-sulphidation occurrences are characterized by extensive zones of advanced argillic alteration, which are variably mineralized, and form a semi-continuous belt that can be traced along strike intermittently for over 100 km, coined the Hickey's Pond-Point Rosie alteration system (O'Brien et al., 1999; *Figure 1-10*). The alteration consists of variable proportions of pyrophyllite, alunite, quartz, specularite, and vuggy silica. These systems occur concentrated in the northern portion of the Burin Peninsula, hosted in Marystown Group volcanics, and include the high-sulphidation prospects examined in this study: Hickey's Pond, Monkstown Road, Tower, and Stewart (*Figure 1-11*). These prospects tend to be situated alongside the plutonic suites arrayed along the anticlinal core of the peninsula – although these junctions are often fault-bounded. The prospects, particularly Monkstown Road, are also spatially associated with the boundary between the Marystown Group felsic volcanics and epiclastic sediments of the Grandy's Pond Arenite Belt subdivision of the Marystown Group; an association possibly analogous to the occurrence of epithermal gold within the Carolina Slate Belt along a similar geological boundary (Feiss et al.,1993; O'Brien et al., 1999; Ayuso et al., 2005).

In contrast to the high-sulphidation prospects, which form regionally extensive alteration belts, the low-sulphidation occurrences are spatially more confined, occurring as isolated deposits. They are characterized by classic epithermal textures that include brecciation, blading, and crustiform and colloform banded veins, containing both quartz and chalcedonic silica, as well as adularia. Prospects of interest for this study include

Heritage, Long Harbour, and Big Easy (*Figure 1-11*). The Heritage prospect is located near Point May, at the southern tip of the peninsula, and nominally, is hosted in volcanic rocks of the Marystown Group. Just west of the peninsula, on the opposing (northern) shore of Fortune Bay, volcanic rocks of the Long Harbour Group host the Long Harbour occurrence. North of the Peninsula near the town of Clarenville, epiclastic sediments of the Musgravetown Group host the Big Easy.

1.7.1.2 Summary of Previous Work

The potential for significant gold deposits in the Burin Peninsula district wasn't fully recognized until the early 1980s, when Hickey's Pond was identified as a gold bearing advanced argillic alteration zone. The Hope Brook Mine in southwestern Newfoundland was discovered around the same time, and recognized to be of great similarity to Hickey's Pond. This prompted extensive gold exploration efforts on the Burin Peninsula by both industry and government throughout the 1980s, leading to the discovery of the many additional high-sulphidation occurrences along the Hickey's Pond-Point Rosie Belt.

Although the occurrence of high-sulphidation epithermal gold mineralization has been well documented since the 1980s, the potential for low-sulphidation epithermal-style gold has really only been recognized within the last decade, with the discovery of Long Harbour in 2004. The low-sulphidation style is increasingly considered highly prospective in the Burin Peninsula district, and throughout the Avalon Zone.

A detailed summary of previous work is provided below for these individual deposits.

Hickey's Pond

Mineralization at Hickey's Pond was first identified in the 1930s and subsequently evaluated for its iron ore potential, due to the presence of abundant specularite contained within quartz veins (Dahl, 1934; Bainbridge, 1934). Further studies by Howland (1938, 1940) dismissed the prospect as a viable iron source, but recognized the presence of alunite. In the late 1970s, pyrophyllite was also identified in association with the alunite,

and the potential for epithermal-related precious metal mineralization was first recognized (Hussey, 1978). In 1982, BP-Selco staked the area around Hickey's Pond and during the following year, conducted a geophysical survey, followed by a small diamond drill program. The results were rather mediocre, the best interval yielding 630 ppb Au over 2 m, and no further work was recommended (McKenzie and Gubins, 1983).

To follow up, the Newfoundland Geological Survey initiated a two-year program to document the mineral occurrence and evaluate the potential for similar occurrences in the surrounding area. During this study, significantly elevated gold grades were identified in grab samples at surface at Hickey's Pond (up to 5.4 g/t; Huard and O'Driscoll, 1985). In addition, the advanced argillic alteration was traced intermittently to both the northeast and southwest alongside the adjacent Swift Current granite, significantly increasing the known extent of the alteration (Huard and O'Driscoll, 1985, 1986). O'Driscoll (1984) also discussed the similarities in the mineralization and advanced argillic alteration occurring at Hickey's Pond with that of similar occurrences in the Carolina Slate Belt, as outlined by Spence et al. (1980). As part of this work, a masters thesis project was completed by Huard (1989), which led to the identification of two main mineralizing events at Hickey's Pond; silicification associated with the development of quartz-pyrite veins, and specularite-rich hydrothermal brecciation, both associated with anomalous gold concentrations. Huard (1989) also recognized the presence of telluride minerals at Hickey's Pond and elsewhere in the region, identifying what was inferred to be calaverite ($AuTe_2$).

In the late 1980s, there was renewed interest by industry. International Corona Corporation conducted further surface sampling and, in 1990, diamond drilling on the property - this time with more promising results. Gold values of up to 12.4 g/t over 1.2 m, and 1.9 g/t over 3.1 m, were recovered from channel sampling and drill core, respectively (Dimmell et al., 1990; Dimmell and MacGillivray, 1992). The property was picked up by Krinor Resources in 1993, but only compilation work was ever completed (Dimmell, 1998).

In the late 1990s, Hickey's Pond was re-evaluated by the Newfoundland Geological Survey, as part of a regional synthesis of the various known prospects. O'Brien et al. (1999) completed detailed alteration mapping, and a comprehensive structural analysis of the property. Over the past few years, the Newfoundland Geological Survey has conducted another regional study of the epithermal gold mineralization in the region, including the Hickey's Pond prospect, with a focus on U/Pb zircon geochronology and detailed alteration mapping using visible infra-red spectrometry (VIRS; Sparkes, 2012; Sparkes and Dunning, 2014; Sparkes et al., 2016).

Since the late 1990s, only limited industry-work has been performed on the property. Western Keltic Mines Inc. held the claims in the early 2000s, and carried out some additional surface sampling in the area (Sexton 2002, 2003). The most recent work to be completed at Hickey's Pond included minor sampling, the acquisition of satellite imagery, and further compilation work, which was performed by Cornerstone Resources between 2007 and 2009 (Dyke 2007, 2009a; Dyke and Pratt, 2008; Labonte, 2010).

Monkstown Road

Following the recognition of the potential for precious metal mineralization at Hickey's Pond in the early 1980s, the surrounding region became of great interest to both industry and governement. In 1983, the Monkstown Road showing was discovered by the Newfoundland Geological Survey, less than 20km down strike (SW) from Hickey's Pond (Tuach, 1984). The showing contains a similar advanced argillic alteration assemblage to that at Hickey's Pond, but is unique in that it contains an abundance of the blue phosphate mineral lazulite ($(Mg,Fe^{2+})Al_2(PO_4)_2(OH)_2$), as first documented by Tuach (1984). In 1983/1984, APEX completed a mapping and surface sampling program centred on this main showing. Only a handful of samples came back with anomalous gold values, the highest being 1.18 g/t (Saunders and Reusch, 1984). In 1985, Kidd Creek Newfoundland Ltd. optioned the Monkstown Road property from APEX and completed additional mapping and lithogeochemical sampling. Only a single sample

yielded an anomalous gold value (8.16 g/t), and additional sampling of the same outcrop was unsuccessful in reproducing any gold anomaly (Degagne and Robertson, 1985).

Since the mid-1980s, only limited work has been done on the property, and there have been no significant precious metals findings. Work has included compilation studies, and additional mapping and sampling. Workers include Corona Corporation in 1989, International Corona Corporation in 1991, prospector, Jeffrey Ralph in 1996, Rockhopper in 1996, GeoVector Management and Western Keltic Mines Inc. in 2002, and finally, Cornerstone Resources between 2007 and 2009 (Dimmell and MacGillivray, 1989; Dimmell et al., 1991; Ralph, 1996; Andrews, 1997; Sexton et al., 2003; Dyke, 2009a; Labonte, 2010).

Tower

The Tower prospect was first discovered in 1985 by Maritec Ltd., for Golden Hind Ventures. Maritec suggested setting up a grid and completing a geophysical survey, and a mapping and sampling program, but these recommendations were never brought to fruition (Reusch, 1985). Over the next couple of years, Cuvier Mines carried out some of the recommendations, setting up a grid, mapping the area, and collecting rock and humus samples. The results were inconclusive and the work ceased in 1987 (McBride, 1987). The claims were held by various workers over the years, but no significant work was done until 2002, when the property was staked by Peter Dimmell and Alex Turpin. They conducted a small prospecting, sampling and trenching program with limited success; their best grab sample yielding only 252 ppb gold (Dimmell, 2003). Comaplex Minerals Corp. picked up the property in 2006, and carried out additional prospecting and trenching. They were successful in collecting the best grab sample in the area to date, yielding 787 ppb gold (Noel, 2006a).

Between 2007 and 2009, Cornerstone Resources picked up the property. They obtained satellite imagery over the area, compiled historical data, and completed a small trenching program which involved trench mapping and channel sampling. Trenching identified a zone of hydrothermal brecciation, and abundant massive silica alteration, but

assays were discouraging; the best sample yielding 62.4 ppb Au over 3m in channel sample. Terraspec analysis was also completed on select samples, identifying alunite, pyrophyllite, illite, muscovite, and topaz around the trenches (Dyke, 2007, 2009a; Dyke and Pratt, 2008).

Stewart

The Stewart prospect was discovered in 1985 by Ralph Stewart, working for Kennco Explorations (Canada), after a sampling program in the region returned samples with gold values up to 1.05 g/t (Stewart, 1986). The property was optioned as a joint venture to Novamin Resources Inc. and Westley Mines Ltd. in the spring of 1986. The companies promptly completed an in depth ground geophysical survey as well as a small mapping and sampling program (Diner, 1986). Later that year, a small drill program, consisting of 4 holes, was carried out. Long intersections of anomalous gold and copper were identified, including 135 ppb Au and 385 ppm Cu over 102 m. Prominent alteration minerals were identified as pyrophyllite, chlorite, silica, and abundant pyrite (Zalnieriunas, 1987).

In 1988, Corona Resources optioned the property. They re-examined and re-sampled drill core from the 1986 drill program, and performed property-wide geological mapping and sampling. Based on their findings, nine small trenches were cleared and subsequently channel sampled, yielding values of up to 1.17 g/t Au over 1 m, and 623 ppb Au over >13m. It was noted that the best samples tend to correspond to strong pyrophyllite, sericite, silica, and alunite alteration and the presence of pyrite and chalcopyrite (Dimmell and MacGillivray, 1990a). In 1990, Corona Resources drilled 3 holes, the best interval measuring 0.25 g/t Au over 63 m, including 0.84 g/t Au over 5 m (Dimmell and MacGillivray, 1990b).

Work ceased for over a decade until the property was staked by Michelle Noel in 2003. It was optioned by Comaplex Minerals Corp. in 2006 for a short time (Noel, 2006b), and picked up by Cornerstone Capital Resources Inc., later that year. Between 2006 and 2008 Cornerstone Resources completed a considerable amount of work on the

property including the acquisition of satellite imagery, improving access to the property, uncovering two trenches, and performing detailed mapping, sampling and alteration studies. Channel sampling in the 800 m long Vinjer trench produced promising results, the best interval measuring 92 ppb Au, 193 ppm Cu, and 19 ppm Mo over 219 m, including 24 m with 228 ppm Au, 535 ppm Cu, and 16 ppm Mo. The best interval recovered from the 70 x 70m Stewart trench measured 555 ppb Au, 826 ppm Cu, and 48 ppm Mo over 12 m (Dyke 2007; Dyke and Pratt, 2008).

Detailed geological mapping by Pratt in 2007 (Dyke and Pratt, 2008), in conjunction with the use of Terraspec spectroscopy, defined a 5.5 km x 700 m wide alteration zone on the property. The alteration was found to be dominated by illite, including lesser topaz, diaspore, and local advanced argillic alteration of silica-alunite-pyrophyllite. Mapping also allowed for the subdivision of the local volcanic stratigraphy, and recognition of two distinct felsic tuffs (the 'Stewart Tuff' and the 'Caribou Tuff'); the latter of which is fairly consistently hydrothermally altered while the other is not. Detailed mapping of the Vinjer trench led to the identification of abundant quartz veins, minor copper sulphides, hydrothermal breccias, possible retrograded potassic alteration, and a previously undocumented quartz diorite body. Together, all of this was interpreted as possible evidence for mineralization closer in affinity to porphyry-style, rather than epithermal. Jeff Hedenquist, highly experienced in porphyry/epithermal environments, was consulted, and after visiting the property agreed that there was potential for porphyry-style gold-copper mineralization on the property (Hedenquist, 2007).

TerraX Minerals acquired the property in 2010, interested in this potential for porphyry-style mineralzation. During that year, compilation work was a main focus, but a property wide prospecting program was also executed. Sampling led to the discovery of a new showing (Forty Creek), where grab samples from angular blocks of quartz yielded gold values up to 59 g/t and silver values up to 2290 g/t. Forty Creek is located 5 km northeast and along strike from the Stewart alteration zone. The program also extended the alteration zone extent, both along and across strike (Setterfield, 2011).

In 2011, the company completed a soil geochemical survey, a deep penetration IP/resistivity survey and a high-resolution airborne magnetic survey (Setterfield and St-Hilaire, 2012). Geophysical anomalies were used as basis for planning a five-hole drill program, which was completed in the fall of 2011. Drill hole ST11-01 produced the best results with a 111 m continuous interval containing 0.13 g/t Au and 0.05% Cu (TerraX Minerals Inc., Press Release, December 16, 2011).

During the following year, work included trenching and sampling of the Forty Creek prospect. Trenching identified a vein set interpreted to be related to the high-grade quartz boulders assayed in 2010. The orientation of the veins was measured, with the intention of identifying future drill hole targets (TerraX Minerals Inc., Press Release, November 15, 2012).

Long Harbour

Prior to 1981, exploration in the Long Harbour area was focused on fluorite (e.g., Smith, 1953; Roley, 1953) and base metal occurrences. However, exploration for base metals in 1981 by Riocanex Inc. identified the first anomalous gold values in the region (Harris, 1981).

In 2003, Cornerstone Capital Resources Inc. began exploring the volcanic rocks of the Long Harbour Group, in the area of northern Fortune Bay. They identified the first known occurrence of low sulphidation-style crustiform-colloform banded chalcedonic silica veins in the western region of the Avalon Zone. In 2003 and 2004, Cornerstone conducted a prospecting and rock sampling program across the region. Although they identified veining and textures suggestive of low-sulphidation-style mineralization, sampling did not return any highly anomalous gold values (Seymour, 2004a; 2004b). Continued prospecting and rock sampling in 2005, led to the discovery of an area of alteration, brecciation, and colloform-crustiform banded quartz veins, continuous over a strike length of ~70m. Samples from this area returned gold values of up to 5.17 g/t from grab sample, and 2.29 g/t over 0.5 m from chip samples (Seymour, 2006).

In 2006, Cornerstone followed up on the promising results of their 2005 program, with continued prospecting and rock sampling in the surrounding area, and trenching and detailed sampling across a 25 m strike length, in the area that returned the highest gold grades. Trenching exposed cockade-style brecciation, colloform-crustiform banded quartz veins, bladed silica pseudomorphing calcite, as well as possible adularia alteration. Almost all of the channel samples returned anomalous gold values, the best interval returning 3.48 g/t Au over 0.9 m (Crewe and Seymour, 2007). No further follow-up work was ever conducted.

Big Easy

Big Easy is the northernmost prospect in the study area, located just northwest of Clarenville. The first positive indication for gold on the property was in the 1980s, when the Newfoundland government performed a regional lake sediment survey, resulting in an anomalous gold value of 10 ppb in a sample taken from Grassy Pond, in the property area (Davenport et al., 1988). GT Exploration Ltd. followed up on the anomalous sample, conducting fieldwork in 1994 and 1995, which included prospecting, mapping and rock sampling. This led to the discovery of an extensive silica-pyrite alteration zone, measuring 1.5 km along strike, and up to 150 m wide. Gold values were consistently weakly anomalous throughout the zone (Saunders, 1996). Work continued through 1996, with continued sampling, mapping and prospecting, yielding similar results to previous years. The work further confirmed the presence of anomalous gold, but did not help to delineate any trends towards higher-grade mineralization (Harris, 1996).

Work did not proceed until 2007, when Alex Turpin staked the property, subsequently optioning it to Cornerstone Resources. During a 2008 field program, Cornerstone extended the alteration zone to a length of 1.7 km and a width of 300-500 m, and recovered grab samples yielding up to 400 ppb Au and 4.6 g/t Ag. Using Terraspec, the alteration zone was determined to be weakly argillic to sub propylitic, and the prospect was interpreted to be of low-sulphidation epithermal affinity (Dyke, 2009b). In 2009, the property was transferred back to Alex Turpin, who conducted additional

sampling from float boulders scattered across the zone, the best samples yielding up to 1 g/t gold and 145 g/t silver (Turpin, 2010)

In 2010 Silver Spruce Resources optioned the property. That year, they constructed a grid over the alteration, carried out a prospecting program and completed an IP/Resistivity survey. Based on these results, five trenches were cleared, uncovering epithermal style alteration and textures including silicification and pyritization, brecciaton, and finely banded quartz veins. Channel sampling resulted in gold grades up to 2.08 g/t over 0.7 m. Dr. Greg Arehart, a recognized expert in epithermal and Carlin-type gold deposits, visited the property later that year and concurred that the various attributes of the showing were consistent with that of an epithermal system (MacGillivray et al., 2011).

Prospecting in early 2011 located a new mineralized alteration zone, about 3.5 km south and along strike of the Big Easy showing (the ET Zone), yielding anomalous gold and silver values and of a similar alteration style to the original prospect. The new zone has been interpreted as a continuation of the original alteration zone, expanding the prospective strike length of alteration to over 5 km (MacGillivray et al., 2011). Later in 2011, a seven-hole drill program was conducted, all holes intersecting anomalous gold and silver values. The best interval occurred in drill-hole, BE-11-3, with 0.87 g/t Au and 33 g/t Ag occurring over 30.5 m, including a 1.5 m interval with 6.05 g/t Au and 174 g/t Ag. Significant values also occurred in drill-hole, BE-11-7, including 7.65 g/t Au and 10 g/t Ag across 1 m, and 319 ppb Au and 13 g/t Ag over 18.6 m (DeLazzer and Dimmell, 2012).

A second phase of drilling was conducted in 2012, consisting of five holes. The most significant interval measured 1.3 g/t Au and 36.7 g/t Ag over 8.7 m, including 1.2m with 7.9 g/t Au and 130 g/t Ag. An airborne, high resolution magnetic and VLF-EM geophysical survey was also conducted during 2012 (Dimmell et al., 2012).

Work in 2013 mostly consisted of compilation studies and evaluation of data by various consultants. Jeffrey Hedenquist, an expert in epithermal precious metal systems,

visited the property and confirmed that the Big Easy prospect has many characteristics of a low-sulphidation epithermal system. A significant finding was confirmation that textures and veins found in outcrop (including potential finely banded sinter), do represent the paleosurface of the system during its formation. This observation would suggest that if high-grade precious metal veins are present in the system, they should still lie below the present surface (Dimmell et al., 2015). U-Pb TIMS dating was carried out on a mafic dyke cross-cutting the mineralization, as part of a BSc Honours thesis by Clarke (2013). An age of 566±2 Ma was measured for the dyke, providing a minimum age constraint for the mineralization.

Exploration in 2014 consisted of additional prospecting, sampling, and a seven-hole drill program. Drilling results were similar to previous years, but also included the intersection of substantial molybdenite mineralization, with Mo values up to 4449 ppm over 0.3 m (Dimmell et al., 2015).

Heritage

The Heritage prospect is the newest discovery of those considered in this study, and located at the southern extent of the study area, at the tip of the Burin Peninsula near Point May. The property was discovered by prospectors Alex Turpin and Albert Stone in 2011, and subsequently optioned by the privately funded, junior exploration company, Puddle Pond Resources Inc. in 2012 (Puddle Pond Resources, Press Release, June 1, 2012). Over the past few years, Puddle Pond Resources Inc. has completed a considerable amount of work on the property, including two drill programs and ongoing geological mapping, prospecting, trenching, and sampling.

In 2012, twelve trenches were cleared over a 1 km strike length section of a presumed 2.5 km epithermal alteration zone. Trenching uncovered significant quartz veining and brecciation across the zone, and channel samples yielded gold values up to 13.1 g/t and silver values up to 320 g/t (interval length not reported; Puddle Pond Resources, Press Release, October 31, 2012). A five-hole drill program was conducted in early 2013 with encouraging results. Some of the best intersections include 2.4 g/t gold

over 0.5 m, and 0.25 g/t gold over 34.83 m. Anomalous silver values were also measured; one of the best intervals yielding 288g/t silver across a 0.4 m interval (Puddle Pond Resources, Press Release, March 21, 2013).

Prospecting and sampling was conducted during the summer in 2013, which identified a new zone (Eagle Zone) of pervasive silicification and quartz veining accompanied by anomalous gold and silver values (Eagle Zone). This zone is inferred to occur over an area of 1000x300 m. Grab samples from the zone yielded up to 2.72 g/t Au and 241.2 g/t Ag (Puddle Pond Resources, Press Release, October 15, 2013). An eight-hole drill program was initiated in the fall of 2013 to test this new zone, once again, with promising results. The best interval contained 5.2 g/t Au and 155 g/t Ag over 5 m (Puddle Pond Resources, Press Release, December 6, 2013). This was followed up with the completion of an IP geophysical survey during the summer of 2014, which identified multiple geophysical anomalies indicative of mineralization potential within the Eagle Zone, defining new future drilling targets (Puddle Pond Resources, Press Release, July 23, 2014).

A 25-hole drill program was completed at the Eagle Zone in 2015, to test the IP anomalies and follow up on any high-grade mineralization intersected during the 2013 drill program. The best intervals included 1.54 g/t Au and 447 g/t Ag over 1.45m, and 1.94 g/t Au and 313 g/t Ag over 1.35m. Drilling results also confirmed that the Eagle Zone is open in both directions beyond a length of 1000m (Puddle Pond Resources, Press Release, November 18, 2015). In the summer of 2016, the company plans to complete a 5000 m drill program to further define mineralization in the Eagle Zone, and also to conduct ground and airborne geophysical surveys (Puddle Pond Resources, Press Release, March 21, 2016).

Note: Since Chapters 2 through 6 are designed to form the basis of free standing papers for future journal publications, some introductory, summary and overview text is repeated in their introductory sections.

CHAPTER 2:
DESCRIPTION OF REGIONAL STRATIGRAPHY AND KEY GEOLOGICAL UNITS ASSOCIATED WITH EPITHERMAL GOLD MINERALIZATION IN THE BURIN PENINSULA REGION

2.1 Introduction

This was designed as a broad, regional scale project, with the primary focus being the economic potential and characterization of the various prospects. Therefore, detailed geological mapping of the region was not within the scope of this study. The aim of this section is to present an overview of the general stratigraphy of the three main geological groups that make up the project area (Marystown, Musgravetown and Long Harbour), as informed by the local host geology of the prospects studied, rather than to provide a comprehensive report or detailed regional map of these groups. More specifically, the purpose of this chapter is to illustrate the volcanic arc affinity of the region, highlighting the prominent lithologies and textures associated with the volcanics and late-syn to post-volcaniclastic sediments that comprise these distinct groups, all three of which are host to epithermal gold occurrences. Key geological units associated with the epithermal-style mineralization at the prospects studied are introduced and discussed as members of their host lithological group. Since most of the samples collected are associated with epithermal mineralization, many have some degree of hydrothermal alteration. However, original igneous textures and minerals are still commonly preserved to varying degrees and provide the basis for rock classification. While some of the hydrothermal alteration may be mentioned herein, a detailed discussion is reserved for the subsequent chapters specifically devoted to describing the high- and low-sulphidation epithermal systems. Alteration and deformation associated with the regional greenschist metamorphism that has affected the entire region will be reviewed here. The term sericite is used throughout this chapter to describe any fine-grained white mica, including muscovite, paragonite or phengite.

The following content incorporates field and petrographic observations and photos acquired as part of this study. The prefix “STA” indicates a station number, as opposed to sample numbers, which don’t include this prefix. Sample numbers starting with “GS”,

were collected by Greg Sparkes (Newfoundland Geological Survey) in 2011 or 2012 during fieldwork related to this project. Any detailed mapping conducted by other authors on the various prospects prior to this study is also included, to supplement the generally coarser sampling done as part of this regional scale project. *Appendix A* can be referred to for more information regarding field work and sampling for this project, including tables of samples (*Table A-1*) and field stations (*Table A-2*), complete with field descriptions and locations.

2.2 Regional Overview

As discussed in *Chapter 1*, the Burin Peninsula region comprises the western portion of the Avalon Zone in Newfoundland and is characterized by wide-spread, late-Neoproterozoic magmatic arc activity that predominantly occurred between ca. 590 to 550 Ma (e.g., Krogh et al., 1988; O'Brien et al., 1995; 1996; Sparkes and Dunning, 2014). Volcanism was associated with arc, arc-adjacent, or continental extensional settings, and is associated with the development of syn- to post-volcanic siliciclastic sedimentary basins of marine, deltaic, and terrestrial affinity (O'Brien et al., 1998, O'Brien et al., 1999). The region is divided into three main lithological groups – Marystown, Musgravetown and Long Harbour (*Figure 2-1*) – which are described in the following sections. The local geology of individual epithermal prospects is described and presented in the context of their respective lithological group.

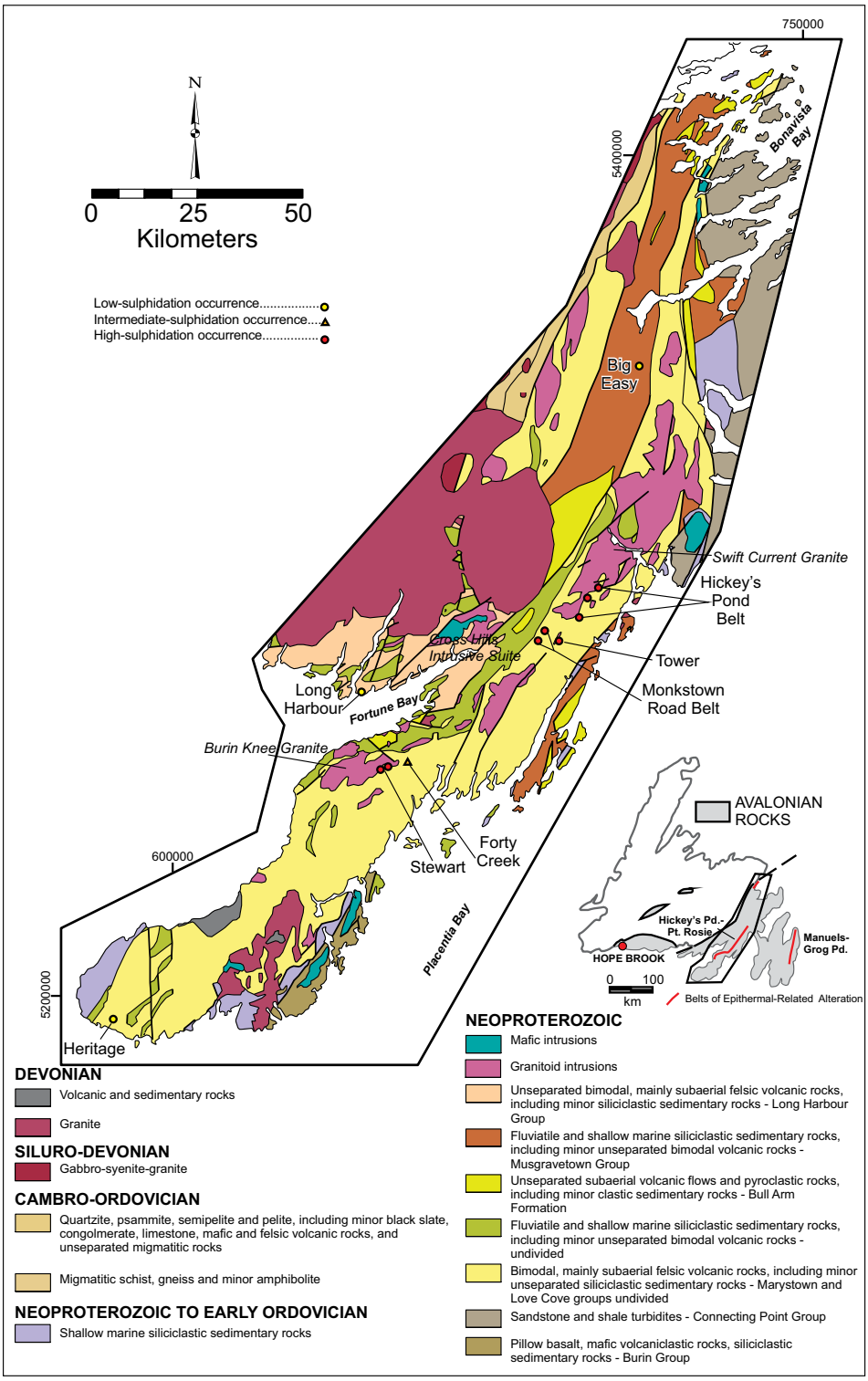

Figure 2-1*: Regional geology map of the western Avalon Zone of Newfoundland, with key epithermal prospects highlighted (modified from Sparkes and Dunning, 2014; O'Brien et al., 1998; coordinates are listed in NAD 27, Zone 21).*

2.2.1 Regional Greenschist Metamorphism and Deformation

All of the Neoproterozoic volcano-sedimentary rocks of the Marystown, Musgravetown and Long Harbour groups underwent greenschist facies metamorphism and transpression-related deformation during the late Silurian-early Devonian, as a result of their accretion to the Laurentian margin (van Staal, 2007; van Staal et al., 2009). The intensity of deformation and greenschist-grade metamorphism generally increases westward, towards the tectonic contact between Avalonia and Ganderia, (Blackwood and Kennedy, 1975; Kennedy et al., 1982; Dallmeyer et al., 1983; O'Brien et al., 1996) which roughly coincides with the western margin of the map in *Figure 2-1*.

2.3 Marystown Group

The majority of the Burin Peninsula is made up of the ca. 590-570 Ma Marystown Group, which makes up the core of a broad-scale N-NE trending anticlinorium (Strong et al., 1978b; O'Brien et al., 1999). The Marystown Group is composed of greenschist-facies subaerial flows and pyroclastics, ranging in composition from basalt through to rhyolite, all of variable calc-alkaline and tholeiitic affinity (Hussey, 1979; O'Brien et al., 1990; 1996; 1999). Although these lithologies would be typical products of caldera-forming eruptions, individual caldera centres or the associated structures, have not yet been explicitly defined. The western margin of the Marystown Group is made up of clastic and epiclastic sediments of the Grandy's Pond Arenite Belt, which separate the Marystown volcanics from the bimodal volcanics of the Long Harbour Group to the west. The Marystown Group has been intruded by a series of high-level, coeval plutons consisting of hornblende-biotite granite, granodiorite, diorite and gabbro (O'Brien et al., 1999). On the northern half of the peninsula, these form a semi-continuous, north-northeast-trending plutonic belt, which includes the 577±3 Ma Swift Current Granite in the north (Tucker, unpublished data; O'Brien et al., 1998), and the 575.5±1 Ma 'Burin Knee Granite' (Sparkes and Dunning, 2014) to the south.

The Marystown Group is host to an extensive belt of high-sulphidation epithermal occurrences, which include the Stewart, Hickey's Pond and Tower prospects. These are

all distributed alongside the plutonic suite and display a variable spatial association with the Grandy's Pond Arenite Belt. The Marystown Group is also, nominally, host to the low-sulphidation Heritage prospect in the south. The main geological units and local geology of the aforementioned prospects, and examples of the Grandy's Pond Arenite Belt and Swift Current Granite are described below. The geology of the Stewart prospect is described in significantly more detail than the other prospects, to complement the more comprehensive lithogeochemical and geochronological sampling performed on the prospect.

2.3.1 Stewart (and Forty Creek) Prospect(s)

A significant portion of the fieldwork conducted for this project was focussed on the Stewart prospect, with samples collected from both surface outcrops and drillcore. As such, a more detailed description of the local geology is provided for the prospect, relative to those in subsequent sections. The majority of samples were collected to assess the hydrothermal alteration and mineralization, but a number of representative samples of the less altered host stratigraphy were also collected. In some instances, however, pervasive hydrothermal alteration and subsequent deformation are prevalent throughout the entirety of a rock unit (e.g., the Caribou Tuff, and the tonalite intrusion) making characterization of the primary host rock more difficult.

The property was mapped in detail in 2007 by Warren Pratt for Cornerstone Resources, and the results are displayed in the geological map shown in *Figure 2-2*. The map has been simplified from its original format, but the unit names and definitions outlined by Pratt remain unchanged. This map was used as the basis for unit identification and sample collection in the field. For consistency, the lithological descriptions that follow generally adhere to the stratigraphy and nomenclature established by Pratt, unless otherwise noted.

The Stewart prospect is situated midway down the peninsula (*Figure 2-1*) near the intrusive contact of a large, high-level plutonic suite, referred to as the 'Burin Knee Intrusive Suite', with adjacent felsic volcaniclastic rocks of the Marystown Group. The

Burin Knee Intrusive Suite has previously been described as consisting of hornblende-biotite granite with lesser felsite and quartz porphyry and is interpreted to be coeval with the Swift Current Granite immediately to the north (O'Brien and Taylor, 1983; O'Brien et al., 1984, 1999). The Stewart prospect is characterized by an extensive, curvilinear zone of advanced argillic alteration, roughly 5.5 km long and 700 m wide, hosting extensive low-grade copper and gold mineralization. The alteration zone is roughly constrained between a lower package of intermediate-mafic volcanics to the southeast, and the Burin Knee Intrusive Suite to the northwest (*Figure 2-2*). However, the margin of the Burin Knee Intrusive Suite contains a 2-3m zone of muscovite-dominated alteration, which is presumably of hydrothermal origin (Sparkes et al., 2012). The lower intermediate-mafic volcanic sequence is also significantly altered - but to an assemblage dominated by chlorite and epidote, most likely related to regional greenschist metamorphism.

Approximately 5 km northeast and along strike of the main Stewart prospect, is the more recently discovered Forty Creek prospect (*Figure 2-1*). This prospect contains a localized cluster of large mineralized boulders of quartz-dominant vein material, highly anomalous in gold and silver. The prospect is centred over a sequence of intermediate volcaniclastic rocks, presumed to represent the on strike extension of the volcaniclastic stratigraphy of Stewart.

2.3.1.1 Lithology, Field Relationships and Petrography of Rock Units at the Stewart Prospect

A penetrative foliation can be traced property-wide, generally striking to the southwest with a variable subvertical dip. Most commonly the fabric dips steeply northwest, with stratigraphy also younging towards the northwest, as interpreted by Pratt (Dyke and Pratt, 2008). Additional evidence to support this interpretation was recognized during fieldwork for this project, including graded bedding fining towards the north-northwest, and sedimentary beds truncated by volcaniclastic rocks towards the north-northwest (*Plate 2-1*). Descriptions of lithology, field relationships and petrography of the main units at Stewart are provided below, in the order of oldest to youngest interpreted ages. Revised lithological names are introduced here, but the units still

correspond to those outlined in *Figure 2-2*, and the nomenclature established by Pratt is also included, displayed in parentheses in the main headings, to avoid any confusion.

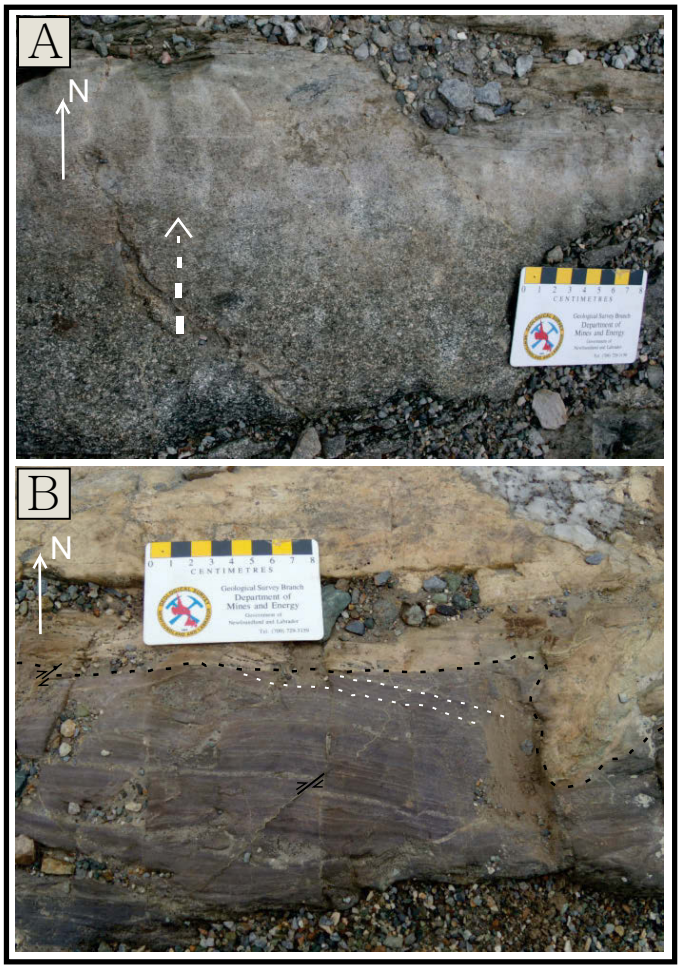

***Plate 2-1**: Indicators of north-northwestward younging direction;*
A) Graded bedding in an epiclastic sediment, fining towards the north (STA-SF-12-025);
B) Well-bedded siltstone with beds (highlighted by dotted white line) truncated by an overlying fine-grained tuff unit towards the north. Also shown is minor dextral displacement along a small northeast trending fault (STA-SF-12-006)

The volcanic stratigraphy includes intermediate-mafic volcanics of the 'Lower Volcanic Unit', a dacitic quartz-feldspar crystal-rich tuff ('Stewart Tuff'), a dacitic quartz crystal-rich tuff ('Caribou Tuff'), and intermediate-mafic volcanics of the 'Upper Volcanic Unit'. Intrusive units include porphyritic andesitic-basalt ('Microdiorite'), a series of porphyritic dacite dykes ('Granite'), tonalite ('Quartz Diorite'), the 'Burin Knee Intrusive Suite' ('Granite') ranging in composition from diorite to granite, and a series of late mafic dykes.

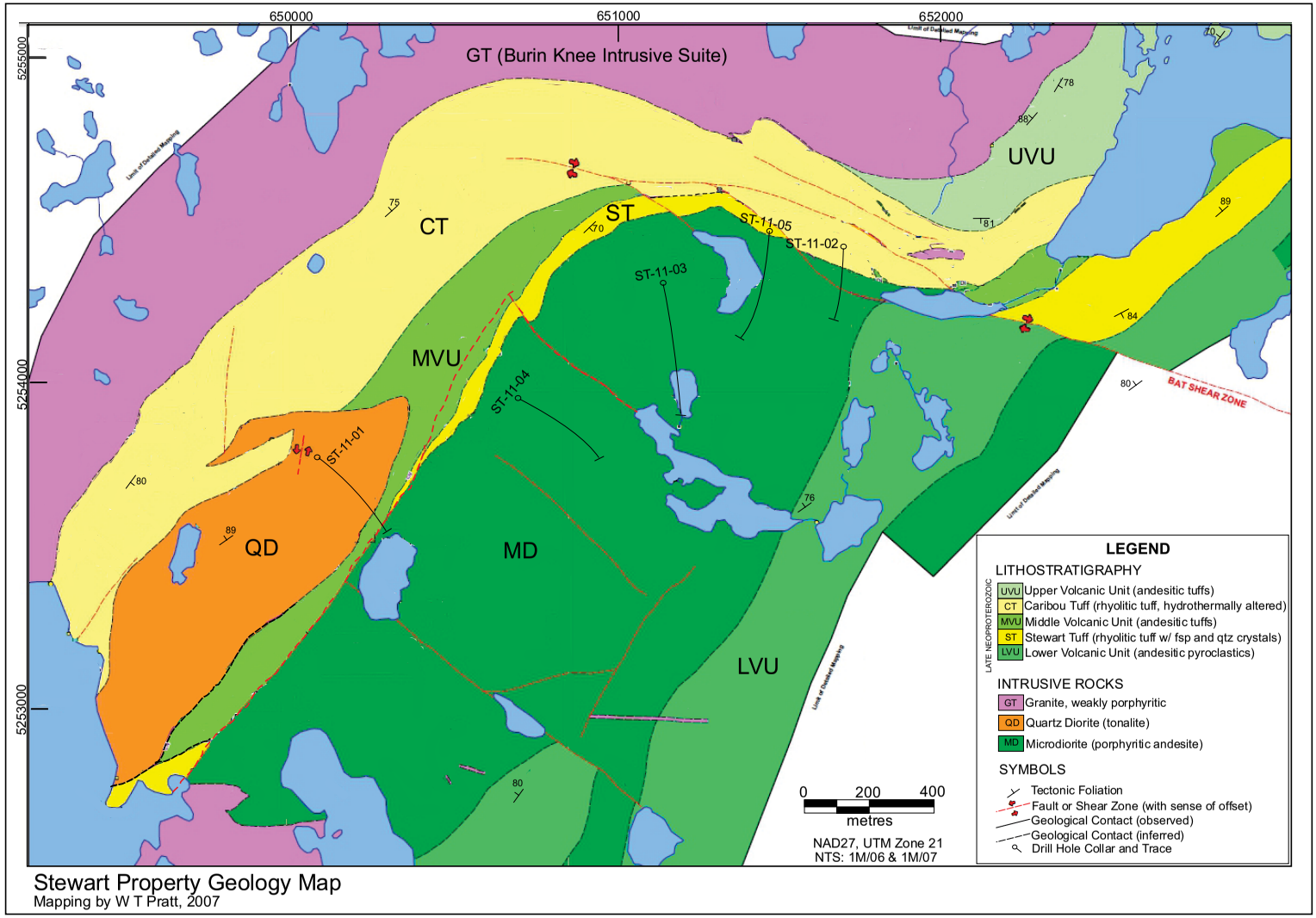

***Figure 2-2**: 1:5000 scale, Stewart Property Geology Map. Displays drill hole traces from TerraX Minerals 2011 drilling program. Mapping was completed in 2007 by Warren Pratt, for Cornerstone Resources (modified from Dyke and Pratt, 2008; coordinates are listed in NAD 27, Zone 21).*

Intermediate-Mafic Volcanics (Lower Volcanic Unit)

The south-southeastern part of the property is comprised of an extensive sequence of intermediate to mafic volcanic rocks, which have been coarsely grouped into one unit, referred to as the Lower Volcanic Unit. It is interlayered with a coarsely-porphyritic andesitic-basalt (described below), the contacts of which are not clearly exposed in the field. This unit is referred to as 'Microdiorite' by Pratt and in current work by TerraX Minerals, and was interpreted by Pratt to represent a series of contemporaneous massive, high-level intrusive sills. Exposure of the Lower Volcanic Unit on surface in the vicinity of the Stewart prospect is fairly limited. However, where it was recognized, it most commonly displayed volcaniclastic textures. Rare examples of what appears to be massive fine-grained basaltic flows were also identified, both in surface outcrops, and as thick intervals intersected at depth during drilling.

The volcaniclastic rocks are andesitic to basaltic in composition and include tuffs, lapilli tuffs, and tuff breccias. They are typically green to grey in colour on both fresh and weathered surfaces, but some outcrops are characteristically maroon to red in colour (*Plate 2-2 A*), suggesting oxidation during deposition, typical of subaerial environments. The more massive tuffs are chloritized and contain variable amounts of plagioclase crystals throughout their matrix (*Plate 2-2 E*). The lapilli tuffs (*Plate 2-2 B-D*) and tuff breccias (*Plate 2-2 A*) contain lapilli and blocks most commonly composed of massive porphyritic andesite to basalt, typically green-grey in colour but occasionally oxidized to a maroon colour (*Plate 2-2 C*). The fragments are contained within a feldspar-phyric, fine-grained matrix raging in composition from andesite to basalt. One sample (GS-11-99; *Plate 2-2 D*) collected from the upper portion of the sequence close to the contact with the overlying felsic volcaniclastics, contains lapilli fragments closely resembling the porphyritic andesitic-basalt sills intruding the sequence. This would suggest that the two units formed relatively contemporaneously, in accordance with Pratt's interpretation.

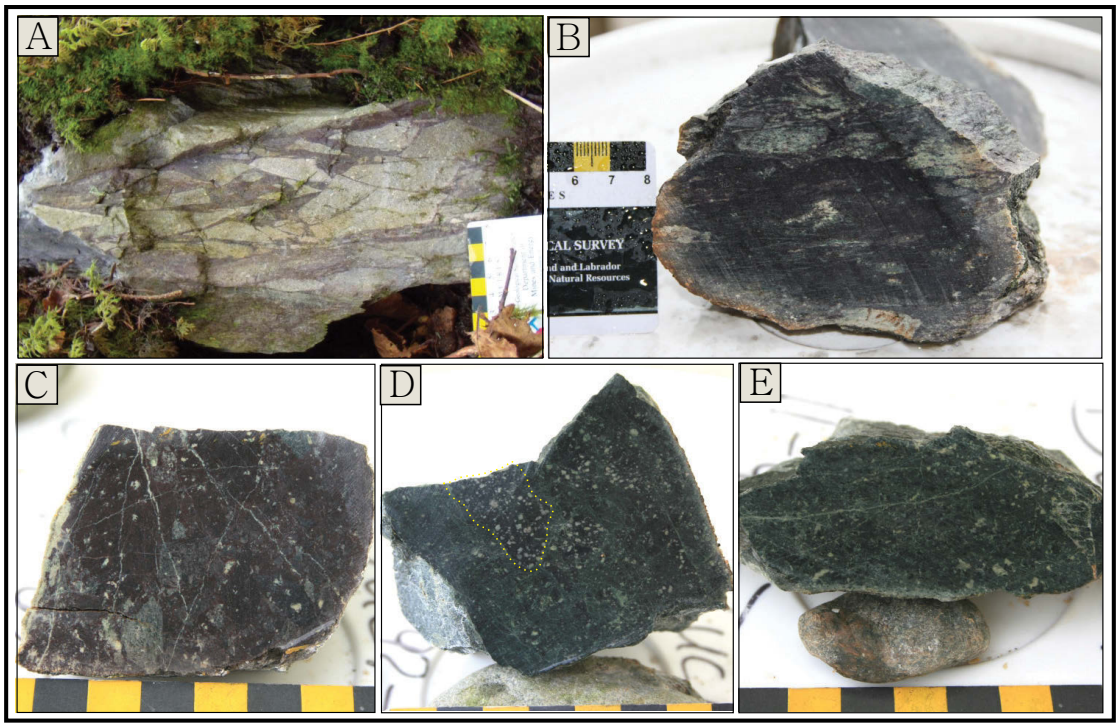

***Plate 2-2**: Representative photos of the intermediate-mafic volcaniclastics of the Lower Volcanic Unit; A) Field photograph of an andesitic lapilli tuff/tuff breccia, with a red, oxidized, fine-grained, variably plagioclase-phyric matrix, hosting subangular plagioclase-phyric andesitic-basaltic clasts, 1-8cm in size (STA-SF-12-135; SF-12-70); B) Andesitic lapilli tuff with an oxidized fine grained plagioclase-phyric matrix containing green, chloritic, subrounded lapilli 1-3cm in size of andesitic-basaltic composition (SF-12-70); C) Andesitic heterolithic lapilli tuff with an oxidized plagioclase-phyric matrix. Lapilli are composed of both green and maroon (oxidized) porphyritic andesite to basalt (GS-11-97); D) Basaltic lapilli tuff with a chloritized, variably plagioclase-phyric matrix containing 1-5cm subround-subangular plagioclase-phyric andesitic-basalt fragments, closely resembling the porphyritic andesitic-basalt/Microdiorite sills (GS-11-99); E) Mafic tuff - sample is pervasively chloritized and contains variable patches of plagioclase phenocrysts (GS-11-95); note that sample is similar in composition to the matrix of D).*

Sample SF-12-70, shown in *Plate 2-2 A&B*, was chosen as a representative sample of the volcaniclastics from the Lower Volcanic Unit for petrography. The section contains about 40% sub-rounded lapilli, ranging in size from 2mm to 3cm, preferentially aligned along a weak pervasive foliation. The surrounding matrix is very fine-grained, and predominantly composed of sericitized feldspars, some of which are weakly porphyritic forming subhedral laths ~30µm in length, and approximately 10% very fine-grained quartz (*Plate 2-3 A*). Most of the lapilli are similar in appearance to the matrix, with a very fine grain size and 15-20% sericitized, lath-shaped plagioclase phenocrysts, slightly better defined than the laths in the matrix. However, the lapilli appear to be more

mafic in composition, displaying weak but pervasive chlorite alteration accompanied by abundant Fe-Ti-oxides (*Plate 2-3 A*). A second type of lapilli fragment is shown in *Plate 2-3 (B-D)*, interpreted to be a welded mafic volcaniclastic. It contains large quartz filled vesicles with undulating margins, smaller epidote and calcite filled vesicles rimmed by quartz, and flattened, wavy fiamme, now composed of chlorite and fine-grained quartz.

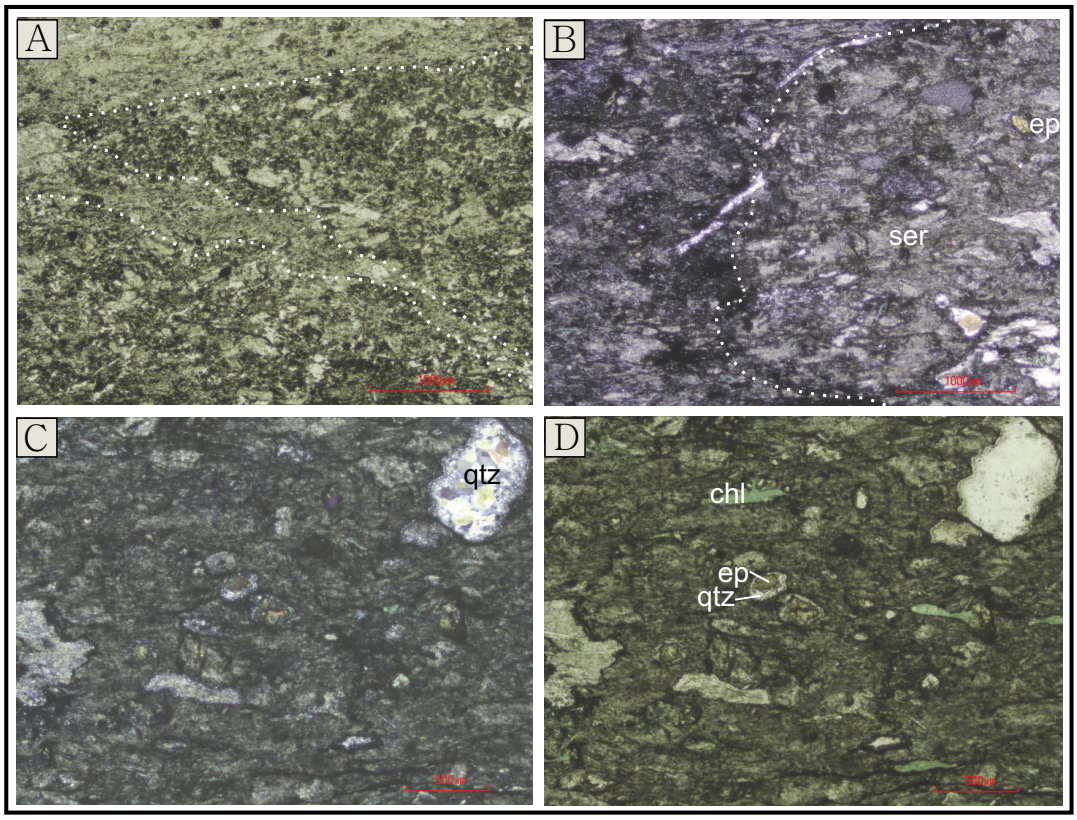

***Plate 2-3**: Photomicrographs of volcaniclastic textures from sample SF-12-70; A) (PPL;2X) Two lapilli fragments (outlined), pervasively altered to chlorite and sericite, with sericitized plagioclase phenocrysts and abundant Fe-Ti-oxides. Matrix is composed of very fine-grained sericitized feldspar and lesser quartz; B) (XPL;2X) Edge of a welded mafic volcaniclastic lapilli fragment is shown (right) within the very fine-grained andesite matrix (left). Lapilli is composed of abundant sericitized plagioclase feldspars, and contains sinuous quartz filled vesicles, smaller epidote and quartz rimmed vesicles, and fiamme, now replaced by fine quartz and chlorite; C) & D)(4X; XPL and PPL respectively) Close-up of large quartz filled vesicle, smaller epidote and calcite filled vesicles rimmed by quartz, and flattened fiamme now filled with chlorite and quartz. ser=sericite, ep=epidote, qtz=quartz, chl=chlorite.*

The massive basaltic flows within the Lower Volcanic Unit are fine grained and green in colour. Characteristic of this unit are fine, black magnetite phenocrysts, approximately 1mm in size, but locally up to 3mm (*Plate 2-4 B*), which occur in addition to locally occurring magnetite veinlets (*Plate 2-4 D*). The flows are pervasively altered to

chlorite, with lesser semi-pervasive epidote, which is more concentrated along fractures and veins (*Plate 2-4*). Although chlorite and epidote can be indicative of propylitic alteration, as part of a hydrothermal alteration zone, the abundant chlorite and epidote alteration found here is more likely the result of regional greenschist metamorphism.

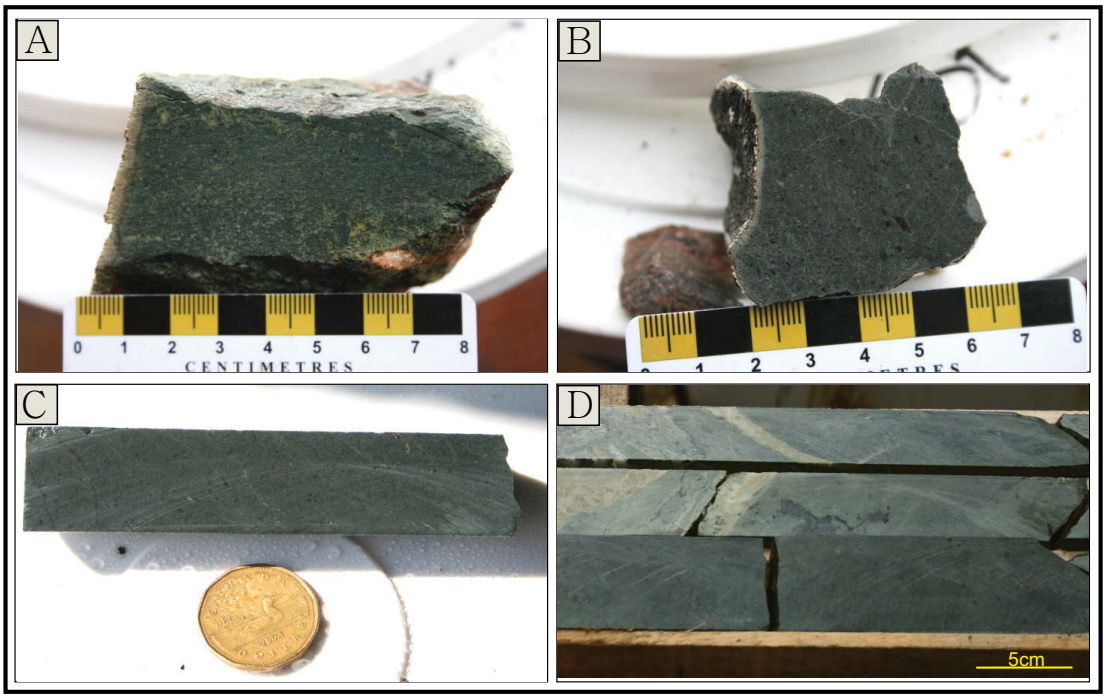

***Plate 2-4**: Representative photos of the massive magnetite-phyric basaltic flows of the Lower Volcanic Unit; A) Fine-grained massive mafic volcanic, with moderate pervasive chlorite alteration, weaker pervasive epidote alteration and epidote altered fractures (GS-12-252); B) Magnetite-phyric massive mafic volcanic with a fine-grained green groundmass with 1-3mm magnetite phenocrysts (GS-12-254); C) Fine-grained massive basalt, with pervasive chlorite alteration, fine fractures of magnetite, and 1-2% 1mm-sized magnetite phenocrysts (SF-12-141; DDH ST-11-03; ~273m); D) Fine-grained massive basalt pervasively altered to chlorite, with 1-2% magnetite phenocrysts up to 3mm in size, and rare magnetite veinlets, and epidote altered fractures and veins (SF-12-139; DDH ST-11-03; ~138m).*

In thin section, the magnetite-phyric massive basaltic flows are very fine grained and comprised of a relatively equigranular matrix of ~60% plagioclase, ~35% clinopyroxene, and up to 5% magnetite (*Plate 2-5*). Plagioclase grains occur as thin sub-euhedral laths displaying simple and polysynthetic twinning. Where measureable, twinning extinction angles indicate a composition of andesine. Clinopyroxene occurs as subhedral, stubby, tabular crystals, with only one cleavage ever evident. Magnetite is evenly distributed throughout the sections and occurs in an abundance of 2-5% as sub-euhedral isometric crystals (*Plate 2-5 E&F*). Sections also contain minor chlorite,

epidote and calcite as products of alteration. Weak pervasive chlorite is dusted throughout the sections, affecting both feldspar and pyroxene grains. Epidote occurs in clusters, scattered throughout (*Plate 2-5 A-B*) and very minor calcite occurs in small isolated patches.

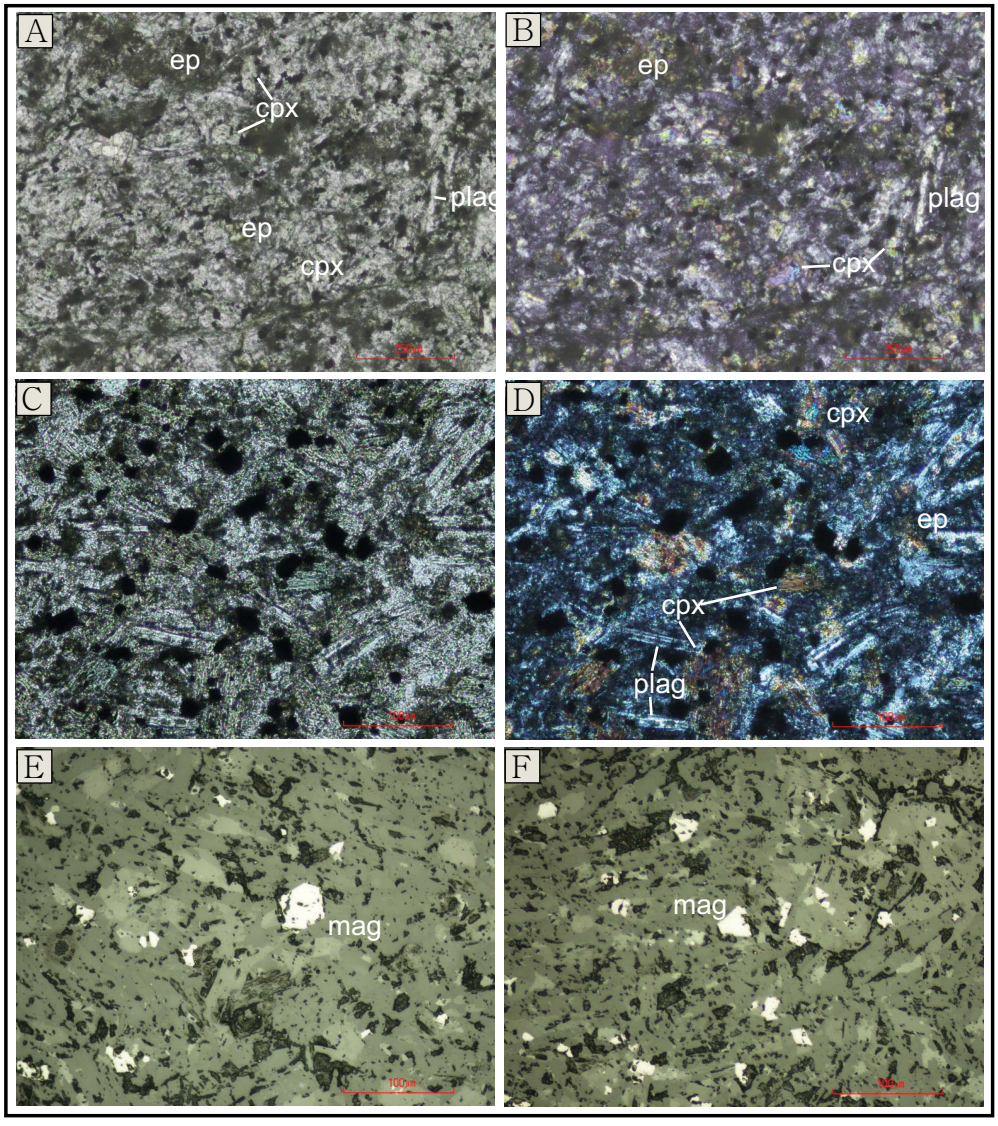

Plate 2-5*: Representative photomicrographs of the massive magnetite-phyric basaltic flows of the Lower Volcanic Unit; A & B)(10X; PPL and XPL, respectively) very-fine grained, matrix of clinopyroxene and plagioclase, with patchy epidote alteration (SF-12-140); C & D)(20X; PPL and XPL, respectively) Very fine-grained, equigranular matrix of subhedral tabular crystals of clinopyroxene and sub-euhedral narrow laths of plagioclase both weakly affected by chlorite alteration, occurring with patches of epidote and disseminated magnetite (opaque) (SF-12-141); E & F) (RL; 20X) Euhedral isometric crystals of magnetite evenly distributed through matrix (SF-12-141). ep=epidote, cpx=clinopyroxene, plag=plagioclase feldspar, mag=magnetite.*

Porphyritic Andesitic-Basalt ('Microdiorite')

The porphyritic andesitic-basalt unit occurs interlayered with, and predominantly confined within, the massive basaltic flows and intermediate-mafic volcaniclastics of the Lower Volcanic Unit. Where observed, contacts are sharp with adjacent units, however diagnostic intrusive characteristics, such as chill margins, were not noted. As previously mentioned, this unit is referred to as 'Microdiorite' by Pratt and in current work by TerraX Minerals, and has been interpreted by Pratt to represent contemporaneous massive, high-level intrusive sills.

The unit is distinctive in appearance, containing coarse 1-4mm plagioclase phenocrysts contained within a very fine-grained dark greenish-grey matrix (*Plate 2-6*). The abundance of phenocrysts varies throughout the unit from 25-50% and there tends to be a bimodal distribution of phenocryst sizes; 0.5-1mm and 2-4mm. Plagioclase phenocrysts are commonly pale green in colour, as a result of epidote-sericite alteration, and occasionally appear zoned, highlighted by the alteration colouration. The unit is cross cut by abundant quartz-epidote veinlets and seems to have been affected to some degree by pervasive silicification.

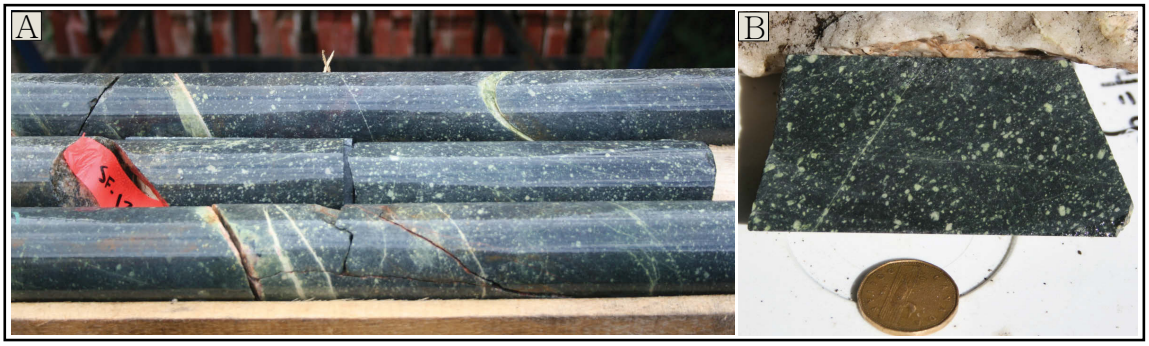

Plate 2-6*: Representative photos of the porphyritic andesitic-basalt (Microdiorite); A) part of a ~37m interval of the unit intersected in drill core, showing abundant quartz-epidote veinlets and porphyritic texture of plagioclase feldspars, altered to epidote-sericite (SF-12-147; DDH ST-11-03; ~57m); B) 1-4mm pale green plagioclase phenocrysts within a very fine-grained green-grey matrix with quartz-epidote veinlets (SF-12-138; DDH ST-11-03; ~64m).*

Sample SF-12-138 from this unit was selected for petrographic analysis (*Plate 2-7*). In thin section, the unit appears extensively altered and shows a significant amount of recrystallization. Groundmass constitutes ~55% of the section, primarily composed of

extremely fine-grained, recrystallized feldspar and quartz. Where the groundmass is locally less altered, it is predominantly composed of very fine-grained laths of plagioclase, displaying polysynthetic twinning. Scattered through the matrix are ~3% (of total) fine-grained, granular crystals of epidote, displaying one strong cleavage, and occurring as square tabs or euhedral, stubby pseudo-hexagonal grains, often rimmed by Fe-Ti-oxides. Orthomagmatic magnetite grains occur as minor (~3%), 0.1-1mm subhedral isometric grains disseminated through the matrix, with exsolution lamellae of ilmenite occurring along the original magnetite cleavage planes (*Plate 2-7 E&F*).

Two types of phenocrysts are present. The first comprises about 25% of the section and are generally coarser-grained (~2mm) and occur as stubby tabular, or pseudo-hexagonal grains (*Plate 2-7 A,B&D*). These grains have been entirely recrystallized to a very fine grained, nondescript mixture of feldspar and quartz with additional replacement by epidote, often highlighting a compositional zonation in these feldspars (*Plate 2-7 D)*. Locally, remnant polysynthetic twinning is still visible. These are interpreted to represent former albite phenocrysts. The second phenocryst type accounts for about 14% of the section and is generally finer-grained than the former (~0.5-1mm), occurring as laths and thin rhombic crystals (*Plate 2-7 A-C*). This type is consistently replaced entirely by chlorite and fine granular grains of epidote in varying proportions. Based on morphology and alteration, these are interpreted as former phenocrysts of a more calcic variety of plagioclase. However, some of the more rhombic-shaped crystals (*Plate 2-7 A&B*) could also represent a former mafic phase such as amphibole, although diagnostic amphibole cleavage is no-longer present.

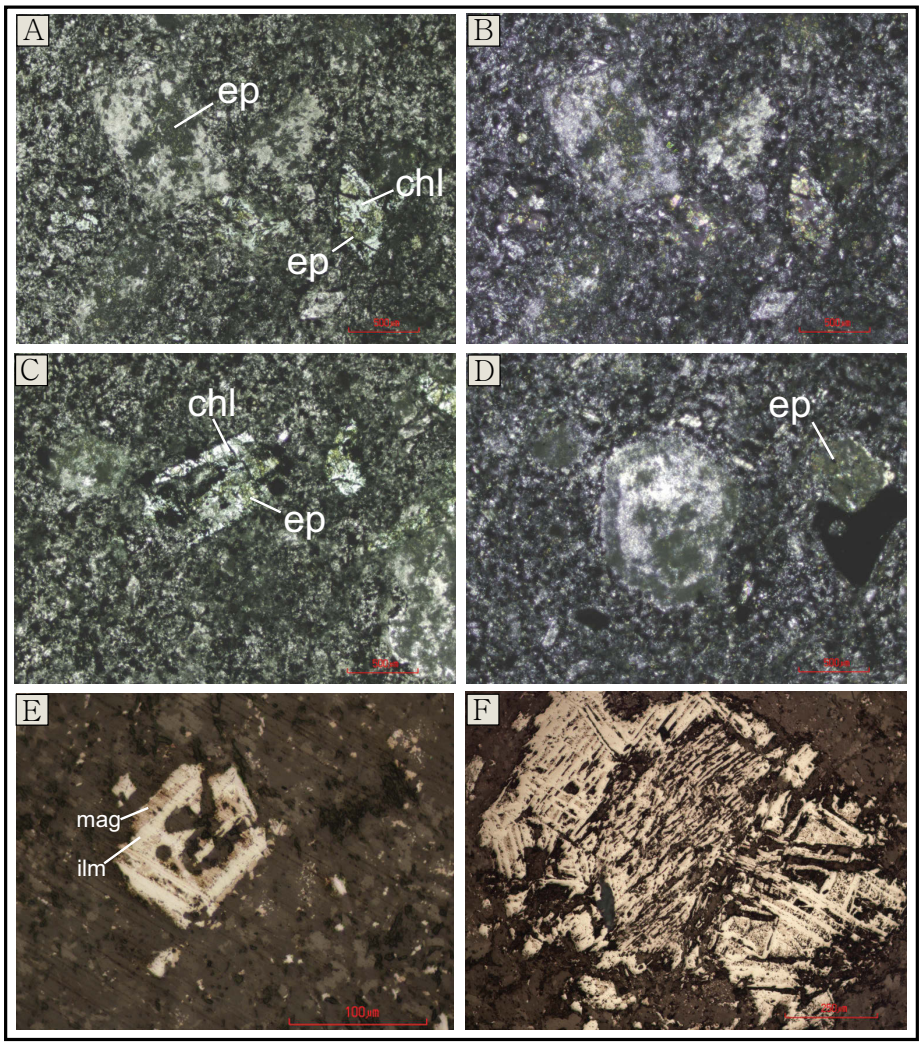

Plate 2-7*: Representative photomicrographs of the porphyritic andesitic-basalt (Microdiorite) from sample SF-12-138; A & B)(4X; PPL and XPL, respectively) Two types of phenocrysts: 1) Albite – coarser, stubby tabular shape, composed of very fine-grained recrystallized feldspar +/-quartz, and epidote; 2) Calcic plagioclase (or amphibole) - Finer-grained, rhombic shape, entirely replaced by chlorite and epidote; C) (4X; PPL) Tabular plagioclase phenocryst (centre) replaced by chlorite and epidote, and more square-shaped albite phenocrysts (far left & far right) recrystallized with very fine-grained epidote; D) (XPL; 4X) Zoned albite phenocryst with very fine-grained recrystallization and a rim altered to very fine-grained epidote; E) (RL; 10X) Orthomagmatic magnetite with ilmenite lamellae; F) (RL; 20X) Orthomagmatic magnetite with ilmenite lamellae. mag=magnetite, ilm=ilmenite, ep=epidote, chl=chlorite.*

Dacitic Quartz-Feldspar Crystal-Rich Volcaniclastic ('Stewart Tuff')

Overlying the Lower Volcanic Unit is the Stewart Tuff, a dacitic quartz-feldspar crystal-rich volcaniclastic unit. Unlike the overlying Caribou Tuff, this unit was relatively unaffected by hydrothermal fluids, and only locally displays signs of

hydrothermal alteration. The unit weathers to a distinctive white colour (*Plate 2-8*), and appears green-grey to pinkish-grey on a fresh surface (*Plate 2-9*). Diagnostic of this unit is the presence of both coarse quartz and feldspar crystals throughout the matrix (*Plate 2-8 A; Plate 2-9*). In outcrop, the unit locally contains horizons rich in subangular-subrounded lapilli and blocks up to 30 cm in size. They are typically aligned with, and stretched in the direction of the regional tectonic foliation (*Plate 2-8*). The clasts are most commonly monolithic, and mafic in composition, weathering to a green or brown colour (*Plate 2-8 C-D; Plate 2-9 D*). Heterolithic horizons do occur locally, and include clasts of medium-grained diorite and pink felsic crystal tuff (*Plate 2-8 B; Plate 2-9 C*).

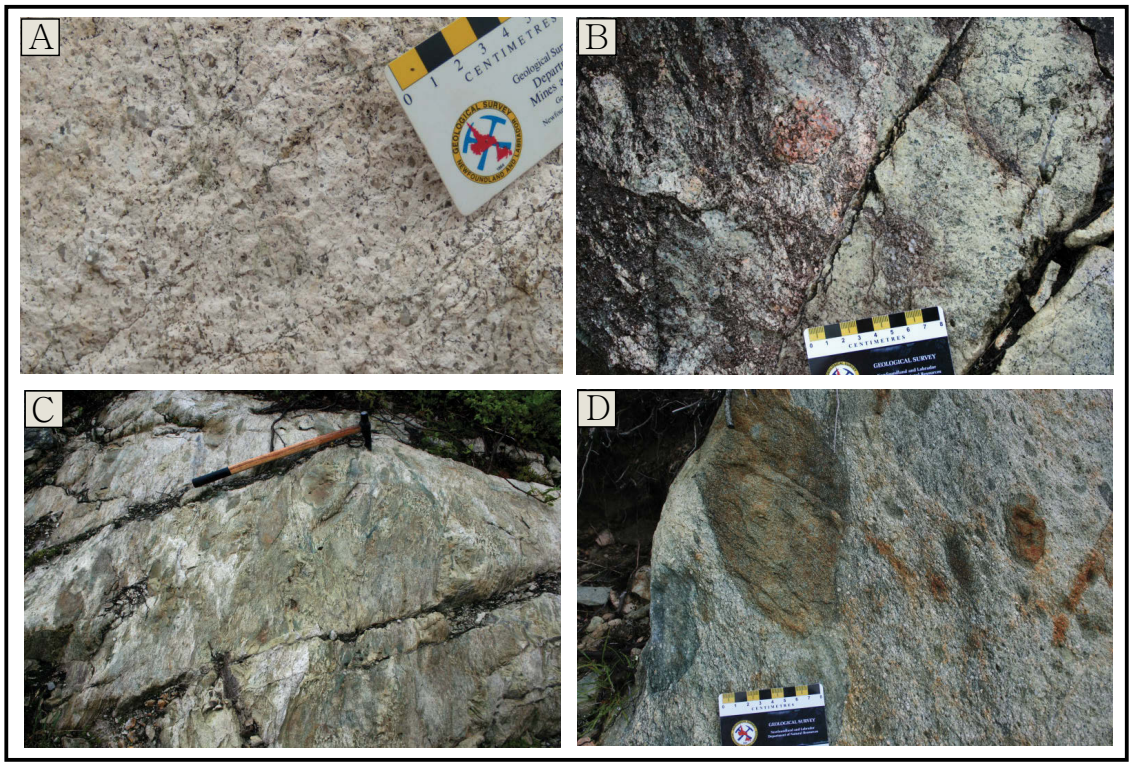

***Plate 2-8**: Representative field photographs of the Stewart Tuff; A) Typical bleached white weathered surface showing coarse quartz and feldspar crystals throughout the matrix (SF-12-43; STA-SF-12-032); B) Pink rhyolitic crystal tuff lapilli fragment (SF-12-43; STA-SF-12-032); C) Bleached white weathered matrix containing abundant fine-grained mafic lapilli and blocks aligned and stretched along foliation. Hammer for scale (STA-SF-12-031); D) Fine-grained mafic lapilli and blocks (SF-12-43; STA-SF-12-032).*

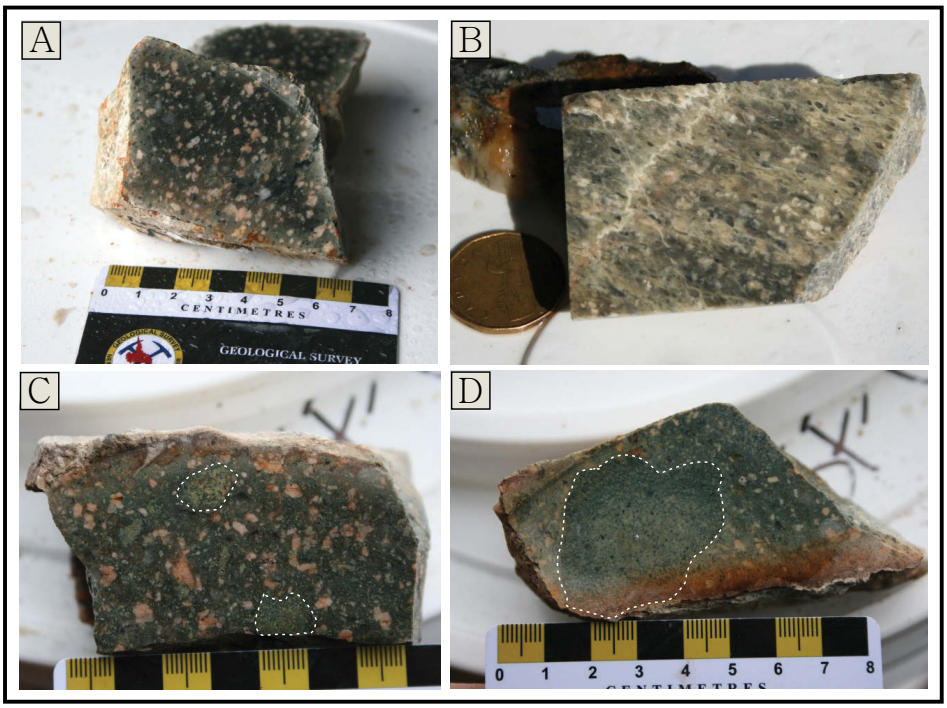

Plate 2-9*: Representative hand sample photos of the Stewart Tuff; A) Dark green-grey siliceous matrix with abundant coarse-grained crystals of quartz and feldspar (SF-12-43); B) Same as previous, with more significant sericite-epidote alteration along foliation and fractures (SF-12-108; DDH ST-11-01; ~435m); C) Quartz and feldspar crystals up to 5mm in size, and fine- to medium-grained dioritic lapilli (GS-12-303; STA-SF-12-102); D) Subrounded, fine-grained mafic lapilli within typical Stewart Tuff matrix (GS-12-272; STA-SF-12-059).*

In thin section, the Stewart Tuff is made up of a very fine-grained matrix of quartz, albite, and potassium feldspar, which accounts for about 60% of the rock (*Plate 2-10*). The remaining 40% includes a variety of crystals and glomerocrysts. Coarse quartz crystals make up about 15% of the sample, ranging in size from 1-3mm. The larger grains tend to form sub-rounded crystals with embayments along their perimeter, filled with the content of the matrix. The smaller grains tend to be more angular, appearing as broken fragments (*Plate 2-10 D*). Quartz also occurs, but less commonly (~6%), as glomerocrysts (*Plate 2-10 A-B*). Albite occurs as individual, euhedral, 1-2mm crystals (~4%; *Plate 2-10 D*), but more commonly in clusters as glomerocrysts (*Plate 2-10 C*), which make up approximately 12% of the section. Albite displays polysynthetic twinning and is very weakly altered to fine grained sericite and epidote. Coarse crystals of potassium feldspar were also identified locally, in trace amounts. Small, 1mm sized laths, now pseudomorphed by epidote and lesser chlorite, also occur in minor amounts (~4%;

Plate 2-10 E-F). This mineral is interpreted to represent a more calcic variety of feldspar, or perhaps a former amphibole, now preferentially replaced by epidote. The unit is crosscut by fine veinlets containing varying amounts of epidote, titanite, apatite, zircon, and sericite.

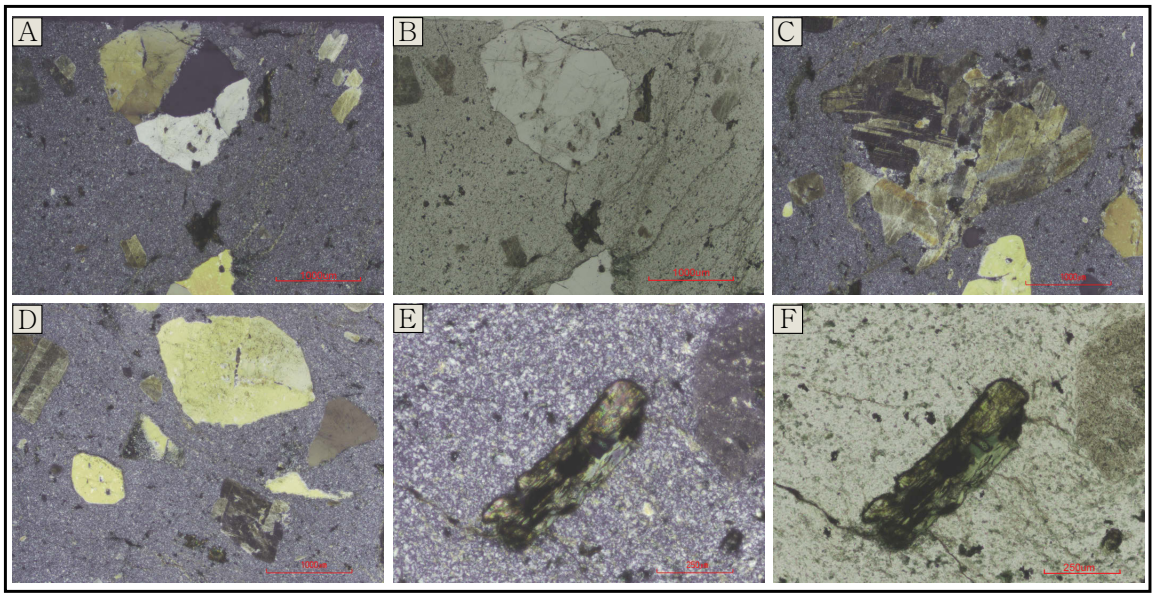

Plate 2-10*: Representative photomicrographs of the Stewart Tuff from sample SF-12-43; A & B) (2X; XPL & PPL, respectively) Quartz glomerocryst and albite crystals in a very fine-grained tuffaceous matrix of quartz, albite, and potassium feldspar; C) (XPL; 2X) Cluster of albite crystals displaying polysynthetic twinning and forming a glomerocryst; D) (XPL; 2X) Crystals of coarse sub-rounded quartz, finer angular quartz, and an albite lath with polysynthetic twinning; E & F) (10X; XPL & PPL, respectively) Finer-grained lath-shaped mineral now pseudomorphed by epidote and chlorite - interpreted as former plagioclase or amphibole.*

Dacitic Quartz Crystal-Rich Volcaniclastic (Caribou Tuff)

The Caribou Tuff is a dacitic quartz crystal-rich volcaniclastic unit that is one of the main host rocks to epithermal alteration and mineralization at the Stewart prospect. It is separated from the underlying Stewart Tuff by the Middle Volcanic Unit of Dyke & Pratt (2008). The entire Caribou Tuff Unit has been affected to some degree by hydrothermal alteration, obscuring the original volcaniclastic textures and making identification difficult in some locations. In outcrop, the unit is commonly weathered to a rust colour from oxidation of abundant sulphides, and is strongly foliated and friable (*Plate 2-11 A*). Fresh surfaces are typically light grey in colour. It is readily distinguishable from the Stewart Tuff based on its crystal content, which is consistently

composed entirely of quartz (*Plate 2-11*) - unlike the Stewart Tuff, which contains both quartz and feldspar crystals. It also commonly contains siliceous, sub-rounded lapilli fragments approximately 1 cm or less in size (*Plate 2-11 A-B*). This also distinguishes the unit from the Stewart Tuff, which commonly contains large mafic blocks in addition to smaller-sized lapilli.

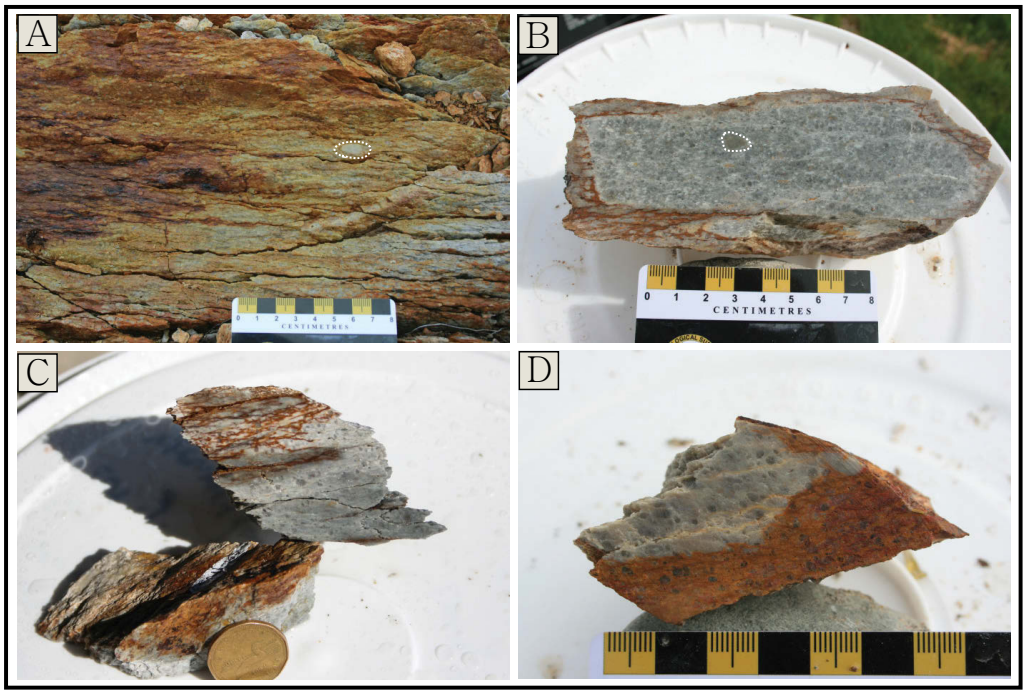

Plate 2-11*: Representative photos of the Caribou Tuff, host to mineralization at Stewart; A) Rusty, friable weathered surface with phyllic alteration, quartz crystals and a single lapilli fragment highlighted (GS-11-167; STA-SF-12-029); B) Relatively unaltered example showing quartz crystals and occasional ~1cm felsic lapilli, one of which is highlighted (GS-11-47); C) Relatively unaltered sample rich in quartz crystals (GS-11-167); D) Pyrophyllite and muscovite altered sample rich in quartz crystals (GS-11-75).*

In thin section, the Caribou Tuff has a very fine-grained quartzo-feldspathic matrix comprising 60% of the sample, which is often dominated by sericite alteration, concentrated along foliation parallel bands (*Plate 2-12*). Quartz crystals (~30%) are suspended throughout the matrix and are most commonly 1-2mm in size. The larger crystals are sub-rounded and often contain rounded matrix embayments (*Plate 2-12 C*). They also occur as sub-euhedral bipyramidal crystals (*Plate 2-12 C*) and as broken, angular fragments (*Plate 2-12 B*). Unlike the Stewart Tuff, quartz does not occur as glomerocrysts - only as individual crystals. Occasional very small (~2mm), sub-rounded lapilli fragments (~7%) are present, predominantly composed of fine granular quartz, but

also containing variable amounts of Fe-Ti-oxides, pyrite, and sericite (*Plate 2-12 D*). About 2-3% sub-euhedral, fine-grained (<0.5mm) pyrite occurs disseminated through the matrix and concentrated along foliation planes (*Plate 2-12 B&D*). Fine-grained, subhedral apatite grains also occur in trace amounts.

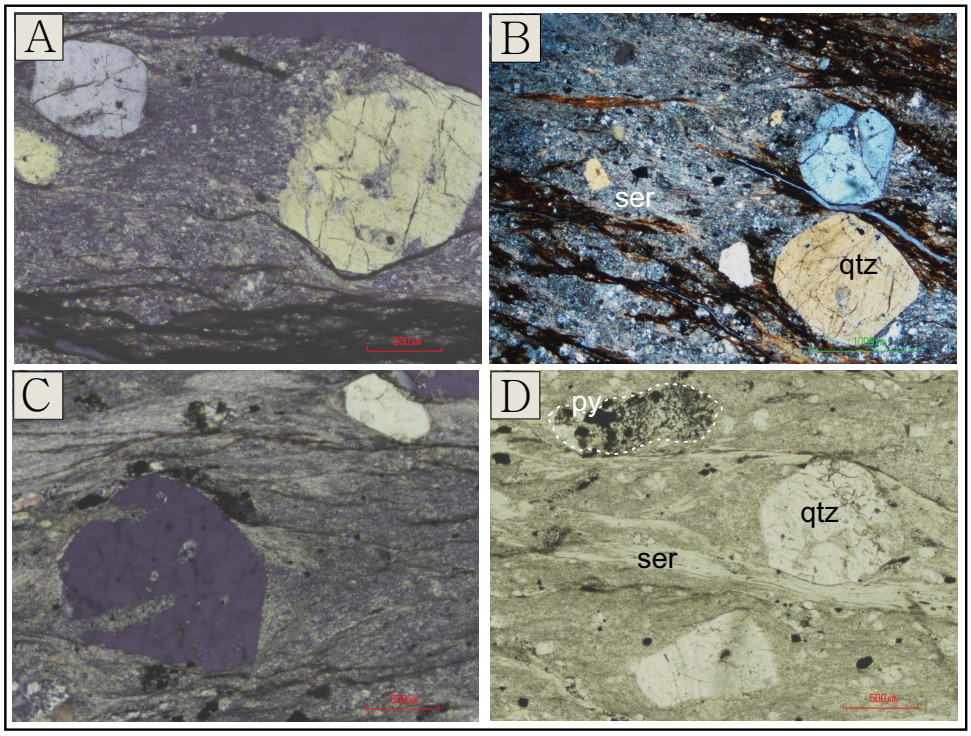

***Plate 2-12**: Representative photomicrographs of the Caribou Tuff; A) (XPL; 4X) Coarse quartz crystals in a very fine-grained, foliated matrix of quartz-feldspar-sericite (GS-11-167); B) (XPL; 2X) Coarse quartz crystals and finer angular quartz fragments within a very fine-grained foliated matrix with sericite and disseminated pyrite (opaque) (GS-11-167); C) (XPL; 4X) Coarse quartz crystal with matrix embayments, and a bipyramidal quartz crystal within a very fine-grained, foliated quartzo-feldspathic matrix with strongly sericitized bands (SF-12-111; DDH ST-11-02; ~91m); D) (PPL; 4X) Quartz crystals, lapilli fragment and disseminated pyrite in a sericite altered matrix. Lapilli fragment is small and composed of fine-grained granular quartz, pyrite and sericite. Sericite is concentrated along foliation planes in matrix (SF-12-111). Ser=sericite, qtz=quartz, py=pyrite.*

Intermediate-Mafic Volcanics (Upper Volcanic Unit)

Overlying the felsic volcaniclastics is a thick package of intermediate to mafic volcanic rocks, which has all been broadly grouped into the Upper Volcanic Unit (Dyke and Pratt, 2008). The unit is dominated by intermediate-mafic volcaniclastic rocks, but also contains lesser massive mafic flows. The samples and outcrops described here occur to the northeast of the mapping limit shown in *Figure 2-2*, but are presumed to represent part of the same unit.

The volcaniclastic rocks range in composition from andesite to basaltic-andesite, and include crystal tuffs and lapilli tuffs. Locally tuff breccia was also identified, containing large blocks up to 50 cm in length. Minor sedimentary layers also occur interbedded with the volcaniclastics, including intervals of feldspar-rich epiclastics and well-bedded siltstone. The volcaniclastic rocks typically appear brownish in colour on weathered surfaces, and medium green-grey on fresh surfaces; however, a thin bed of distinctive maroon-coloured lapilli tuff was identified locally (*Plate 2-13*).

***Plate 2-13**: Interval of maroon-coloured basaltic-andesitic lapilli tuff (centre) interbedded with green-grey feldspar-rich epiclastic sediments/crystal tuff. Oval pits are weathered out mafic lapilli (STA-SF-12-27; SF-12-27).*

Most of the volcaniclastic rocks identified in the field contain abundant, variably epidotized feldspar crystals up to 4mm in size, dispersed throughout their otherwise very fine-grained matrices. Some of the lapilli tuffs are monolithic, containing only chloritized

mafic fragments (*Plate 2-14 A-B*), while others are heterolithic, hosting: 1) pale beige-green, siliceous, fiamme-like fragments; 2) fine-grained mafic fragments; and 3) fine-grained felsic fragments (*Plate 2-14 C*). Lapilli are typically 1-3cm in size, but are locally as small as 2mm, and as large as blocks (>6.4cm).

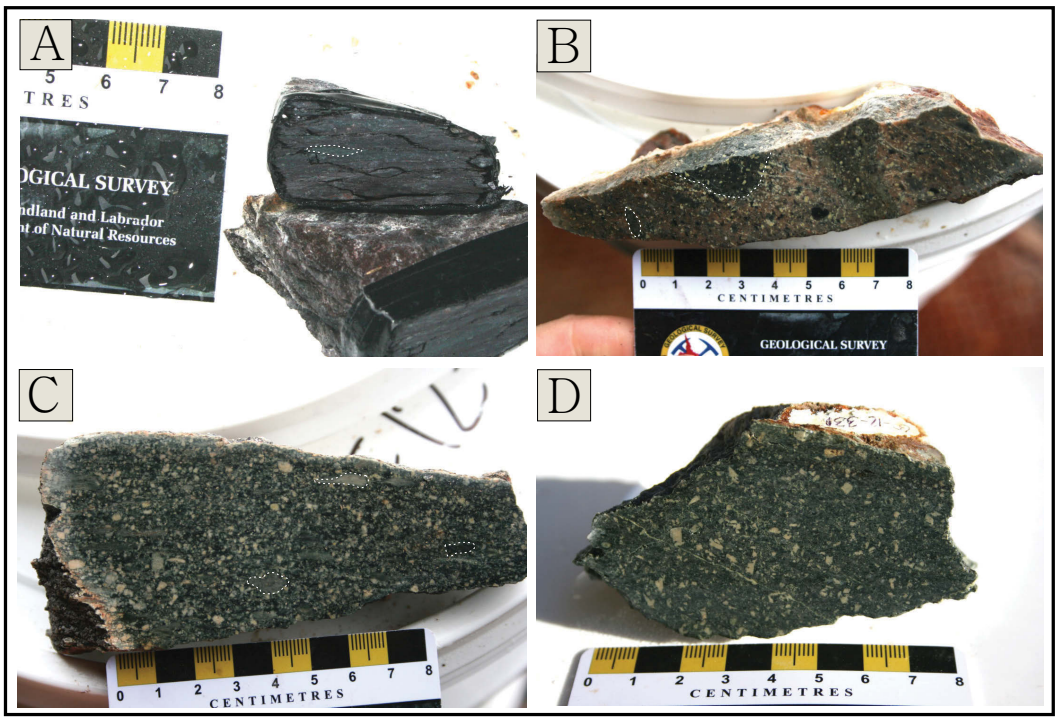

***Plate 2-14**: Representative photos of the intermediate-mafic volcaniclastics of the Upper Volcanic Unit; A) Basaltic-andesitic lapilli tuff, with 2mm-3cm chloritized mafic fragments stretched along the foliation within a fine-grained, oxidized maroon matrix (SF-12-27; STA-SF-12-27); B) Andesitic feldspar-crystal-rich lapilli tuff. Lapilli are 1-3cm, sub-rounded and composed of a fine-grained, plagioclase-phyric, chloritized mafic rock (GS-12-301; STA-SF-12-098); C) Basaltic-andesitic feldspar-crystal-rich heterolithic lapilli tuff. Three types of lapilli are highlighted: 1) pale beige-green, siliceous, fiamme-like; 2) fine-grained mafic; and 3) fine-grained felsic (GS-12-311; STA-SF-12-107); D) Basaltic-andesitic feldspar-crystal tuff. Feldspar crystals are up to 4mm and variably epidotized (GS-12-331; STA-SF-12-127).*

Sample SF-12-27 (*Plate 2-13* and *Plate 2-14 A*) was selected for petrographic analysis. In thin section the sample appears strongly foliated and deformed and is significantly affected by alteration related to regional greenschist metamorphism. A very fine-grained matrix accounts for ~45% of the section, composed of sericite, chlorite, feldspar and quartz, with fine-grained disseminated hematite crystals throughout (*Plate 2-15*). Sitting within the matrix are coarse rounded clusters of titanite (~10%), which are up

to 2mm in size, occurring with minor epidote and hematite, and containing abundant quartz inclusions. There are also ~5% similarly sized euhedral rhombic- to hexagonal-shaped grains of epidote containing quartz inclusions. Epidote may be a pseudomorphic replacement of former titanite or amphibole based on the distinct rhombic crystal morphology.

Stretched and rounded lapilli ranging from 2-30 mm in size make up the remaining 40% of the section. Most commonly, lapilli are mafic in composition and strongly altered to chlorite, containing abundant fine- to medium-grained subhedral prisms of epidote (separate from the coarser rhombic grains) and minor sericite (*Plate 2-15 A-B*). A second, much less common type of lapilli is also present, containing abundant very fine-grained hematite crystals, remnant albite phenocrysts, and quartz filled cavities within a very fine-grained feldspathic matrix (*Plate 2-15 C*).

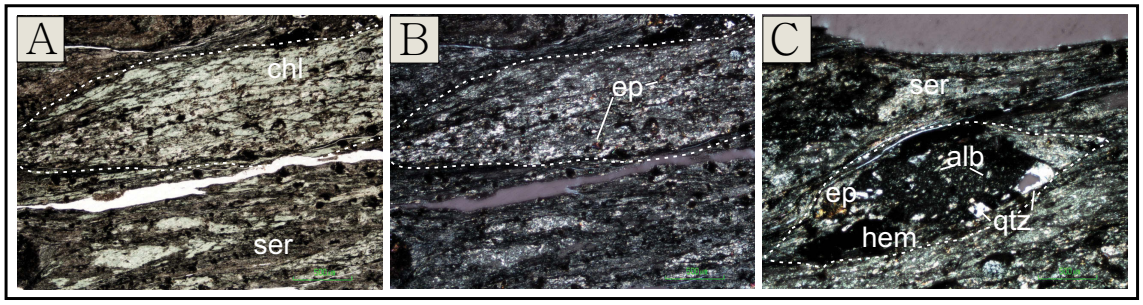

***Plate 2-15**: Representative photomicrographs of the intermediate-mafic volcaniclastics of the Upper Volcanic Unit from sample SF-12-27; A & B) (4X; PPL & XPL, respectively) Portion of a 3 cm lapilli fragment, strongly altered to chlorite and containing fine-grained subhedral epidote crystals. Matrix is quartzo-feldspathic but significantly altered to sericite. Oxides are mostly hematite; C) (XPL; 4X) Sheared lapilli fragment composed of a plagioclase-phyric mafic rock with quartz filled cavities and abundant Fe-oxide (hematite). alb=albite, ep=epidote, hem=hematite, ser=sericite, qtz=quartz.*

Massive mafic volcanic rocks were also identified within the unit and are interpreted to represent massive basaltic flows. They are fine-grained, green in colour, pervasively altered to chlorite and are frequently cross cut by fine epidote veinlets (*Plate 2-16*). They commonly contain 2-3mm amygdules filled with quartz and epidote, but vesicles up to 10 cm, partially filled with quartz were identified locally.

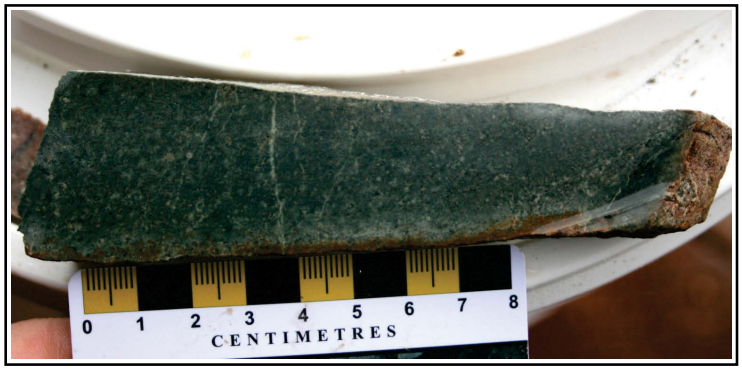

***Plate 2-16**: Representative hand sample photo of the massive basaltic flows of the Upper Volcanic Unit. Sample is fine-grained and massive with trace pyrite and moderate pervasive chlorite alteration. Also contains minor 2-3mm amygdules filled with epidote and quartz. (GS-12-288; STA-SF-12-083).*

Porphyritic Dacite Dykes ('Granite')

Feldspar-phyric dacite dykes most evidently occur crosscutting the Lower Volcanic Unit and the Microdiorite. Two are shown in *Figure 2-2* striking roughly E-W in the southern portion of the map, grouped in with the 'Granite' intrusions. A third was found during fieldwork for this project about one kilometer north of the longest one shown in *Figure 2-2*, crosscutting the Microdiorite unit (GS-12-255; STA-SF-12-41). The dyke was ~3m wide with contacts oriented at 130/30, and composed of a very fine-grained, pink feldspar and quartz matrix with 15% white feldspar phenocrysts (*Plate 2-17 D*). The same lithology was also identified in drill core recovered from DDH ST-11-03, where it crosscuts both the massive mafic volcanics of the Lower Volcanic Unit and the Microdiorite (*Plate 2-17 A*). In drill core the unit ranges from pink to grey in colour and contains variable amounts (5-15%) of white feldspar phenocrysts, 1-3mm in size, scattered throughout a very fine-grained quartzo-feldspathic matrix (*Plate 2-17 A-C*). The unit appears to have undergone some degree of silicification.

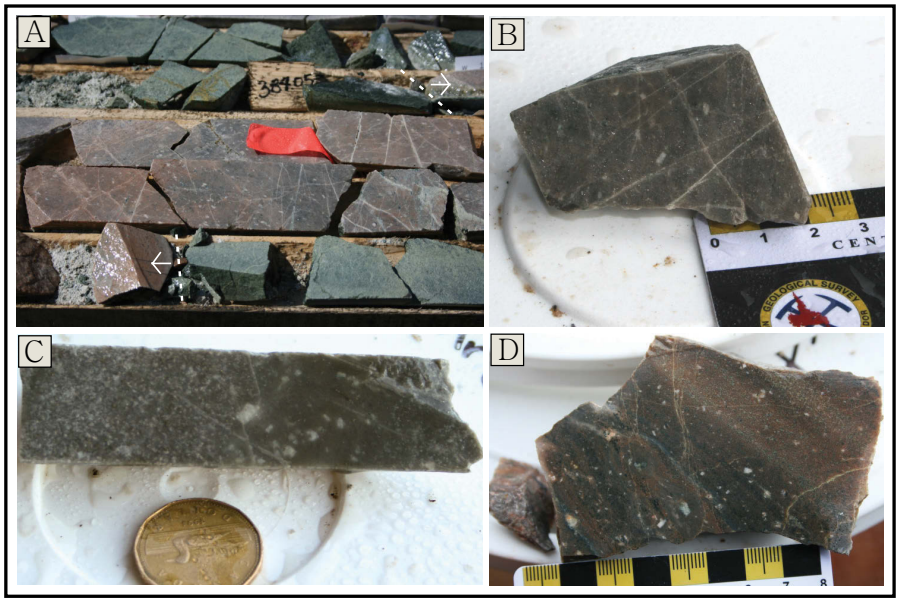

Plate 2-17*: Representative photos of the porphyritic dacite dykes; A) ~2.5m interval of a pink to grey feldspar-phyric dacite dyke cross cutting the massive mafic flows of the Lower Volcanic Unit (SF-12-144; DDH ST-11-03; ~385.5m); B) 6-8% feldspar phenocrysts up to 3mm in size within a very fine-grained grey-pink quartz-rich matrix (SF-12-144); C) 1-3mm white feldspar phenocrysts varying in abundance from 5-15% within a very fine-grained grey matrix. Unit appears to be silicified (SF-12-142; DDH ST-11-03; ~377m); D) 15% white feldspar phenocrysts 1-2mm in size, within a very fine-grained, pink and grey layered siliceous matrix (GS-12-255; STA-SF-12-041).*

Based on crosscutting relationships, these dykes are obviously younger than the Lower Volcanic Unit and Microdiorite intrusives, and could be contemporaneous with the overlying felsic volcaniclastics as a subvolcanic counterpart, since they were not identified crosscutting any of the overlying volcanic stratigraphy. It is also possible that these dykes are associated with the Burin Knee Intrusive Suite.

In thin section, 80% of the sample is made up of a very fine-grained matrix of quartz, potassium feldspar, and albite. Phenocrysts, and more abundant glomerocrysts of albite comprise ~18% of the sample with individual crystals ranging in size from <0.5mm-2mm displaying both polysynthetic and simple twinning (*Plate 2-18*). They have been altered to varying degrees to epidote and minor titanite and chlorite, some laths entirely pseudomorphed and others only partially replaced (*Plate 2-18 C&D*). Some phenocrysts have not been replaced by secondary minerals, but have been partially recrystallized to a much finer grain size. Locally, faint remnant grain boundaries can be made out in the fine-grained matrix, of former phenocrysts that have undergone

substantial recrystallization to a finer grain size, making them almost indiscernible from the matrix (*Plate 2-18 B*). The phenocryst abundance therefore may have been substantially higher in the original rock. 2-3% pyrite occurs disseminated throughout the matrix and along small fractures where it occurs with chlorite and epidote. Trace euhedral zircon crystals occur throughout.

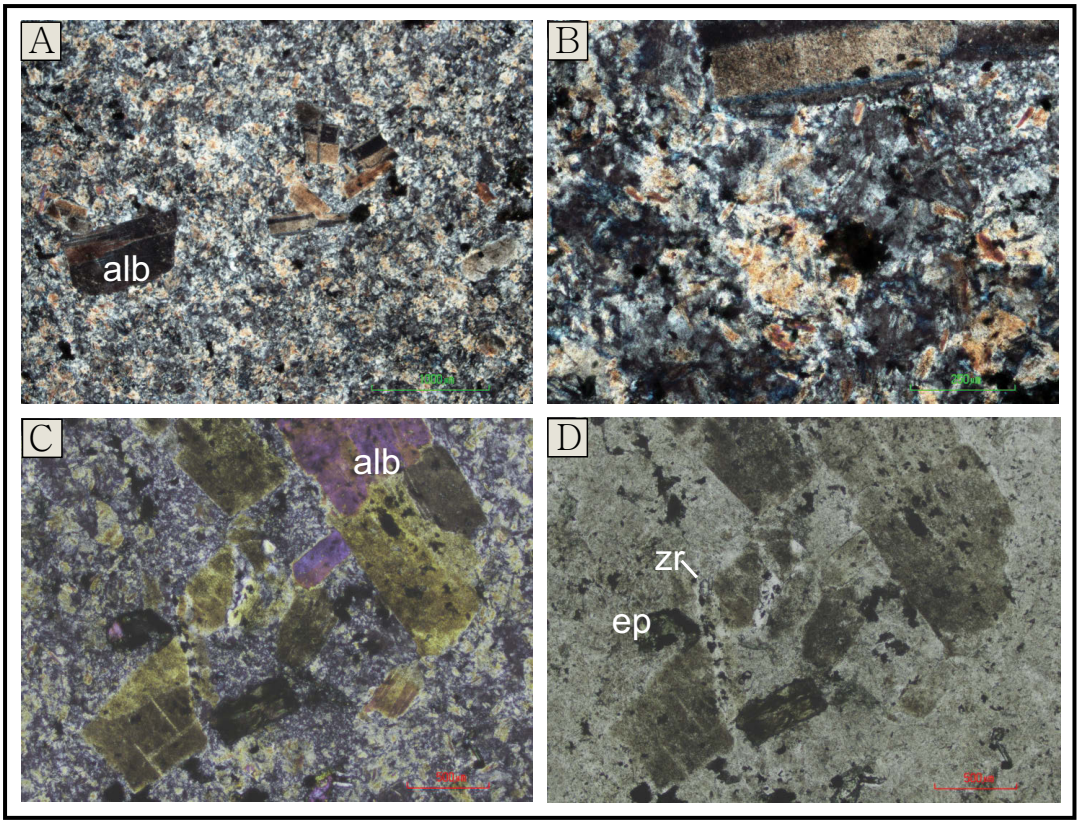

Plate 2-18*: Representative photomicrographs of the porphyritic dacite dykes from sample SF-12-144: A) (2X; XPL) Glomerocryst and coarse phenocryst of albite within a very fine-grained matrix of potassium feldspar, quartz, and albite. Opaque minerals are mostly pyrite; B) (10X; XPL) Close-up displaying the very fine-grained matrix of potassium feldspar, quartz and albite and in centre-left a possible remnant recrystallized albite phenocryst; C&D) (4X; XPL and PPL, respectively) Close-up of glomerocryst with albite altering to epidote, two of which have been entirely replaced. One small euhedral zircon appears more clearly in the PPL image. alb=albite, zr=zircon, ep=epidote.*

Tonalite (Quartz-Diorite/Tonalite)

The tonalite intrusive body occurs in the western portion of *Figure 2-2*, and is one of the principle hosts to Au-Cu mineralization at Stewart, the other main host being the Caribou Tuff. It was first identified as an intrusion, separate from the surrounding altered

felsic volcaniclastics, by Pratt during mapping in 2007. It has an elongate shape, parallel to the regional foliation and intrudes into the volcanic stratigraphy of the Stewart Tuff, Middle Volcanic Unit and Caribou Tuff. Clear intrusive contacts between these units are not present in the field, and even when observed in drill core, are ambiguous due to the intensity of overprinting hydrothermal alteration and deformation present.

It is unclear whether the tonalite represents a component of the extensive Burin Knee-Swift Current intrusive suites or is a separate intrusive unit. It is quite probable that it is part of the above mentioned intrusive suites, however, it is described here separately as it is a key host rock at Stewart and unique in that it is the only felsic plutonic rock on the property that has been affected so significantly by hydrothermal alteration.

In outcrop, the unit is weathered to a distinctive rusty orange colour as a result of oxidation of the abundant sulphides hosted within the unit (*Plate 2-19A*). Where the unit is intensely hydrothermally altered, igneous textures are not well preserved, and the rock hosts a phyllic to advanced argillic alteration assemblage, which appears light grey to beige on a fresh surface. Towards the core of the intrusive body, the unit becomes less altered and less deformed, and fresher rock surfaces exhibit a grey-green colour and primary igneous textures become more apparent (*Plate 2-19*). In these examples, the unit is medium grained, containing distinctive rounded quartz grains and abundant chloritized laths, both 1-2mm in size, but up to 4mm locally (*Plate 2-19 C*). Surrounding these grains is a less distinct interstitial grey material, presumably composed of quartz and feldspar. Frequently crosscutting the unit, are fine quartz veinlets with diffuse boundaries, and fine fractures of chlorite and pyrite.

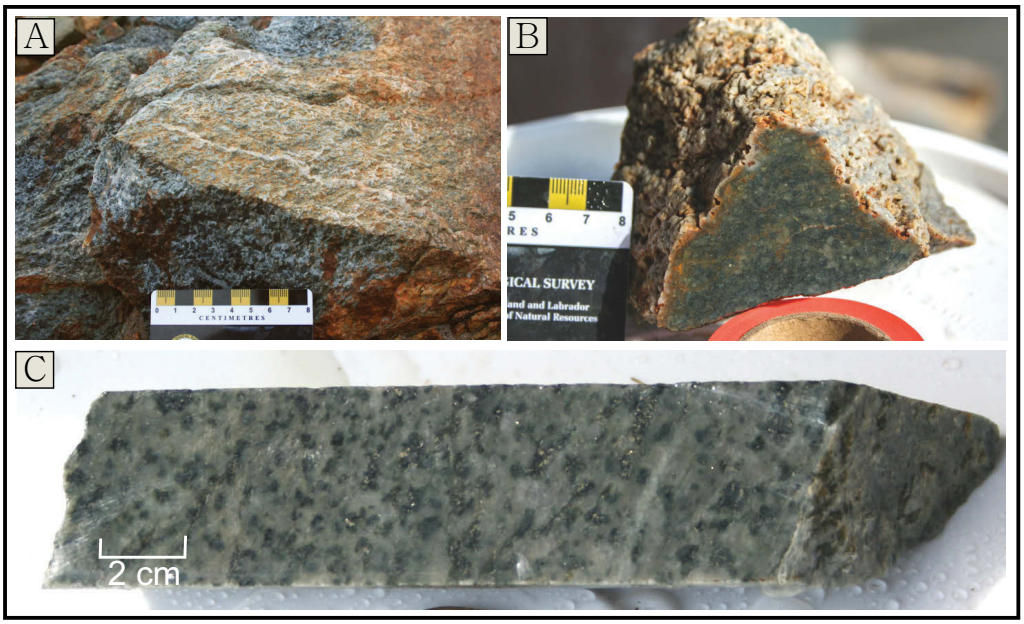

***Plate 2-19**: Representative photos of relatively unaltered samples of tonalite, host to mineralization at Stewart; A) Rusty orange weathered surface with quartz veining and a green and white, chloritic fresh rock face (STA-SF-12-029); B) Stockwork quartz-veining through chlorite altered tonalite (SF-12-39; STA-SF-12-029); C) Relatively unaltered and undeformed sample showing medium grained chlorite altered laths and rounded quartz crystals. Quartz veining and chlorite-pyrite fractures crosscut the unit (SF-12-84; DDH ST-11-01; ~141m).*

Multiple examples of this unit, displaying varying degrees of alteration, were selected for petrographic analysis (*Plate 2-20*). Overall, 50-60% of the sample is made up of a fine-grained granular quartz matrix, rounded quartz phenocrysts 1-2mm in size comprise 10-20%, and the remaining 30-40% is made up of 1-4mm, lath-shaped and completely altered phenocrysts, of former feldspar and amphibole. Characteristic of this unit, and distinguishing it from the adjacent, also significantly altered, Caribou Tuff, is its quartz groundmass which, although fine-grained, is still much coarser and granular than any of the felsic volcaniclastics. The unit also lacks embayments in its quartz phenocrysts, which is a common feature in both felsic volcaniclastic units (the Stewart and Caribou tuffs).

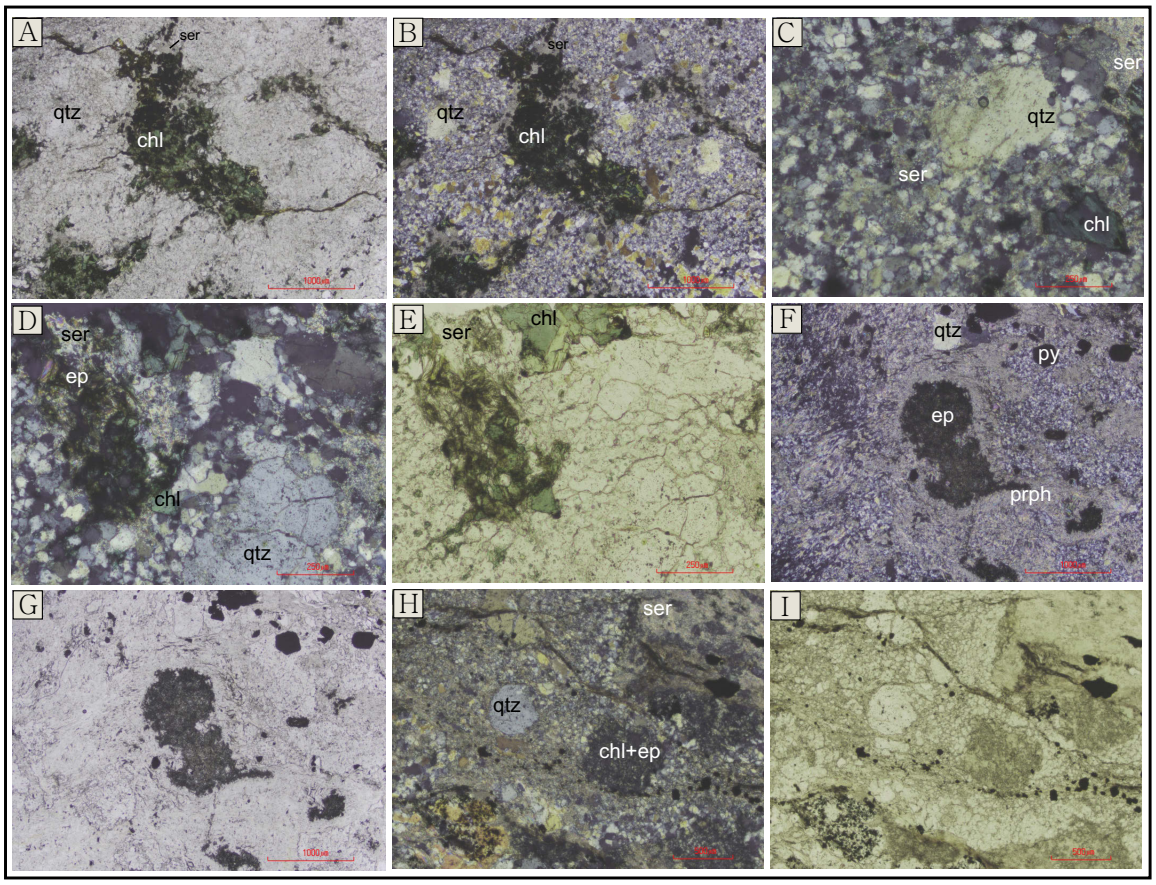

***Plate 2-20**: Representative photomicrographs of the tonalite host rock at Stewart; A&B) (2X; PPL and XPL, respectively) 1-2mm former amphibole altered to chlorite and minor sericite around its perimeter. Also contains pyrite and Fe-oxides. Smaller rounded quartz phenocrysts also occur within fine-grained crystalline quartz matrix (SF-12-39); C) (10X; XPL) Close-up of 0.5mm rounded quartz phenocryst and granular matrix of quartz with sericite alteration (SF-12-39); D&E) (10X; XPL and PPL, respectively) ~1mm rounded quartz phenocryst (bottom right) and a remnant 0.75mm feldspar lath completely replaced by epidote,and lesser sericite, chlorite and quartz, both sitting in a matrix of fine-grained granular quartz (SF-12-39); F&G) (2X; XPL and PPL, respectively) Disseminated pyrite, 0.5mm quartz phenocrysts and 0.5-2mm former feldspar laths completely replaced by epidote (core) and overprinted by pyrophyllite (rim) within a fine-grained granular quartz matrix (SF-12-42) H&I) (4X; XPL and PPL, respectively) 0.5mm rounded quartz phenocrysts and 0.5-2mm former feldspar laths completely altered to epidote and lesser sericite and chlorite within granular quartz matrix (SF-12-84; DDH ST-11-01; ~141m); chl=chlorite, qtz=quartz, ser=sericite, ep=epidote, py=pyrite, prph=pyrophyllite.*

One of the least altered and deformed samples collected from the tonalite is shown in *Plate 2-20 (A-E)*. In this sample, the crystalline quartz groundmass is clearly visible, containing only minor sericite alteration. Former feldspar laths are predominantly altered to epidote, with minor sericite locally altering the periphery of the grains, and former amphibole crystals are altered to chlorite, pyrite and various oxides. In *Plate 2-20 H & I*, the tonalite displays strong alteration to a phyllic assemblage dominated by sericite, and

in *Plate 2-20 F & G* the tonalite is altered to an advanced argillic assemblage. In the latter, pyrophyllite is abundant throughout the groundmass, which has promoted more substantial deformation during subsequent metamorphism. Here, the former feldspars show initial replacement by epidote, which is overprinted by pyrophyllite, encasing the phenocrysts.

Burin Knee Intrusive Suite ('Granite')

The Burin Knee Intrusive Suite extends across the entire northern portion of the map in *Figure 2-2* (labeled as Granite), intruding the volcanic stratigraphy, and marking the western and northern boundary of the hydrothermal alteration zone at Stewart. It is also found outcropping in the southwestern portion of the mapping area and as a small isolated body within the boundaries of the Caribou Tuff in the northeast. Although not sampled in detail, distinct phases were still evident, with compositions ranging from granite to diorite.

The more granitic examples include those found along the shore in the southwest and the isolated body sitting within the Caribou Tuff in the northeast (*Figure 2-2*). These more granitic intrusives weather to light colours, from white-beige to light pink, and appear distinctively pink on a fresh surface (*Plate 2-21*). They are medium grained overall, with crystals locally up to 4mm of quartz and variably epidotized feldspar within a finer groundmass of quartz and potassium feldspar. Small clots of chlorite occur locally and are presumably altered former biotite or amphibole crystals (*Plate 2-21 C*).

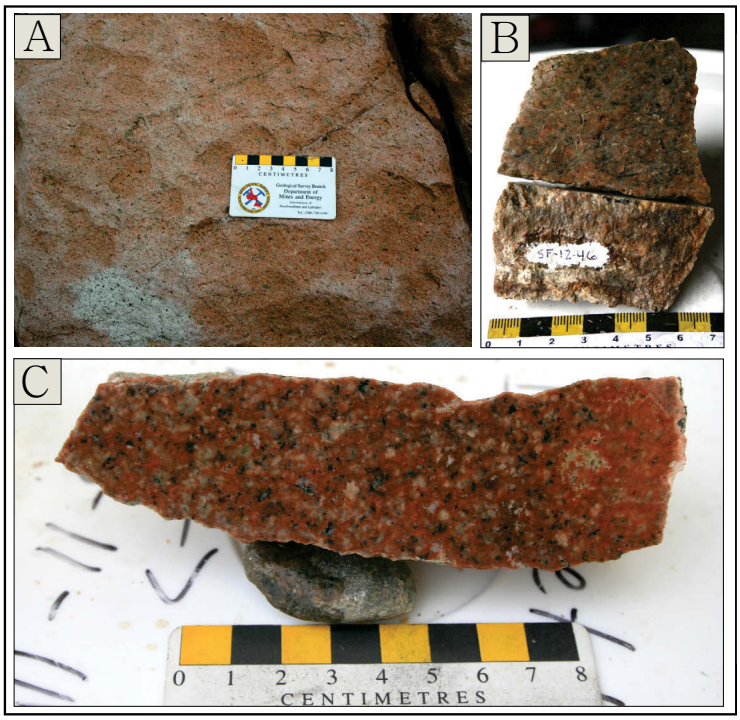

***Plate 2-21**: Representative photos of the more granitic examples of the Burin Knee Intrusive Suite; A) White to light pink weathering of a medium grained granite from the southwest corner of mapping area (GS-12-266; STA-SF-12-053); B) Pink, medium grained granite with fine epidote veinlets. Taken from the isolated body sitting within the Caribou Tuff towards the northeast (SF-12-46; STA-SF-12-034); C) Pink, medium grained granite with epidotized feldspars, fine epidote veinlets, and ferromagnesian minerals altered to chlorite (southwest) (GS-11-94).*

Two samples were selected for petrographic analysis, and both display significant micro-granophyric texture, comprising up to 60% of the section (*Plate 2-22*). Medium-grained quartz (20%) is often intergrown with similarly sized potassium feldspar grains (15%), sutured together by diffuse and irregular grain boundaries (*Plate 2-22 A&E*), which are enclosed by finer quartz-potassium feldspar intergrowths of the prevalent micro-granophyric texture. Potassium feldspar commonly displays diagnostic tartan twinning. Laths of albite (~10%) occur either as individual phenocrysts or, less commonly, as glomerocrysts. They are typically 0.75-1mm in size and when relatively unaltered, display polysynthetic twinning and weak micro-antiperthitic texture locally (*Plate 2-22E*). When laths lie along late fractures, they tend to be replaced entirely by an assemblage of mostly sericite and epidote with minor Fe-Ti-oxides (*Plate 2-22 D*). Filling the fractures is a similar assemblage of sericite, epidote, chlorite, titanite, and rutile. Rare 0.5mm laths occur which have been altered to sericite and chlorite in varying proportions, with patches of titanite elongated parallel to the crystal axis (*Plate 2-22 F*). The sericite in this case is interpreted as phengite, based on its darker yellow colour in PPL and slightly higher birefringence. These laths might be former feldspars preferentially altered along late fractures, or a former ferromagnesian mineral phase.

Trace amounts of fine-grained subhedral apatite, and very fine-grained euhedral zircon occur throughout.

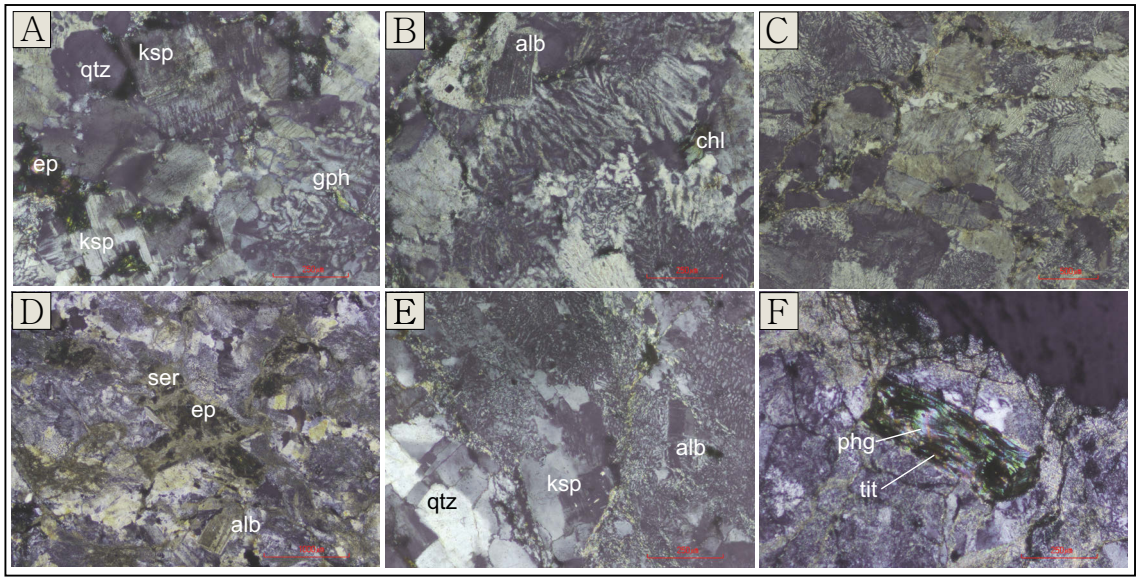

***Plate 2-22**: Representative photomicrographs of granitic examples of the Burin Knee Intrusive Suite; A) (10X; XPL) Quartz and potassium feldspar grains intergrown with irregular boundaries and surrounded by micro-granophyric texture. Potassium feldspar displays tartan twinning and sample is crosscut by epidote veinlets (GS-12-266; STA-SF-12-053); B) (10X; XPL) Small lath of albite surrounded by potassium feldspar and further surrounded by microgranophyric texture (GS-12-266); C) (4X; XPL) 85% micro-granophyric texture surrounding occasional quartz and potassium feldspar grains and crosscut by sericite-chlorite-epidote veinlets (GS-12-266); D) (2X; XPL) Relatively unaltered albite lath with polysynthetic twinning, besides albite laths along fractures altered to epidote-Fe-Ti-oxides-sericite, surrounded by microgranophyric texture and crosscut by sericite-epidote-chlorite-titanite-rutile veinlets (SF-12-46; STA-SF-12-034); E) (10X; XPL) Albite with weak micro-antiperthitic texture and intergrown potassium feldspar and quartz crystals with diffuse irregular grain boundaries, surrounded by micro-granophyric texture (SF-12-46); F) (10X; XPL) 0.5mm lath shaped mineral altered to sericite(phengite) and titanite (dark, high relief patches) and minor chlorite – former ferromagnesian mineral or feldspar preferentially altered along fractures (SF-12-46); ep=epidote, qtz=quartz, alb=albite, ser=sericite, ksp=potassium feldspar, gph=granophyric texture, chl=chlorite, tit=titanite, phg=phengite.*

In the western portion of the map (*Figure 2-2*) along the periphery of the pluton where it shares a contact with the Caribou Tuff, the unit appears fine- to medium-grained and closer to granodiorite in composition. It weathers to a light pink colour, and appears a similar pinkish grey colour on a fresh surface (*Plate 2-23 A&B*). In thin section, the granodiorite is fine- to medium-grained, and generally, fairly equigranular (*Plate 2-23 D&E*). The composition varies across the section but overall contains between 40-60% albite laths, variably altered to calcite, sericite and epidote or locally, finely recrystallized.

Quartz (25-40%) occurs as sub-euhedral individual crystals, but also as coarse, anhedral interstitial filling. Potassium feldspar (~10-15%) occurs as sub-euhedral tabular-shaped crystals commonly displaying perthitic texture (*Plate 2-23 F*) and possibly tartan twinning locally. It also occurs as anhedral masses partially intergrown with quartz, and locally displays weakly developed micro-granophyric texture (*Plate 2-23 F*). Approximately 5-7% former ferromagnesian minerals are present as narrow laths and tabs now composed of chlorite, and minor epidote and Fe-Ti-oxides. They locally show remnant cleavages intersecting at ~120/60°, diagnostic of an amphibole (Plate 2-23 C).

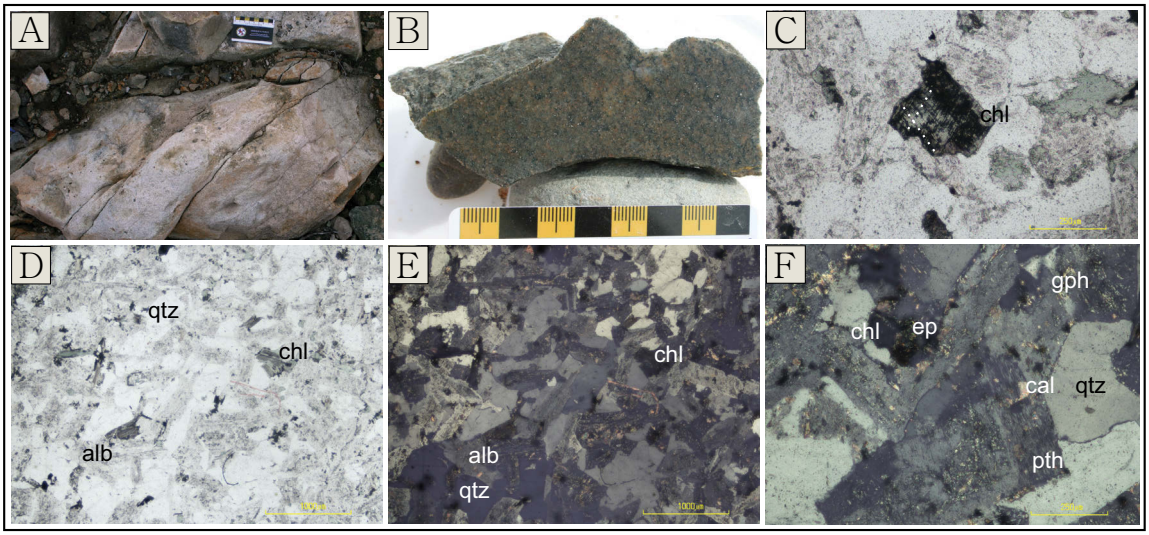

***Plate 2-23**: Representative photos and photomicrographs of the granodioritic phase of the Burin Knee Intrusive Suite from sample GS-11-52); A) Light pink weathered surface of the fine- to medium-grained granodiorite along periphery of southern contact with the Caribou Tuff; B) Light grey-pink fresh surface; C) (10X; PPL) Small grain of former amphibole altered to chlorite and oxides, showing diagnostic ~120/60° cleavage; D&E) (2X; PPL & XPL, respectively) Fine- to medium-grained, fairly equigranular portion of sample containing evident quartz, albite, and chloritized former amphibole crystals; F) (10X; XPL) Potassium feldspar showing perthitic texture, intimately occurring with quartz, and weakly developed microgranophyric texture where they are intergrown. Patches of calcite, epidote and chlorite alteration present. chl=chlorite, qtz=quartz, alb=albite, pth=perthitic texture, ep=epidote, cal=calcite, gph=granophyric texture.*

A distinct diorite phase also occurs, located in the northeast about 125m north of the isolated granitic body that lies within the Caribou Tuff. This unit is fine- to medium-grained, green-grey in colour, and contains abundant coarse acicular mafic phenocrysts, up to 1cm in size, which are altered to chlorite (*Plate 2-24 A*).

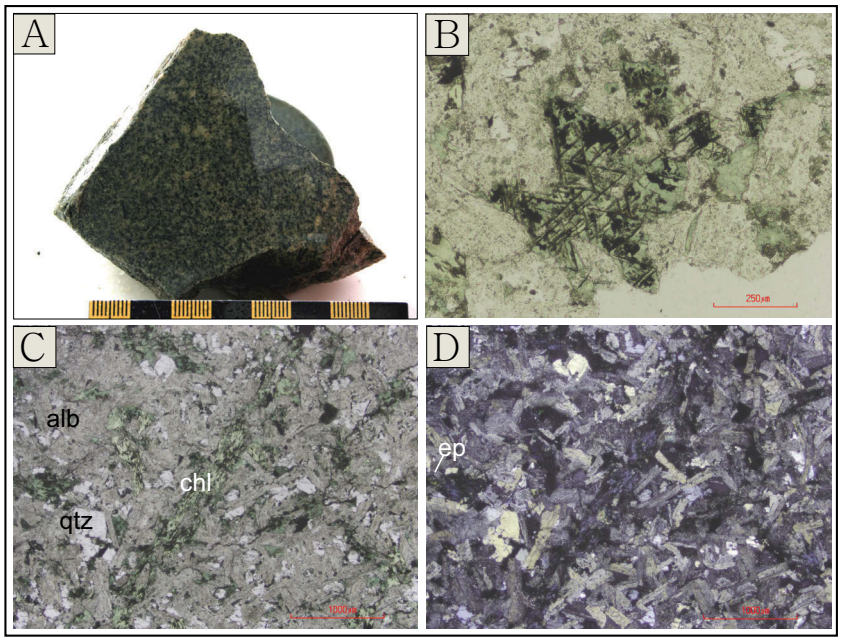

Plate 2-24*: Representative photos and photomicrographs of the dioritic phase of the Burin Knee Intrusive Suite from sample SF-12-44; A) Green fresh surface of the fine- to medium-grained diorite with acicular mafic phenocrysts; B) (10X; PPL) Close-up of chlorite-altered grain showing ~120/60° cleavage directions (highlighted by presence of oxide minerals), diagnostic of amphiboles; C&D) (2X; PPL & XPL, respectively) Fine- to medium-grained cumulate textured groundmass of albite and minor quartz, containing coarse, acicular phenocrysts of chlorite, after actinolite. alb=albite, qtz=quartz, chl=chlorite, ep=epidote.*

The diorite is primarily made up of fine- to medium-grained interlocking laths of albite (~80%) forming a cumulate texture (*Plate 2-24 C&D*). Albite has been altered to sericite, and also often appears as fine, recrystallized masses at high magnification. Quartz (5-15%) forms as both subhedral grains and as an anhedral interstitial filling between the feldspars. The most distinctive feature of this unit is the coarse, acicular mafic crystals that comprise ~10-15% of the section, composed of chlorite and lesser epidote and Fe-Ti-oxides (*Plate 2-24*). These are interpreted as former actinolite crystals based on their acicular crystal habit, and the 120/60° cleavage intersections displayed locally, usually highlighted by the presence of oxides along the cleavage planes (*Plate 2-24 B*). Trace amounts of feldspar, displaying no twinning and a more tabular shape, were identified locally, and interpreted as alkali-series feldspars. Minor epidote and calcite occur as a patchy alteration, and trace pyrite is disseminated throughout.

Mafic Dykes

Mafic dykes are one of the youngest features found at the Stewart prospect. They are narrow (~1m) and rare in outcrop, so are not represented in the scale of mapping displayed in *Figure 2-2*. They are dark grey-green on both weathered and fresh surfaces, fine-grained, massive and otherwise featureless (*Plate 2-25*). *Plate 2-25 A* shows a relatively unaltered mafic dyke crosscutting the hydrothermally altered tonalite, with a sharp contact. This indicates that the mafic dyke is not only younger than the volcanic and plutonic stratigraphy, but also postdates the hydrothermal alteration and mineralization. Similar mafic dykes were identified in drill core (e.g., SF-12-102; DDH ST-11-02; ~49m). These dykes are fine-grained and chloritic, and crosscut the hydrothermally altered Caribou Tuff. They contain about 2% disseminated pyrite, and are crosscut by multiple sets of opaque white-beige quartz-feldspar-epidote veins. The veins appear to be syn-tectonic, resulting from extensional stress, and not related to the hydrothermal system at Stewart.

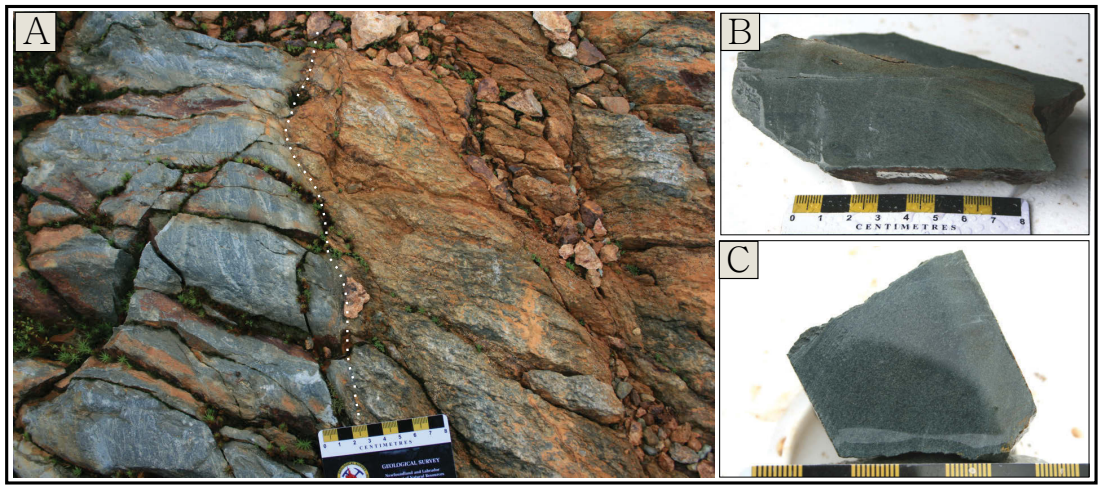

Plate 2-25*: Representative photos of the crosscutting mafic dykes; A) Fine-grained massive and unaltered mafic dyke crosscutting hydrothermally altered tonalite. Contact highlighted by dotted line (STA-SF-12-029; SF-12-41/GS-11-33); B) Fresh surface of the fine-grained, chloritic, massive mafic dyke (SF-12-41); C) Fresh surface of the fine-grained, chloritic, massive mafic dyke (GS-11-33).*

A single sample, from the outcrop displayed in *Plate 2-25 A*, was selected for petrographic analysis. In thin section, the unit appears weakly foliated and significantly altered from its primary assemblage. The groundmass is pervasively altered to fine-grained chlorite and lesser sericite and quartz, with patchy epidote alteration and ~5%

fine-grained rutile disseminated throughout. Remnant lath-shaped feldspar phenocrysts occur, and make up ~25% of the section (*Plate 2-26 A&B*). They vary in size, the maximum length being approximately 1mm, and have been entirely replaced by chlorite and lesser epidote and Fe-Ti-oxide. Fine-grained anhedral grains of quartz are present scattered throughout the matrix, comprising 10-15% of the section (*Plate 2-26 C&D*).

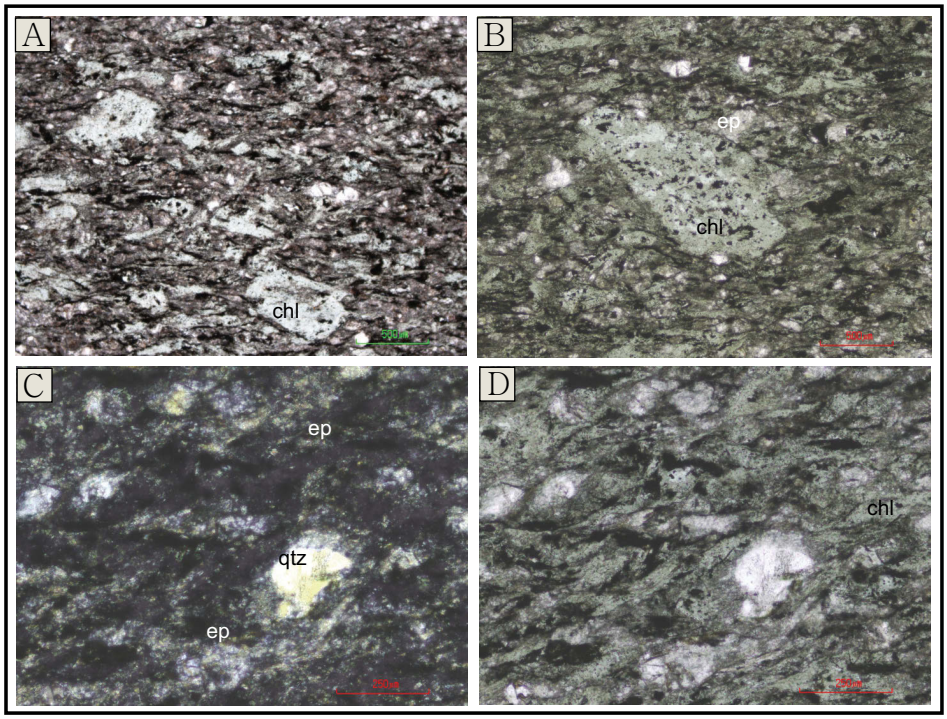

***Plate 2-26**: Representative photomicrographs of the crosscutting mafic dykes from sample SF-12-41; A) (4X; PPL) Feldspar lath phenocrysts altered to chlorite within a foliated groundmass dominated by chlorite, rutile, epidote and sericite; B) (4X; PPL) 1mm sized feldspar lath-shaped phenocryst altered to chlorite and lesser epidote and Fe-Ti-oxides. Bright white grains are quartz; C&D) (10X; XPL & PPL, respectively) Fine anhedral quartz grains scattered through the groundmass in abundance of up to 15% locally. Patchy epidote alteration is evident here. chl=chlorite, ep=epidote, qtz=quartz.*

2.3.1.2 Brief Description of Intermediate Volcaniclastic Rocks at the Forty Creek Prospect

The stratigraphy immediately adjacent to the mineralized quartz boulders at the Forty Creek prospect is very similar to some of the volcaniclastic stratigraphy found at Stewart, just 5 km to the southwest. The rocks are intermediate to mafic in composition and include feldspar crystal tuffs (*Plate 2-27 B*), separated by horizons of lapilli tuff. Lapilli tuff units contain rounded, intermediate-felsic lapilli, 1-6cm in size, but locally up

to 10 cm (blocks), hosted within a fine-grained chloritic and plagioclase-phyric matrix (*Plate 2-27 A*).

***Plate 2-27**: Representative photos of the intermediate-mafic volcaniclastic rocks from Forty Creek (STA-SF-12-114); A) Mafic-intermediate lapilli tuff with rounded felsic lapilli in a chloritic, feldspar-phyric matrix; B) Weathered surface of an intermediate feldspar crystal tuff.*

2.3.1.3 Overview of Local Structure

Most of the Stewart property has been affected by a penetrative foliation, generally striking to the southwest and dipping steeply northwest. However, the dip is variable, from subvertical to steeply southeast (*Figure 2-3*). This fabric is interpreted to have occurred during the Silurian-Devonian when regional greenschist metamorphism and ductile deformation occurred. Rocks affected by hydrothermal alteration prior to deformation, tend to be much more deformed due to their high mica content making them more susceptible to deformation. The penetrative fabric is made evident by lapilli fragments and micaceous minerals, which have been stretched and aligned parallel to the foliation (e.g., *Plate 2-8 C&D; Plate 2-12*).

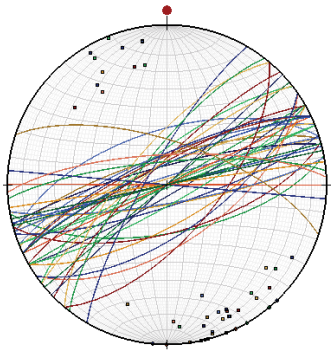

***Figure 2-3**: Stereonet of all foliations collected in the Stewart-Forty Creek area. Foliation predominantly striking southwest and dipping steeply towards the northwest.*

Pratt identified a major shear zone on the property, which he referred to as the Bat Shear Zone (*Figure 2-2*). It is a vertical, southeast-striking structure with both dextral and vertical displacement, which has caused the regional foliation to diverge locally, parallel to the shear direction (Dyke and Pratt, 2008).

In addition to this major structure, evidence for local smaller scale faulting and shearing occurs across the property. In the west, indicators for sinistral strain striking towards the north-northeast include a folded mineralized quartz vein (*Plate 2-28 D*) and 30cm brittle displacement of a ptygmatically folded quartz vein (*Plate 2-28 E*). Across the property, indicators of dextral strain can also be found, possibly associated with the main Bat Shear Zone. Evidence includes sigmoidal-shaped breccia fragments (*Plate 2-28 A*), and prevalent kink-banding (*Plate 2-28 B&C*). At Forty Creek towards the northeast, a quartz vein parallel to a west-southwest foliation is sheared and boudinaged with sigma-shaped boudins indicative of a dextral shear sense (STA-SF-12-114).

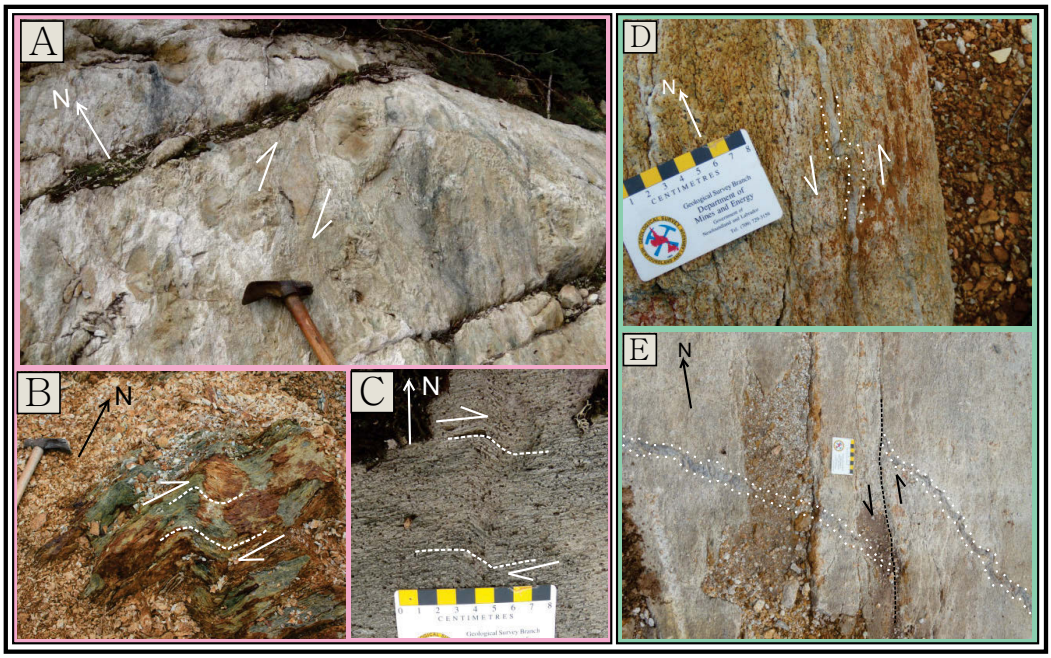

***Plate 2-28**: Representative photos of small-scale shear and fault indicators at Stewart; A-C) Examples of dextral shear sense indicators including sigmoidal-shaped breccia fragments (A; STA-SF-12-031) and kink-banding (B; STA-SF-12-028 & C; STA-SF-12-024); D&E) Examples of local N-NE sinistral shear and fault sense indicators in the western portion of the property, including a folded mineralized vein (D; STA-SF-12-035) and 30cm displacement of a ptygmatically folded quartz vein (E; STA-SF-12-030).*

2.3.2. Hickey's Pond Prospect

The Hickey's Pond prospect is located at the northern end of the Burin Peninsula, along the southeastern margin of the Swift Current Granite (*Figure 2-2*). The prospect is small, but well exposed, containing a central vuggy silica core (yielding grab samples of up to 60.4 g/t Au), surrounded by an extensive halo of advanced argillic alteration. The prospect is overthrust from the northwest, and bound by the southwest-striking and steeply northwest-dipping Hickey's Brook Fault (Huard, 1989), shown in *Figure 2-4*. The southeastern extent of mineralization is not exposed at surface, but within approximately 100m of the advanced argillic alteration halo, the rocks have graded back into unaltered felsic volcaniclastics towards the southeast (Huard, 1989).

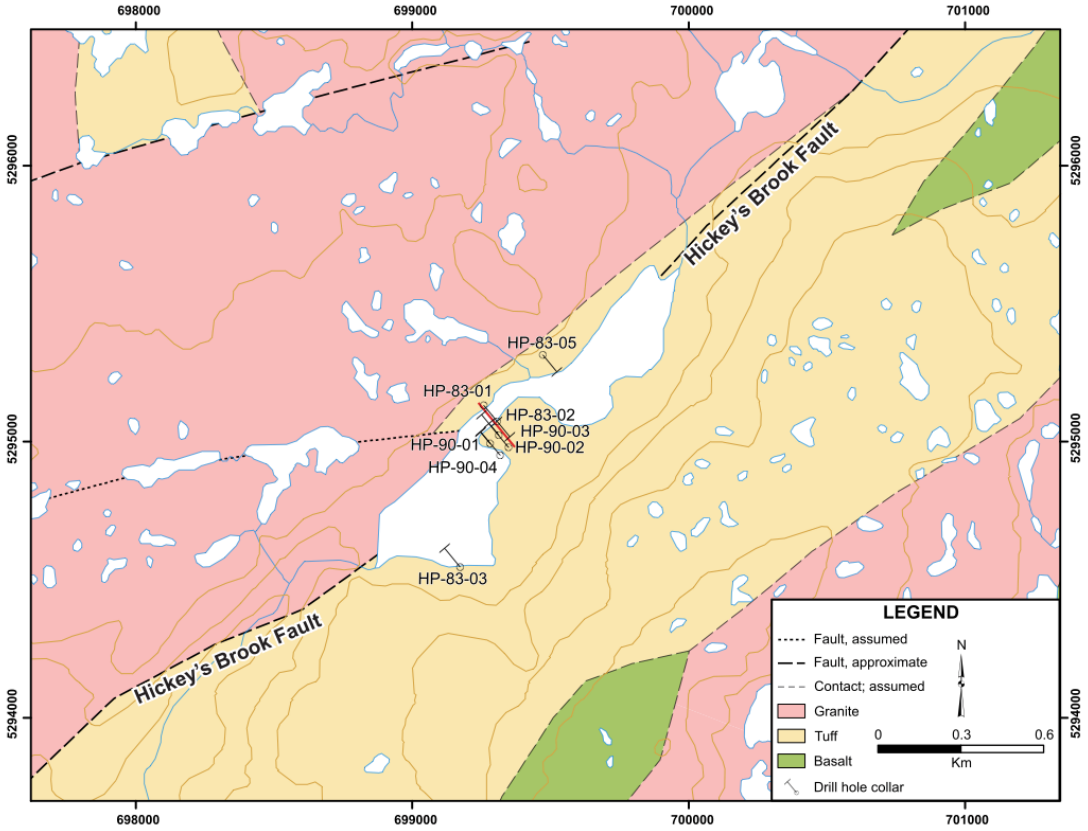

***Figure 2-4**: Compilation map outlining the geology surrounding the Hickey's Pond prospect (data from Huard and O'Driscoll, 1986; O'Brien et al., 1999; Sexton et al., 2003; Sparkes et al., 2016) The red line denotes the location of a cross-section included in Chapter 5. (From Sparkes et al., 2016).*

2.3.2.1 Brief Description of Volcaniclastic Host Rocks

The Hickey's Pond prospect is broadly hosted in high-strain, greenschist-grade felsic pyroclastic rocks of the Marystown Group (O'Brien et al., 1999; *Figure 2-4*). The stratigraphy exposed in the immediate vicinity of the prospect is however, significantly altered and deformed. In high-sulphidation systems, vuggy silica typically occupies the core of the alteration zonation, and is the result of highly acidic fluids extensively leaching the host rocks leaving predominantly silica residue. This is essentially what is found in outcrop at Hickey's Pond. An advanced argillic alteration, enveloping the vuggy silica zone, contains an abundance of soft minerals, and has been strongly affected by regional deformation. For both of these reasons, most of the original igneous textures are now obscured in the hydrothermally altered rocks exposed at Hickey's Pond.

To the southeast of Hickey's Pond, the closest adjacent unaltered rocks have been mapped as felsic crystal tuffs (Huard, 1989). Towards the northwest, the immediately adjacent rocks in the hanging wall of the Hickey's Brook Fault are comprised of a sequence of felsic volcaniclastics that are much less deformed, and relatively unaltered, compared to those at Hickey's Pond (O'Brien et al., 1999; Sparkes et al., 2016). The volcaniclastics are dominated by lapilli tuffs, containing well-defined cm-scale lapilli fragments and sub-euhedral phenocrysts of feldspar and lesser quartz within a fine-grained quartz-rich matrix. The unit is moderately foliated and altered to a greenschist assemblage of sericite, chlorite and epidote (Sparkes et al., 2016; *Plate 2-29 A*). Proximal to the Hickey's Brook Fault, but further northwest, the volcaniclastics are intruded by the Swift Current Granite (Huard, 1989; O'Brien et al., 1999).

A thin section from the vuggy silica zone at Hickey's Pond, displays what is interpreted here as a remnant lapilli fragment, suggesting a volcaniclastic origin for the host rocks. The lapilli fragment is 1cm in length, sub-rounded and, although its mineral composition is identical to that of the surrounding predominantly quartz-altered groundmass, is discernible by its overall finer grain size (Plate 2-29 B).

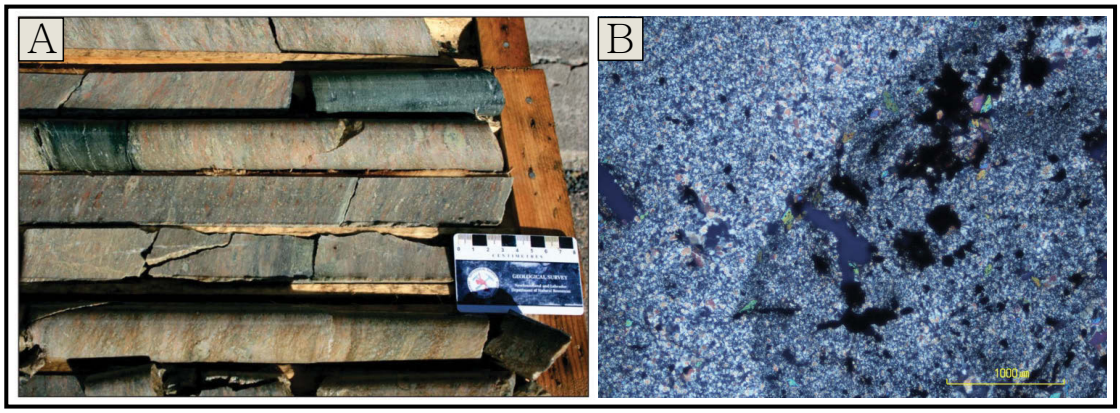

***Plate 2-29**: Representative photo and photomicrograph of volcaniclastic rocks at the Hickey's Pond prospect; A) Foliated felsic lapilli tuff from the northwestern side of Hickey's Pond, occurring in the hanging wall of the Hickey's Brook Fault (DDH HP-83-01, ~22m; from Sparkes et al., 2016; B) (2X; PPL) Possible remnant lapilli fragment preserved in the vuggy silica zone, distinct from the surrounding matrix by its finer grain size (SF-12-152).*

2.3.2.2 Overview of Local Structure

The following is summarized from the structural interpretations presented by O'Brien et al. (1999), unless otherwise noted.

The rocks at Hickey's Pond have undergone intense deformation as a result of multiple deformation events, all of which have affected the hydrothermal alteration assemblage. A southwest-northeast trending and steeply northwest-dipping foliation occurs, containing a moderately to steeply southwest-plunging stretching lineation. Local isoclinal folds occur, plunging steeply to the southwest, with axial planes parallel to foliation. Huard (1989) noted a c-s fabric occurring locally, indicative of a reverse sense of motion, synonymous with motion along the adjacent Hickey's Brook Fault. These initial structures are further deformed by open, moderately-steeply northeast-plunging folds and shallow southwest-plunging folds. The overall strain intensity tends to increase westward towards the Hickey's Brook Fault.

2.3.3 Tower Prospect

The Tower prospect is also located centrally on the northern Burin Peninsula, about 15 km southwest and along strike of Hickey's Pond (*Figure 2-2*). The prospect consists of a northeast-southwest trending belt of advanced argillic alteration, up to 1km

in length and 200m in width (Sparkes et al., 2014), host to weakly anomalous gold (up to 179 ppb) and molybdenum (203 ppm; Dimmell, 2003). The alteration zone is inferred to be confined, both to the east and west, by two faults, based on lineations elucidated through VLF surveying conducted by Hayes (2000). Despite the strong hydrothermal alteration, igneous textures are still visible locally within the altered rocks, and are suggestive of a felsic-intermediate volcaniclastic host rock.

2.3.3.1 Lithology and Petrography of Volcaniclastic Host Rocks

Outside of the main alteration zone, the intensity of hydrothermal alteration dissipates quickly, and adjacent outcrops clearly display original igneous compositions and textures. Approximately 100 m southwest of the main alteration zone, the unaltered rocks are intermediate to felsic in composition and include crystal and lapilli tuffs (e.g., *Plate 2-30 A*).

Rocks from the perimeter of the alteration zone are weakly altered to silica, pyrite and sericite, but are still clearly identifiable as felsic crystal tuffs (*Plate 2-30 B&C*). They contain both feldspar and quartz crystals and occasional lapilli fragments, which are all readily discernible, despite oxidative weathering (*Plate 2-30 B*). In thin section this weakly altered unit contains 35-45% crystals and ~5% lapilli dispersed through a very fine-grained, moderately foliated, quartz-sericite matrix. The crystal content is dominated by albite, which is typically 1-3mm in size, and occurs as irregular anhedral grains to euhedral crystals, which are variably recrystallized, rimmed by quartz, and altered to sericite. Quartz crystals are typically finer (<0.5mm) and subangular. Lapilli are usually slightly coarser-grained than the matrix, but still fine-grained, with feldspar laths occurring in a finer, quartz-rich matrix. Locally, lapilli are also composed of very fine-grained silica (*Plate 2-30 C).*

Remnant volcaniclastic textures are also found locally within the advanced argillic alteration zone, the protolith here is, therefore, presumed similar to the adjacent relatively unaltered volcaniclastic units. *Plate 2-30 D* displays a photomicrograph of a sample, collected from within the advanced argillic zone, with well-preserved igneous textures

that classify it as a crystal tuff. It contains ~1mm quartz crystals with embayed margins, as well as sub-euhedral bipyramidal quartz crystals within a recrystallized, silicic matrix. There are also what appear to be remnant feldspar crystals that have undergone complete recrystallization, making them difficult to discern from the matrix, but still distinctive, especially in plane-polarized light.

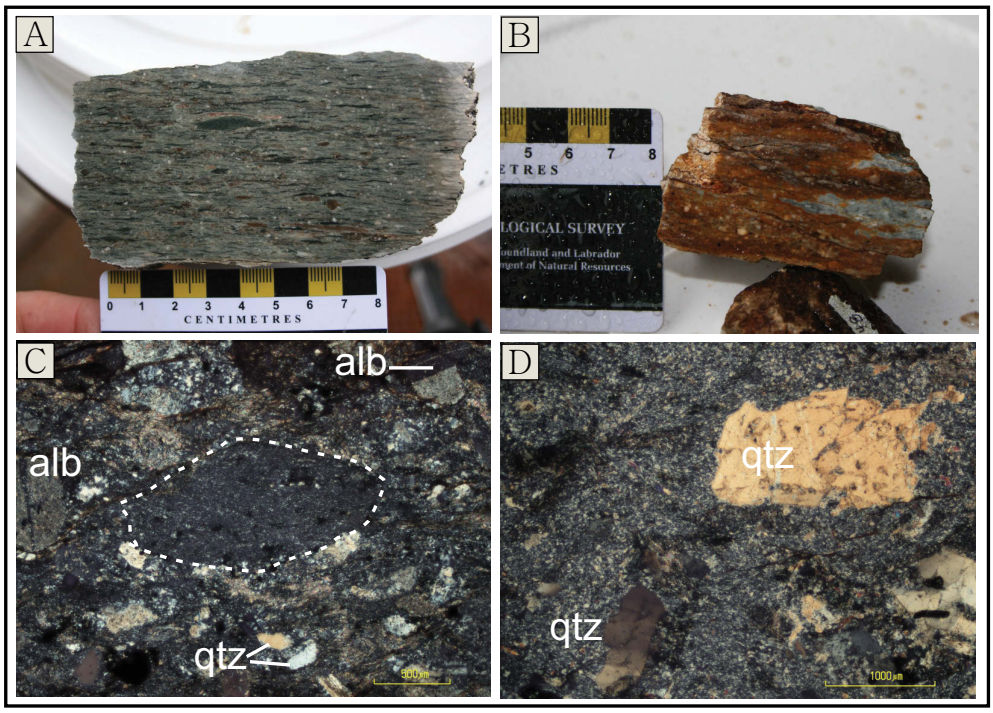

Plate 2-30*: Representative photos and photomicrographs of the intermediate-felsic volcaniclastic host rocks at Tower; A) Relatively unaltered, foliated intermediate lapilli tuff with 3mm-2cm lapilli and feldspar crystals suspended in a fine-grained matrix, from ~100m southwest of the alteration zone (GS-12-219; STA-SF-12-012); B) Intermediate-felsic feldspar-quartz-crystal tuff from perimeter of alteration zone (SF-12-23; STA-SF-12-019); C) (4X; XPL) Intermediate-felsic crystal tuff from perimeter of alteration zone with subhedral albite crystals, finer angular quartz fragments, and a small very fine-grained siliceous lapilli fragment (outlined; SF-12-23); D) (2X; XPL) Felsic crystal tuff from within the advanced argillic alteration zone, containing coarse 2mm quartz crystals with rounded embayments along their margins and sub-euhedral bipyramidal quartz crystal within a very fine-grained, recrystallized matrix. Remnant recrystallized feldspars also occur but are difficult to see – e.g. one lies to the right and roughly parallel to the bipyramidal quartz crystal (SF-12-07; STA-SF-12-009). qtz=quartz, alb=albite.*

2.3.3.2 Overview of Local Structure

The property contains a strong penetrative fabric, striking southwest and dipping steeply towards the northwest (*Figure 2-5*). Folding occurs locally with varying intensity and complexity, but overall shallowly plunging towards the east-northeast. Evidence for

shearing with a relative dextral sense of motion is abundant throughout the property. Silica veins are all strongly boudinaged, and exhibit dextral-sense shear indicators including asymmetrically shaped boudins, rotated boudins, and 'Z' folding (Plate 2-31).

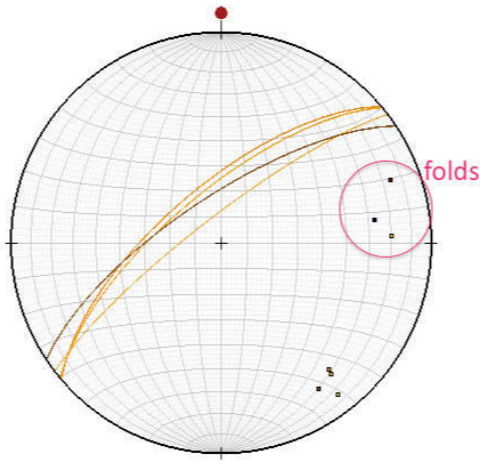

***Figure 2-5**: Stereonet showing southwest-striking, steeply-northwest-dipping foliation. Circle contains lineation measurements for shallowly east-northeast plunging local folding.*

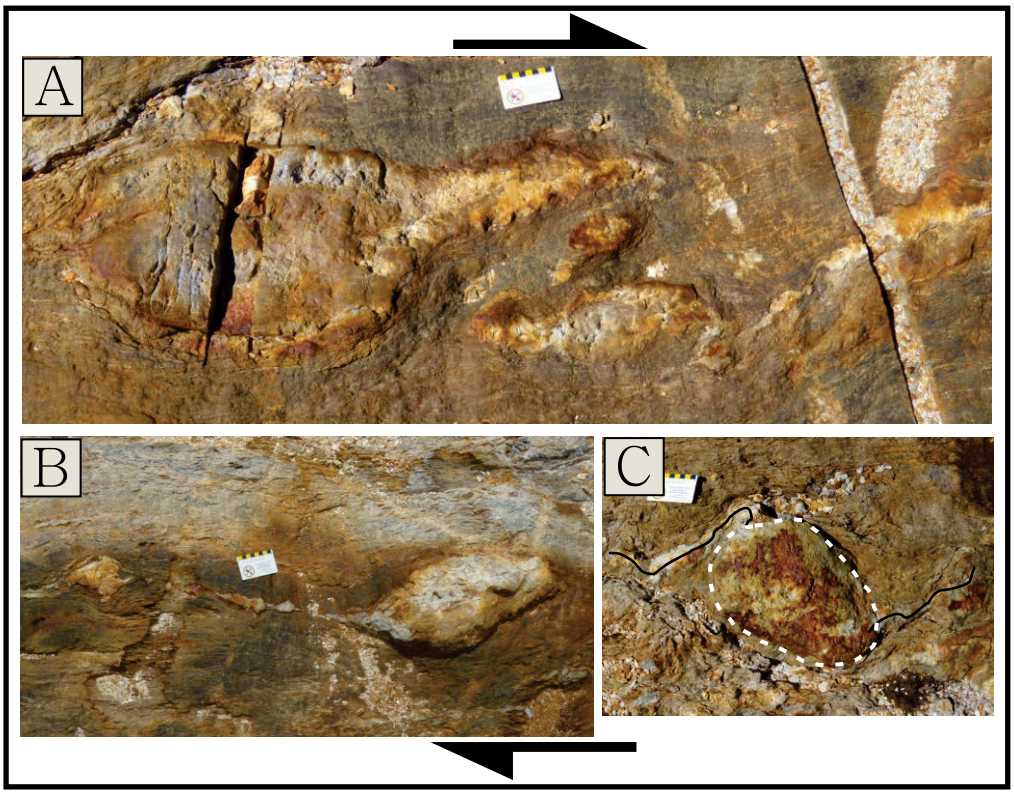

***Plate 2-31**: Representative photos of the dextral sense shear indicators at Tower (STA-SF-12-009; STA-SF-12-010); A) Boudinaged silica vein with asymmetric boudins and overall 'Z' folding shape; B) Boudinaged silica vein with asymmetric boudins; C) Silica boudin which has been rotated dextrally. Boudin is outlined in dashed white line, and quartz tails are marked by the thin black lines.*

2.3.4 Lithology and Petrography of the 'Grandy's Pond Arenite Belt'

The 'Grandy's Pond Arenite Belt' spans the northern half of the Burin Peninsula along its western edge, overlying the volcanics of the Marystown Group (*Figure 2-2*). The belt is predominantly composed of feldspathic-lithic arenites with subordinate fine polymictic conglomerates that are locally interbedded with thin pyroclastic units, and thus interpreted to represent intra-formational epiclastic deposits (O'Brien & Nunn, 1980). The boundary between the felsic volcanics to the east, and epiclastics to the west, is important, as there is an empirical spatial association between this boundary and the occurrence of high-sulphidation epithermal mineralization in the region. Furthermore, this lithological contact may be analogous to similar geological boundaries considered highly prospective for gold within the Carolina Slate Belt (Feiss et al.,1993; O'Brien et al., 1999; Ayuso et al., 2005).

Two outcrops from within this unit were visited during fieldwork. At these locations, the unit contains abundant fine to medium-grained euhedral feldspar crystals within thick layers of green-grey feldspathic arenite. This lithology is weakly bedded, containing thin, subordinate layers of silt, and of coarser lithic arenite (*Plate 2-32 B*). Locally, the unit displays distinctive horizons of crossbedding (*Plate 2-32 A*).

In thin section, the main groundmass enclosing the various coarser constituents is fine-grained and predominantly composed of albite and epidote, with lesser quartz. The groundmass also contains layers rich in chlorite, epidote, sericite and magnetite (*Plate 2-32 C&D*). Magnetite occurs as sub-euhedral crystals and its overall abundance is ~2%.
The unit is weakly sorted and bedded. As an example, 0.5-1mm subangular-angular fragments of quartz crystals occur in abundance of 5-10%, but only along distinct horizons (*Plate 2-32 C*). Albite crystals are abundant (~20%), occurring as euhedral crystals and angular-subrounded crystal fragments, 1-2mm in size (*Plate 2-32 C*). They typically display polysynthetic or simple twinning and locally display a micro-antiperthitic texture. Untwinned alkali feldspars were also identified, but only locally. Feldspars are variably altered to sericite and epidote.

The representative thin section for this unit (*Plate 2-32*) is particularly rich in lithic fragments, which range in abundance from 20-40%. Fragments are subrounded and up to 4mm in size. They are typically of igneous origin and felsic-intermediate in composition, made up of a fine quartzo-feldspathic groundmass containing slightly coarser feldspar laths, and locally include minor amounts of chlorite, zircon and magnetite (*Plate 2-32 C&D*). Flat, elongate fragments also occur, consisting entirely of sericite (*Plate 2-32 C*) or of very fine-grained quartz (*Plate 2-32D*).

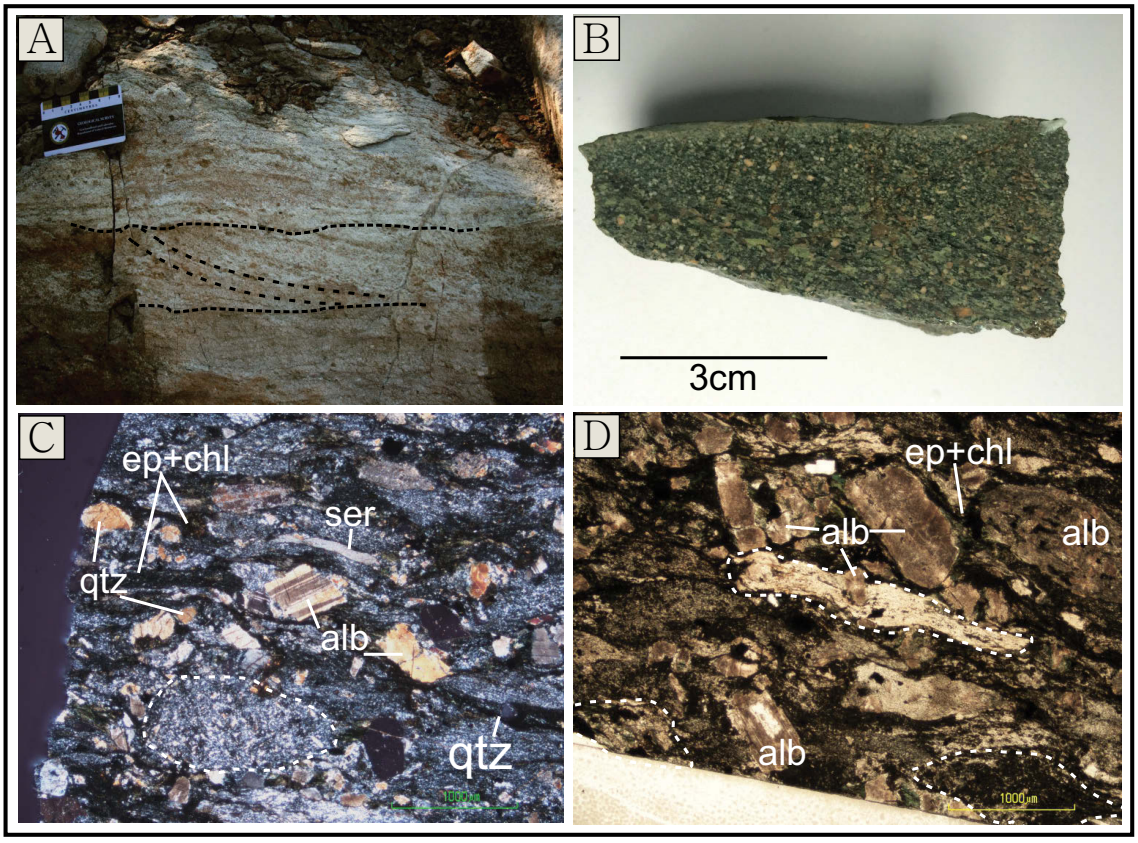

Plate 2-32*: Representative photos and photomicrographs of the 'Grandys Pond Arenite Belt'; A) Outcrop-scale photo displaying cross bedding identified locally (highlighted by thin black dashed lines) (SF-12-149); B) Fresh surface showing weak bedding in the unit, with a coarser, more lithic-rich layer at the bottom and a finer-grained layer with abundant euhedral feldspar at the top (SF-12-148); C) (2X; XPL) Fine-grained groundmass of albite-epidote-quartz with thin dark layers rich in chlorite-epidote-sericite-magnetite. Sparse fragments of quartz crystals occur along a single horizon. Fragments include a typical felsic-intermediate igneous fragment (outlined with a dashed white line) and a flat elongate one composed of sericite. Twinned albite crystals and fragments are scattered throughout (SF-12-148); D) (2X; PPL) Various sub-euhedral grains of weakly altered feldspar occurring with various types of lithic fragments, including a flat, elongate, very fine-grained, quartz-rich one, and fragments near the bottom containing magnetite (highlighted by dashed white lines) (SF-12-148). ep=epidote, chl=chlorite, alb=albite, ser=sericite, qtz=quartz.*

2.3.5. Lithology and Petrography of the 'Swift Current Granite'

The 'Swift Current Granite' is a large, high-level plutonic suite located at the top of the Burin Peninsula (*Figure 2-2*). The suite intrudes, and is roughly coeval with volcanics of the Marystown Group, and consists of hornblende-biotite granite, diorite and gabbro (O'Brien et al., 1999). The suite is part of a larger, semi-continuous plutonic belt extending southwest to the 'Burin Knee Granite'. The high-sulphidation epithermal prospects occurring on the Burin Peninsula generally lie along the eastern margin of this larger plutonic suite. A sample collected along the Burin Highway within the town of Swift Current was chosen as a representative example of the suite, and is displayed in *Plate 2-33*.

In hand sample, the unit appears coarse grained, containing an abundance of pink, potassium feldspar locally displaying perthitic textures, and lesser grey quartz and white feldspar (*Plate 2-33 A*). Pale green sericite-epidote alteration occurs along fine fracture networks throughout, and variably alters the feldspars. Fine-grained, dark mafic minerals occur in relatively low abundance, often spatially associated with the epidote-sericite alteration.

In thin section, the sample is composed of 40-45% coarse-grained potassium feldspar with variably developed perthitic texture, up to 8mm in size (*Plate 2-33 C&D*). Quartz (~35%) is also fairly coarse-grained, generally between 4-6mm. Albite (20-25%) occurs as 2-3mm sized laths, variably altered to sericite and lesser epidote and chlorite. Albite is relatively more fine-grained than the other main constituents, and is often found as inclusions within coarse potassium feldspar grains (*Plate 2-33 C&D*). Fine-grained tabs of biotite are found locally, but biotite has for the most part, been replaced by chlorite, with a total abundance of about 3-5% (*Plate 2-33 B*). Trace titanite is found as 0.5mm euhedral crystals (*Plate 2-33 B*), as well as trace zircon as finer-grained euhedral crystals. Fine fractures filled with epidote, chlorite and minor sericite crosscut the sample.

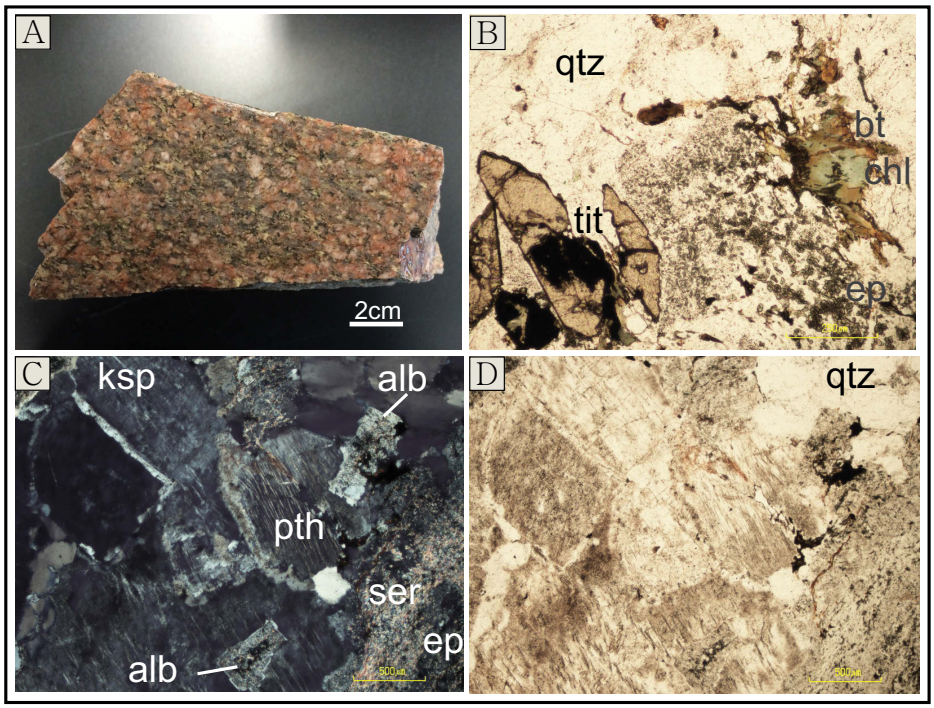

Plate 2-33*: Representative photos and photomicrographs of the 'Swift Current Granite' from sample SWC-2; A) Hand sample of coarse grained granite; B) (10X; PPL) Medium-grained euhedral titanite crystals and tabs of biotite being replaced by chlorite; C&D) (4X; XPL & PPL, respectively) Laths of albite weakly altered to epidote and sericite occurring as inclusions within coarser potassium feldspar with weakly developed tartan twinning and perthitic texture. ksp=potassium feldspar, pth=perthitic texture, ser=sericite, ep=epidote, alb=albite, qtz=quartz, tit=titanite.*

2.3.6 Heritage Prospect

The Heritage prospect is located in the southernmost part of the Burin Peninsula (*Figure 2-2*), distant from the previously discussed examples of the Marystown Group. Unlike the other prospects discussed so far, which are host to high-sulphidation epithermal mineralization, the mineralization found at Heritage is of the low-sulphidation epithermal-style. Despite the variable, but extensive silicification present, original igneous textures are much better preserved at the Heritage prospect than at the aforementioned occurrences. This is because the hydrothermal fluids associated with low-sulphidation systems are more neutral than their high-sulphidation counterparts, therefore the host rocks did not undergo the same acid-leaching process and subsequent replacement, preventing the wholesale obliteration of original mineralogy and igneous

textures. Instead, the hydrothermal system is imprinted on the host rocks as extensive networks of quartz veins and breccias, along with pervasive silicification.

2.3.6.1 Lithology, Field Relationships and Petrography of Rock Units

A very general overview of the litho-stratigraphy at Heritage is described below - with what is currently interpreted as units from oldest to youngest, with stratigraphy younging towards the northwest. Evidence for this is contained locally in sedimentary horizons, and includes graded bedding fining upwards towards the northwest, and fragments of older strata within an overlying unit along a shallowly-northwest-dipping contact (*Plate 2-34*). The stratigraphy includes a thick sequence of andesitic pyroclastics, and more locally occurring rhyolitic crystal tuffs, interbedded sandstones and conglomerates, and porphyritic-amygdaloidal basalts. All of these units are crosscut by a series of narrow mafic dykes. A detailed property map outlining these units is currently being produced by G. Woodland as part of a M.Sc. project on the Heritage property.

***Plate 2-34**: Shallowly northwest dipping contact between a lower grey-green sandstone and an upper red laminated siltstone. Stratigraphy is younging towards the northwest with the dip direction based on the presence of green clasts of the lower unit above the contact within the overlying red siltstone.*

Andesitic Pyroclastics

The andesitic pyroclastic rocks are the main host to epithermal mineralization at the Heritage prospect. They vary significantly across the property, occurring as crystal tuffs, lapilli tuffs, and tuff breccias and contain both monolithic and heterolithic populations of clasts. Overall, the sequence generally tends to become finer with less

abundant clasts towards the northwest, grading from heterolithic tuff breccias to fairly massive feldspar-crystal tuffs.

On the eastern side of the prospect, pyroclastic textures are well exposed in one of the exploration trenches referred to as the Ridge Trench (*Plate 2-35 A&B*). The rocks are composed of heterolithic andesitic tuff breccias with blocks up to 60cm in size, and lapilli and blocks together comprising up to 75% of the rock. The most commonly occurring fragments include a red oxidized andesitic lapilli tuff, and variations of massive andesitic feldspar-crystal tuffs, which occur as grey and relatively unaltered, or as red-oxidized, and green-chloritized equivalents. Minor rhyolitic crystal tuff and amygdaloidal basalt fragments also occur. A 50cm volcanic bomb is also locally preserved, which displays a thin chilled margin and is surrounded by some form of concentrically zoned reaction halo (*Plate 2-35B*).

Towards the west, monolithic lapilli tuffs and more massive feldspar-crystal tuffs become more common. The lapilli tuffs contain mm- to cm-scale fragments composed of massive andesitic feldspar-crystal tuffs within a finer-grained matrix of similar composition *(Plate 2-35 C&D)*. Typically the fragments are more green and chloritic while the matrix is more red and oxidized, but this differential alteration pattern is variable, with the opposite occurring locally, or neither showing distinctive colouration/alteration. Horizons of massive porphyritic andesite, interpreted as feldspar-crystal tuffs, also occur (*Plate 2-35 E&F*). Once again, this massive unit appears both as a grey-green variety, and a more red/oxidized variety. This difference in alteration is interpreted as reflecting original variations in depositional setting from a subaerial to shallow lacustro-marine environment, and may have been accentuated further by the local hydrothermal activity.

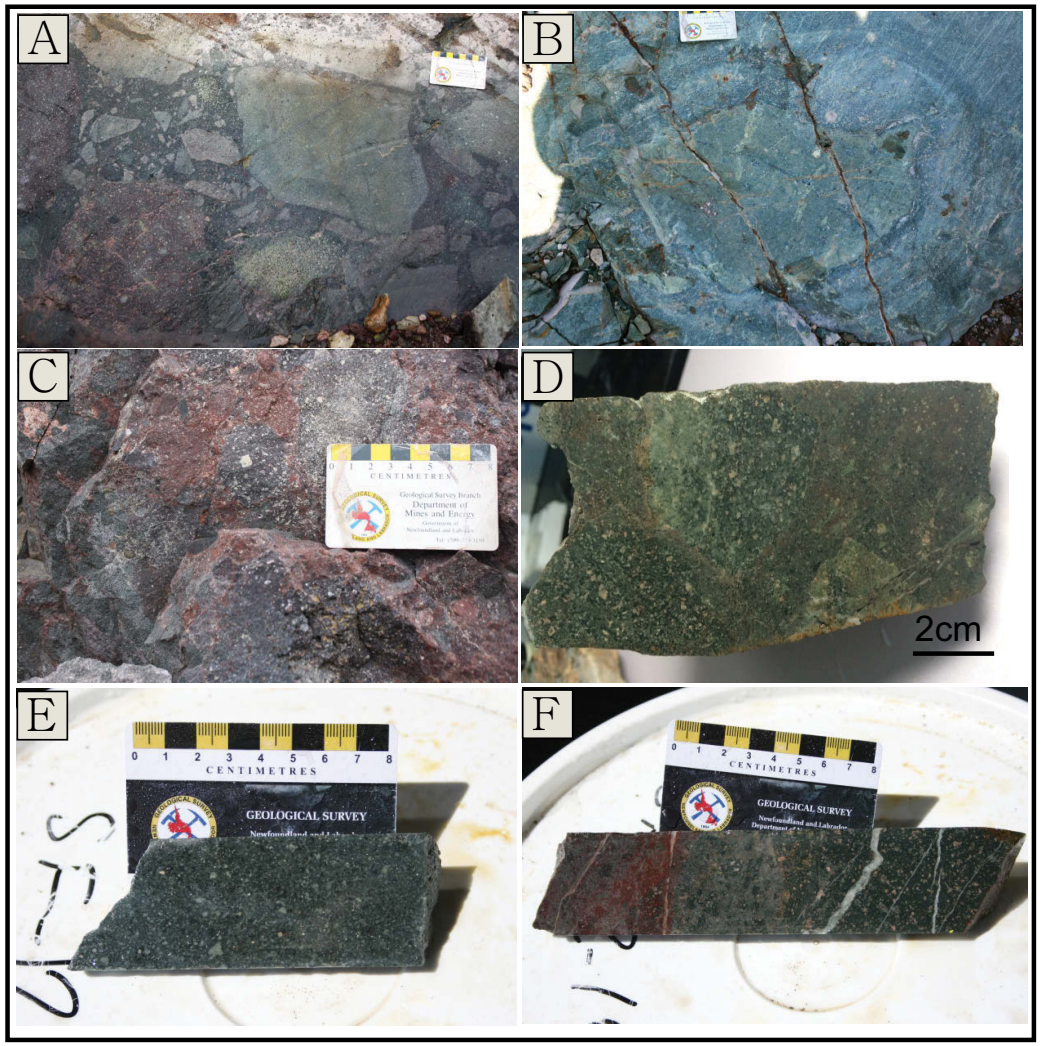

***Plate 2-35**: Representative photos of the andesitic pyroclastic rocks, which are the main hosts to mineralization at the Heritage prospect; A) Heterolithic andesitic tuff breccia shown in the Ridge trench; B) 50cm volcanic bomb located in the Ridge trench; C) Monolithic andesitic porphyritic lapilli tuff, with grey lapilli within a red oxidized finer-grained matrix of similar composition from southwestern portion of property; D) Fresh surface of a sample similar to the previous outcrop photo from the Zaxis trenches, with green porphyritic andesite lapilli within a more red, finer-grained similarly composed matrix. Fragments are monolithic but locally variably altered, and sample has been affected by silicification (SF-13-180); E) Green-grey, massive, andesitic feldspar-crystal tuff affected by silicification (SF-13-172; HD-01-13; ~32m); F) Green massive andesitic feldspar-crystal tuff affected by silicification and hydrothermal brecciation on left side (SF-13-162; HD-05-13; ~23m.*

Sample *SF-13-180*, a monolithic lapilli tuff from the Zaxis Trench, was selected for petrographic analysis as it was one of the least altered examples of the host lithology (although still somewhat silicified), and because of its overall homogeneity in texture and composition (*Plate 2-36*). The thin section contains a single population of subangular

ash-lapilli rock fragments from <0.5mm to 15mm in size, accounting for up to 50% of the sample (*Plate 2-36 A&B*). The fragments contain ~20% phenocrysts of albite displaying polysynthetic twinning, which sit in a finer matrix of albite laths, abundant chlorite, minor sericite and fine- to medium-grained subhedral grains of Fe-Ti-oxides with titanite (*Plate 2-36 E*). Feldspar phenocrysts often show total replacement by chlorite, although some are predominantly replaced by calcite with lesser chlorite and quartz (*Plate 2-36 C&D*). Although the fragments may vary in macroscopic appearance, in thin section they simply display variable degrees of alteration to a more sericite dominated assemblage, while still the same original rock type as the chlorite-dominated fragments. The matrix surrounding the ash-lapilli fragments shows significant alteration due to hydrothermal silicification and is predominantly composed of very-fine-grained quartz and lesser sericite with ~20% feldspar phenocrysts that are finer-grained than those occurring in the fragments. Feldspar phenocrysts in the matrix are most commonly replaced by quartz but locally also display alteration to chlorite, calcite and sericite. They sometimes display remnant simple twinning, which could be representative of albite or a more potassic alkali-feldspar variety, but the silicification and finer grain size makes this difficult to discern (*Plate 2-36 E*). Apatite is quite abundant throughout the sample (~2-3%) occurring in both fragments and matrix.

In thin section, the more massive crystal tuffs appear to be closer to a dacitic composition than andesitic (*Plate 2-35 E&F*), despite the abundance of chlorite alteration visible in hand sample. This observation is based on the feldspar content, which is dominated by alkali-series feldspars. The two samples analyzed in thin section have both been affected by hydrothermal alteration, predominantly silicification. They contain ~30% feldspar phenocrysts and glomerocrysts within a fine-grained matrix of quartz, chlorite and sericite. The feldspar phenocrysts in sample *SF-13-172* have for the most part been replaced by quartz, calcite, and chlorite but locally still display remnant compositional zoning and simple twinning. These are interpreted as sanidine phenocrysts. The feldspar crystals in sample *SF-13-162* are not as significantly altered and clearly show two types of feldspar. The finer-grained feldspar comprising the

glomerocrysts consistently display simple twinning and are interpreted as sanidine (*Plate 2-36 F*). The coarser-grained phenocrysts are generally untwinned and locally display weak perthitic texture, further emphasized by partial preferential silicification of a single phase (*Plate 2-36 F*). Quartz also rims some of the coarse feldspar phenocrysts locally. These coarser grains are interpreted as a variety of potassium-rich alkali-feldspar.

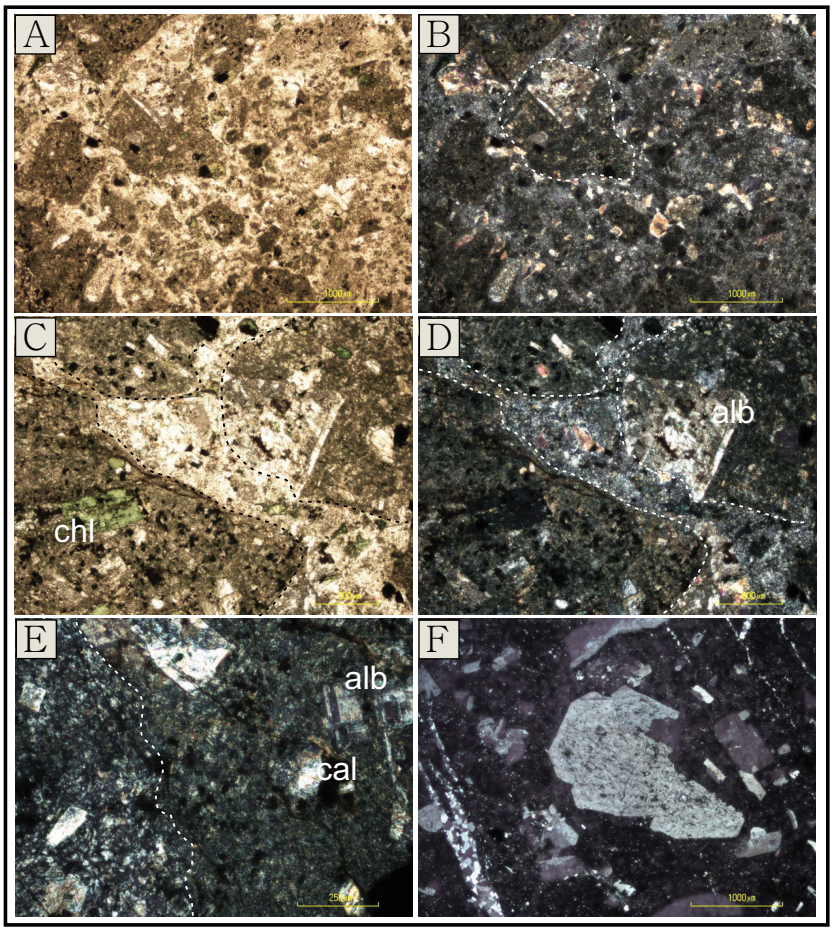

***Plate 2-36**: Representative photomicrographs of the andesitic pyroclastic rocks at Heritage: A-E) monolithic andesitic lapilli tuff (SF-13-180) & F) massive porphyritic andesite-dacite (SF-13-162); A&B) (2X; PPL & XPL, respectively) Various chlorite altered feldspar-phyric lapilli (3mm-3cm) within a finer-grained feldspar-phyric matrix; C&D) (4X; PPL & XPL, respectively) Close-up view showing matrix (centre) and surrounding lapilli. Lapilli are coarser-grained and more chloritic, matrix quartz-rich; E) (10X; XPL) Close-up of chloritic lapilli fragment (right) and matrix (left). Fragment contains albite phenocrysts with polysynthetic twinning, matrix contains two finer feldspar phenocrysts, the upper left one displaying simple twinning. Small pockets of calcite alteration in both; F) (2X; XPL) Coarse phenocrysts of untwinned alkali feldspar rimmed by quartz, medium-grained short laths of alkali feldspar displaying weak perthitic texture, and smaller glomerocrysts of sanidine in a very fine-grained matrix of quartz and lesser chlorite. chl=chlorite, alb=albite, cal=calcite.*

Rhyolitic Crystal Tuff

Rhyolites are not evident at surface in the immediate vicinity of the main prospect, but minor rhyolitic horizons intercalated with the more massive andesites are intersected in drillcore. Rhyolites have also been previously mapped to the north of the main Heritage prospect (O'Brien et al., 1977). A sample collected from drill core is shown in *Plate 2-37 A*. The unit is pink in colour and contains abundant coarse-grained quartz crystals, as well as green, sericite and chlorite altered lath-shaped feldspar crystals. In thin section the sample consists of a very fine-grained quartzo-feldspathic matrix altered to sericite (70%), containing ~20% coarse-grained quartz crystals and 10% medium- to coarse-grained feldspar crystals. The quartz crystals range from 1-4mm in size. The coarser grains tend to occur as sub-euhedral square- or pseudohexagonal- shaped grains containing rounded embayments along their perimeter, or as angular fragments. Smaller grains include euhedral bipyramidal crystals and subangular fragments. Feldspars are ~1-3mm in size, occurring as subhedral laths, locally as glomerocrysts, and have been entirely replaced by very fine-grained sericite and lesser chlorite. Although this felsic horizon could represent a porphyritic intrusive phase, the rounded embayments along the edges of the euhedral quartz grains is more characteristic of an extrusive volcaniclastic rock.

Plate 2-37*: Representative photos and photomicrographs of the rhyolitic crystal tuffs at Heritage from SF-13-163 (HD-05-13; ~65m); A) Light pink fresh surface of a rhyolitic tuff containing crystals of quartz and green-altered-feldspar; B&C) (2X; PPL & XPL, respectively) Coarse sub-euhedral quartz crystals with rounded embayments along their margins and coarse feldspar crystals which have been completely replaced by very fine-grained sericite and chlorite, within a very fine-grained sericite-altered quartzo-feldspathic matrix. Qtz=quartz, fsp=feldspar.*

Interbedded Sandstones and Conglomerates

A sequence of sediments occurs predominantly west of, and overlying the extensive andesitic pyroclastics. They are predominantly composed of thick interbedded layers of sandstone and pebble conglomerate, which locally display weak graded bedding, ranging in colour from green-grey to red (*Plate 2-38A*). Beds of red laminated siltstone also occur locally (*Plate 2-34; Plate 2-38A*). The conglomerates are typically redder in colour than the sandstones, and are generally poorly sorted. They contain an abundance of sub-euhedral feldspar crystals and a variety of subangular-subrounded pebbles (1-20mm) and, overall, appear to be of epiclastic origin. The pebbles most commonly include grey porphyritic andesite, pink rhyolite, and red siltstone (*Plate 2-38 B&C*).

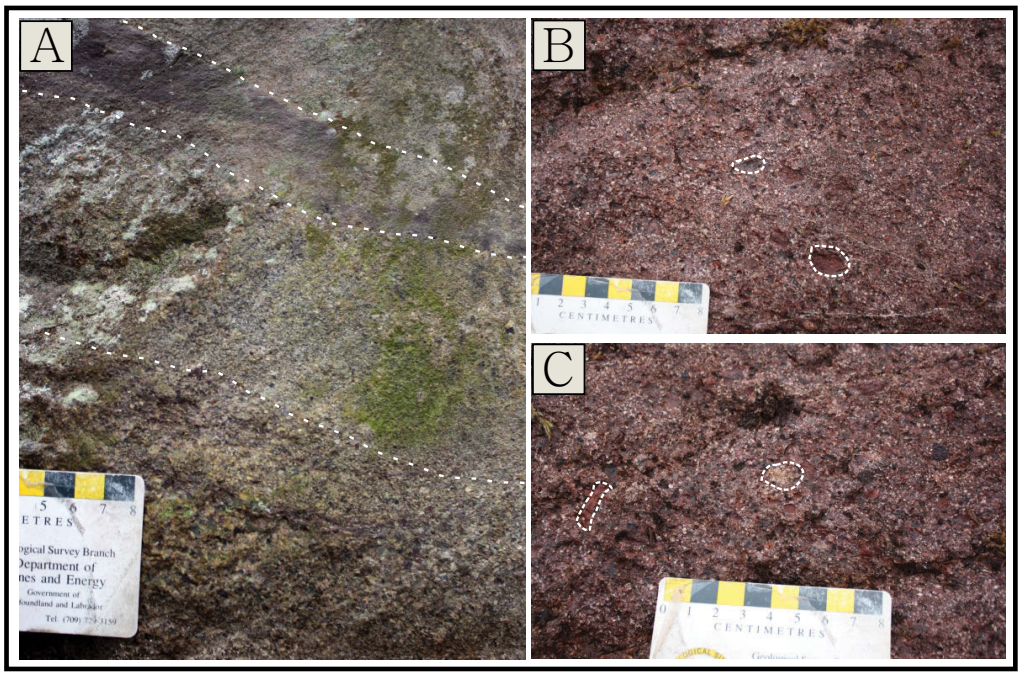

***Plate 2-38**: Representative photos of sandstones and conglomerates at Heritage; A) Weak graded bedding with a coarser-lithic-rich layer at the bottom, fining upwards towards a thin red silt layer (outlined) near the top; B&C) Examples of the red, poorly-sorted conglomerates with some pebbles highlighted.*

Porphyritic-Amygdaloidal Basalt

Further west, and overlying and partially intercalated with the sediments, are porphyritic and amygdaloidal basalts. Similar to all of the above stratigraphy, these basalts show differential alteration containing both green (chloritic) and red (oxidized)

subtypes (*Plate 2-39 A&B*). In addition, these basalts also locally contain distinctive, irregularly-shaped, red jasperoid clasts interpreted to have formed as a chemical sediment in a submarine environment (*Plate 2-39 B*). Sometimes the red jasper material also appears as fine veinlets, presumably as a result of later remobilization. The basalts are both porphyritic and amygdaloidal, containing feldspar crystals up to ~5mm and amygdules up to ~1cm in length. The feldspar phenocrysts are often altered to epidote, and amygdules typically filled with chlorite, quartz or calcite.

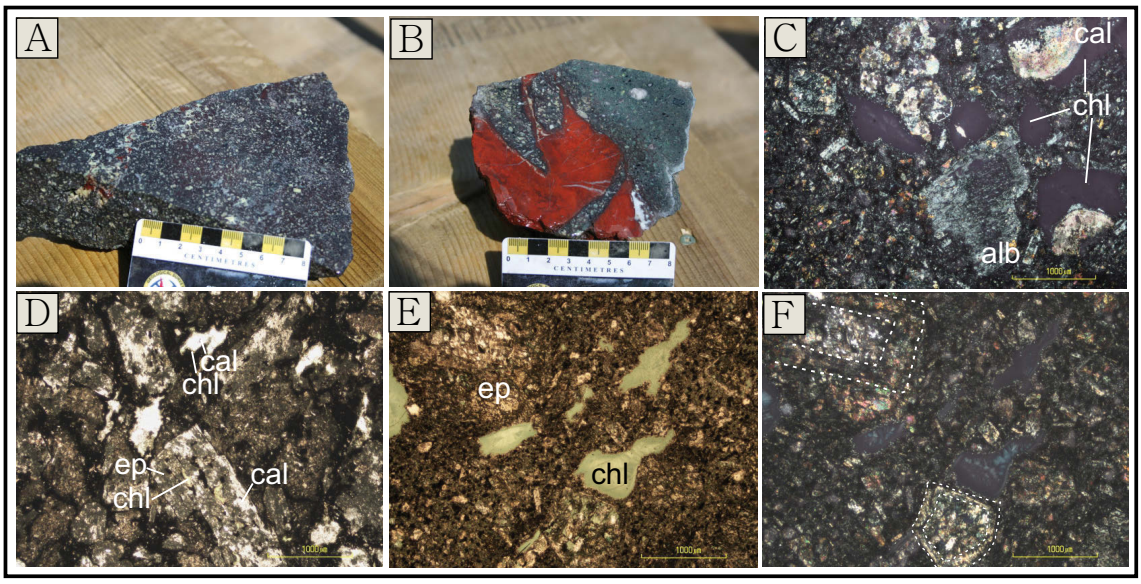

***Plate 2-39**: Representative photos and photomicrographs of the porphyritic amygdaloidal basalt at Heritage; A) Maroon to green coloured fresh surface of porphyritic basalt; (SF-13-185/HBQ1); B) Green (right) and maroon (left) colour variations in the basalt, which also contains a distinctive red jasperoid clast, and coarse amygdules evident on the right (HBQ2); C) (2X; XPL) Colloform amygdule filling of calcite followed by chlorite. Also showing zoned albite phenocryst and chlorite-epidote altered groundmass (HBQ3B); D) (2X; PPL) Amygdules lined by chlorite and filled with calcite, and feldspar phenocrysts significantly replaced by epidote, chlorite and calcite, within an Fe-Ti-oxide-rich matrix (SF-13-185/HBQ1); E&F) (2X; PPL & XPL, respectively) Irregularly shaped chlorite filled amygdules, and coarse zoned feldspar phenocrysts replaced by epidote, chlorite and calcite (zoning outlined by dotted lines) (HBQ3B). cal=calcite, chl=chlorite, alb=albite, ep=epidote.*

In thin section, the matrix of this unit is made up of fine laths of albite and pervasive chlorite and epidote alteration. Where samples are more maroon in colour, the matrix contains an increased abundance of Fe-Ti-oxides (*Plate 2-39 D*). Amygdules are irregular in shape and most commonly rimmed by calcite and filled with chlorite, but the opposite also occurs (*Plate 2-39 D&E*). Locally, the amygdules show colloform filling

textures (*Plate 2-39 C*). Feldspar phenocrysts have been substantially altered to varying proportions of epidote, chlorite and calcite, but remnant polysynthetic twinning occurs locally and indicates albite as the dominant phenocryst phase. Phenocrysts also display weak crystal zonation, highlighted by variations in their alteration assemblages (*Plate 2-39 E&F*).

Mafic Dykes

A number of narrow mafic dykes occur across the Heritage property. They appear most obviously in the exploration trenches where they crosscut, and contrast with, hydrothermal quartz veining and brecciation (*Plate 2-40*). They are typically 1-2m in width, fine-grained, and appear brown on a weathered surface and green on a fresh surface. At the core of the dykes, feldspar phenocrysts are abundant (*Plate 2-41 C*), but diminish towards the outer margins where amygdules and vesicles become prevalent (*Plate 2-41 B*). The dykes are generally magnetic, strike north-south to slightly northwest-southeast with a subvertical dip, and are definitively post-mineralization based on strong crosscutting relationships, including the presence of angular hydrothermal breccia xenoliths contained within them locally (*Plate 2-40 A-C*).

However, a single mafic dyke occurring in the Whalesback Trench indicates a slightly different temporal relationship with the epithermal mineralization. Although the dyke crosscuts the majority of the hydrothermal veining and brecciation, minor anastomosing hydrothermal quartz veining occurs within the outer margins of the dyke. This suggests that the dyke is late syn- to post-mineralization, and possibly representative of a separate, older generation of mafic dyke. The dyke is non-magnetic and was recorded as striking in a north-northeast direction (*Plate 2-40 D*).

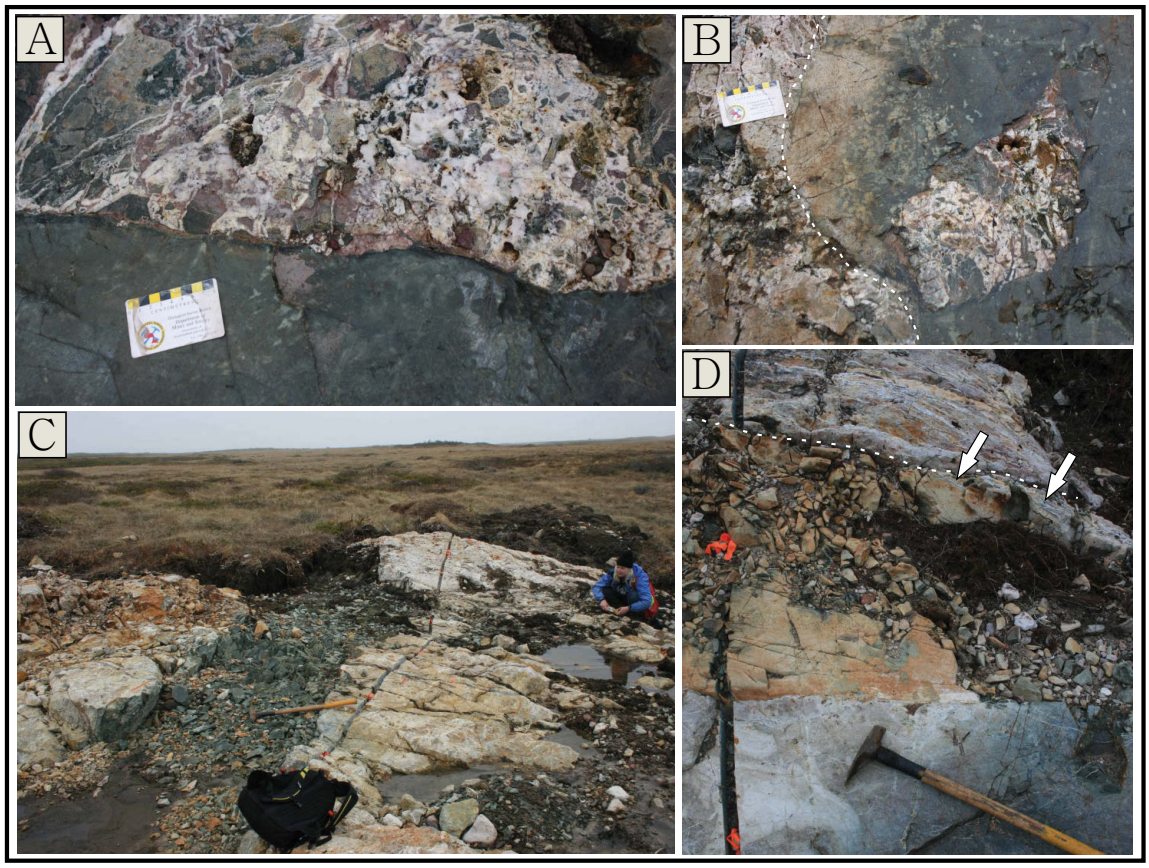

***Plate 2-40**: Representative photos of the mafic dykes at Heritage; A) Mafic dyke clearly crosscutting a hydrothermal breccia in the Ridge Trench (SF-13-178); B) Xenolith of hydrothermal breccia contained within the crosscutting dyke in the Ridge Trench (SF-13-178); C) Mafic dyke crosscutting veining and hydrothermal brecciation in L1 Trench (SF-13-161); D) Mafic dyke at the Whalesback Trench, which crosscuts the majority of hydrothermal veining, but locally is crosscut along its margins by fine silica veins (Pointed out by white arrows) (SF-13-179).*

Multiple examples of the mafic dykes were selected for petrographic analysis. Generally, the dykes contain approximately 30% phenocrysts and glomerocrysts of albite, which are usually 1-2mm in size, but locally up to 4mm (*Plate 2-41 D, E &G*). They are typically replaced by varying proportions of calcite and chlorite, or locally display fine-grained quartz-feldspar replacement. Weak compositional zoning is seen in some of the feldspars, and locally, clear polysynthetic twinning is still evident (*Plate 2-41 E&G*). The surrounding matrix is fine-grained and predominantly composed of albite laths and clots of chlorite, with local epidote and patchy calcite alteration. Amygdules are common and are rounded, to irregular and elongate in shape. They are typically filled with chlorite and calcite; one lining the cavity and the other filling the remaining void. In contrast, the

dyke from the Whalesback Trench shows colloform quartz lining amygdules occurring with calcite (*Plate 2-41 F*) – more evidence of late syn-mineralization timing for this dyke. Trace chalcopyrite and magnetite is found disseminated throughout all of the dykes, with the exception of the Whalesback dyke, where euhedral pyrite seems to occur in lieu of magnetite.

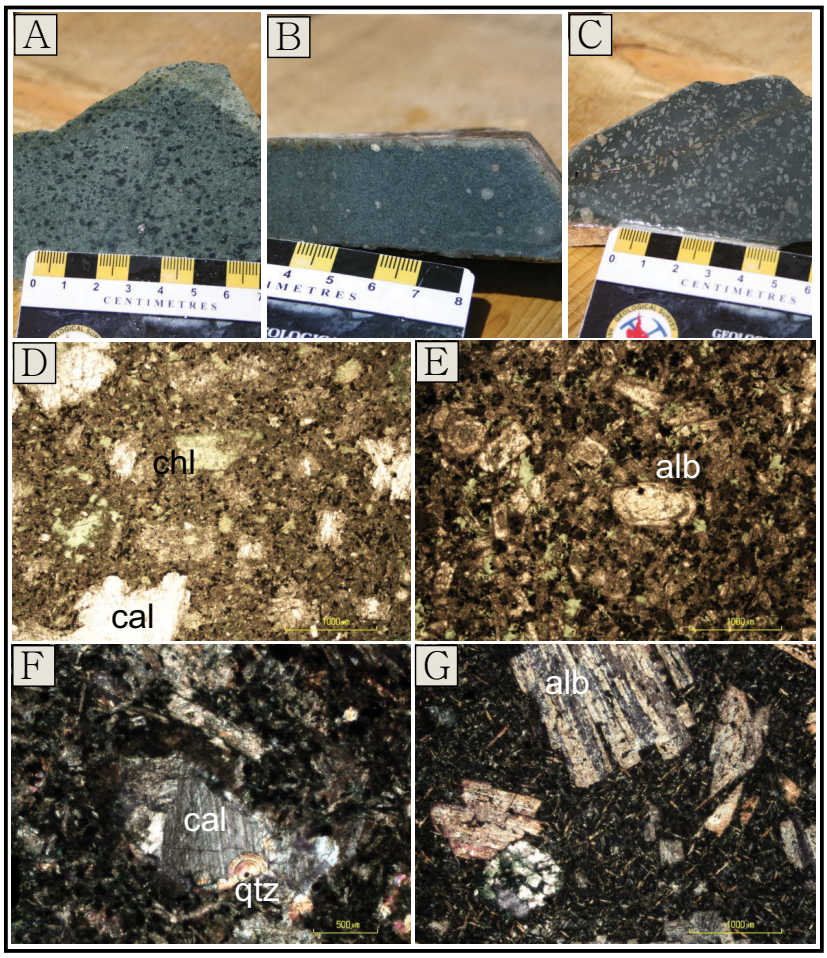

Plate 2-41*: Representative photos and photomicrographs of the mafic dykes at Heritage; A) Chlorite-altered feldspar phenocrysts and chlorite-filled amygdules in a fine-grained matrix. Dyke crosscuts mineralization in L1 Trench (SF-13-161); B) Calcite filled amygdules from the outer margin of dyke crosscutting mineralization in the Ridge Trench (SF-13-178); C) Feldspar-phyric core of the mafic dyke, crosscutting mineralization in the Ridge Trench (SF-13-178); D) (2X; PPL) Chlorite and calcite altered feldspar phenocrysts and glomerocrysts, and minor irregularly-shaped chlorite amygdules (SF-13-161); E) (2X; PPL) Weakly zoned albite phenocrysts altered to calcite, lesser chlorite, or finely recrystallized. Clots of chlorite throughout (SF-13-164; HD-05-13; ~50m); F) (2X; XPL) Colloform quartz lining an amygdule which is further filled with calcite (SF-13-179; Whalesback Trench); G) (2X; XPL) Albite glomerocrysts with polysynthetic twinning, individual phenocrysts, and chlorite-calcite-filled amygdule in bottom left, all in a fine-grained matrix of mostly albite and chlorite (SF-13-178). chl=chlorite, cal=calcite, alb=albite, qtz=quartz.*

2.3.6.2 Overview of Local Structure

The stratigraphy surrounding the Heritage prospect is relatively undeformed, with only a weak penetrative foliation present, striking southwest and dipping moderately towards the northwest (*Figure 2-6 A*). Sedimentary bedding strikes parallel to the foliation, but with a consistently shallower dip angle, slightly oblique to the foliation (*Figure 2-6 B*). Contacts, where noted, parallel the more shallowly dipping sedimentary bedding. Evidence for minor faulting was noted across the property, generally striking towards the southwest with a steep to subvertical northwest dip.

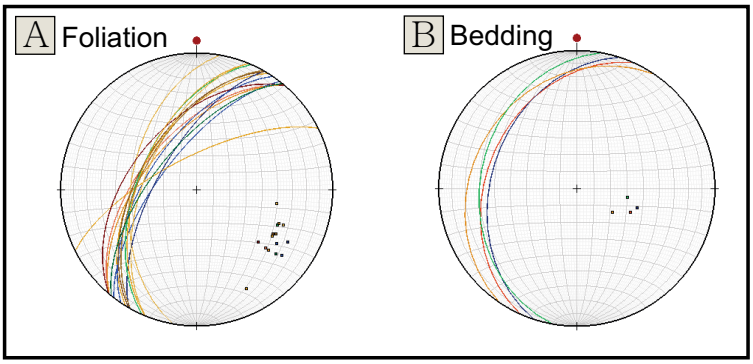

***Figure 2-6**: Stereonets displaying, A) Foliation and B) Bedding measurements at Heritage. Foliation strikes southwest and dips moderately to the northwest. Bedding is slightly oblique to the foliation, striking the same way, but dipping shallowly to the northwest.*

2.4 Musgravetown Group

Flanking the Marystown Group along its eastern margin, and also occurring as a continuous belt north of the Burin Peninsula towards Bonavista Bay, is the ca. 570 Ma Musgravetown Group (*Figure 2-1*). This group is primarily composed of fluviatile and shallow marine epiclastic sedimentary rocks, which display an overall transition from subaerial to shallow marine deposition (O'Brien et al., 1996; 1999) Minor subaerial, bimodal volcanics also occur throughout the sequence - rhyolite from the base of the Rocky Harbour Formation, which occurs in the upper portion of the overall Musgravetown Group succession, has been dated at 570 +5/-3 Ma (O'Brien et al., 1989; Dunning, unpublished data; O'Brien and King, 2004).

The stratigraphy includes red, alluvial conglomerates and sandstones at the base, which are overlain by subaerial bimodal volcanics. The volcanics are succeeded by shallow marine and fluvial sandstones, which coarsen and redden upwards into red sandstones and boulder conglomerates, and eventually are covered by shallow marine sandstones and quartz arenites, of possible Cambrian age (O'Brien & Knight, 1988; O'Brien et al., 1996).

The Musgravetown Group is host to the Big Easy low-sulphidation epithermal-gold prospect. The prospect occurs in the upper portions of the Musgravetown stratigraphy, within the sediments nominally overlying the bimodal volcanics.

2.4.1 Big Easy Prospect

The Big Easy prospect is located west of Clarenville, just south of the Trans-Canada Highway on the southwest side of Thorburn Lake. The prospect contains an ~1km long zone of silicic alteration hosted primarily in interbedded sandstones and pebble conglomerates of epiclastic origin (*Figure 2-7*). Mineralization occurs in networks of narrow, finely banded silica veins, where it is concentrated in thin dark Ag-Au-rich bands.

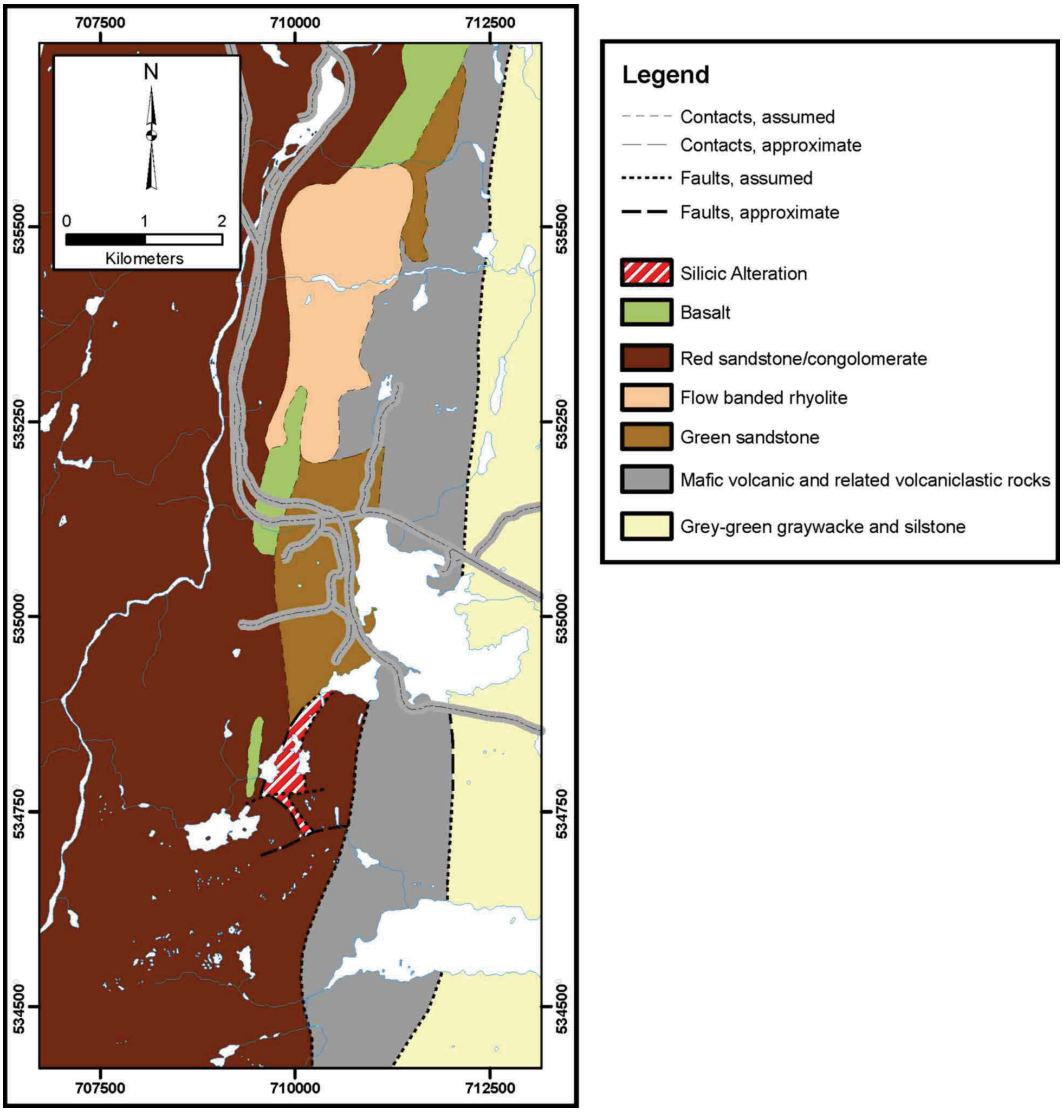

Figure 2-7*: Map of the geology surrounding the Big Easy prospect (marked by silicic alteration) southwest of Thorburn Lake. The flow banded rhyolite to the north is centred on another prospect known as the West Princess prospect, which hosts anomalous copper mineralization (From Layne et al., 2016).*

2.4.1.1 Lithology, Field Relationships and Petrography of Rock Units

The majority of mineralization at Big Easy is hosted in interbedded epiclastic sandstones and polymictic pebble conglomerates. Where the sediments are unaffected by silicification, they appear red in colour, in contrast to the sediments directly affiliated with mineralization which are green in colour and chloritic, becoming more grey in colour with increasing silicification. Locally occurring within these sediments are volcaniclastic horizons of a distinctive andesitic accretionary lapilli tuff unit. Lower in

the sequence, red flow banded rhyolite is found locally along a faulted contact at depth in drill core. Similar red flow banded rhyolite can be found outcropping more extensively towards the north where it occurs on a neighbouring copper prospect known as West Princess (*Froude et al., 2002; Figure 2-7*). The volcano-sedimentary stratigraphy is cross cut by a series of narrow mafic dykes. All of these units are discussed in greater detail below.

'West Princess' Flow Banded Rhyolite

The flow-banded rhyolite described here was collected from drill core from the West Princess prospect, which occurs approximately 5km north of Big Easy. The rhyolite is predominantly brick red in colour and contains distinct flow banding textures. Banding is further defined by two distinct finely intercalated lithologies; one is brick red, very fine-grained, and massive, and the other is greyer in colour and contains fine-grained white feldspar phenocrysts (*Plate 2-42 A*).

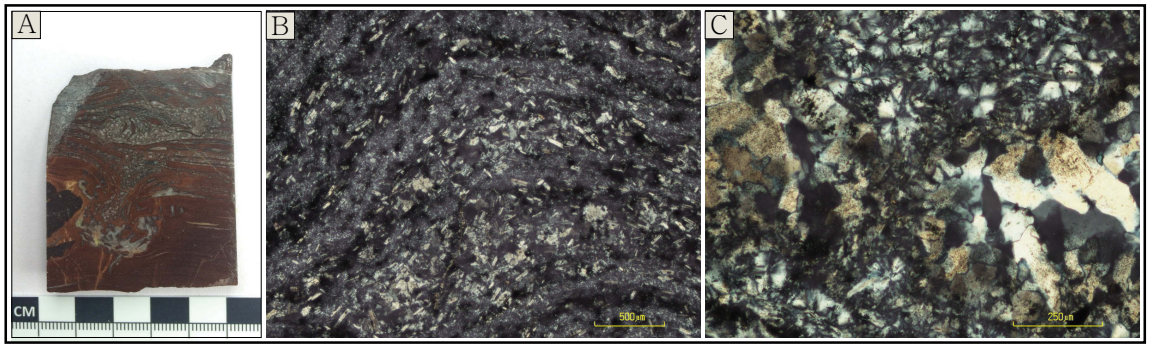

***Plate 2-42**: Representative photo and photomicrographs of the flow banded rhyolite from the nearby West Princess prospect (sample 'WPR'); A) Fresh surface showing flow banding and distinct layers of very fine-grained red siliceous material and maroon-grey feldspar-phyric layers; B) (4X; XPL) Flow banding with alternating layers of very fine-grained silica, and fine-grained quartz-feldspar with albite phenocrysts; C) (10X; XPL) Local development of layers of fine-grained quartz displaying spherulitic texture (top and bottom), alternating with layers of coarser, polycrystalline clusters of quartz.*

In thin section the same flow banding is apparent, with bands of very fine-grained quartz (and lesser feldspar) alternating with fine-grained quartzo-feldspathic bands containing ~25% albite phenocrysts and fine patches of epidote and calcite alteration (*Plate 2-42 B*). Separating these bands are thin, discontinuous layers rich in oxides. There are local variations in the composition and texture of the flow banding. For

example, in *Plate 2-42 C,* layers of spherulitic quartz occur with quartz forming fine-grained radiating bundles, which alternate with layers of coarser polycrystalline quartz clusters.

Sandstone and Polymictic Pebble Conglomerate

Polymictic pebble conglomerates, and lesser interbedded sandstones are the dominant host lithologies at the Big Easy prospect. More distal to the mineralization, the sediments appear red in colour (*Plate 2-43 A*), whereas the sediments directly adjacent to the mineralization are green in colour (*Plate 2-43 B*), becoming greyer with increasing (hydrothermal) silicification (*Plate 2-43 C*). The pebble conglomerates are polymictic, containing angular to subrounded pebbles typically 1-10mm in size, but up to 3-4cm locally. The pebbles commonly consist of pink porphyritic rhyolite, grey andesite, and beige chert (*Plate 2-43 C*).

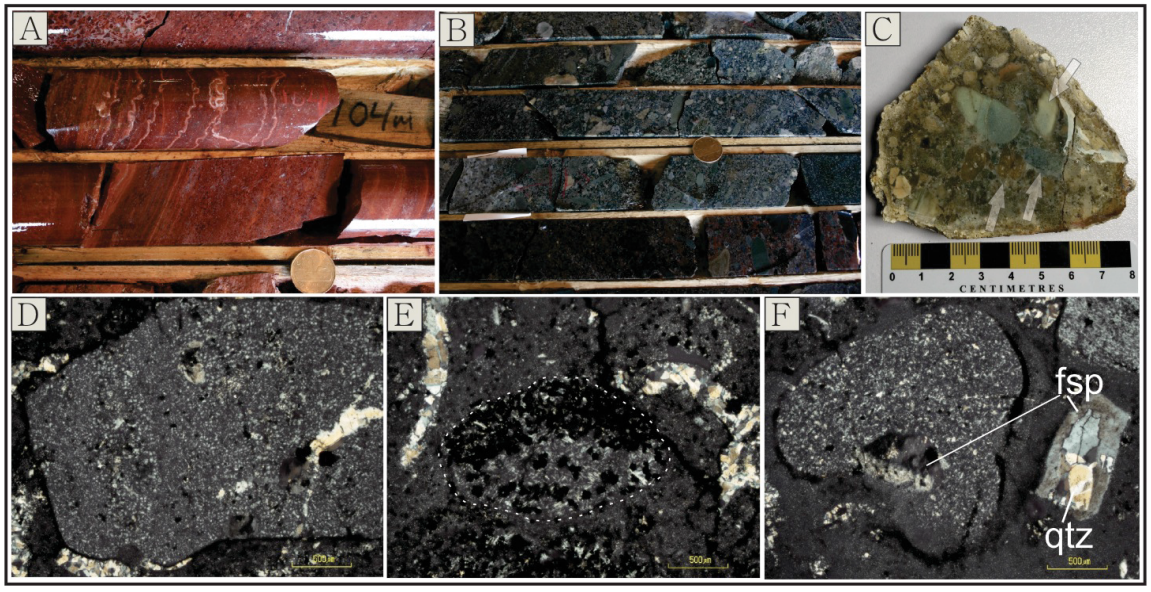

Plate 2-43*: Representative photos and photomicrographs of the sandstones and conglomerates at Big Easy; A) Red well-bedded sandstones, more distal to mineralization (drill hole BE-11-01; ~104m); B) Green, chloritic, polymictic pebble conglomerates proximal to mineralization (drill hole BE-11-01; ~40m); C) Fresh surface of silicified conglomerate showing various subrounded clasts, including porphyritic rhyolite (pink), andesite (grey), and chert (beige), all highlighted by arrows; D) (4X; XPL) Subangular rhyolitic clast with feldspar phenocrysts and weak flow banded texture (MC-12-06); E) (4X; XPL) ~1mm subrounded clast of andesite dominated by albite laths and opaque pyrite (MC-12-06); F) (4X; XPL) Subrounded ~2mm rhyolitic clast with alkali feldspar phenocryst, and untwinned alkali feldspar in the matrix being replaced by quartz (MC-12-06). fsp=feldspar, qtz=quartz. Sample MC-12-06 is from the collection of Matt Clarke (Honours B.Sc. thesis at Memorial University).*

A silicified example of the conglomerate was selected for petrographic analysis. The groundmass is well-bedded and composed almost entirely of quartz, presumably of hydrothermal origin. Very fine-grained beds containing (<1mm) angular crystal fragments alternate with coarser-grained beds containing crystal fragments up to 2mm and subrounded lithic clasts, 3-10mm in size. The crystal fragments are composed of quartz, and lesser alkali feldspar and albite. Feldspars are commonly replaced by quartz (*Plate 2-43 F*), but where they aren't, display remnant simple twinning or are untwinned. The lithic clasts include feldspar-phyric rhyolite locally displaying weak flow banding textures (*Plate 2-43 D&F*), andesite containing albite laths and pyrite (*Plate 2-43 E*), and very fine-grained, cherty clasts.

Andesitic Accretionary Lapilli Tuff

Local horizons of andesitic accretionary lapilli tuff occur within the extensive clastic sedimentary sequence. This unit is very distinctive in appearance, containing abundant rounded, concentrically zoned lapilli, generally grading outward from a coarser-grained core to a finer-grained rim (*Plate 2-44 A*). The cores of the lapilli typically contain green fragments, which are also found elsewhere in the sample without accretionary rims. This unit occurs within the main alteration zone and is consistently silicified and pyritiferous.

In thin section the groundmass is a very fine-grained, and generally indiscernible, mixture of ash and fragments. Coarser constituents include euhedral or angular fragments of quartz crystals (~5%), fine-grained subhedral pyrite (5-7%) and various other fragments (~20%) typically 1-3mm in size. These fragments include a rounded very fine-grained to aphanitic variety, and a green irregularly shaped variety composed of a very fine-grained mixture of chlorite, sericite and calcite (*Plate 2-44 C*). The dominant constituents suspended in the matrix are the much larger accretionary lapilli, which are up to 2cm in size, and account for ~25% of the thin section. Similar to what can be seen macroscopically, they contain a coarser core consisting predominantly of the green rock fragments and angular quartz crystals, which grades outwards into a finer grain size

resembling the matrix, and is rimmed by the very fine-grained to aphanitic material which is also found making up the smaller rounded fragments (*Plate 2-44 B*).

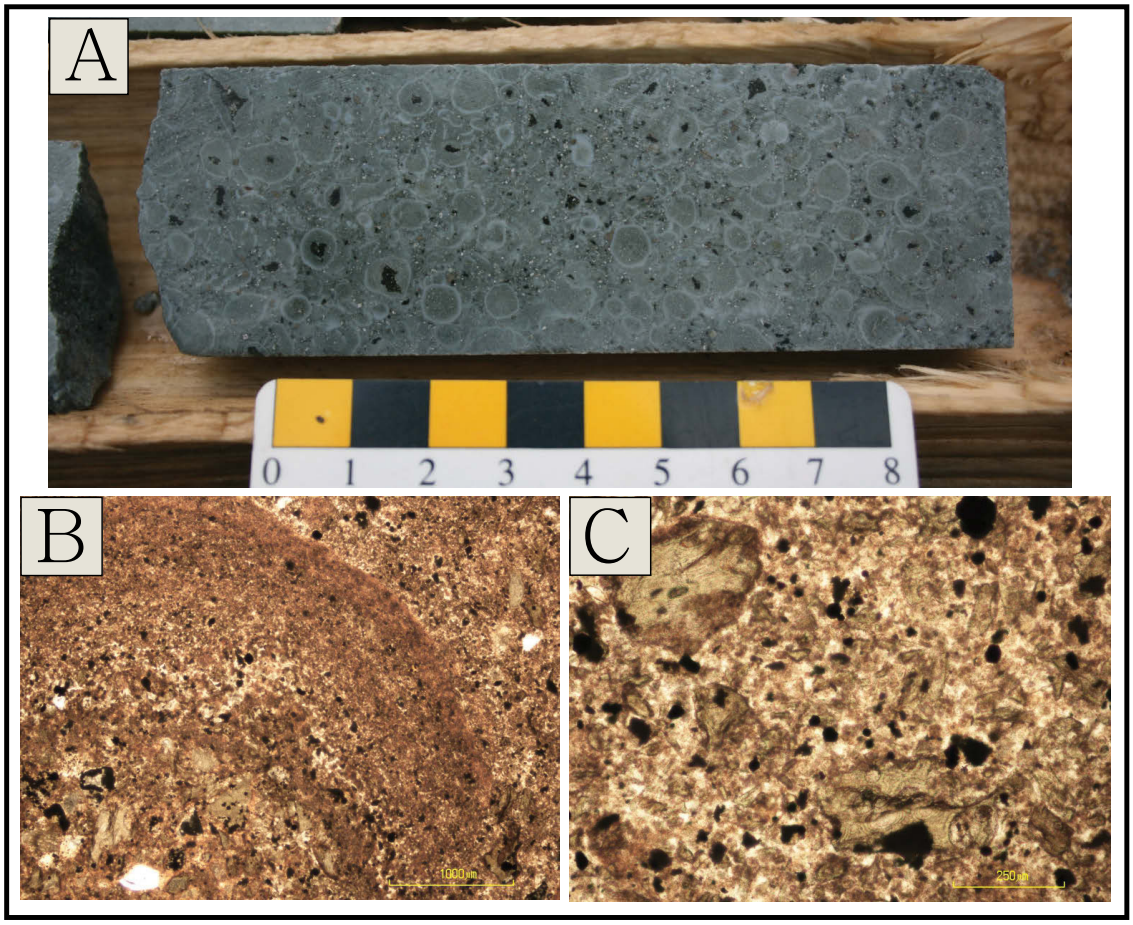

Plate 2-44*: Representative photo and photomicrographs of the andesitic accretionary lapilli tuff unit at Big Easy from sample SF-13-181; A) Fresh surface of the silicified unit, showing abundant (~75%) accretionary lapilli and 5-7% pyrite mineralization; B) (2X; PPL) Displays the grading within the accretionary lapilli, with a core of coarser rock fragments and quartz crystals, fining outward to a grain size/composition similar to the groundmass, and rimmed by a very fine-grained-aphanitic material; C) (10X;PPL) Close-up view of green rock fragments composed of very fine-grained mixture of chlorite-sericite-calcite. Opaque minerals predominantly pyrite.*

Mafic Dykes

Mafic dykes are found crosscutting the sediments and mineralization at various intersections in drill core and are fine-grained, green and chloritic (*Plate 2-45 A*). They are locally crosscut by fine quartz veins. However, these veins appear syn-tectonic in origin and postdate the hydrothermal activity related to epithermal mineralization. In thin

section, these dykes contain ~20% euhedral lath-shaped phenocrysts and glomerocrysts of plagioclase feldspar, up to 2mm in length (*Plate 2-45 B&C*). Despite being variably replaced by calcite and chlorite, feldspars commonly still display polysynthetic twinning and lesser simple twinning. A low extinction angle between the polysynthetic twinning pairs is indicative of oligoclase. No distinguishable former mafic phases are evident. The groundmass is fine-grained and composed predominantly of laths of plagioclase and fine-grained Fe-Ti-oxides, surrounded by semi-pervasive chlorite, and lesser calcite, alteration. Fine-grained an-subhedral quartz grains also occur locally. This mineral assemblage indicates a composition of andesite to basalt. The sample is crosscut by fine, syn-tectonic calcite-quartz-chlorite veining.

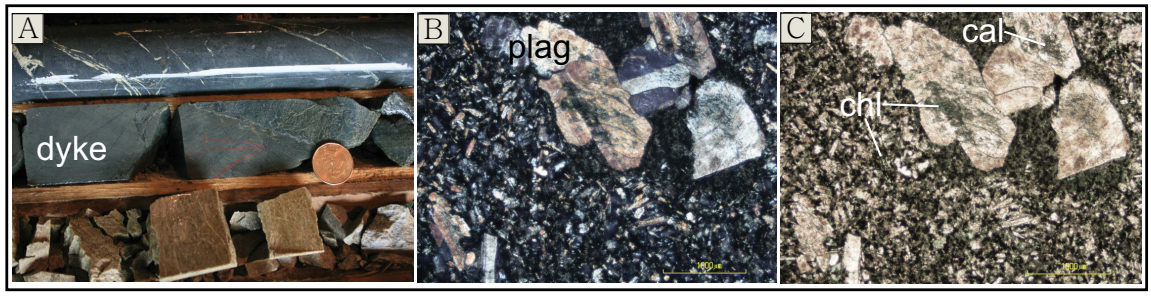

Plate 2-45*: Representative photo and photomicrographs of the mafic dykes crosscutting the volcano-sedimentary stratigraphy at Big Easy; A) Fine-grained, chloritic mafic dyke (left) crosscutting sediments (right) in drill core (BE-11-01; top of hole); B&C) (2X; XPL and PPL, respectively) Lath-shaped plagioclase (oligoclase) phenocrysts and glomerocrysts variably altered to calcite and chlorite within a fine-grained matrix of albite, chlorite, calcite, Fe-Ti-oxides, and trace quartz (MC-12-01; BE-11-03; ~10m). cal=calcite, chl=chlorite, plag=plagioclase feldspar. Sample MC-12-01 is from the collection of Matt Clarke (Honours B.Sc. thesis at Memorial University).*

2.5 Long Harbour Group

Overlying the Marystown Group to the west and north is the ca. 570-550 Ma Long Harbour Group (*Figure 2-1*). The Long Harbour Group is dominated by subaerial felsic volcanics of alkaline to peralkaline affinity, with lesser bimodal horizons and siliciclastic sedimentary rocks (O'Brien et al., 1995). The Long Harbour Group can be further subdivided into a lower volcanic sequence (Belle Bay Formation), a middle clastic sedimentary unit (Anderson's Cove Formation), an upper volcanic sequence (Mooring Cove Formation), and an upper clastic sedimentary sequence (Recontre Formation) (Williams, 1971; O'Brien et al., 1995).

The Belle Bay Formation is a subaerial, bimodal volcanic rock suite, predominantly composed of pink to purple rhyolites, which include flow-banded, massive, porphyritic, spherulitic and tuffaceous varieties. Locally, rhyolite is interlayered with massive to amygdaloidal basalt, and minor epiclastic sediments. The conformably-overlying Anderson's Cove Formation, is a thin clastic sedimentary unit with red sandstone and pebble conglomerate occurring at its base, followed by a sequence of grey-green sandstones, siltstones and shale. The Anderson's Cove sediments conformably pass into volcanic rocks of the Mooring Cove Formation, consisting of flow-banded rhyolite, rhyolite tuff and amygdaloidal basalts, as well as minor red to grey sandstones. Alluvial clastic sediments of the Recontre Formation occur at the top of the Long Harbour Group and conformably overly the Mooring Cove Formation. The formation consists of locally crossbedded purple, grey and red sandstones, pebble conglomerates, and red argillite beds (Williams, 1971; O'Brien et al., 1995).

Rhyolite of the Belle Bay Formation is host to the low-sulphidation epithermal mineralization found at the Long Harbour prospect, and is described in greater detail immediately below.

2.5.1 Long Harbour Prospect

The Long Harbour prospect is located along the northern shore of Fortune Bay, west of the Burin Peninsula (*Figure 2-2*). The shoreline is distinctive in appearance, made up of high, barren cliffs of rhyolite, with very little vegetative cover *(Plate 2-46)*. Gold mineralization occurs within a network of banded quartz-adularia veins and breccias, which are continuous over a strike length of approximately 70 metres. The veins and breccias are hosted in an extensive flow-banded rhyolite unit.

Plate 2-46*: Aerial view looking roughly west, from northeast of the Long Harbour prospect, showing barren hills of rhyolite of the Belle Bay Formation in the background, and a thicker vegetative cover over the Recontre Formation in the foreground.*

2.5.1.1 Lithology and Petrography of Flow Banded Rhyolite

The flow-banded rhyolite, host to low-sulphidation epithermal gold-mineralization at Long Harbour, consists of fine, mm-scale, red and pink bands, with banding generally striking in a north-northeast direction (*Plate 2-47 A&B*). Phenocrysts of dark grey quartz and light pink feldspar, typically 1mm in size or less, are visible as sparsely distributed grains in hand sample (*Plate 2-47 B*).

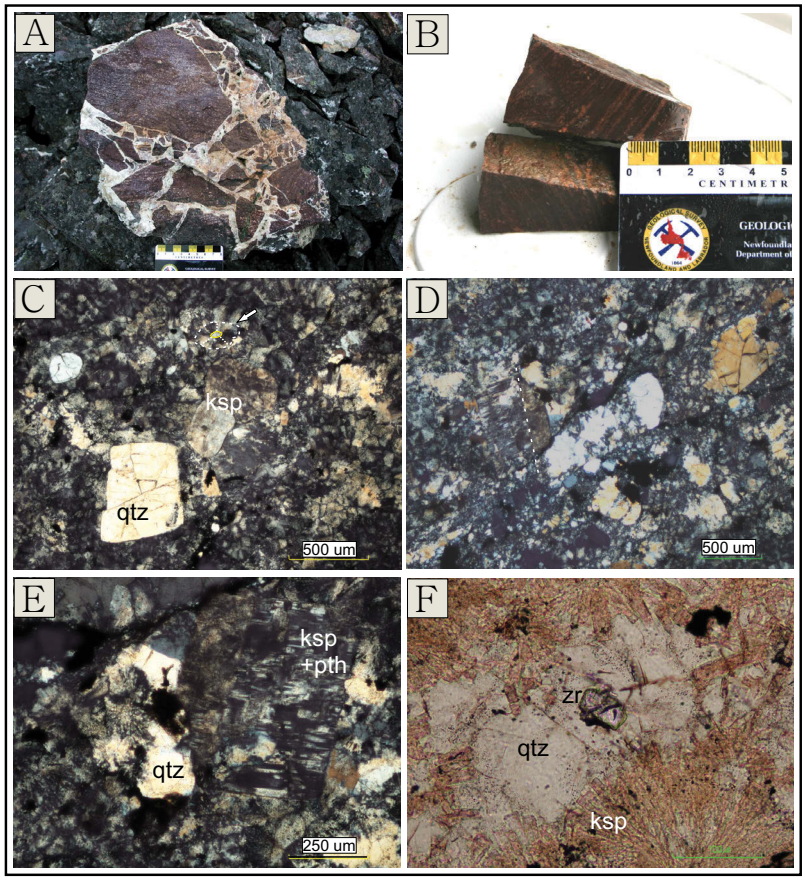

Plate 2-47*: Representative photos and photomicrographs of the flow-banded rhyolite host rock at Long Harbour (SF-12-56; STA-SF-12-116); A) Hydrothermal brecciation of red flow-banded rhyolite; B) Hand sample showing fine banding and small phenocrysts; C) (4X; XPL) Various sizes of quartz and microperthitic potassium-feldspar phenocrysts within a very fine-grained matrix of potassium feldspar, quartz, and albite; D) (4X; XPL) Potassium feldspar with microperthitic texture and remnant simple twinning, highlighted by dashed white line; E) (10X; XPL) Potassium feldspar (orthoclase) showing perthitic texture, adjacent to a quartz phenocryst partially overgrown by spherulitic texture, both within a very fine grained devitrified matrix of potassium feldspar with lesser quartz and albite; F) Spherulitic texture with euhedral tabs of potassium feldspar in small radiating bundles growing into coarser quartz, and occasionally nucleating around fine quartz phenocrysts. qtz=quartz, ksp=potassium feldspar pth=microperthitic texture, zr=zircon.*

In thin section, a very fine-grained matrix of potassium feldspar, lesser quartz, and minor albite accounts for 65-70% of the section. At high magnification, a weak, patchy spherulitic texture is visible, where euhedral tabs of potassium feldspar occur in small radiating bundles, occasionally nucleating around fine quartz phenocrysts (*Plate 2-47 F*). Locally the texture intrudes into what appear to be (former) phenocrysts of coarser quartz (*Plate 2-47 E*). Quartz phenocrysts occur concentrated in discontinuous layers, which is what partially defines the fine banding in the rock. They are typically 1mm or less in size

and make up ~25% of the section. Coarser quartz grains occur as sub-euhedral square-shaped crystals, while finer ones are more anhedral and subrounded (*Plate 2-47 C*). Potassium feldspar phenocrysts (interpreted to be orthoclase) also occur in abundance of 5-10%. They are similar in size to the quartz phenocrysts, forming sub-euhedral square- to short tabular-shaped crystals, which locally display simple twinning, and often contain a patchy microperthitic texture (*Plate 2-47 C-E*). Subhedral crystals of hematite with rutile lamellae are disseminated throughout the matrix and locally display a subhedral hexagonal shape. Trace stubby euhedral prisms of zircon were also identified (*Plate 2-47 F*).

2.6 Discussion

The textures and lithologies presented in this chapter as representatives of the Marystown, Musgravetown and Long Harbour groups are clearly indicative of volcanic arc environments. However, significant variations between the three groups are evident.

The volcanic rocks of the Marystown group range in composition from basalt to rhyolite, but are dominated by more intermediate compositions of andesite to dacite. Pyroclastic textures dominate the sequences, although massive flows are also present, typically basaltic in composition. These lithologies are indicative of a mature arc undergoing very active subduction-related volcanism. Sedimentary horizons occur interbedded with the pyroclastic rocks, or overlying them (e.g., the Grandy's Pond Arenite Belt) and include siltstones, sandstones and pebble conglomerates deposited in a fluvial setting - based on the presence of locally developed graded bedding and cross bedding. However, they also appear to be closely related spatially and temporally with the volcanism, and therefore epiclastic in nature - based on the angularity of clasts and the abundance of volcanic derived debris they contain.

The volcanic rocks of both the Long Harbour and Musgravetown groups are dominated by red rhyolites with lesser mafic volcanics comprising a more bimodal suite, in contrast to the wider range of compositions that occur in the Marystown Group. Flow

banding and spherulitic textures are common in the rhyolites of both groups. Both groups also contain abundant accumulations of clastic sediments separating, and overlying the volcanic horizons. Similar to the Marystown Group, the sediments are both fluviatile and epiclastic in origin, displaying well-developed bedding, and a range in clast shapes, from round to angular, with clasts predominated by volcanic-derived detritus. The presence of bimodal volcanism is indicative of a later stage of arc-volcanism, and the abundance of clastic sediments could be representative of either intra-caldera, or late-stage intra- or back-arc extensional basin fill.

The variation in oxidation found to occur within individual units occurs throughout the Marystown Group, and more locally at the Big Easy prospect in the Musgravetown Group, and could be interpreted as a change in depositional setting from subaerial to shallow-marine. However, the greener, more "reduced" facies at Big Easy is more likely a consequence of the localized near-surface hydrothermal activity related to the epigenetic mineralization found there.

These generalized themes and interpretations are explored in more detail in *Chapter 3*.

CHAPTER 3: MAJOR AND TRACE ELEMENT LITHOGEOCHEMISTRY

3.1 Introduction

Major and trace element lithogeochemical analyses were carried out on 36 samples from across the project area, focused around the main epithermal prospects of interest. Fresher rock units were collected for host rock geochronology (see *Chapter 4*), as well as representative samples of lithologies proximal to and hosting epithermal alteration zones and mineralization. The main objectives were to further classify rock units, including those collected for geochronology, characterize the rocks within the volcanic arc environment, identify relationships between rock units on a deposit scale, and, on a more regional scale, characterize any distinct geochemical signatures of the Marystown, Musgravetown and Long Harbour Groups, and any contrasting or correlative trends between them. At prospects such as Tower and Hickey's Pond, where the exposed host rocks are almost uniformly intensely altered, geochemical analyses aided the determination of protolith host lithologies.

A description of the methods used for sample preparation and analysis are provided in *Appendix B*. The complete geochemical data used for interpretation, including supplemental datasets, is described and included in *Appendix C*. Analyses of standards and duplicates for quality control purposes can be found in *Appendix D*.

The following content is structured in parallel to *Chapter 2*, beginning with a geochemical summary of the Marystown Group, followed by the Musgravetown and Long Harbour Groups. Geochemical analyses of the local lithologies at prospects of interest, and of any other important units described in *Chapter 2*, are presented individually, but within the context and as representative examples of, the larger lithological group in which they are contained. Each section includes rock classification diagrams, major element data, and trace element data (including tectonic discrimination diagrams), followed by a brief interpretation of the presented data. The chapter is concluded with a regional synthesis comparing the geochemical characteristics of the three main lithological groups.

All samples have been affected to some degree by alteration associated with greenschist facies metamorphism. Under these conditions, potentially mobile elements include certain major elements (Ca, Na and K) and low field strength trace elements (Rb, Ba and Sr). Many samples are also affected to some degree by hydrothermal alteration, since they were primarily collected proximal to epithermal gold prospects. Under these hydrothermal conditions, potentially mobile elements, in addition to those previously mentioned, include Si, Mn, Mg and Fe. Samples that have been most intensely altered, to an advanced argillic alteration assemblage associated with the high-sulphidation epithermal environment, also show mobility in the high field strength (HFSE) and rare earth elements (REE) including Y, La, Ce, Pr, Nd, Sm, Eu, Gd, Dy, Ho, Er, Yb and Lu, all of which are traditionally considered to be immobile in other contexts. Intensely altered samples are included in certain plots, but labeled as 'Advanced Argillic Alteration' to demonstrate the element mobility discussed above. However, they are for the most part not included in plots, nor used for interpretation of the igneous rock suites. Weakly altered host rock samples, displaying discernable primary igneous textures that still enable rock identification, are still used for interpretation, and have been grouped into one of the main lithologies.

The classification diagrams of Pearce (1996) and Winchester and Floyd (1977), both of which avoid the use of alkali elements, are presented and used to determine rock compositions. The diagram of Pearce (1996) is used as the primary classification diagram, as it relies entirely on immobile trace elements, which are the least susceptible to the effects of alteration. The diagram of Miyashiro (1974) is used to elucidate tholeiitic and calc-alkaline fractionation trends.

Major element data are shown on Harker-type variation plots, plotted against SiO_2, as it provides the greatest dispersion in values for this dataset. Despite some local enrichments associated with hydrothermal alteration (silicification), samples generally display SiO_2 distributions consistent with igneous fractionation. For prospects with a greater abundance of mafic rocks, the major element data is also plotted against Mg#, as a differentiation index, to accommodate the smaller range of SiO_2 in mafic rocks. Fe is

plotted as "total Fe as FeO" (FeO*) for the purposes of the Harker-type diagrams, as well as the classification diagram of Miyashiro (1974). Since we focussed on plots of highly incompatible elements for the purpose of discriminating sample suites in this study, no detailed discussion of Fe_2O_3-FeO apportionment in whole rock samples is included here.

Trace element data are then presented for each locale using multi-element primitive mantle-normalized spider diagrams, and tectonic discrimination diagrams. Bivariate plots and bivariate ratio plots are also included for prospects where sampling is more substantial, to enable the discussion of regional-scale correlations.

REE and HFSE data are shown on multi-element extended REE spider diagrams, normalized to the primitive mantle values of Sun and McDonough (1989). The REE patterns are used to group related rock units, and to identify any anomalous trends, to further characterize them within the volcanic arc environment. In general, flatter trends (lower LREE to HREE ratios) are suggestive of a more juvenile magma source or primitive arc environment, while an increase in slope (enrichment in LREE relative to HREE ratio) correlates with a more mature arc system (e.g., Condie, 1989). Arc rocks typically have lower abundances of HFSE and show enrichment in the incompatible elements Th and LREE (Murphy, 2007), resulting in negative Nb and Ti anomalies on the spider diagrams. The presence of a negative Eu anomaly is the result of extensive plagioclase fractionation in more evolved magmas.

Mafic rocks are plotted on the tectonic discrimination diagram for basalts of Cabanis and Lecolle (1989). Felsic rocks are plotted on the tectonic discrimination diagram for granites of Pearce et al. (1984). The primary purpose of these plots is to test for genetic relationships, and highlight correlations between rock units in this geographically extensive sample set. Therefore, volcanic and plutonic rocks are plotted together.

In terms of petrogenesis, arc systems are relatively complex, and magma compositions reflect the influence of multiple processes, including fractional crystallization, partial melting, magma mixing, crustal contamination and crustal

assimilation; they are rarely formed through simple fractionation alone (Murphy, 2007). There is a general progression towards more felsic compositions with increasing arc maturity and crustal thickness. Most often, mafic arc-magmas are found to be derived from the mantle, felsic arc-magmas derived from partial melting of the crust, and intermediate arc-magmas from either fractionation of a more mafic parent, or by magma mixing of mafic and felsic end members (e.g. Eichelberger 1975; Gill 1981; Carmichael 2002). These processes are reflected in trace element abundances, used here to identify correlations and possible genetic relationships between rock units on a deposit scale (where sampling is sufficient), and to highlight any contrasting or correlative trends amongst the lithological groups on a more regional scale.

Incompatible trace element plots using REEs and HFSEs, including Gd, Eu, Yb, La, Sm, Zr, Ce, Y, Th and Nb (normalized to primitive mantle values of Sun and McDonough, 1989) are plotted against fractionation indices of SiO_2, or Zr. When SiO_2 is used, the SiO_2 content of hydrothermally silicified samples has been adjusted based on the compositional shifts between the classification diagrams of Pearce (1996) and Winchester and Floyd (1977). Linear trends on these bivariate plots are indicative of a related suite of rocks. Various incompatible trace element ratios are also used to further define any correlations. Since fractional crystallization does not significantly affect these highly incompatible trace element ratios, they should remain constant if a suite of rocks is derived from the same source, and related solely through simple fractionation. Therefore, variations are indicative of source heterogeneity or the influence of other magma differentiation processes, including partial melting, crustal contamination or magma mixing.

3.2 Marystown Group

3.2.1 Stewart

Stewart is one of several high-sulphidation prospects hosted within the Marystown Group volcanics (*Figure 2-1*). In more recent years the potential for porphyry-style mineralization has been recognized at the prospect (Hedenquist, 2007), and it has been inferred that porphyry-style mineralization is overprinted by advanced argillic alteration

related to the high-sulphidation system. Therefore, lithogeochemistry may, in some cases, reflect a combination of multiple magmatic-hydrothermal alteration events in addition to greenschist facies metamorphism.

There are six felsic units and five intermediate-mafic units discussed in this section, corresponding to the Stewart rock units outlined in *Chapter 2*. The felsic volcanic rocks include; the dacitic quartz-feldspar crystal-rich volcaniclastics (Stewart Tuff), and the dacitic quartz crystal-rich volcaniclastics (Caribou Tuff host rock). Felsic intrusive units include; the porphyritic dacite dykes, and the various phases of the Burin Knee Intrusive Suite (BKIS), which have been subdivided into tonalite (host rock), diorite-granodiorite and granite. The mafic volcanic rocks include; massive basaltic flows and intermediate-mafic volcaniclastics of the Lower Volcanic Unit, and the intermediate-mafic volcaniclastics of the Upper Volcanic Unit. Mafic intrusive units include; the porphyritic andesitic-basalt, and the fine-grained mafic dykes.

Six geochronology samples were collected from Stewart: 1) Dacitic quartz-feldspar crystal-rich volcaniclastic ('Stewart Tuff'; SF-12-43); 2) Dacitic quartz crystal-rich volcaniclastic ('Caribou Tuff'; GS-11-167); 3) Basaltic-andesitic lapilli tuff ('Upper Volcanic Unit'; SF-12-27); 4) Porphyritic dacite dyke (SF-12-144); 5) Granite of the BKIS (SF-12-46); 6) Crosscutting mafic dyke (SF-12-41). These samples will be highlighted in the following content, and will generally appear labeled in the geochemical plots. Sample SF-12-142 is an equivalent sample to SF-12-144, and is used as the representative sample for geochemistry.

3.2.1.1 Rock Type Classification

In the classification diagram of Pearce (1996; *Figure 3-1a*) samples plot in compositional fields consistent with the field and petrographic observations discussed in *Chapter 2*. The massive basaltic flows and intermediate-mafic volcaniclastics of the Lower Volcanic Unit, and the porphyritic andesitic-basalt intrusive, plot together within the *basalt* field. Approaching the andesite field, the mafic dykes (SF-12-41) occur clustered together, and occurring on the cusp of the *basalt-andesite* fields are the

intermediate-mafic volcaniclastics of the Upper Volcanic Unit (SF-12-27). The Stewart (SF-12-43) and Caribou (GS-11-167) Tuffs occur tightly clustered at the boundary between the *andesite* and *dacite-rhyolite* fields. The porphyritic dacite dykes (SF-12-142) are of similar composition to these latter two units, occurring at the base of the *dacite-rhyolite* field. Samples of the tonalite unit, presumed a part of the BKIS, generally overlap with samples of Stewart and Caribou Tuff, just below the boundary between *andesite* and *dacite-rhyolite*. A single sample of the diorite phase from the BKIS plots in the centre of the *andesite* field, and a single sample of granodiorite from the BKIS plots along the boundary between the *andesite* and *dacite-rhyolite* fields. The granitic samples of the BKIS plot within the *dacite-rhyolite* field. These units lie primarily within the broad *subalkaline* field. The intensely hydrothermally altered samples ('Advanced Argillic Alteration') are displaced to the right into the alkaline and ultra-alkaline fields (increased Nb/Y).

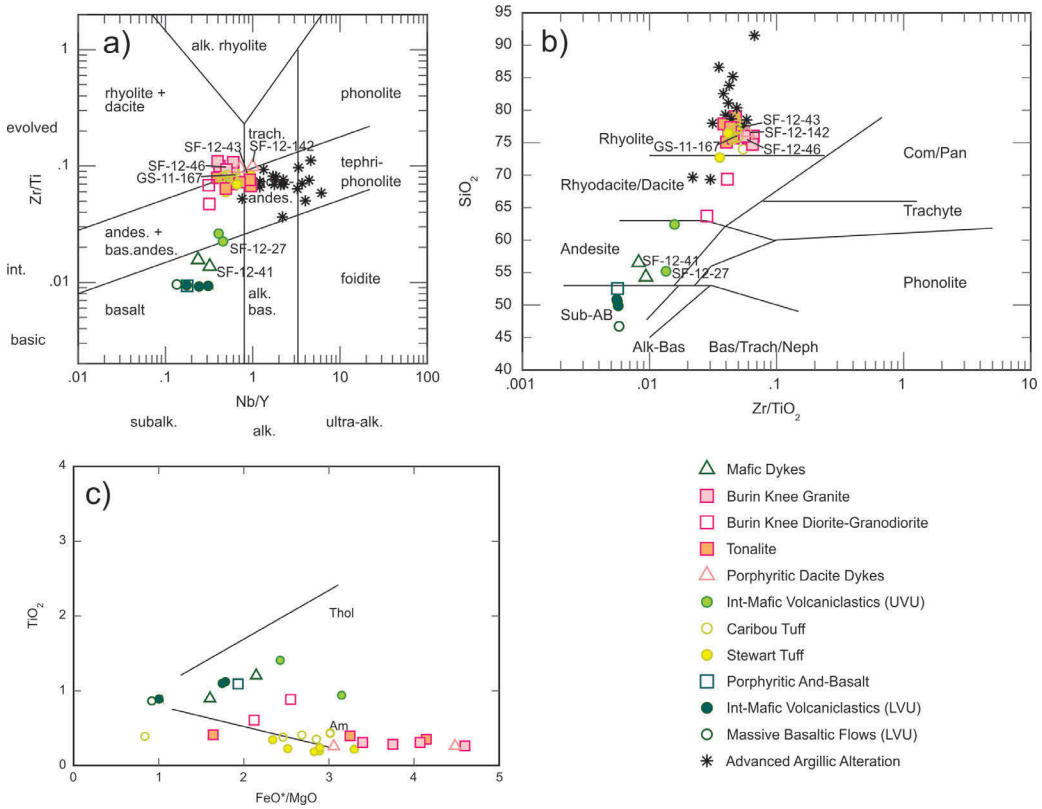

Figure 3-1*: Classification diagrams for Stewart samples; a) Zr/Ti vs. Nb/Y (Pearce, 1996; after Winchester and Floyd, 1977); b) SiO_2 vs Zr/TiO_2 (Winchester and Floyd, 1977); c) Miyashiro (1974). Thol=tholeiitic, Am=calc-alkaline.*

In the diagram of Winchester and Floyd (1977; *Figure 3.1b*) the samples comprise a single, *sub-alkaline* field trend. Samples show a general systematic shift upwards into nominally more felsic compositions from those defined in *Figure 3.1a*. Most of the advanced argillic alteration samples are displaced into the upper *rhyolite* field with SiO_2 values from >77 and 93% (silicification).

When plotted on the classification diagram of Miyashiro (1974; *Figure 3-1c*) the mafic volcanic rocks of the lower volcanic unit and the mafic dykes generally follow the positively sloped *tholeiitic* trend line. In contrast, the intermediate to felsic volcanic and intrusive rocks adhere to the negatively sloped *calc-alkaline* trend line.

3.2.1.2 Major Element Geochemistry

The major element compositions of all the samples are plotted against SiO_2 on Harker-type variation diagrams in *Figure 3-2*. Overall, the samples can be seen forming a single trend on most of the plots, and significant compositional overlap occurs between the Stewart Tuff, Caribou Tuff, porphyritic dacite dykes, tonalite, and granites.

Strong negatively sloped linear trends can be seen in the plots of MgO, FeO* and CaO. Advanced argillic alteration samples show deviations from these main trends with significant MgO and CaO depletion, and slightly increased FeO* values. The tonalite (host rock) also shows slight variations with lower CaO, and elevated FeO* values. Similarly, the mafic dyke sample (SF-12-41) that crosscuts the tonalite unit plots with significantly lower CaO, and higher FeO* values. Lastly, the andesitic lapilli tuff of the 'Upper Volcanic Unit' (SF-12-27) plots as an outlier on the CaO plot, at slightly lower values.

TiO_2, Al_2O_3, MnO and P_2O_5 form strong, slightly curved trends, beginning with slightly positive (to flat) slopes at lower SiO_2, and transitioning to negative slopes as samples become more SiO_2 enriched. In the MnO plot, the advanced argillic alteration samples deviate from the main trend, showing considerable depletion in Mn. Some of the Caribou Tuff and tonalite samples also show minor variance from the main MnO trend, to lower values. On the plot of P_2O_5, two samples plot as significantly higher outliers; GS-11-195 (diorite), and SF-12-115 (vuggy silica alteration).

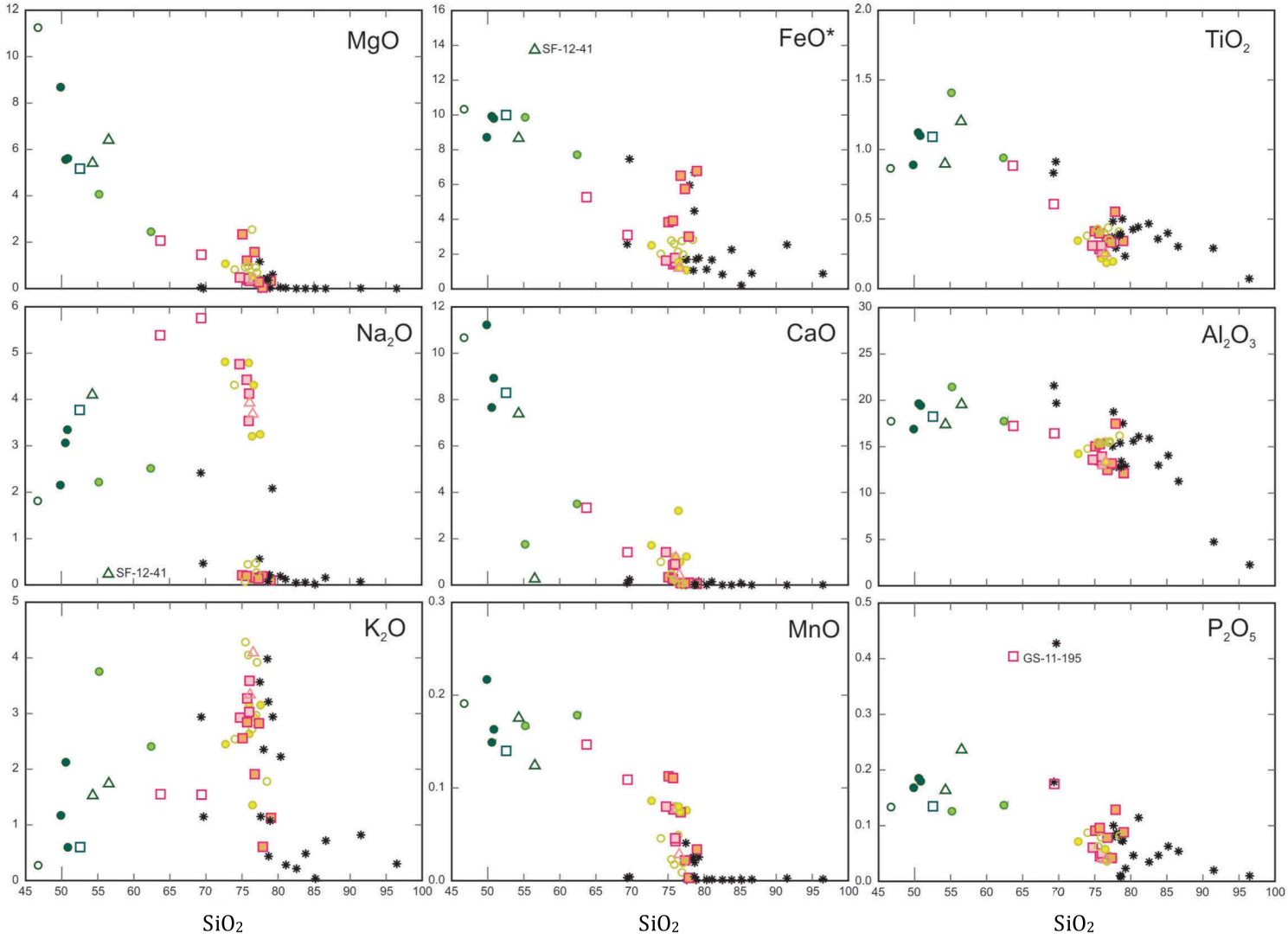

***Figure 3-2**: Major element data (wt. %) for Stewart samples, plotted against SiO_2. Symbols as in Figure 3-1.*

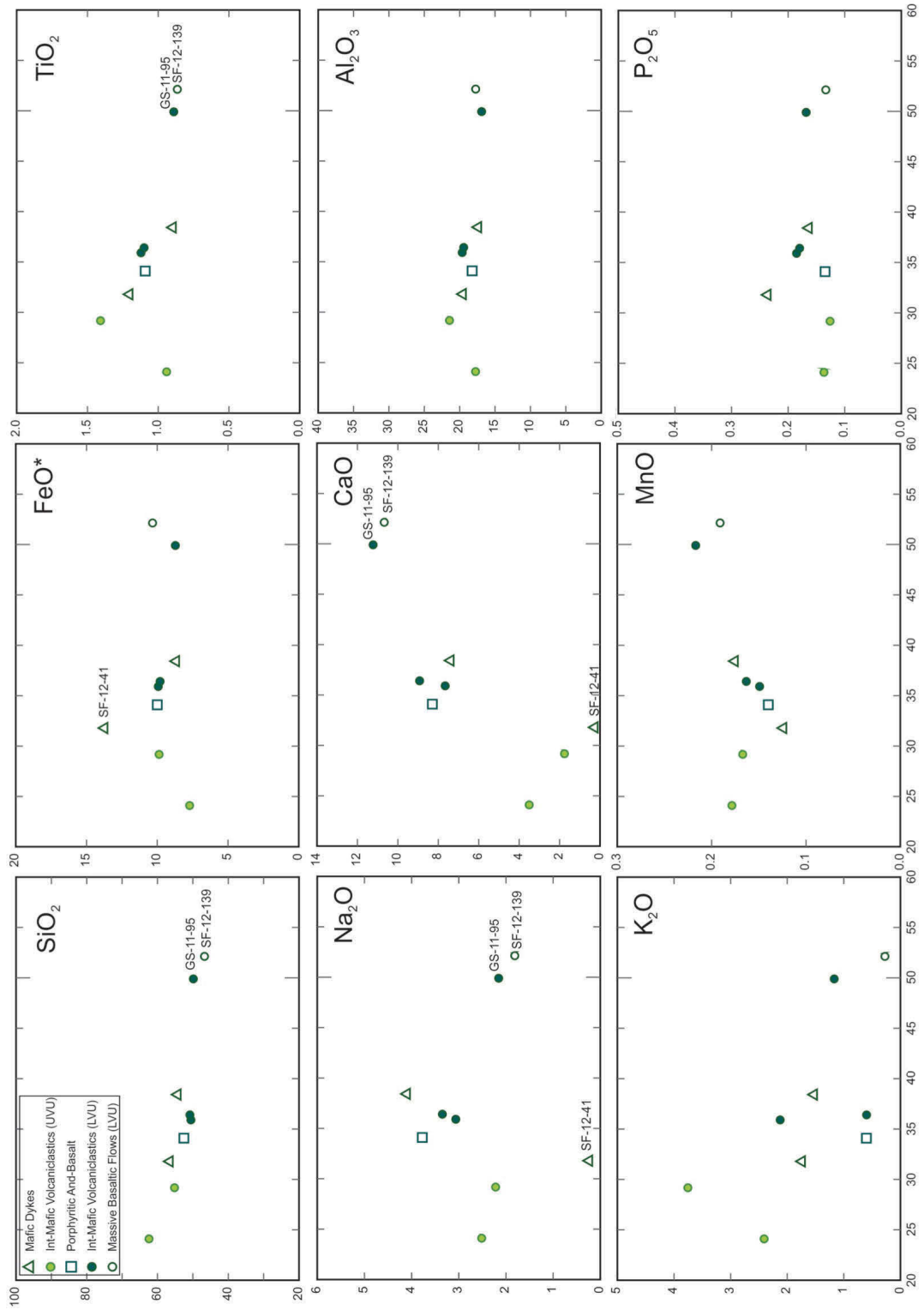

***Figure 3-3**: Major element data (wt. %) for Stewart intermediate-mafic volcanic and intrusive rocks plotted against Mg#.*

The plots of Na_2O and K_2O both show weak positively sloped trends, but with significant scatter. Samples of advanced argillic alteration, tonalite, and Caribou Tuff show significant depletion in Na_2O, as does mafic dyke sample SF-12-41. The remaining samples in the Na_2O plot, and all samples in the K_2O plot show considerable unsystematic variations in the elements.

The major oxides for the intermediate-mafic samples are also plotted against Mg# - a greater variant than SiO_2 for mafic rocks (*Figure 3-3*). The same trends and variations as displayed on the SiO_2 plots are generally evident. In addition, the massive basaltic flow unit (SF-12-139) clusters with a mafic tuff sample (GS-11-95) of the volcaniclastic unit.

3.2.1.3 Trace Element Geochemistry

Intermediate-mafic rock samples are plotted on extended primitive mantle-normalized REE diagrams (*Figure 3-4 a)-f)*). The massive basaltic flow (*b*) and intermediate-mafic volcaniclastics (*c*) of the Lower Volcanic Unit, and the porphyritic andesitic-basalt (*d*) intruding them, overlap and show very similar REE patterns. These are relatively flat, containing a moderate negative Nb anomaly and a small negative Zr anomaly.

Compared to the mafic-intermediate rocks of the Lower Volcanic Unit, the intermediate-mafic volcaniclastics (*e*) of the Upper Volcanic Unit show a more pronounced negative Nb anomaly and a steeper overall REE pattern. This unit also contains a slight negative Ti anomaly.

The REE patterns of the mafic dykes (*f*) plot intermediate to the rocks of the Lower and Upper Volcanic Units. The slope of the REE-pattern is parallel to those of the Lower Volcanic, but at slightly higher abundances. The dykes also contain a small negative Zr anomaly, similar to those of the Lower Volcanic Unit. However, the dykes also display a much more significant negative Nb anomaly, congruous with that of the Upper Volcanic Unit, as well as a small negative Ti anomaly.

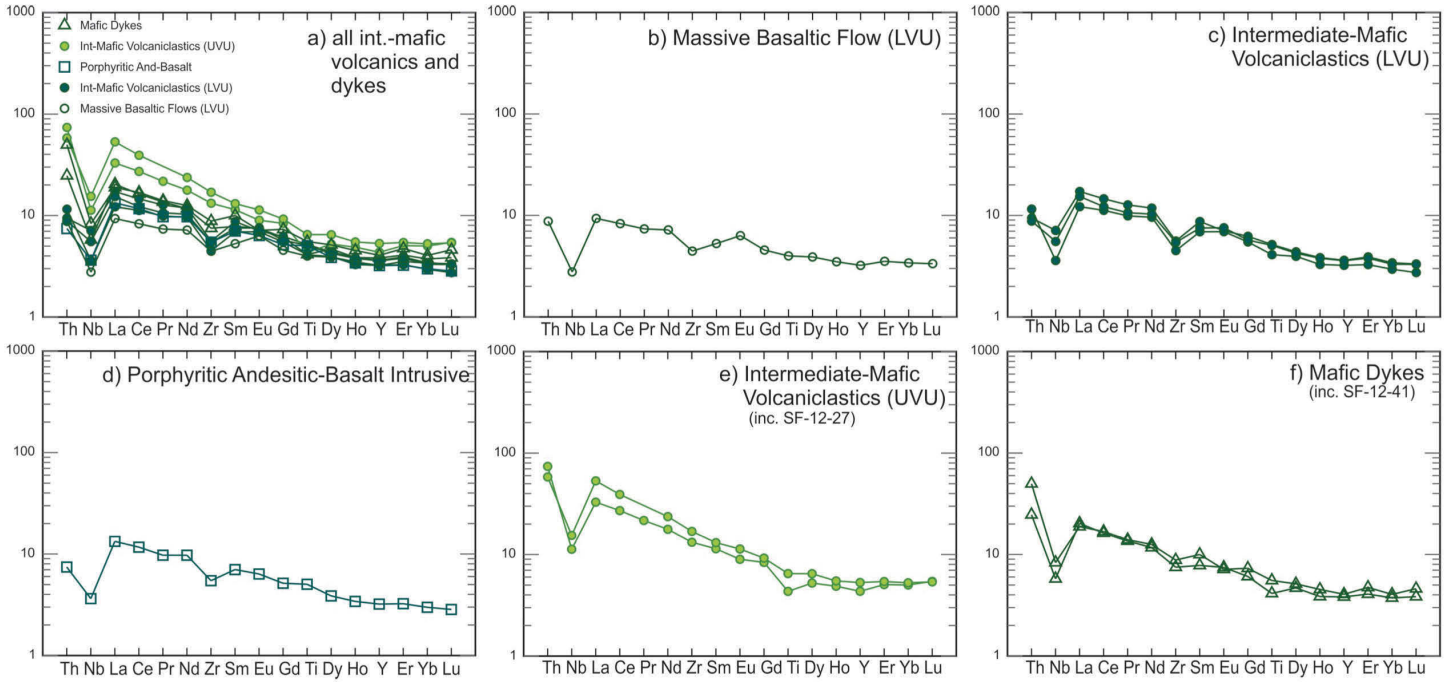

Figure 3-4*: Extended REE patterns for Stewart intermediate-mafic rocks, normalized to primitive mantle values of Sun and McDonough (1989); a) All intermediate-mafic samples at Stewart; b) Single sample of the massive basaltic flow from the Lower Volcanic Unit; c) Three samples from the intermediate-mafic volcaniclastics of the Lower Volcanic Unit; d) Single sample of the porphyritic andesitic-basalt intrusive; e) Two samples of the intermediate-mafic volcaniclastics from the Upper Volcanic Unit; f) Two samples of fine-grained, crosscutting mafic dykes.*

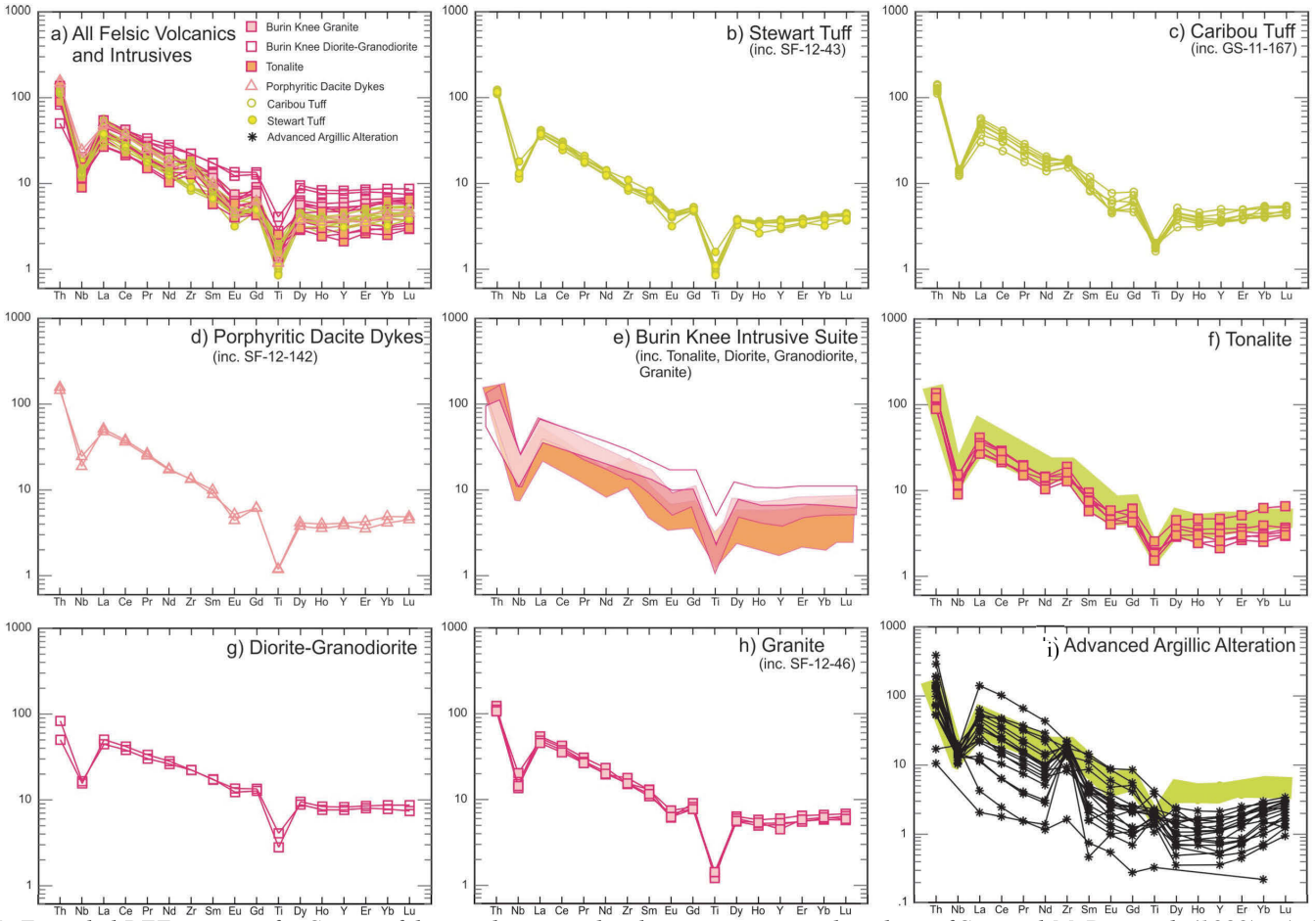

Figure 3-5: *Extended REE patterns for Stewart felsic rocks, normalized to primitive mantle values of Sun and McDonough (1989); a) All felsic samples; b) Six samples of the Stewart Tuff (dacitic quartz-feldspar crystal-rich volcaniclastic); c) Seven samples of Caribou Tuff (dacitic quartz crystal-rich volcaniclastic) host rock; d) Two samples of the porphyritic dacite dykes; e) All samples of the BKIS, including diorite-granodiorite, tonalite, and granite; f) Six samples of tonalite host rock overlaid on Caribou Tuff (green); g) Sample of diorite and granodiorite; h) Four samples of granite; i) Samples of intense advanced argillic alteration within Caribou Tuff and Tonalite units, overlaid on relatively unaltered to weakly altered Caribou Tuff for comparison.*

Felsic rock samples are also plotted on extended primitive mantle-normalized REE diagrams (*Figure 3-5*). All of the felsic samples display similar, overlapping and parallel REE patterns, as well as negative Nb and Ti anomalies (*Figure 3-5a*). The slopes of the REE-patterns of the felsic rocks are very similar to that of the intermediate-mafic volcaniclastics of the Upper Volcanic Unit, and more inclined than those of the Lower Volcanic Unit and porphyritic andesitic-basalt intrusive (*Figure 3-4).*

The Stewart Tuff (*b*) and porphyritic dacite dykes (*d*) share almost identical REE patterns, with a significant negative Ti anomaly and a smooth LREE trend, and a small negative Eu anomaly. The Caribou Tuff (*c*) differs only slightly from these two units, displaying a smaller negative Ti anomaly, and a small positive Zr anomaly.

All of the BKIS units are shown together in *Figure 3-5e,* and individually in *Figure 3-5f* through *h*. The tonalite (*f*) REE patterns are almost identical to those of the Caribou Tuff (shown shaded in green), including the same positive Zr anomaly and smaller negative Ti anomaly. The tonalite differs in that it displays greater variance in HREEs, extending both slightly higher and lower than the Caribou Tuff.

The REE-patterns of the BKIS granites (*h*) plot directly above and parallel to those of the BKIS tonalite (*f*), but do not contain a positive Zr anomaly and include a more significant negative Ti anomaly. The BKIS diorite-granodiorites (*g*), which are slightly more mafic than both the tonalite and granite units, plot with overall higher REE values, particularly the HREEs, and display a shallower overall slope, with a slightly smaller negative Nb anomaly.

Samples of the Caribou Tuff and tonalite host rocks that have been intensely altered to an advanced argillic assemblage are plotted in Figure 3-5i, along with relatively unaltered to only weakly altered examples of the Caribou Tuff for comparison. Relative to the less altered Caribou Tuff, all samples of the advanced argillic alteration show depletion in HREEs and Y, and a majority of samples also show depletion in the middle REEs. Most samples display LREEs consistent with the Caribou Tuff, but some still show significant depletion, and one sample shows apparent enrichment.

Figure 3-6 displays various bivariate incompatible trace element plots. *Figure 3-6 a-b* display La_N and Th_N plotted against fractionation indices of Zr and SiO_2, respectively. Both plots display a strong positive linear trend.

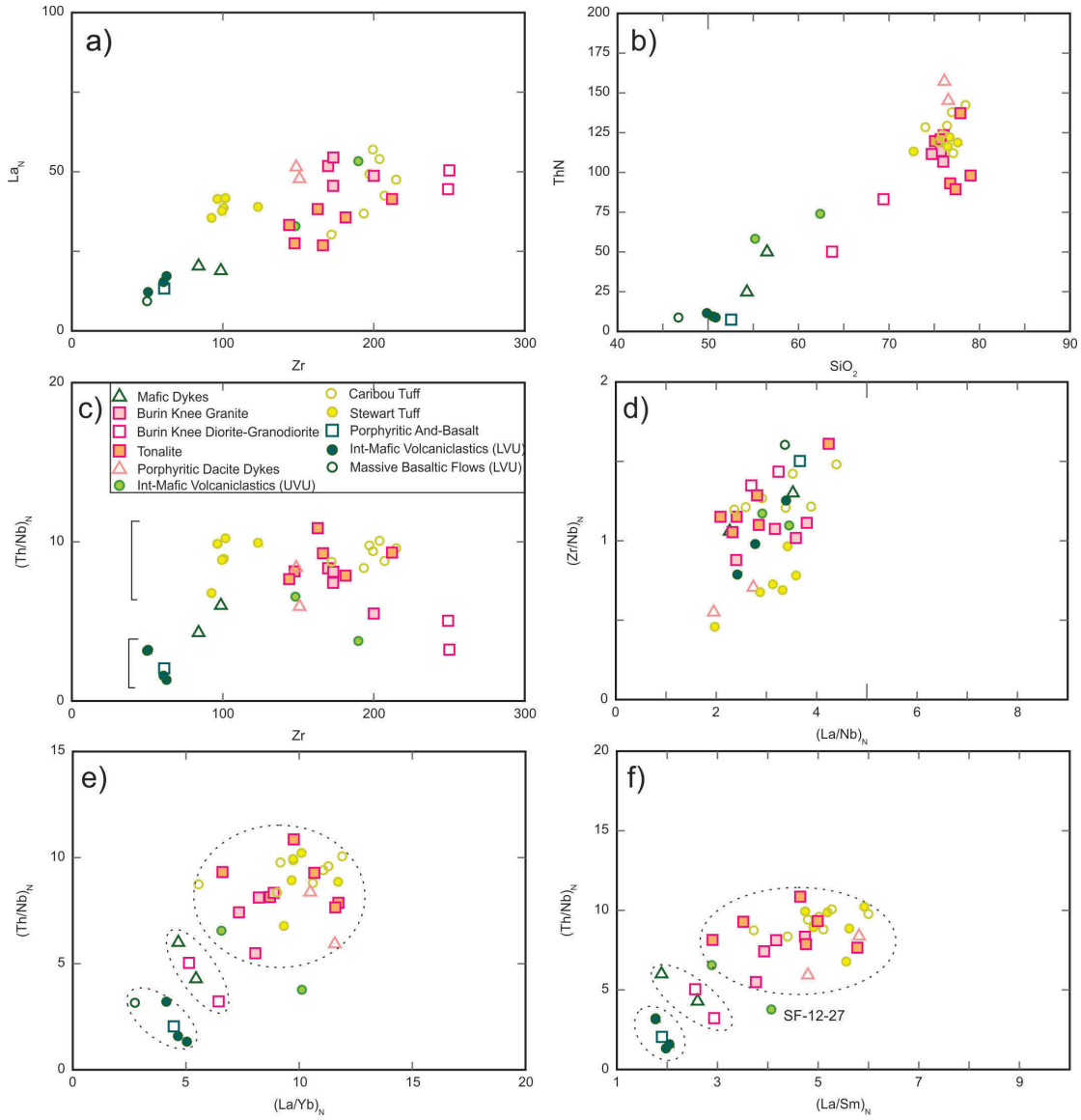

Figure 3-6*: Bivariate incompatible trace element plots. All elements normalized to primitive mantle values of Sun and McDonough (1989); a) La plotted against Zr as a fractionation index; b) Th plotted against SiO_2 as a fractionation index; c) Th/Nb plotted against Zr; d-f) ratio-ratio plots of Zr/Nb vs. La/Nb(d), Th/Nb vs. La/Yb (e), and Th/Nb vs. La/Sm (f). Dashed ellipses enclose correlative rock units.*

The incompatible trace element ratio of $(Th/Nb)_N$ is plotted against Zr in *Figure 3-6c*. The plot displays two main horizontal trends; the mafic volcanics and mafic intrusive of the Lower Volcanic Unit plotting together at lower ratios, and the felsic volcanics and

most of the BKIS plotting together at higher ratios. The cross-cutting mafic dykes, the diorite-granodiorite, and sample SF-12-27 of the Upper Volcanic Unit largely plot intermediate to these two main trends.

In the bivariate ratio-ratio plots of $(Zr/Nb)_N$ vs. $(La/Nb)_N$, $(Th/Nb)_N$ vs. $(La/Yb)_N$ and $(Th/Nb)_N$ vs. $(La/Sm)_N$ (*Figure 3-6 d-f*), samples consistently form a single, broad, linear-trending cluster. However, in the latter two plots, the samples can be further subdivided into three subgroups: 1) The mafic flows and volcaniclastics of the Lower Volcanic Unit and the porphyritic andesitic basalt; 2) The cross-cutting mafic dykes and the diorite and granodiorite of the BKIS; and 3) The felsic volcaniclastics, dacite dykes, one sample of the intermediate volcaniclastics of the Upper Volcanic Unit, and tonalites and granites of the BKIS. Sample SF-12-27 of the Upper Volcanic Suite plots as a slight outlier to the main clusters.

The intermediate-mafic rocks are plotted on the tectonic discrimination diagram for basalts of Cabanis and Lecolle (1989) in *Figure 3-7a*. All samples plot in the field of *calc-alkali volcanic-arc basalts*, except for the massive basaltic flow of the Lower Volcanic Unit, which lies in the *volcanic-arc tholeiite* field (VAT). The felsic rocks are plotted on the tectonic discrimination diagram for granites of Pearce et al. (1984) in *Figure 3-7b*. All of the samples plot in the same field of *volcanic-arc granites and syn-collisional granites (VAG+syn-COLG)*.

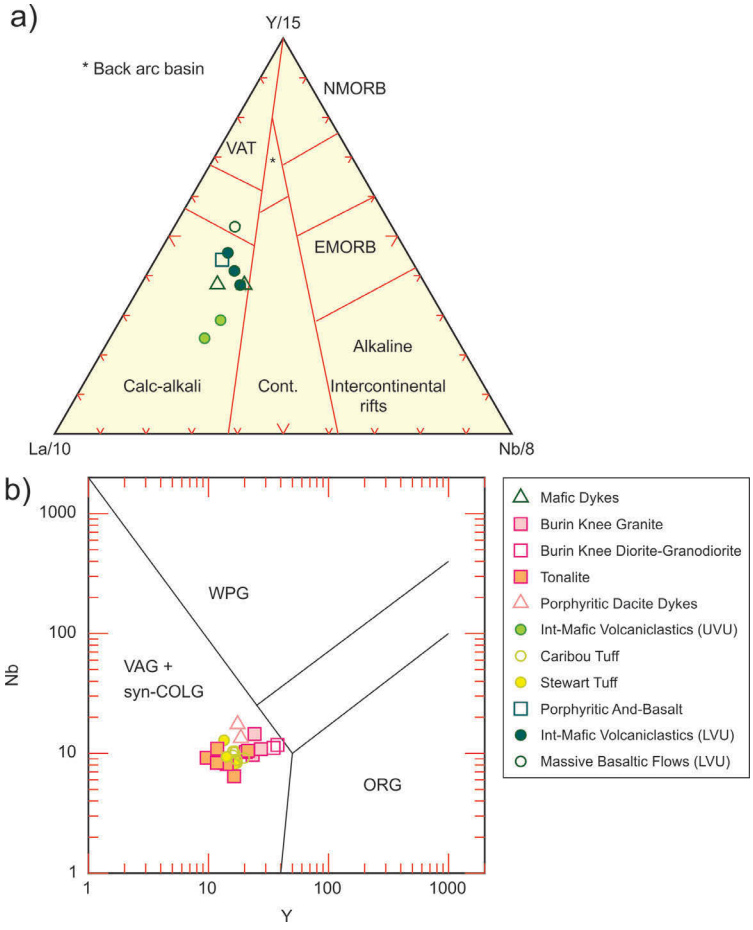

Figure 3-7*: Tectonic discrimination diagrams; a) Intermediate-mafic samples from Stewart plotted on the tectonic discrimination diagram for basalts of Cabanis and Lecolle, 1989. Calc-alkali=calc-alkali volcanic arc basalts, VAT=volcanic-arc tholeiites, Cont=continental basalts;*
b) Felsic samples from Stewart plotted on the tectonic discrimination diagram for granites of Pearce et al., 1984. WPG=within plate granite, VAG=volcanic-arc granite, syn-COLG=syn-collisional granites, ORG=ocean-ridge granites.

3.2.1.4 Stewart Interpretation

The extreme mobility of elements under high-sulphidation epithermal conditions is demonstrated in *Figures 3-1, 3-2* and *3-5,* which include samples that have been intensely altered to an advanced argillic assemblage. In the plots displaying major element oxide data (*Figures 3-1b & 3-2*), these altered samples show significant elevations in SiO_2 and minor elevations in FeO*, most likely due to the presence of pyrite and/or specular hematite. Significant depletions in other major elements include MgO, Na_2O, CaO and MnO, presumably a result of the alteration of original mineral species to silica and K-rich clays that now comprise the bulk of these rocks. The Caribou Tuff and tonalite rock units are unaltered to weakly altered relative to the 'advanced argillic alteration' samples, and show similar element mobility trends but to a far lesser extent. The mafic dyke sampled for geochronology (SF-12-41) which crosscuts the tonalite unit,

and seemingly the advanced argillic alteration in outcrop, might not be truly post-alteration, as it deviates from the main trend lines in *Figure 3-2* systematically with the other hydrothermally altered samples. In the extended REE plot in *Figure 3-5*, advanced argillic samples show depletion in HREEs, Y, and middle REEs, and occasional positive and negative fluctuations in the LREEs; all of which are traditionally deemed immobile. This is due to the highly acidic nature of these high-sulphidation hydrothermal fluids, drastically leaching the original host rock and removing these elements. The depletion in Y is also apparent in *Figure 3-1a,* causing the nominal shift of altered samples into the alkaline and ultra-alkaline fields.

On the major element oxide plots in *Figure 3-2* elements that showed non-linear scatter, as opposed to the more systematic variations resulting from the hydrothermal alteration, include Na_2O, K_2O, and to a less extent, CaO. These variations are interpreted to be the result of metasomatism during later greenschist-grade metamorphism.

The rock types at Stewart range from basalt to dacite according to the rock type classification diagram of Pearce (1996), which is generally consistent with field and petrographic observations. The shift of samples into more felsic fields in the diagram of Winchester and Floyd (1977) is most likely a result of the significant hydrothermal alteration affecting the property, as evidenced by the significant relative enrichment in SiO_2 in the samples of advanced argillic alteration. Samples might also be affected by weak ambient silicification associated with greenschist-facies metamorphism.

All of the samples form single linear trends on the rock classification diagrams, the Harker major oxide diagrams, and the bivariate trace element plots, and are therefore interpreted to represent a single volcanic suite derived from a single source and related, at least partially, by fractional crystallization. All of the samples also show geochemical signatures indicative of subduction-related magmatism (e.g. negative Nb and Ti anomalies) consistent with formation in a volcanic arc environment. This is also portrayed in the tectonic discrimination diagrams shown in *Figure 3-7*. These arc-signatures tend to become more pronounced moving upwards through stratigraphy, in

conjunction with the progressive enrichment in LREE relative to HREE (increase in REE pattern slopes), illustrating a progression in arc maturity from the Lower Volcanic Unit (including the andesitic-basalt intrusive) through to the overlying felsic volcanics and intrusives. This is also reflected in their respective subdivisions on the bivariate trace element ratio-ratio plots (*Figure 3-6 e-f*). The broad linear-trending cluster formed amongst all the samples indicates an overall genetic relationship between all of the rock units. However, within this trend, the mafic rocks of the Lower Volcanic Unit cluster tightly at lower values, indicating a close relationship through fractional crystallization, while the felsic volcanics plot at progressively higher values. The latter effect is interpreted to be the result of an increased influence of contamination and/or partial melting of the crust in the formation of the felsic rocks during the evolution and maturation of the arc. This subdivision is also evident on the classification diagram of Miyashiro (1977) where the mafic flows and volcaniclastics of the Lower Volcanic Unit, and the porphyritic andesitic-basalt intrusive, adhere to a separate tholeiitic trend representing a more juvenile phase of arc volcanism, while the remaining, generally felsic, rocks follow a calc-alkaline trend.

Overall, the various felsic volcanic and intrusive rock units at Stewart share very similar REE-patterns and are presumably all closely related rock units (*Figure 3-5*). REE-patterns of the porphyritic dacite dykes are almost identical to those of the Stewart Tuff, and based on additional cross-cutting relationships, the dykes potentially represent a subvolcanic equivalent of the Stewart Tuff, occurring as feeder dykes to the unit. A geochemical affinity is also evident between the Caribou Tuff and the tonalite, which share a unique small positive Zr anomaly; and similarly, the tonalite may represent a subvolcanic equivalent to the Caribou Tuff. Some of the tonalite samples show slight depletion and variation in HREEs relative to the Caribou Tuff, but this is interpreted to be a minor effect of hydrothermal-related HREE mobilization, even in these relatively unaltered samples.

The REE-patterns of the tonalites, and granites of the BKIS share similar overall patterns and have parallel slopes. The granite REE-patterns plot directly above and

parallel to those of the tonalite (*Figure 3-5e*), which is compatible with these units being related through fractional crystallization. The diorites-granodiorites however, which are slightly more mafic than both the tonalite and granite units, counter-intuitively plot higher than both units, and are noticeably enriched in HREEs, in addition to displaying a shallower overall slope and smaller negative Nb anomaly. This indicates that they aren't related to the rest of the intrusive suite exclusively by simple fractional crystallization. They also plot as a separate cluster on the incompatible trace element ratio-ratio plots, clustered with the mafic dykes (*Figure 3-6*), implying a possible genetic relationship. On extended REE diagrams (*Figures 3-4 & 3-5*) the diorites-granodiorites plot higher than the mafic dykes, but with similarly-sized negative Nb anomalies and parallel REE-pattern slopes. The diorite-granodiorite unit therefore appears to represent a distinct phase of the BKIS, affected to a greater extent by upper crustal contamination. This is supported by the observation of the unique presence of actinolite in both the diorite and granodiorite samples (*Chapter 2*), which isn't a typical primary mineral phase in felsic intrusive suites. Diorite sample GS-11-195 shows a distinct elevation in P_2O_5 concentration (*Figure 3-2*), which could also be the result of crustal contamination. Alternatively, the diorite-granodiorite and mafic dykes could have formed from magma mixing of the mafic and felsic endmembers of the suite, given their intermediate position on the ratio-ratio plots (*Figure 3-6 e-f*). If the diorites-granodiorites are in fact related to the mafic dykes, perhaps they represent a slightly later phase of the intrusive suite, given that the mafic dykes cross-cut the tonalite.

3.2.2 Hickey's Pond and Tower

Hickey's Pond and Tower are adjacent high-sulphidation prospects that occur on the northern Burin Peninsula along the eastern margin of the Swift Current Granite (*Figure 2-1*). Two samples from Tower (SF-12-104 & GS-11-54) contain primary igneous features and are not significantly altered. However, the remaining samples collected from these locations are for the most part significantly altered, predominantly to an advanced argillic assemblage. This has obvious and significant effects on both major and trace element chemistry, as demonstrated in *Section 3.2.1*. As such, the discussion on

the lithogeochemical characteristics of these two prospects is brief and combined, and a section on major element chemistry is not included due to the small number of fresh samples available.

One sample (SF-12-150) was selected for U-Pb geochronology from the Hickey's Pond prospect. This sample is from the central Au-enriched vuggy silica zone, consisting mostly of quartz, ore minerals and Fe-Ti-oxides, and was not analyzed for major or trace elements because of this high-degree of leaching and alteration. However, an equivalent sample (GS-11-457) collected from the same narrow zone is included and explicitly labeled in the plots below.

3.2.2.1 Rock Type Classification

On the classification diagram of Pearce (1996; *Figure 3-8*) the host rocks at Hickey's Pond range from *basalt* to *andesite*, and at Tower, from *andesite* to *rhyodacite*. Sample GS-11-457 (equivalent to geochronology sample SF-12-150), when projected to lower Nb/Y to account for leaching, plots as an *andesite* to *basaltic-andesite*. Although all of the Hickey's Pond samples are significantly altered, one sample (GS-11-461) appears to be relatively least altered, with Y remaining immobile, and plots in the *subalkaline* field proper, along with the two least altered Tower samples (SF-12-104 & GS-11-154).

3.2.2.2 Trace Element Geochemistry

The three relatively unaltered samples of intermediate-felsic volcanic rocks recognized above are plotted on an extended REE diagram normalized to primitive mantle (*Figure 3-9a*). These samples overlap, display distinct negative Nb and Ti anomalies, and a moderately sloped trend enriched in LREE relative to HREE. Intensely altered samples are also plotted on an extended REE diagram, shown in *Figure 3-9b*. The samples of advanced argillic alteration display consistent depletions in the HREEs, Y and middle REEs, and rare depletions in the LREEs relative to the unaltered samples shown in yellow (from *Figure 3-9a*).

The relatively unaltered felsic-intermediate volcanics are plotted on the tectonic discrimination diagram for granites of Pearce et al. (1984) in *Figure 3-10*. The samples plot in the field of *volcanic-arc granites and syn-collisional granites (VAG+syn-COLG)*.

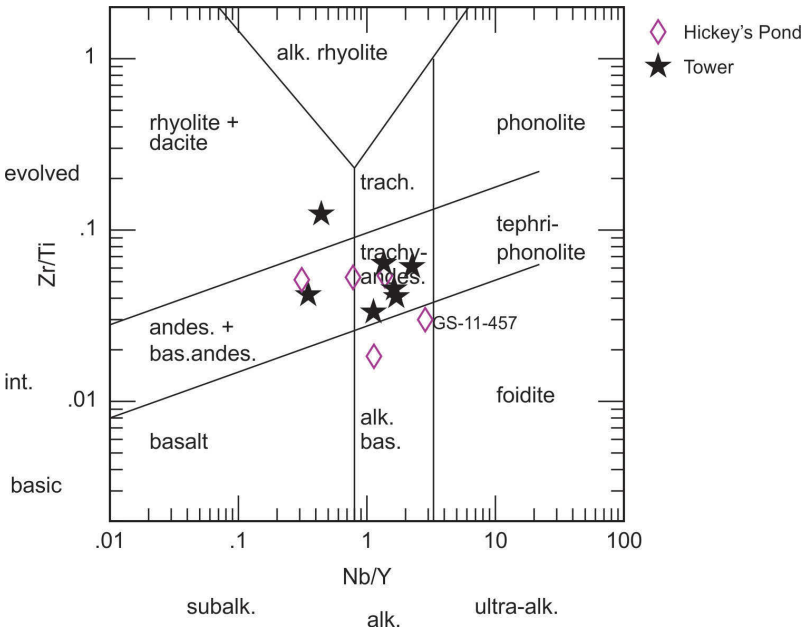

***Figure 3-8**: Classification diagram of Pearce (1996; after Winchester and Floyd, 1977) for Hickey's Pond and Tower samples.*

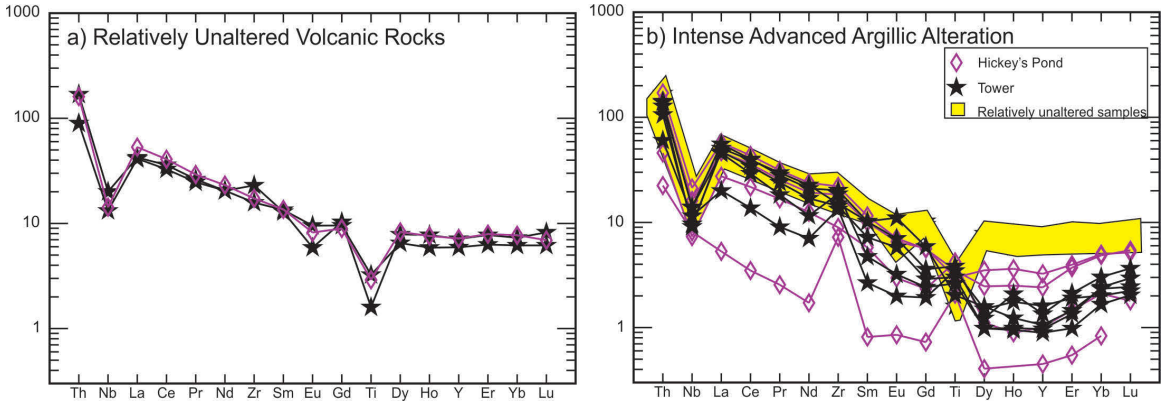

***Figure 3-9**: Extended REE patterns for rocks from the Hickey's Pond and Tower prospects, normalized to primitive mantle values of Sun and McDonough (1989); a) Three relatively unaltered felsic-intermediate volcanics (Tower: SF-12-104 & GS-11-154; Hickey's Pond: GS-11-461); b) Nine samples of intense advanced argillic alteration.*

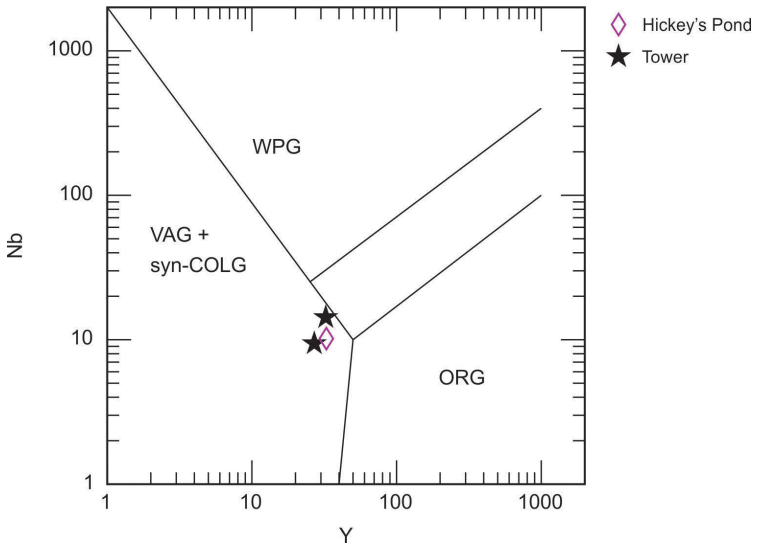

***Figure 3-10**: Tectonic discrimination diagram for granites of Pearce et al. (1984) for felsic-Intermediate volcanic rocks from Hickey's Pond and Tower. WPG=within plate granite, VAG=volcanic-arc granite, syn-COLG=syn-collisional granites, ORG=ocean-ridge granites.*

3.2.2.3 Hickey's Pond and Tower Interpretation

Similar to Stewart, mobilization of Y and REEs is evident in the samples of advanced argillic alteration (*Figure 3-9b*). This is due to the highly acidic nature of these high-sulphidation hydrothermal fluids, which leach the original host rock and remove these elements. The depletion in Y is also evident in *Figure 3-8*, where all of the altered samples appear shifted into the alkaline field.

The Hickey's Pond samples are all strongly affected by advanced argillic alteration and do not show any clear primary igneous textures. However, one sample (GS-11-461) appears to be relatively less altered based on its resistance to trace element mobilization, plotting as a subalkaline andesite in *Figure 3-8* and displaying an expected REE-pattern (*Figure 3-9a*). If the Y depletion of the other altered samples is accounted for, and the samples are projected to the left in the classification diagram, the host rocks at Hickey's Pond fall in a compositional range of basalt to andesite.

Two of the Tower samples collected adjacent to the main prospect are relatively unaltered (SF-12-104 & GS-11-154), displaying primary igneous textures, and plot as rhyodacite and andesite, respectively. The remaining altered host rock samples, when projected to the left on the classification diagram also plot with similar compositions, ranging from andesite to dacite.

The REE-patterns of the three relatively unaltered samples are coincident with the (intermediate)-felsic volcanics at Stewart, displaying a moderately sloped trend enriched in LREE relative to HREE with distinct negative Nb and Ti anomalies - all features indicative of subduction zone-related magmatism. Also consistent with Stewart, the samples plot in the volcanic arc and syn-collisional granite field in the tectonic discrimination diagram in *Figure 3-10.*

3.2.3 Heritage

The Heritage prospect is a low-sulphidation style deposit situated in the southernmost Burin Peninsula (*Figure 2-1*). The prospect is nominally hosted within Marystown Group volcanics. Limited lithogeochemical sampling was completed here, in support of geochronological determinations, so the dataset below is focussed on key hosts for epithermal mineralization, and later cross-cutting dykes, as outlined in *Chapter 2*. Three units are discussed in this section: a porphyritic andesite pyroclastic unit (geochronology sample SF-13-180), porphyritic amygdaloidal basalt, and later cross-cutting mafic dykes. The andesite pyroclastic is the predominant host rock at Heritage, and was explicitly sampled for geochronology for this reason.

3.2.3.1 Rock Type Classification

On the classification diagram of Pearce (1996; *Figure 3-11a*) the andesite pyroclastic host rock plots within the *andesite* field, and the amygdaloidal basalts cluster in the upper *sub-alkaline basalt* field. The mafic dykes overlap the amygdaloidal basalts within the *sub-alkaline basalt* field, but show slightly more vertical variation, with one mafic dyke (SF-13-178) plotting closer to the *basaltic andesite* field. In the classification diagram of Winchester and Floyd (1977; *Figure 3-11b*) the andesite pyroclastic host rock is shifted into the *dacite-rhyodacite* field, and the basalts are shifted to a composition of *basaltic andesite*. The mafic dykes plot similarly to the previous figure with two in the *basalt* field and one plotting as a basaltic *andesite*. In *Figure 3-11c*, the andesite pyroclastic lies close to the nominal *calc-alkaline* trend line, with the remainder of the samples plotting as a flat array between the *calc*-alkaline and tholeiitic trend lines.

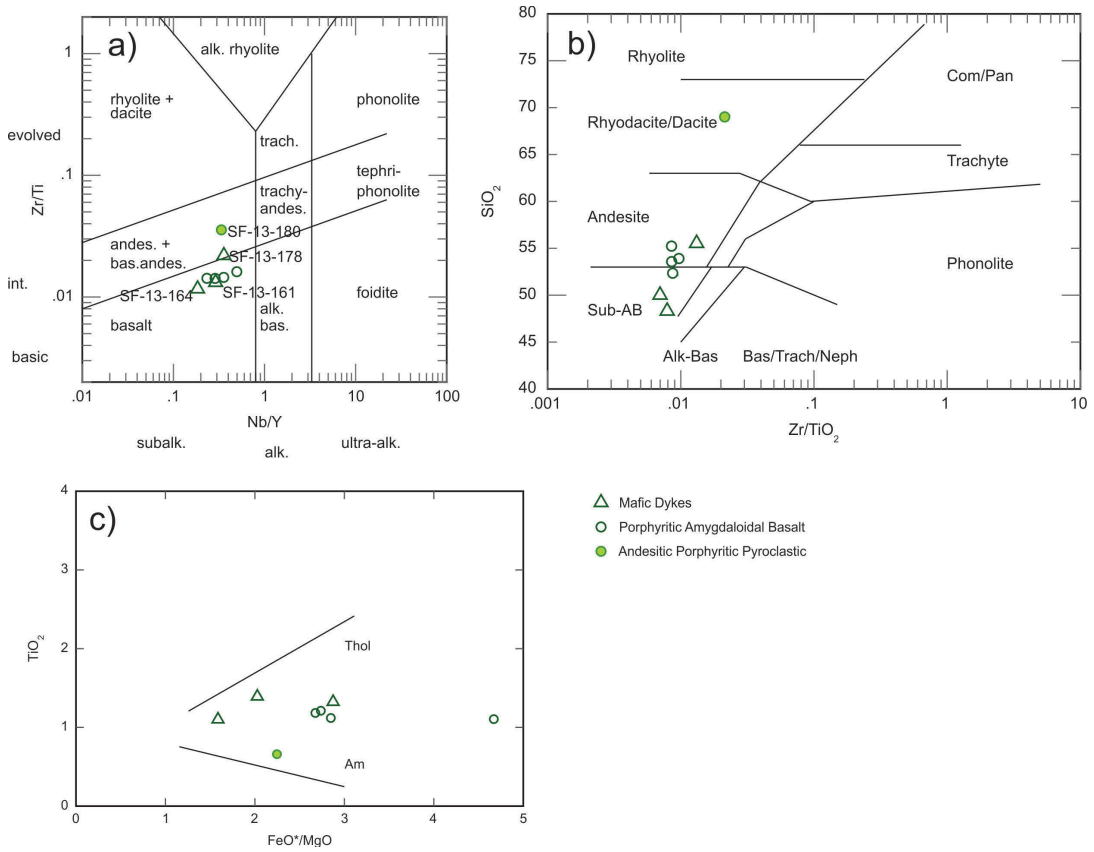

Figure 3-11*: Classification diagrams for intermediate-mafic volcanic and intrusive samples from Heritage; a) Zr/Ti vs. Nb/Y (Pearce, 1996; after Winchester and Floyd, 1977); b) SiO_2 vs. Zr/TiO_2 (Winchester and Floyd, 1977); c) Classification diagram of Miyashiro (1974). Thol=tholeiitic, Am=calc alkaline.*

3.2.3.2 Major Element Geochemistry

The major element compositions of all the samples are plotted against SiO_2 on Harker-type major element variation diagrams in *Figure 3-12*. Sample SF-13-180, as the main host rock at Heritage, is also known, from field and petrographic evidence, to be strongly silicified as a consequence of areally extensive, pervasive hydrothermal alteration. To account for this, it is also shown in *Figure 3-12* projected to a lower SiO_2 value based on its compositional shift between the classification diagrams in *Figure 3-11a-b*. Most of the plots display a linear trend developed amongst the samples.

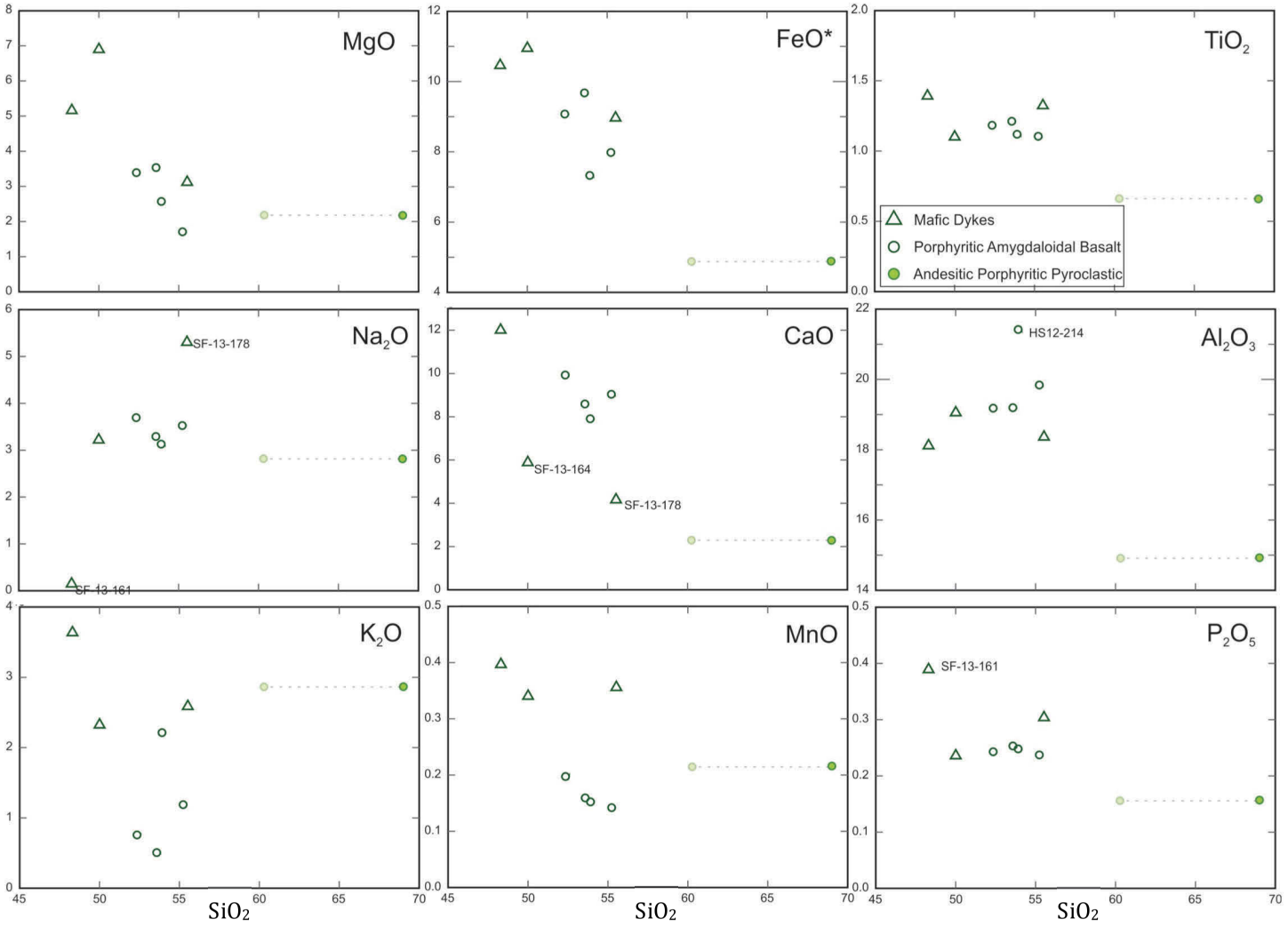

***Figure 3-12**: Major element data (wt. %) for Heritage samples, plotted against SiO_2. Andesite pyroclastic sample (SF-13-180) is also projected to lower SiO_2, assuming an originally andesitic composition that was altered by hydrothermal silicification.*

Negatively sloped trends are evident in the plots of MgO, FeO*, and CaO, with only minor deviations present, typically in mafic dyke samples. In the plot of MgO, one dyke (SF-13-164) plots slightly off-trend at higher values, and on the CaO plot, two mafic dykes (SF-13-164 & SF-13-178) plot with slightly lower values. Negatively sloped, curved trends are displayed for TiO_2, Al_2O_3 and P_2O_5. Basalt sample HS12-214 plots at elevated Al_2O_3 values, and mafic dyke sample SF-13-161 plots at distinctly higher P_2O_5 values, relative to the main trend lines. A relatively flat trend line is evident in the plot of Na_2O, with the exception of mafic dyke sample SF-13-178 displaying a significantly higher concentration, and mafic dyke sample SF-13-161 displaying a significantly lower concentration. Significant scatter occurs in the plots of K_2O and MnO, with no apparent trend line.

3.2.3.3 Trace Element Geochemistry

The intermediate-mafic samples are plotted on extended primitive mantle-normalized REE diagrams in *Figure 3-13 a)-e)*. When plotted together (*a*), all of the samples generally overlap, each containing a clear negative Nb anomaly. The andesite pyroclastic (*b*) has a slightly shallower overall REE-pattern slope, enriched in HREEs relative to all but one of the other samples. The andesitic pyroclastic also contains a strong negative Ti anomaly. The basalts and mafic dykes (*Figure 3-13c-e*) display almost identical REE patterns and contain a slight negative Zr anomaly not evident in the andesite pyroclastic. Mafic dyke sample SF-13-178, with a slightly more felsic composition (basaltic andesite), plots above the basaltic flows and basaltic mafic dykes, but with a parallel slope and matching REE-pattern.

Figure 3-14 displays a series of bivariate incompatible trace element plots. *Figures 3-14 a* through *c* show Th_N, Nb_N, and La_N plotted against SiO_2 as a fractionation index. Similar to the major oxide element plots in *Figure 3-12,* SF-13-180 is also shown projected to a lower SiO_2 value to account for silicification due to hydrothermal alteration. With this adjusted value, all of the plots show positive linear trends.

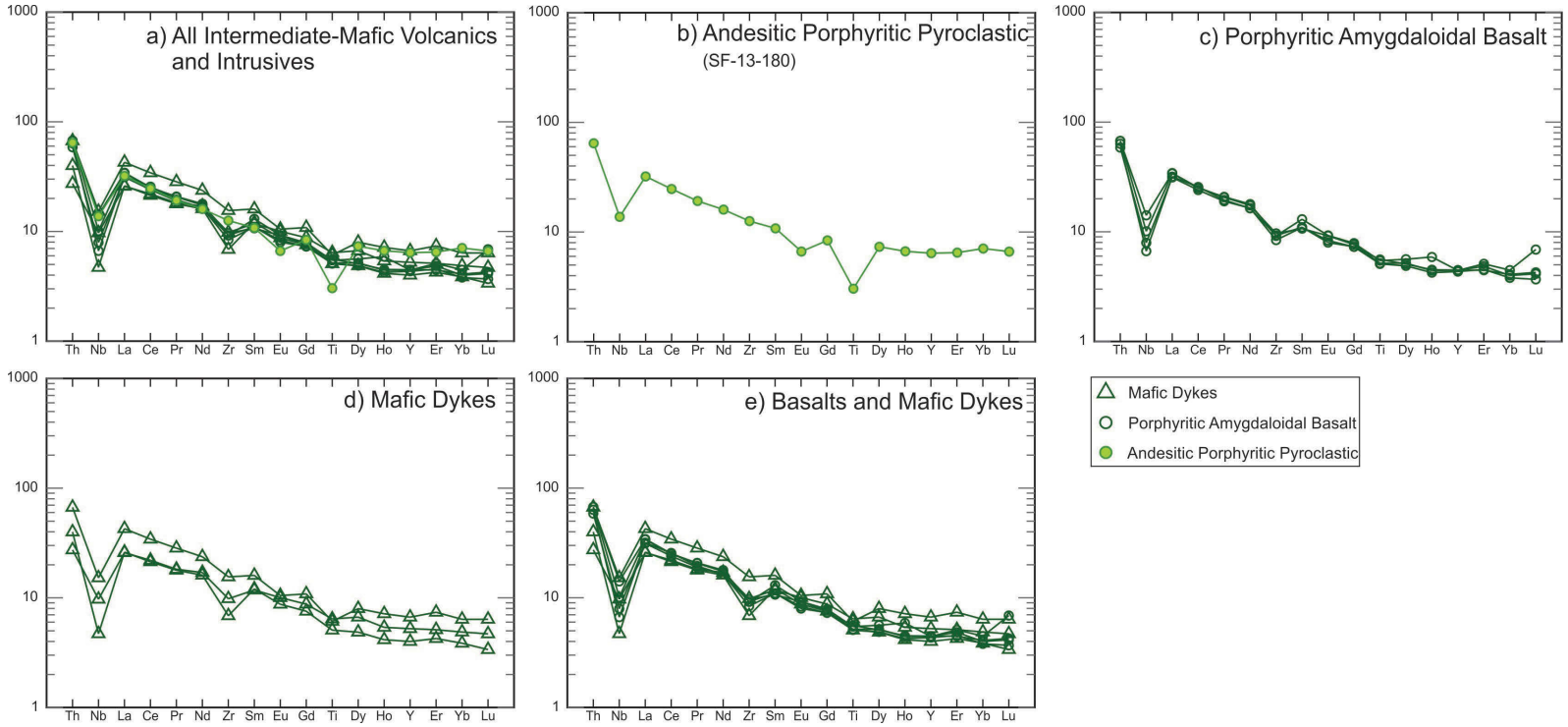

***Figure 3-13**: Extended REE patterns for all samples at Heritage, normalized to primitive mantle values of Sun and McDonough (1989); a) All samples; b) Single sample of andesite pyroclastic (host lithology and geochronology sample SF-13-180); c) Four samples of porphyritic amygdaloidal basalt; d) Three samples of mafic dyke; e) Basalts and mafic dykes plotted together showing overlapping REE patterns.*

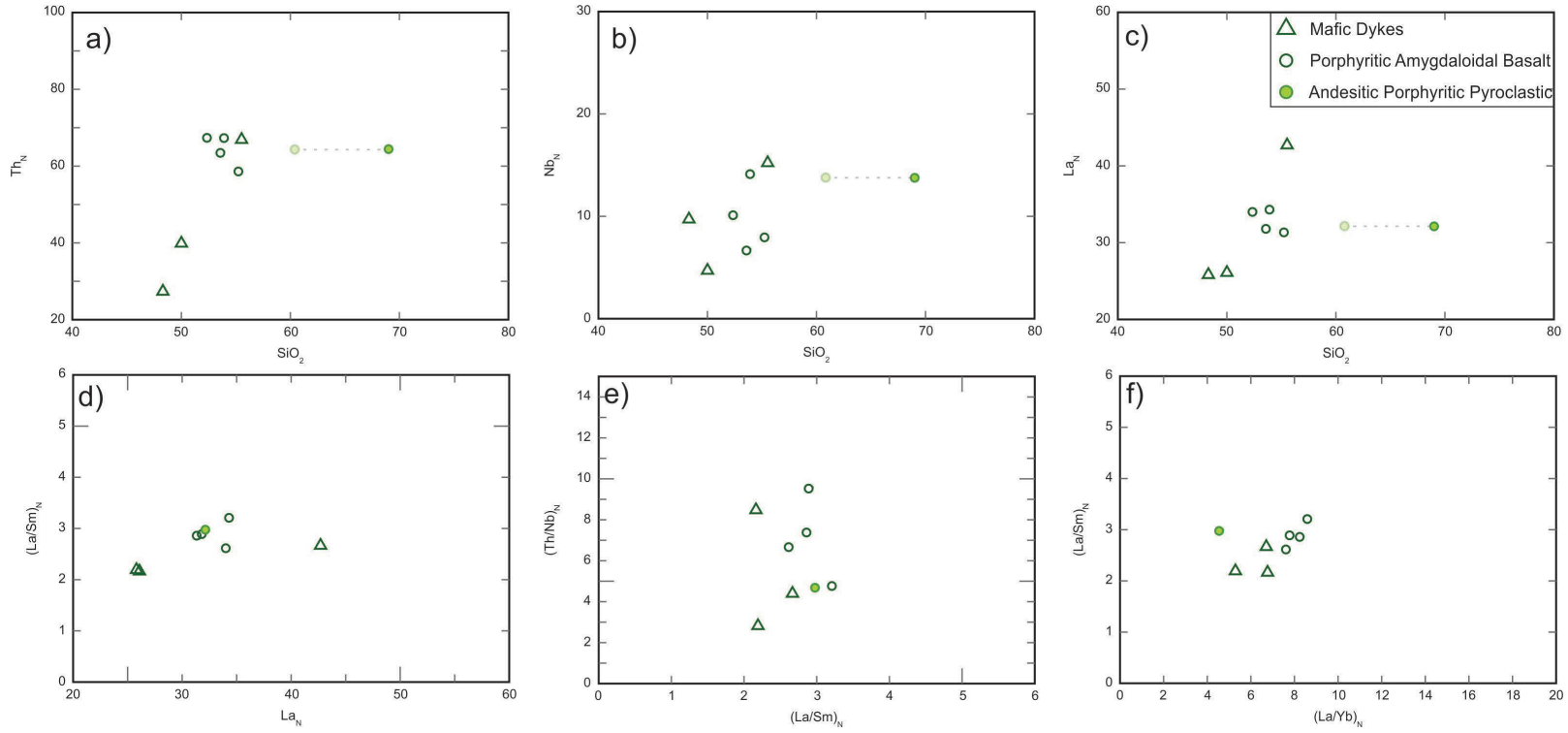

***Figure 3-14**: Bivariate incompatible trace element plots for Heritage samples. All elements normalized to primitive mantle values of Sun and McDonough (1989); a) Th plotted against SiO_2 as a fractionation index; b) Nb plotted against SiO_2 as a fractionation index; c) La plotted SiO_2 as a fractionation index; d) La/Sm plotted against La; e&f) Ratio-ratio plots of Th/Nb vs. La/Sm (d), and La/Sm vs. La/Yb (e).*

The incompatible trace element ratio of $(La/Sm)_N$ is plotted against La_N in *Figure 3-14d*, and samples form a single horizontal trend. In the bivariate ratio-ratio plot of $(Th/Nb)_N$ vs. $(La/Sm)_N$ (*Figure 3-14e*) samples form a single broad cluster overall, but with some scatter evident in the $(Th/Nb)_N$ values. In the bivariate ratio-ratio plot of $(La/Sm)_N$ vs. $(La/Yb)_N$ (*Figure 3-14f*) samples form a clustered pattern overall, with the andesite pyroclastic plotting in a position slightly removed from the main group.

When plotted on the tectonic discrimination diagram of Cabanis and Lecolle (1989), samples plot entirely within the field of *calc-alkali volcanic-arc basalts* (*Figure 3-15*).

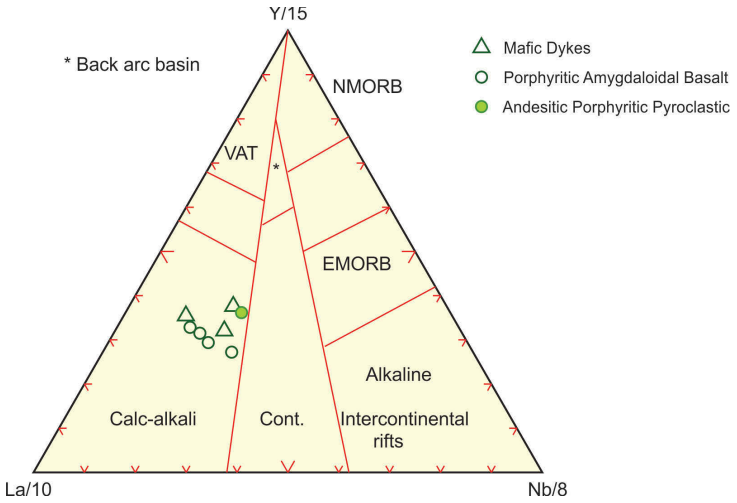

***Figure 3-15**: Tectonic discrimination diagrams for basalts of Cabanis and Lecolle, 1989. Calc-alkali=calc-alkali volcanic arc basalts, VAT=volcanic-arc tholeiites, Cont=continental basalts.*

3.2.3.4 Heritage Interpretation

Trends in some diagrams presented here are not overly defined due to the limited set of samples. However some informative correlations can still be deduced.

Unlike those for the high-sulphidation deposits discussed above, the hydrothermally altered host rock at Heritage (SF-13-180) does not show any significant biases in major or trace element abundance, except for a distinct elevation in SiO_2. Therefore, these low-sulphidation fluids may be inferred to have had a much lower impact on element mobility than their adjacent high-sulphidation counterparts.

Some of the mafic rocks show minor variations in MgO, Na_2O, and CaO values, and all of them display fairly significant variations in K_2O. This is interpreted to be the result of metasomatism during post-depositional greenschist facies metamorphism.

The units sampled from Heritage range in composition from basalt to andesite according to the classification diagram of Pearce (1996), consistent with field and petrographic observations. The porphyritic andesite pyroclastic appears shifted into a compositional field of rhyodacite on the classification diagram of Winchester and Floyd (1977), but this is a result of strong silicification (evident petrographically) associated with the local hydrothermal alteration.

When the andesite pyroclastic host rock sample (SF-13-180) is projected back towards lower SiO_2 values, all of the samples generally form single linear trends on the rock classification diagrams, the Harker major oxide diagrams, and the bivariate trace element plots, and are therefore interpreted to represent a single volcanic suite derived from a single source, and related, at least partially, by fractional crystallization. The flat trend line produced on the La/Sm vs. La plot, and clustering of samples on the ratio-ratio plots provides further indication that these rocks are part of a single suite and more specifically, related through simple fractional crystallization. On the ratio-ratio plot of $(La/Sm)_N$ vs. $(La/Yb)_N$ the andesitic pyroclastic unit plots at a slightly lower La/Yb ratio, which could indicate the influence of another magma differentiation process but, overall, appears closely related to the mafic rocks. Since the andesite pyroclastic is a product of explosive volcanism, slight variations in chemistry might also be caused by the presence of foreign rock fragments (older lithologies) incorporated during deposition. The minor variations in Th/Nb values within this suite in *Figure 3-14e* could reflect the influence of crustal contamination or magma mixing. However, this seems unlikely, since most of the variation occurs within the basalt samples, which were all collected from one large outcrop within a single stratigraphic horizon, and shouldn't show significant petrogenetic variability. Given that each sample of basalt was collected individually and analyzed at different times and at different labs, the minor fluctuations in Th/Nb ratios might simply reflect analytical reproducibility.

All of the Heritage samples show geochemical signatures indicative of subduction-related magmatism, including a moderately-sloped REE-pattern and a negative Nb anomaly. The andesite pyroclastic also shows a negative Ti anomaly. All of these features are consistent with formation in a volcanic arc environment, which is also demonstrated in the tectonic discrimination diagram shown in *Figure 3-15*. The mafic dykes exhibit correlative REE patterns with the basaltic flows. Therefore, these dykes likely represent feeder dykes to the basaltic flows that overlie the intermediate pyroclastic rocks that the dykes crosscut.

3.2.4 Grandy's Pond Arenite Belt

The 'Grandy's Pond Arenite Belt' (GPAB) spans the northern half of the Burin Peninsula along its western edge (*Figure 2-1*), overlying the volcanics of the Marystown Group. The belt is predominantly composed of feldspathic-lithic arenites and lesser fine polymictic conglomerates of epiclastic affinity, locally interbedded with thin pyroclastic units. Geochemical data for two samples of arenite (including geochronology sample SF-12-148) is presented here. Although these are water-lain sediments, they are clearly volcanic-derived, and data are presented in the same manner as in the other sections of this Chapter, allowing a test for affiliation with the Marystown Group, or other volcanic protoliths, as their main detrital source.

3.2.4.1 Rock Type Classification

On both of the classification diagrams shown in *Figure 3-16*, samples of arenite plot in the compositional range of *andesite* to *dacite*.

3.2.4.2 Trace Element Geochemistry

Samples are plotted on an extended primitive mantle-normalized REE diagram in *Figure 3-17a*, displaying moderately sloped, parallel REE-patterns and containing distinct negative Nb and Ti anomalies. Sample SF-12-149 also displays small positive anomalies in Zr and Eu. When plotted on the tectonic discrimination diagram for granites of Pearce

et al. (1984), samples plot in the field of *volcanic-arc granites and syn-collisional granites* (*VAG+sun-COLG*; *Figure 3-17b*).

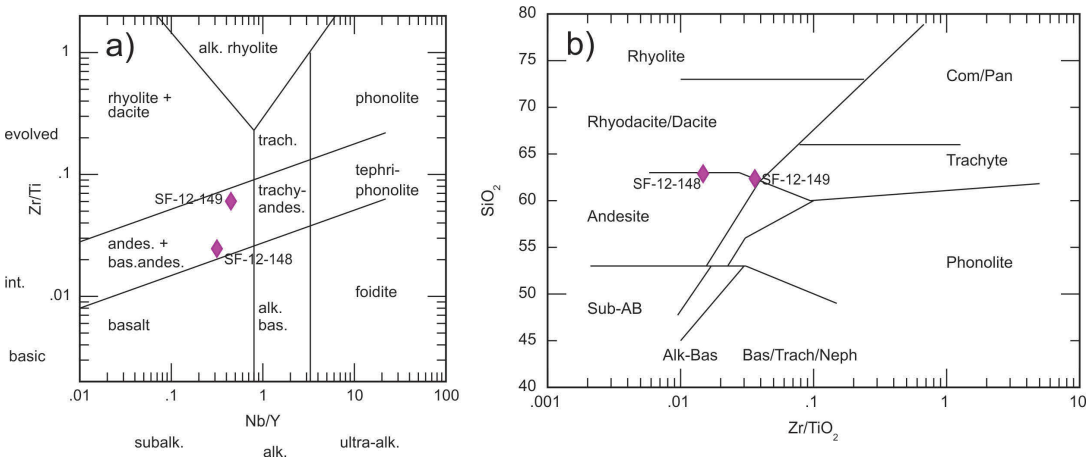

Figure 3-16*: Classification diagrams for epiclastic sediments of the Grandy's Pond Arenite Belt; a) Zr/Ti vs. Nb/Y (Pearce, 1996; after Winchester and Floyd, 1977); b) SiO_2 vs. Zr/TiO_2 (Winchester and Floyd, 1977).*

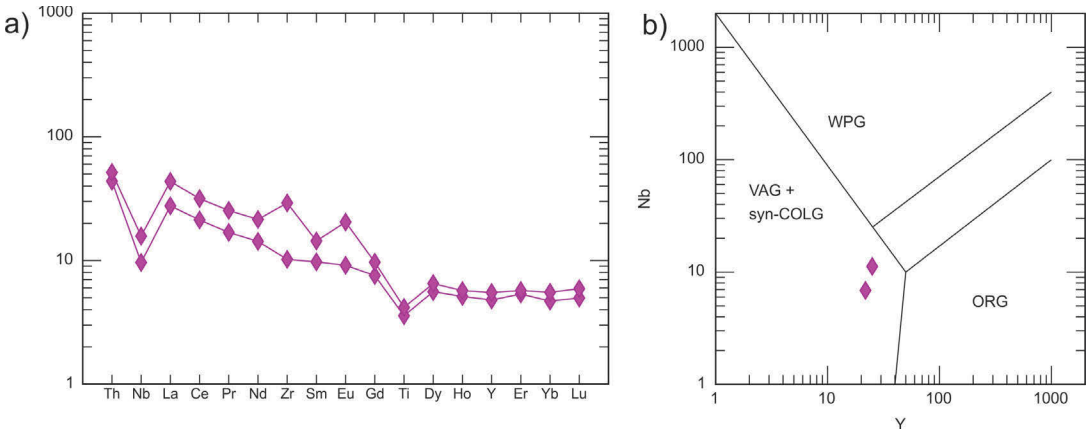

Figure 3-17*: Trace element plots for epiclastic sediment samples of the Grandy's Pond Arenite Belt; a) Extended REE patterns, normalized to primitive mantle values of Sun and McDonough (1989); b) Tectonic discrimination diagram for granites of Pearce et al. (1984). WPG=within plate granite, VAG=volcanic-arc granite, syn-COLG=syn-collisional granites, ORG=ocean-ridge granites.*

3.2.4.3 Grandy's Pond Arenite Belt Interpretation

Although these are sedimentary rocks, they appear, from field and petrographic evidence, to be derived predominantly from volcanic material, and are treated as such to characterize them relative to the surrounding volcanic rocks, and to test their affiliation with volcanics of the Marystown Group. The two samples plot as andesite to dacite in

composition; a similar range to other volcanic rocks of the Marystown Group from this study (e.g., Stewart, Hickey's Pond, Tower). They also display very similar REE patterns to the Marystown volcanics, including moderate slopes and distinct negative Nb and Ti anomalies, suggestive of subduction related magmatism, and consistent with a volcanic arc environment. They also plot in the same field as the Marystown volcanics on tectonic discrimination diagrams, in the field of volcanic arc and syn-collisional granites. The consistency between the two samples on trace element plots, particularly in their REE patterns, demonstrates that the sediments most likely are derived from a relatively homogenous single source, of volcanic affinity.

3.2.5 Swift Current Granite and Other Regional Plutons

Major pre-Cambrian plutons intruding Marystown volcanics along the length of the peninsula, and proximal to known hydrothermal activity, are discussed in this section. Samples include granite from the Swift Current Intrusive Suite (SCIS), granite, granodiorite and diorite from the Burin Knee Intrusive Suite (BKIS; discussed in *Section 3.2.1*, above), and diorite and granodiorite (SCB-2) from the Seal Cove pluton located on the southwestern shore of the peninsula near the town of Garnish. The Seal Cove pluton is introduced here as it is one of the closest plutons to the Heritage prospect, with the exception of the extensive Devonian-aged granites of the St. Lawrence Intrusive Suite, and is also discussed in the following chapter on U-Pb geochronology. Although presumably part of the BKIS, the tonalite host rock from Stewart is not included, since it displays significant hydrothermal related HREE mobilization (even the very weakly altered samples of tonalite show minor variations and depletions in HREEs as demonstrated in *Section 3.2.1*, above).

3.2.5.1 Rock Type Classification

Regional plutonic rocks are plotted on rock classification diagrams in *Figures 3-18a-b*. The SCIS granites plot as *rhyolites*, the Seal Cove granodiorite as *rhyodacite-rhyolite*, the BKIS granodiorite as *rhyodacite*, the BKIS diorite as *dacite-andesite*, and the Seal Cove diorite as *andesite*, all following a *subalkaline* trend. When plotted on the

classification diagram of Miyashiro (1974; *Figure 3-18c*), samples follow a *calc-alkaline* trend.

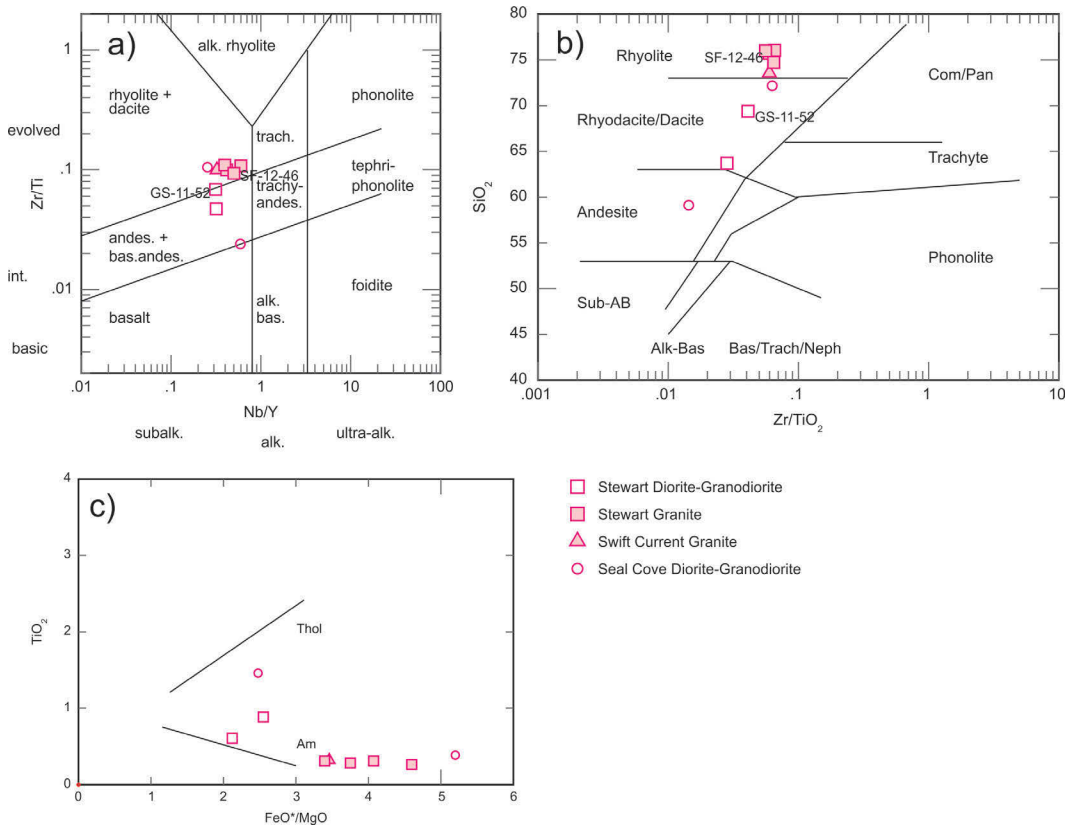

Figure 3-18*: Classification diagrams for samples of major regional plutonic suites that intrude Marystown volcanics on the Burin Peninsula, plotted on various classification diagrams; a) Zr/Ti vs. Nb/Y (Pearce, 1996; after Winchester and Floyd, 1977); b) SiO2 vs Zr/TiO2 (Winchester and Floyd, 1977); c) classification diagram of Miyashiro (1974). Thol=tholeiitic, Am=calc alkaline.*

3.2.5.2 Major Element Geochemistry

The major element compositions of all the plutonic samples are plotted against SiO_2 on Harker major element diagrams in *Figure 3-19.* A strong linear trend is evident in most of the plots. MgO, FeO*, CaO, and P_2O_5 all display strong negatively sloped linear trends. A single outlier occurs in the plot of P_2O_5, with the sample of BKIS diorite (GS-11-195) plotting at anomalously high concentrations. TiO_2 forms a slight upward sloping, curved trend, and Al_2O_3 and MnO form strong downward sloping, curved trends. The plots of K_2O and Na_2O display weak positive-sloping trends, with significant variation and scatter in values.

3.2.5.3 Trace Element Geochemistry

Samples are plotted on extended primitive mantle-normalized REE diagrams (*Figure 3-20 a) - h)*). The REE patterns of all of the samples (*a*) are generally parallel, and overlapping, with only slight variation in HREEs present. All samples also display clear negative Nb and Ti anomalies. Samples are then subdivided on subsequent plots both by location (*b-d*) and by rock type (*e-g*). When subdivided by rock type, the REE-patterns of similarly composed rocks from different localities display very similar, overlapping patterns. A gradual increase in the negative Nb and Ti anomalies and overall slope of the REE-pattern occurs progressively from diorite through granodiorite to granite.

Figure 3-21 displays various bivariate incompatible trace element plots. The samples form slightly positive linear trends when La_N and Th_N are plotted against SiO_2 as a fractionation index (*Figure 3-21 a-b*). The incompatible trace element ratio of $(La/Sm)_N$ is plotted against La_N in *Figure 3-21c.* Samples form a roughly horizontal trend, with samples clustered within a fairly narrow range of La/Sm values.

In the bivariate incompatible trace element ratio-ratio plots of $(La/Sm)_N$ vs. $(La/Yb)_N$, $(Th/Nb)_N$ vs. $(La/Yb)_N$, and $(Zr/Nb)_N$ vs. $(La/Nb)_N$ (*Figure 3-21 d-f*), samples consistently form a single, broad, sometimes linear-trending cluster. The Swift Current granite (SWC-2) displays an anomalously high Th/Nb value in *Figure 3-21e*.

When plotted on the discrimination diagram of Pearce et al. (1984), these intermediate-felsic plutonic rocks plot in the field of *volcanic-arc granites and syn-collisional granites* (*VAG+syn-COLG*; *Figure 3-22*).

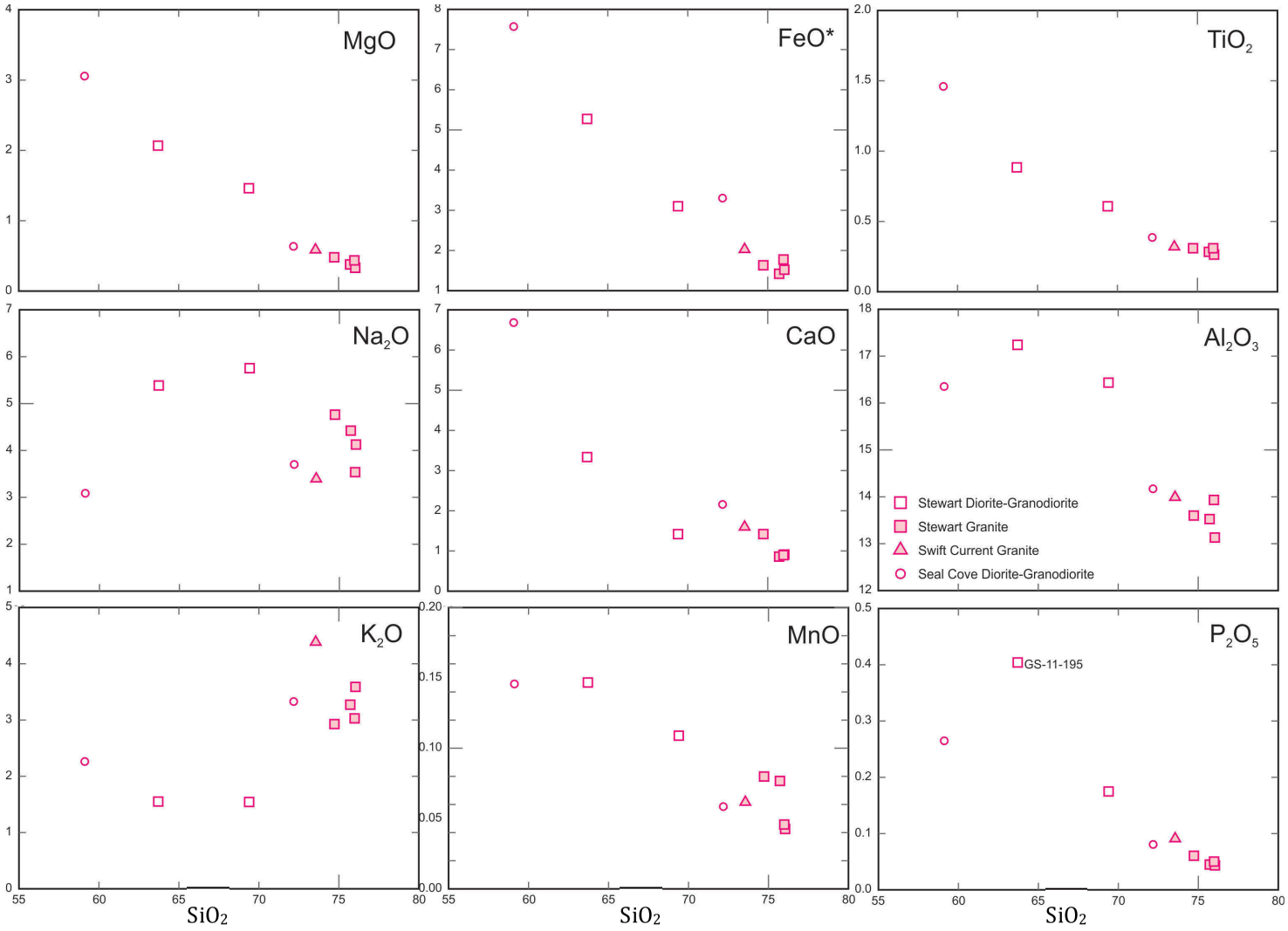

***Figure 3-19**: Major element data (wt. %) for major regional plutonic rocks, plotted against SiO_2.*

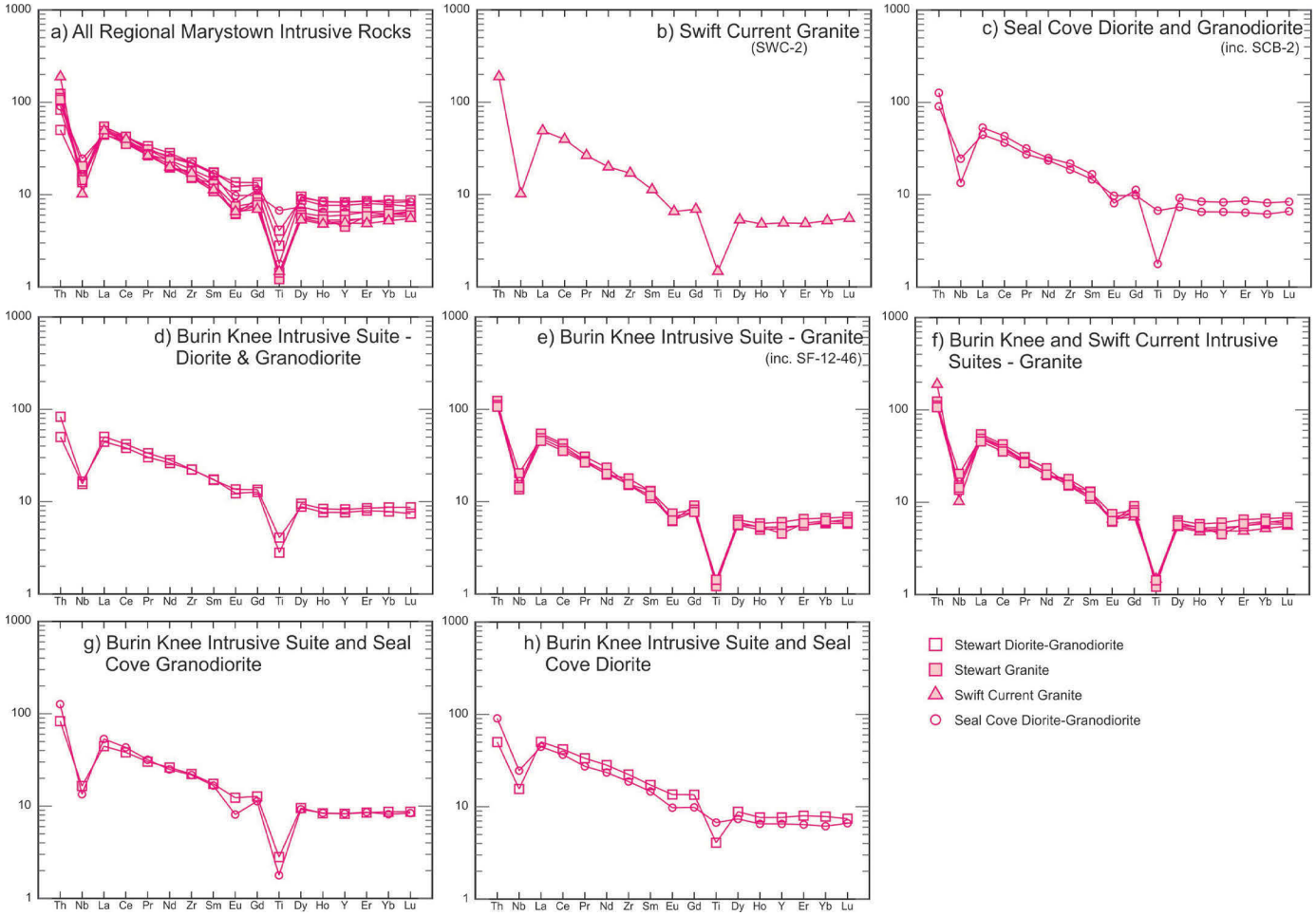

Figure 3-20: *Extended REE plots of regional plutonic rocks, normalized to primitive mantle values of Sun and McDonough (1989); a) All samples; b) Single sample of the Swift Current granite (SWC-2); c) Two samples from the Seal Cove pluton of diorite and granodiorite (including sample SCB-2, discussed in Chapter 4); d) Two samples of diorite and granodiorite from the BKIS (same as Figure 3-5g); e) Four samples of granite from the BKIS (including geochronology sample SF-12-46; same as Figure 3-5h); f) Granite from Swift Current and BKIS plotted together; g) Granodiorite from BKIS and Seal Cove plotted together; h) Diorite from the BKIS and Seal Cove plotted together.*

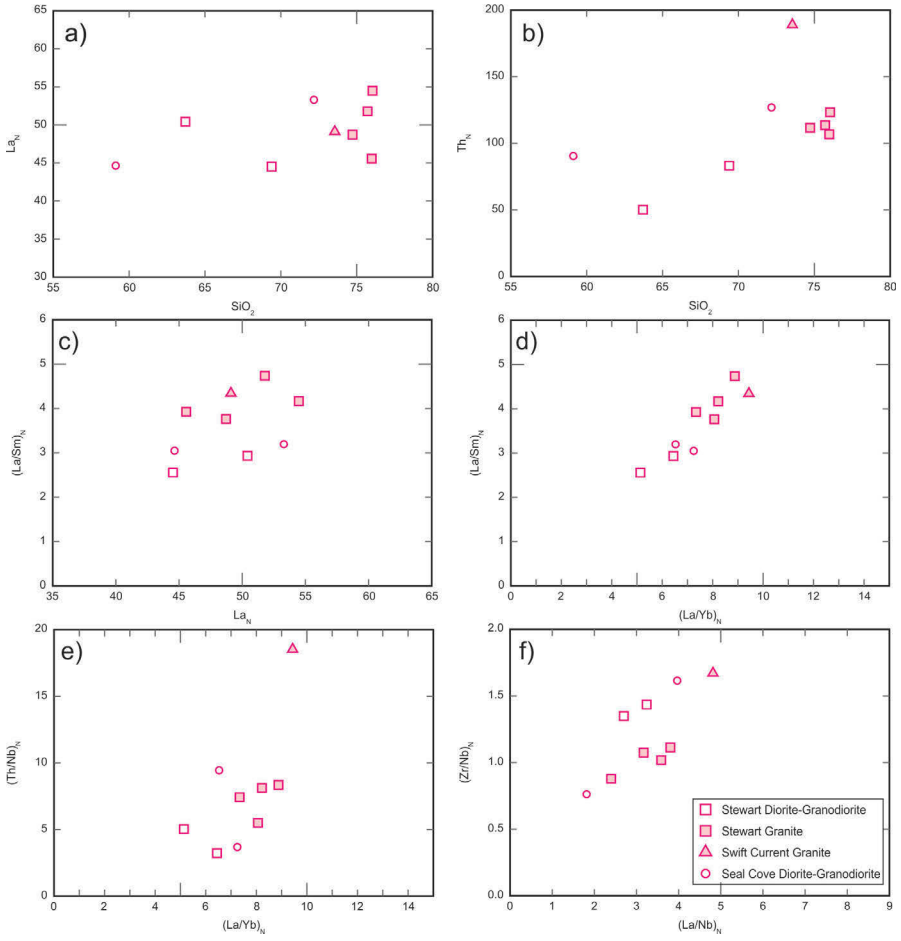

Figure 3-21*: Bivariate incompatible trace element plots for regional plutonic rocks. All elements normalized to primitive mantle values of Sun and McDonough (1989); a) La plotted against SiO_2 as a fractionation index; b) Th plotted against SiO_2 as a fractionation index; c) La/Sm vs. La; d-f) Ratio-ratio plots of La/Sm vs. La/Yb (d), Th/Nb vs. La/Yb (e), and Zr/Nb vs. La/Nb (f).*

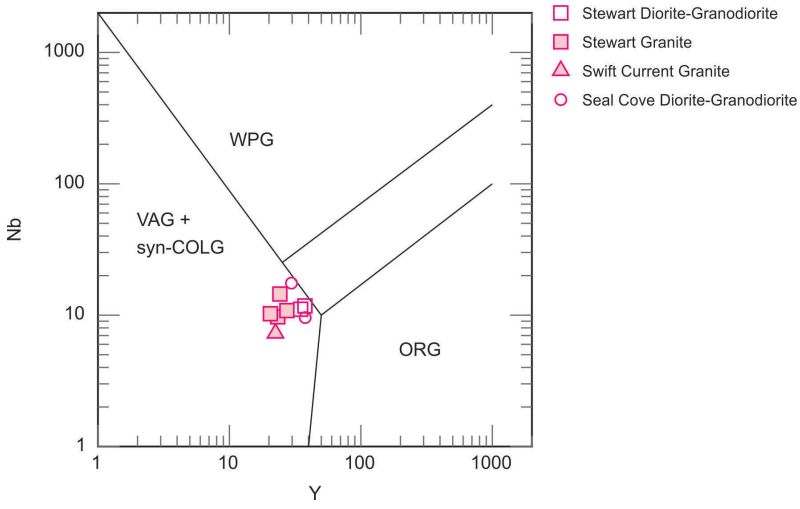

Figure 3-22*: Tectonic discrimination diagram for granites of Pearce et al. (1984). WPG=within plate granite, VAG=volcanic-arc granite, syn-COLG=syn-collisional granites, ORG=ocean-ridge granites.*

3.2.5.4 Swift Current Granite and Other Regional Plutons Interpretation

The plutonic rocks range in composition from andesite to rhyolite and plot along a subalkaline trend on the classification diagrams in *Figure 3-18,* consistent with field and petrographic observations and synonymous with their classification as diorite, granodiorite and granite. Single linear trends are evident on the rock classification diagrams, Harker major oxide diagrams, and bivariate trace element plots. Therefore, despite their broad geographical distribution, these samples appear to represent a related suite of plutonic rocks, originally derived from a single source, related to some extent through simple fractional crystallization, and of calc-alkaline affinity.

All of the samples also show geochemical signatures indicative of subduction-related magmatism, including a moderately sloped REE-pattern and presence of negative Nb and Ti anomalies. All of these features are consistent with formation in a volcanic arc environment, which is also demonstrated in the tectonic discrimination diagram of Pearce et al. (1984) where samples plot as volcanic arc granites. The gradual increase in negative Nb and Ti anomalies and overall slope of the REE-patterns seen occurring from diorite through granodiorite to granite might represent a temporal progression in arc maturity.

The Swift Current Granite displays significantly higher Th/Nb values than other plutonic rocks, but is otherwise very similar in chemistry. This might indicate the influence of more appreciable wall rock contamination from country rocks in this sample which was collected near the inferred roof of the pluton.

3.3 Musgravetown Group

3.3.1 Big Easy

The Big Easy prospect is a low-sulphidation style deposit situated approximately 50 km north of the peninsula proper, just northwest of the town of Clarenville (*Figure 2-1*). It is hosted primarily in interbedded sandstones and pebble conglomerates of epiclastic origin, and minor volcaniclastics, included within the Musgravetown Group.

Ten samples from Big Easy are presented in this section, four of which are hydrothermally altered. The altered samples are strongly silicified, and contain variable amounts of chlorite and pyrite. Four lithological subdivisions are discussed; hydrothermally altered (epiclastic) sandstones, andesitic accretionary lapilli tuff host rocks, flow banded rhyolite from Big Easy drill core and from the neighbouring West Princess prospect, and cross-cutting mafic dykes. Sandstones are included in the dataset and described relative to the other volcanic rocks since they are epiclastic in nature and appear derived from the adjacent volcanic rocks.

Two geochronology samples were collected from vicinity of the Big Easy prospect; one from the andesitic accretionary lapilli tuff (SF-13-181), and another from the West Princess rhyolite (GS-WPR). Sample MC-BE12-2 is an equivalent of MC-12-01, an intermediate composition dyke that was age-dated in 2012 (Clarke, 2013), and will also be discussed in *Chapter 4*.

3.3.1.1 Rock Type Classification

On the classification diagram of Pearce (1996; *Figure 3-23a*), samples generally form a *subalkaline* trend, with the West Princess rhyolites plotting in the *dacite-rhyolite* field, the altered sandstones ranging from *basaltic andesite* to *dacite*, the accretionary andesitic tuff plotting as an *andesite*, and the cross-cutting mafic dykes ranging from *basalt* to *basaltic andesite*. On the classification diagram of Winchester and Floyd (1977; *Figure 3-23b*), the mafic dykes and West Princess rhyolites plot in similar fields, but the hydrothermally altered sandstones and accretionary tuff are shifted into more felsic compositional fields, particularly SF-13-181 and GS-11-329. The flow banded rhyolite from Big Easy drill core (sample GS-13-021; DDH BE-11-05) plots at the boundary between *subalkaline* and *alkaline rhyolite* in *Figure 3-23a*, but plots distinctly as an *alkaline rhyolite* in *Figure 3-23b*.

On the classification diagram of Miyashiro (1974; *Figure 3-23c)*, the subalkaline sandstones and volcanic rocks plot along a *calc-alkaline* trend, while the mafic dykes

adhere to a more *tholeiitic* trend. One of the West Princess rhyolite samples is not shown as it plots with an extreme FeO*/MgO ratio, but still along trend with the other samples.

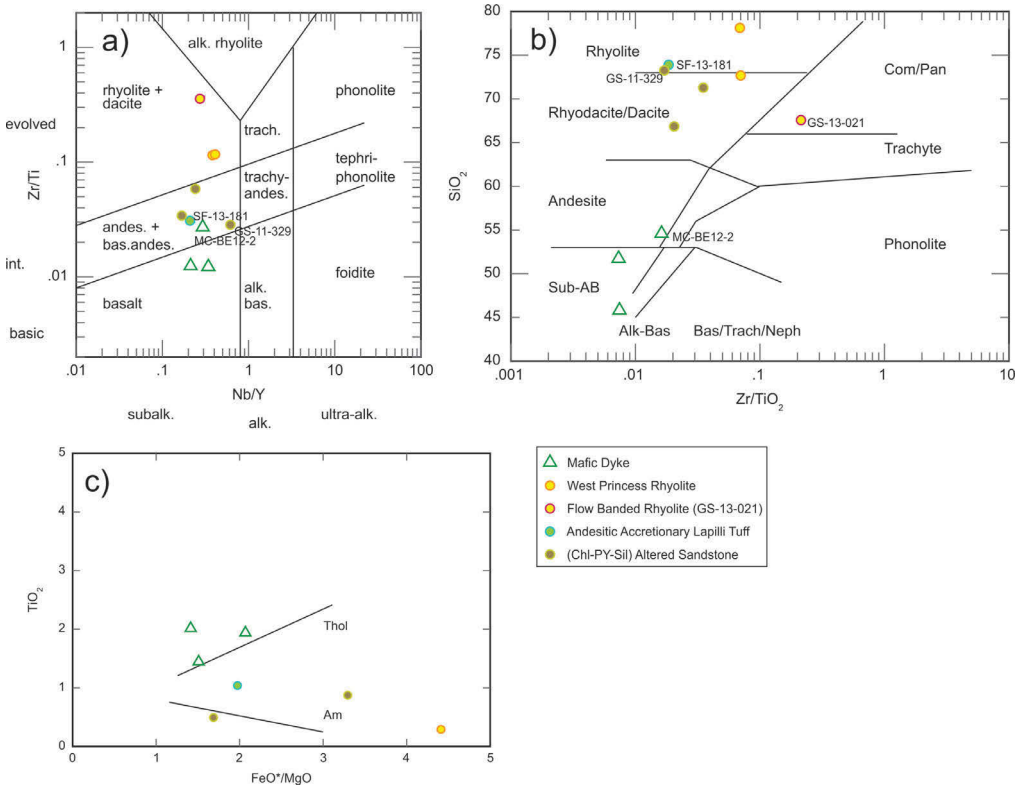

Figure 3-23*: Classification diagrams for Musgravetown Group volcanics and sediments and cross-cutting mafic dykes from Big Easy; a) Zr/Ti vs. Nb/Y (Pearce, 1996; after Winchester and Floyd, 1977); b) SiO_2 vs Zr/TiO2 (Winchester and Floyd, 1977); c) classification diagram of Miyashiro (1974). Thol=tholeiitic, Am=calc alkaline.*

3.3.1.2 Major Element Geochemistry

Samples are plotted on Harker-type major element variation diagrams in *Figure 3-24*. Sample SF-13-181 is known from field and petrographic evidence to be strongly silicified by hydrothermal activity. To account for this, it is also shown in *Figure 3-24* projected to a lower SiO_2 value based on its compositional shift between the classification diagrams in *Figure 3-23 a-b*. GS-11-329 is also strongly silicified, but is not projected to lower SiO_2 values, since it fairly consistently plots as an outlier in *Figure 3-24*, regardless of this shift in SiO_2.

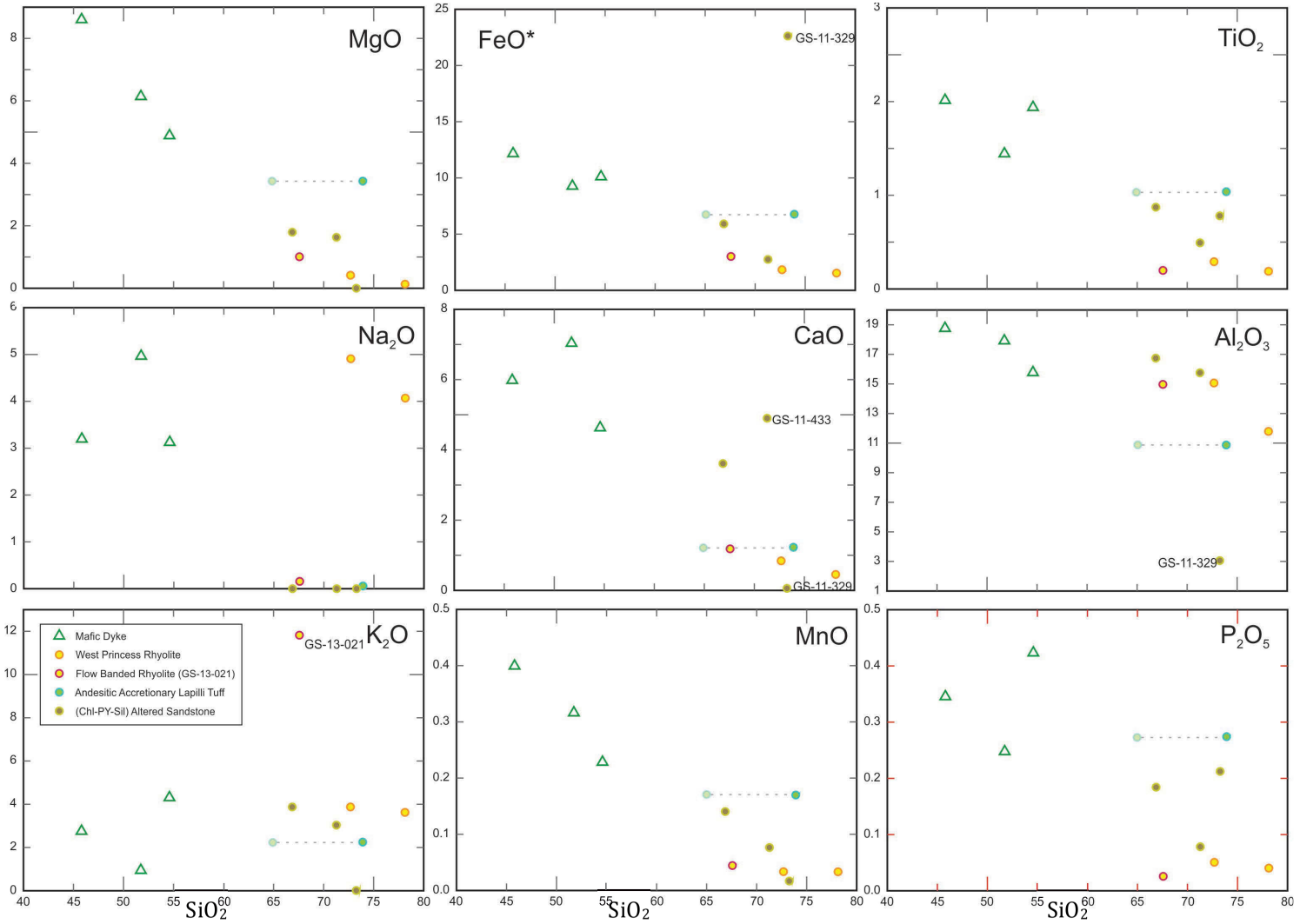

***Figure 3-24**: Major element data (wt. %) for Musgravetown Group volcanics and sediments and cross-cutting mafic dykes from the Big Easy prospect.*

For the most part, samples form distinct linear trends. Negatively sloped trends occur in the plots of MgO, FeO*, TiO_2, CaO, Al_2O_3, MnO, and P_2O_5. Outliers include GS-11-329 which shows anomalously high FeO*, and anomalously low MgO, Al_2O_3 and CaO concentrations, GS-11-433 with elevated CaO, and SF-13-181 with low Al_2O_3.

A weak positively sloped trend is evident for samples of the West Princess rhyolite and mafic dykes on the plot of Na_2O, although neither appears to be affected by hydrothermal alteration petrographically. In contrast, rhyolite sample GS-13-021, also apparently unaffected by hydrothermal alteration, shows significant depletion. The hydrothermally altered sediments and tuff show similar depletion of Na_2O.

A fairly flat trend is produced on the plot of K_2O, with the exception of GS-11-329 (depleted), and GS-13-021 (considerably enriched).

3.3.1.3 Trace Element Geochemistry

Samples are plotted on primitive mantle-normalized extended REE diagrams in *Figure 3-25 a) – e)*. The andesitic tuff (*a*) shows a shallow to moderately sloping REE-pattern with small negative Nb and Ti anomalies. The sandstones (*b*) plot similarly to the tuff, but with more pronounced negative Nb and Ti anomalies, and one sample (GS-11-329) showing distinct HREE depletion. The two units are plotted together for comparison in *Figure 3-25e* (GS-11-329 excluded), where their REE patterns show significant overlap.

Rhyolite from the West Princess prospect and from Big Easy drill core (GS-13-021) show distinct REE-patterns (*Figure 3-25c*). The West Princess rhyolite samples display a moderately sloping REE-pattern with distinct negative Nb and Ti anomalies and a minor negative Eu anomaly. Rhyolite sample GS-13-021 shares a similar negative Nb anomaly, but is enriched in HREE relative to the West Princess samples, forming a flatter overall REE-pattern, and contains considerably larger negative Ti and Eu anomalies.

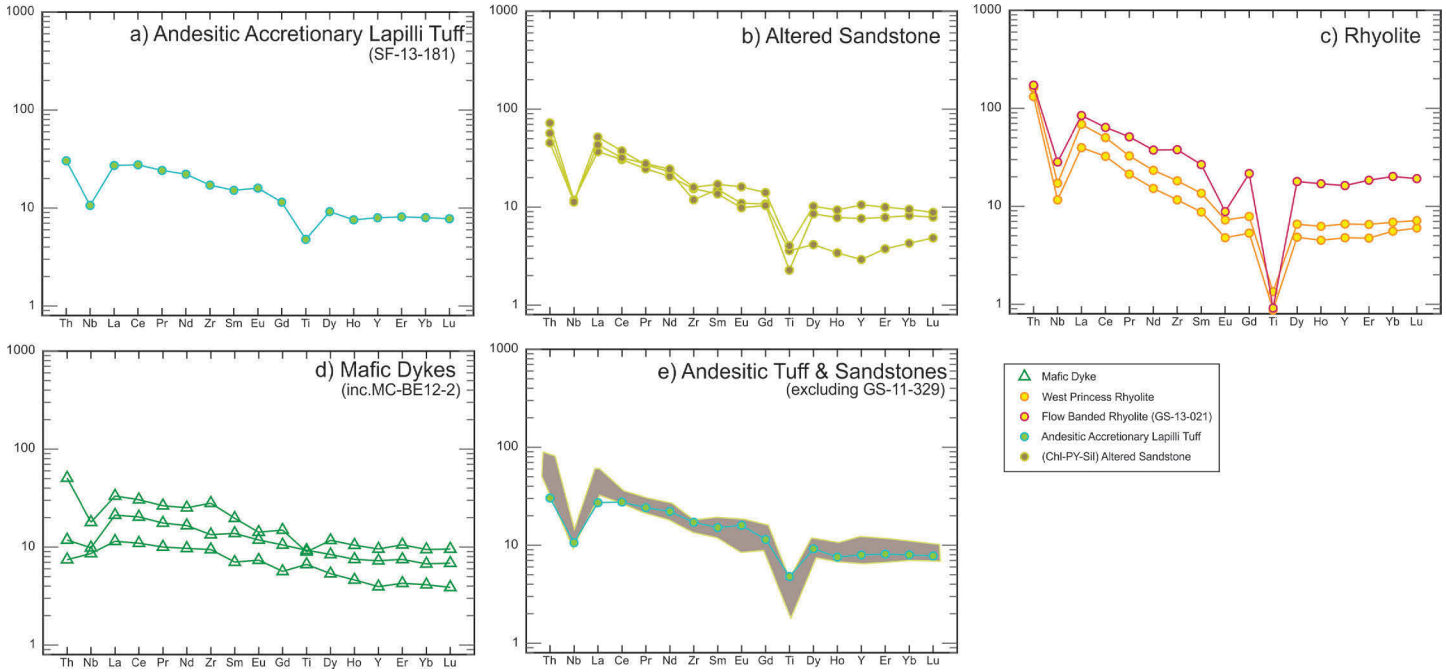

***Figure 3-25**: Extended REE plots for epiclastic sediments, volcanic rocks and mafic dykes from the Big Easy prospect, normalized to primitive mantle values of Sun and McDonough (1989); a) Andesitic accretionary lapilli tuff host rock (geochronology sample SF-13-181); b) Epiclastic sandstone host rocks variably altered to chlorite and silica and containing variable pyrite mineralization (sample GS-11-329 with abundant pyrite); c) Flow banded rhyolite from Big Easy drill core (DDH BE-11-05; GS-13-021) and two samples of flow banded rhyolite from the West Princess prospect (geochronology sample GS-WPR); d) Cross-cutting mafic dykes; e) Andesitic tuff (a) plotted over epiclastic sandstones (b) (excluding GS-11-329).*

The mafic dykes (*d*) form relatively flat REE patterns. The basaltic samples are for the most part devoid of any anomalous peaks or troughs, while the basaltic-andesite (MC-BE12-2) displays a small, but distinct negative Nb anomaly, and minor negative Eu and Ti anomalies.

Various bivariate incompatible trace element plots are shown in *Figure 3-26*. Most Samples form positive linear trends when the incompatible trace elements Nb_N and La_N are plotted against fractionation indices of La_N and SiO_2, respectively (*Figure 3-26 a-b*). Rhyolite sample GS-13-021 forms above the main trend line in both plots, and mafic dyke sample MC-BE12-2 plots slightly above the trend line in *Figure 3-26a*. *Figure 3-26c* highlights the negative Eu anomaly by plotting EuN against Eu* (where $Eu^* = \sqrt{(Sm_N x Gd_N)}$). Once again, the samples form a linear trend, except rhyolite GS-13-021, which plots as a distinct outlier to this main trend. In the bivariate incompatible trace element ratio-ratio plot of $(Zr/Nb)_N$ vs. $(La/Nb)_N$ (*Figure 3-26 d*) all samples form a single cluster.

The mafic dykes are plotted on the tectonic discrimination diagram for basalts in *Figure 3-27a*. The basaltic samples plot in the field of *continental basalt*, and the andesitic basalt sample (MC-BE12-2) plots at the triple-point boundary between *calc-alkali volcanic arc basalt*, *continental basalt*, and *volcanic arc tholeiite*. The sandstones and intermediate to felsic volcanic rocks are plotted together on the tectonic discrimination diagram for granites in *Figure 3-27b*. The sandstones, andesitic tuff, and West Princess rhyolite samples all plot together in the field of *volcanic arc and syn-collisional granites* (*VAG+syn-COLG*), and rhyolite sample GS-13-021 plots separately in the field *of within plate granites* (*WPG*).

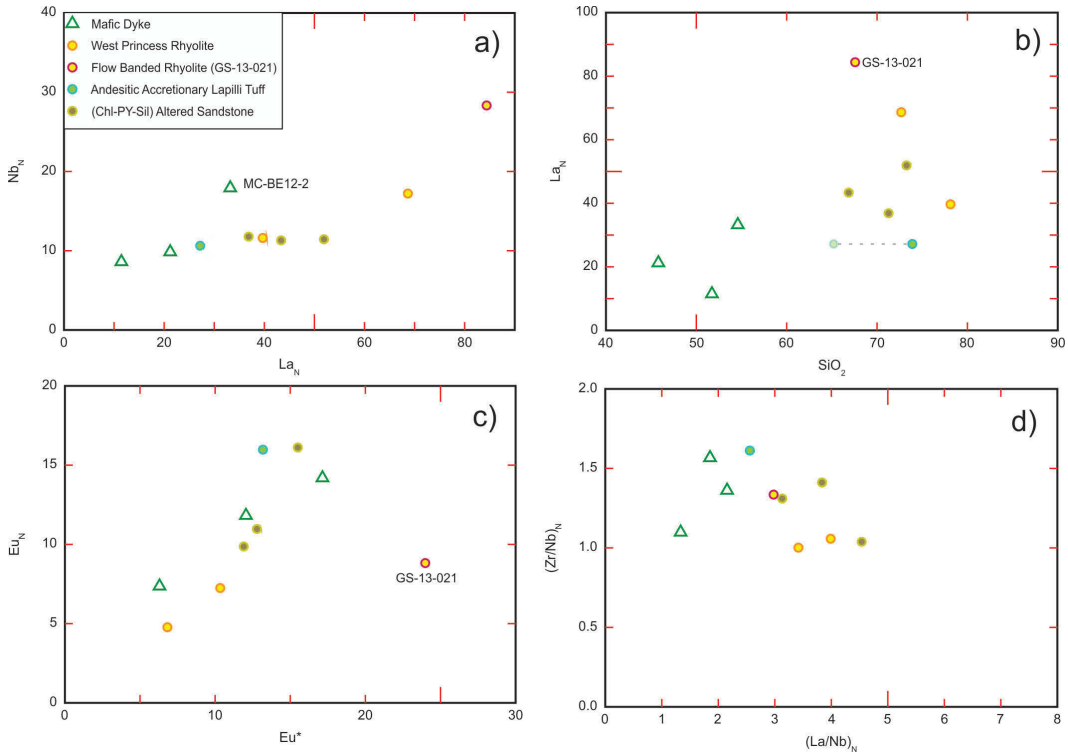

***Figure 3-26**: Bivariate incompatible trace element plots for volcanic and epiclastic sedimentary rocks, and cross-cutting mafic dykes of the Musgravetown Group from the Big Easy (and West Princess) prospect. All elements normalized to primitive mantle values of Sun and McDonough (1989); a) Nb plotted against La; b) La plotted against SiO_2 as a fractionation index; c) Eu vs. Eu* (where Eu*= $\sqrt{(Sm_N x Gd_N)}$), plotted to highlight Eu anomalies; d) Ratio-ratio plot of Zr/Nb vs. La/Nb.*

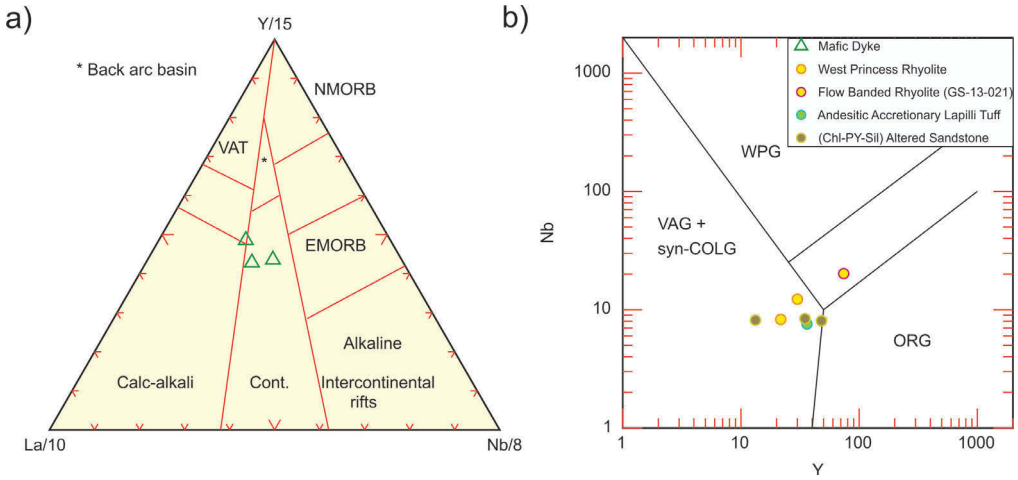

***Figure 3-27**: a) Mafic dykes cross-cutting Musgravetown volcano-sedimentary rocks, plotted on the tectonic discrimination diagram for basalts of Cabanis and Lecolle (1989) (Calc-alkali=calc-alkali volcanic arc basalts, VAT=volcanic-arc tholeiites, Cont=continental basalts); b) Intermediate-felsic volcanic rocks and epiclastic sediments of the Musgravetown Group plotted on the tectonic discrimination diagram for granites of Pearce et al. (1984) (WPG=within plate granites, VAG=volcanic-arc granite, syn-COLG=syn-collisional granites, ORG=ocean-ridge granites).*

3.3.1.4 Big Easy Interpretation

On the classification diagram of Pearce (1996) volcanic rocks from the West Princess prospect plot as rhyodacite, the accretionary lapilli tuff plots as andesite, the sandstones vary from basaltic andesite to dacite, and the mafic dykes plot as basalt (and one sample as basaltic andesite) – but all lie along a subalkaline trend. These rock classifications are generally consistent with field and petrographic observations. On the classification diagram of Winchester and Floyd (1977), unaltered samples plot similarly, but the hydrothermally altered epiclastic sandstones and accretionary tuff are shifted to more felsic compositions, particularly SF-13-181 and GS-11-329. This is the result of significant silicification associated with the hydrothermal alteration. Here, the effects of hydrothermal alteration are also evident in other major oxides, demonstrated particularly well by the anomalous concentrations present in the most altered sample, GS-11-329. Element mobility associated with hydrothermal alteration includes FeO* enrichment from pyrite mineralization, and significant depletion in MgO, Al_2O_3, CaO, Na_2O and K_2O. Na_2O is perhaps the most mobile under these conditions, since all of the hydrothermally altered rocks show significant depletion in this element. Sample GS-11-329 also displays HREE depletion (*Figure 3-25b*) presumably related to the hydrothermal alteration, which is empirically similar to that noted for samples affected by advanced argillic alteration associated with the high-sulphidation systems.

On the classification diagrams, rhyolite sample GS-13-021 plots separately from the other rhyolites and along a separate, alkaline trend from all of the other samples. It also has a distinctly higher K_2O concentration than all of the other samples (Figure 3-24), further demonstrating its alkalinity. GS-13-021 is an outlier on most of the bivariate trace element plots (*Figure 3-26*) and lies in the separate field for within plate granite on the tectonic discrimination diagram for granites (*Figure 3-27b*). Based on this evidence, this unit is interpreted to represent a distinct volcanic phase, unrelated to the other volcanic and epiclastic rocks. This is further demonstrated on the extended-REE plot in *Figure 3-25c*, where this sample shows significant HREE enrichment and considerably larger negative Eu and Ti anomalies relative to the other rhyolites. Furthermore, this extended-

REE pattern, and the position of the sample in the within plate granite field, are extremely similar to the rhyolites of the Long Harbour Group (presented below in *Section 3.4*). Although this rhyolite occurs lower in the stratigraphy at the Big Easy prospect, it occurs only in fault-bounded contact with the host epiclastic sediments, permissive of inclusion in the younger Long Harbour Group.

The remaining samples generally form single linear trends on the rock classification diagrams, Harker major oxide diagrams, and bivariate trace element plots. The intermediate to felsic volcanics and epiclastic sediments are interpreted to represent a single volcanic suite derived from a single source. All of these units display distinct negative Nb and Ti anomalies compatible with their formation in a volcanic arc environment, further supported by their designation as volcanic arc and syn-collisional granites on the tectonic discrimination diagram for granites (*Figure 3-27b*). The andesitic tuff and epiclastic sandstones show overlapping patterns while the West Princess rhyolites show similar but steeper REE-patterns interpreted to be the result of LREE enrichment during the progression of arc maturity. The REE-patterns of these lithologies are similar to those of the Marystown Group, and are also of calc-alkaline affinity based on the classification diagram of Miyashiro (1974).

Despite their linear correlations with the other samples, the mafic dykes might not be as closely related. The basaltic andesite dyke (MC-BE12-2) contains a small negative Nb anomaly, demonstrating an affiliation with subduction zone related magmatism, but plots at the triple junction between calk-alkaline volcanic arc basalt, volcanic arc tholeiite, and continental basalt. The two basaltic dykes do not show distinct negative Nb anomalies, and plot completely within the continental basalt field. All of the dykes also appear to be of tholeiitic affinity based on the classification diagram of Miyashiro (1974). The dykes are interpreted as being associated with late-arc extension, subsequent to active subduction. All of the samples cluster on the incompatible trace element ratio-ratio plot in *Figure 3-26d,* which typically would indicate a genetically closely related suite of rocks. However, these more detailed lines lines of evidence support the subdivision of units as described above.

3.4 Long Harbour Group

3.4.1 Long Harbour

The Long Harbour prospect is a low-sulphidation style deposit situated on the northern shore of Fortune Bay (*Figure 2-1*), and hosted in volcanics of the Long Harbour Group. Only one rock type is present in the immediate vicinity of the prospect, hosting the mineralized veins – a flow banded rhyolite, which was sampled for lithogeochemistry and geochronology (SF-12-56). To present a broader representation of the Long Harbour Group, other Long Harbour volcanics were included, collected from approximately 20 km northeast of the prospect. Two rock types are represented in the following content: 1) rhyolites (flow banded, massive and volcaniclastic varieties), which account for the majority of the volcanic rocks that make up the Long Harbour Group, and 2) cross-cutting mafic dykes.

3.4.1.1 Rock Type Classification

On the classification diagram of Pearce (1996; *Figure 3-28a*) volcanic rocks of the Long Harbour Group plot in the field of *alkaline rhyolite* and the cross-cutting mafic dykes plot in the *subalkaline* fields of *basalt* and *basaltic andesite*. Samples plot similarly on the classification diagram of Winchester and Floyd (1977; *Figure 3-28b*). The subalkaline mafic dykes are also plotted on the classification diagram of Miyashiro (1974) in *Figure 3-28c*, where they adhere to a *tholeiitic* trend.

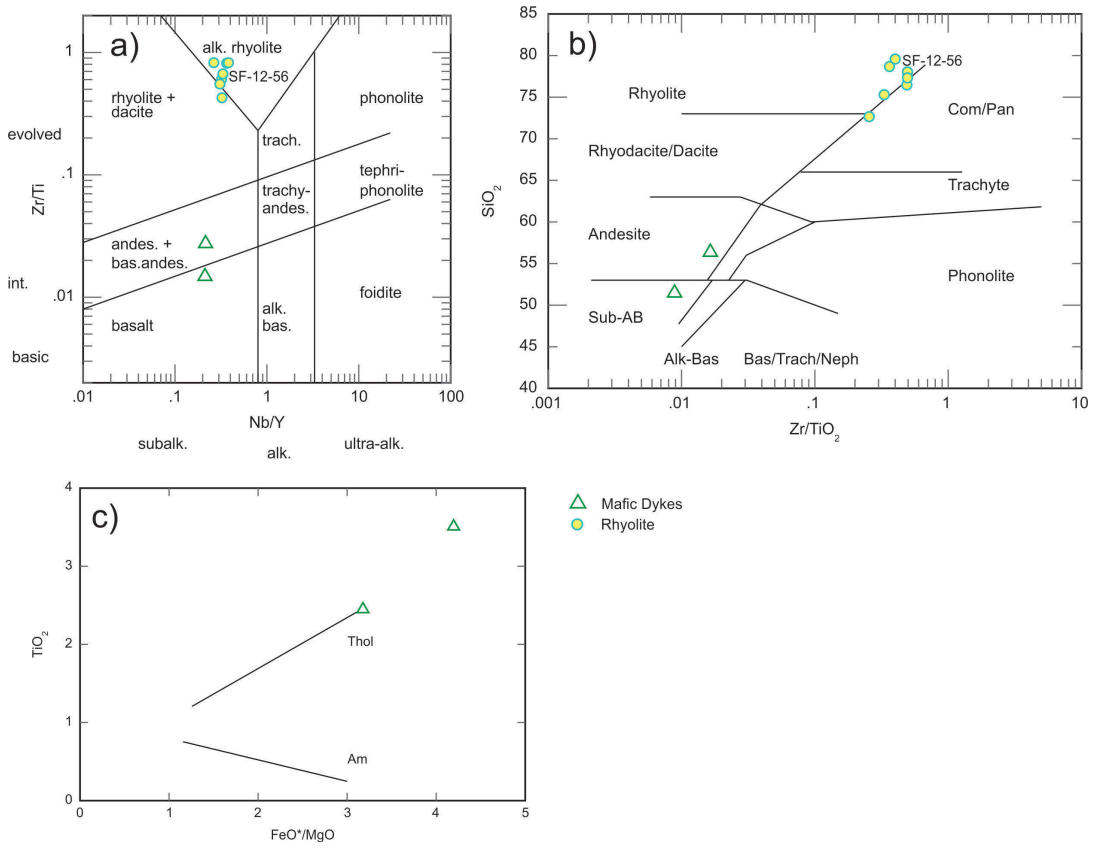

Figure 3-28*: Classification diagrams for volcanic and intrusive rocks of the Long Harbour Group; a) Zr/Ti vs. Nb/Y (Pearce, 1996; after Winchester and Floyd, 1977); b) SiO_2 vs Zr/TiO_2 (Winchester and Floyd, 1977); c) classification diagram of Miyashiro (1974). Thol=tholeiitic, Am=calc alkaline.*

3.4.1.2 Major Element Geochemistry

The major element compositions of all samples are plotted against SiO_2 on Harker-type major element variation diagrams in *Figure 3-29*. Despite the small sample size, and limited compositional variation, the samples generally define linear trends

Negatively sloped trends are evident in the plots of FeO*, TiO_2, CaO, and MnO, without any outliers. A strong trend is also displayed in the plot of Al_2O_3, where samples form a negatively sloping, curved trend line. A positive trend is present in the plot of K_2O, with only one sample of rhyolite, GS-11-362, plotting at a slightly lower concentration.

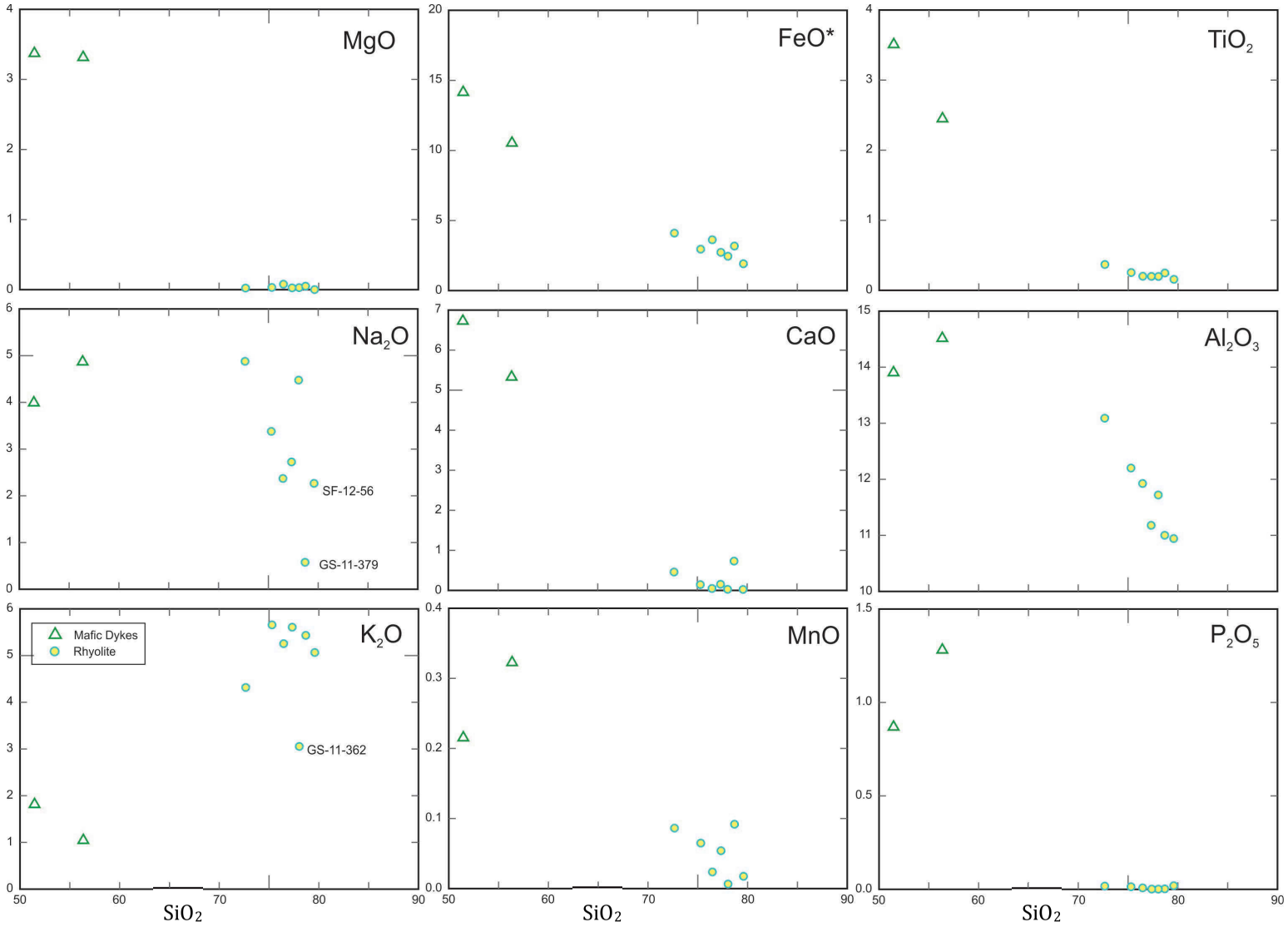

***Figure 3-29**: Major element data (wt. %) for volcanic rocks of the Long Harbour Group, plotted against SiO_2.*

A clear trend is not evident in the plot of Na_2O, which displays significant variation amongst samples of rhyolite. MgO and P_2O_5 display an overall negative correlation, but a clear trend line is not present, as the rhyolites show significant depletion in both elements.

3.4.1.3 Trace Element Geochemistry

The Long Harbour Group rhyolites and cross-cutting mafic dykes are plotted on primitive mantle-normalized extended REE diagrams in *Figure 3-30*. The rhyolites form an overall shallowly sloping REE pattern with a low LREE to HREE ratio (*a*). They contain a small negative Nb anomaly, a large negative Ti anomaly, and variable positive Zr and negative Eu anomalies. Based on these patterns, the rhyolites can be further subdivided into two groups, shown in *Figure 3-30 b-c*. The first group, including samples of red and grey volcaniclastic and flow-banded rhyolites, displays higher LREEs and smaller positive Zr and negative Eu anomalies (*b*). The second group, which includes red massive and flow-banded rhyolites, displays lower LREEs and more significant positive Zr and negative Eu anomalies (*c*).

The mafic dykes form a shallowly sloping, relatively flat REE pattern. They display small negative Nb anomalies and one sample displays a small negative Ti anomaly.

Figure 3-31 displays various bivariate incompatible trace element plots. Samples form positive linear trends when the incompatible trace elements Nb_N and Th_N are plotted against fractionation indices of Zr and SiO_2, respectively (*Figure 3-31a-b*). The incompatible trace element ratio of $(La/Sm)_N$ is plotted against La_N in *Figure 3-31c,* where samples form a strong horizontal linear trend, showing very little variation in $(La/Sm)_N$ values. In the bivariate incompatible trace element ratio-ratio plots of $(La/Sm)_N$ vs. $(La/Yb)_N$, $(Th/Nb)_N$ vs. $(La/Sm)_N$, and $(Zr/Nb)_N$ vs. $(La/Nb)_N$ (*Figure 3-31d-f*), samples consistently plot as a single cluster.

The mafic dykes are plotted on the tectonic discrimination diagram for basalts in *Figure 3-32a*, where they plot at the triple-point boundary between *calc-alkali volcanic arc basalt*, *continental basalt*, and *volcanic arc tholeiite*. The rhyolites plot in the lower portion of the *within plate granite* field (*WPG*) on the tectonic discrimination diagram for granites in *Figure 3-32b*.

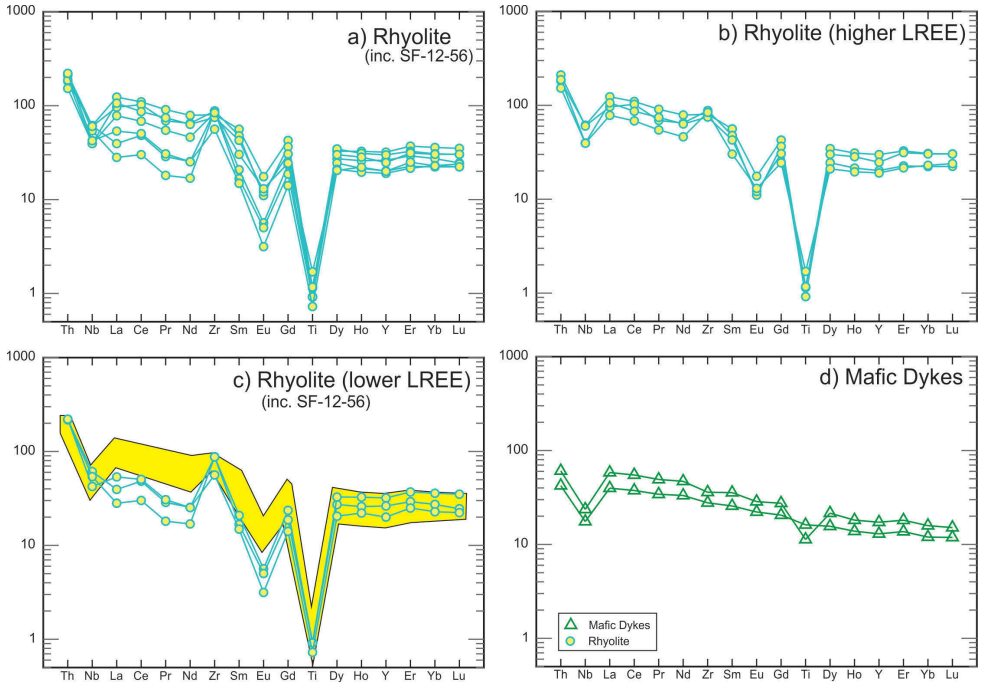

***Figure 3-30**: Extended REE plots for volcanic and intrusive rocks of the Long Harbour Group, normalized to primitive mantle values of Sun and McDonough (1989); a) Rhyolites, including geochronology sample SF-12-56; b) Sub-group of rhyolites containing higher LREE concentrations and smaller positive Zr and negative Eu anomalies. Rock types include red and grey volcaniclastic and flow banded rhyolite; c) Sub-group of rhyolites containing lower LREE concentrations and larger positive Zr and negative Eu anomalies, plotted over REE patterns from b. Rock types include red massive and flow banded rhyolites, and include geochronology sample SF-12-56; d) Mafic dykes.*

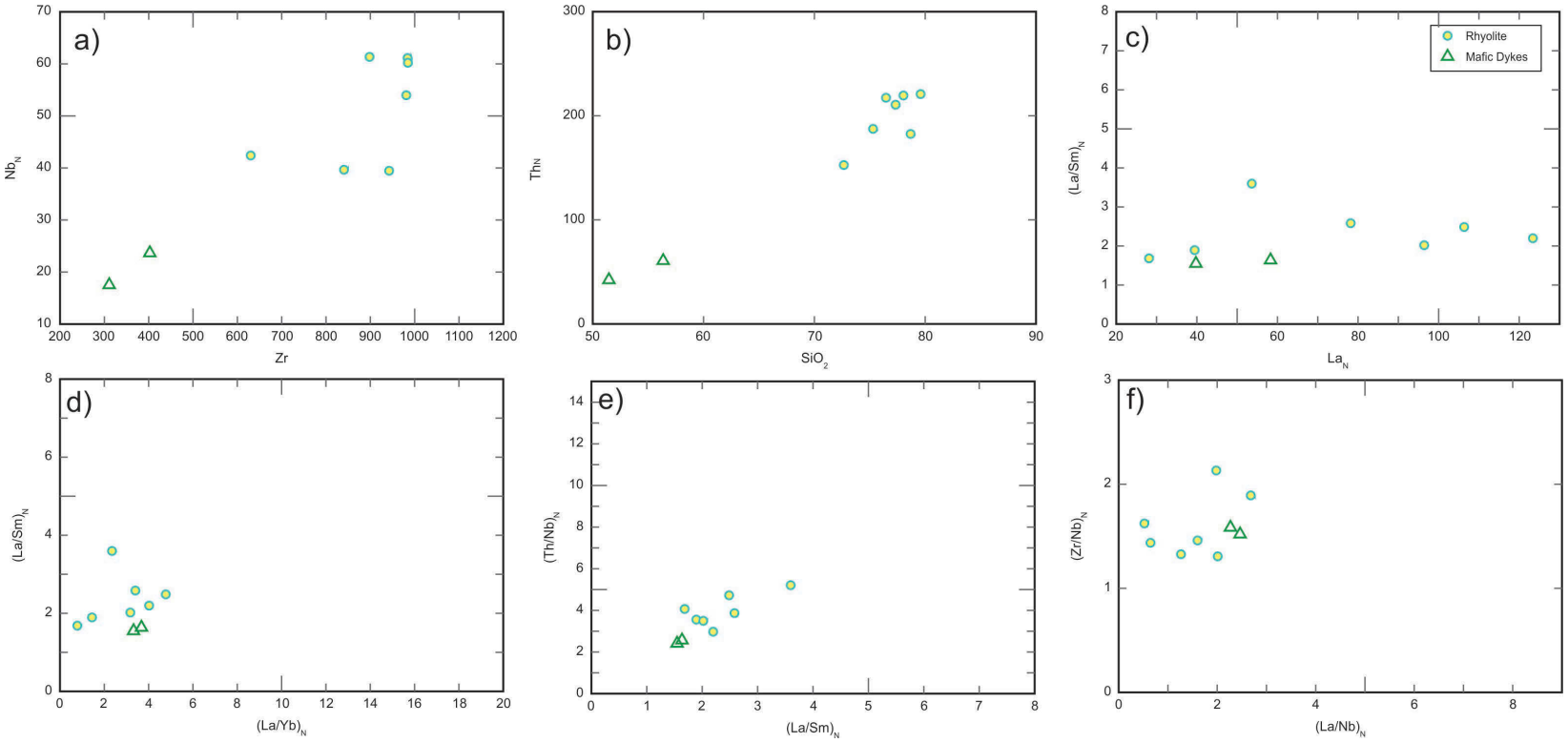

Figure 3-31*: Bivariate incompatible trace element plots for rocks of the Long Harbour Group. All elements normalized to primitive mantle values of Sun and McDonough (1989); a) Nb plotted against Zr as a fractionation index; b) Th plotted against SiO_2 as a fractionation index; c) La/Sm vs. La; d-f) Ratio-ratio plots of La/Sm vs. La/Yb (d), Th/Nb vs. La/Sm (e), and Zr/Nb vs. La/Nb (f).*

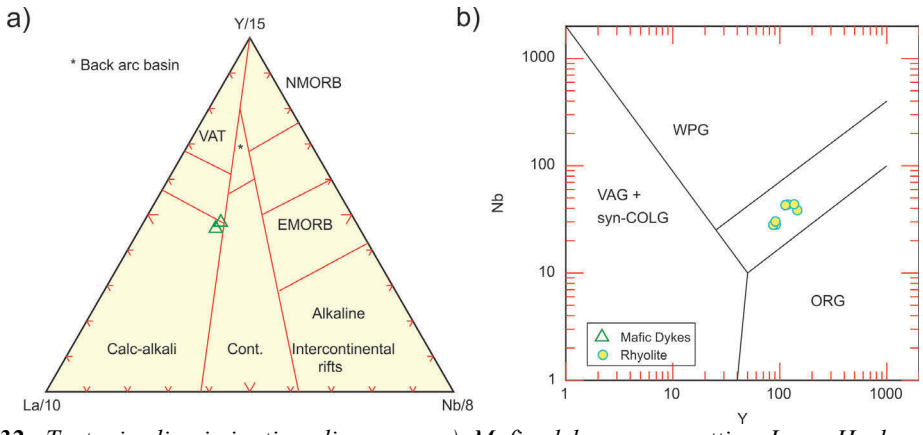

***Figure 3-32**: Tectonic discrimination diagrams; a) Mafic dykes cross-cutting Long Harbour volcanics plotted on the tectonic discrimination diagram for basalts of Cabanis and Lecolle, 1989. Calc-alkali=calc-alkali volcanic arc basalts, VAT=volcanic-arc tholeiites, Cont=continental basalts; b) Long Harbour rhyolites plotted on the tectonic discrimination diagram for granites of Pearce et al., 1984. WPG=within plate granite, VAG=volcanic-arc granite, syn-COLG=syn-collisional granites, ORG=ocean-ridge granites.*

3.4.1.4 Long Harbour Interpretation

The geochemical signatures of rocks from the Long Harbour Group are distinctly different from those of the Marystown and Musgravetown Groups, and represent a bimodal assemblage of alkaline rhyolites, and tholeiitic basalt to basaltic andesite dykes.

Although not directly related through fractional crystallization, the rhyolites and later mafic dykes appear to be derived from a single source, based on the strong linear trends formed on the Harker major oxide diagrams, and the bivariate trace element plots. The consistent La/Sm values produced, and tight clustering of samples on incompatible trace element ratio-ratio plots, provides further indication that these rocks are genetically related, despite their compositional polarity.

The rhyolites are alkaline and contain a high concentration of silica (~80% SiO_2). All rhyolites share consistent small negative Nb anomalies, large negative Ti anomalies, and a relatively flat overall REE-pattern (compared to the calc-alkaline volcanics of the Marystown Group) as a result of HREE enrichment. The rhyolites can be subdivided into two groups based on LREE content and magnitude of positive Zr and negative Eu

anomalies. However, they are interpreted to represent a genetically related progression, whereby progressive fractionation of LREE-containing mineral phases and plagioclase lead to lower LREE content and a more substantial negative Eu anomaly (*Figure 3-30*). The rhyolites are significantly depleted in MgO and P_2O_5 on major element plots (*Figure 3-29*), interpreted to be a result of their high silica content and high degree of fractionation. They also show significant variation in Na_2O content, a result of metasomatism during subsequent greenschist facies metamorphism.

The mafic dykes are basalt to basaltic andesite in composition and plot as subalkaline tholeiites on classification diagrams (*Figure 3-28*). They display relatively flat REE patterns (*Figure 3-30*), with the exception of a small negative Nb anomaly, consistent with a more juvenile tholeiitic magma association

This suite of rocks is interpreted to have formed during a late stage of arc volcanism in an extensional tectonic regime, possibly within a back arc environment. This is indicated by the consistent presence of small negative Nb anomalies in the REE patterns of the bimodal rock types, and in the overall bimodal nature of the assemblage. This is also consistent with the tectonic discrimination diagrams (*Figure 3-32*), where rhyolites are classified as within plate granites, perhaps forming in association with more well developed continental crust of a mature arc system, further removed from the leading edge of the subduction zone in a more distal back arc environment. Similarly, mafic dykes plot at the boundary between calc-alkaline arc basalts, continental basalts, and arc tholeiites, representing more juvenile mafic magmas, interpreted to be intruding as extension-related dykes. Furthermore, these dykes are geochemically similar to those crosscutting the Musgravetown Group and are interpreted to be correlative.

3.5 Discussion

The purpose of this final section is to compare and contrast some of the main geochemical features outlined above for the Marystown, Musgravetown, and Long Harbour Groups. Hydrothermally altered samples discussed above as showing evidence of significant trace element mobility have been omitted from further discussion. This

includes GS-11-329 epiclastic sediment (Big Easy), and all of the tonalite samples from Stewart. All of the data presented for the Marystown Group including the Stewart, Tower, Hickey's Pond and Heritage prospects, Grandy's Pond Arenite Belt, and regional plutonic rocks is synthesized and discussed first, as this was the group examined in most detail. This is followed by a final discussion integrating all of the Burin Peninsula data, and highlighting important correlations and relationships between the Marystown, Musgravetown, and Long Harbour Groups.

3.5.1 Marystown Regional Synthesis

All of the rock units analyzed from prospects of the regionally extensive Marystown Group show geochemical signatures diagnostic of subduction zone-related magmatism, and consistent with formation in an arc environment.

Extended REE plots comparing volcanic, sedimentary and intrusive rocks of the Marystown Group, as collected from the different prospects/geographic locations on the Burin Peninsula, are shown in *Figure 3-33*. Mafic Volcanic Rocks (*a*) from Stewart and Heritage each display particularly distinct REE-patterns. The mafic flows and volcaniclastics of the Lower Volcanic Unit, and the porphyritic andesitic-basalt intrusive at Stewart are geochemically distinct, not only from the mafic rocks at Heritage, but from all other sampled lithologies in the Marystown Group - displaying relatively flat REE-patterns with small negative Nb anomalies. They are interpreted to represent a more juvenile phase of arc volcanism, perhaps in an ocean island arc setting, with compositions closer to volcanic-arc tholeiites. In contrast, the mafic volcanics (flows) from Heritage are calc-alkaline volcanic arc basalts, displaying an enrichment in LREE and more pronounced negative Nb anomaly, relative to the mafic volcanics at Stewart. These are considered to be representative of a more mature phase of arc volcanism.

Intermediate Volcanic Rocks (*b*) from all four of the prospects in the Marystown Group show nearly identical, overlapping REE-patterns, and are similar in morphology to the REE-patterns of the Heritage mafic volcanics in (a), with the exception of a stronger negative Ti anomaly.

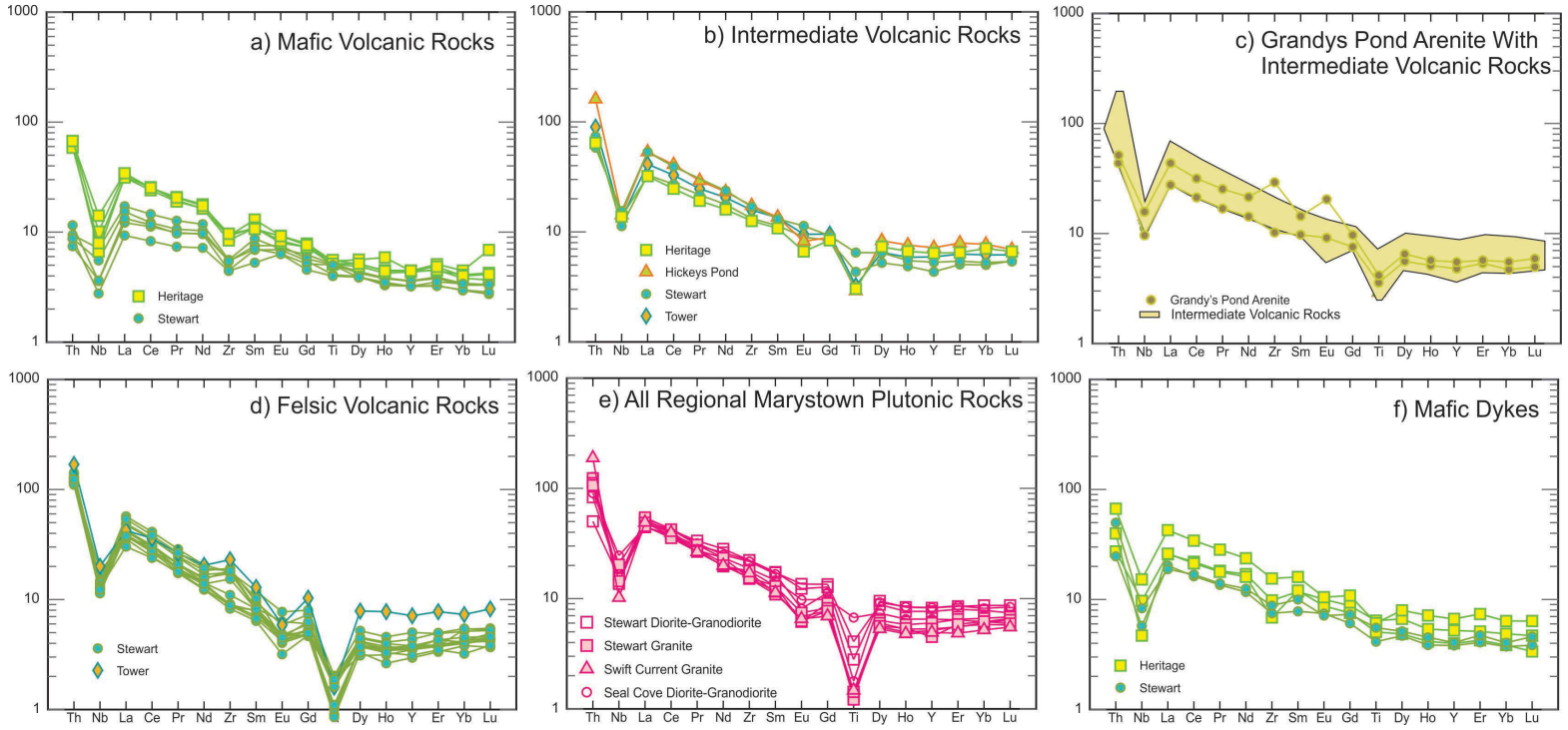

Figure 3-33*: Extended REE plots for volcanic, epiclastic-sedimentary, and intrusive rocks of the Marystown Group, normalized to primitive mantle values of Sun and McDonough (1989); a) Mafic volcanic rocks; b) Intermediate volcanic rocks; c) Epiclastic sediments of the Grandy's Pond Arenite Belt plotted over intermediate volcanic rocks from b; d) Felsic volcanic rocks; e) Regional plutonic rocks; f) Mafic dykes.*

The epiclastic sediments of the Grandy's Pond Arenite Belt are plotted over REE-patterns of the Intermediate Volcanic Rocks from (*b*) in *(c)*, and also show correlative patterns. These sediments are therefore likely derived predominantly from mafic to intermediate volcanic rocks of the Marystown Group. The elevated Zr and Eu in sample SF-12-149 are likely a consequence of modest preferential concentration of zircon and plagioclase clasts during sedimentation.

The Felsic Volcanic Rocks in (*d*) were predominantly sampled from Stewart, but one additional rhyodacite was collected from Tower. When plotted together, the felsic samples display very similar REE-patterns, with the exception of slightly higher HREEs present in the Tower sample. The REE-patterns of the felsic volcanic rocks show an overall increase in slope between the LREEs and HREEs, and more pronounced negative Nb and Ti anomalies, relative to the patterns of the mafic to intermediate Marystown rocks. The presence of these pronounced arc signatures occurring in conjunction with a shift to more felsic compositions is interpreted to represent a progression in arc maturity within a consanguineous volcanic suite.

Plutonic Rocks (*e*) spanning the Burin Peninsula, and ranging in composition from diorite to granite also show very similar, generally overlapping REE-patterns, and appear to represent a closely related suite of plutonic rocks. Their patterns are also correlative with those of the felsic volcanics.

Mafic Dykes (*f*) from the Heritage and Stewart prospects all display similarly shaped and parallel REE-patterns, including distinct negative Nb anomalies, and plot with a systematic shift upwards corresponding to a compositional gradient from basalt to basaltic andesite. They are interpreted to represent a single, related group of mafic intrusives, and although they cross-cut some of the volcanic rock, they appear closely related to the overall volcanic-arc derived stratigraphy of the Marystown Group.

The bivariate incompatible trace element ratio-ratio plots shown in *Figure 3-33 a-d* display overall clustering patterns of samples, indicating a genetic relationship amongst all of the rock units sampled from the Marystown Group. The Swift Current granite plots

at anomalously high Th/Nb values (*Figure 3-33 c-d*), but otherwise plots consistently with the other samples of the Marystown Group. The anomalous Th/Nb value is most likely the result of wallrock contamination of this sample by Marystown Group volcanics.

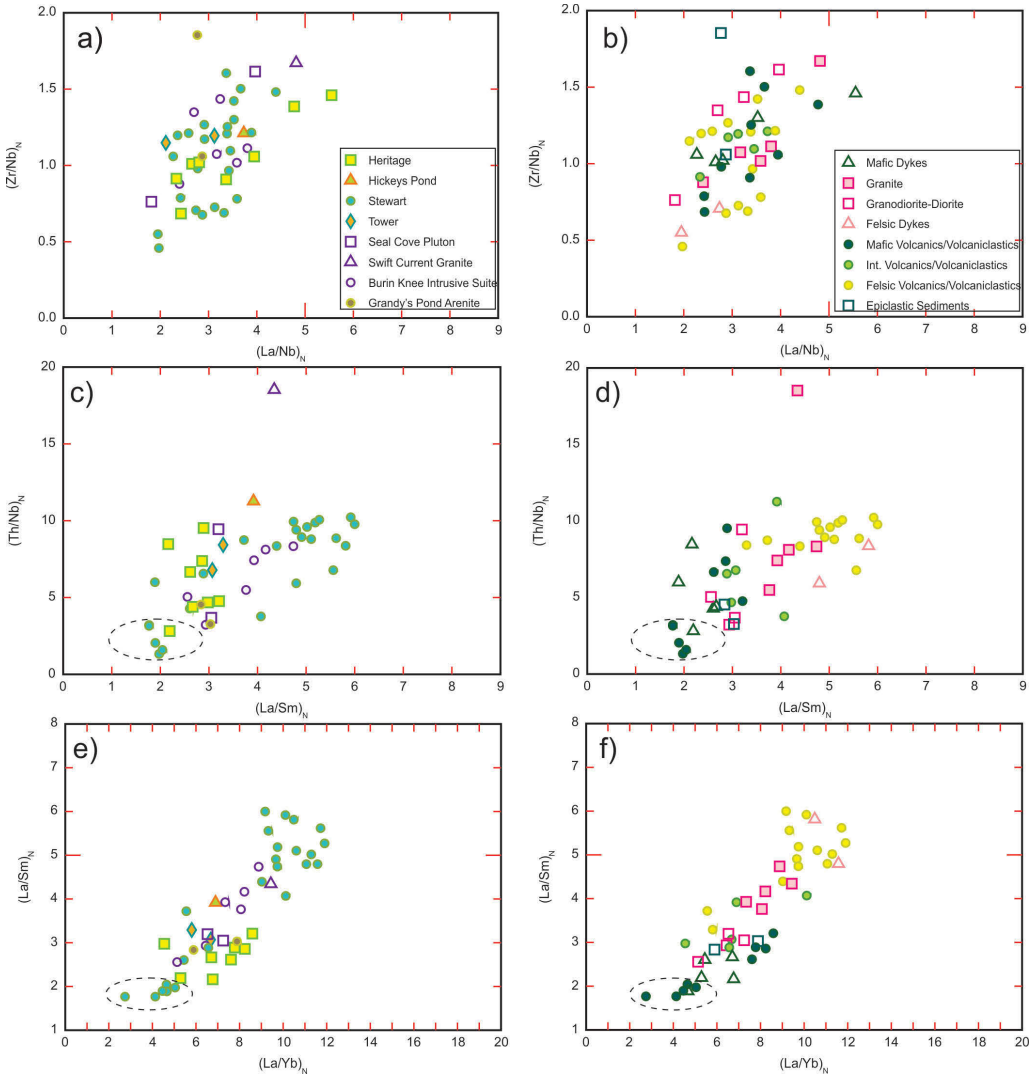

Figure 3-34*: Bivariate incompatible trace element ratio-ratio plots for volcanic, epiclastic-sedimentary, and intrusive rocks of the Marystown Group. All elements normalized to primitive mantle values of Sun and McDonough (1989). Samples are plotted and subdivided both by geographic/deposit location and by rock type; a&b) Zr/Nb vs. La/Nb; c&d) Th/Nb vs. La/Sm; e&f) La/Sm vs. La/Yb.*

The interpreted progression in arc maturity, depicted by changes in REE-patterns between mafic and felsic volcanic rocks, is further illustrated in *Figure 3-34 e-f,* where La/Sm (a measurement of LREE enrichment) is plotted against La/Yb (a measurement of overall REE slope). Mafic rocks from the Lower Volcanic Unit at Stewart, interpreted as

more juvenile arc tholeiites, plot in a distinct cluster towards the bottom left (highlighted by dashed ellipse). The remaining volcanic and intrusive rocks form a positive linear trend with a general transition from mafic and intermediate compositions into more felsic compositions at higher values. A variety of magma differentiation processes are inevitably responsible for this linear variation, including varying degrees of fractional crystallization, contamination, partial melting or magma mixing, nevertheless, the sampled lithologies of the Marystown Group appear to represent a single regional-scale volcanic arc-related suite.

3.5.2 Regional Synthesis of the Marystown, Musgravetown and Long Harbour Groups

Volcanic rocks of the Marystown and Long Harbour Groups display very distinct geochemical trends, representative of two discrete volcanic suites. This is particularly evident when felsic volcanic rocks are plotted on extended REE plots, as shown in *Figure 3-35*. The Marystown/Musgravetown felsic volcanics comprise *Group 1*, and the Long Harbour felsic volcanics are subdivided into *Groups 2 &3*.

The Marystown/Musgravetown Felsic Volcanics (*Group 1*) show REE-patterns typical of mature volcanic arc rocks, including moderately sloped trends and substantial negative Nb anomalies, resulting from subduction related processes. In contrast, the Long Harbour Felsic Volcanics (*Groups 2&3*) display much smaller negative Nb anomalies, flatter overall trends, and significant negative Eu anomalies, and are interpreted to have formed during late stage arc volcanism in an extensional tectonic regime, possibly within a back arc environment (*Section 3.3.1*). As discussed in *Section 3.3.1,* the latter two groups, although showing some distinct geochemical features, are considered to be closely affiliated and related through progressive fractional crystallization.

Volcanic and epiclastic rocks of the Musgravetown Group generally appear to be consanguineous with rocks of the Marystown Group, and therefore likely formed in a similar maturing volcanic arc environment. This is demonstrated in *Figure 3-35b* and

Figure 3-36a, where samples of flow banded rhyolite (from the West Princess prospect) and the andesitic tuff host rock at the Big Easy prospect display REE-patterns that overlap with those of compositionally equivalent rocks of the Marystown Group. In addition, REE-patterns of the epiclastic sediments of the Musgravetown Group overlap with those of the epiclastic sediments of the Grandy's Pond Arenite Belt (*Figure 3-36b*), which also exhibits an affiliation with the volcanics of the Marystown Group.

Sample GS-13-021, a flow banded rhyolite from drill core at the Big Easy prospect, was collected as a possible representative of Musgravetown volcanics. However, this unit consistently displays geochemical signatures synonymous with those of the Long Harbour Group (e.g. *Figure 3-35c*). This rhyolite occurs lower in the stratigraphy at the Big Easy prospect, along a fault-bounded contact with the host sediments, and is interpreted as a possible subsurface extension of the Long Harbour Group, emplaced via faulting.

Three subdivisions of mafic dykes, interpreted to represent separate generations, can be identified across the region from extended REE plots (*Figure 3-37*). The mafic dykes cross-cutting volcanic rocks of the Marystown Group (*Figure 3-37b*) are all calc-alkaline and appear to be closely affiliated with subduction zone related magmatism and with the surrounding volcanic-arc-derived stratigraphy of the Marystown Group (*Section 3.5.2*). A second group of mafic dykes (*Figure 3-37c*) cross-cuts both the Long Harbour and Musgravetown Groups. These are tholeiitic and appear to be affiliated with late extension-related-magmatism of the Long Harbour Group, with the corollary that the cross-cut Musgravetown Group rocks must be older than the Long Harbour Group. A third group of mafic dykes (*Figure 3-37d*), also of tholeiitic affinity, shows similar REE-patterns to 'Group 2' mafic dykes, but does not display the negative Nb anomaly contained in every other sampled rock unit. Therefore, it is interpreted to not have formed in association with subduction zone related magmatism, and may mark a cessation in arc-volcanism in the region.

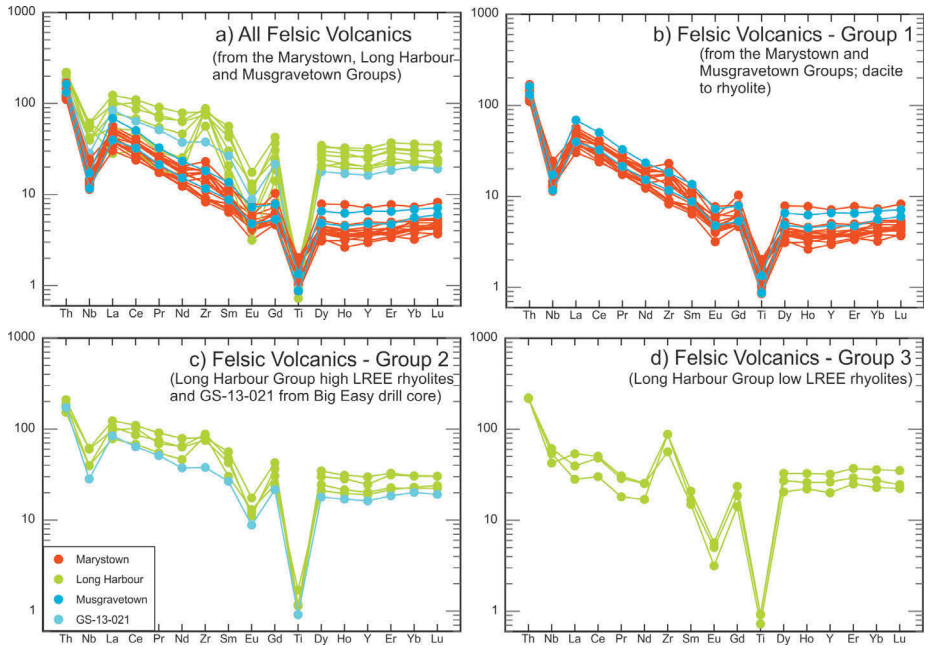

***Figure 3-35**: Extended REE plots for all felsic volcanic rocks (dacite to rhyolite flows and volcaniclastics) from the Marystown, Musgravetown and Long Harbour Groups, normalized to primitive mantle values of Sun and McDonough (1989); a) All felsic volcanic rocks; b) Group 1 felsic volcanics – flow banded rhyolite from the Musgravetown Group (including geochronology sample GS-WPR) and dacitic-rhyolitic volcaniclastics of the Marystown Group (including geochronology samples SF-12-43, GS-11-167, SF-12-142) ; b) Group 2 felsic volcanics – flow banded and volcaniclastic rhyolites from Long Harbour and sample GS-13-021 (flow banded rhyolite) from Big Easy drill core; c) Group 3 felsic volcanics – flow banded rhyolites from Long Harbour (including geochronology sample SF-12-56).*

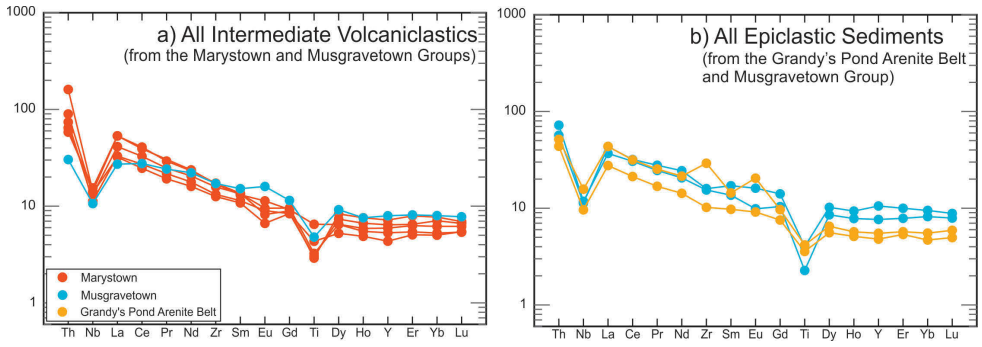

***Figure 3-36**: Extended REE plots for all sampled intermediate volcaniclastic rocks and epiclastic sediments, normalized to primitive mantle values of Sun and McDonough (1989); a) All intermediate volcaniclastic rocks from the Marystown Group (including geochronology samples SF-12-27 and SF-13-180) and Musgravetown Groups (including geochronology sample SF-13-181); b) All epiclastic sediments from the Grandy's Pond Arenite Belt (including geochronology sample SF-12-148) and Musgravetown Group.*

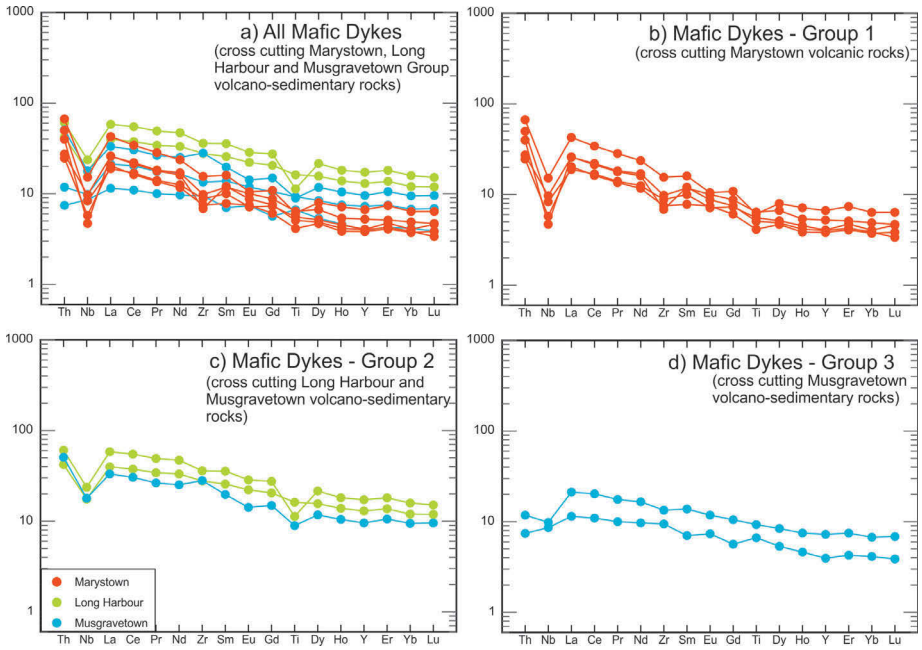

Figure 3-37*: Extended REE plots for mafic dykes (basalt to basaltic andesite) cross-cutting the Marystown, Musgravetown and Long Harbour Groups, normalized to primitive mantle values of Sun and McDonough (1989); a) All mafic dyke samples; b) Group 1 mafic dykes – calc-alkaline dykes, cross-cutting and associated with arc-volcanism of the Marystown Group; c) Group 2 mafic dykes – tholeiitic dykes cross-cutting the Long Harbour and Musgravetown Groups (MC-BE12-2), associated with late-arc-extensional tectonics of the Long Harbour Group; d) Group 3 mafic dykes – late post-arc tholeiitic dykes crosscutting Musgravetown Group.*

All of these regional correlations are also illustrated below on bivariate trace element plots (*Figure 3-38*) and tectonic discrimination diagrams (*Figure 3-39*).

Volcanic and intrusive rocks of the Marystown Group, epiclastic sediments of the Grandy's Pond Arenite Belt, and volcanic and epiclastic rocks of the Musgravetown Group form a single linear trend on bivariate trace element plots and cluster together on incompatible trace element ratio-ratio plots. The various units are interpreted to be a related suite of rocks, representative of various facies within a regionally extensive volcanic arc environment, and recording a complex combination of magma differentiation processes typical of arc environments and subduction zones, and a general progression in arc maturity. This progression is particularly evident in *Figure 3-38c* where a gradual enrichment in La/Sm correlates with a systematic shift in rock composition from basalt to rhyolite. A similar pattern is displayed in the incompatible trace element ratio-ratio plot of Th/Nb vs. La/Yb (*Figure 3-38f*).

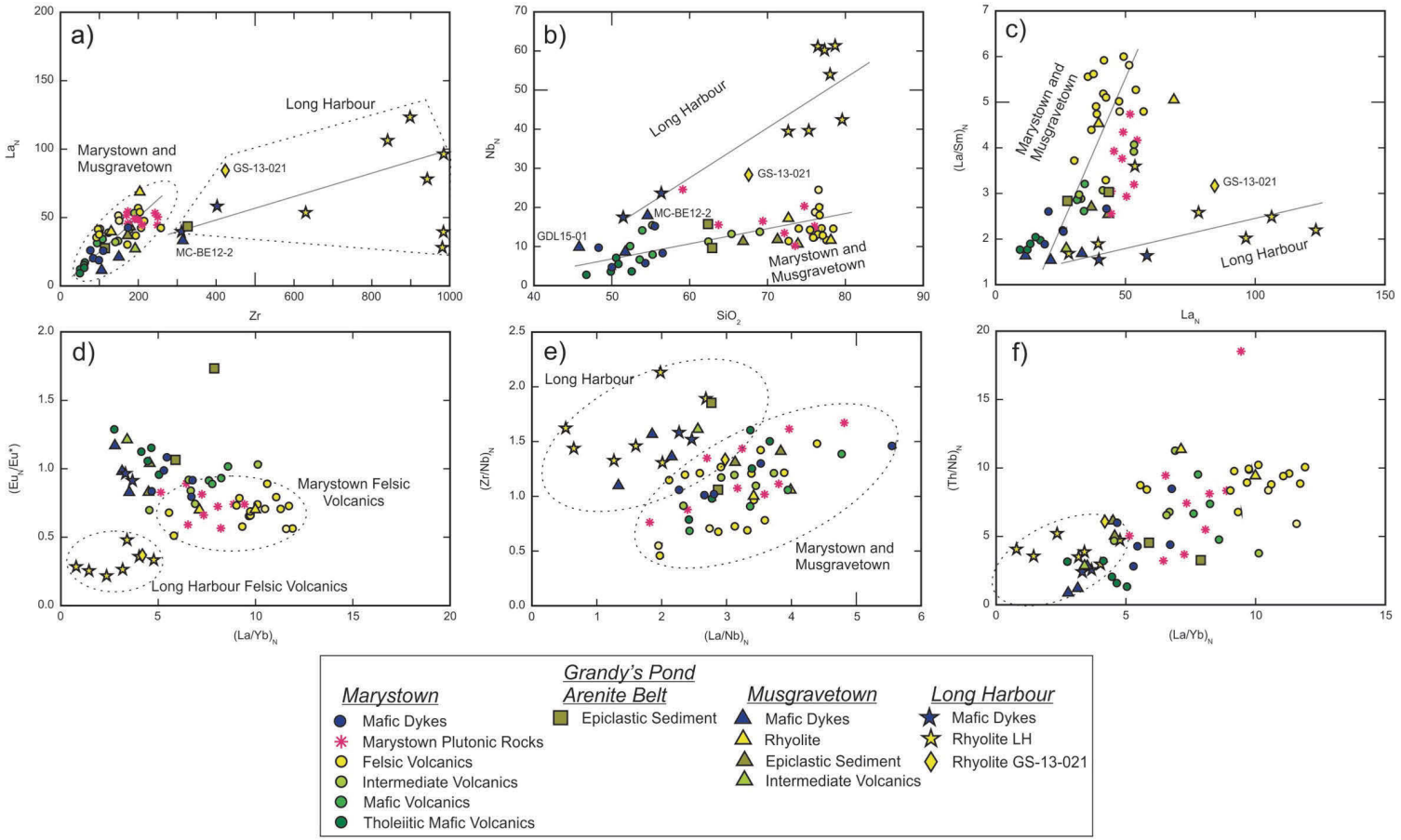

***Figure 3-38**: Bivariate incompatible trace element plots for volcanic, epiclastic-sedimentary, and intrusive rocks of the Marystown, Musgravetown and Long Harbour Groups, and Grandy's Pond Arenite Belt. All elements normalized to primitive mantle values of Sun and McDonough (1989); a) La plotted against Zr as a fractionation index; b) Nb plotted against SiO_2 as a fractionation index; c) La/Sm vs. La; d-f) Ratio-ratio plots of Eu_N/Eu^* vs. La/Yb (d), Zr/Nb vs. La/Nb (e), and Th/Nb vs. La/Yb (f). Plots show distinct trends and clusters between Long Harbour volcanics (including mafic dykes cross-cutting Long Harbour and Musgravetown rocks, and sample GS-13-021 from Big Easy), and Marystown and Musgravetown volcanics, sediments and intrusives (including Grandy's Pond Arenite Belt).*

The relationship amongst these units is further demonstrated when plotted on tectonic discrimination diagrams. Intermediate to felsic volcanic and plutonic rocks, and epiclastic sedimentary rocks of similar composition cluster tightly in the field of volcanic arc granites on the tectonic discrimination diagrams for granites (*Figure 3-39 b-c*). On the tectonic discrimination diagram for basalts (*Figure 3-39a*) the tholeiitic basalts and basaltic andesites from the Lower Volcanic Unit at the Stewart prospect plot with compositions closer to the volcanic-arc tholeiites field (labeled as '1' in inset). As discussed in *Section 3.5.1* these are interpreted as an earlier, more juvenile phase of arc volcanism, possibly in an ocean island arc setting. Other basaltic and basaltic andesite volcanic rocks of the Marystown Group, plot further into the calc-alkali volcanic-arc field (labeled as '2' in inset) representing a progression to a more mature phase of arc volcanism, and overall appear to be compositionally and genetically related to the mafic dykes cross-cutting the Marystown Group.

In contrast, volcanic and intrusive rocks of the Long Harbour Group (including sample GS-13-021) and mafic dykes cross-cutting the Long Harbour and Musgravetown Groups form a single linear trend on bivariate trace element plots and cluster together on incompatible trace element ratio-ratio plots, with slopes and positions distinct from trends formed by the volcano-sedimentary rocks of the Marystown-Musgravetown Groups.

Unlike the Marystown-Musgravetown rocks, the Long Harbour Group rocks do not show any significant variation in incompatible trace element ratios between the mafic and felsic rocks (e.g. *Figures 3-38 c&f*) indicating magma differentiation occurred primarily through simple fractional crystallization. This is also illustrated in *Figure 3-38d* which highlights the strong negative Eu anomaly displayed in rhyolites of the Long Harbour Group. Although these rocks were not generated through a complex set of processes typical of arc environments, they still display an affiliation with them, indicated by their small characteristic negative Nb anomalies (*Figure 3-35 c-d*). This suite of rocks is interpreted to have formed during the late stages of arc volcanism, more distal to the trench and arc, in an extensional back-arc environment, further indicated by the bimodal compositional distribution and the alkaline affinity of the Long Harbour volcanic rocks.

Consistent with this model, the Long Harbour rhyolites plot as within plate granites on the tectonic discrimination diagrams for granites (*Figure 3-39 b-c*).

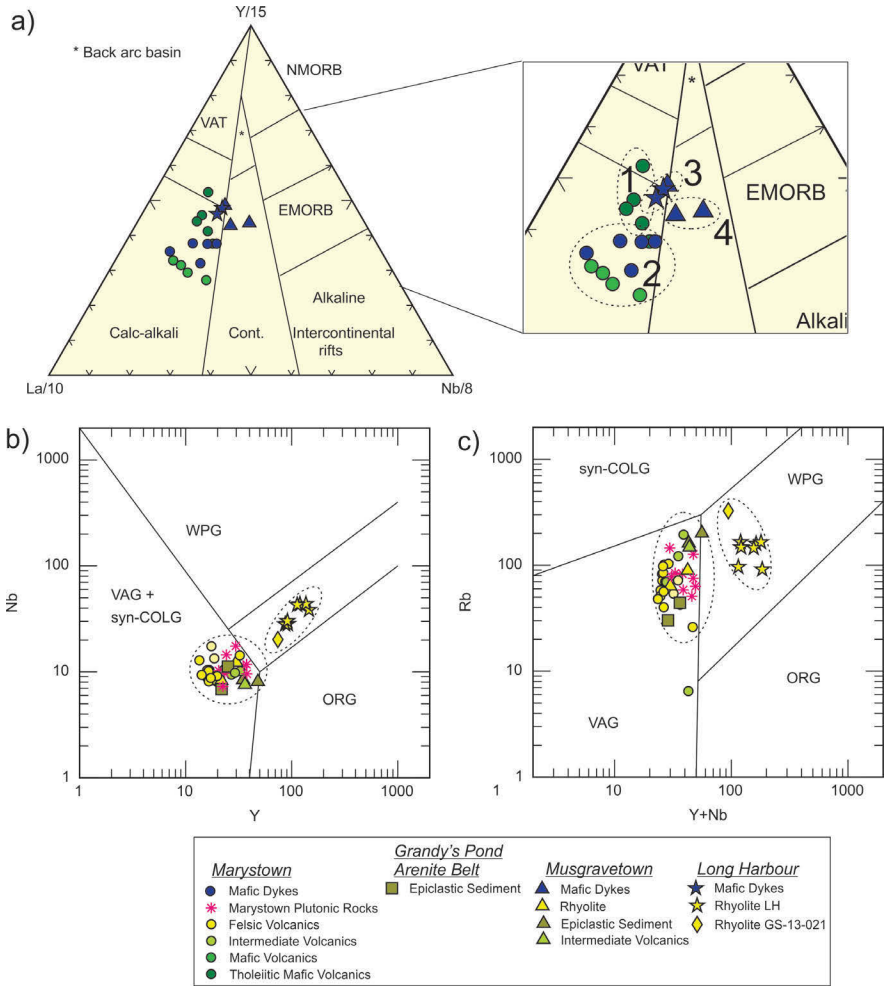

Figure 3-39*: Tectonic Discriminatino compilation plots of volcanic, epiclastic-sedimentary, and intrusive rocks of the Marystown, Musgravetown and Long Harbour Groups, and Grandy's Pond Arenite Belt; a) Basaltic flows and mafic dykes plotted on the tectonic discrimination diagram for basalts of Cabanis and Lecolle (1989) with rock unit subdivisions highlighted in the inset image. 1=Juvenile arc-tholeiites of the Marystown Group, 2=More mature arc-basalts and associated mafic dykes of the Marystown Group, 3=Late extension-related tholeiitic mafic dykes cross-cutting the Long Harbour and Musgravetown Groups, 4=Late post-arc tholeiitic mafic dykes cross-cutting the Musgravetown Group. Calc-alkali=calc-alkali volcanic arc basalts, VAT=volcanic-arc tholeiites, Cont=continental basalts; b&c) Intermediate-felsic volcanic and plutonic rocks and epiclastic sediments plotted on the tectonic discrimination diagrams for granites of Pearce et al. (1984) using Nb vs. Y (b) and Rb vs. Y+Nb (c). WPG=within plate granites, VAG=volcanic-arc granite, syn-COLG=syn-collisional granites, ORG=ocean-ridge granites.*

The tholeiitic mafic dykes cross-cutting the Long Harbour and Musgravetown Groups, presumably representative of a more juvenile magma source, appear to be coincident with this late extensional back arc environment and therefore related to Long

Harbour magmatism. A first group shows minor arc signatures (Group 2; *Figure 3-37c*) and plots in the field of volcanic arc tholeiites on the tectonic discrimination diagram for basalts (*Figure 3-39a*; '3' in inset). The second, presumably later, group records the disappearance of any arc signature (Group 3; *Figure 3-37d*), and plots in the field of continental basalts on the same tectonic discrimination ('4' in inset).

CHAPTER 4: U/Pb ZIRCON CA-TIMS GEOCHRONOLOGY

4.1 Introduction and Previous Work

U/Pb zircon ages were determined by CA-TIMS (Chemical Abrasion-Thermal Ionization Mass Spectrometry) for a variety of samples from across the Burin Peninsula region. The purpose of this geochronological study was to not only to contribute to a more complete knowledge of the regional stratigraphy of the Burin Peninsula and Avalon Zone but, also, to more specifically constrain the ages of the precious metal bearing epithermal systems.

Until recently, only a handful of U/Pb zircon ages had been published for the area. Most of the work was completed in the 1980s and 1990s when there was renewed interest in the area after the initial discovery of these epithermal precious metal systems. These earlier samples were prepared for analysis using physical abrasion (Krogh, 1982); the standard technique at that time. This work proposed an age of 577 ±3 Ma for the plutonism associated with the high sulphidation epithermal systems on the Burin Peninsula, based on a sample of the Swift Current Granite (O'Brien et al., 1998). In addition, five samples were analyzed to provide a proposed age range of 590-565Ma for volcanic rocks of the Marystown Group (O'Brien et al., 1999; McNamara et al., 2001), which comprise the bulk of the peninsula and are host to both high- and low- sulphidation mineralization. The Long Harbour Group, located on the northern shore of Fortune Bay, and host to low-sulphidation epithermal mineralization, was sampled at the base and top of its stratigraphic succession, providing a proposed age range of 570-550 Ma (O'Brien et al., 1995). An alkaline gabbro of the Cross Hills Intrusive Suite, intruding the Long Harbour Group, was dated at 547 +3/-6 Ma (Tuach, 1991). Finally, one sample was taken just west of the Bonavista Peninsula, from what was then considered the Bull Arm Formation at the base of the Musgravetown Group, giving that group a maximum age of 570 +5/-3 Ma (O'Brien et al., 1989). However, the stratigraphy there was later interpreted as representing the lower part of the overlying Rocky Harbour Formation, leaving the maximum age of the Musgravetown Group relatively unconstrained (O'Brien and King, 2004).

In more recent years, the technique for U/Pb zircon dating has been improved in accuracy by the use of chemical abrasion in place of physical abrasion, before final sample dissolution. Employing this new technique, a number of ages were recently published by Sparkes and Dunning, (2014) and Sparkes et al. (2016): At the Stewart prospect, a granodiorite (*GS-11-52*), part of the 'Burin Knee Intrusive Suite' (BKIS) and associated with the extensive belt of granitoid plutonism that traverses the pensinsula, gave an age of 575 ±1 Ma. In addition, a "quartz diorite" (the Stewart tonalite described in this thesis) that hosts advanced argillic alteration and mineralization at Stewart gave an age of 577 ±1.4 Ma. Both of these ages correlate well with the previous date by O'Brien et al. (1998) for the Swift Current Granite. Three felsic volcanic samples were collected from; the southern Burin Peninsula, the northern part of the peninsula near the Tower prospect, and midway down the peninsula. These yielded overlapping ages of 576.8 ±2.6 Ma, 576.2 ±2.8 Ma, and 574.4 ±2.5 Ma, respectively, implying a narrow age range for the Marystown Group volcanics as a whole. The last of these three samples listed was, in fact, an archived sample that had previously given an age of 608 Ma (Krogh et al., 1988). At the Hickey's Pond prospect, samples of the advanced argillic alteration and of a felsic volcaniclastic rock adjacent to the main alteration zone, yielded ages of 586 ±3 Ma and 585.8 ±1.7 Ma, respectively. A granodiorite sample from an area mapped as part of the Cross Hill Intrusive Suite gave an age of 581 ±1.5 Ma, significantly older than the previous date by Tuach (1991) for the gabbro of the Cross Hill Intrusive Suite (547 +3/-6 Ma). Lastly, a granitic intrusion on the southern end of the peninsula at the Peters Brook prospect was dated at 635 ±2 Ma, revealing the presence of a previously unrecognized magmatic event in the area.

Other CA-TIMS U/Pb ages recently determined for rocks in the Burin Peninsula area include: a basaltic andesite dyke cross-cutting the Musgravetown Group host of mineralization at the Big Easy Prospect (MC-12-01/MC-BE12-2), and a granodiorite from a plutonic suite near Seal Cove on the southwest side of the peninsula (SCB-2). The dyke was collected from drill core as part of a B.Sc. thesis at Memorial University and yielded an age of 566 ±2 Ma (Clarke, 2013). The granodiorite was collected in

association with this project, and yielded an age of 685 ±3.5 Ma (Layne, G.D., 2016, unpublished data); revealing another previously unrecognized magmatic event on the Burin Peninsula, but one recorded in plutonic rocks on the Connaigre Peninsula to the west (O'Brien et al, 1995).

The locations and final U/Pb ages of samples from previous work and from the current study are summarized in *Figure 4-1*, and UTM's from the current study are provided in *Table 4-1*.

4.2 Sampling

In the summer of 2012 and the fall of 2013, a total of thirteen samples collected from both surface outcrops and drill core were processed for geochronological work. Eleven yielded zircon of a quality and quantity suitable for analysis. An additional sample was added to the project in 2015, collected from drill core, giving a total of twelve samples processed for zircon U/Pb CA-TIMS analysis.

All samples were collected proximal to the main epithermal showings. Primary candidates for sampling included host rocks to mineralization, cross cutting lithologies, potential plutonic parents to the hydrothermal activity, and any unique marker units within the broader stratigraphy.

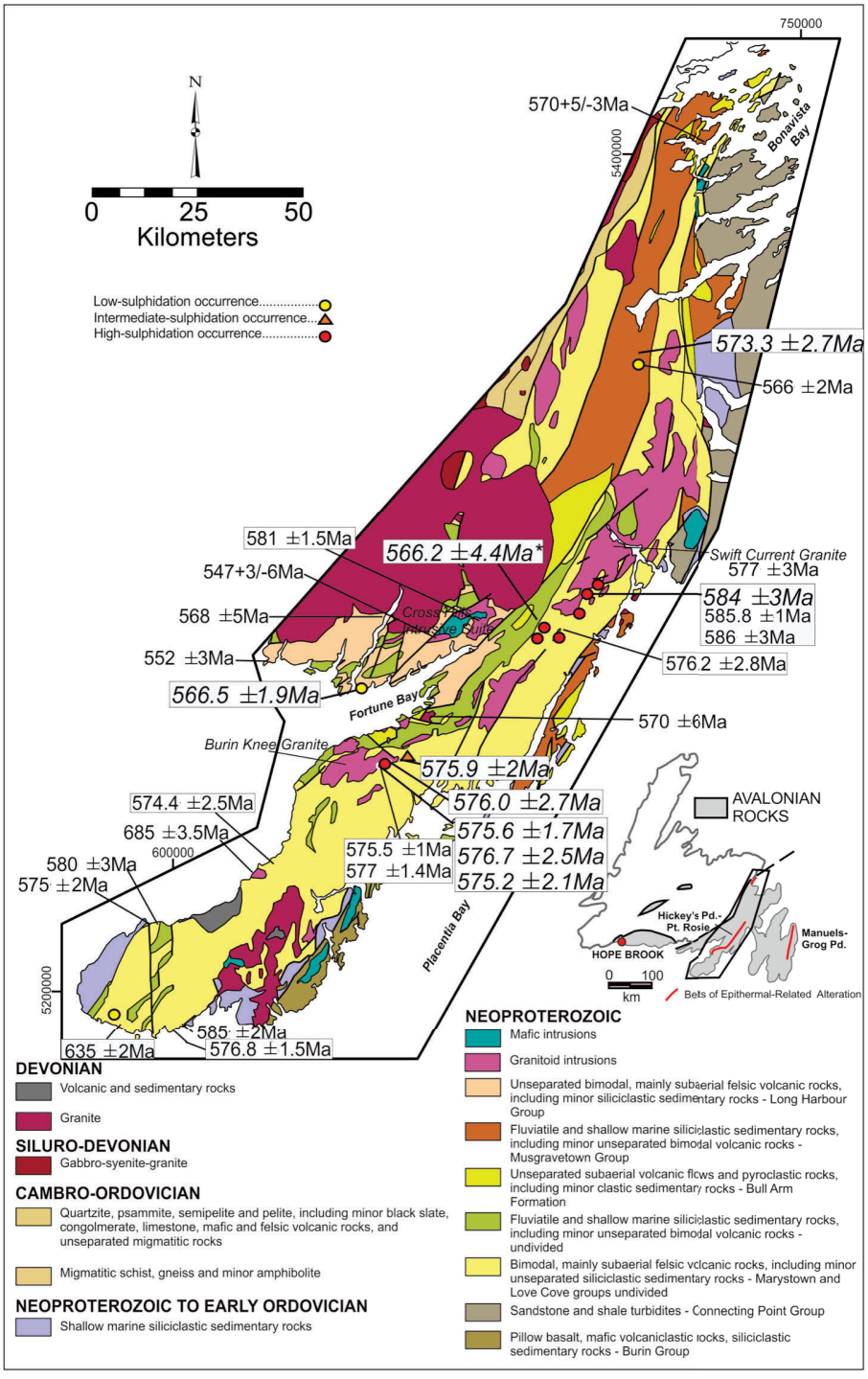

***Figure 4-1**: Regional geology map of the western Avalon Zone of Newfoundland, displaying locations and final U/Pb ages of regional geochronology sampling. Data generated from this study is listed in the large, italicized font in borders. Dates from Sparkes and Dunning (2014) and Sparkes et al. (2016) are listed in borders. Other listed ages are compiled from: Tuach, 1991; O'Brien et al., 1989; O'Brien et al., 1995; O'Brien et al., 1998; McNamara et al., 2001; Clarke, 2013; Kellett, 2014; Layne, 2016, unpublished data. Key epithermal prospects also shown (modified from Sparkes and Dunning, 2014; O'Brien et al., 1998; coordinates are listed in NAD 27, Zone 21; '*'indicates a preliminary result*).

4.3 Analytical Procedure

Rock samples were first crushed and pulverized, and the heavier minerals separated out by gravity and water flow using a Wilfley table. Samples were then sieved to -40 mesh size, and the remaining fine material reduced using a magnet. Heavy minerals were further isolated using high-density methylene iodide (MI; S.G.=3.3) in a separatory funnel. The remaining heavy-mineral fraction was then passed through a Frantz magnetic separator to progressively remove any highly magnetic material, leaving a small fraction of potentially zircon-rich material.

This remaining fraction was examined in alcohol under a microscope and zircons were individually picked using tweezers and sorted based on appearance and quality; the clearest and most euhedral crystals being selected for analysis. A small number of grains were also set aside for cathodoluminescence (CL) imaging. The grains to be analyzed were chemically abraded using the Mattinson (2005) chemical abrasion, thermal ionization mass spectrometry (CA-TIMS) technique, where grains are first annealed for 36 hours in an oven at 1000°C and then etched in concentrated hydrofluoric acid at 200°C for a few hours. This procedure removes any damaged portions of the crystal, which may have experienced Pb loss, which would bias the age determination.

Final zircon fractions of 2-5 grains were selected based on morphology and quality after etching, and washed in distilled nitric acid, followed by double distilled water, then loaded into Krogh- type TEFLON dissolution bombs. A $^{205}Pb/^{235}U$ tracer and distilled hydrofluoric acid was added to the bomb, which was then sealed and placed in an oven at 210°C for 5 days to dissolve the zircon crystals. Pb and U were isolated by performing ion exchange chemistry following the methods of Krogh (1973), but using modified columns, and only one tenth the reagent volumes reported in that paper. The resulting Pb and U were collected in a clean beaker with a single drop of ultrapure phosphoric acid.

Lead and uranium isotopic analysis was performed in the Department of Earth Sciences at Memorial University by Dr. Greg Dunning. Samples were loaded on

outgassed single Re filaments with silica gel and dilute phosphoric acid and measured using a MAT 262 mass spectrometer. The faraday cups were calibrated with NBS 981 lead standard and the ion-counting secondary electron multiplier (SEM) detector was calibrated against the faraday cups by measurement of known Pb isotopic ratios. Pb and U concentrations were measured by peak jumping on the SEM. A series of datasets were collected for each sample, measured from 1400 to 1550°C for Pb and 1550 to 1640°C for U. The best datasets were combined to produce a mean value for each isotopic ratio.

The measured ratios were corrected for Pb fractionation of 0.1% per amu and U fractionation of 0.03% per amu, determined from repeat measurements of NBS standards. They were also corrected for laboratory procedure blanks (1-2pg for Pb, and 0.3pg for U) and for common lead above the laboratory blank, with Pb composition predicted using the two-stage model of Stacey and Kramers (1975) for the age of the sample. The decay constants of Jaffey et al. (1971) were used to calculate the ages, with uncertainties calculated and reported as two sigma. Final ages were determined and reported as the weighted average of the $^{206}Pb/^{238}U$ ages calculated using ISOPLOT, with uncertainties reported at the 95% confidence interval.

4.4 Results

Results are presented in general chronological order from oldest to youngest, based on geochronology results, field relationships, and geochemical observations. Most of the samples yielded small, prismatic zircon grains, which appear to represent a single-age igneous population displaying fine igneous growth zoning (*Plate 4-1*). This is further indicated by the isotopic data, which are primarily concordant and overlapping *(Table 4-1; Figure 4-2*). There are however some exceptions to this, which are discussed accordingly.

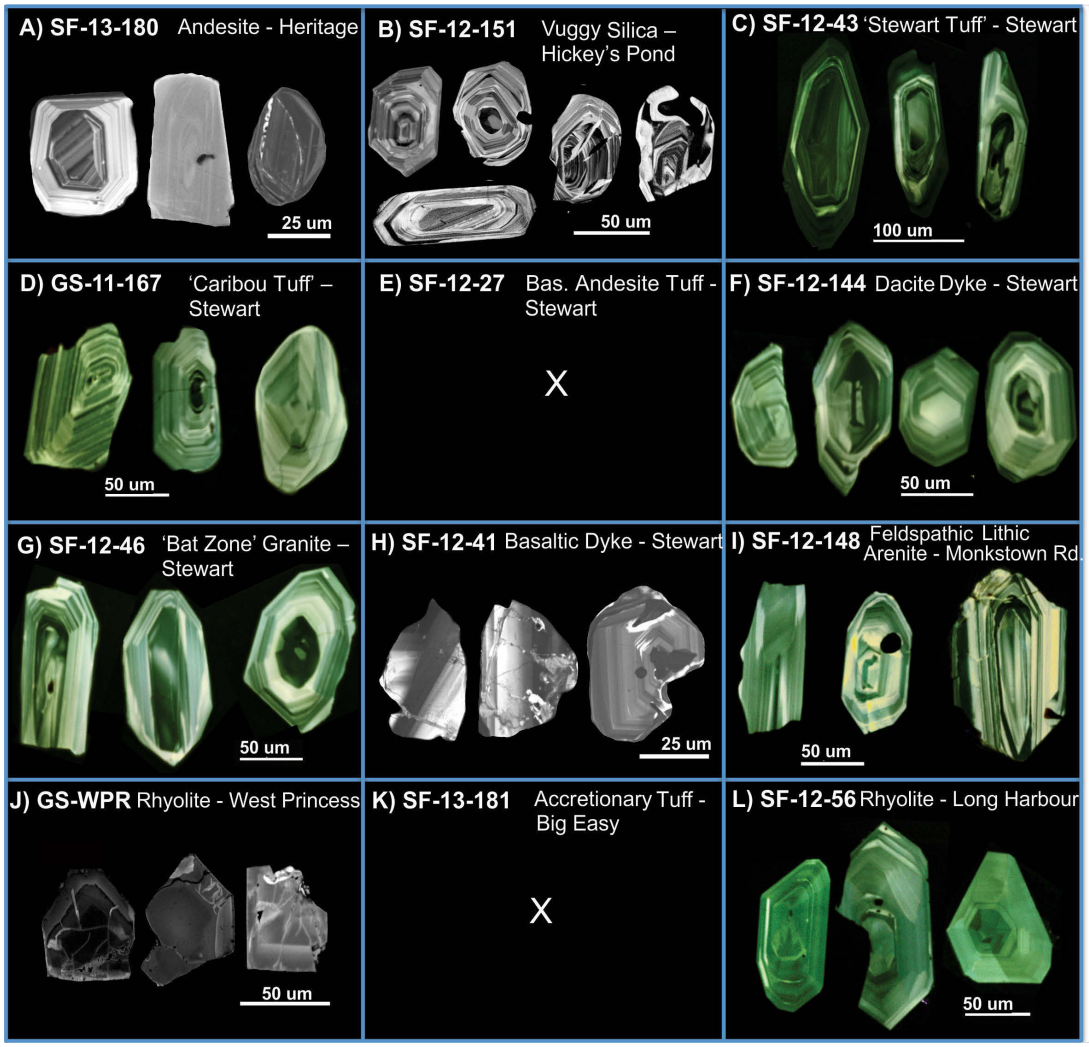

Plate 4-1*: Cathodoluminescence (CL) images of zircon crystals, highlighting the occurrence of igneous growth-zoning. Images are generally representative of the grain type analyzed from each sample, except for SF-12-41 (H) and GS-WPR (J), which did not contain abundant zircon. For these two samples, only lower quality grains and crystal fragments were available for imaging, while the best quality grains were processed for age dating. For samples SF-12-27 (E) and SF-13-181 (K), zircon grains were so sparse as to preclude CL on additional grains. These latter two samples are displayed as blank frames to preserve symmetry with subsequent plates (Plates 4-2 and 4-3).*

Fraction	Concentration Measured				Corrected Atomic Ratios								Age (Ma)		
	Weight	U	Pb rad	total common Pb	$^{206}Pb/^{204}Pb$	$^{208}Pb/^{206}Pb$	$^{206}Pb/^{238}U$	±	$^{207}Pb/^{235}U$	±	$^{207}Pb/^{206}Pb$	±	$^{206}Pb/^{238}U$	$^{207}Pb/^{235}U$	$^{207}Pb/^{206}Pb$
	(mg)	(ppm)	(ppm)	(pg)											
SF-13-180: Pyroclastic Andesite - Heritage (585186E, 5196930N)															
Z1 6 sml prm	0.006	101	14.3	2	2941	0.1902	0.12881	58	1.566	80	0.08817	32	781	957	1386
Z2 2 sml prm	0.002	57	6.6	3	286	0.2065	0.10577	60	0.8824	206	0.06051	130	648	642	622
Z3 2 sml prm	0.002	47	5.9	2	335	0.2407	0.11196	88	0.954	164	0.0618	94	684	680	667
Z4 2 sml prm	0.002	52	6.4	5	175	0.2133	0.11255	94	0.9633	196	0.06208	114	688	685	677
Z5 1 sml prm	0.001	66	8.3	2	201	0.3521	0.10424	72	0.8659	200	0.06024	128	639	633	612
SF-12-151: Vuggy Silica - Hickey's Pond (699317E, 5295024N)															
Z1 5 clr euh prm	0.005	183	20.6	18	326	0.3156	0.09483	50	0.7779	88	0.0595	60	584	584	585
Z2 2 clr euh prm	0.002	24	2.7	2	183	0.2813	0.09581	140	0.7733	732	0.05854	514	590	582	550
SF-12-43: Dacitic 'Stewart Tuff' - Stewart (650857E, 5254413N)															
Z1 1 lrg flat prm	0.002	330	35.9	3	1367	0.2913	0.09339	64	0.7618	90	0.05916	58	576	575	573
Z2 1 sml equant prm	0.002	110	11.8	1	793	0.2713	0.09324	128	0.766	158	0.05959	104	575	577	589
Z3 2 euh prm	0.003	117	12.4	4	588	0.2594	0.09329	56	0.7623	110	0.05926	80	575	575	577
Z4 1 euh prm	0.002	316	35.3	1	2735	0.3313	0.09333	84	0.7617	74	0.05919	46	575	575	574
GS-11-167: Dacitic 'Caribou Tuff' - Stewart (649789E, 5253902N)															
Z1 3 clr euh prm	0.005	78	8.5	2	926	0.299	0.09359	86	0.7644	91	0.05924	60	577	577	576
Z2 1 clr euh prm	0.002	260	28.1	1	2077	0.2839	0.09324	102	0.7621	90	0.05927	54	575	575	577
Z3 3 clr euh prm	0.005	82	8.9	2	1051	0.2825	0.09369	60	0.7635	80	0.05911	54	577	576	571
SF-12-27: Basaltic Andesite Volcaniclastic - Stewart (655388E, 5256169N)															
Z1 2 med prm	0.003	123	13.4	3	671	0.2911	0.09356	84	0.7656	102	0.05935	70	577	577	580
Z2 2 clr euh med prm	0.003	84	9.6	5	341	0.3063	0.09673	42	0.8017	168	0.06011	116	595	598	608
Z3 2 clr prm	0.003	70	7.7	3	456	0.3115	0.09356	80	0.7622	92	0.05908	62	577	575	570
Z4 2 clr prm	0.003	160	19.1	3	999	0.4245	0.09337	44	0.7649	72	0.05941	48	575	577	582
SF-12-144: Porphyritic Dacite Dyke - Stewart (DDH ST-11-03, 385m)															
Z1 4 clr euh prm	0.006	50	5.6	3	585	0.3332	0.09328	60	0.7624	74	0.05928	50	575	575	577
Z2 2 clr euh prm	0.003	97	10.7	1	1934	0.3146	0.09328	66	0.7603	70	0.05912	54	575	574	571
Z3 5 clr euh prm	0.007	67	7.4	4	848	0.3288	0.09329	52	0.7622	80	0.05926	54	575	575	576
Z4 4 clr euh prm	0.006	70	7.8	1	3310	0.3294	0.09371	58	0.7641	54	0.05914	34	577	576	572
SF-12-46: 'Bat Zone' Granite - Stewart (652055E, 5254398N)															
Z1 3 clr prm	0.003	92	10.3	5	373	0.3258	0.09339	70	0.7663	226	0.05951	162	576	578	586
Z2 2 clr prm	0.002	26	3.1	2	178	0.4039	0.09346	104	0.7628	378	0.05919	270	576	576	574
Z3 1 clr prm	0.001	130	15.6	5	172	0.4246	0.09359	84	0.7633	316	0.05915	224	577	576	573
Z4 2 clr prm	0.002	27	3.2	11	47	0.3963	0.09335	148	0.7731	1102	0.06007	792	575	582	606
SF-12-41: Cross Cutting Basaltic Dyke - Stewart (650144E, 5253611N)															
Z1 3 clr euh prm	0.003	653	76.2	8	1629	0.1571	0.11109	58	0.9616	52	0.06278	26	679	684	701
Z2 2 clr euh prm	0.002	1111	253.9	4	8724	0.1002	0.2229	114	2.8278	138	0.09201	18	1297	1363	1468
Z3 2 clr euh prm	0.002	170	22.6	3	900	0.0923	0.13302	54	1.2625	86	0.06883	38	805	829	894
Z4 2 clr prm	0.002	277	36.1	6	611	0.3234	0.10939	46	0.9326	108	0.06183	64	669	669	668

SF-12-148: Grandy's Pond Arenite Belt - Monkstown Rd (686115E, 5289941N)															
Z1 1 lrg sharp prm	0.002	104	13.7	2	714	0.604	0.0918	74	0.7445	118	0.05882	90	566	565	560
Z2 2 sml clr prm	0.002	78	8.1	8	132	0.263	0.0914	68	0.7266	118	0.05765	82	564	555	517
GS-WPR: Flow Banded Rhyolite - West Princess (DDH WP-01-003)															
Z1 2 clr sml prm	0.002	79	8.6	6	163	0.2986	0.09297	62	0.7584	250	0.05916	180	573	573	573
Z2 1 clr prm	0.001	88	9.9	6	103	0.3423	0.09303	72	0.7553	148	0.05888	106	573	571	563
Z3 2 clr prm	0.002	87	9.2	8	143	0.2496	0.09477	60	0.7623	294	0.05834	208	584	575	543
SF-13-181: Andesitic Accretionary Lapilli Tuff - Big Easy (DDH BE-12-8; 67m)															
Z1 2 sml clr prm	0.002	59	6.4	32	42	0.1728	0.10158	124	0.8305	750	0.05929	498	624	614	578
Z2 2 sml clr prm	0.002	63	6	4	215	0.2057	0.0877	84	0.7036	362	0.05819	278	542	541	537
Z3 4 clr prm	0.004	25	2.6	4	145	0.3029	0.08971	52	0.7254	200	0.05865	150	554	554	554
Z4 1 clr prm	0.001	35	4.2	7	47	0.4232	0.09488	210	0.7812	976	0.05972	746	584	586	593
Z5 2 clr prm	0.002	92	9.8	10	123	0.3163	0.08998	78	0.7315	192	0.05896	144	555	557	566
Z6 2 clr prm	0.002	52	5.3	8	95	0.2629	0.08925	90	0.72	304	0.05851	232	551	551	549
SF-12-56: Flow Banded Rhyolite - Long Harbour (645256E, 5272243N)															
Z1 2 short 2:1 prm	0.002	147	14.4	7	277	0.19	0.09161	70	0.7451	188	0.05899	136	565	565	567
Z2 2 short prm	0.002	53	5.4	4	190	0.2177	0.09136	104	0.7508	258	0.05961	190	564	569	589
Z3 5 clr sml prm	0.005	95	9.6	3	832	0.2191	0.09193	44	0.7455	30	0.05881	18	567	566	560
Z4 4 clr sml prm	0.004	86	8.7	2	1043	0.2097	0.09227	92	0.7469	96	0.05871	66	569	566	556
Z5 3 clr sl prm	0.003	35	3.6	2	406	0.202	0.09256	64	0.7516	252	0.05889	184	571	569	563

Table 4-1*: U/Pb data from rocks from the Burin Peninsula, northern Fortune Bay, and Clarenville area. UTMs listed for each sample location are provided in NAD 27, Zone 21 coordinates. All zircon was chemically abraded (Mattinson, 2005) prior to dissolution. Weights of grains were estimated, with potential uncertainties of 25-50% for these small samples. Atomic ratios corrected for fractionation, spike, laboratory blank of 0.6-2 picograms (pg) common lead, and initial common lead at the age of the sample calculated from the model of Stacey and Kramers (1975), and 0.3 pg U blank. Two sigma uncertainties are reported after the ratios and refer to the final digits.*
rad–radiogenic; Z-zircon; 2, 4, etc.-number of grains in analysis; prm-prism; sml-small; euh-euhedral; frag-fragments; clr-clear; equ-equant.

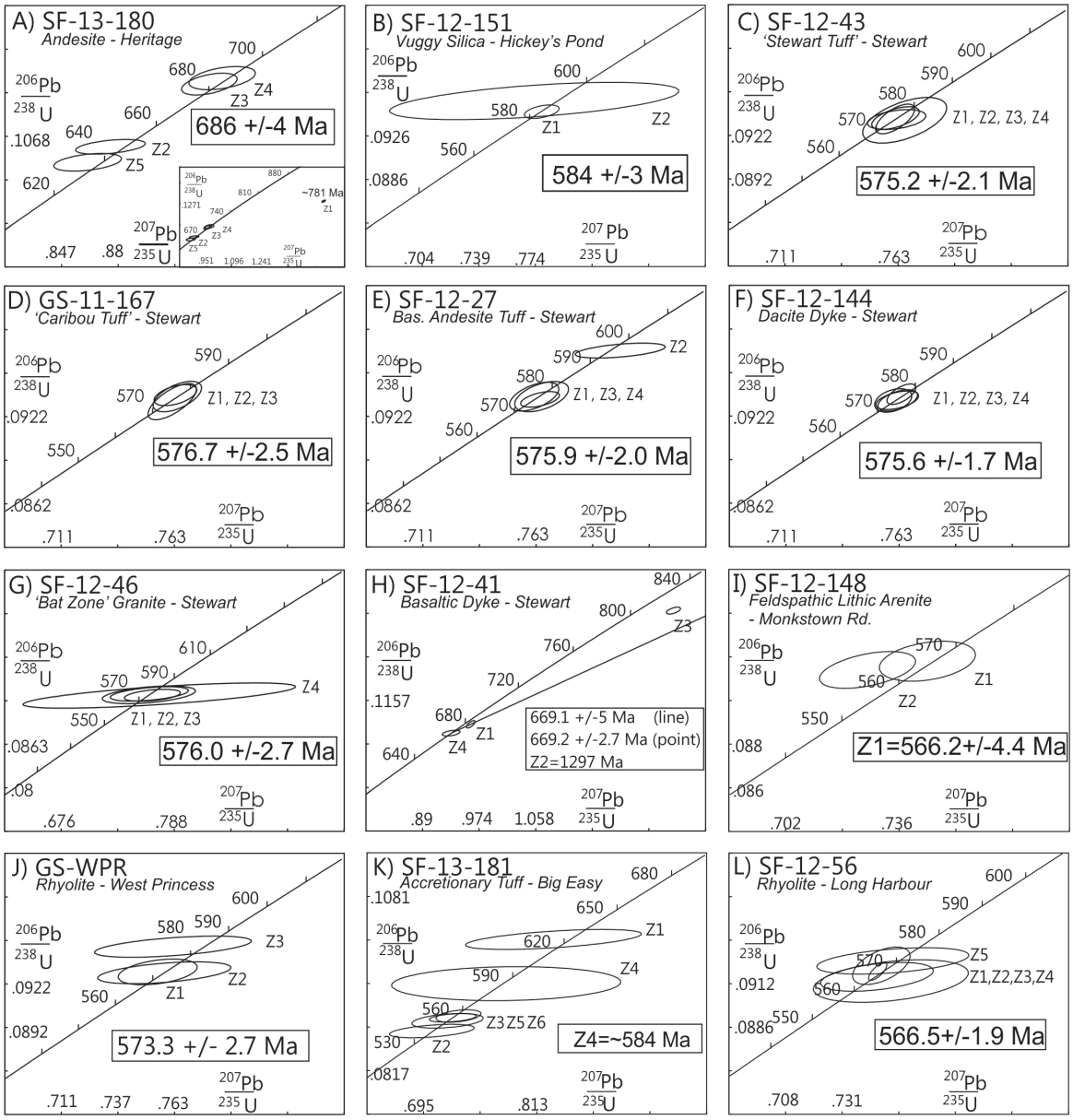

***Figure 4-2**: Concordia diagrams of U/Pb results of zircon analyses from samples from the Burin Peninsula, northern Fortune Bay, and Clarenville area. Error ellipses are at the 2σ level. Refer to Table 4-1 for sample locations and descriptions.*

4.4.1 Neoproterozoic Volcanic Rocks of the Marystown Group

4.4.1.1 Pyroclastic Andesite Host Rock at the Heritage Prospect (SF-13-180)

The Heritage prospect is a low-sulphidation epithermal Au-Ag prospect located in the southernmost part of the Burin Peninsula. The hydrothermal system is imprinted into the host rocks as extensive networks of quartz veins and breccias, along with pervasive

silicification. Andesitic pyroclastic rocks are the main host to the epithermal alteration and mineralization.

Sample *SF-13-180* was collected from the 'Zaxis Trench', and selected for its relatively unaltered and homogeneous composition. It is an andesitic lapilli tuff containing a monolithic population of mm- to cm-scale lapilli fragments, and local block-sized fragments (*Plate 4-2 A*). Fragments are composed of massive andesitic feldspar-crystal tuffs and sit within a matrix of similar composition, but generally of a finer grain size. Typically the fragments are green and altered to chlorite and sericite, and the matrix is reddish, oxidized, and strongly silicified. However, this differential alteration pattern is variable, with the opposite relationship occurring locally, or neither component showing distinctive colouration/alteration.

The sample yielded a relatively small population of zircon crystals that were tiny, clear, and prism shaped, with slightly rounded edges locally (*Plate 4-3 A*). Cathodoluminescence (CL) images display clear igneous growth zoning, however one grain also displays a distinct xenocrystic core (*Plate 4-1 A*). Two fractions (Z3 & Z4) of 2 grains each are concordant and overlapping, and yield a weighted average $^{206}Pb/^{238}U$ age of 686 ±4 Ma (MWSD=0.84; *Figure 4-2 A*). Two other fractions (Z2 & Z5) of 1 to 2 grains are concordant, plotting at 648 Ma and 639 Ma, while a single fraction (Z1) of 6 grains is discordant at an age of 781 Ma. The weighted average age of 686 ±4 Ma corresponds with the age determined recently for a granodiorite sample (SCB-2) located near Seal Cove on the southwestern Burin Peninsula of 685 ±3.5 Ma (Layne, G.D., 2016, unpublished data). The youngest measured age (fraction Z5 at 639 Ma) corresponds to the age of the Peter Brook granite (Sparkes and Dunning, 2014), lying proximal to the Heritage prospect. A definitive age cannot be determined for the host rocks at Heritage based on this sample (see *Section 4.5: Discussion*).

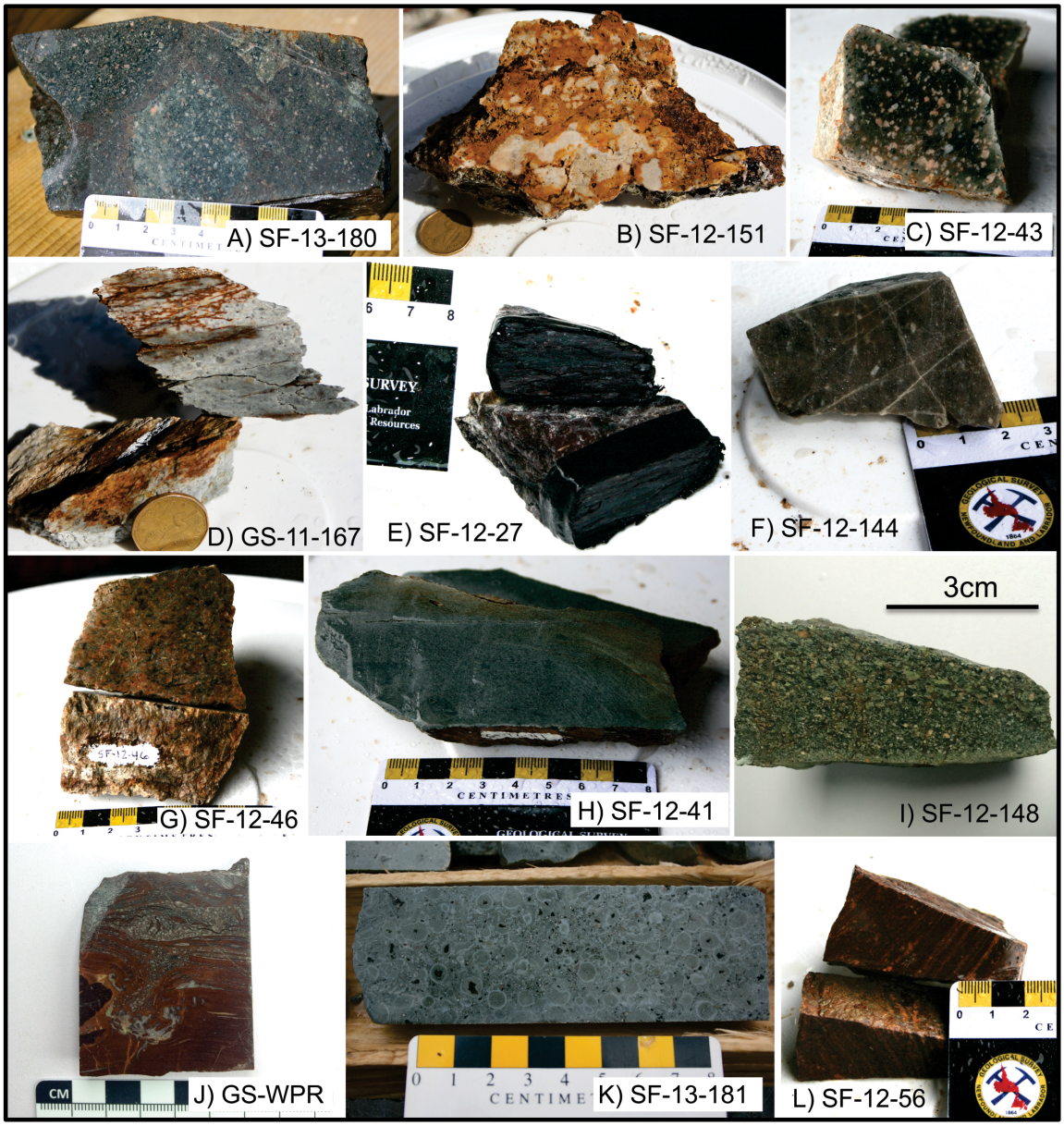

***Plate 4-2**: Representative photos of samples selected for zircon U/Pb geochronology; A) Andesitic lapilli tuff host rock at Heritage prospect; B) Vuggy silica host rock at Hickey's Pond prospect; C) Dacitic 'Stewart Tuff' from the Stewart prospect; D) Dacitic 'Caribou Tuff' host rock at Stewart prospect; E) Basaltic andesite lapilli tuff from the 'Upper Volcanic Unit' at Stewart prospect; F) Dacitic porphyritic dyke from the Stewart prospect; G) 'Bat Zone' granite from the Stewart prospect; H) Basaltic dyke cross cutting tonalite host rock at the Stewart prospect; I) Epiclastic feldspathic-lithic-arenite from the Grandy's Pond Arenite Belt (Monkstown Rd); J) Flow banded rhyolite from the West Princess prospect, adjacent to the Big Easy prospect; K) Andesitic accretionary lapilli tuff host rock at Big Easy prospect; L) Flow banded rhyolite host rock at Long Harbour prospect.*

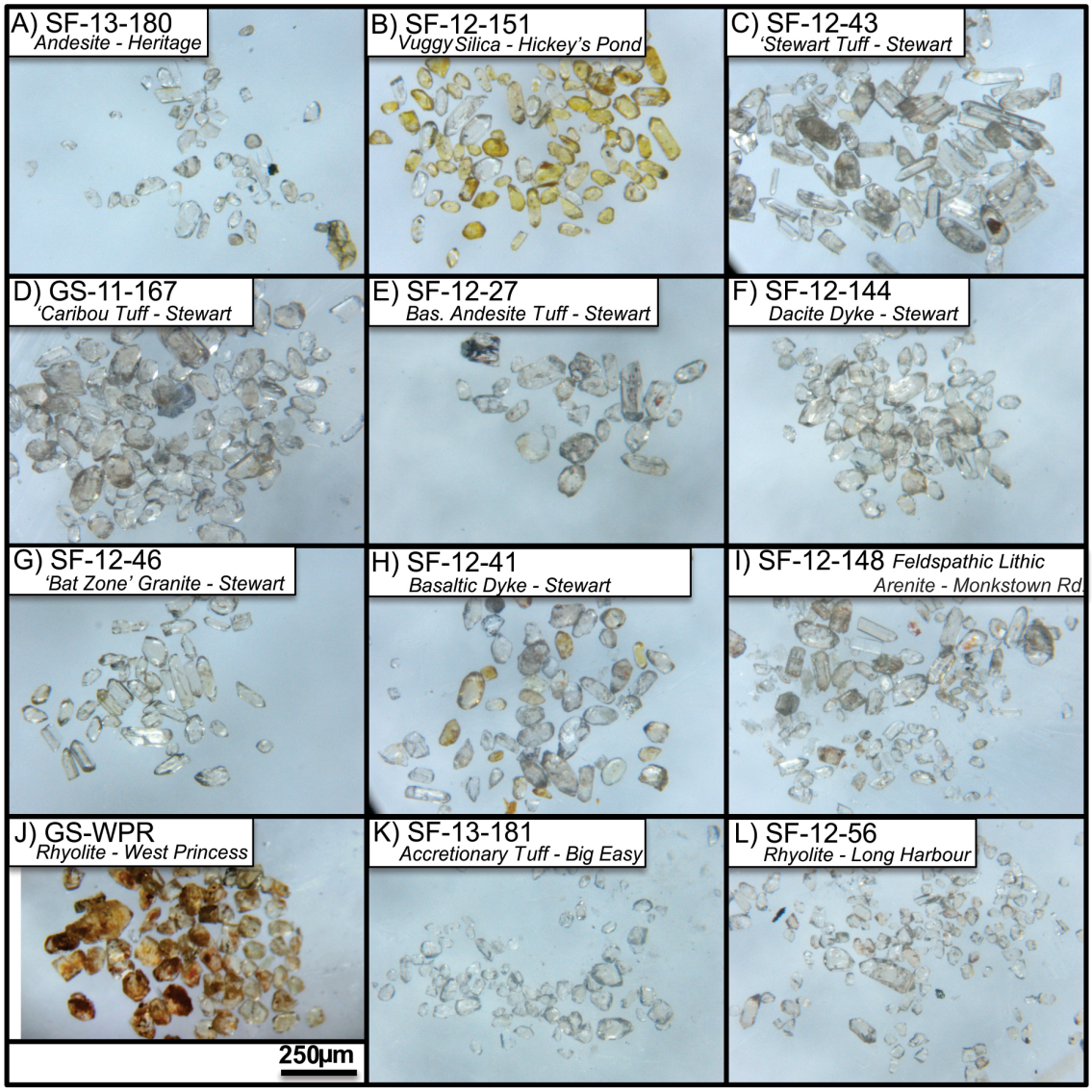

***Plate 4-3**: Photomicrographs of zircon from each of the samples selected for U/Pb geochronology.*

4.4.1.2 Vuggy Silica Host Rock at the Hickey's Pond Prospect (SF-12-151)

The Hickey's Pond prospect is located in the northern portion of the Burin Peninsula, along the southeastern margin of the Swift Current Granite. The prospect is small, but the main alteration envelope is well exposed, containing a central vuggy silica core (yielding gold grades in grab sample of up to 60.4 g/t) surrounded by a halo of advanced argillic alteration. The prospect is overthrust from the northwest, and bound by

the southwest-striking and steeply northwest-dipping Hickey's Brook Fault (Huard, 1989).

Sample *SF-12-151* (*Plate 4-2 B*) was collected from the central vuggy silica zone. It is primarily composed of fine quartz with lesser alunite, rutile and zircon scattered throughout the quartz matrix. The sample is strongly oxidized, with abundant hematite lining vugs, after primary pyrite-tennantite mineralization.

The sample yielded abundant small, euhedral, prism-shaped zircon, and a few more stubby sub-rounded grains, which are clear to yellow in colour from iron staining (*Plate 4-3 B*), and in CL images display clear igneous growth zoning (*Plate 4-1 B*). Two grains also display some unique features in the CL images of *Plate 4-1 B*, including zircon-filled fractures and lobate irregular crystal zonation, possibly corresponding to the minor population of stubby sub-rounded grains, and might represent the presence of hydrothermal overgrowth. Two fractions, Z1 (5 grains) and Z2 (2 grains), containing euhedral prismatic grains, are concordant and overlapping in the Concordia diagram of *Figure 4-2 B*, above. The final age is determined using only fraction Z1, which yielded a much more precise analysis, with a $^{206}Pb/^{238}U$ age of 584 ±3 Ma (*Figure 4-2 B*). This age is consistent with two recently published ages from the prospect, one of which corresponds with the same vuggy silica zone as SF-12-151. Three fractions were analyzed from this sample (SJOB-97) and were reported as concordant and overlapping yielding a weighted average $^{206}Pb/^{238}U$ age of 586 ±3Ma (MSWD=0.026; Sparkes et al., 2016; *Figure 4-3*).

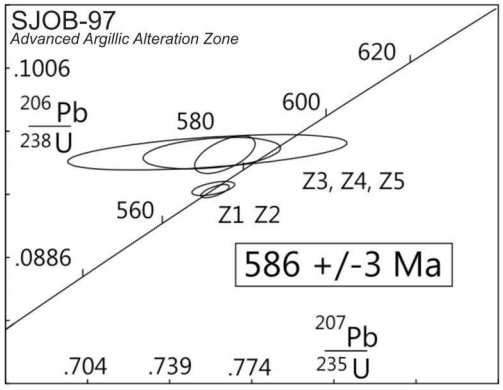

***Figure 4-3**: Concordia diagram of U/Pb results of new zircon analyses for sample SJOB-97 from the advanced argillic zone at the Hickey's Pond prospect (from Sparkes et al., 2016). SJOB-97 is analogous to SF-12-151. Analyses of Z1 and Z2 fractions were carried out using the physical abrasion technique of Krogh (1982) yielding an age of 572 ±1.5Ma (O'Brien et al., 1999). Fractions Z3, Z4, Z5 were measured using CA-TIMS by Sparkes et al. (2016) at 586 ±3Ma. Error ellipses are at the 2σ level (modified from Sparkes et al., 2016).*

It was noted that some of the zircon grains from the vuggy silica zone at the Hickey's Pond prospect (*SF-12-151*) display unique textures and growth patterns in CL images, which are not present in other zircon grains from relatively unaltered rock samples from elsewhere across the region (*Plate 4-1 B*). Most notably these features include zircon-filled fractures cross cutting formerly crystallized zircon grains, and lobe-shaped zonations around the outside of grains, surrounding an igneous core and truncating igneous growth zoning. To test the affiliation of these textural anomalies in zircon with the presence of high-sulphidation epithermal alteration, additional CL imaging of zircon grains from the advanced argillic zone at the Tower prospect was undertaken.

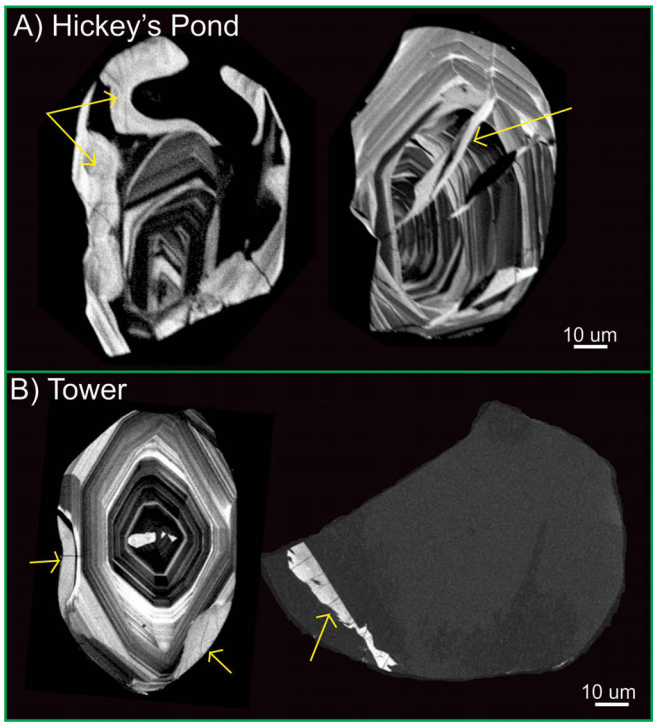

***Plate 4-4**: Cathodoluminescence (CL) images of zircon crystals from: A) Hickey's Pond and B) Tower displaying textures and overgrowths interpreted to be of possible hydrothermal origin. Regions pointed out by yellow arrows.*

Although not abundant, similar features were identified in some zircon grains from the advanced argillic alteration zone at the Tower prospect. *Plate 4-4 A* displays the two previously discussed zircon grains from the Hickey's Pond prospect (sample *SF-12-151*) and *Plate 4-4 B* shows two zircon grains from the Tower prospect (*SF-12-22*) with overgrowth and crack-filling features. The first grain from Tower shows two bright,

lobe-shaped overgrowths truncating igneous growth zoning on the left and bottom right sides of the grain. The second grain from Tower shows a bright zircon filled fracture cross-cutting a non-luminescent zircon grain. It is proposed that both features represent a hydrothermal overgrowth associated with the high-sulphidation epithermal alteration.

4.4.1.3 Dacitic 'Stewart Tuff' at the Stewart Prospect (SF-12-43)

The Stewart prospect is located midway down the peninsula, along the southeastern margin of a large, high-level plutonic suite referred to as the 'Burin Knee Intrusive Suite' (BKIS). The prospect is considered to represent a collapsed porphyry system overprinted by high-sulphidation epithermal-style alteration and mineralization. It is characterized by an extensive, curvilinear zone of advanced argillic alteration, roughly 5.5 km long and 700 m wide, hosting broad, low-grade copper and gold mineralization. The alteration zone is roughly constrained between a lower package of intermediate-mafic volcanics ('Lower Volcanic Unit') to the southeast, and the BKIS to the northwest.

Sample *SF-12-43* is a dacitic quartz-feldspar crystal tuff, part of the 'Stewart Tuff' unit, positioned above and northwest of the intermediate-mafic rocks of the 'Lower Volcanic Unit', and below the 'Caribou Tuff' host unit. The 'Stewart Tuff' unit is locally rich in lapilli- and block-sized clasts, but sample SF-12-43 is free of clasts, and made up of a fine-grained siliceous matrix containing medium to coarse-grained quartz and feldspar crystals (*Plate 4-2 C*).

The sample yielded a single population of abundant medium-sized, clear, elongate, euhedral zircon prisms (*Plate 4-3 C*), which display clear igneous growth zoning in CL images (*Plate 4-1 C*). Four fractions of 1 to 2 grains each are concordant and overlapping and yield a weighted average $^{206}Pb/^{238}U$ age of 575.2 ±2.1 Ma (MWSD=0.025; *Figure 4-2 C*).

4.4.1.4 Dacitic 'Caribou Tuff' Host Rock at the Stewart Prospect (GS-11-167)

Sample *GS-11-167* is a dacitic quartz-crystal tuff, from the 'Caribou Tuff' unit at the Stewart prospect. The unit stratigraphically overlies the 'Stewart Tuff' and is one of

the main host rocks to high-sulphidation epithermal alteration and mineralization. The entire unit has been affected to some degree by hydrothermal alteration, ranging from a phyllic to an advanced argillic assemblage, and is generally pyritiferous. The unit is typically strongly foliated, and appears gossanous on weathered surfaces due to the weathering of the prevalent sulphides (predominantly pyrite). Siliceous, sub-rounded lapilli fragments approximately 1 cm or less in size are common throughout the unit.

Sample *GS-11-167* is a relatively unaltered example of the 'Caribou Tuff', moderately altered to a phyllic assemblage, and containing ~2% pyrite (*Plate 4-2 D*). It is made up of a fine-grained quartz-rich matrix containing abundant coarse-grained quartz crystals and occasional siliceous lapilli.

The sample yielded a single population of abundant medium to large-sized, clear, euhedral zircon prisms (*Plate 4-3 D*), which display clear igneous growth zoning in CL images (*Plate 4-1 D*). Three fractions of 1 to 3 grains each are concordant and overlapping and yield a weighted average $^{206}Pb/^{238}U$ age of 576.7 ±2.5 Ma (MWSD=0.29; *Figure 4-2 D*).

4.4.1.5 Basaltic Andesite Tuff at the Stewart Prospect (SF-12-27)

Sample *SF-12-27* was collected approximately two kilometers northeast of the main Stewart showing, and is interpreted to be part of the intermediate to mafic 'Upper Volcanic Unit', overlying the felsic volcanics (e.g., Stewart and Caribou Tuffs). The sample is a lapilli tuff of basaltic andesite composition, with green chloritic 2-20mm lapilli occurring in a fine-grained maroon matrix (*Plate 4-2 E*).

The sample yielded a very small population (~20 grains) of small to medium-sized, generally clear, euhedral zircon prisms and some crystal fragments (*Plate 4-3 E*). CL imaging was not completed on this sample due to the limited quantity of usable zircon grains extracted. Three fractions of 2 grains each (Z1, Z3, Z4) are concordant and overlapping and yield a weighted average $^{206}Pb/^{238}U$ age of 575.9 ±2.0 Ma (MWSD=0.13; *Figure 4-2 E*). Another fraction of 2 grains (Z2), is concordant at 595

Ma. This shift to an older age from the other 3 fractions is most likely the result of the presence of at least one inherited older zircon core in this fraction (*Table 4-1*).

4.4.2 Neoproterozoic Intrusive Rocks of the Marystown Group

4.4.2.1 Porphyritic Dacite Dyke at the Stewart Prospect (SF-12-144)

Sample *SF-12-144* is a feldspar-phyric dacite dyke collected from drill core (DDH: ST-11-03). The unit is found in both drill core and in surface exposures cross cutting the porphyritic basaltic-andesite intrusive ('Microdiorite') and mafic rocks of the 'Lower Volcanic Unit'. These dykes are about 3m wide and typically strike towards the southwest. Sample SF-12-144 is composed of a very fine-grained pink to grey siliceous matrix containing 15% feldspar phenocrysts (*Plate 4-2 F*).

The sample yielded a single population of abundant small, clear, euhedral zircon prisms (*Plate 4-3 F*), which display clear igneous growth zoning in CL images (*Plate 4-1 F*). Four fractions of 2 to 5 grains each are concordant and overlapping and yield a weighted average $^{206}Pb/^{238}U$ age of 575.6 ±1.7 Ma (MWSD=0.54; *Figure 4-2 F*).

4.4.2.2 Granite from the 'Bat Zone' at the Stewart Prospect (SF-12-46)

Sample *SF-12-46* is a medium-grained pink granite (*Plate 4-2 G*). It was collected from a small granite body, intruding into the hydrothermally altered volcanic rocks in the northeast portion of the Stewart property, referred to as the 'Bat Zone'. This small isolated granite is interpreted to be part of the larger BKIS.

The sample yielded a single population of abundant small, clear, elongate, euhedral zircon prisms (*Plate 4-3 G*), which display clear igneous growth zoning in CL images (*Plate 4-1 G*). Four fractions of 1 to 3 grains each are concordant and overlapping and yield a weighted average $^{206}Pb/^{238}U$ age of 576 ±2.7 Ma (MWSD=0.053; *Figure 4-2 G*). This is consistent with the ages 575 ±1 Ma and 577 ±1.4 Ma, reported for other phases of the BKIS (Sparkes and Dunning, 2014).

4.4.2.3 Basaltic Dyke Cross Cutting Tonalite Host Rock at the Stewart Prospect (SF-12-41)

Sample *SF-12-41* was collected from a 1m wide mafic dyke which cross cuts the tonalite host unit (dated at 577 ±1.4 Ma; Sparkes and Dunning, 2014) in the Vinjer trench. The sample is fine-grained, massive, dark grey-green in colour, and basaltic in composition (*Plate 4-2 H*).

The sample yielded a small and slightly variable population of zircon (*Plate 4-3 H*). The crystals range from very tiny to medium-sized, and in quality from clear euhedral prisms to cloudy fragments. Some grains are yellow in colour, and some show sub-rounded edges. Typically this would not qualify a sample as a good candidate for geochronology. However, this particular sample is important for providing a minimum age constraint on the alteration and mineralization at the Stewart prospect, so the best quality zircon were selected for analysis. The few remaining lower quality grains and fragments were used for CL imaging, and although they are not fully representative of the measured fractions, still display igneous growth zoning (*Plate 4-1 H*).

Four fractions of 2 to 3 grains each produced four discordant points, which fall upon a Discordia line with a lower intercept of 669.1 ±5 Ma. This is controlled by a concordant point at an age of 669.2 ±2.7 Ma (Z4; *Figure 4-2 H*). The other fractions produce ages of 679 Ma, 805 Ma, and 1297 Ma. Clearly, based on crosscutting relationships, these ages are not representative of the dyke itself, and most likely represent the ages of inherited zircon from older crustal rocks.

4.4.3 Neoproterozoic Epiclastic Sedimentary Rocks of the Grandy's Pond Arenite Belt (SF-12-148)

The 'Grandy's Pond Arenite Belt' spans the northern half of the Burin Peninsula along its western edge, overlying the volcanics of the Marystown Group. The belt is predominantly composed of feldspathic-lithic arenites with subordinate fine polymictic conglomerates, which are locally interbedded with thin pyroclastic units.

Sample *SF-12-148* was collected along Monkstown Road in the vicinity of the Tower and Monkstown Rd. high-sulphidation epithermal prospects. The sample is predominantly composed of abundant fine to medium-grained euhedral feldspar crystals defining weakly bedded layers of green-grey feldspathic-arenite. Thin subordinate layers of silt, and coarser lithic-arenite also occur interbedded throughout (*Plate 4-2 I*).

The sample yielded an abundant but variable population of zircon (*Plate 4-3 I*). Grains range from very tiny to medium-sized, appear both clear and cloudy, and occur as both euhedral crystals and incomplete fragments. The euhedral crystals include both elongate and stubby prisms. The variation in the zircon population of this sample is expected, based on its origin as an epiclastic-sedimentary rock, where all contained zircon is detrital by definition, and presumed derived from adjacent sources. The youngest population of zircon is representative of a maximum age of deposition for the sedimentary unit, and the age of its volcanic source. Alternatively, if any zircons represent an ash composition this would yield the actual age of deposition and nearby volcanism. Despite some variation in the overall zircon population, all samples display clear igneous growth zoning in CL images (*Plate 4-1 I*).

Preliminary results for sample *SF-12-148* include two fractions of 1 to 2 grains each that are discordant, but partially overlap at ages of 566 and 564 Ma (*Figure 4-2 I*). As a preliminary age estimate, the more precise measurement of 566.2 ±4.4 Ma from fraction Z1 is used. Based on these results, more determinations are planned, to better elucidate a maximum age for this unit.

4.4.4 Neoproterozoic Volcanic Rocks of the Musgravetown Group

4.4.4.1 Flow Banded Rhyolite at the West Princess Prospect (GS-WPR)

The West Princess prospect is west of the town of Clarenville and approximately 5km north of the Big Easy prospect, and occurring within the stratigraphy of the Musgravetown Group. Sample *GS-WPR* is a flow banded rhyolite which was collected from drill core at the West Princess prospect. It was collected for geochronology after

attempts to date samples from within the Big Easy prospect were unsuccessful in extracting adequate zircon populations for analysis. This would include sample SF-13-181 described below (*Section 4.4.4.2*).

The *GS-WPR* rhyolite is predominantly red in colour and contains very distinct flow banding textures (*Plate 4-2 J*). The banding is defined by two distinct finely intercalated lithologies; one is red, very fine-grained, massive and siliceous, and the other is grey in colour and contains fine grained white feldspar phenocrysts.

The sample yielded a limited quantity of a single population of clear to yellow (oxide stained), small-sized, euhedral zircon prisms and fragments (*Plate 4-3 J*). Because the amount of zircon was limited, the best quality grains were reserved for analysis and only the low quality fragments were used for CL imaging, and thus are not fully representative of the measured grains. Despite some inclusions and fractures, these grains still display igneous growth zoning (*Plate 4-1 J*). Two fractions of 1 to 2 grains each (Z1, Z2) are concordant and overlapping and yield a weighted average $^{206}Pb/^{238}U$ age of 573.3 ±2.7 Ma (MWSD=0.016; *Figure 4-2 J*). This age is older than, but overlapping within error of the previously determined lower age constraint of 570 +5/-3 Ma for the Rocky Harbour Formation, which comprises the upper portions of the Musgravetown Group (O'Brien et al., 1989; O'Brien and King, 2004). A third fraction of 2 grains (Z3) yielded a concordant point at 584 Ma.

4.4.4.2 Andesitic Accretionary Lapilli Tuff Host Rock Horizon at the Big Easy Prospect (SF-13-181)

The Big Easy prospect is a low-sulphidation epithermal Au-Ag deposit, located west of Clarenville, and just south of the Trans-Canada Highway on the southwest side of Thorburn Lake. The prospect contains a ~1km long zone of silicic alteration hosted primarily in interbedded sandstones and pebble conglomerates of epiclastic origin. Mineralization occurs within networks of narrow, finely banded silica veins, permeating the pervasively silicified host rocks.

Sample *SF-13-181* is an andesitic accretionary lapilli tuff, which was collected from drill core at the prospect (DDH BE-12-8). The unit occurs as multiple thin horizons within the extensive clastic sedimentary sequence, host to the hydrothermal alteration and mineralization. This unit is very distinctive in appearance, containing abundant rounded, concentrically zoned lapilli, generally grading outward from a coarser-grained core to a finer-grained rim (*Plate 4-2 K*). The sample is pyritiferous and strongly silicified.

The sample yielded a small population of very tiny to small-sized, clear, euhedral zircon prims and fragments (*Plate 4-3 K*). Due to this limited population of very small grains, CL imaging was not completed on the sample. Six fractions of 1-4 grains each produced seemingly concordant, but widely dispersed ages at 624, 584, 555, 554, 551, and 542 Ma (*Figure 4-2 K*). The older fractions (Z1 and Z4) are consistent with older known volcanic sequences in the region, however the younger 542-555 Ma fractions are considered anomalous since this rock is conformable with a sequence crosscut by a 566 ±2 Ma basaltic andesite dyke (Clarke, 2013). Every fraction contained a high common to radiogenic lead ratio (*Table 4-1)* and the range and predominant shift to younger ages is very likely the result of lead loss in these tiny grains. These results are thus deemed preliminary, with further analyses pending to try to better constrain the age of this distinct marker horizon.

4.4.5 Neoproterozoic Volcanic Rocks of the Long Harbour Group

4.4.5.1 Flow Banded Rhyolite Host Rock at the Long Harbour Prospect (SF-12-56)

The Long Harbour prospect is located immediately west of the Burin Peninsula, along the northern shore of Fortune Bay, hosted within flow banded rhyolites of the Belle Bay Formation. It is a low-sulphidation epithermal system, with gold mineralization occurring within a network of banded quartz-adularia veins and breccias, continuous over a strike length of approximately 70 metres.

Sample *SF-12-56* is an example of the flow banded rhyolite host rock, and was collected adjacent to the main zone of hydrothermal veining. The rhyolite consists of fine,

mm-scale, red and pink bands containing fine-grained phenocrysts of dark grey quartz and light pink feldspar (*Plate 4-2 L*).

The sample yielded a single population of abundant, predominantly small, clear, short, euhedral zircon prisms (*Plate 4-3 L*), which display clear igneous growth zoning in CL images (*Plate 4-1 L*). Four fractions of 2 to 5 grains each (Z1-Z4) are concordant and overlapping and yield a weighted average $^{206}Pb/^{238}U$ age of 566.5 ±1.9 Ma (MWSD=0.77; *Figure 4-2 L*). This is consistent with previously determined ages for other members of Long Harbour Group, with ages of 568 ±5 Ma and 552 ±3 Ma, measured from the base and top of the Long Harbour Group succession, respectively (O'Brien et al., 1995; Tucker unpublished data). A fifth fraction of 3 grains (Z5) yields a slightly older concordant point at 571 Ma. This fraction is not used in the final age calculation as it is significantly older than the tight cluster of other analyses and may contain an inherited zircon core.

4.5 Discussion

All of the newly measured U-Pb zircon ages are summarized together with all relevant ages from previous published studies, in *Figure 4-4*. The few samples described above that yielded inconclusive preliminary results (*SF-13-181, Big Easy Accretionary Lapilli Tuff*), or ages interpreted to be representative of xenocrystic (*SF-12-41, Stewart Cross-Cutting Dyke*) or pyroclastic (*SF-13-180, Heritage Andesite Pyroclastic*) inclusions of older zircon, are discussed further in this section but not illustrated in *Figure 4-4*.

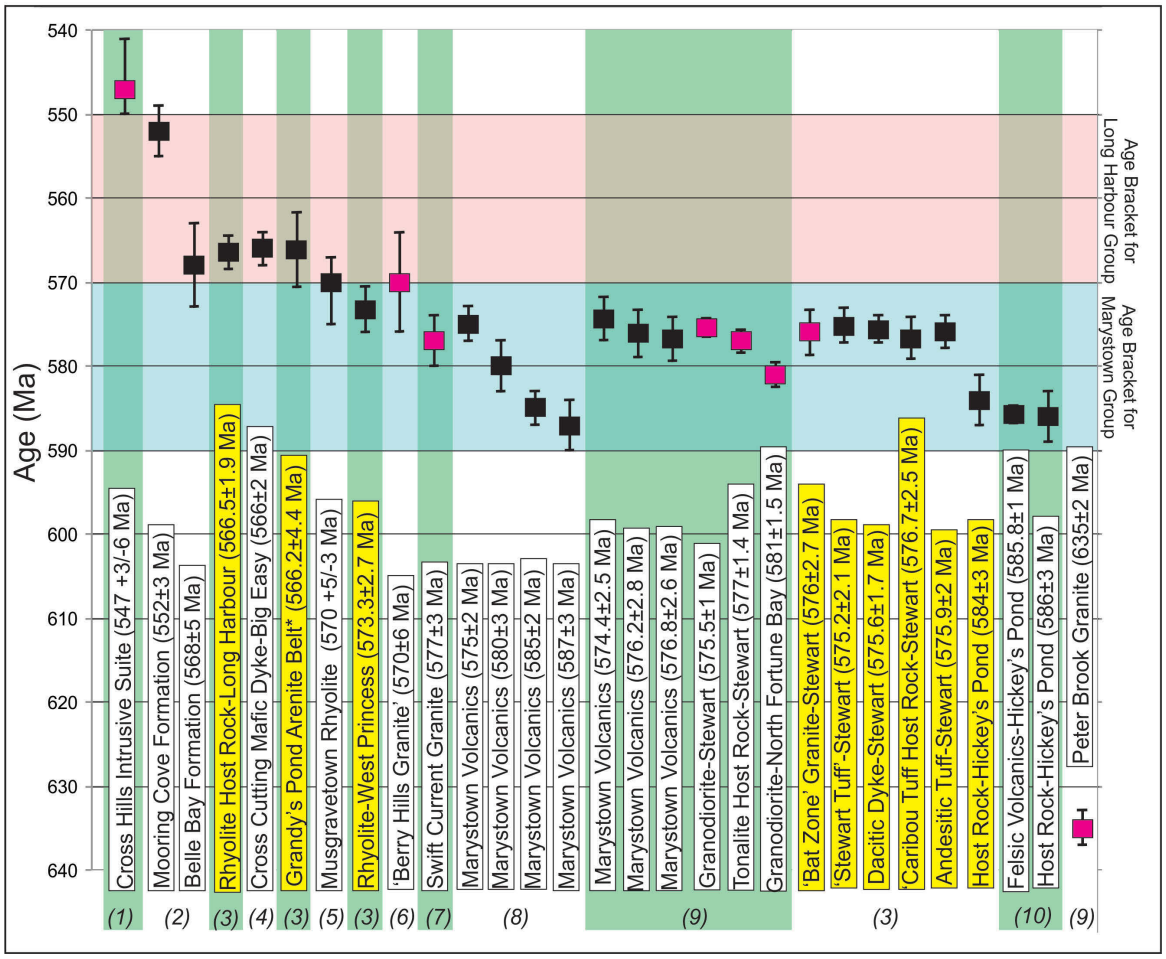

Figure 4-4*: Summary of relevant U/Pb geochronological data from the Burin Peninsula, northern Fortune Bay, and Clarenville areas. Also shown (right margin) are the regional age brackets for the Marystown Group (pale blue) and Long Harbour Group (pale pink). Numbers at the bottom of the plot correspond to the listed publications containing the data: 1) Tuach, 1991; 2) O'Brien et al., 1995; 3) this study (also highlighted in yellow); 4) Clarke, 2013; 5) O'Brien et al., 1989; 6) Kellett, 2014; 7) O'Brien et al., 1998; 8) McNamara et al., 2001; 9) Sparkes and Dunning, 2014; 10) Sparkes et al., 2016. Pink boxes indicate felsic plutonic rocks.*

4.5.1 Volcanic and Intrusive Rocks of the Marystown Group

Heritage Prospect

The 686 ±4 Ma age calculated from two overlapping and concordant fractions, measured for the pyroclastic andesite host rock (SF-13-180) at the Heritage prospect corresponds with the age of plutonic rocks near Seal Cove on the southwest Burin Peninsula, recently dated at 685 ±3.5 Ma (Layne, G.D., 2016, unpublished data). If this represents the true igneous age of the pyroclastic host rock, this would record a period of

arc volcanism previously unrecognized on the Burin Peninsula – although arc volcanism of this age (ca. 685-670 Ma) *has* been identified within the broader Avalon Zone, as represented in the Tickle Point Formation on the Connaigre Peninsula, west of the Burin Peninsula (e.g., Swinden and Hunt, 1991; Tucker, 1991, unpublished data; O'Brien et al., 1992; O'Brien et al., 1994). However, there are two younger fractions analyzed from this same sample. The youngest fraction (Z5) yielded an age of 639 Ma, coincident with the 635 ±2 Ma age of the Peter Brook granite, located proximal to the Heritage prospect (*Figure 4-4*; Sparkes and Dunning, 2014). If this Z5 fraction represents the true age, the slightly older Z2 fraction, yielding an age of 648 Ma, might be explained as the combination of an older ~686 Ma inherited zircon core with ~635 Ma age zircon overgrowth. This would be nominally consistent with the presence of xenocrystic cores identified in CL images (*Plate 4-1 A*).

Alternatively, the andesite may have contained a primary population of very fine-grained zircon not represented in the measured fractions, which were instead dominated by coarser grained zircon inherited from underlying felsic plutonic rocks. Given the similarity of geochemical signatures of the volcanic rocks at Heritage with other volcanic rocks of the Marystown Group, and their seeming lateral continuity with Marystown Group stratigraphy in field exposure, they are less likely to be part of an older, unique volcanic arc sequence. Our current interpretation is that the calculated ages for *SF-13-180* represent the inherited ages of xenoliths of country rock picked up during eruption of this predominantly pyroclastic unit, and that the Heritage prospect host rocks are contemporaneous with other rocks of the Marystown Group. However, further work is underway to develop a less equivocal age, and to elucidate this relationship, by dating non-pyroclastic felsic lithologies at Heritage.

Hickey's Pond Prospect

Two fractions were measured for sample SF-12-151 from highly altered host rocks at Hickey's Pond, the more precise fraction (Z1; *Figure 4-2B*) yielding an age of 584 ±3 Ma. This correlates with the recently published ages from Hickey's Pond of 586

±3 Ma for similarly highly altered rocks, and 585.8 ±1.7 Ma for less altered felsic volcanics inferred to be located within the hanging wall of the Hickey's Brook Fault, immediately adjacent to the deposit (Sparkes et al., 2016). In sum, the determinations for the two samples from the advanced argillic alteration zone provide an interpreted *maximum* age for mineralization at the prospect of 585 ±2 Ma (*Figure 4-5*), since epithermal deposits cannot pre-date their volcanic host rocks.

The recognition and characterization of hydrothermal zircon is a highly contentious topic, and the diagnostic features remain relatively ambiguous. Hydrothermal zircon occurrences are typically described in literature as having a "spongy" texture and to be enriched in high field strength elements, REE, common lead, and F relative to magmatic zircon (e.g., Watson et al., 1997; Hoskin et al. 1998; Hoskin, 1999). The grains from the Hickey's Pond (and Tower) showing(s), do not display a spongy texture, but display other unique textures, the presence of which appears to correlate with the occurrence of high-sulphidation epithermal alteration. These zircon display unique zircon overgrowths, as fracture filling or lobes around the grain perimeter, which are not present in any of the other relatively unaltered rocks of various origins sampled across the region. Therefore, these unique features are interpreted to possibly represent hydrothermal overgrowths, related to water-rich-trace element enriched-siliceous hydrothermal fluids of the high-sulphidation epithermal systems. However, further quantitative analysis using Secondary Ion Mass Spectrometry (SIMS) or microprobe to determine isotopic and trace element compositions would need to be completed to more adequately identify a hydrothermal origin for these zircon overgrowths, as qualitative observations alone are not sufficient. The presence of hydrothermal zircon is important though, as it provides a means to directly date mineralizing events.

The younger, but highly precise, ages of the older physical abrasion determinations of zircon from the vuggy silica zone at Hickey's Pond (fractions Z1, Z2 of SJOB-97; *Figure 4-3*), are potentially a consequence of analyzing fractions with lower-U cores of circa 585 Ma residual from the volcanic host rocks, which were volumetrically predominantly overgrown with higher-U rims of hydrothermal zircon (preferentially

removed from later samples analyzed using chemical abrasion). This interpretation would provide an estimated age of 572 ±1.5 Ma for the high-sulphidation mineralization at Hickey's Pond (*Figure 4-5*), or at least a more precise maximum age for mineralization, as this result could represent a mixed age to some extent.

Stewart Prospect

All volcanic rock samples from the Stewart prospect overlap within error at 576 ±1 Ma (*Figure 4-4*) and are indicative of abundant arc volcanism occurring over a relatively short period of time. Granite intruding the altered volcanic rocks at Bat Zone, and considered to be part of the BKIS, gave an age of 576 ±2.7 Ma, which is contemporaneous with the volcanic stratigraphy and with previously dated phases of the BKIS, including 575 ±1 Ma granodiorite and 577 ±1.4 Ma tonalite (Sparkes and Dunning, 2014). Furthermore, these ages are correlative with the 577 ±3 Ma Swift Current Granite on the north end of the peninsula (O'Brien et al., 1998). This 574-579 Ma age of plutonism is thus strongly inferred as parental to the precious metal high-sulphidation system at Stewart, which is hosted in the 576 ±1 Ma volcanic rocks within the Marystown Group.

The 575.6 ±1.7 Ma dacitic dykes that cross-cut the 'Lower Volcanic Unit' are the same age as the main felsic volcanic stratigraphy at Stewart, and geochemically resemble the 'Stewart Tuff' unit. They are therefore interpreted as possible feeder dykes to this unit. The corollary is that the 'Lower Volanic Unit' is in fact finitely older than the overlying felsic volcanic stratigraphy hosting mineralization at Stewart, and confirms a north-westward younging direction on the property.

The mafic dyke (*SF-12-41*) cross-cutting the 577 ±1.4 Ma (Sparkes and Dunning, 2014) tonalite host rock did not yield a logically consistent age, since all zircon fractions recorded dates significantly older than the tonalite it cross-cuts. Therefore, the dated zircon did not crystallize from the mafic dyke itself, but are interpreted to have been stoped from older lower crust by the mafic magma prior to intrusion, and represent the ages of older basement rocks. This is also indicated by the subrounded shapes of the

zircon, suggesting some degree of corrosion during this inheritance process. This sample was therefore not successful in providing a *minimum* age estimate for the deposit.

The age of high-sulphidation mineralization at Stewart is constrained to a *maximum* age of 576 ±2.5 Ma; the age of the volcanic 'Caribou Tuff' host rock (*Figure 4-5*). However, the high-sulphidation mineralization is likely penecontemporaneous with the Caribou Tuff, since the porphyry-style mineralization and the high-sulphidation mineralization at Stewart would appear filial, and linked to the 576 ±2.7 Ma Bat Zone granite, and/or the 575.5 ±1 Ma Stewart granodiorite (Sparkes and Dunning, 2014) that lie in close proximity.

4.5.2 Grandy's Pond Arenite Belt

Sample *SF-12-148* is still pending further measurements for refinement, but out of the two measured fractions, the more precise one is used as a preliminary age for the unit at 566.2 ±4.4 Ma. Since this is a sedimentary unit, the zircon are detrital and the youngest age is used to determine a *maximum* age for deposition. The ages are also expected to be representative of the ages of the volcanic rocks that comprise the unit.

The 566.2 ±4.4 Ma age is younger than the tightly constrained ages of volcanic rocks of the Marystown Group, but similar to the age determined for the Long Harbour Group. Based on these preliminary ages alone, this would imply that the arenite was, at least in part, derived from the younger Long Harbour volcanic rocks. However, bulk samples of the Grandy's Pond Arenite Belt (GPAB) display geochemical signatures that are closely correlative with the Marystown volcanics (*Chapter 3*), and quite distinct from those of Long Harbour. In one scenario, the GPAB could have been formed predominantly by erosion of an adjacent highland of Marystown Group rocks, but included components of volcanic ash ejecta from actively erupting volcanoes ca. 566 Ma, contemporaneous with the Long Harbour Group. Alternatively, it is possible that this age represents a minimum age for the Marystown volcanism. In either case, the GPAB records a facies change between the pyroclastic rocks of caldera centres undergoing very active arc volcanism ca. 575 Ma to a more distal setting, with intermittent volcanic

contributions (as indicated by thin interbedded pyroclastic units), and shedding and re-deposition of volcanic material, further re-worked by fluvial processes (indicated by cross bedding) ca. 566 Ma.

The GPAB is intruded by a number of plutonic rocks (e.g. O'Brien and Nunn, 1980; Kellett, 2014), but these are largely of undocumented age or affiliation. If these were the same suite of plutonic rocks as the Swift Current Granite and BKIS, this would constrain the GPAB to an age contemporaneous with the volcanic rocks of the Marystown Group. A single age has recently been determined for the 'Berry Hills Granite'. This pluton (formerly considered Devonian) cross-cuts GPAB sediments near the town of St. Bernard's - and yielded a SHRIMP U/Pb age of 570 ±6 Ma (Kellett, 2014). Unfortunately, this determination does not allow a conclusive assignment of either a Marystown or Long Harbour Group age to this pluton. More analyses are underway on sample SF-12-148 to confirm this initial ca. 566 Ma age estimate for the GPAB. Obviously, a more precise determination by CA-TIMS for the Berry Hills Granite would be desirable as well.

4.5.3 Volcanic Rocks of the Musgravetown Group

West Princess Prospect

Sample *GS-WPR* was collected for geochronology after attempts on two other samples from the Big Easy prospect (including *SF-13-181*) were unsuccessful in yielding adequate zircon populations for analysis. Sample *GS-WPR*, a flow banded rhyolite conformable with the Musgravetown epiclastic sediments, yielded an age of 573.3 ±2.7 Ma, which is older than the post-570 Ma Rocky Harbour Formation near the top of the succession. This new age is, marginally younger, but consistent with the period of volcanism represented in the Marystown Group on the Stewart prospect. In addition, volcanic and epiclastic rocks of the Musgravetown and Marystown Groups exhibit similar geochemical signatures (*Chapter 3*). Given these data, the Musgravetown Group is interpreted to overlap in time with the Marystown Group, with Musgravetown Group rocks formed within the same regional volcanic arc, but reflecting a facies change to

clastic-sedimentary dominated sequences (epiclastics) in an intra-caldera setting, resulting from contemporaneous, or marginally younger, erosion of the arc volcanics.

Big Easy Prospect

A conclusive age was not determined for the andesitic accretionary lapilli tuff conformable with the host rock stratigraphy at Big Easy (*SF-13-181*). This was an important sample, as its age would provide a maximum age for mineralization at the prospect, which has already been constrained to a *minimum* age of 566 ±2 Ma (Clarke, 2013; *Figure 4-5*) of a mafic dyke which cross cuts the mineralized sequence.

Additional fractions are currently in queue for measurement to hopefully refine the current data, which includes six fractions producing a wide range of ages. Being a volcaniclastic rock, the presence of multiple ages isn't unusual since older zircon can be incorporated as xenocrysts or xenoliths. However, the fractions did not produce any overlapping points to indicate a dominant age-population. The grains were very tiny and of low quality containing very high common to radiogenic Pb ratios (*Table 4-1*) resulting in larger error in some measurements. Because the grains were so small, they were also etched for less time than a typical sample would be, potentially leaving large portions of crystal behind containing significant lead loss. Fractions Z2, Z3, Z5, and Z6 are interpreted to be the result of significant lead loss, plotting along concordia at younger ages between 542 and 555 Ma. The hosting volcano-sedimentary sequence cannot be this young since it is cross cut by a 566 ±2 Ma mafic dyke (Clarke, 2013).

The oldest fractions, Z1 and Z4, yield ages that correlate with the ages of other regional volcanic sequences. Fraction Z1, at 624 Ma is the result of zircon inheritance, with xenocrysts or xenoliths derived from older crustal rocks. Ca. 620 Ma volcanic and co-magmatic plutonic rocks occur on the Avalon Peninsula within the Harbour Main Group and Holyrood Intrusive Suite (e.g., Krogh et al., 1988; Sparkes et al., 2005).

Fraction Z4 at ~584 Ma might also be the result of zircon inheritance, alternatively, it could be representative of the rocks true age, since it correlates with the

age of host rocks at the Hickey's Pond prospect of the Marystown Group, of which Musgravetown Group rocks appear to be akin to. If this is the true age of volcanism, the timing of mineralization becomes confined between ~584 and 566 Ma, however, further measurements are necessary to conclusively determine an age.

Our current interpretation, as summarized in Figure 4-5, is that Big Easy has a definitive *minimum* age of 566 Ma based on the cross-cutting dyke, but is likely affiliated with the 570-580 Ma plutonism of the Swift Current and Burin Knee Intrusive Suites, as evidenced by the presence of the 573.3 ±2.7 Ma West Princess Rhyolite in the nearby Musgravetown Group stratigraphy.

4.5.4 Volcanic Rocks of the Long Harbour Group

Long Harbour Prospect

Flow banded rhyolite from the Belle Bay Formation of the Long Harbour Group (*SF-12-56*) produced an age of 566.5 ±1.9 Ma. This age is consistent with previously published ages from the base and top of the group (O'Brien et al., 1995; Tucker unpublished data) and is distinctly younger than volcanic rocks of the Marystown and Musgravetown Groups.

The age of the Long Harbour rhyolite corresponds to the age of the mafic dyke cross cutting mineralization at the Big Easy prospect (Clarke, 2013). This age correlation is also consistent with geochemical results (*Chapter 3*), where the Long Harbour rhyolites and mafic dykes cross cutting rocks of both the Long Harbour and Musgravetown Groups displayed similar geochemical signatures and tectonic affinity

The 566.5 ±1.9 Ma age of the rhyolite host rock provides a *maximum* age for mineralization at the Long Harbour prospect. In terms of the regional study area, the low-sulphidation mineralization at Long Harbour thus currently stands as unique in terms of age, and its affiliation with a separate, alkaline, episode of arc volcanism (*Figure 4-5*).

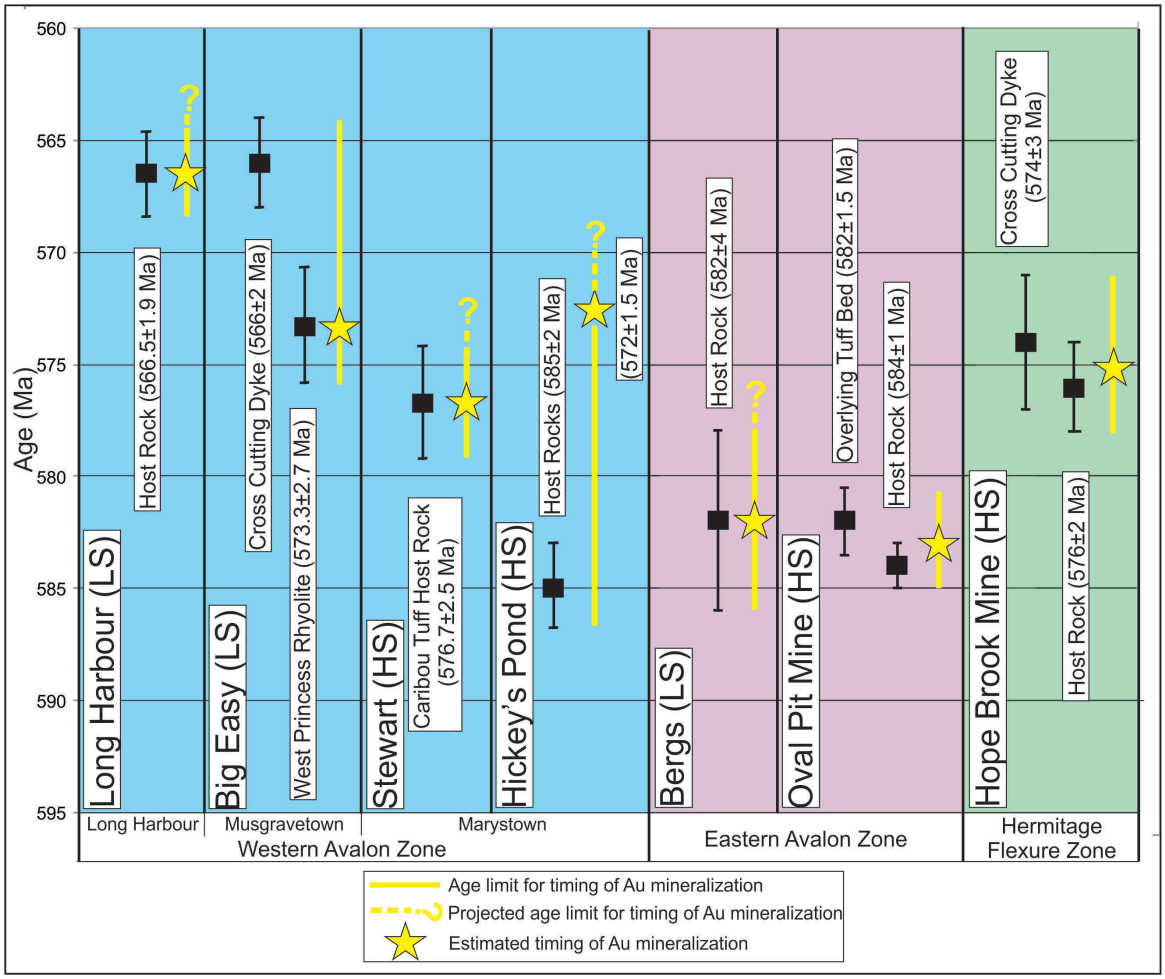

***Figure 4-5**:Summary table showing age constraints on the timing of epithermal-style mineralization and alteration within the Avalon Zone of Newfoundland. LS=low-sulphidation; HS=high-sulphidation. Additional data compiled from: Dube et al., 1998; Sparkes et al., 2005; Clarke, 2013; Sparkes et al., 2016.*

4.6 Summary of Main Findings

-A *maximum* age for mineralization of *585 ±2 Ma* was determined at Hickey's Pond, but an age of *572 ±1.5 Ma* is interpreted as an estimate for the timing of the high-sulphidation mineralization, based on the earlier age determination analyzed using physical abrasion (O'Brien et al., 1999) and the presence of hydrothermal zircon at the prospect.

-An overall age of *576 ±1 Ma* was determined for the volcanic stratigraphy at Stewart, indicating abundant arc volcanism occurring over a relatively short period of time, and also contemporaneous with plutonic rocks of the Burin Knee Intrusive Suite and Swift Current Granite. A north-westward younging direction of the volcanic stratigraphy was also determined based on age dating and cross-cutting relationships

-A *maximum* age for mineralization of *576 ±2.5 Ma* (age of Caribou Tuff host rock) was determined at Stewart, which is also an estimate for the timing of mineralization itself, given that the porphyry-style mineralization and high-sulphidation mineralization at Stewart appear filial, and linked to the proximal Bat Zone granite and Stewart granodiorite that lie in close proximity and of similar age (~576 Ma).

-the Grandy's Pond Arenite Belt has been assigned a preliminary age of *566 ±4.4 Ma*, with further analyses underway.

-A *minimum* age for mineralization of *566 ±2 Ma* was previously determined at Big Easy (Clarke, 2013), but the low-sulphidation mineralization itself is interpreted to be affiliated with the 570-580 Ma plutonism of the Swift Current and Burin Knee Intrusive Suites, as evidenced by the presence of the *573.3 ±2.7 Ma* West Princess Rhyolite in the nearby Musgravetown Group stratigraphy.

-A *maximum* age for mineralization of *566.5 ±1.9 Ma* was determined at Long Harbour. Regionally, the low-sulphidation mineralization at Long Harbour currently stands as unique in terms of age, and its affiliation with a separate, alkaline, episode of arc volcanism

CHAPTER 5: CHARACTERISTICS AND SULPHUR ISOTOPE SIGNATURES OF HIGH-SULPHIDATION EPITHERMAL AU MINERALIZATION OF THE BURIN PENINSULA

5.1 Introduction

Both high- and low-sulphidation precious metal bearing epithermal systems occur throughout the Burin Peninsula region of the Western Avalon Zone. The high-sulphidation prospects are found concentrated on the peninsula itself, hosted within volcanic rocks of the Marystown Group, and form an extensive belt of hydrothermal alteration that can be traced intermittently for over 100 km, known as the Hickey's Pond-Point Rosie alteration system. The potential for significant gold mineralization in the Burin Peninsula district wasn't fully realized until the early 1980s, when the Hickey's Pond prospect was identified as a gold bearing advanced argillic alteration zone. The Hope Brook Mine in southwestern Newfoundland was discovered around the same time, and recognized to be of great similarity to Hickey's Pond. This prompted extensive gold exploration efforts on the Burin Peninsula by both industry and government throughout the 1980s, leading to the discovery of the many additional high-sulphidation occurrences along the Hickey's Pond-Point Rosie belt.

The main high-sulphidation prospects of interest in this study are the Hickey's Pond, Stewart, Tower, and Monkstown Road prospects, their locations shown in *Figure 5-1*. Directly adjacent to the Stewart prospect is the Forty Creek showing, tentatively interpreted to represent an intermediate-sulphidation style epithermal system. Currently, not much is known about the showing, but given its close proximity to, and potential genetic relationship with the Stewart prospect, it is discussed as part of this chapter. Also apparent at the Stewart prospect is the potential for additional porphyry-style mineralization. Reevaluation of the property in recent years has led to the interpretation that the deposit represents porphyry-style gold-copper mineralization, overprinted by advanced argillic alteration associated with a related, telescoped high-sulphidation epithermal system (e.g., Hedenquist, 2007; Dyke and Pratt, 2008).

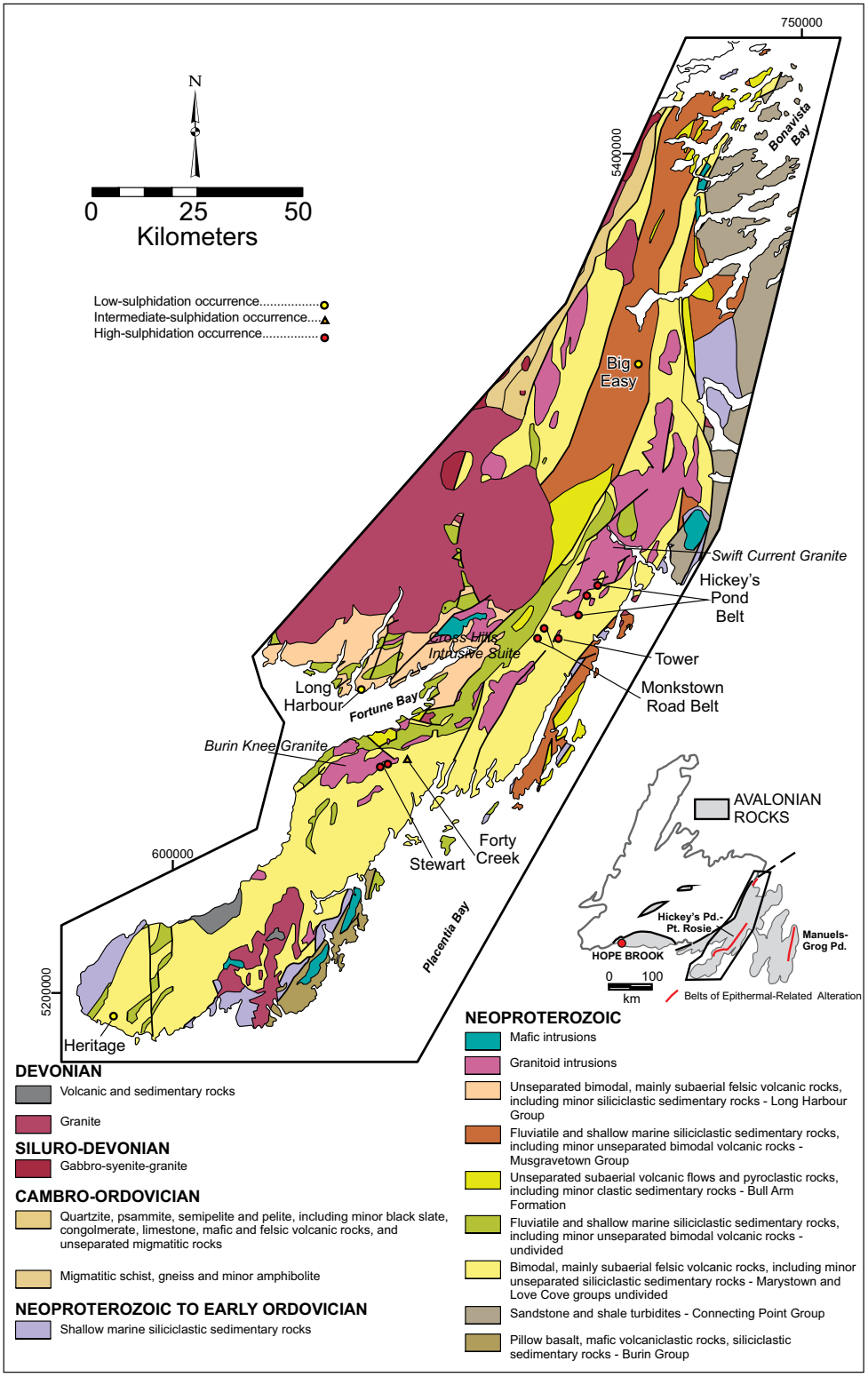

***Figure 5-1**: Regional geology map of the western Avalon Zone of Newfoundland with key epithermal prospects highlighted (modified from Sparkes and Dunning, 2014; O'Brien et al., 1998; coordinates are listed in NAD 27, Zone 21).*

The main objectives of examining these high-sulphidation occurrences were to further characterize these systems within the epithermal realm (and porphyry-style realm at Stewart), and to determine what might make some occurrences more prospective than others for gold, despite their seemingly similar alteration assemblages and extents. To accomplish this it was important to determine the mineralogy and distribution of the alteration and ore assemblages, examine the deportment of gold at each prospect, and where possible, develop a paragenetic sequence. This was done using a combination of petrography, visible infra-red reflectance spectroscopy (VIRS), and scanning electron microscopy with energy dispersive X-ray spectrometry (SEM-EDX). The fine-grained nature of gold and of the micas and clay minerals commonly formed in these low-temperature environments makes them difficult to identify with the microscope alone, so VIRS and SEM-EDX are imperative for accurate identification. These methods also allow for the distinction between potassic- and sodic-dominated alunite, the latter of which forms at higher temperatures and is more typically associated with auriferous hydrothermal systems (e.g., Stoffregen and Cygan, 1990; Dill, 2001). A preliminary sulphur isotope study was also conducted for the high-sulphidation prospects, the objectives and methods of which are discussed separately in *Section 5.9*.

At Hickey's Pond, VIRS data were collected at regularly spaced intervals through archived drill core to produce an alteration map in cross section (work was conducted in collaboration with Greg Sparkes of the NL Geological Survey). To accompany the alteration mapping, a detailed analysis of ore mineralogy in the four highest-grade gold zones was also completed. A summary of this work can be found in the recent publication by Sparkes et al. (2016), and the accompanying VIRS spectral data in the open-file report by Sparkes et al. (2015). Alteration mapping is particularly important in these high-sulphidation systems since well-defined alteration zoning is produced during their formation, which can be used to indicate the orientation of the system and the location of potential high-grade gold zones.

At the remaining prospects (Stewart, Forty Creek, Tower, and Monkstown Road) VIRS data were used to identify alteration only in specific samples of interest, as detailed

alteration mapping has already been completed at the Tower, Stewart, and Monkstown Road prospects, by Sparkes (2012) and Sparkes and Dunning (2014).

A comprehensive summary of previous work and detailed descriptions of the local geology at each of the prospects, is provided in *Chapter 1* (*Section 1.7.1.2*) and *Chapter 2*, respectively. The geology of the Monkstown Road prospect is also introduced here to highlight the unique alteration that occurs there, although it is hosted in similar volcaniclastic stratigraphy to the nearby Tower and Hickey's Pond prospects. The results of this investigation on high-sulphidation alteration and mineralization are presented below, following a brief description of methodology and a discussion of the characteristics and genesis of high-sulphidation epithermal gold systems. A summary of the results of this chapter, highlighting the main characteristics of each deposit as well as those of the idealized models for low-, intermediate- and high-sulphidation epithermal, and porphyry deposits, can be found in *Table E-1* of *Appendix E*.

5.2 Methods

Representative samples of alteration, mineralization and veining were collected from outcrop and drill core at the various prospects. Sampling was primarily focused in areas containing the highest grades of gold, based on historical reports. Representative samples were cut into 30 μm thick polished thin sections. A more detailed description of sampling procedures, and tables summarizing sample attributes (*Table A-1*) and field station data (*Table A-2*), including descriptions and locations can be found in *Appendix A*.

A TerraSpec® Pro portable visible infra-red reflectance spectrometer was used to collect VIRS spectra, a procedure that does not require any special sample preparation. Archived drill core from the Hickey's Pond prospect was also analyzed, with VIRS spectra collected at 1m intervals. The spectra were interpreted using TSG™ Pro software (Ver. 7.1.0.062), programmed to identify the two most dominant minerals in a sample based on its spectral characteristics. The results from the automated software were then verified through manual interpretation using reference spectra. The TSG™ Pro results of individual samples can be viewed in *Table 1* of *Appendix A*, listed under the headings of

Alteration 1 and *Alteration 2*. A more detailed discussion of VIRS methods and applications and of the portable device itself can be found in Kerr et al. (2011).

A subset of representative samples was then selected for SEM-EDX analysis. The 30um thick, polished thin sections were carbon coated and analyzed using a FEI MLA 650 FEG scanning electron microscope (SEM), equipped with energy dispersive X-ray spectrometry (EDX), based on silicon drift detector (SDD) technology, at the MAF-IIC Microanalysis Facility at Memorial University. Images and data were typically acquired using an accelerating voltage of 15kV, with some analyses done at 25 kV. Quantax Esprit version 1.9 software was used for analyzing X-ray spectra, and the interactive peak-to-background ZAF (PB-ZAF) method was used for elemental quantification. Quantification data was calculated as normalized atomic % concentrations and mineral identification was done manually using the atomic ratios. Examples of spectra from some of the key ore minerals can be found in *Appendix G.*

5.3 Setting, Characteristics and Genesis of High-Sulphidation Epithermal Gold Systems

Unless otherwise noted, the following content has been extracted and compiled from the comprehensive reviews of epithermal systems presented by White and Hedenquist (1995), Hedenquist et al. (2000) and Sillitoe and Hedenquist (2003), and references therein. A general overview of the epithermal environment is described first, followed by a more detailed discussion of the high-sulphidation end-member.

5.3.1 Overview of the Epithermal Environment

Epithermal gold deposits are broadly defined as hydrothermal deposits formed at shallow depths (generally <1km) from surface, and at relatively low temperatures (<300°C). These deposits are precious metal dominated (Au ± Ag), but can also contain appreciable amounts of base metals such as Cu, Pb, or Zn. They are associated with convergent plate margins, most commonly forming coevally with arc magmatism during subduction, and during post-subduction extension. Epithermal deposits can be divided into two main end-members: high-sulphidation and low-sulphidation – and the former is

the focus of this chapter. The classification is based on the sulphidation state, essentially the range in T-fS_2 space indicated by the hypogene sulphide assemblage (Barton and Skinner, 1967; Barton, 1970; Einaudi et al., 2003; *Figure 5-2*). A third subdivision of intermediate-sulphidation has been introduced in recent years, which reflects an ore assemblage indicative of a sulphidation-state intermediate to that of the two original end members (Hedenquist et al., 2000).

5.3.2 Deposit Setting and Characteristics

High-sulphidation deposits typically occur during active subduction, roughly simultaneous with related calc-alkaline arc volcanism, and hosted within subaerial, andesitic to rhyolitic volcaniclastic rocks. They are typically located proximal to volcanic vents where magmatic vapours discharge at surface as high-temperature acidic fumaroles, and overlie shallowly emplaced degassing oxidized intrusions. These intrusions are not only spatially related, but also genetically linked to the high-sulphidation deposits, providing a source of heat and volatiles, and can themselves also generate and host porphyry-style mineralization at depth (Arribas, 1995; *Figure 5-3*). Many examples of contemporaneous porphyry and high-sulphidation deposits have been documented (e.g. Sillitoe, 1999), most notably the example of Lepanto (Arribas et al., 1995).

High-sulphidation deposits exhibit strong alteration zoning, most typically radiating from a central, vuggy, residual silica core that hosts the highest ore grades. Alteration grades outwards to an advanced argillic alteration assemblage of quartz-alunite±kaolinite, followed by an argillic assemblage of illite-smectite, which is surrounded by more distal, and less diagnostic, phyllic and propylitic assemblages (*Figure 5-4*). In the presence of higher temperatures and pressures of deeper deposits, pyrophyllite can occur in the place of alunite, and dickite in the place of kaolinite. Topaz and tourmaline may also be present in high temperature zones and indicate the presence of F and B in the acidic hydrothermal fluids (Taylor, 2007).

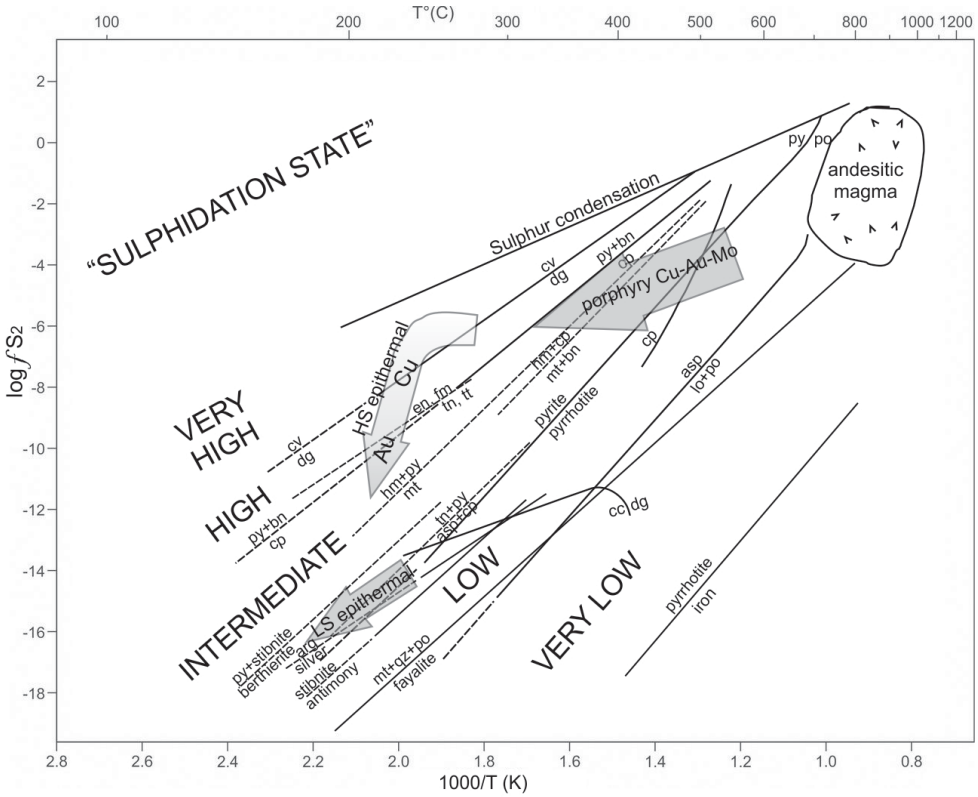

Figure 5-2*: Log fS_2-1000/T diagram illustrating fluid environments in porphyry Cu deposits, and high- and low-sulphidation epithermal Au-Ag deposits in terms of a series of possible cooling paths. Fluid environments are based on sulphide assemblages and temperatures discussed in Einaudi et al., 2003, and sulphidation reactions from Barton and Skinner (1979). High-sulphidation arrow displays early Cu-rich high-sulphidation state assemblage, followed by a Au-rich stage at intermediate sulphidation states. arg=argentite, asp=arsenopyrite, bn=bornite, cc=chalcocite, cp=chalcopyrite, cv=covellite, dg=digenite, en=enargite, fm=famatinite, hm=hematite, lo=lollingite, mt=magnetite, py=pyrite, po=pyrrhotite, qz=quartz, tn=tennantite, tt=tetrahedrite (modified from Einaudi et al., 2003).*

Disseminated or replacement-style mineralization is formed most commonly, facilitated by the porous and permeable nature of the volcaniclastic host rocks (Hedenquist et al., 2000). Mineralized veins, stockworks and hydrothermal breccias also occur frequently. These deposits tend to contain an abundance of high-sulphidation state sulphides (and sulphosalts), including pyrite, enargite, luzonite, famatinite, covellite, tennantite and tetrahedrite (Einaudi et al., 2003). Gold typically occurs as native-gold, electrum, or as various gold-tellurides.

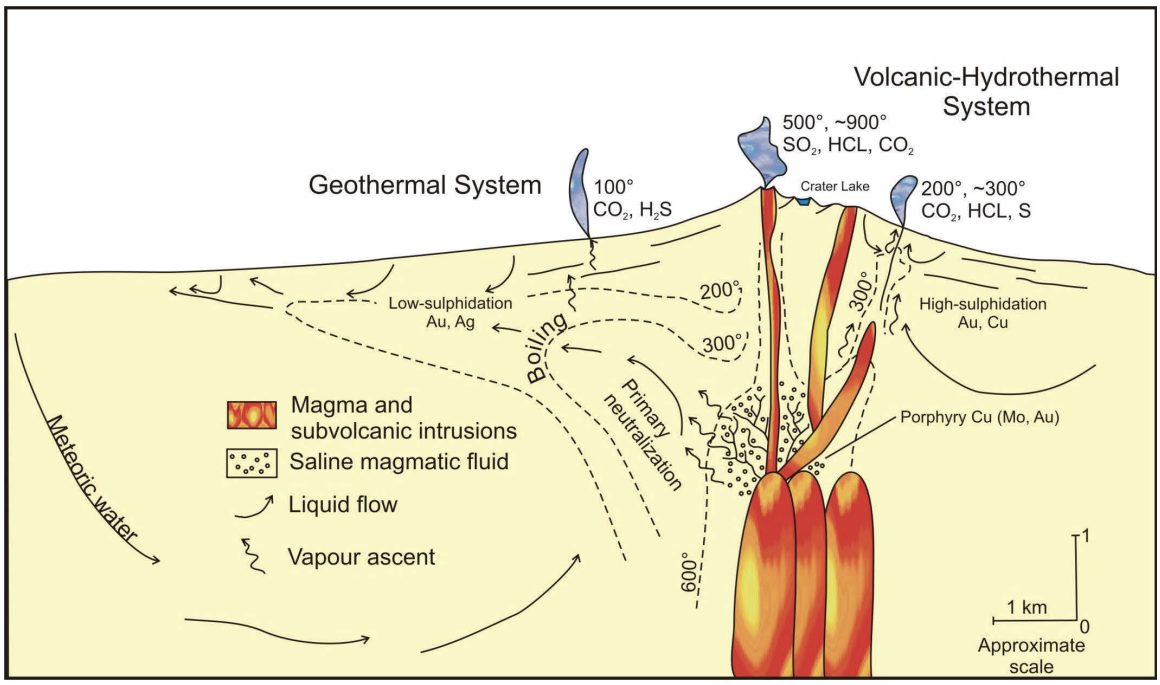

***Figure 5-3**: Schematic illustrating the environments in which high-sulphidation (volcanic-hydrothermal) and low-sulphidation (geothermal) deposits form, and their spatial relationship to the main parent intrusion driving the systems. Within this environment, the parent intrusion also commonly spawns porphyry-style mineralization at depth. Fluid and vapour flow paths and basic mixing and physiochemical gradients are also shown (From Hedenquist and Lowenstern, 1994).*

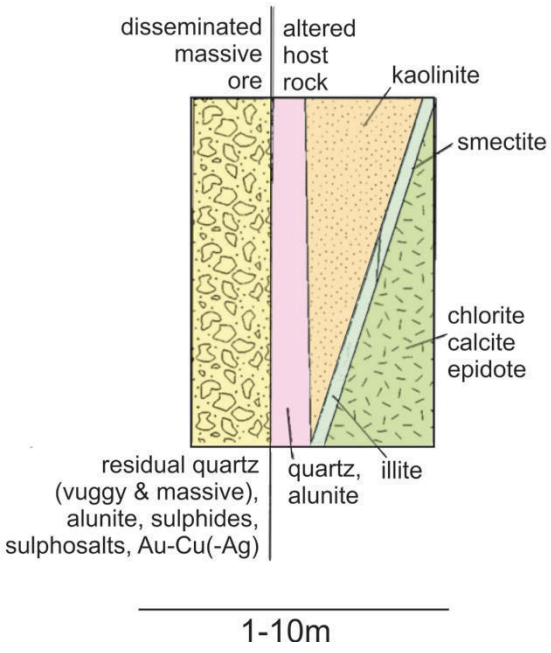

***Figure 5-4**: Diagram depicting the typical alteration zoning present in high-sulphidation epithermal deposits, grading outwards from the vuggy silica high-grade ore zone, to quartz-alunite+/-kaolinite (advanced argillic), to illite-smectite (argillic), to phyllic and propylitic assemblages (modified from Cooke and Simmons, 2000)*

5.3.3 Metal Source, Fluid Characteristics and Deposit Genesis

When melting of the mantle wedge occurs during subduction, due to a decreased melting temperature from hydration, and decompression melting from convection, sulphides in the upper mantle are partially consumed and can contribute metals to magmas ascending into the crust (Hedenquist and Lowenstern, 1994). Metals can also enter magmas from melting of the crust and mass transfer from the subducting slab (Hedenquist and Lowenstern, 1994).

As magma slowly ascends, and fractional crystallization occurs, the melt becomes enriched with H_2O and incompatible elements, including metals such as gold (Hedenquist and Lowenstern, 1994). As magma approaches shallower depths, the decrease in pressure causes fluids to exsolve, which sometimes further subdivide into two phases at progressively lower pressures: 1) a low density, low salinity vapour containing compounds such as CO_2, SO_2, H_2S, and HCl; and 2) a dense, hypersaline liquid (brine) rich in Cl, Cu and other chlorophile elements (Hedenquist and Lowenstern, 1994), both of which can contain gold.

High-sulphidation deposits display a strong genetic relationship to magmatism and it is generally accepted that magma is the main metal source and heat source driving the system (e.g. Hedenquist and Lowenstern, 1994; White et al., 1995; Sillitoe and Hedenquist, 2003). For high-sulphidation-style deposits to form it is crucial that an oxidized, intermediate, calc-alkaline magma is emplaced at shallow crustal levels, within a few km of surface, and that deep seated structural conduits such as faults and fractures are present to accommodate the rapid ascent of fluids.

The current genetic model is still based on Arribas's (1995) two-stage model adapted from White (1991). The first stage involves the rapid ascent of an acidic, magmatic vapour phase derived from two-phase separation of the exsolved magmatic fluid, which upon reaching very shallow levels reacts with shallow water aquifers causing the disproportionation of magmatic SO_2 to form H_2SO_4 and H_2S. The acidic (pH <2), oxidized H_2SO_4 fluid causes the extensive leaching responsible for the formation of

vuggy silica alteration (Hedenquist and Lowenstern, 1994; Cooke and Simmons, 2000). The fluids become progressively more neutralized moving outwards from the vuggy silica core due to wall rock interaction and/or dilution by meteoric waters causing the observed characteristic alteration zoning (Taylor, 2007).

The second stage is the mineralizing stage, which exploits the porosity created in the first stage to precipitate gold and other metals. Unlike the first stage, the second stage fluids may have several possible origins, and these may vary from deposit to deposit. There are three possible origins proposed for the second stage mineralizing fluid:

1) An acidic, oxidized, highly saline brine, in which metals get carried as chloride complexes and deposit at shallow depths due to dilution, cooling, reduction, and/or pH increase from mixing with ground waters. This would originate from the denser brine phase of an exsolved magmatic fluid.

2) An acidic, reduced, low-salinity fluid, with gold transported as an AuHS(aq) (bisulphide complex), formed from mixing of magmatic vapour and lesser meteoric fluids at depth. Approaching shallow depths, this fluid type can mix with ground water, inducing oxidation, sulphate stable conditions, and the precipitation of gold as shown in *equation 1* below (Cooke and Simmons, 2000);

$$AuHS(aq) + 4H_2O \rightarrow Au(s) + SO_4^{2-} + 2H^+ + 3.5H_2 \quad (1)$$

3) A similar acidic vapour phase as the first stage, with gold transported as sulphide and/or chloride species. Similar to above, at shallow depths the vapour can mix with ground water inducing oxidation and precipitating gold.

5.4 Hickey's Pond

The Hickey's Pond prospect is situated along the southeastern margin of the Swift Current Granite, hosted in intermediate to felsic volcaniclastic rocks of the Marystown Group (*Figure 5-5*). The prospect is small, but well exposed, containing a central vuggy silica core surrounded by an extensive halo of advanced argillic alteration, and then more distal phyllic alteration. The alteration is overthrust from the northwest, and bounded by the southwest-striking and steeply northwest-dipping Hickey's Brook Fault (*Figure 5-5*). Relatively unaltered, and much less deformed, felsic volcaniclastic rocks occur in the hanging wall, directly adjacent to the advanced argillic alteration and are intruded by the Swift Current Granite further to the northwest (O'Brien et al., 1999; Sparkes et al., 2016). The southeastern extent of the alteration is not exposed but inferred to be truncated by a faulted contact (Sparkes et al., 2016).

Within the extensive Hickey's Pond-Point Rosie alteration belt, the Hickey's Pond prospect has yielded the highest gold grades to date (up to 60.4 g/t gold in grab sample). It is for this reason that the property was assessed in the greatest detail, to try to better understand the local controls on gold mineralization. Sampling at the prospect was focussed on four main zones, each containing unique textures and mineral assemblages, which historically have yielded some of the highest gold grades, both at surface and at depth. The zones are referred to be their distinctive identifying properties: 1) Vuggy Massive Silica (surface exposure; *Figure 5-5*), 2) Pyrite-Quartz-Alunite (62-64m depth in DDH HP-90-03; *Figure 5-6*), 3) Hydrothermal Specularite Breccia (surface exposure; *Figure 5-5*), and 4) Specularite-Quartz-White Mica (~117m depth in DDH HP-90-02; *Figure 5-6*). For clarity, 'specularite' is used throughout this chapter when referring to the grey, crystalline, metallic form of hematite associated with the hydrothermal alteration, and 'hematite' is reserved for describing the red, earthy form, typical of oxidative weathering.

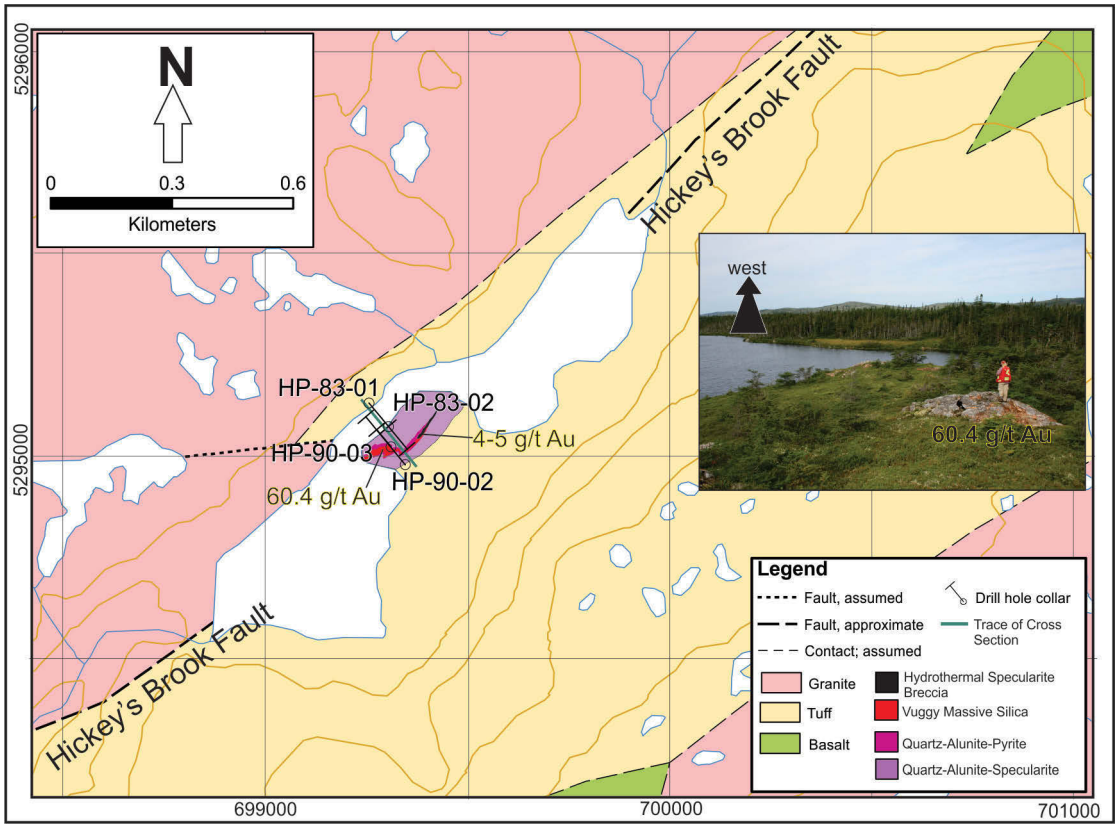

***Figure 5-5**: Compilation map outlining the geology surrounding the Hickey's Pond prospect (modified from Sparkes et al., 2016, data from Huard and O'Driscoll, 1986; O'Brien et al., 1999; Sexton et al., 2003).*

5.4.1 Alteration Zoning and Hydrothermal Textures

A clear zonation of high-sulphidation-related alteration is exposed at surface, grading outwards from a central massive to vuggy silica core to a more extensive halo of an advanced argillic assemblage dominated by quartz-alunite, followed by more distal phyllic alteration (*Figure 5-5*).

The siliceous core consists of grey to beige massive silica, containing discontinuous patches of vuggy-textured silica (*Plate 5-1 A, C, D*). Silica is the main constituent, typically ~90%, making up the fine-grained matrix and also occurring as coarser grains in clusters with Na-alunite, as comb-texture-quartz lining vugs, and locally as veinlets (± sulphides and alunite). 5-15% alunite occurs intergrown with quartz; finely disseminated throughout the silica matrix, clustered with quartz filling vugs, and within quartz-sulphide veinlets. Up to 5% rutile also occurs and also appears related to

the primary hydrothermal quartz-alunite assemblage. This alteration corresponds with the '*Vuggy Massive Silica*' ore assemblage described in *Section 5.4.3*.

The advanced argillic alteration is dominated by quartz-alunite and transitions from a pyrite-rich assemblage (*Plate 5-1 B*) to a more laterally extensive specularite-rich one (*Plate 5-1 E*) extending outwards from the central silica core. Both varieties are highly deformed and contain alternating, discontinuous bands of variable grain size and composition, including a finer-grained assemblage dominated by quartz (70-80%) with lesser Na-alunite, and a coarser-grained assemblage with roughly equal proportions of quartz and Na-alunite. Both horizons contain pyrite and/or specularite, and trace rutile. Locally within the specularite-bearing zones, the finer-grained assemblage appears to make up a main groundmass, with the coarser-grained assemblage forming isolated clusters, and seams, which encompass small rafts of the former.

Local exposures of hydrothermal breccia occur centrally within the overall alteration halo, adjacent on the northeast of the central vuggy silica zone (*Figure 5-5*). The breccia is relatively undeformed and contains strongly silica altered angular fragments with minor Na-alunite (5-7%) and trace rutile, which are fractured and surrounded by an assemblage of 50-60% quartz, 30-40% specularite, 10-20% Na-alunite, and minor rutile (*Plate 5-1 F*). Some alunite grains show irregular zoning, with portions of the crystals composed of the Ca- and Sr-phosphate minerals woodhouseite and svanbergite, respectively, which are isostructural with alunite. This alteration corresponds to the '*Hydrothermal Specularite Breccia'* ore assemblage described in *Section 5.4.3*.

Analysis of alteration in the subsurface, based on VIRS of drill core, shows that the advanced argillic alteration is contained within the footwall of the northwesterly dipping Hickey's Brook Fault (*Figure 5-6*). At the top of drillhole HP-83-01, collared on the northwest side of Hickey's Pond, felsic volcaniclastic rocks of the hanging wall contain a propylitic alteration assemblage consisting of phengite, iron-magnesium chlorite, and epidote, representative of a regional greenschist metamorphic assemblage.

Approximately 30 m downhole, an abrupt change occurs, with an increase in intensity of the penetrative fabric and shift to a phyllic alteration assemblage containing muscovite, and lesser paragonite.

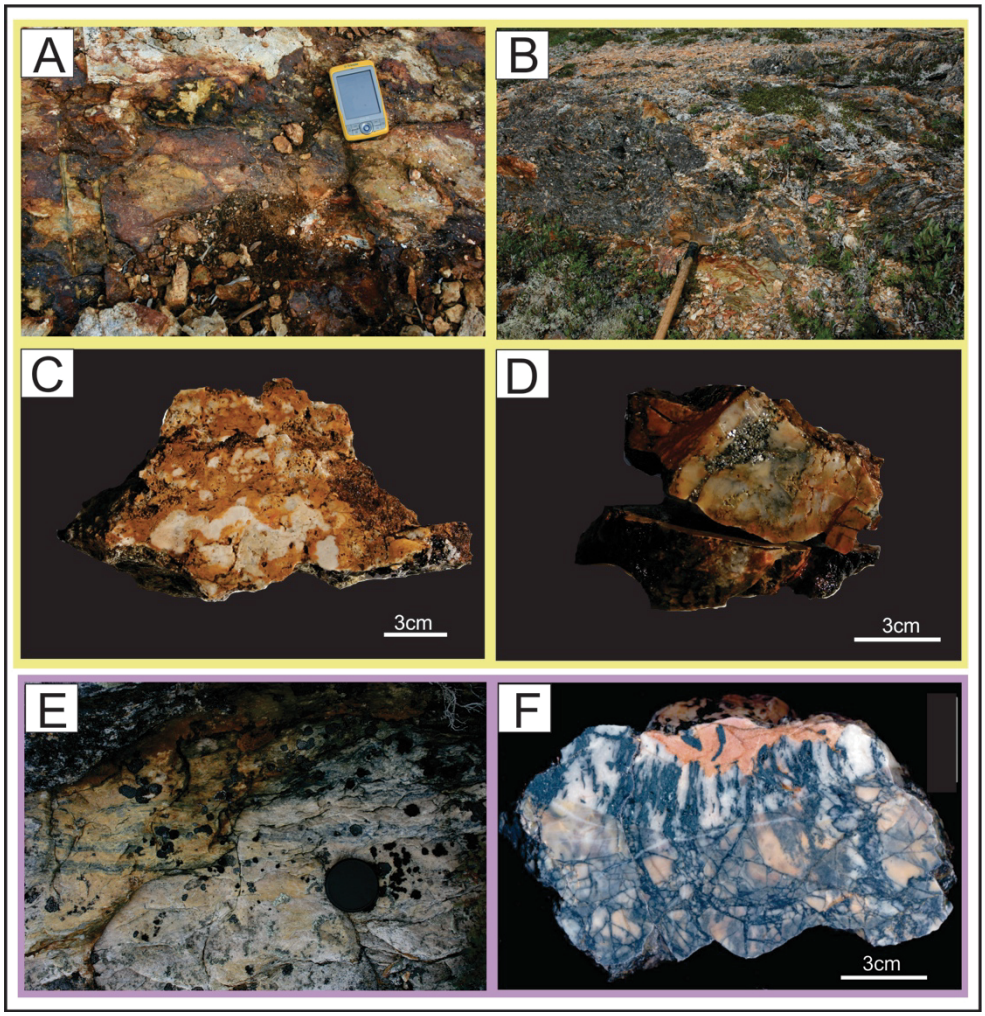

Plate 5-1*: Representative photos of high-sulphidation-related alteration assemblages and textures found at surface at the Hickey's Pond prospect. A-D (yellow frames) are pyrite dominated assemblages and E&F (purple frames) are specularite dominated assemblages: A) 'Vuggy Massive Silica' zone found at surface, strongly oxidized and yielding up to 60.4 g/t gold; B) Advanced argillic alteration assemblage of quartz-alunite-pyrite surrounding the vuggy massive silica zone. Outcrop is friable and oxidized; C) Hand sample from the 'Vuggy Massive Silica' zone displaying vuggy silica textures (SF-12-151); D) Hand sample from the 'Vuggy Massive Silica' zone (A) displaying local enrichment in sulphides, including sulphide veinlets of pyrite and tennantite cross-cutting more massive silica (SF-12-152; 60.4 g/t Au); E) Advanced argillic alteration assemblage of quartz-alunite-specularite surrounding both the vuggy silica core and quartz-alunite-pyrite alteration assemblage (lens cap for scale); F) Hand sample of the 'Hydrothermal Specularite Breccia' located centrally within the overall alteration halo, adjacent and northeast of the central vuggy silica zone (SF-13-183/OB-98-41; 5.4 g/t Au).*

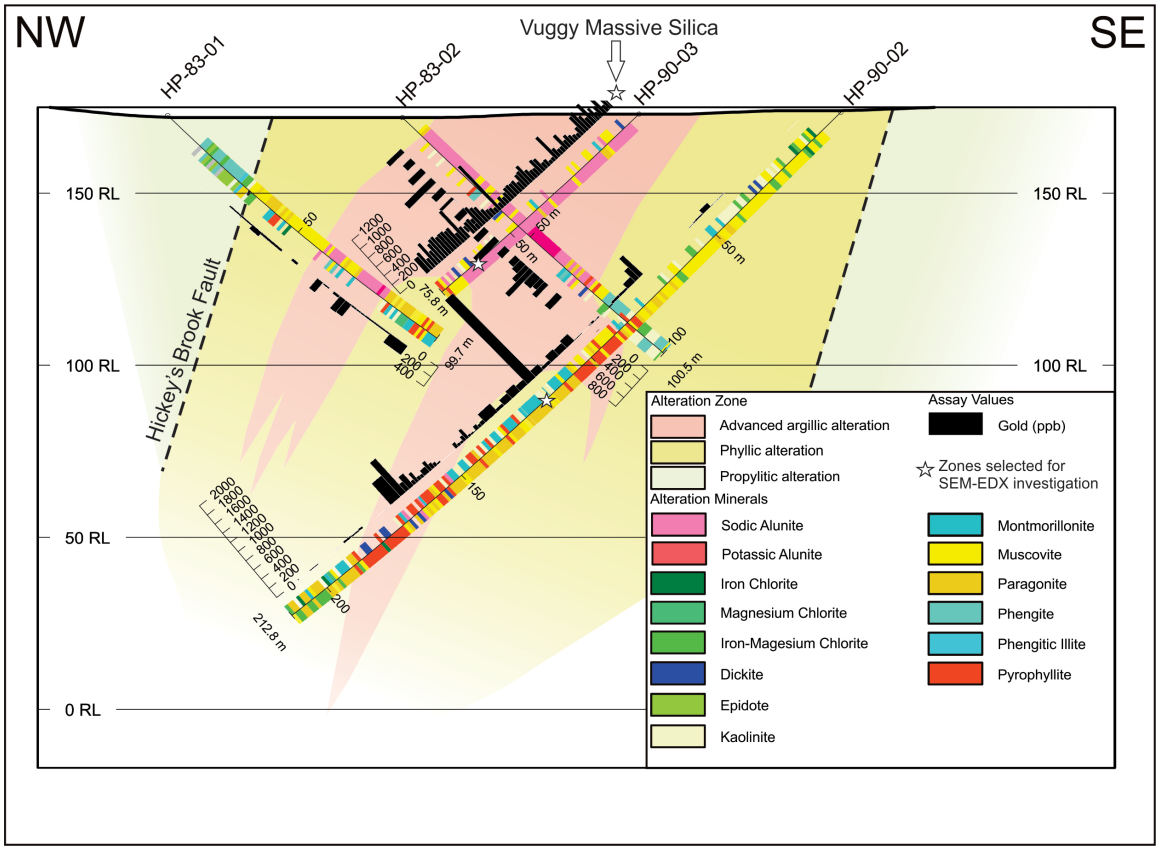

***Figure 5-6**: Schematic cross-section illustrating the subsurface distribution of the main alteration assemblages present at the Hickey's Pond prospect. VIRS data was collected, and is displayed, at 1m intervals. The dominant mineral phase detected is shown on the right-hand side, and the secondary mineral, if present, is shown on the left-hand side of the drillhole trace. White stars indicate the locations of detailed investigations of ore mineralogy, corresponding with elevated gold concentrations. The cross-section location is shown in Figure 5-5 (modified from Sparkes et al., 2016).*

The main zone of advanced argillic alteration can be outlined based on VIRS data (*Figure 5-6*) and occurs centrally within the halo of phyllic alteration, with a coalescing boundary. The advanced argillic alteration is dominated by Na-alunite, but at deeper vertical depths becomes dominated by pyrophyllite with lesser dickite. A more detailed petrographic investigation of this VIRS-defined alteration zone was completed locally on a short interval from drillhole HP-90-03 at 62-64m depth, the alteration of which corresponds with the '*Pyrite-Quartz-Alunite*' ore assemblage described in *Section 5.4.3*. This interval is strongly deformed and predominantly composed of a fine-grained quartz-dominated groundmass that is intercalated and folded with discontinuous bands of coarser-grained quartz, Na-alunite (locally up to 85%), and pyrite. The coarser-grained assemblage also forms distinct clusters, and comb-texture quartz locally occurs lining

small cavities, both of which might be representative of a hydrothermal-related vuggy-texture, however the strong deformation across the interval makes identification of such textures difficult. Rutile is also present throughout the interval.

Based on VIRS data, the phyllic alteration bounding the advanced argillic alteration at lower depths and towards the southeast, is dominated by paragonite, with lesser muscovite (*Figure 5-6*). This phyllic alteration assemblage is locally host to the highest-grade gold mineralization intersected in drillcore; an association not typical of most high-sulphidation gold systems. Consequently, a more detailed petrographic investigation was completed for the gold-enriched interval in drillhole HP-90-02 at ~117m depth, which contains the *'Specularite-Quartz-White Mica'* ore assemblage described in *Section 5.4.3*. Similar to the advanced argillic zones, the interval is highly deformed and predominantly composed of a fine-grained quartz-dominated groundmass containing coarser-grained discontinuous bands (locally defining a weak breccia texture) and clusters, and irregularly shaped, rounded cavities lined with comb-textured quartz (*Plate 5-2*). The latter two textures, again, are interpreted as possible vuggy silica textures. However, unlike the advanced argillic alteration zones, alunite is not present, although woodhouseite and minor svanbergite (typically as intergrown crystal zonations) are present, phases isostructural with alunite, but not readily detectable by VIRS. These minerals are associated with the coarser-grained assemblage of quartz, specularite, rutile, and white mica. SEM-EDX analyses determined paragonite to be the dominant phase of white mica, consistent with VIRS data. It also identified the presence of minor muscovite and possible illite (the latter not specifically identified with VIRS).

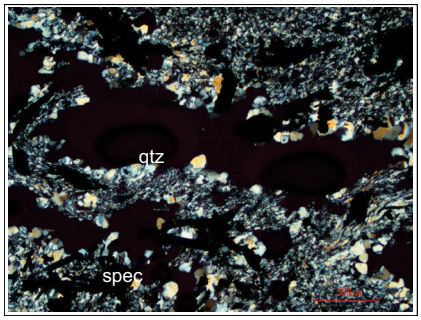

***Plate 5-2**: Photomicrograph (4X; XPL) showing clusters of coarser-grained specularite and quartz and irregularly shaped cavities lined by comb-textured quartz, possibly indicative of hydrothermal-related vuggy silica texture (SF-15-189). spec=specularite, qtz=quartz.*

5.4.2 Mineralization: Mineralogy, Associations and Paragenesis

As previously outlined, four distinct alteration zones, all of which are auriferous to some extent, were analyzed in detail to assess the deportment of gold at the Hickey's Pond prospect. The four zones are representative of mineralization at surface and at depth, and contain both pyrite- and specularite-dominated assemblages. These two Fe-phases are closely associated with mineralization, but only rarely found to coexist. An extensive assortment of opaque minerals, including sulphides, sulphosalts, selenides, tellurides, and native metals, were identified in each of the zones, and are summarized in *Table 5-1*. The specific occurrence and paragenesis of these minerals is discussed in greater detail below, within the context of the four defined ore zones.

Vuggy Massive Silica

The highest gold grades at the Hickey's Pond prospect occur at surface within massive silica alteration, locally displaying vuggy textures, and associated with alunite, pyrite, and rutile. The sulphide content is highly variable throughout this zone. Sulphide-poor areas contain Fe-oxides (predominantly hematite) with distinctive boxwork and colloform textures with cubic- and dodecahedron-shaped cross sections representative of pseudomorphs after a primary hypogene sulphide assemblage of ~1-3% pyrite (*Plate 5-3*). Locally, Fe-oxides contain trace As and Sb interpreted as a residue of minor primary tennantite, and intact hessite (Ag_2Te) occurs locally, disseminated in the massive silica alteration. Fe-oxides are also present as late vug and fracture fill locally associated with acanthite (Ag_2S), naumannite (Ag_2Se), and tiemannite (HgSe). Gold mineralization occurs as relatively coarse (up to 40 μm) grains of native gold, contained within pockets of colloform hematite (after pyrite; *Plate 5-3*). The coarse gold grains typically contain minor amounts of Ag (up to 2 at. %) and are microcrystalline in texture. Locally, hematite occurs interstitially to the microcrystalline texture and the gold/hematite grains are cross cut by fine fractures of pure native gold (*Plate 5-3*).

	Pyrite Dominated		Specularite Dominated	
	Vuggy Massive Silica	Pyrite-Quartz-Alunite	Hydrothermal Specularite Breccia	Specularite-Quartz-White Mica
AU MINERALIZATION				
Native Au	X	X	X	X
Calaverite $AuTe_2$	X		X	X
Fischesserite Ag_3AuSe_2	X			
Electrum (Au, Ag)	X			X
SULPHIDES/SULPHOSALTS				
Tennantite $Cu_6[Cu_4(Fe,Zn)_2]As_4S_{13}$	X	X		
Te-rich Tennantite		X		X
As-rich Pyrite		X		
Enargite Cu_3AsS_4	X			
Wittichenite Cu_3BiS_3		X		
Bornite Cu_5FeS_4	X	X		
Chalcopyrite $CuFeS_2$	X	X		X
Covellite CuS	X	X		
Chalcocite Cu_2S	X			
Acanthite Ag_2S	X			X
Cinnabar HgS		X		X
Galena PbS			X	
Stephanite Ag_5SbS_4			X	
TELLURIDES				
Tsumoite BiTe	X	X	X	X
Hessite Ag_2Te	X	X		X
Native Te	X			X
Coloradoite HgTe				X
SELENIDES				
Klockmannite CuSe			X	X
Bellidoite Cu_2Se			X	X
Umangite Cu_3Se_2			X	
Laitakarite Bi_4Se_3			X	
Bohdanowiczite $BiAgSe_2$			X	X
Grundmannite $CuBiSe_2$			X	X
Clausthalite PbSe				X
Naumannite Ag_2Se	X			X
Tiemannite HgSe	X	X		X
Native Se		X		X
OTHER				
Native Bi			X	

***Table 5-1**: Summary of the sulphide, sulphosalt, telluride, and selenide minerals, and native metals identified at the Hickey's Pond prospect within the four main zones of anomalous gold mineralization.*

Areas within the massive to vuggy silica alteration enriched in sulphides, contain up to 20% pyrite and tennantite, occurring together as disseminations in the siliceous groundmass, as blebby vug filling, and in small (<1cm wide) cross-cutting folded veinlets with quartz and minor alunite (*Plate 5-4 A*). Minor enargite and bornite occur with pyrite and tennantite in some of the finer vugs, where these primary copper minerals have been largely replaced by chalcopyrite, covellite and chalcocite (*Plate 5-4 B&C)*. Pyrite commonly contains inclusions of bornite. Tennantite hosts a wide variety of inclusions including bornite, hessite (Ag_2Te), calaverite ($AuTe_2$), native tellurium, tsumoite (BiTe), and, less commonly, naumannite (Ag_2Se) and native gold (*Plate 5-4 D*). Tennantite is commonly replaced by various Fe-As-Sb-oxides.

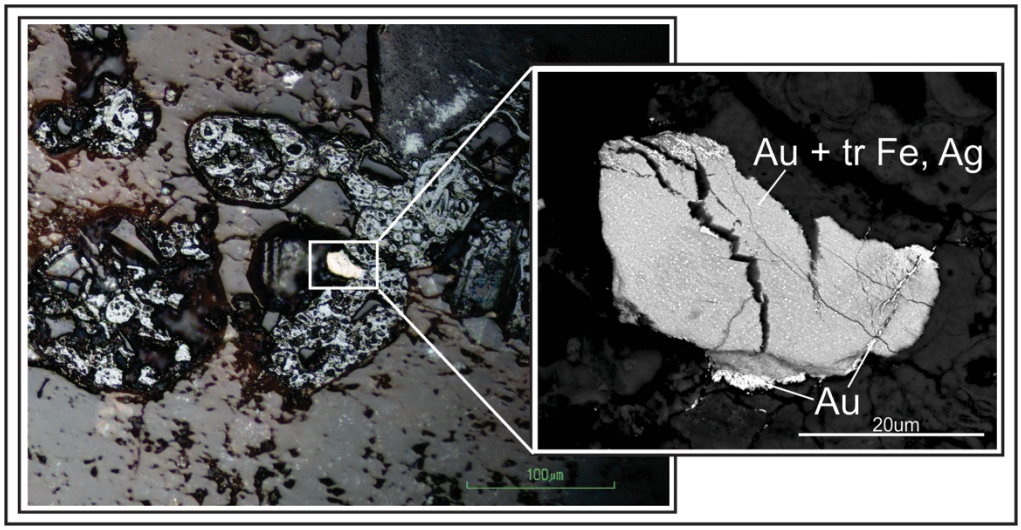

Plate 5-3*: Reflected light (20X) and BSE SEM (inset) photomicrographs of sulphide-poor vuggy silica from surface at Hickey's Pond (SF-12-150). Boxwork- and colloform-textured Fe-oxides occurring as pseudomorphic replacements of cubic- and dodecahedron-shaped primary hypogene pyrite, and surrounding coarse grain of native gold (Au). Gold grain contains minor amounts of silver (Ag) as well as microcrystalline interstitial hematite (Fe), and is cross cut by fine fractures of pure native gold (white).*

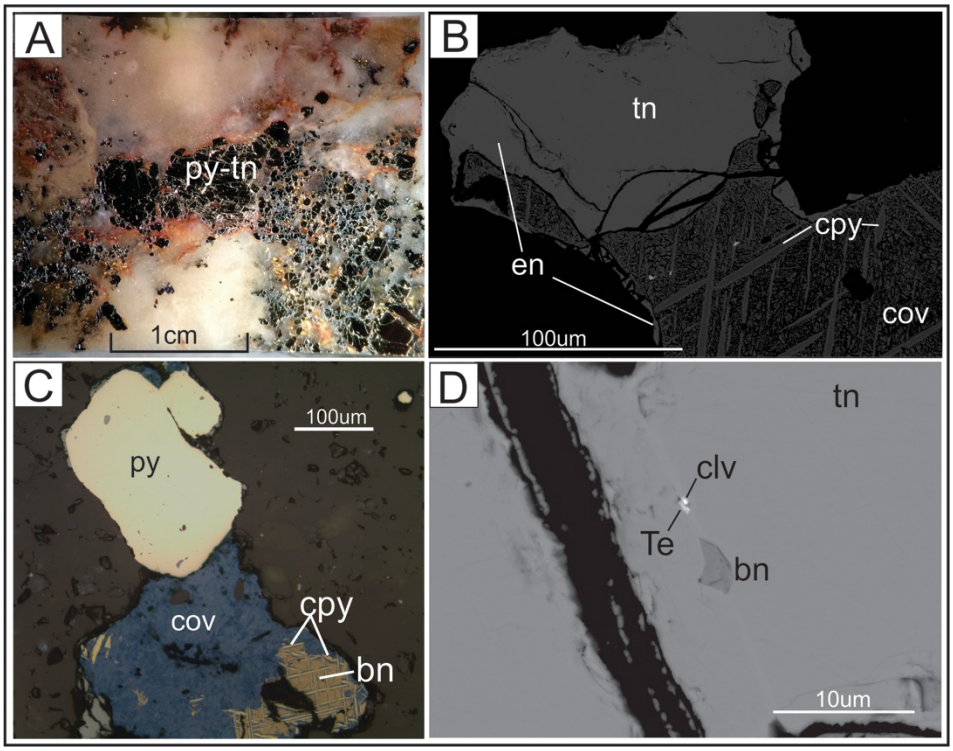

Plate 5-4*: Representative photos and photomicrographs from the sulphide-rich portion of the vuggy massive silica zone (SF-12-152); A) polished surface showing folded pyrite-tennantite(-quartz-alunite) vein cross-cutting massive silica matrix; B) BSE-SEM image of intergrown tennantite (tn) and minor enargite (en) filling a small vug in the silica matrix with replacement by chalcopyrite (cpy) and covellite (cov); C) reflected light (20X) image of pyrite (py), minor tennantite (bottom left), and bornite (bn) filling a small vug. Bornite displays exsolution lamellae of chalcopyrite, and is replaced by covellite; D) BSE-SEM image of bornite, and intergrown calaverite (clv) and native Te inclusions within tennantite.*

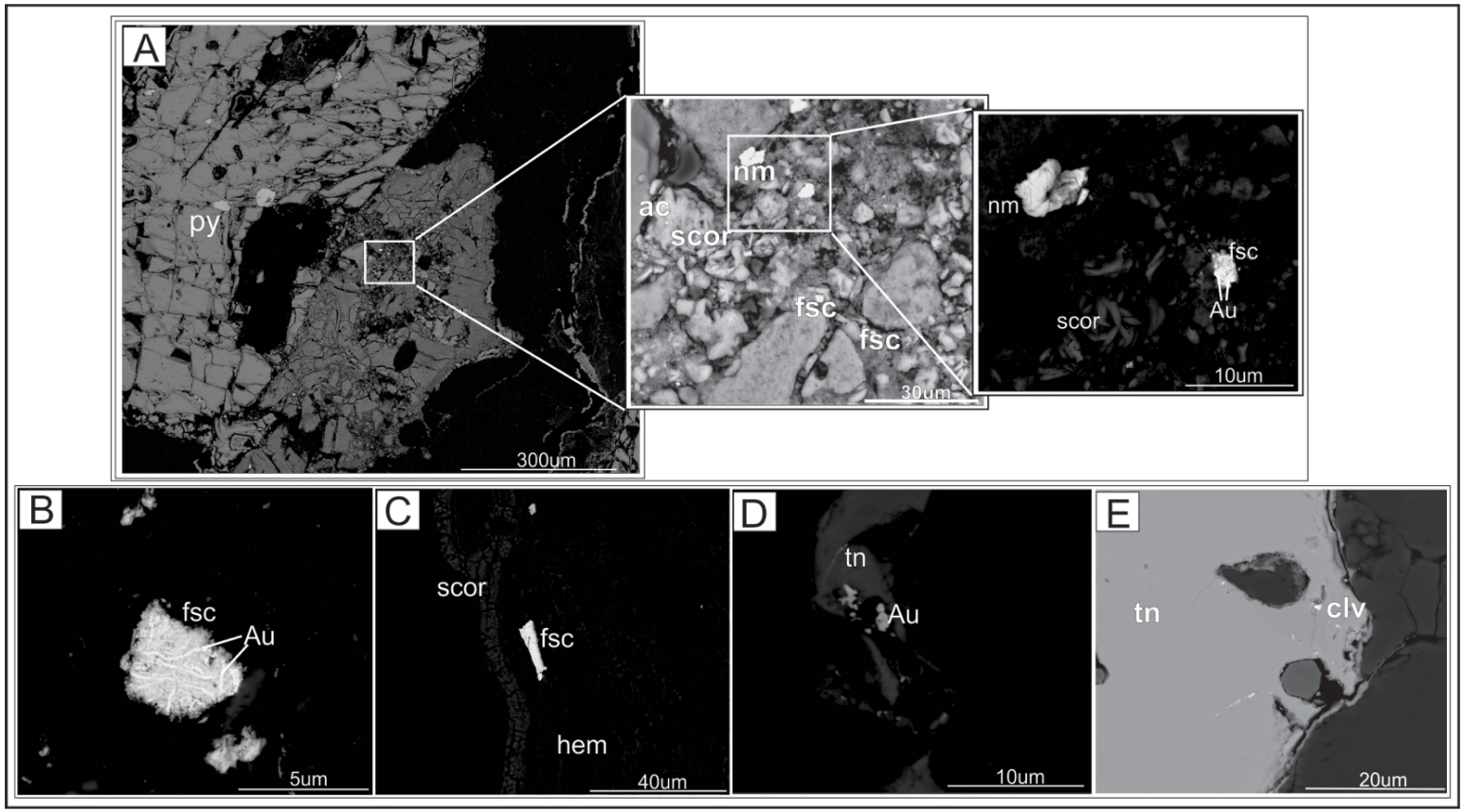

***Plate 5-5**: Representative BSE-SEM images of gold mineralization in the sulphide-rich vuggy massive silica zone (SF-12-152); A) Brecciated fragments of Fe-As-Sb-oxide (former tennantite) surrounded by scorodite-rich (scor) matrix, containing precious metal mineralization, including selenides (fischesserite-fsc, and naumannite-nm), native Au, and acanthite (ac); B) Fischesserite with white ribbons of native Au occurring in a fine-grained, oxidized, hematite breccia; C) Elongate fischesserite grain contained within colloform layers of hematite (hem) and scorodite (scor) lining a fracture; D) Very fine-grained native Au, as inclusions within (or intergrowths with) tennantite (tn); E) Calaverite (clv) inclusions within tennantite.*

The sulphide-enriched variant of the vuggy massive silica zone is associated with the highest gold grades at the prospect, with up to 60.4 g/t Au recovered from grab sample. Gold is present in a variety of phases, the most abundant being fischesserite (Ag_3AuSe_2). Fischesserite occurs within: 1) Fine scorodite ($FeAsO_4•2H_2O$)-hematite-angelellite ($Fe_4(AsO_4)_2O_3$) breccias with naumannite and minor native gold (*Plate 5-5 A&B)*, and 2) Colloform layers of hematite and scorodite, which line fractures and cavities (*Plate 5-5 C)*. Native gold is less common, occurring in association with tennantite, as fine (<4μm) irregularly shaped inclusions (or intergrowths) (*Plate 5-5 D)*, as well as in fractures in tennantite grains. Gold also occurs as the gold-telluride, calaverite, which occurs as tiny (<1μm) inclusions in tennantite (*Plate 5-5 E*). Rare electrum occurs as fine (~2μm) grains in oxidized fractures.

These observations and their suggested temporal relationships for mineralization in the vuggy massive silica alteration zone are summarized in *Figure 5-7.*

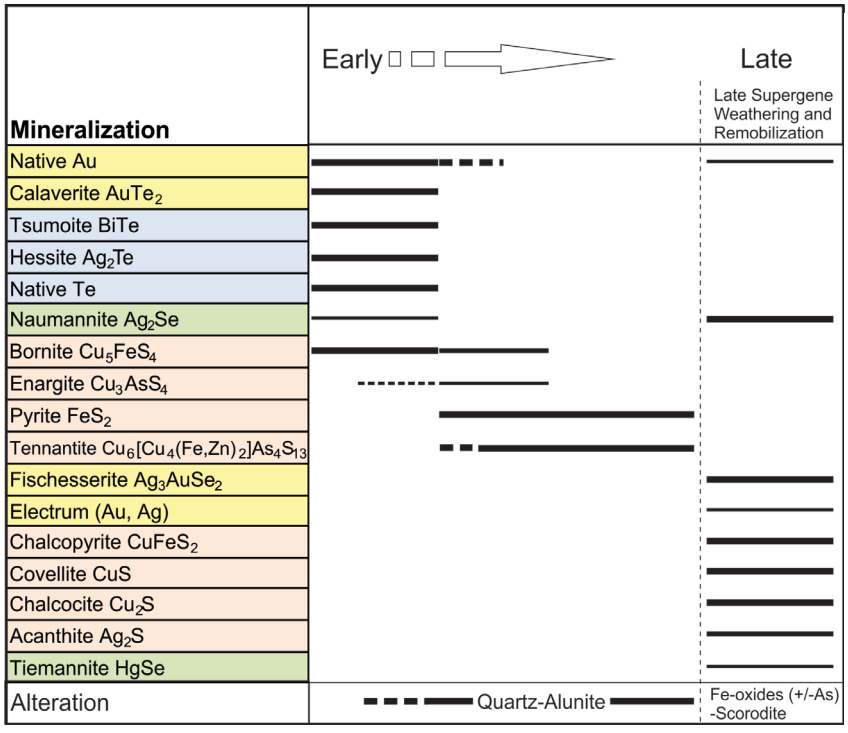

Figure 5-7*: Paragenetic sequence for mineralization in the vuggy massive silica zone at the Hickey's Pond prospect. Colours as in Table 5-1. Line thickness is representative of relative frequency of occurrence. Mineral occurrence lines in the 'late supergene weathering and remobilization' column are not representative of their relative timing, but as a group, late, relative to the main hypogene assemblage.*

Pyrite-Quartz-Alunite (62-64m depth in DDH HP-90-03)

Anomalous gold grades occur throughout the advanced argillic alteration of drillhole HP-90-03. The 62-64m interval discussed in this section is situated immediately down-hole from one of the best intersections, which yielded 1 g/t Au over 1m (Dimmel et al., 1992).

Pyrite is the most prevalent opaque mineral phase, ranging in abundance from 1-10%, occurring as fine disseminations along the foliation, and clustered with coarser-grained quartz and Na-alunite, which appear to be filling vugs. Locally, alunite crystals display patchy internal phosphatic zoning of woodhouseite/svanbergite. Pyrite grains commonly display distinct cores and rims, the cores typically displaying minor enrichment in As (*Plate 5-6 A*). Pyrite grains commonly contain inclusions of bornite, tsumoite (BiTe), tennantite, a Te-rich variety of tennantite, wittichenite (Cu_3BiS_3), and hessite (Ag_2Te) (*Plate 5-6 A-D*). In the Te-rich variety of tennantite, Te appears to be substituting for As, based on semi-quantitative SEM-EDX data. Both varieties of tennantite, and occasionally tsumoite and bornite, also occur in minor amounts intergrown with pyrite along pyrite grain boundaries (*Plate 5-6 B, D, E*). Chalcopyrite and covellite are also present along the same pyrite grain boundaries but occur as replacements of tennantite or bornite and are not part of the hypogene sulphide assemblage (*Plate 5-6 B&F*). Gold mineralization is not robust across this interval, but was found to occur as very fine-grained native gold, directly associated with both pyrite and alunite (*Plate 5-6 F&G*).

Locally, breccias are developed in which hydrothermally altered fragments are surrounded by fine, colloform-banded Fe-oxides and lesser kaolinite, which also pseudomorphically replace adjacent pyrite grains. Native selenium, tiemannite (HgSe), and cinnabar (HgS) also occur in association with the oxidized breccias, and are most commonly found concentrated along thin fractures within the Fe-oxides (*Plate 5-6 H&I*).

These observations and their suggested temporal relationships for mineralization in the pyrite-quartz-alunite subsurface alteration zone are summarized in *Figure 5-8.*

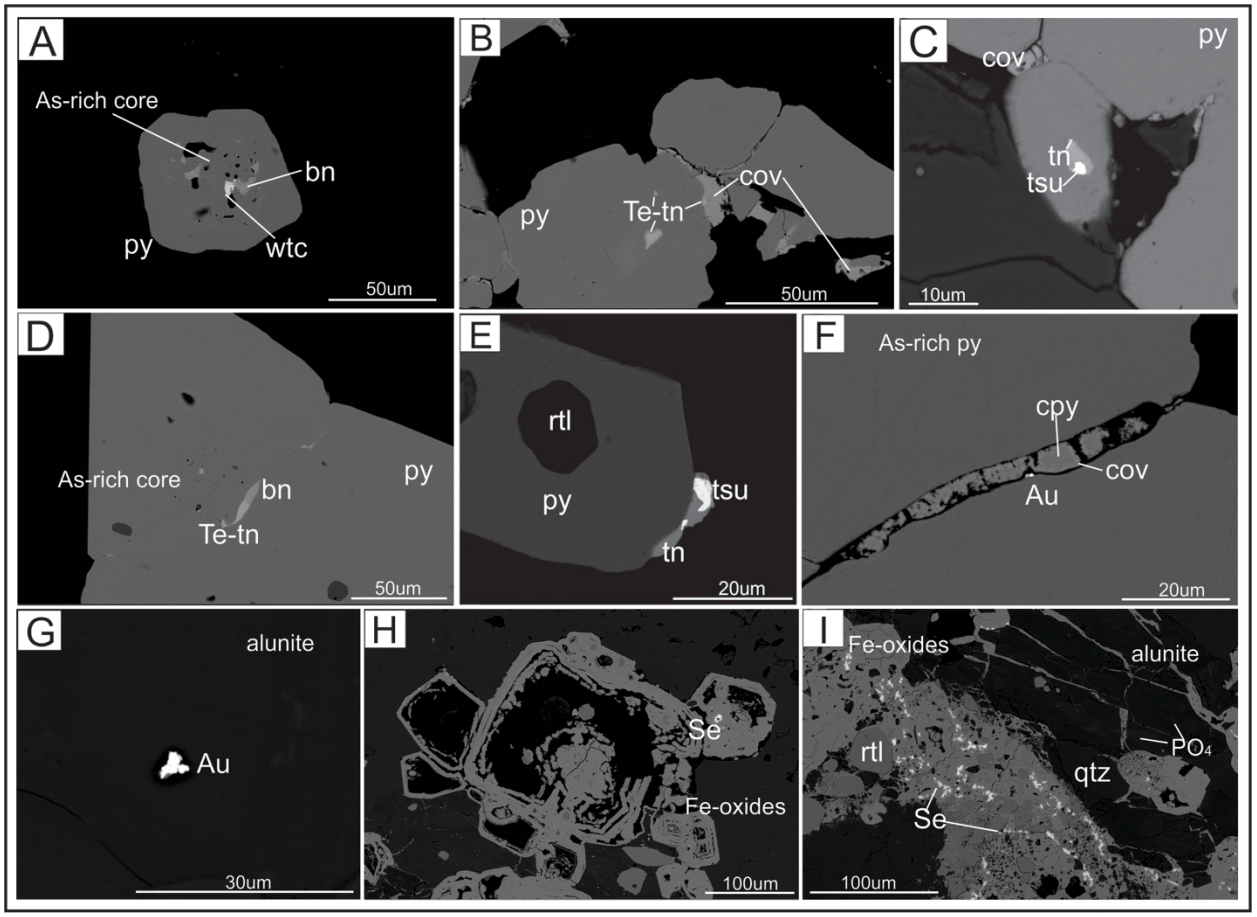

***Plate 5-6**: Representative BSE-SEM images of mineralization in the pyrite-quartz-alunite zone; A) Pyrite (py) with an arsenic- and inclusion-rich core. Inclusions are bornite (bn) and wittichenite (wtc) (SF-15-191); B) Pyrite with inclusions of Te-rich tennantite (Te-tn). Minor Te-tennantite also occurs along pyrite grain boundaries, most of which has been replaced by late covellite (cov) (SF-15-194); C) Inclusion of tsumoite (tsu) and tennantite (tn) within pyrite (SF-15-192); D) Te-tennantite and bornite occurring as an intergrowth with pyrite along a faint pyrite grain boundary (SF-15-194); E) Tennantite and tsumoite along edge of pyrite grain (rtl=rutile) (SF-15-192); F) As-rich pyrite with chalcopyrite (cpy) and covellite (after tennantite or bornite) along a pyrite grain boundary and adjacent to a tiny inclusion of native Au in pyrite (SF-15-191); G) Native Au within coarse grain of alunite (SF-15-194); H) Colloform-banded Fe-oxides pseudomorphically replacing pyrite proximal to late oxide-breccias, containing local patches of native Se (SF-15-193); I) Hydrothermally altered breccia fragments of rutile (rtl), quartz (qtz) and alunite, surrounded by a matrix of colloform-banded Fe-oxides, occasional laths of kaolinite, and fine fractures of native Se. Lighter patches in alunite crystals is phosphatic (woodhouseite/svanbergite) zoning (SF-15-193).*

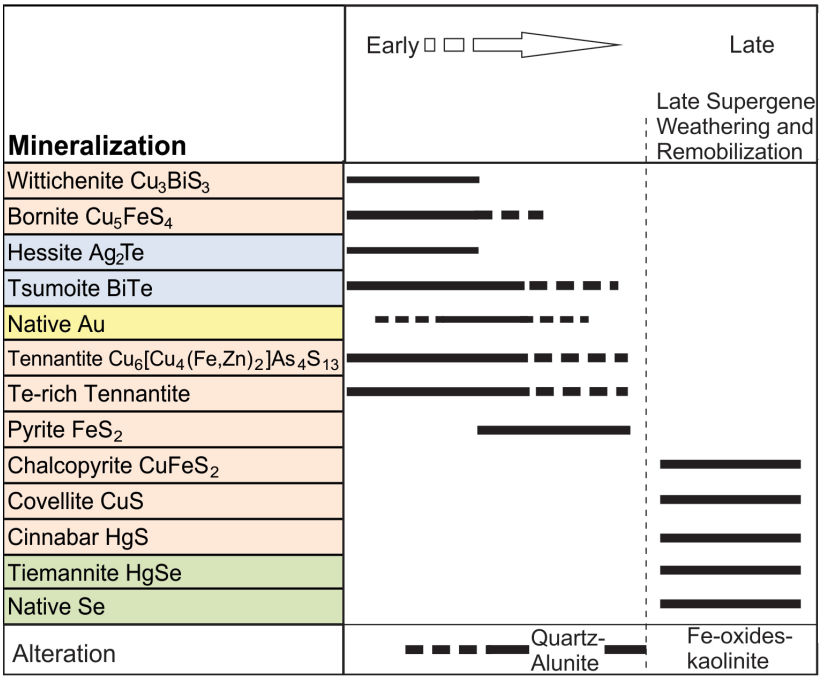

***Figure 5-8**: Paragenetic sequence for mineralization in the pyrite-quartz-alunite zone at the Hickey's Pond prospect. Colours as in Table 5-1. Line thickness is representative of relative frequency of occurrence. Mineral occurrence lines in the 'late supergene weathering and remobilization' column are not representative of their relative timing, but as a group, late, relative to the main hypogene assemblage.*

Hydrothermal Specularite Breccia

Gold grades of up to 5.4 g/t Au have been recovered in grab samples from the hydrothermal specularite breccias exposed at surface (e.g. O'Brien et al., 1999). In these zones, strongly silicified fragments are brecciated and encompassed by fine specularite-rich seams.

In addition to quartz, the brecciated fragments also contain minor alunite, and local disseminated pyrite, typically intergrown with covellite or chalcocite (*Plate 5-7 A*). Based on the mineralogical relationships observed in the other mineralized zones, these copper minerals are interpreted as late-stage replacements of other primary hypogene copper minerals such as bornite or tennantite.

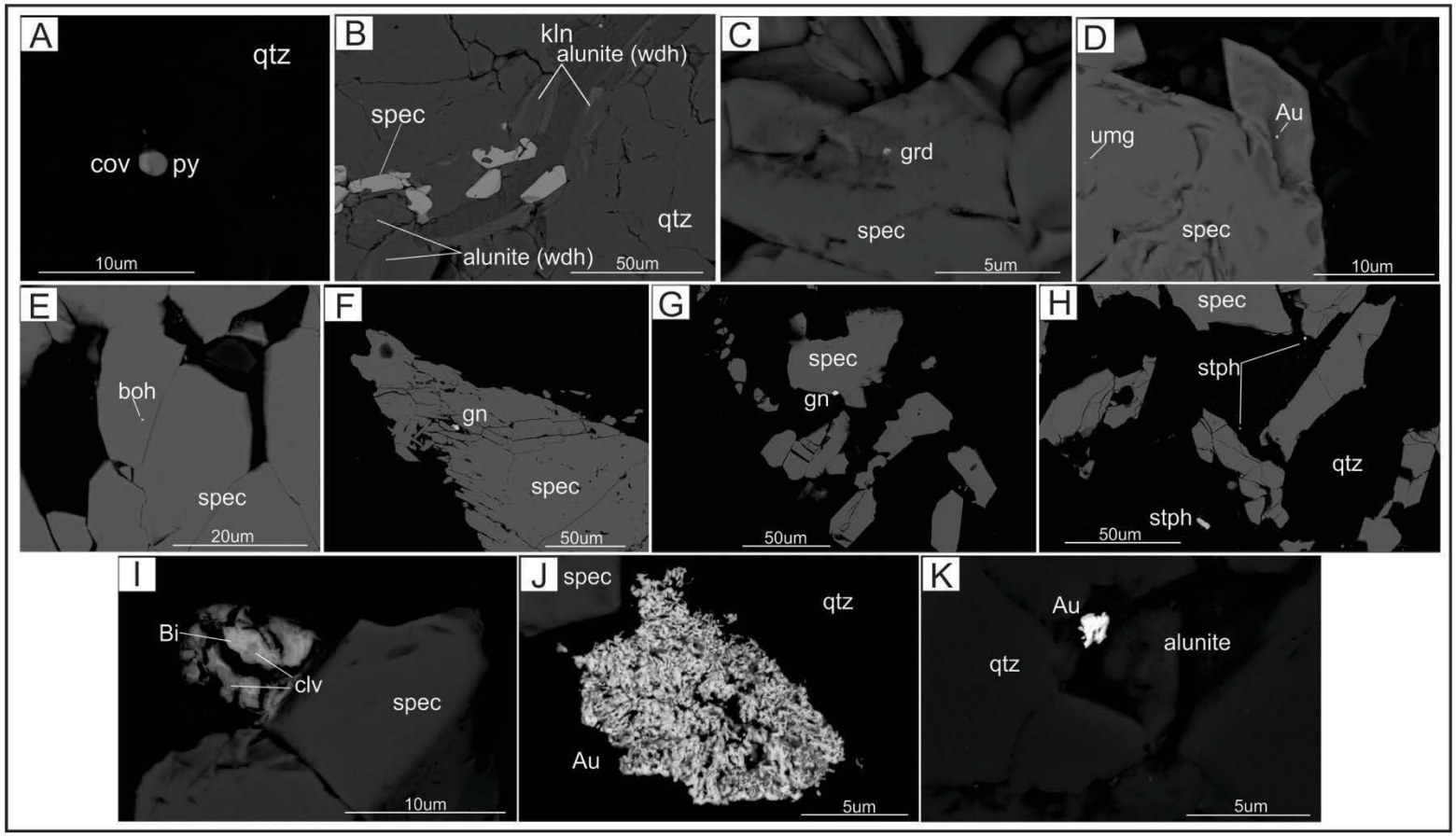

Plate 5-7*: Representative BSE-SEM images of mineralization in the hydrothermal specularite breccia zone at surface (SF-15-183); A) small inclusion of pyrite (py) and covellite (cov) within a brecciated silica(-alunite) altered fragment; B) Specularite (spec) breccia seam associated wtih Na-alunite showing phosphatic zoning (woodhouseite-wdh), cross-cutting quartz; C) Grundmannite (grd) inclusion in specularite; D) Au and umangite (umg) inclusions in specularite; E) Bohdanowiczite (boh) inclusion in specularite; F) Galena (gn) occurring within a cavity in a coarse specularite grain; G) Galena occurring with specularite in a breccia seam; H) Grains of stephanite (stph) associated with specularite and quartz in a breccia seam (SF-15-184);I) Grain of intimately intergrown calaverite (clv) and native Bi growing on edge of specularite; J) Microcrystalline grain of gold in breccia seam associated with specularite; K) Au growing between crystals of alunite in breccia seam.*

The breccia seams are predominantly composed of quartz, specularite, Na-alunite (±woodhouseite/svanbergite zoning), and minor rutile, with specularite accounting for 30-40% of the assemblage (*Plate 5-7 B*). An assemblage of minor minerals rich in Se, Cu and Bi occur throughout the breccia seams as tiny inclusions within specularite. Minerals include klockmannite (CuSe), bellidoite (Cu_2Se), umangite (Cu_3Se_2), grundmannite ($CuBiSe_2$), laitakarite (Bi_4Se_3), bohdanowiczite ($BiAgSe_2$), tsumoite (BiTe), and native Au (*Plate 5-7 C-E*). Small grains of galena (PbS) and stephanite (Ag_5SbS_4) commonly occur within the seams; stephanite is found disseminated throughout, while galena typically shows a closer affinity with specularite (*Plate 5-7 F-H*).

Gold most commonly occurs as native Au, closely associated with, and generally positioned adjacent to specularite, or less commonly alunite, within the breccia seams (*Plate 5-7 J&K*). The grains are small, ranging in size from 2-20μm, and typically show a microcrystalline texture. As previously noted, native Au also occurs locally as small inclusions within the specularite. Gold was also identified locally as the gold-telluride mineral calaverite, where it was found intimately intergrown with native Bi along the margin of a specularite crystal (*Plate 5-7 I*).

These observations and their suggested temporal relationships for mineralization in the hydrothermal specularite breccia mineralized zone are summarized in *Figure 5-9*.

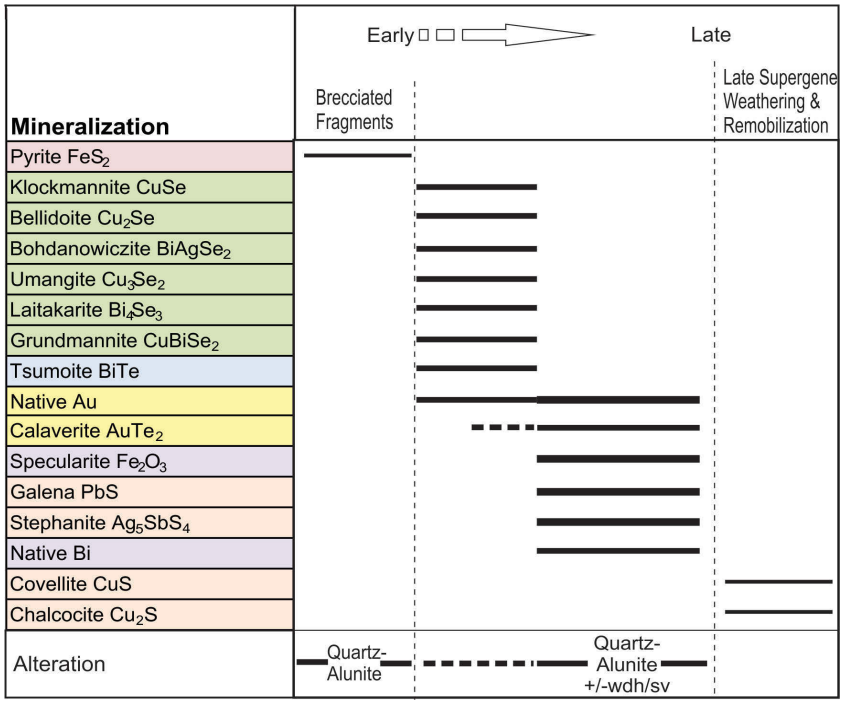

***Figure 5-9**: Paragenetic sequence for mineralization in the hydrothermal specularite breccia zone at the Hickey's Pond prospect. Colours as in Table 5-1. Line thickness is representative of relative frequency of occurrence.*

Specularite-Quartz-White Mica (117m depth in DDH HP-90-02)

The highest gold grades encountered during drilling, occur in drillhole HP-90-02, the best intersection yielding 1.96 g/t Au over 1m at an approximate depth of 117m (Dimmel et al., 1992). This intersection corresponds with the presence of abundant specularite and a phyllic alteration assemblage of predominantly paragonite, based on VIRS. However, further petrographic work showed that the alteration is dominated by quartz with lesser rutile, woodhouseite (-svanbergite), and minor paragonite, and possible illite.

Specularite accounts for up to 35% of the alteration assemblage, generally occurring as relatively coarse acicular grains. It is concentrated in discontinuous bands, defined by the deformation fabric, along with rutile, white mica, and phosphates, and in clusters with relatively coarse-grained quartz, which appear to be filling vugs. A weak breccia texture is locally developed, where the specularite-rich bands encompass rounded

portions of the finer-grained quartz-rich matrix, which also contains minor disseminated specularite as fine-subhedral grains.

A diverse assemblage of tellurides and selenides was identified across this interval. Calaverite ($AuTe_2$), hessite, coloradoite (HgTe), native Te, klockmannite (CuSe), bellidoite (Cu_2Se), and bohdanowiczite ($BiAgSe_2$) were found to occur as fine disseminated grains within the fine-grained quartz-dominated matrix (*Plate 5-8 A&B*). A similar assemblage including hessite, coloradoite, native Te, klockmannite, bohdanowiczite, chalcopyrite, tsumoite, grundmannite ($CuBiSe_2$), and clausthalite (PbSe) occur as inclusions within specularite (*Plate 5-8 C-F*). Locally, a tellurium-rich variety of tennantite occurs as relatively coarse grains intergrown with specularite (*Plate 5-8 D*).

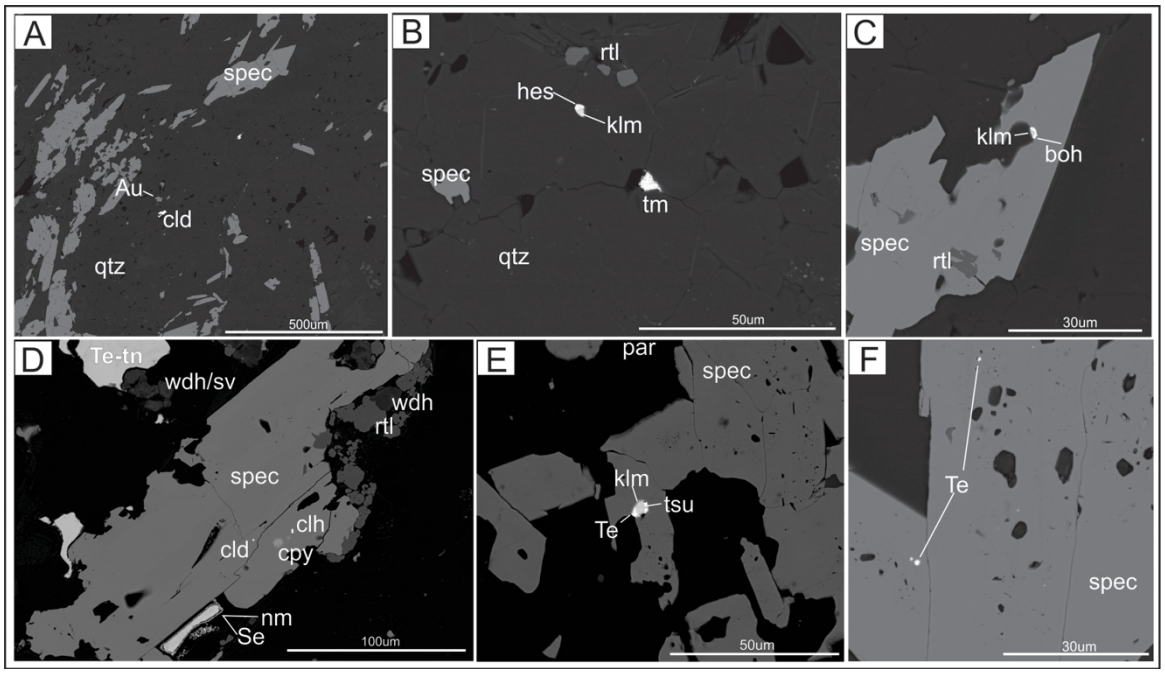

Plate 5-8*: Representative BSE-SEM images of opaque-mineral assemblage in the specularite-quartz-white mica zone (SF-15-189); A) Fine-grained coloradoite (cld) and very fine-grained native Au occurring within the fine-grained quartz (qtz)-dominated matrix, surrounded by bands of coarser specularite (spec); B) Intergrown hessite (hes) and klockmannite (klm) inclusion within the quartz matrix occurring with fine-grained disseminated specularite and rutile (rtl). A late cross-cutting fracture is locally filled with tiemannite (tm); C) Inclusion of klockmannite and bohdanowiczite (boh) within coarse specularite; D) Specularite intergrown with Te-tennantite (Te-tn), rutile (rtl) and woodhouseite (wdh), and containing inclusions of coloradoite (cld), clausthalite (clh), and chalcopyrite (cpy). Te-tennantite is overgrown by late naumannite (nm) and native Se; E) Inclusion of native Te, klockmannite, and tsumoite (tsu) within specularite associated with paragonite (SF-15-190); F) Inclusions of native Te in specularite.*

Gold predominantly occurs as native gold, and is most commonly found within the specularite-rich clusters and deformed bands, but occasionally within the quartz-rich groundmass (*Plate 5-9*). Gold is closely associated with specularite or less commonly, rutile (*Plate 5-9 F*). Gold grains range in size from 2-10μm, but locally as large as 40μm, are microcrystalline in texture, and often show an internal layering pattern (e.g. *Plate 5-9 G, I, J*). Gold also occurs as electrum, which was identified locally filling late fractures, and as calaverite inclusions in specularite.

A late stage assemblage of Hg- and Ag-selenides and sulphides is found filling fractures and lining cavities (*Plate 5-8 B&D*). This assemblage includes cinnabar (HgS), tiemannite (HgSe), acanthite (Ag_2S), naumannite (Ag_2Se), and native selenium. Tiemannite (HgSe) and cinnabar (HgS) are often also found rimming grains of native Au (*Plate 5-9 I*).

These observations and their suggested temporal relationships for mineralization in the specularite-quartz-white mica subsurface alteration zone are summarized in *Figure 5-10.*

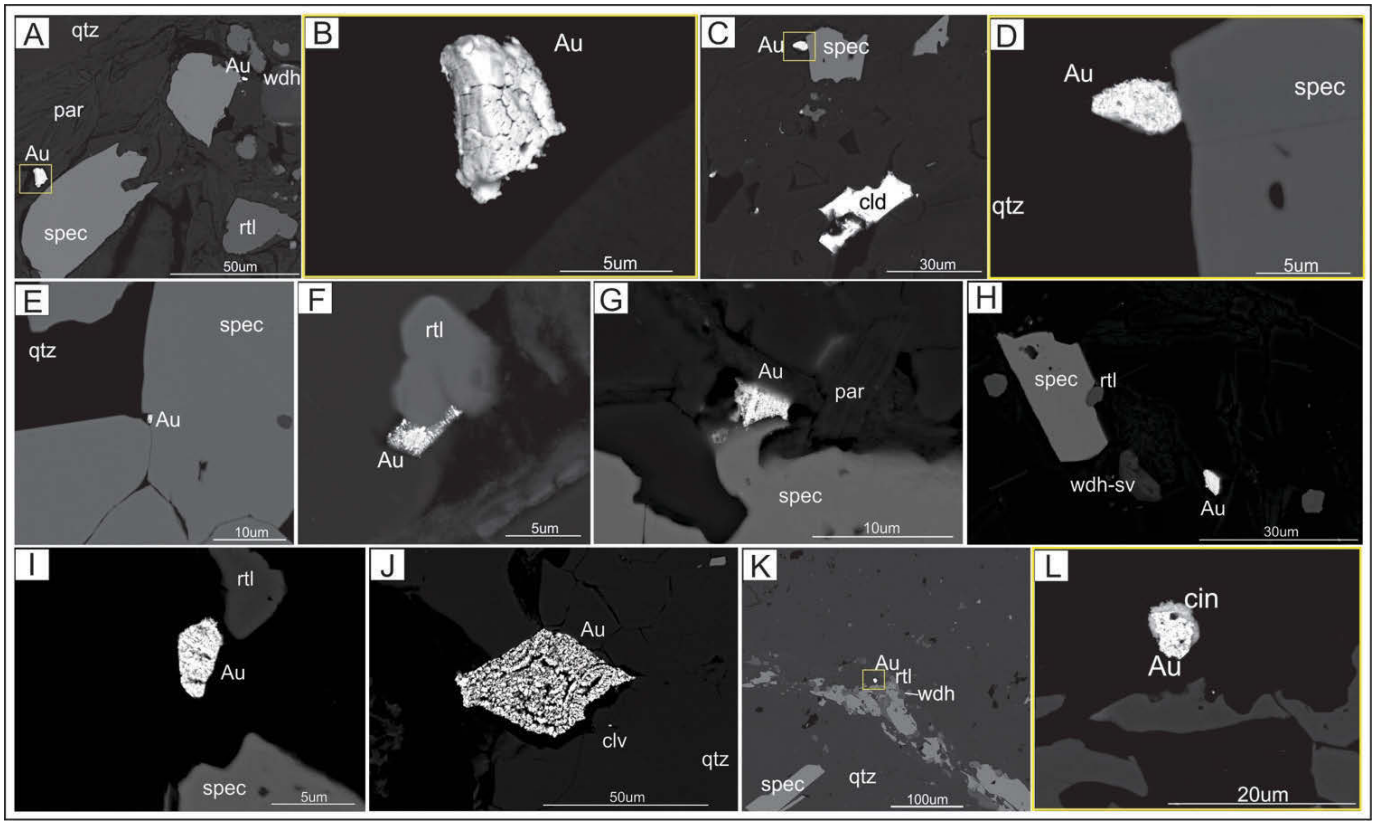

***Plate 5-9**: Representative BSE-SEM images of gold mineralization in the specularite-quartz-white mica zone (SF-15-189); A&B) Native Au occurring within a specularite band, associated with specularite (spec), rutile (rtl), quartz (qtz), paragonite (par), and woodhouseite (wdh); C&D) Microcrystalline grain of native Au associated with specularite and proximal to coloradoite (cld), occurring in the fine quartz groundmass; E) Native gold within a cluster of coarse specularite; F) Native Au partially intergrown with rutile within a coarse specularite band (SF-15-190); G) Native Au with a layered texture, occurring with specularite and adjacent to paragonite in a specularite band; H) Native Au within a band of specularite, rutile, quartz and zoned woodhouseite (wdh)-svanbergite (sv) crystals; I) Native Au with a layered texture; J) Coarse (40um) grain of native Au within quartz-rich matrix, showing layered texture, and adjacent to a tiny grain of calaverite (clv) (SF-15-190); K&L) Native Au rimmed by late-stage cinnabar (cin) and occurring within a coarse specularite-quartz-rutile-woodhouseite band.*

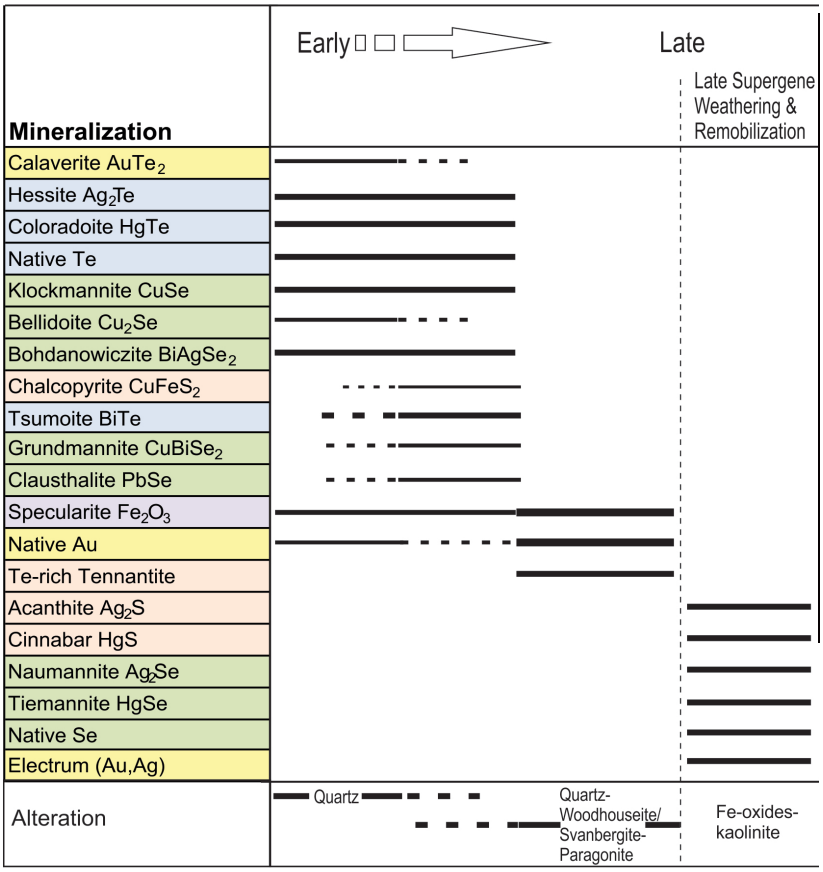

***Figure 5-10**: Paragenetic sequence for mineralization in the specularite-quartz-white mica zone at the Hickey's Pond prospect. Colours as in Table 5-1. Line thickness is representative of relative frequency of occurrence.*

5.4.3 Interpretation

With the exception of the 'specularite-quartz-white mica' zone, the highest gold grades at the Hickey's Pond prospect occur in association with an advanced argillic alteration assemblage dominated by quartz and Na-alunite. The 'specularite-quartz-white mica' zone contains minor paragonite, indicative of a phyllic assemblage, however, it is dominated by quartz alteration, and also contains the Ca- Sr-phosphates, woodhouseite and svanbergite, which are isostructural with alunite. These phosphate minerals were also identified locally as zonations in alunite crystals in the 'hydrothermal specularite breccia' zone, and more rarely in the 'pyrite-quartz-alunite' zone. Although not typically described in the core epithermal literature, these phosphate minerals have been identified at many high-sulphidation deposits and are considered to be overlooked constituents of a hypogene advanced argillic assemblage (e.g. Stoffregen and Alpers, 1987; Hikov, 2004; Milu et al., 2004). Therefore, the 'specularite-quartz-white mica' zone is interpreted as an

extension of the advanced argillic zone, which is consistent with the anomalous gold grades present, and the recognition of possible vuggy silica textures.

In the pyrite-rich zones, there is a general transition from an earliest hypogene assemblage of native Au, Ag-Bi-Au-tellurides, and Cu-sulphides (bornite and lesser enargite) to a slightly later hypogene assemblage dominated by pyrite and tennantite with minor native Au. This is succeeded by a later assemblage of Au-Ag-Hg-selenides and Ag-Hg-sulphides, occurring as open-space filling in fractures and oxidized breccias, associated with Fe-oxides (+/-As), kaolinite, and scorodite. Late chalcopyrite, covellite, and chalcocite also occur as replacements of primary hypogene Cu-sulphides.

In the specularite-rich zones, there is a general transition from an earliest assemblage of Au, Au-Ag-Bi-Hg-tellurides, and Cu-(Bi-Ag-Pb)-selenides to a syn- to slightly later assemblage dominated by specularite, with minor tennantite and native Au. Although not present in the breccia at surface, the 'specularite-quartz-white mica' zone contains a late assemblage rich in Ag-Hg-selenides and Ag-Hg-sulphides, occurring as open-space filling in fractures and surrounding grains of the main hypogene assemblage.

These two generalized sequences are overall quite similar, with the exception that Cu-selenides and specularite occur in the specularite-rich zones in lieu of Cu-sulphides and pyrite in the pyrite-rich zones. While the pyrite- and specularite-dominated assemblages could represent two distinct hydrothermal fluids, they are instead interpreted as the result of a single fluid precipitating different mineral phases under changing redox conditions over time, leading to these local variations in the occurrence of Cu- and Fe-phases.

There is evidence for multiple episodes of hydrothermal activity at the prospect. The most notable is the local development of the hydrothermal specularite breccia, where specularite-seams cross-cut silicified and locally pyritiferous fragments. Further evidence includes the presence of quartz-pyrite-tennantite veins, which crosscut earlier replacement style mineralization. The latter observation also demonstrates an evolution in fluid chemistry over time, where minerals of higher sulphidation state (bornite and enargite)

are cross-cut by tennantite, a relatively lower sulphidation state mineral (*see Figure 5-2)*. The presence of distinct cores and rims of different compositions in pyrite is also indicative of this.

The late Au-Ag-Hg-selenide and Ag-Hg-sulphide assemblage is interpreted to be the result of late weathering and supergene processes. The assemblage could alternatively be associated with a later, unique hydrothermal event, but the close association with Fe-oxides (±As), kaolinite and scorodite within colloform banding, boxwork replacement textures and oxidized breccias support the former interpretation. The dissolution of primary hypogene ore leads to the formation of solution collapse breccias and the mobilization of dissolved components, which in this case are dominated by Au-Ag-Se(-Hg-S), and subsequent re-precipitation. This appears to be an important process for gold-enrichment at the Hickey's Pond prospect, where fischesserite was found to be the dominant phase of gold in the highest-grade gold sample (SF-12-152) collected from the prospect to date. Elsewhere, native gold of hypogene origin is the dominant phase, yielding lower, but still highly anomalous gold grades.

In summary, Hickey's Pond is the result of a succession of hydrothermal events as part of a single hydrothermal system, associated with a progressively evolving hydrothermal fluid. Gold occurs as native gold as part of a hypogene assemblage of characteristic high-sulphidation minerals (e.g. enargite, tennantite, pyrite, specularite). An important, and in some places the predominant Au-bearing phase is the selenide mineral fischesserite, which occurs as a result of late, secondary supergene enrichment.

5.5 Tower

The Tower prospect is located approximately 11 km southwest and along strike of the Hickey's Pond prospect (*Figure 5-1*), hosted in intermediate volcaniclastic rocks of the Marystown Group. It contains similar alteration assemblages to that of the Hickey's Pond prospect, but is only weakly anomalous in gold (up to 179 ppb) with additional minor enrichments in Mo (up to 203 ppm Mo; Dimmell, 2003). The advanced argillic alteration zone is ~150-200m wide and at least 500m in length, striking in a northeast-

southwest direction and bounded on both sides by fault structures (Hayes, 2000; Sparkes et al., 2014).

VIRS alteration studies conducted by Dyke and Pratt (2008) and Sparkes et al. (2014) found the advanced argillic assemblage at the Tower prospect to be dominated by Na-alunite, with lesser pyrophyllite and muscovite, and local topaz, the presence of which is indicative of a relatively high temperature of formation (>260°C; Sparkes et al., 2014; Reyes, 1990). Sparkes et al. (2014) also documented an alunite-pyrite assemblage locally overprinting an alunite-specularite-pyrophyllite one, the former, associated with elevated Au, Cu, Mo and Se values relative to the latter.

For this project, representative samples were collected from hydrothermal veins and distinct horizons within the advanced argillic alteration zone. The objectives were to assess the ore and alteration assemblages, identify any key features or relationships amongst them, and to determine any notable differences to the alteration and ore, style and mineralogy found at the auriferous Hickey's Pond prospect.

5.5.1 Alteration Zoning and Hydrothermal Textures

Similar to Hickey's Pond, the advanced argillic alteration at Tower can be broadly subdivided based on the presence of pyrite versus specularite. Locally the minerals coexist, but typically form within distinct, foliation-parallel horizons with Na-alunite and less commonly, pyrophyllite, within the strongly deformed alteration zone.

Alunite makes up the majority of the alteration zone, occurring as euhedral crystals within deformed bands of >80% alunite with minor quartz, inter-banded with layers of very fine-grained quartz (>80%) and lesser alunite. In the pyritic zones, the alunite bands tend to be thinner and variably coalescent *(Plate 5-10 A&B*). In the specularite zones, the same style of alunite banding occurs, in addition to much thicker banding, more consistent with the main deformation fabric (*Plate 5-10 C*). Both the alunite- and quartz-dominated horizons host pyrite and/or specularite.

Pyrophyllite occurs locally, typically found at the northeastern and southwestern extents of the main alteration zone exposed at surface. It occurs similarly to alunite, as foliation-parallel bands, alternating with fine-grained quartz-rich bands. The pyrophyllite alteration is also host to both pyrite and specularite mineralization (*Plate 5-10 D-F*).

Scattered throughout the alteration zone are blocks, up to 1m wide, of grey to beige massive silica, enveloped by advanced argillic alteration and boudinaged and stretched to varying degrees, parallel to the main foliation (*Plate 5-10 G&H*). Despite being intensely silicified, when viewed petrographically, primary igneous-volcaniclastic textures can still be identified, including quartz and rare remnant feldspar phenocrysts, and polycrystalline quartz fragments. The blocks also contain deformed segments of quartz veinlets, and minor alunite- (and locally pyrophyllite) banding. They typically contain minor pyrite and only rarely specularite.

Two types of hydrothermal breccias are developed locally. In the first, coarse-grained seams of up to 70% specularite with additional quartz and alunite surround fragments of similar composition, though much finer-grained and with significantly less specularite (~10%) (*Plate 5-10 I*). In the second type, very-fine grained topaz and lesser rutile brecciate quartz-rich fragments containing up to 10% euhedral, zoned crystals of intergrown alunite and woodhouseite (*Plate 5-10 J&K*). Outside of this breccia zone, topaz also occurs locally within the alunite and pyrophyllite altered wallrock, and silicified blocks, as identified by VIRS.

White quartz veining is abundant, occurring as <1-10 cm wide, discontinuous and boudinaged segments within the strongly deformed advanced argillic alteration (*Plate 5-10 L*), and within the silicified blocks. They are almost exclusively composed of quartz, but locally contain coarse-grained alunite, pyrite and/or specularite (*Plate 5-10 E*).

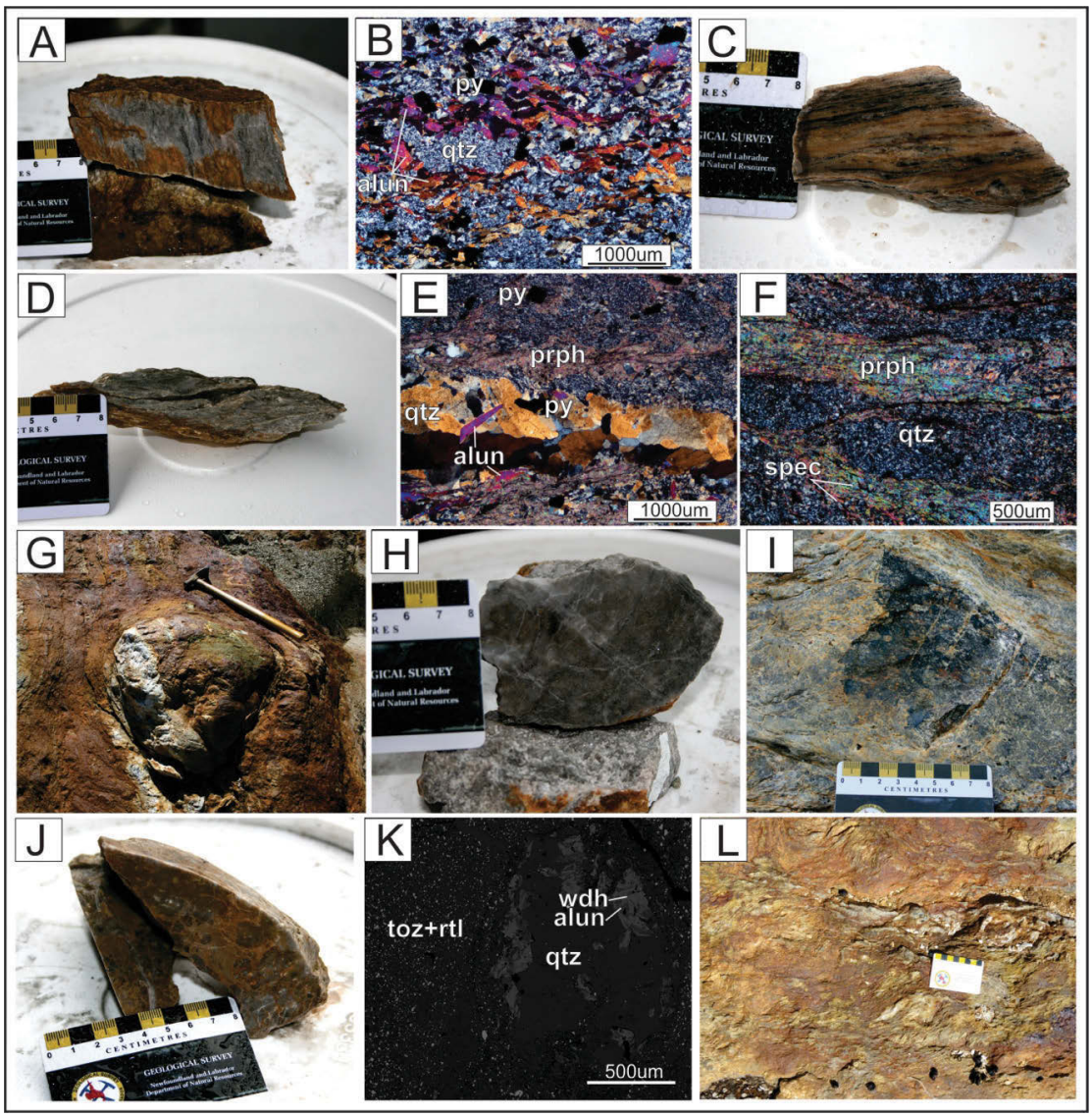

***Plate 5-10**: Representative photos and photomicrographs of alteration and hydrothermal textures at the Tower prospect; A) Hand sample of foliated altered bands of quartz and alunite. Darker bands are pyrite-rich (SF-12-10); B) Transmitted light (XPL;2X) image of foliated coalescing bands of alunite(alun)-pyrite (py) and quartz (qtz) (SF-12-15); C) Hand sample of thicker foliated bands of specularite-quartz and alunite (SF-12-22); D) Hand sample of foliated altered bands of pyrophyllite and quartz containing pyrite and with minor quartz-alunite-pyrite veining (SF-12-01); E) Transmitted light (XPL;2X) image of quartz-alunite-pyrite vein hosted within foliated matrix with thin pyrophyllite (prph) and quartz-rich bands and pyrite. Pyrophyllite appears to overprint veining (SF-12-01); F) Transmitted light (XPL;4X) image of foliated pyrophyllite and quartz banding hosting specularite (spec) (SF-12-25); G) Outcrop photograph of ~75cm silicified block enveloped within quartz-alunite-pyrite alteration (STA-SF-12-010); H) Hand sample of grey massive silica alteration from silicified block (SF-12-09); I) Outcrop photograph of locally developed hydrothermal breccia with specularite (>80%) encompassing quartz-rich clasts with minor specularite (STA-SF-12-009); J) Hand sample of locally developed hydrothermal breccia with topaz+/-rutile encompassing quartz-rich fragments with up to 10% alunite-woodhouseite (SF-12-19d); K) SEM-BSE image of quartz fragment with erratically zoned crystals of alunite (darker) and woodhouseite (wdh;brighter) contained within breccia matrix of topaz(toz)+/-rutile(rtl) (SF-12-19a); L) Outcrop photograph of white, 1-2cm wide quartz veining, folded and locally boudinaged (STA-SF-12-010).*

5.5.2 Mineralization: Mineralogy and Associations

Pyrite and specularite persistently occur throughout the advanced argillic zone in an abundance of 1-15% as fine- to medium-grained disseminations within foliated bands of alteration (*Plate 5-10 B&F*).

Pyrite associated with zones of alunite alteration typically displays distinct inclusion-rich cores, and smooth outer rims (*Plate 5-11 A*). The grains range in shape from anhedral and partially corroded to, more rarely, euhedral; the more anhedral tending to be directly intergrown with alunite. Pyrite associated with zones of pyrophyllite alteration, tends to be more subhedral to euhedral with less abundant inclusions, and does not contain distinct cores and rims (*Plate 5-11 B*). Both styles of pyrite are associated with chalcopyrite, which commonly occurs as inclusions and locally as interstitial fill along pyrite grain boundaries (*Plate 5-11 A, C, E*). Minor, very fine-grained barite also occurs in both, disseminated with pyrite or as inclusions within it. Tennantite was identified locally as interstitial fill along pyrite grain boundaries associated with alunite alteration within a silicified block (*Plate 5-11 D).* Tsumoite (BiTe) was also identified locally as inclusions in pyrite associated with pyrophyllite alteration (*Plate 5-11 E).* The tsumoite inclusions also contain variable amounts of selenium, presumably from another minor coexisting Bi-Te-Se phase.

Specularite generally occurs as euhedral acicular crystals. Unlike pyrite, it was not found to occur with any other sulphide, sulphosalt, or telluride minerals. In addition to its occurrence as disseminations throughout the groundmass, it also occurs locally as a coarse-grained breccia matrix (*Plate 5-10 I*). Both specularite and pyrite also locally occur within multiple generations of white quartz veins, as relatively coarse grains associated with alunite (*Plate 5-10 E; Plate 5-11 F).*

The samples that yielded the most anomalous gold grades (117, 56 and 35 ppb Au) are associated with pyrite, quartz and alunite, occurring within altered wallrock or grey silica pods. In contrast, the specularite horizons typically yielded Au values at or below the detection limit of 1 ppb.

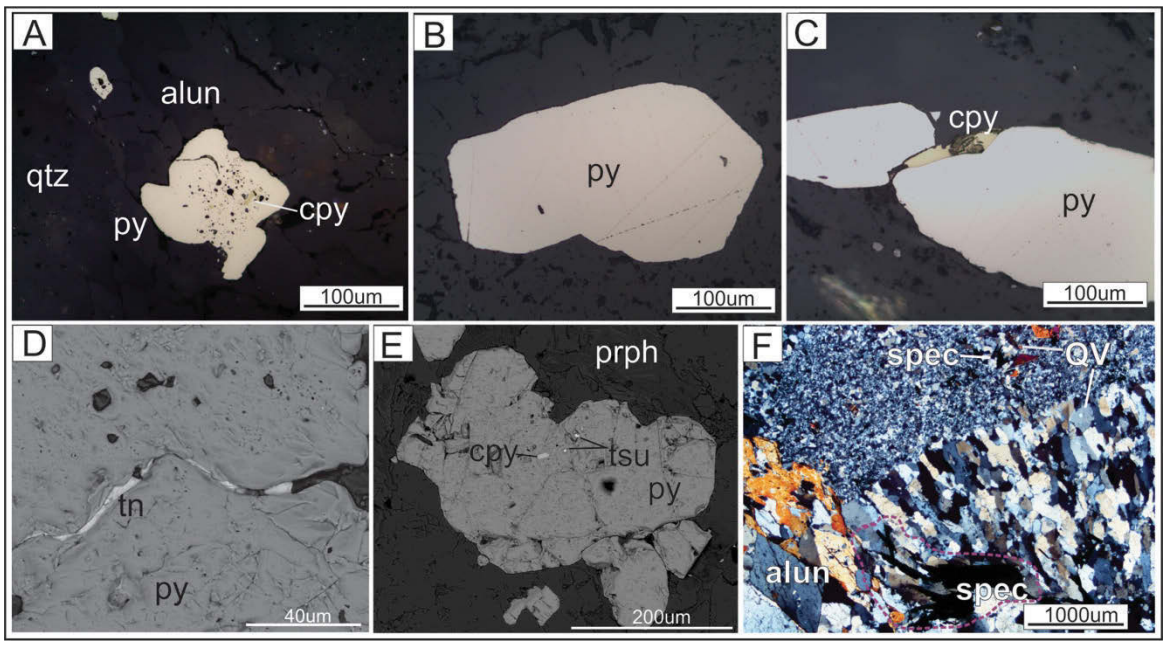

Plate 5-11*: Representative photomicrographs of mineralization at the Tower prospect; A) Reflected light (20X) image of anhedral pyrite (py) with inclusion-rich cores and smooth rims within quartz (qtz)-alunite (alun) alteration. Pyrite contains inclusions of chalcopyrite (cpy) (SF-12-09); B) Reflected light (20X) image of subhedral to euhedral pyrite grain within pyrophyllite and quartz alteration (SF-12-01); C) Reflected light (20X) image of chalcopyrite forming at grain boundaries between subhedral pyrite grains in pyrophyllite-quartz alteration (SF-12-01); D) BSE-SEM image of tennantite (tn) occurring along grain boundaries between anhedral pyrite grains in quartz-alunite alteration (SF-12-09); E) BSE-SEM image of cluster of subhedral pyrite grains containing inclusions of chalcopyrite and tsumoite (tsu) within pyrophyllite (prph) alteration (SF-12-01); F) Transmitted light (XPL;2X) image of three generations of quartz veining (QV) +/-alunite, containing acicular specularite (spec; locally highlighted by dashed purple line) (SF-12-08).*

5.5.3 Interpretation

The advanced argillic alteration, ore assemblage and ore textures at the Tower prospect are characteristic of a high-sulphidation epithermal system, and very similar to those developed at the Hickey's Pond prospect. In particular, the quartz-alunite-dominated alteration and the corresponding hypogene mineralization assemblage, which includes pyrite, specularite, chalcopyrite, tennantite and Bi-tellurides. Tower differs in that it contains topaz, indicative of a relatively higher temperature of formation, and does not display a well-defined central vuggy massive silica zone. What is exposed on surface at the Tower prospect is interpreted to have formed deeper in the epithermal system than that exposed at the Hickey's Pond prospect, below what may have been the main horizon of mineralization, presumably within a vuggy silica zone. The silicified blocks, which

correspond to some of the most gold-anomalous horizons on the property, are interpreted to be the dismembered remnants of a pre-existing massive silica alteration zone.

The Tower prospect is the result of many generations of hydrothermal activity, based on the presence of two types of hydrothermal breccias, overprinting alteration assemblages (e.g. topaz after quartz-alunite), the development of cores and rims in pyrite, and abundant cross-cutting quartz veining.

5.6 Monkstown Road

The Monkstown Road prospect is situated south of the Swift Current Granite, adjacent and to the west of the Tower prospect (*Figure 5-1*), and is hosted within intermediate to felsic volcaniclastic rocks. The prospect is part of a northeast-southwest trending zone of advanced argillic alteration, of which the phyllosilicate-rich portions have been significantly affected by deformation. It became an area of exploration interest after the discovery of gold at the Hickey's Pond prospect, due to its close proximity, and similar advanced argillic alteration assemblage. The advanced argillic alteration at the Monkstown Road prospect is largely barren, but has locally yielded anomalous gold values of up to 1.18 g/t in grab sample (Saunders and Reusch, 1984).

This prospect was not evaluated in great detail, but is included to highlight its somewhat unique alteration assemblage. A single sample was evaluated petrographically (SF-12-153) and described below.

5.6.1 Alteration Mineralogy

The most distinctive feature at the Monkstown Road prospect, is the presence of the bright blue phosphate mineral lazulite ($MgAl_2(PO_4)_2(OH)_2$; *Plate 5-12*). The mineral occurs as sub- to euhedral crystals within quartz-specularite veins, bounded by pyrophyllite at its margins (*Plate 5-13 A&B*), and is deformed within a greater envelope of advanced argillic alteration dominated by alunite, pyrophyllite, quartz and specularite. Within the pyrophyllite-rich vein margins, the phosphate minerals woodhouseite and

svanbergite are common. They occur locally intergrown with lazulite (*Plate 5-13 C*), but most commonly as individual subhedral crystals with distinct svanbergite cores and woodhouseite rims (*Plate 5-13 C-E*). Barite is also a common mineral phase throughout the sampled zone (*Plate 5-13 F*).

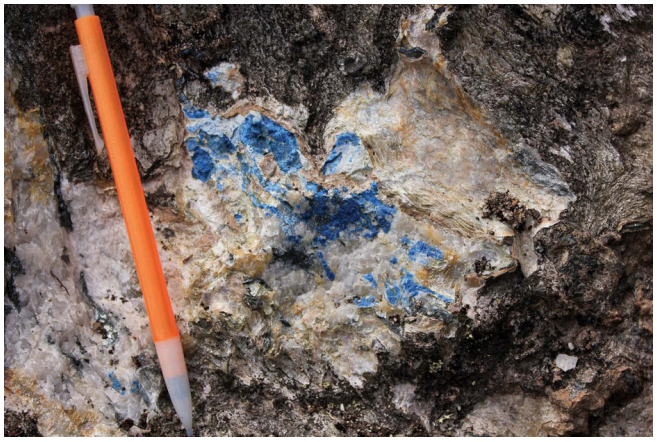

***Plate 5-12**: Blue lazulite ($MgAl_2(PO_4)_2(OH)_2$) occurring as part of the advanced argillic alteration assemblage at the Monkstown Road prospect. Additional alteration in photo includes quartz, specularite, alunite, and pyrophyllite.*

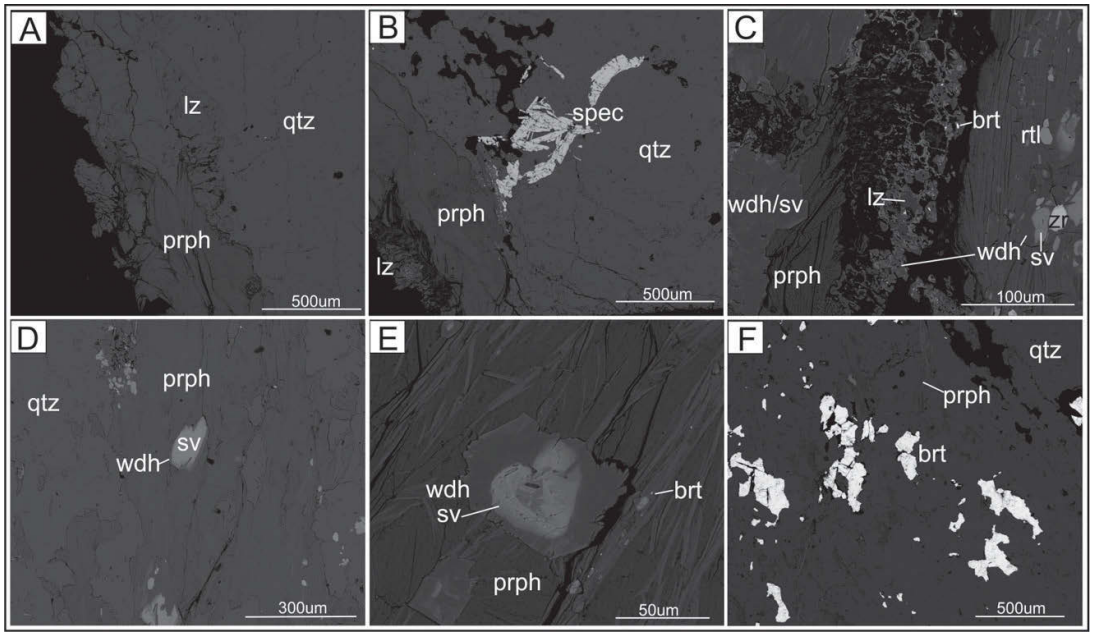

***Plate 5-13**: Representative BSE SEM images of alteration and mineralization at the Monkstown Road prospect (SF-12-153); A) Coarse subhedral crystal of lazulite (lz) within a quartz (qtz) vein bounded by pyrophyllite (prph) (lazulite is slightly darker than surrounding quartz); B) Lazulite within pyrophyllite, bounding quartz-specularite (spec) veining; C) Anhedral mass of intergrown lazulite (primarily in core) and woodhouseite (wdh) (and minor svanbergite) containing small inclusions of barite (brt), encompassed by a seam of pyrophyllite. Massive woodhouseite with svanbergite (sv) zoning occurs on the left, and on the right, distinctly zoned crystals of woodhouseite with svanbergite cores occur with zircon (zr) and rutile (rtl); D) Quartz, pyrophyllite, and svanbergite/woodhouseite alteration; E) Distinctly zoned phosphate crystal with svanbergite core and woodhouseite rim within pyrophyllite with minor barite; F) Coarse-grained barite occurring within quartz-pyrophyllite alteration.*

5.7 Stewart

The Stewart prospect is situated midway down the Burin Peninsula (*Figure 5-1*) near the intrusive contact of the large 'Burin Knee' intrusive suite (BKIS), with adjacent felsic volcaniclastic rocks of the Marystown Group. The Stewart prospect is characterized by an extensive, curvilinear zone of advanced argillic alteration, roughly 5.5 km long and 700 m wide, roughly bounded by a lower package of intermediate-mafic volcanic rocks to the southeast and the intrusive contact of the BKIS to the northwest. Unlike the Hickey's Pond, Tower, and Monkstown Road prospects – which host an advanced argillic alteration assemblage dominated by Na-alunite – the advanced argillic alteration at Stewart is dominated by pyrophyllite. The prospect is host to broad, low-grade copper and gold mineralization and minor enrichments in molybdenum. Some of the best intervals include 1.17 g/t Au over 1m, and 826 ppm Cu and 48 ppm Mo over 12m, recovered from channel samples in the alteration zone (Dimmell and MacGillivray, 1990a; Dyke and Pratt, 2008).

Alteration and mineralization is primarily hosted in two units; a dacitic quartz crystal tuff (the 'Caribou Tuff') and a small tonalite body intruding into the felsic volcanic sequence. The identification of this intrusive body during exploration work in 2007, in addition to the presence of abundant quartz veins containing minor copper sulphides, and possible retrograded potassic alteration, was tentatively inferred to represent the presence of a collapsed porphyry-system, with advanced argillic alteration overprinting porphyry-style mineralization (Dyke and Pratt, 2008; Sparkes, 2012). Follow up work by Sparkes (2012) included a detailed VIRS alteration study, which identified discrete alteration zoning at the prospect but the evidence for a superimposed epithermal and porphyry system remained unclear.

The main objective for this project was to further characterize the Stewart prospect in the context of the porphyry-epithermal environment, by evaluating the main ore assemblages present, the deportment of gold, and any associations between mineralization, veining, and alteration. Sampling generally focused on zones of elevated

copper and gold values based on previous work, and on mineralized quartz veining, which typically corresponded to pyrophyllitized zones within the Stewart tonalite.

5.7.1 Alteration and Hydrothermal Quartz Veining

The detailed VIRS alteration study completed by Sparkes (2012), found the alteration at Stewart to be dominated by either pyrophyllite or illite. Both alteration types are found in each of the hosting units, but Sparkes (2012) found the pyrophyllite to be more prevalent in the tonalite, and the illite more prevalent in the Caribou Tuff.

The host units are generally moderately to strongly foliated, with illite and pyrophyllite concentrated along bands parallel to the foliation (*Plate 5-14 A*). Both types of alteration are associated with variable degrees of silica alteration; where silicification is prevalent, host rocks are foliated less-intensely. Pyrophyllite also occurs as a semi-pervasive replacement of the groundmass and as veins up to 2cm wide (*Plate 5-14 B&C*). These thick pyrophyllite veins are typically devoid of sulphides and contain minor dickite. Woodhouseite commonly occurs within bands of pyrophyllite as fine-grained euhedral crystals, often accompanied by xenotime (YPO_4) and minor svanbergite, and is locally associated with mineralization (*Plate 5-14 D&E*).

Local rafts of less intensely altered and deformed tonalite occur within the pyrophyllite-dominated alteration. Primary igneous textures are preserved in these rafts, which have been predominantly altered to Fe-chlorite and variable amounts of silica (*Plate 5-14 F*). It is these zones that were formerly interpreted by Dyke and Pratt (2008) as zones of potassic alteration associated with deeper level porphyry-related alteration, which had undergone retrograde alteration to chlorite during metamorphism. Fe-chlorite also occurs localized within mineralized quartz veining, contained within a broader zone of pyrophyllite alteration.

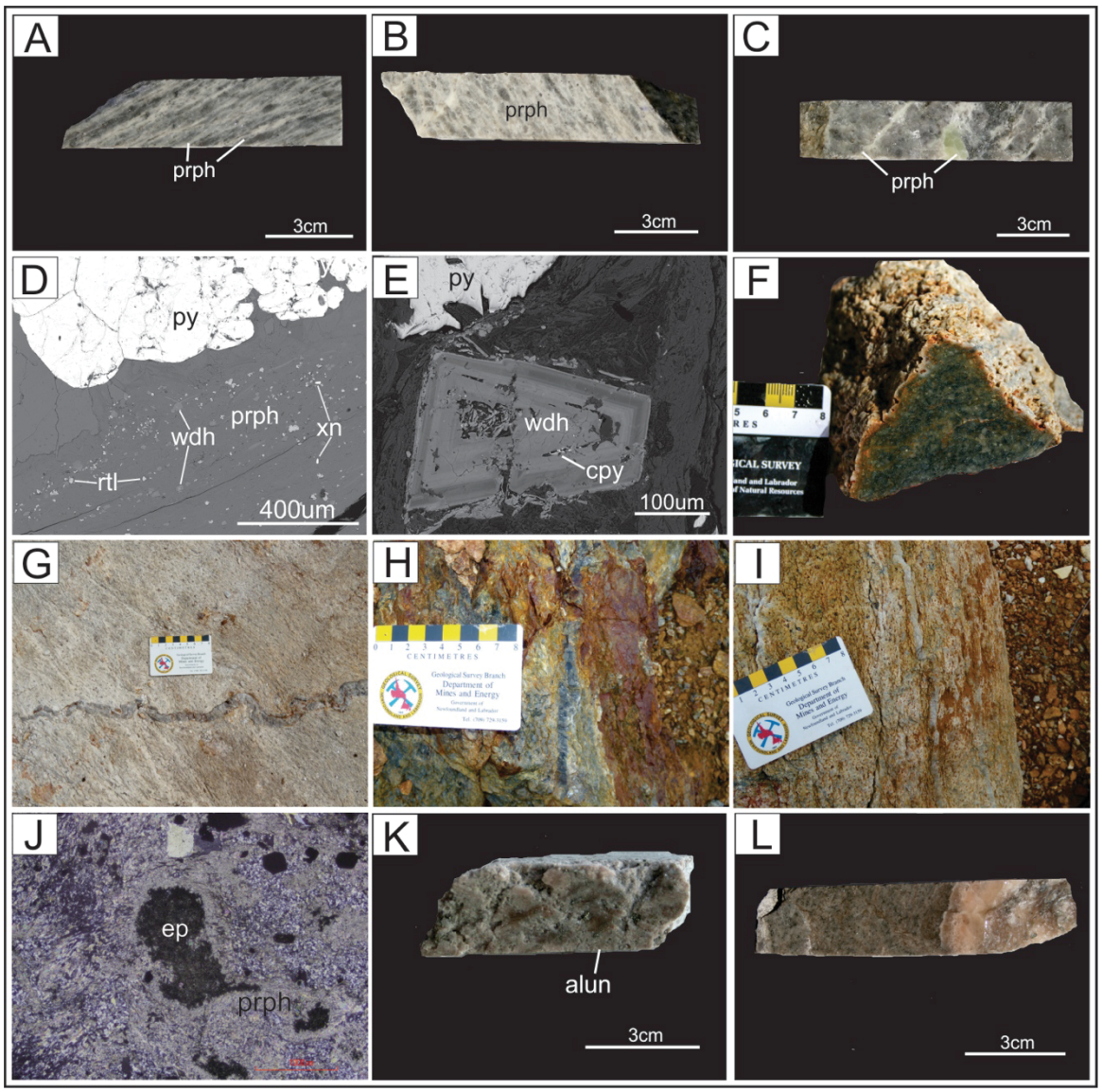

Plate 5-14*: Representative photos and photomicrographs of alteration and hydrothermal veining at the Stewart prospect; A) Pyrophyllite (prph) alteration concentrated along foliation-parallel bands (SF-12-73); B) Semi-pervasive pyrophyllite alteration (SF-12-85); C) Up to 1.5cm wide beige-yellow coloured pyrophyllite veins (SF-12-71); D) BSE-SEM image of a foliation-parallel pyrophyllite band associated with coarse-grained pyrite (py) and containing very-fine-grained rutile (rtl) and the phosphate minerals woodhouseite (wdh) and xenotime (xn) (SF-12-118); E) BSE-SEM image of a euhedral, zoned crystal of woodhouseite associated with pyrite and containing inclusions of chalcopyrite (cpy) (SF-12-76); F) Fe-chlorite (-silica) altered tonalite occurring as a raft within an envelope of pyrophyllite alteration (SF-12-39); G) Ptygmatically folded quartz vein within pyrophyllite-dominated alteration (SF-12-42); H) Grey quartz vein within silicified wallrock (SF-12-28); I) Stockwork quartz veining within chlorite-altered tonalite (SF-12-35); J) Transmitted light (XPL; 2X) image of a former feldspar phenocryst positioned adjacent to quartz veining, replaced by epidote (ep) and further overprinted by pyrophyllite (SF-12-42); K) Locally developed vuggy silica textures associated with an alteration assemblage of quartz-alunite, occurring towards the northeast from the main mineralized zone (SF-12-119); L) 2cm wide alunite vein (SF-12-122).*

Quartz veining is abundant throughout the tonalite unit, occurring in both the pyrophyllite and chlorite altered horizons, with veins ranging from 1-5cm in width (*Plate 5-14 G&H*). Stockwork-style veining is also locally developed (*Plate 5-14 I*). There are multiple generations of quartz veining, the relationships of which are complex, especially due to adjacent groundmass silicification and later deformation. Quartz veins are locally brecciated by seams of pyrophyllite, or crosscut along their margins by fine fractures of pyrophyllite. Conversely, quartz veins locally crosscut pyrophyllite in the host groundmass. Adjacent to the margins of some quartz veins within the pyrophyllite-altered tonalite, former feldspar laths have been completely replaced by epidote, and further overprinted by pyrophyllite alteration (*Plate 5-14 J)*.

The hydrothermal alteration found at the main prospect extends eastward to what is referred to as the 'Bat Zone', where the hydrothermal alteration locally transitions into a quartz-alunite dominated assemblage, associated with locally developed vuggy silica textures in drill core (*Plate 5-14 K*). Alunite most commonly occurs as veins, up to 4cm wide (*Plate 5-14 L*). Contrary to the typical high-sulphidation epithermal model, this assemblage does not contain anomalous gold grades on the Stewart property.

5.7.2 Mineralization: Mineralogy and Associations

The main sulphide assemblages found to occur within the extensive alteration zone at the Stewart prospect include pyrite, pyrite-chalcopyrite, pyrite-chalcopyrite-specularite, chalcopyrite-galena, and molybdenite-pyrite. Most of the assemblages are associated with pyrophyllite or fine-grained white mica alteration (typically identified by VIRS as muscovite). The pyrite-chalcopyrite-specularite and chalcopyrite-galena assemblages, and occasionally pyrite-chalcopyrite, also occur intergrown with Fe-chlorite. Most of the abundant quartz veining that occurs across the property is barren of any sulphide mineralization, with sulphide minerals only present as later cross cutting fracture-filling. However, two types of quartz-sulphide veins containing assemblages of pyrite-chalcopyrite and chalcopyrite-galena were identified locally.

Pyrite is abundant throughout the extensive alteration zone at Stewart, and multiple generations are evident based on morphology and occurrence. Pyrite can be coarsely subdivided into two main morphologies; 1) anhedral to subhedral pyrite, containing inclusion rich cores and smooth outer rims, ranging from a fine to coarse-grain size (*Plate 5-15 A*), and 2) fine-grained euhedral pyrite (*Plate 5-15 D&E*). When it is the only sulphide, pyrite typically occurs as the former, disseminated and clustered within the main groundmass, disseminated within foliated bands of pyrophyllite and fine-grained white mica (*Plate 5-15 B*), and within barren quartz veins as a later infill, exploiting points of weakness, typically along the central axis of the vein (*Plate 5-15 C*). This morphology of pyrite is often also associated with minor chalcopyrite, present as inclusions in the cores of grains or occasionally as later interstitial fill. Minor barite, galena and specularite are also present locally as inclusions in pyrite cores.

The fine-grained euhedral variety of pyrite typically occurs with chalcopyrite ± chlorite, or with chalcopyrite, specularite and chlorite. These assemblages occur as fine disseminations and networks of very fine fractures, cross cutting barren quartz veins and the host groundmass (*Plate 5-15 D-F*).

Pyrite and chalcopyrite also occur as quartz-sulphide veinlets (~1cm), with chalcopyrite (± minor galena and cassiterite) occurring interstitially to tightly clustered aggregates of sub- to euhedral pyrite grains (*Plate 5-15 G&H*). A second type of quartz-sulphide veining is present locally, with relatively coarse-grained, intergrown blebs of chalcopyrite, galena, and chlorite contained within ~2cm wide quartz veins (*Plate 5-15 I&J*).

Molybdenite occurs fairly consistently throughout the alteration zone, but in very low abundance. It is typically very fine-grained, occurring within foliated bands or seams of very fine-grained pyrophyllite (± white mica), associated, and locally intergrown, with fine-grained, disseminated anhedral pyrite grains, the majority of which display cores and rims (*Plate 5-15 K&L*).

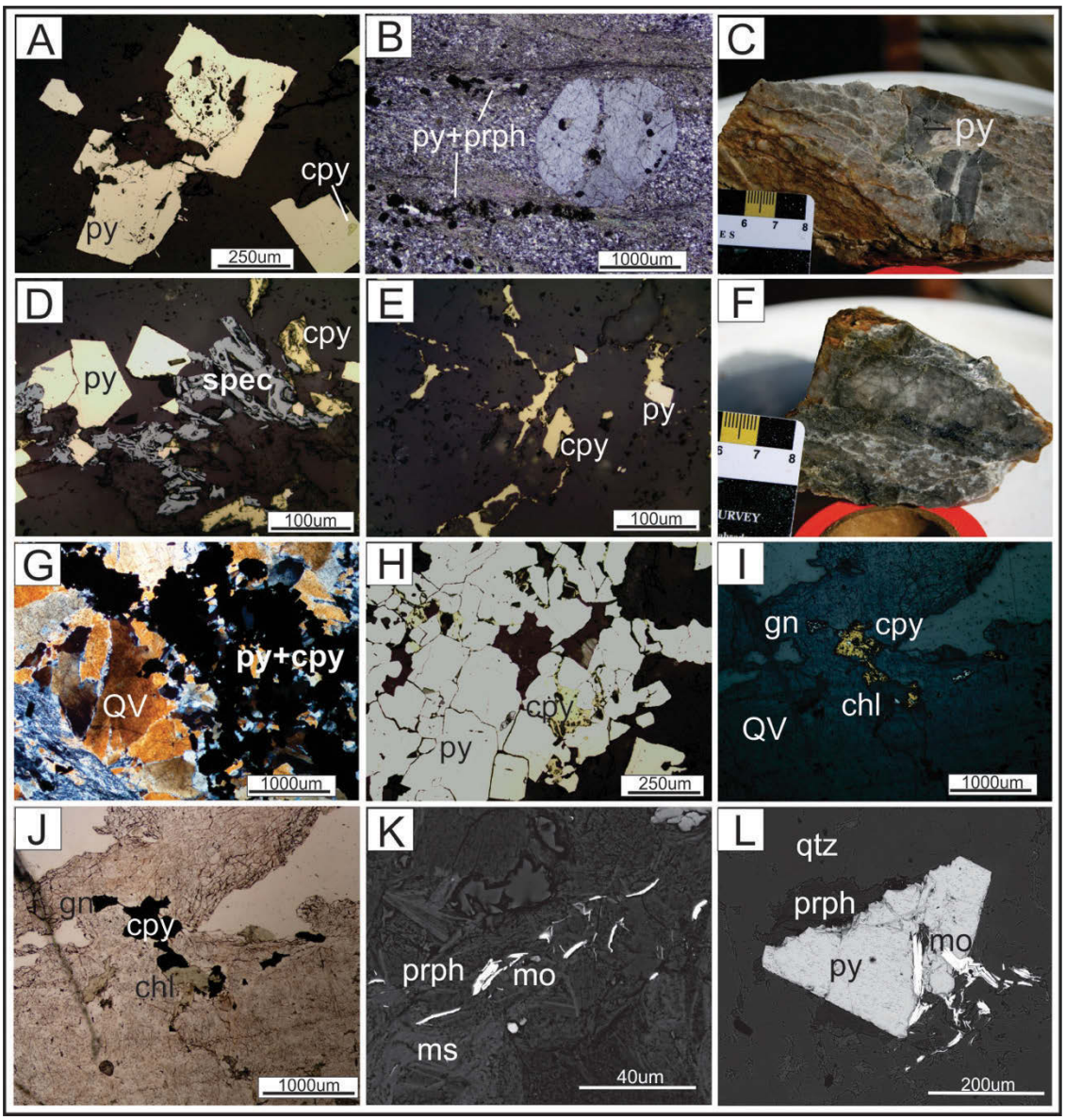

Plate 5-15*: Representative photos and photomicrographs of sulphide mineralization at the Stewart prospect; A) Reflected light (10X) image of subhedral pyrite (py) grains with inclusion-rich cores containing chalcopyrite (cpy), and smooth rims (SF-12-28); B) Transmitted light (XPL;2X) image of pyrite within foliation-parallel bands of pyrophyllite (prph) (SF-12-73); C) Deformed quartz veining with pyrite occurring as later fracture filling along the veins central axis (SF-12-42); D) Reflected light (20X) image of euhedral pyrite occurring with specularite (spec) and chalcopyrite (cpy) within a fine fracture (SF-12-28); E) Reflected light (20X) image of euhedral pyrite occurring with chalcopyrite within a network of fine fractures (SF-12-32A); F) Hand sample of the former, showing the sulphide fracture network crosscutting both the groundmass and white quartz veining (SF-12-32A); G) Transmitted light (XPL;2X) image of quartz-sulphide veining containing pyrite and chalcopyrite (QV=quartz vein; SF-12-83); H) Reflected light (10X) image of the quartz-pyrite-chalcopyrite veins, with aggregates of subhedral pyrite surrounded by interstitial chalcopyrite (SF-12-83); I&J) Reflected and transmitted light (PPL; 2X) images of intergrown chalcopyrite, galena (gn) and chlorite (chl) occurring within white quartz veining (SF-12-86); K) BSE-SEM image of very fine-grained molybdenite (mo) within a pyrophyllite seam, with minor muscovite (ms; SF-12-78); L) BSE-SEM image of intergrown molybdenite and pyrite (SF-12-78).*

Precious metal mineralization was not identified in any of the analyzed samples. However, the three grab samples yielding the highest gold grades (up to 1.5 g/t Au) collected as part of this study, also yielded corresponding enrichments in molybdenum, and contained minor molybdenite identifiable in thin section. Other shared characteristics of these samples include diffuse quartz veining associated with wallrock silicification within a broad envelope of pyrophyllite alteration, the presence of anhedral pyrite with inclusion-rich cores, and a fine-grained assemblage of chalcopyrite-euhedral pyrite ± specularite ± chlorite.

5.7.3 Interpretation

Alteration and mineralization at the Stewart prospect records a complex and seemingly protracted hydrothermal event, resulting in multiple generations of quartz veining, occurring intermittently with advanced argillic alteration, multiple generations of pyrite mineralization, and the occurrence of local alteration overprints. However, the occurrence of a pyrophyllite-dominated alteration assemblage with the characteristic high-sulphidation assemblage pyrite – specularite ± chalcopyrite, in association with anomalous gold values, provides fairly unequivocal evidence for a high-sulphidation epithermal system. However, evidence for an underlying porphyry system remains ambiguous.

Chlorite occurs within at least one set of quartz veins intergrown with galena and chalcopyrite, and elsewhere crosscuts quartz veins as fine fracture filling with specularite, pyrite and chalcopyrite. The presence of chlorite directly associated with Cu-mineralization on the property is not typical of a high-sulphidation environment, and could perhaps be an indication of the presence of an underlying porphyry environment.

Further evidence for the presence of a porphyry-type hydrothermal system at the Stewart prospect is the occurrence of epidotized feldspars associated with hydrothermal quartz veining, overprinted by pyrophyllite alteration. It is possible that this represents distal propylitic alteration and veining from a porphyry system, later overprinted by advanced argillic alteration from an epithermal system.

While the presence of molybdenite can be a strong indication for porphyry-style mineralization, it is also not uncommon for it to occur in high-sulphidation epithermal environments. In addition, the molybdenite at Stewart consistently occurs with high-sulphidation-related pyrophyllite, and is therefore most likely related to the epithermal environment.

The phosphate mineral woodhouseite commonly occurs in association with pyrophyllite, and is also interpreted to be part of the hypogene advanced argillic alteration assemblage.

5.8 Forty Creek

Prospecting along strike of the main Stewart prospect led to the 2010 discovery of the Forty Creek showing, located approximately 5 km to the northeast (*Figure 5-1*). The showing consists of a localized accumulation of angular mineralized boulders of quartz vein material, which contain up to 59 g/t Au and 2290 g/t Ag (TerraX Minerals Inc., Press Release; December 20, 2010). The mineralization has yet to be identified in situ, but is presumably hosted in adjacent, and regionally abundant intermediate volcaniclastic rocks. Given its close proximity to the extensive alteration zone at Stewart, it is interpreted to be related to the overall hydrothermal system, and has been suggested to represent an intermediate-sulphidation style of mineralization. The main objective for this prospect was to identify the alteration and ore assemblage, and the deportment of gold, as possible indications of an epithermal-related genetic origin.

5.8.1 Alteration, Ore Mineralogy and Paragenesis

Mineralization occurs in massive white quartz boulders associated with Fe-Mg-chlorite and muscovite, as determined by VIRS, occurring in patches and along fractures (*Plate 5-16 A*). These minerals have been identified across the region in association with greenschist-related alteration as a result of regional metamorphism, and are not necessarily representative of a localized hydrothermal assemblage.

The ore assemblage is composed of sulphide and telluride minerals, with gold and silver occurring as sylvanite ($(Au,Ag)_2Te_4$), petzite (Ag_3AuTe_2) and hessite (Ag_2Te). The main recurring ore mineral associations are pyrite, sphalerite-chalcopyrite ± galena, hessite-petzite ± chalcopyrite-sphalerite ± altaite (PbTe), and hessite-sylvanite.

Pyrite is a relatively minor phase but occurs as sub- to euhedral disseminated grains, often spatially associated with blebs of chalcopyrite-sphalerite ± galena (*Plate 5-16 C*). Locally, pyrite contains very minor overgrowths of sphalerite and galena along its perimeter, and elsewhere is completely encompassed by hessite (associated with petzite-chalcopyrite-sphalerite; *Plate 5-16 D*).

Chalcopyrite-sphalerite ± galena occur as coarse, blebby intergrowths within quartz (*Plate 5-16 B&C*). Galena is commonly partially replaced by a late assemblage of covellite and anglesite, which form distinct colloform banded textures and locally contain minor naumannite (*Plate 5-17 A-C*).

Hessite and petzite occur together as fine disseminated grains within the quartz groundmass (*Plate 5-16 E*). Similar small grains of hessite and petzite also occur with the addition of minor, but intimately intergrown chalcopyrite, sphalerite, and altaite (*Plate 5-16 F*). Hessite, petzite, chalcopyrite and sphalerite are also found intergrown as coarse blebs, locally encompassing disseminated pyrite grains (*Plate 5-16 D*).

Hessite is also associated with the Au-Ag-telluride mineral sylvanite. Sylvanite is the dominant phase, hosting small irregular patches of hessite either as intergrowths or exsolution textures. They tend to form relatively coarse, elongate, anhedral grains sporadically distributed along fracture networks. Altaite typically surrounds these coarse grains and fills the fine connecting fractures (*Plate 5-16 G*). Altaite was also locally identified surrounding blebby sphalerite-chalcopyrite. Native tellurium, chalcocite, and minor acanthite occur as replacements of altaite, the chalcocite often displaying dendritic textures (*Plate 5-17 D-F)*.

The temporal relationships of the described ore assemblages at Forty Creek are summarized in *Figure 5-11*.

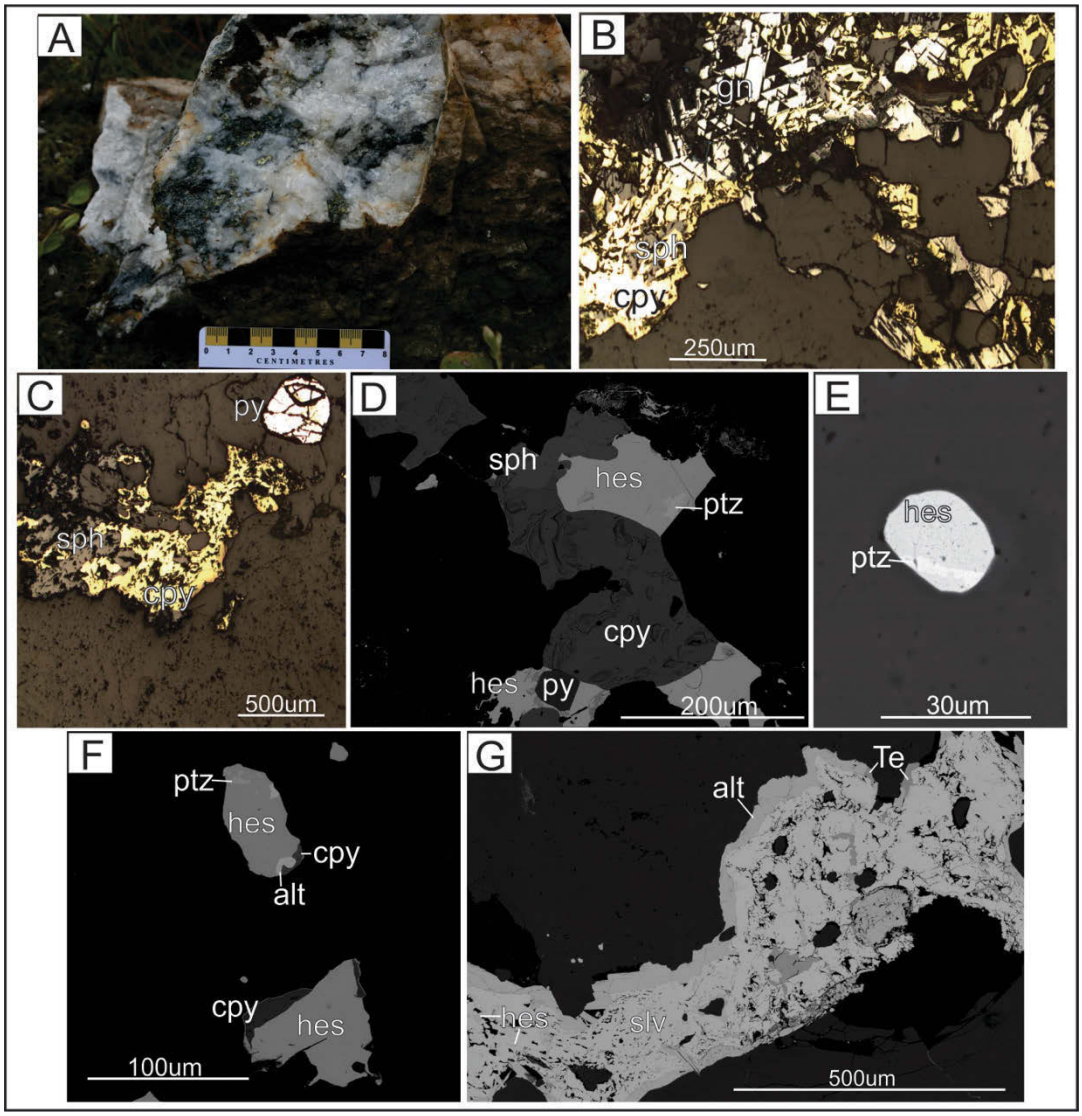

Plate 5-16: *Representative photos (A), photomicrographs (B&C), and BSE SEM images (D-G) of mineralization at the Forty Creek showing; A) Typical grab sample from the prospect, showing abundant chlorite and sulphides hosted in white quartz; B) Reflected light (10x) image of intergrown blebby sulphides of chalcopyrite (cpy), galena (gn) and sphalerite (sph) (SF-12-50a); C) Reflected light (5x) image of intergrown chalcopyrite and sphalerite, and proximal subhedral pyrite (py) grain (SF-12-50a); D) Intergrown, blebby hessite (hes), petzite (ptz), chalcopyrite and sphalerite, with hessite encompassing former disseminated pyrite grain (SF-12-50c); E) Fine disseminated grain of hessite with band of petzite (40crkNTR); F) Fine grains of hessite intergrown with minor petzite, chalcopyrite, and altaite (alt) (SF-12-50c); G) Coarse grain of predominantly sylvanite (slv) containing irregular patches of slightly darker hessite (hes), all surrounded by altaite with minor native Te (SF-12-50c).*

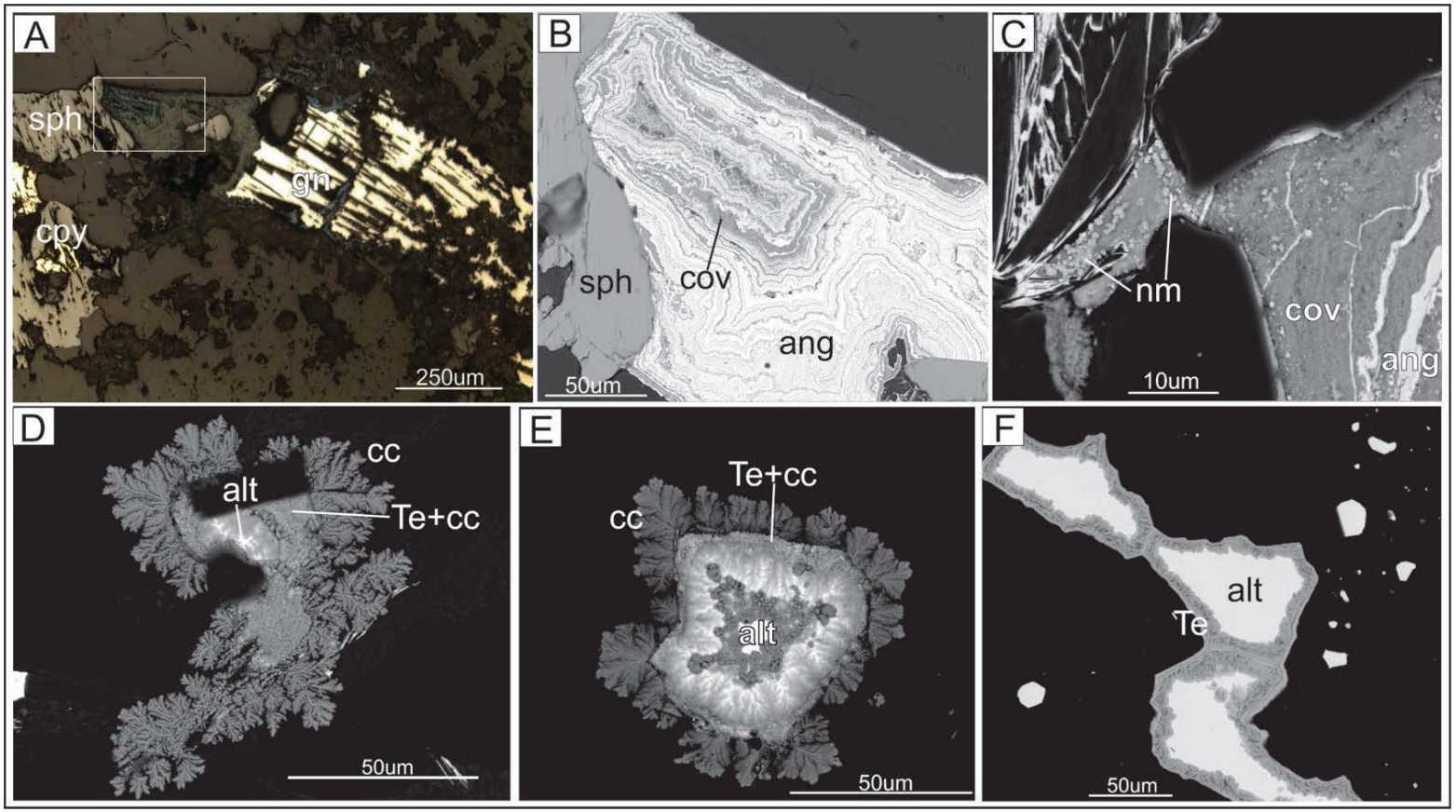

Plate 5-17*: Representative photomicrographs (A) and BSE SEM images (B-F) of the mineralogy and related textures resulting from late supergene processes and weathering at Forty Creek; A) Reflected light (10X) image of galena (gn) being replaced by an assemblage of covellite and anglesite. Outlined box is shown as closeup in B) (SF-12-50a); B) Detailed image of colloform bands of covellite (cov) and anglesite (ang) replacing galena (SF-12-50a); C) Minor, very fine-grained naumannite (nm) forming with covellite (SF-12-50a); D&E) Altaite (alt) being replaced by native Te and chalcocite (cc), and surrounded by dendritic chalcocite; F) Altaite forming along fracture and being replaced along its perimeter by native Te (40crkNTR).*

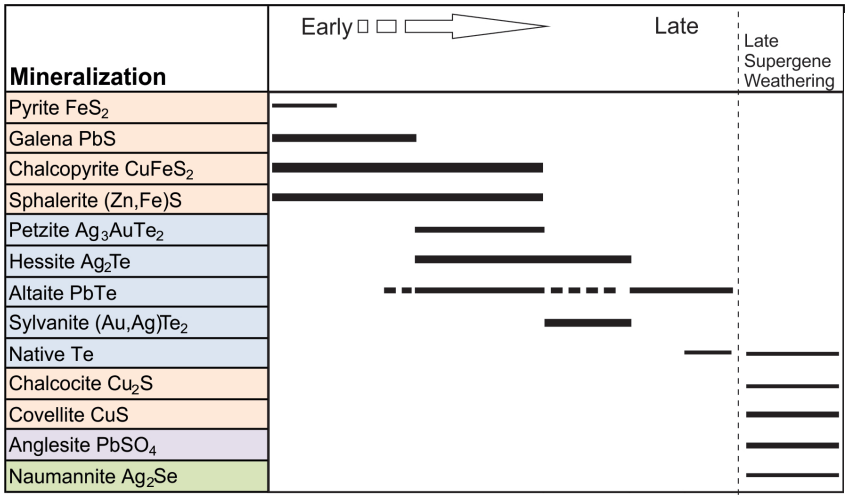

***Figure 5-11**: Paragenetic sequence for mineralization at the Forty Creek prospect. Colours as in Table 5-1. Line thickness is representative of relative frequency of occurrence. Mineral occurrence lines in the 'late supergene weathering' column are not representative of their relative timing, but as a group, late, relative to the main hypogene assemblage.*

5.8.2 Interpretation

The Ag-Au-Pb-Te-Zn-Cu rich assemblage could be representative of epithermal-related mineralization, as these are commonly enriched elements in these systems. The enrichment of Ag relative to Au is common for both intermediate- to low-sulphidation types, while the presence of abundant tellurides and lack of selenides is generally more suggestive of an intermediate-sulphidation style. However, the ore assemblage alone, without the identification of diagnostic hydrothermal alteration minerals or an understanding of the context of the veining, is not enough to definitively deduce a genetic model.

5.9 Sulphur Isotopes ($\delta^{34}S$)

Sulphur isotope studies were conducted on sulphides from the various high-sulphidation epithermal prospects occurring within the Hickey's Pond-Point Rosie alteration belt. This was done to characterize the isotopic signature of these regional epithermal deposits and to identify any local variations (indicative of a different sulphur source), and correlations between the $\delta^{34}S$ values and local gold concentrations. At Stewart it was important to test for the presence of a bimodal population, which could provide further evidence for the coexistence of a high-sulphidation system overprinting an underlying porphyry system. The Forty Creek showing was also analyzed to compare

its isotopic signature to the adjacent Stewart prospect as well as the other high-sulphidation prospects in the region, to gain more insight into its genetic origins and potential association with the extensive belt of epithermal alteration.

Relevant sulphur isotope data for precious metal epithermal systems are relatively limited. However, published studies on high-sulphidation deposits typically report values averaging around 0‰, similar to porphyry deposits, and broadly indicative of a magmatic sulphur source, but ranging from -7 to +7‰ (e.g. Arribas et al., 1995; Bethke et al., 2005; Fifarek and Rye, 2005). Despite their close magmatic association, high-sulphidation systems, and to a slightly lesser degree, porphyry systems, show a broad range of $\delta^{34}S$ values. This is due to the sub-equal proportions of oxidized (SO_2) and reduced (H_2S) sulphur species in the fluids, particularly in oxidized, low pH systems, coupled with their relatively low temperature of formation (Ohmoto, 1972; Seal, 2006). Crustal contamination of the source magmas can also affect the sulphur isotopic composition of the magmatic hydrothermal system (Seal, 2006).

Determinations of $\delta^{34}S$ were performed on grains of pyrite, chalcopyrite and galena using the Cameca IMS 4f Secondary Ion Mass Spectrometer (SIMS) at the MAF-IIC Micoanalysis Facility of Memorial University, following the methodology of Brueckner et al. (2015). At the Hickey's Pond prospect, pyrite was analyzed from within the high-grade vuggy massive silica zone. At the Tower prospect, grains of both pyrite and chalcopyrite were analyzed from within the main advanced argillic alteration zone. Grains of pyrite, chalcopyrite, and galena were analyzed at both the Stewart and Forty Creek prospects. At Stewart, sulphide grains were selected to represent different styles of quartz veining and both chloritic and advanced argillic alteration, and at Forty Creek, the selected grains were associated with auriferous white quartz veining. A table summarizing the individual $\delta^{34}S$ values is included in *Appendix F*.

5.9.1 Results

The $\delta^{34}S$ values from grains of pyrite, chalcopyrite and galena, from all of the analyzed deposits are plotted together in *Figure 5-12*. The high-sulphidation prospects appear to form a single population ranging from -6.8 to +5.9‰ with an average of -0.6‰. The $\delta^{34}S$ values from the Forty Creek deposit plot at distinctively lower values, ranging from -10.5 to -5.3‰, with an average of -7.8‰. The data from each deposit are also presented individually, below, to highlight any deposit-specific trends.

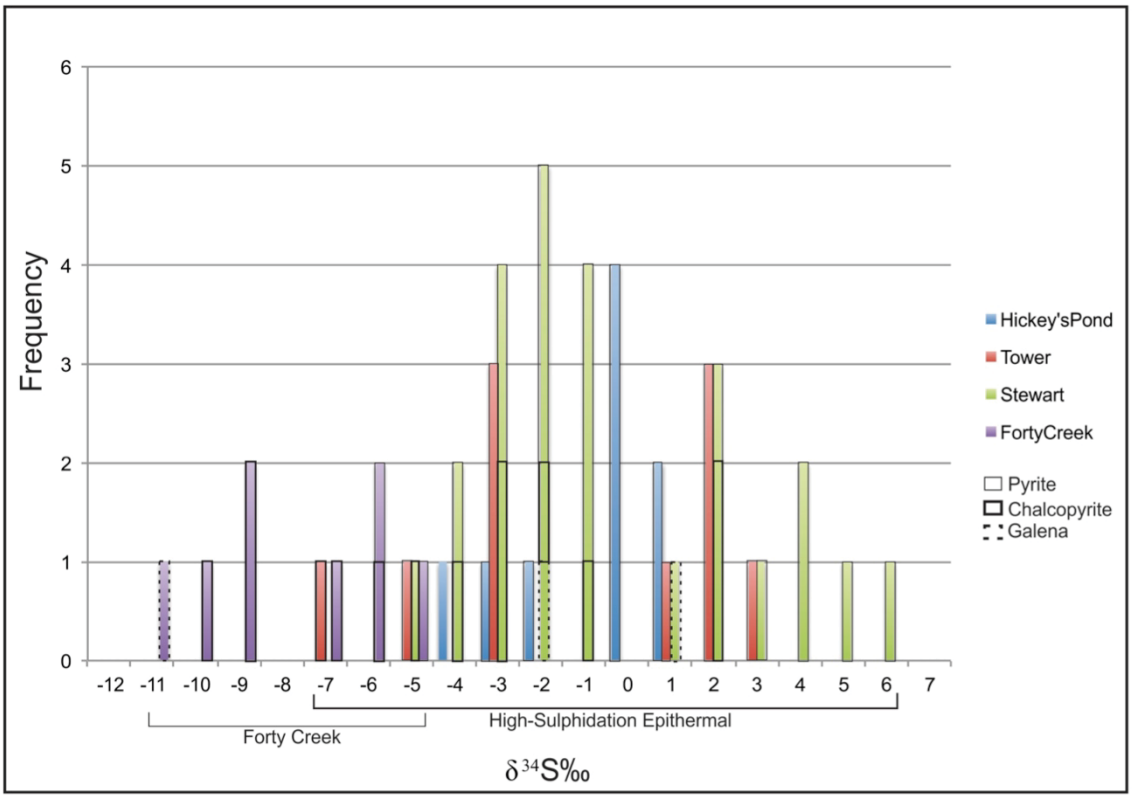

Figure 5-12*: Histogram for sulphides (pyrite, chalcopyrite, and galena) hosted within the high-sulphidation epithermal Hickey's Pond, Tower, and Stewart prospects (n=44), as well as the Forty Creek "intermediate-sulphidation" veins (n=8). $\delta^{34}S$ values of the high-sulphidation prospects range from -6.8 to +5.9‰ and average at -0.6‰. Bin width=1‰.*

Hickey's Pond

The results of analyses on pyrite grains from the vuggy massive silica zone at the Hickey's Pond prospect are displayed in *Figure 5-13*. The $\delta^{34}S$ values range from -3.7 to +1.4‰, with an average of -0.7‰. Overall, the data appear to form a single population. However, there is some additional correlation with specific occurrences of pyrite; the lighter values representative of finer-grained vug filling, and the heavier values with later, cross cutting quartz-sulphide veins. Both types of pyrite are associated with alunite alteration.

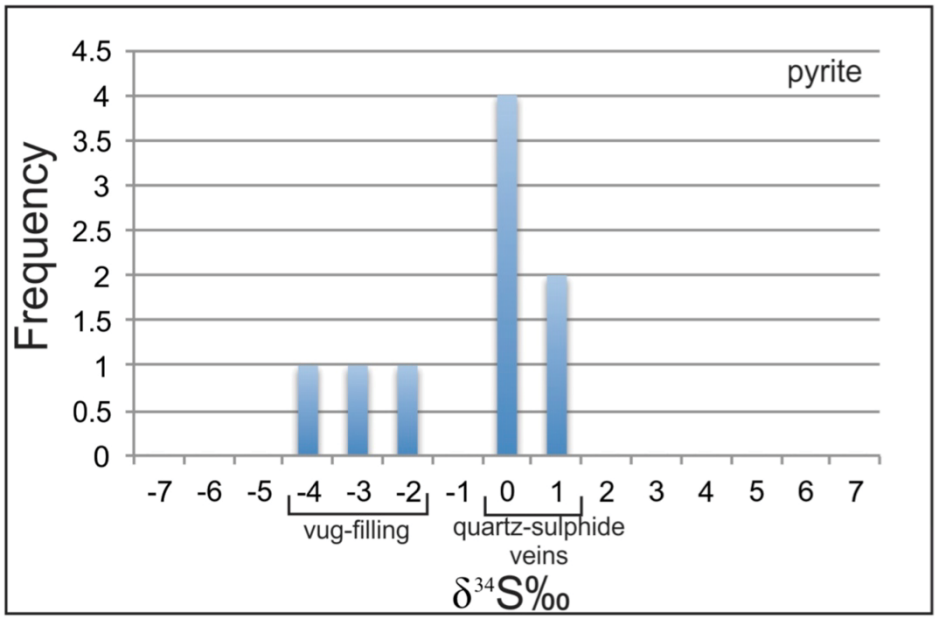

Figure 5-13*: Histogram for pyrite hosted within the vuggy massive silica zone associated with alunite at the Hickey's Pond prospect. $\delta^{34}S$ values range from -3.7 to +1.4‰ with an average of -0.7‰ (n=9; Bin width=1‰). Lighter values associated with finer-grained vug filling, and heavier values with later cross cutting quartz-sulphide veins.*

Tower

The results of analyses on pyrite and chalcopyrite grains from the advanced argillic alteration zone at the Tower prospect are displayed in *Figure 5-14*. The $\delta^{34}S$ values for pyrite range from -4.6 to +3.0‰, with an average of -0.6‰. A single chalcopyrite grain yielded a value of -6.8‰. Two populations of $\delta^{34}S$ values are evident, which correspond with specific petrographic observations. The negative values for pyrite

and chalcopyrite correspond to subhedral to euhedral pyrite grains hosted in pyrophyllite-quartz alteration. The positive values correspond to anhedral pyrite displaying cores and rims, developed within alunite-quartz alteration.

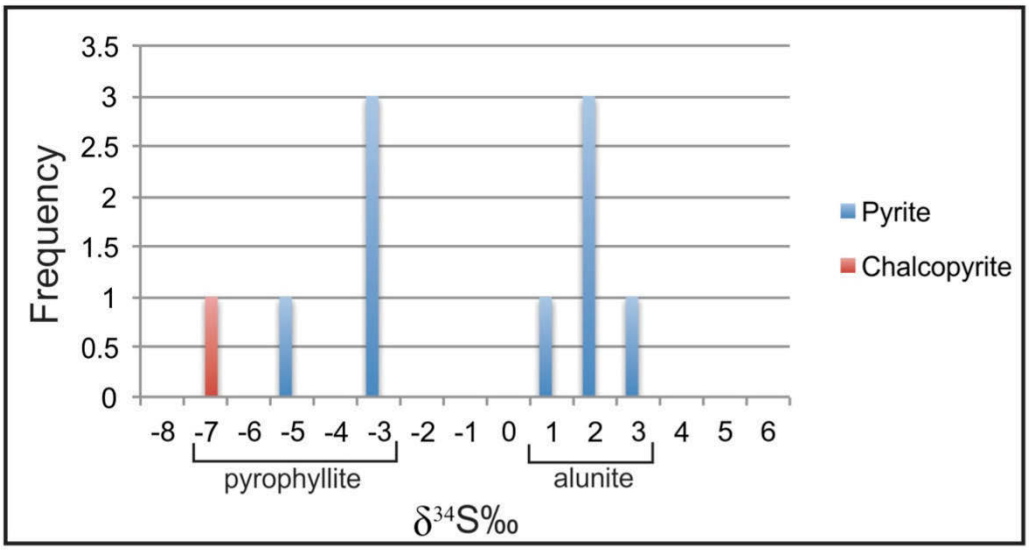

Figure 5-14*: Histogram for pyrite and chalcopyrite hosted within the advanced argillic alteration zone at the Tower prospect. $\delta^{34}S$ values for pyrite range from -4.6 to +3.0‰ with an average of -0.6‰ (n=9; Bin width=1‰). A single $\delta^{34}S$ value of -6.8‰ was measured from chalcopyrite, giving a total average of -1.2‰ (n=10). Negative values associated with subhedral to euhedral pyrite occurring within pyrophyllite-quartz alteration, and positive values with anhedral pyrite with cores and rims within alunite-quartz alteration.*

Stewart

The results of analyses on pyrite, chalcopyrite and galena grains from veining and wallrock from within the pyrophyllite-dominated advanced argillic alteration envelope at the Stewart prospect are displayed in *Figure 5-15*. The $\delta^{34}S$ values for all minerals range from -4.6 to +5.9‰, with an average of -0.4‰. The analyses form a bimodal distribution, separated only by a small gap at 0‰. The sulphide minerals analyzed were generally associated with either pyrophyllite-white mica alteration or chlorite alteration. The pyrite displaying cores and rims and associated with pyrophyllite-white mica alteration are widely distributed through both populations. Chalcopyrite ± pyrite ± specularite associated with chlorite is confined to the negative population, but chalcopyrite and galena associated with chlorite in quartz veins overlaps with the former, and spans both populations.

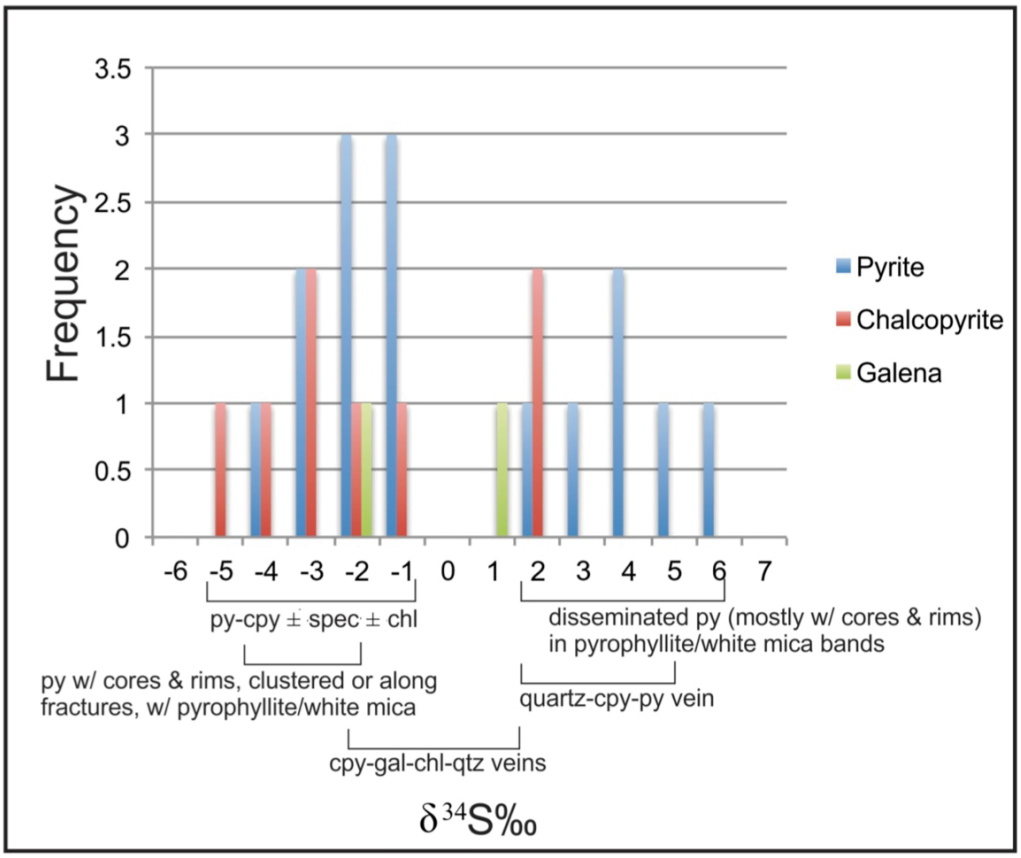

Figure 5-15*: Histogram for pyrite, chalcopyrite and galena hosted within the advanced argillic alteration envelope at the Stewart prospect. $\delta^{34}S$ values of all analyses range from -4.6 to +5.9‰ with an average of -0.4‰ (n=25; Bin width=1‰). Two subtle populations are formed, but with no specific alteration or morphological distinctions defining them. Pyrite associated with pyrophyllite and white mica occurs throughout both groups, as does the chalcopyrite-chlorite association.*

The stable isotope fractionation between two substances should approach zero at infinite temperatures (Bigeleisen and Mayer, 1947); conversely, the fractionation between two substances becomes more variable at lower temperatures. Given that high-sulphidation epithermal systems form at relatively low temperatures (<300°C), the differences in sulphur fractionation between different mineral phases becomes more pronounced. Since the dataset at Stewart contains multiple analyses from three different sulphide minerals, $\delta^{34}S$ values were also recalculated at a hypothetical temperature of 200°C, based on the experimentally derived temperature dependent equilibrium sulphur isotope fractionation factors presented in *Table 1* and *Figure 2* of Seal (2006; and references therein). The results are presented in *Figure 5-16*. $\delta^{34}S$ values of all analyses

range from -6.2 to +4.0‰ with an average of -1.1‰ (n=25; Bin width=1‰) and form a single, slightly asymmetric population. Analyses of intergrown pyrite and chalcopyrite from within a quartz-sulphide vein now plot directly adjacent. Chlorite- and pyrophyllite-associated measurements now overlap and span most of the total range. Pyrite associated with pyrophyllite-white mica shows the greatest variation.

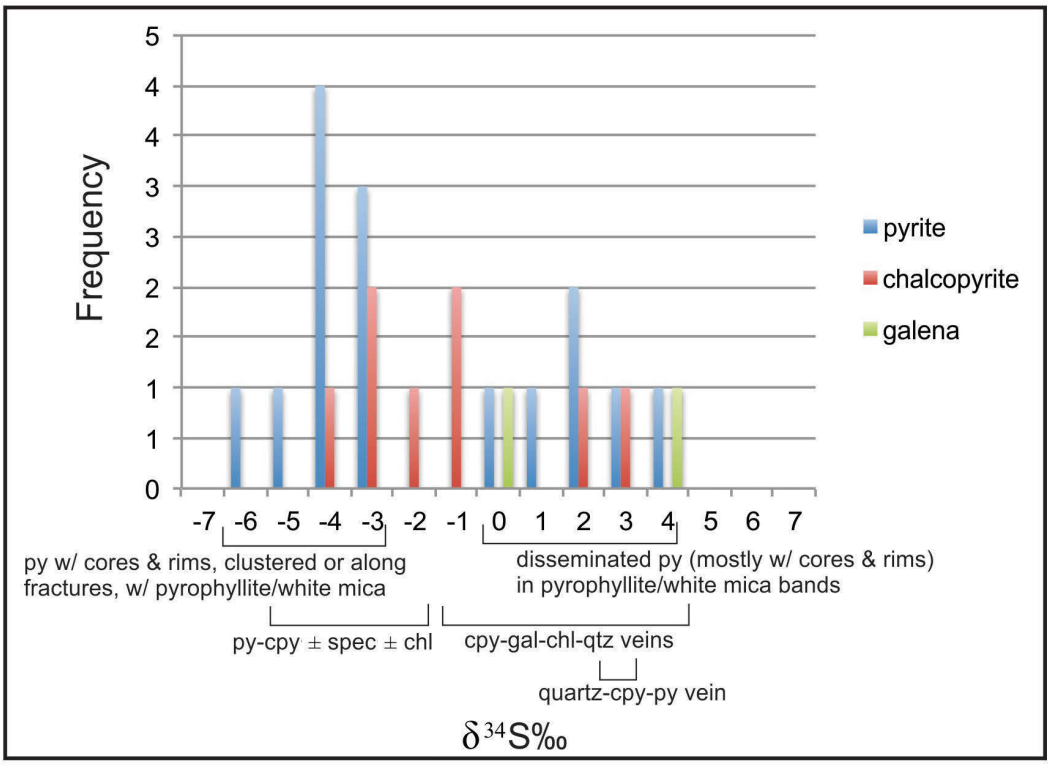

***Figure 5-16**: Histogram for pyrite, chalcopyrite and galena hosted within the advanced argillic alteration envelope at the Stewart prospect, recalculated at a formation temperature of 200°C, based on the experimentally derived temperature dependent equilibrium sulphur isotope fractionation factors presented in Table 1 and Figure 2 of Seal (2006; and references therein). $\delta^{34}S$ values of all analyses range from -6.2 to +4.0‰ with an average of -1.1‰ (n=25; Bin width=1‰) and form a single population.*

Forty Creek

The results of analyses on pyrite, chalcopyrite and galena grains from massive white quartz boulders at the Forty Creek showing are displayed in *Figure 5-17*. The $\delta^{34}S$ values range from -10.5 to -5.3‰, with an average of -7.8‰. The data form a single population, with distinctly lighter values than the nearby high-sulphidation epithermal deposits.

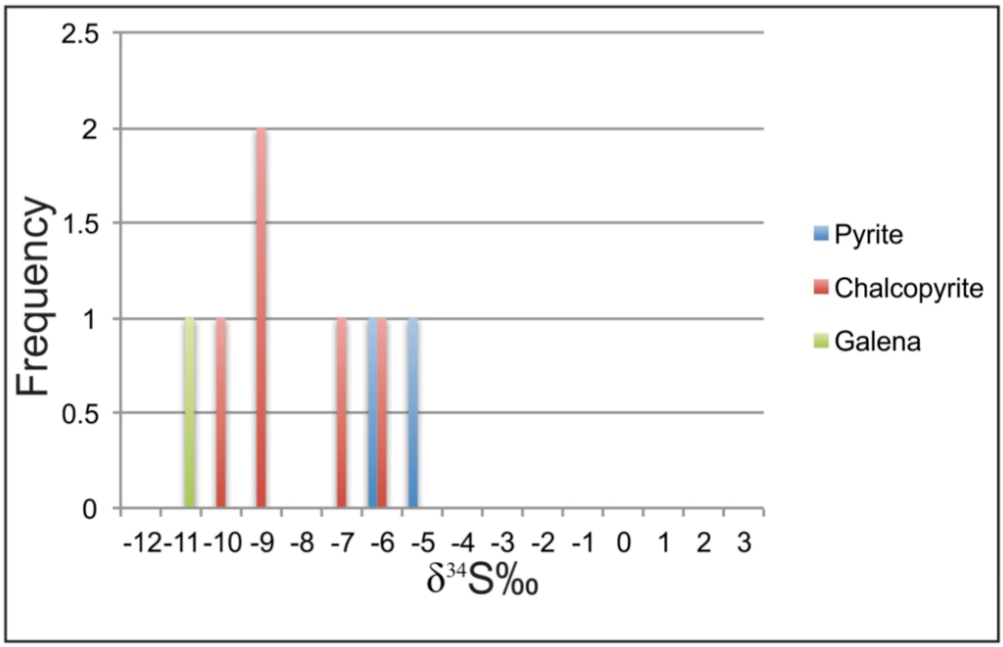

Figure 5-17*: Histogram for pyrite, chalcopyrite and galena hosted within massive white quartz veining in boulders at the Forty Creek showing. $\delta^{34}S$ values for all minerals form a single population ranging from -10.5 to -5.3‰ with an average of -7.8‰ (n=8; Bin width=1‰).*

5.9.2 Interpretation

As a whole (*Figure 5-12*), the high-sulphidation prospects of the Hickey's Pond-Point Rosie advanced argillic alteration belt (not including the Forty Creek prospect) appear to form a single population with $\delta^{34}S$ ranging from -6.8 to +5.9‰ with an average of -0.6‰. These values are indicative of a magmatic sulphur source, consistent with the high-sulphidation genetic model. This range in values is also consistent with the range of isotopic sulphur values measured from other high-sulphidation epithermal deposits (e.g. Arribas et al., 1995; Bethke et al., 2005; Juliani et al., 2005).

When evaluated separately, some deposits show additional detailed trends. Both Tower and Hickey's Pond show fluctuations in $\delta^{34}S$ interpreted to be representative of mineralization under changing physicochemical conditions during the evolution of a dynamic epithermal system. Hickey's Pond shows an overall single population of $\delta^{34}S$ values, but a transition from lighter isotopic values in earlier, finer grained pyrite filling vugs to heavier values in later, coarser-grained quartz-sulphide veining. Two populations are present at the Tower prospect, which could simply be the result of a small sample size. However, the populations directly correlate with different styles of pyrite and different alteration assemblages; subhedral to euhedral pyrite and associated chalcopyrite within pyrophyllite alteration yield negative values, and more anhedral pyrite with cores and rims within alunite alteration yield positive values. While both are ultimately derived from the same magmatic sulphur source, these two populations are suggestive of the presence of at least two generations of mineralization, precipitating under changing physicochemical conditions.

Pyrite, chalcopyrite and galena from the Stewart prospect show the largest variation in $\delta^{34}S$ values, ranging from -4.6 to +5.9‰, with an average of -0.4‰ and also form a weakly bimodal population. There does not appear to be a clear distinction in the characteristics of mineralization between the two groups to elucidate the presence of both porphyry- and epithermal-style mineralization. Pyrite with cores and rims associated with high-sulphidation-related pyrophyllite-white mica alteration spans the entire range of values. There is a slight correlation with the textural occurrence of this pyrite; the positive values generally disseminated, and the negative values clustered in the matrix or along fractures. While these might represent separate generations of pyrite mineralization, they are all associated with the high-sulphidation system. Analyses of mineralization associated with chlorite alteration also span both populations of $\delta^{34}S$ values.

The recalculated data, accounting for natural isotopic fractionation between cogenetic mineral phases at lower temperatures, forms a single population, and is perhaps a better representation of the isotopic sulphur signature at the Stewart prospect. The

chlorite and high-sulphidation-related pyrophyllite assemblages overlap, and both span most of the $\delta^{34}S$ range in values. Similar to Tower and Hickey's Pond, the range in values is interpreted to be the result of multiple generations of mineralization precipitating under changing temperature and redox conditions in an evolving high-sulphidation epithermal system. While this does not rule out the possibility for porphyry mineralization (the isotopic signature of a genetically related porphyry system could yield very similar values), the results do not provide any definitive evidence in this respect.

Sulphur isotopic values from the Forty Creek showing range from -10.5 to -5.3‰, with an average of -7.8‰, which is significantly lighter than the values measured at the adjacent high-sulphidation epithermal deposits. These more negative values are indicative of a different sulphur source for mineralization at Forty Creek, and most likely the result of a unique genesis, unrelated to the regionally developed epithermal mineralization. The negative values might also indicate a sulphur source influenced to some degree by biogenically derived sulphur, however there are no obvious sedimentary horizons in the proximal country rocks that might have been the source.

5.10 Discussion

Regional Implications

The Hickey's Pond, Tower and Stewart prospects are all hosted in similar intermediate to felsic volcaniclastic rocks of the Marystown Group. These rocks and the adjacent regional plutons implicated as parents for the hydrothermal activity, consistently yield U-Pb zircon ages of ca. 575 Ma (*Chapter 4*) and, based on lithogeochemistry, are associated with subduction-related magmatism (*Chapter 3*). In addition, the deposits all contain similar ore mineralogy (i.e., pyrite, specularite, chalcopyrite, galena, tennantite), and similar, but variably developed, alteration assemblages (i.e., quartz-alunite, pyrophyllite). This extensive belt of high-sulphidation alteration and mineralization is therefore interpreted to be the result of hydrothermal activity related to ca. 575 Ma volcanism-plutonism.

Indicators for Gold Mineralization

Hickey's Pond is the most gold enriched prospect associated with high-sulphidation epithermal mineralization in the region. In addition to gold, Hickey's Pond is also significantly enriched in tellurium and selenium relative to the other high-sulphidation prospects, which appears to play a key role in the local concentration of gold. In addition to native gold, gold occurs as the Au-telluride, calaverite, and the Au-Ag-selenide, fischesserite. Calaverite is the third most abundant phase of gold, and occurs as part of the hypogene high-sulphidation assemblage with native Au. Cu-Ag-Bi-selenide minerals also occur as part of this early hypogene assemblage. Fischesserite is the second most abundant phase of gold and is interpreted to have formed from the mobilization and re-precipitation of selenium, silver and gold from the primary hypogene assemblage, as a result of weathering and supergene processes. Therefore, the presence of a gold, selenium and tellurium enriched hypogene fluid, and the conditions for a supergene environment to occur, were important factors for gold enrichment at the Hickey's Pond prospect.

Forty Creek is also enriched in tellurium (and minor selenium) and contains significant concentrations of gold and silver. Whether or not Forty Creek is directly related to the belt of high-sulphidation epithermal occurrences, it further suggests that tellurium and selenium enrichments are important indicators for gold mineralization in the region.

The association of high-grade gold mineralization with vuggy silica is well documented in high-sulphidation systems. The preservation of a well-developed central vuggy massive silica zone at the Hickey's Pond prospect, corresponding to the highest grades of gold is consistent with this, and appears to be an important feature for gold mineralization in the region. The Tower prospect is very similar to Hickey's Pond, containing quartz-alunite-dominated alteration and a hypogene mineralization assemblage that includes pyrite, specularite, chalcopyrite, tennantite and Bi-tellurides. Tower differs in that it contains topaz, indicative of a higher temperature of formation, and does not

contain a central vuggy massive silica zone, but rather remnant blocks of one. It is interpreted to have formed deeper in the epithermal system, below the main horizon of mineralization in the silicified core; a feature that is only obviously preserved at Hickey's Pond.

Gold enrichment at Stewart is relatively minor, however, anomalous gold values tend to occur associated with the presence of molybdenite.

Occurrence of Phosphate Minerals

In addition to the typical advanced argillic alteration, dominated by alunite or pyrophyllite, previously undocumented Ca-Sr-phosphate minerals, woodhouseite and svanbergite were also identified at each of the high sulphidation prospects as part of the advanced argillic assemblage. Although not typically described in the core epithermal literature, these phosphate minerals are iso-structural with alunite, have been identified at many high-sulphidation deposits, and are considered to be overlooked constituents of a hypogene advanced argillic assemblage (e.g. Stoffregen and Alpers, 1987; Hikov, 2004; Milu et al., 2004).

Evidence for Porphyry-Style Mineralization at Stewart

The occurrence of a pyrophyllite-dominated alteration assemblage with the characteristic high-sulphidation minerals pyrite, chalcopyrite and specularite, in association with anomalous gold values, provides fairly unequivocal evidence for a high-sulphidation epithermal system. Evidence for an underlying porphyry system remains ambiguous. However, potential indicators of porphyry-style mineralization include the presence of Fe-chlorite associated with Cu-mineralization, possibly retrograded from a potassic assemblage, and the overprinting of epidote associated with hydrothermal quartz veining by pyrophyllite. Although molybdenite, a mineral not found at the other high-sulphidation prospects, could be an indication of a porphyry system, it tends to occur directly associated with pyrophyllite, and therefore most likely associated with the epithermal system.

Sulphur Isotopes

Pyrite ± chalcopyrite ± galena from all of the high-sulphidation prospects analyzed from within the Hickey's Pond-Point Rosie advanced argillic alteration belt, yield a similar range of $\delta^{34}S$ values, forming a single population with values ranging from -6.8 to +5.9‰ with an average of -0.6‰. These values are indicative of a magmatic sulphur source, consistent with the high-sulphidation genetic model. This range in values is also consistent with isotopic sulphur values measured from other high-sulphidation epithermal deposits (e.g. Arribas et al., 1995; Bethke et al., 2005; Juliani et al., 2005). Local variations in $\delta^{34}S$ associated with specific alteration assemblages or sulphide morphologies are interpreted to be representative of multiple generations of sulphide mineralization, precipitating under changing physicochemical conditions during the evolution of a dynamic epithermal system.

Mineralization at Forty Creek

The Ag-Au-Pb-Zn-Cu rich assemblage, the high silver to gold ratio and the presence of abundant tellurides are likely indicators for formation in an intermediate-sulphidation epithermal environment. However, the $\delta^{34}S$ values measured at Forty Creek are significantly lower than the nearer 0‰ magmatic signatures of the surrounding high-sulphidation prospects, yielding an average $\delta^{34}S$ of -7.8‰. This indicates a different sulphur source for mineralization at Forty Creek, potentially one influenced to some degree by biogenically derived sulphur. The relationship between Forty Creek, the Stewart prospect and other regionally developed high-sulphidation occurrences remains uncertain.

CHAPTER 6: CHARACTERISTICS OF LOW-SULPHIDATION EPITHERMAL AU MINERALIZATION IN THE BURIN PENINSULA REGION

6.1 Introduction

In addition to high-sulphidation epithermal systems, precious metal bearing, low-sulphidation epithermal systems also occur across the Burin Peninsula region. The potential for this style of gold mineralization to occur in the Western Avalone Zone was only fully recognized within the past decade, and therefore has become highly prospective. The three most significant occurrences to date are the Heritage, Big Easy and Long Harbour prospects, their locations shown in *Figure 6-1*. These are all hosted in different rock types and within separate lithological groups; Heritage is hosted in volcaniclastic rocks of the Marystown Group, Big Easy in epiclastic sediments of the Musgravetown Group, and Long Harbour in flow banded rhyolite of the Long Harbour Group. Compared to the high-sulphidation prospects (*Chapter 5*), which contain highly variable concentrations of gold (e.g., Hickey's Pond with 60.4 g/t Au and Monkstown Road with only weakly anomalous concentrations), the low-sulphidation deposits all have yielded fairly significant gold grades and with more consistent reproducibility.

The Long Harbour prospect was evaluated in the greatest detail since very little is known about the prospect and historical work has been minimal, primarily due to its remoteness from roadways. The mineralization and alteration at Heritage was sampled and analyzed in some detail, but was not treated as a main focus since concurrent work is being done on the deposit as part of a M.Sc. thesis by G. Woodland at Memorial University. The description of the Big Easy prospect is primarily based on field observations, with reference to data from a B.Sc. thesis by M. Clarke (2013) and recent work by Layne et al. (2016), and is included to characterize regional variations amongst the low-sulphidation occurrences.

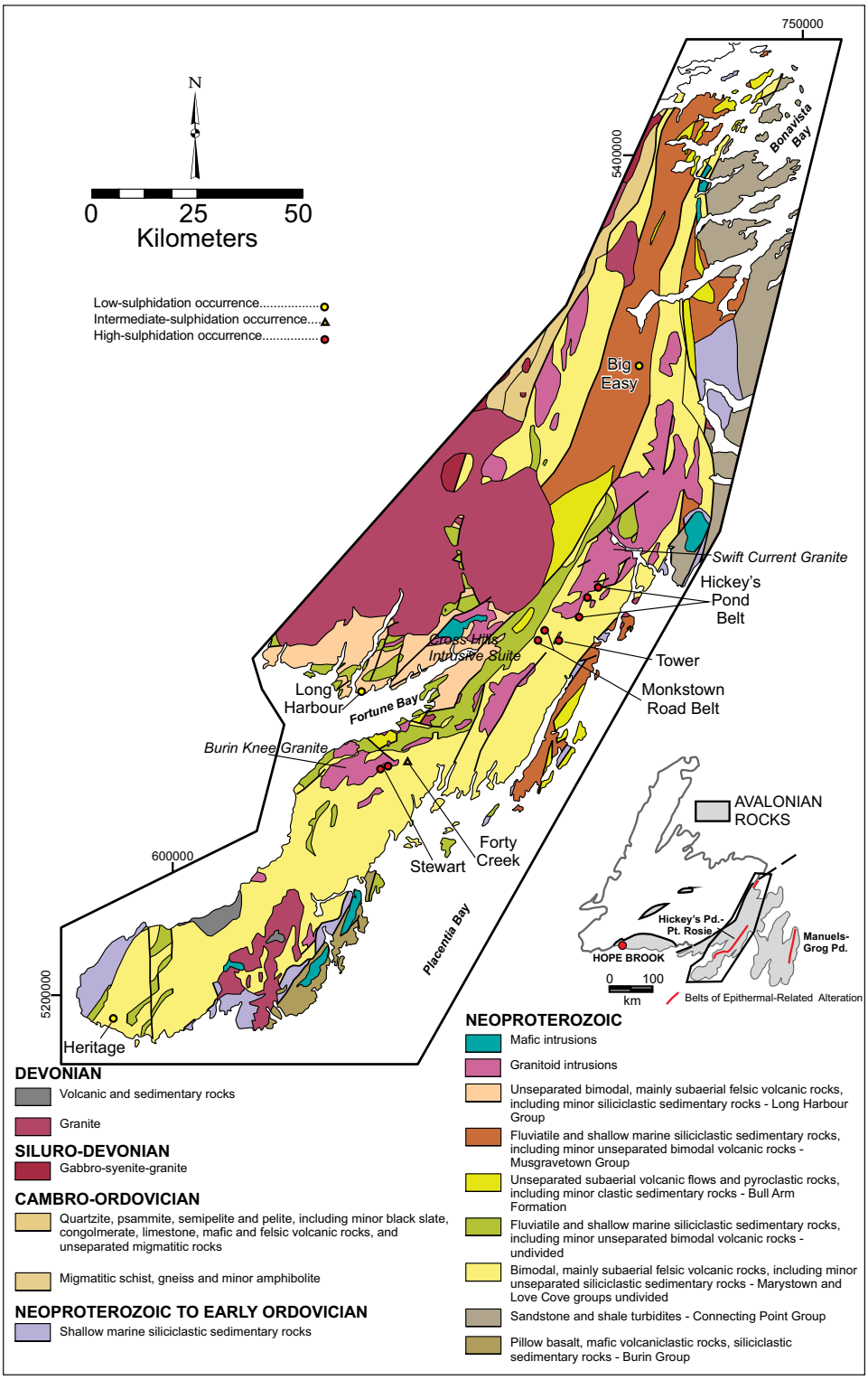

Figure 6-1*: Regional geology map of the western Avalon Zone of Newfoundland with key epithermal prospects highlighted. Low sulphidation occurrences at Big Easy, Heritage and Long Harbour are shown as yellow dots (modified from Sparkes and Dunning, 2014; O'Brien et al., 1998; coordinates are listed in NAD 27, Zone 21).*

The objectives of evaluating these low-sulphidation systems were i) to further characterize them within the epithermal environment by identifying the main alteration and ore assemblages and any key hydrothermal textures, and ii) to try to determine the occurrence and timing of gold at each deposit. To accomplish this, representative samples of veining, mineralization and alteration were collected from each prospect, and evaluated using petrography, visible infra-red reflectance spectroscopy (VIRS), and scanning electron microscopy with energy dispersive X-ray spectrometry (SEM-EDX). The procedures implemented for VIRS and SEM-EDX are described under *Methods* (*Section 5.2*) in *Chapter 5*. Similar to high-sulphidation systems, both gold and alteration minerals are typically very fine-grained in low-sulphidation deposits, making VIRS and SEM-EDX very useful tools for mineral identification. Low-sulphidation systems do not form laterally extensive alteration halos like their high-sulphidation counterparts, but still contain characteristic alteration assemblages.

A comprehensive summary of previous work and detailed descriptions of the local geology at each of the three prospects is provided in *Chapter 1* (*Section 1.7.1.2*) and *Chapter 2*, respectively. The results of this investigation on low-sulphidation-style alteration and mineralization in the Burin Peninsula region are presented below, following a summary of the general characteristics and genesis of low-sulphidation epithermal gold systems.

6.2 Setting, Characteristics and Genesis of Low-Sulphidation Epithermal Gold Systems

Unless otherwise noted, the content in this section has been extracted and compiled from the comprehensive reviews of epithermal systems presented by White and Hedenquist (1995), Hedenquist et al. (2000) and Sillitoe and Hedenquist (2003), and references therein. A general overview of the epithermal environment is described first, followed by a more detailed discussion of the low-sulphidation end-member.

6.2.1 Overview of the Epithermal Environment

Epithermal gold deposits are defined as hydrothermal deposits formed at shallow depths (generally <1km) from surface, and at relatively low temperatures (<300°C). These deposits are precious metal dominated (Au±Ag), but can also contain appreciable amounts of base metals such as Cu, Pb, or Zn. They are associated with convergent plate margins, most commonly forming coevally with arc magmatism during subduction, and during post-subduction extension. Epithermal deposits can be divided into two main end-members: high-sulphidation and low-sulphidation, the latter of which is the focus of this chapter. The classification is based on the sulphidation state, essentially the range in T-fS_2 space indicated by the hypogene sulphide assemblage (Barton and Skinner, 1967; Barton, 1970; Einaudi et al., 2003; *Figure 6-2*). A third subdivision, intermediate-sulphidation, has been introduced in recent years, which reflects an ore assemblage indicative of a sulphidation-state intermediate to that of the two original end members (Hedenquist et al., 2000).

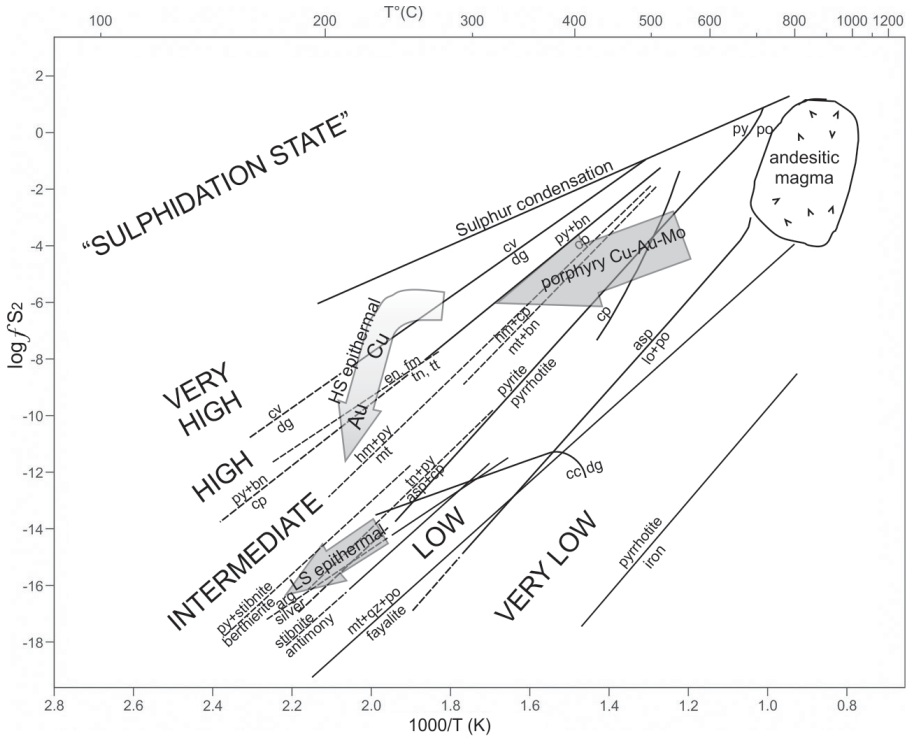

Figure 6-2*: Log fS_2-1000/T diagram illustrating fluid environments in porphyry Cu deposits, and high- and low-sulphidation epithermal Au-Ag deposits in terms of a series of possible cooling paths. Fluid environments are based on sulphide assemblages and temperatures discussed in Einaudi et al., 2003, and sulphidation reactions from Barton and Skinner (1979). High-sulphidation arrow displays early Cu-rich high-sulphidation state assemblage, followed by a Au-rich stage at intermediate sulphidation states. Low-sulphidation arrow shows the general domain for this deposit type (<300°C). arg=argentite, asp=arsenopyrite, bn=bornite, cc=chalcocite, cp=chalcopyrite, cv=covellite, dg=digenite, en=enargite, fm=famatinite, hm=hematite, lo=lollingite, mt=magnetite, py=pyrite, po=pyrrhotite, qz=quartz, tn=tennantite, tt=tetrahedrite (modified from Einaudi et al., 2003).*

6.2.2 Deposit Setting and Characteristics

Low-sulphidation deposits tend to form during late- or post-subduction related extension, or even rifting, within intra- near- or back-arc environments, including continental arcs, and are most commonly hosted in bimodal volcanic suites. Generally, they do not display a direct spatial affiliation with underlying intrusions as clearly as their high-sulphidation counterparts do - occurring as much as 5-6 km away from a magmatic source (*Figure 6-3*). Any exsolved magmatic fluids involved combine with meteoric waters and undergo significant water-rock interactions at depth during a prolonged ascent, allowing for equilibration with the host rocks. The resulting fluid is near-neutral, weakly saline, and reduced, with a composition dominated by meteoric water; the original

magmatic input now only a minor constituent. These systems commonly generate hot springs as a surficial signature.

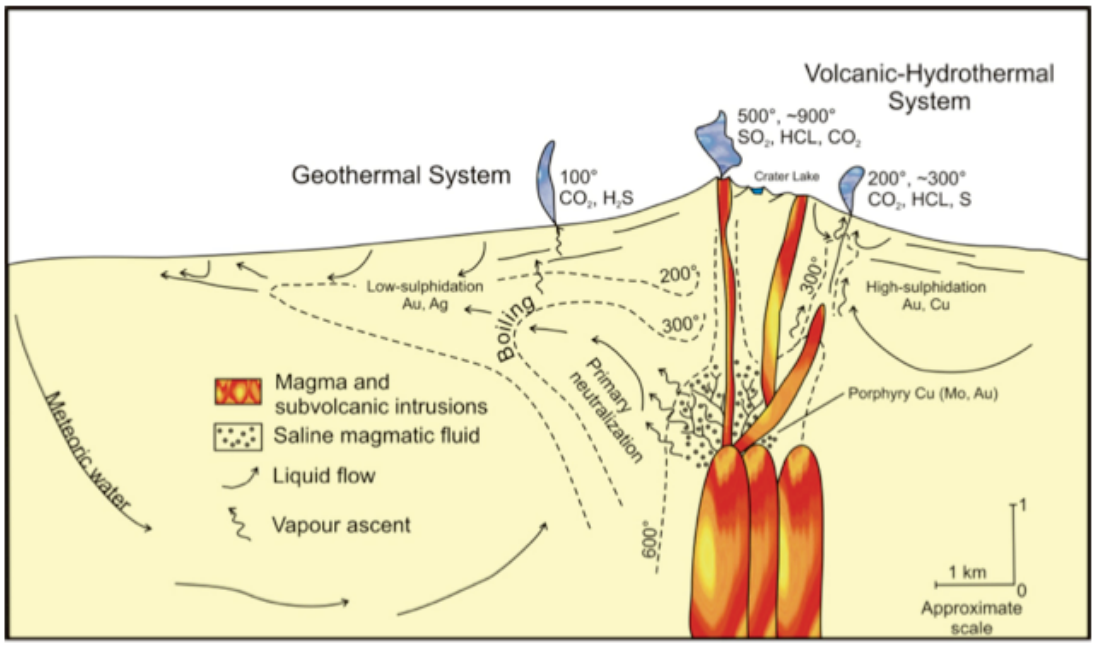

Figure 6-3*: Schematic illustrating the environments in which high-sulphidation (volcanic-hydrothermal) and low-sulphidation (geothermal) deposits form, and their spatial relationship to the main parent intrusion driving the systems. Within this environment, the parent intrusion also commonly spawns porphyry-style mineralization at depth. Fluid and vapour flow paths and basic mixing and physiochemical gradients are also shown (From Hedenquist and Lowenstern, 1994).*

Low-sulphidation deposits are more spatially confined, with alteration and mineralization more discretely contained within networks of veins and brecias, in contrast to the extensive alteration zoning developed in high-sulphidation deposits. *Figure 6-4* (after Hedenquist et al., 2000) summarizes the characteristic features and general components of low-sulphidation deposits. Characteristic vein-filling minerals include quartz, adularia and chalcedony, typically forming as crustiform and colloform banding. Calcite may occur as blades in zones of boiling. *Figure 6-4* also portrays the typical outward progression of wallrock alteration assemblages in vein selvages from phyllic to argillic to propylitic, which generally occurs on a centimetre to metre scale. These deposits tend to host a low-sulphidation state assemblage of that includes pyrite or pyrrhotite, chalcopyrite and arsenopyrite (Einaudi et al., 2003; *Figure 6-2*). Gold typically occurs as electrum, native gold, or Au-Ag-selenides, hosted within the cavity

filling veins and breccias. Silver typically occurs as native silver and/or acanthite and/or electrum, and Ag/Au ratios are often very high.

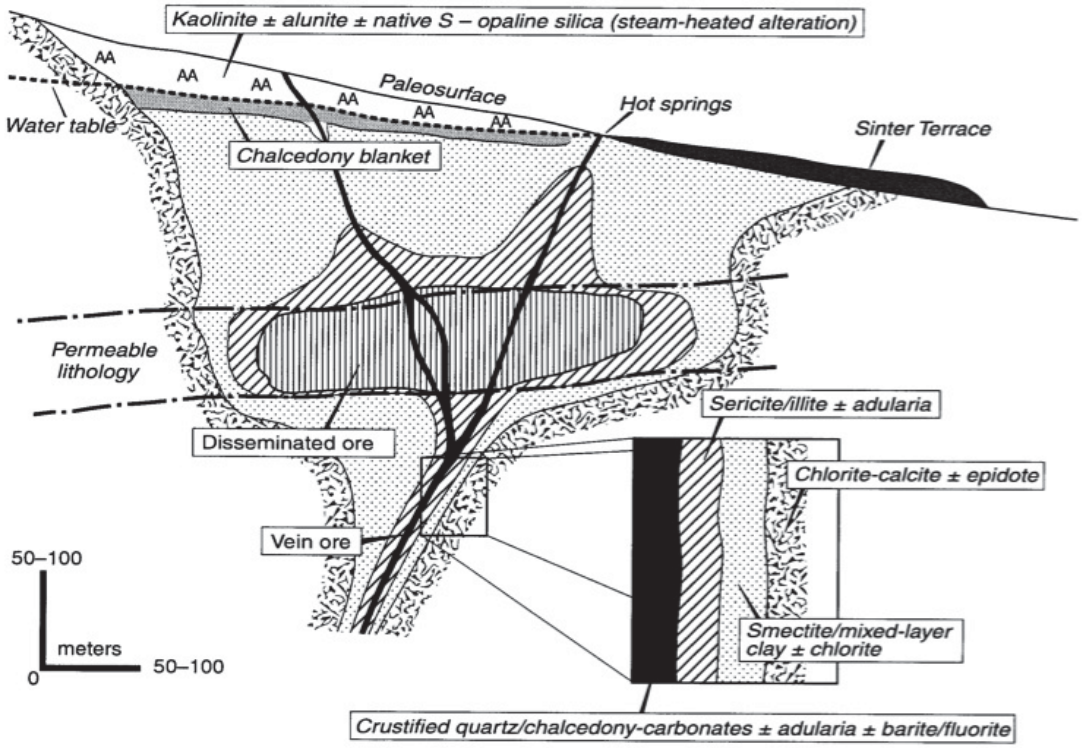

***Figure 6-4**: Generalized schematic of a low-sulphidation system, including typical alteration zonation and distribution of characteristic features (From Hedenquist et al., 2000).*

6.2.3 Metal Source, Fluid Characteristics and Deposit Genesis

When melting of the mantle wedge occurs during subduction, due to a decreased melting temperature from hydration and decompression melting from convection, sulphides within the upper mantle are partially consumed and can contribute metals to magmas ascending into the crust (Hedenquist and Lowenstern, 1994). Metals can also enter magmas from melting of the crust and mass transfer from the subducting slab (Hedenquist and Lowenstern, 1994).

As magma slowly ascends, and fractional crystallization occurs, the melt becomes enriched with H_2O and incompatible elements, including metals such as gold (Hedenquist and Lowenstern, 1994). As magma approaches shallower depths, the decrease in pressure

causes fluids to exsolve, which may further subdivide into two phases at shallow crustal pressures (<2000 bars): 1) a low density, low salinity vapour containing compounds such as CO_2, SO_2, H_2S, and HCl; and 2) a dense, hypersaline liquid (brine) rich in Cl, Cu and other chloridophile elements (Hedenquist and Lowenstern, 1994), both of which can contain dissolved gold.

A visible association between low-sulphidation epithermal mineralization and the underlying parent intrusion is not always evident. However, it is generally accepted that intrusions occurring as much as 5-6 km away, can still act as the main heat and metal source for these systems. Exsolved magmatic fluid from the distal intrusion becomes incorporated with meteoric waters and slowly ascends to surface, undergoing significant wall-rock interactions on route. These interactions can contribute additional metals to the fluid from leaching of the basement rocks, and eventually result in the equilibration of the fluid with the host rocks, yielding a near-neutral pH, reduced fluid. In fluids of this nature, gold is typically dominantly transported as $Au(HS)_2^-$ (Cooke and Simmons, 2000).

As pressure decreases during ascent towards the surface, the fluid may eventually boil as it reaches shallow depths, converting dissolved CO_2 into a vapour and resulting in the precipitation of bladed calcite. In addition to the loss of CO_2 during boiling, the sulphide ligand responsible for transporting gold is also lost to the vapour phase, inducing gold saturation and subsequent precipitation.

6.3 Heritage

The Heritage prospect is located on the southernmost tip of the Burin Peninsula (*Figure 6-1*). Mineralization is hosted within a thick sequence of andesitic volcaniclastic rocks of the Marystown Group, ranging from massive crystal tuffs to heterolithic pyroclastic breccias. The prospective zone is approximately 3.9 km in length and up to 1 km wide, marked by pervasive silicification and anomalous Au-Ag values.

The Eagle Zone, discovered during drilling in the prospective area by Puddle Pond Resources in 2013 has been drilled to a vertical depth of 160 m, and remains open at

depth, and along strike for >1000 m. Drill results to date include 10.60 m grading 3.44 g/t gold and 18.15 g/t silver, including 2.60 m grading 7.34 g/t gold and 257.55 g/t silver (Exploration and Development Highlights 2015: Newfoundland and Labrador Department of Natural Resources).

6.3.1 Alteration and Hydrothermal Textures

The most common alteration minerals associated with Ag-Au mineralization at the Heritage prospect (as identified with VIRS) are the white micas phengite and phengitic illite, representative of a phyllic alteration assemblage. Muscovite and Fe-Mg-chlorite also occur, but are consistently identified across the region, and are presumed to be associated with regional greenschist metamorphism.

A pervasive silicification affects the prospective zone. Within this silica envelope, hydrothermal quartz breccias, including cockade-style breccia, are extensively developed (*Plate 6-1 A*). Multiple generations of quartz and silica veins are also recognized across the silicified zone, typically oriented in one of three directions; NNE-SSW, NE-SW and NW-SE (*Plate 6-1 B*). Veins are typically <1-6 cm in width and locally display fine quartz-chalcedony banding (*Plate 6-1 C*). Veins occasionally display a weak peach-pink colouration, which locally was identified with SEM-EDX as adularia, occurring as euhedral prismatic crystals (*Plate 6-1 D*). Blading is a common texture at the Heritage prospect, and locally very well developed, with blades up to 4 cm long (*Plate 6-1 E*). Petrographic analysis of blading indicates a composition of quartz and calcite (*Plate 6-1 F*). Calcite was also found hosting fine grains of galena surrounding sphalerite masses. Both of these styles of calcite appear to be of hydrothermal origin. Calcite also occurs filling late fractures (e.g., *Plate 6-1 D*) and is prevalent in surrounding lithologies unaffected by hydrothermal alteration, therefore, this latest calcite is also presumed to be a result of regional greenschist metamorphism.

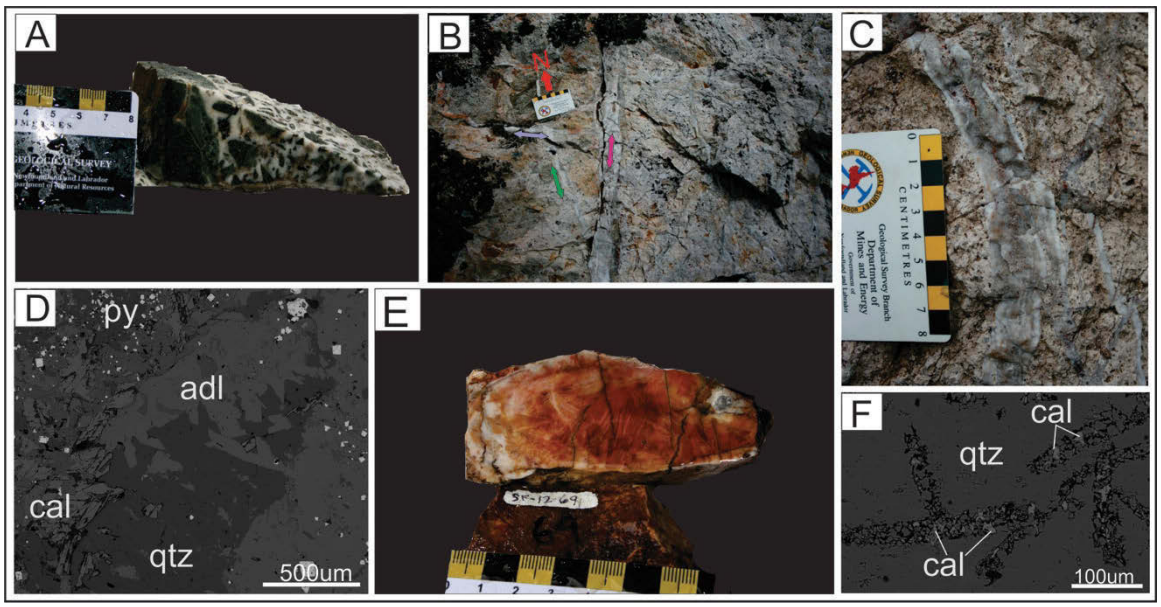

***Plate 6-1**: Representative photos and photomicrographs of alteration mineralogy and hydrothermal textures at the Heritage prospect; A) Sample of cockade-style breccia (SF-12-68); B) 'Whales Pod' Trench showing three directions of quartz-silica veining marked by coloured arrows: ~NE-SW (pink), N-S (green), and NW-SE (purple). Red arrow is north (585783E, 5196748N); C) Quartz-chalcedonic silica banded vein (585793E, 5196758N) in outcrop; D) BSE-SEM image of quartz (qtz)-adularia (adl) vein. Adularia crystals are euhedral. Calcite (cal) formed along later cross cutting fractures. Groundmass is rich in pyrite (py) (SF-13-158); E) Coarse bladed texture (SF-12-69); F) BSE-SEM image of blading composed of calcite (lighter grey) and quartz (SF-13-155b).*

6.3.2 Mineralization: Mineralogy, Associations and Paragenesis

Pyrite is the most abundant sulphide mineral associated with the hydrothermal mineralization. It generally occurs disseminated within the silicified wallrock adjacent to veining, and to a lesser extent within the veins themselves, as either fine-grained euhedral crystals, or coarse-grained corroded and euhedral grains (*Plate 6-2 A*), representative of at least two generations of pyrite. Pyrite contains various ore minerals as inclusions including chalcopyrite, galena, acanthite, sphalerite and arsenopyrite (*Plate 6-2 A-B*). Locally, the coarser-grained corroded type of pyrite contains fine-grained inclusions of galena and acanthite, and shows partial replacement by sphalerite (*Plate 6-2 C*). Locally pyrite is intergrown with chalcopyrite and sphalerite (*Plate 6-2 D*). More commonly sub- to euhedral pyrite grains are found surrounded by anhedral masses of sphalerite, and both are cross cut by fractures filled with galena (*Plate 6-2 E*). However, sphalerite and galena also occur together locally as fracture fillings in pyrite. Elsewhere, anhedral sphalerite grains are enveloped in calcite containing fine grains of galena (*Plate 6-2 F*). Locally

acanthite was found as euhedral, acicular crystals nucleating around fine grains of pyrite (*Plate 6-2 G*). Portions of the acanthite crystals also contain inclusions of native silver (*Plate 6-2 H*). These observations and the implied paragenesis for ore mineralization at Heritage are summarized in *Figure 6-4.*

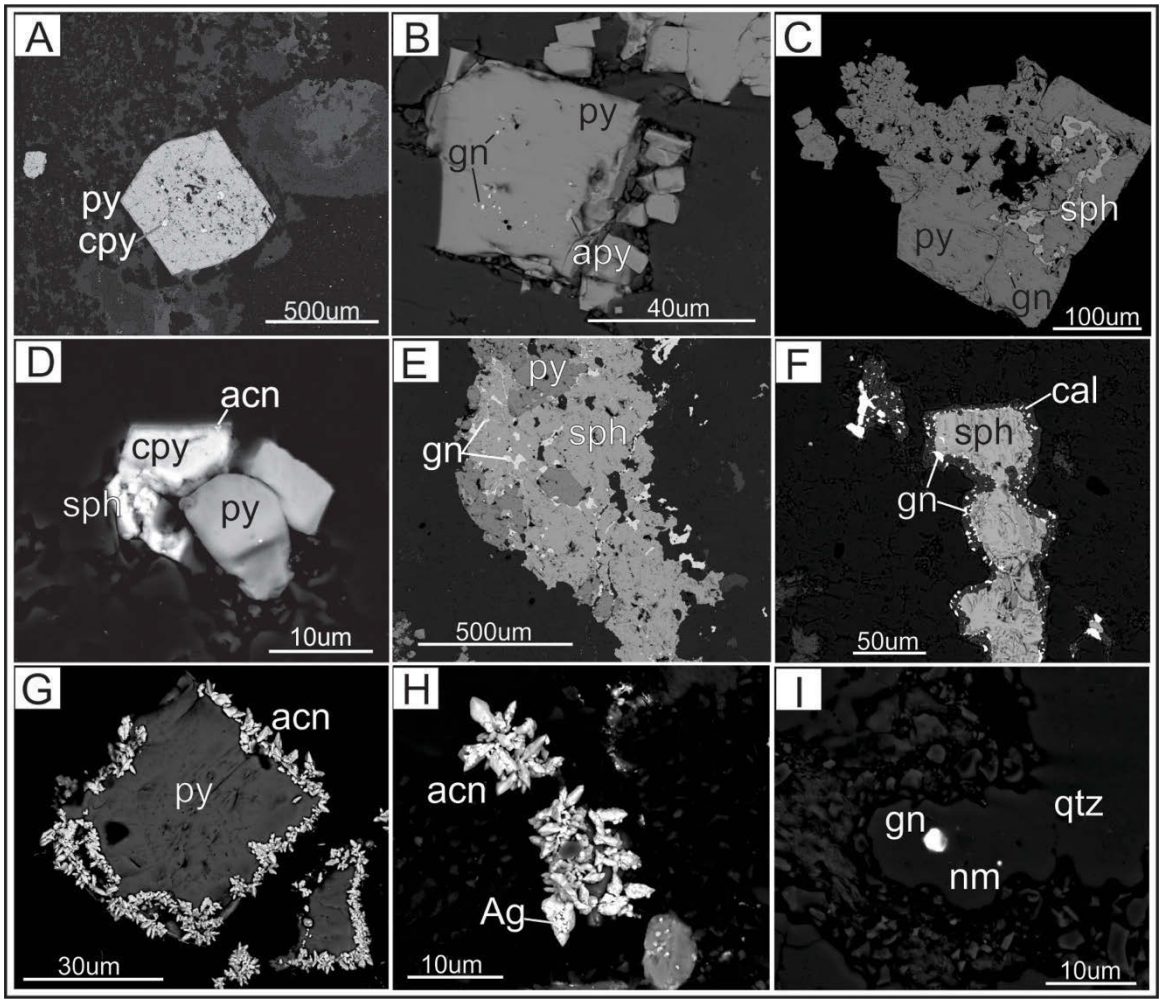

Plate 6-2*: Representative BSE-SEM photomicrographs of mineralization at the Heritage prospect; A) Coarse-grained euhedral and partially corroded pyrite (py) grain with chalcopyrite (cpy) inclusions as later fill (SF-13-156); B) Fine-grained euhedral pyrite containing inclusions of galena (gn) and arsenopyrite (apy) (SF-13-166); C) Coarser-grained, corroded, subhedral pyrite containing inclusions of galena (and finer acanthite) and showing filling/replacement by sphalerite (sph) (SF-13-160); D) Fine-grained, intergrown pyrite, chalcopyrite and sphalerite, containing very fine-grained inclusions of acanthite (can; brightest white) (SF-13-156); E) Fine-grained subhedral grains of pyrite encompassed by anhedral mass of sphalerite, and both crosscut by fine fractures of galena (SF-13-177); F) Anhedral sphalerite rimmed by calcite (cal; dark grey) and galena (SF-13-168); G) Euhedral acicular crystals of acanthite nucleated on fine-grained euhedral pyrite (SF-13-158); H) Close-up of euhedral acanthite showing brighter spots composed of native Ag (SF-13-158); I) Fine-grained inclusions of galena and naumannite (nm) in quartz (qtz) associated with quartz-calcite blading (SF-12-155b).*

A separate fine-grained, disseminated, silver-enriched assemblage also occurs and is closely associated with calcite-quartz blading, and therefore appears empirically linked to fluid boiling. Ore minerals include hessite (Ag_2Te), acanthite, naumannite (Ag_2Se), chalcopyrite, native Bi, galena, and stibnite (Sb_2S_3) (*Plate 6-2 I*). The timing of this assemblage relative to the overall sequence is unclear, but the sulphides are still diagnostic of a low-sulphidation environment.

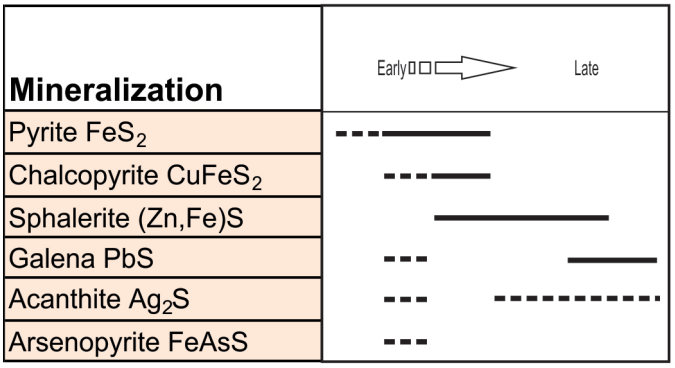

***Figure 6-5**: Basic paragenetic sequence for mineralization at the Heritage prospect. The relative timing of the "boiling-related" Ag-rich assemblage found disseminated within bladed textures was not clear and is not included here.*

6.4 Big Easy

The Big Easy prospect is located just north of the Burin Peninsula proper - west of Clarenville on the southwest side of Thorburn Lake. The prospect contains a ~1.5 km long zone (100 to 500 m wide) of silicic alteration hosted in epiclastic sediments of the Musgravetown Group. The sediments primarily comprise interbedded sandstones and pebble conglomerates. One of the best drill intersections to date yielded 0.87 g/t Au and 33.5 g/t Ag over 30.5m, which includes 6.05 g/t Au and 174 g/t Ag over 1.5m (Silver Spruce Resources News Release, May 3, 2011). The alteration and hydrothermal textures are described here based on field observations, but the additional details of the mineralization have been summarized from recent work by Layne et al. (2016) and a B.Sc. thesis by M. Clarke (2013).

6.4.1 Alteration and Hydrothermal Textures

The host sedimentary units are intensely silicified, and contain an argillic alteration assemblage of illite-smectite based on VIRS analyses. Discrete quartz veining is abundant crosscutting the silicified zone, with veins typically ranging in width from 2 to 15cm, and occurring in multiple orientations. Crustiform banding is well developed in many of the quartz veins, with bands composed of quartz, silica and adularia (*Plate 6-3A*). Blading of adularia-quartz is also locally developed within the quartz veins (*Plate 6-3B*). Hydrothermal quartz breccias are also observed, and sometimes display cockade-breccia texture, with quartz sequentially enveloping the host fragments. One of the most interesting features of this prospect is the presence of banded chalcedonic silica sinter exposed at surface (*Plate 6-3 C*), which is a record of hot spring activity on the paleosurface.

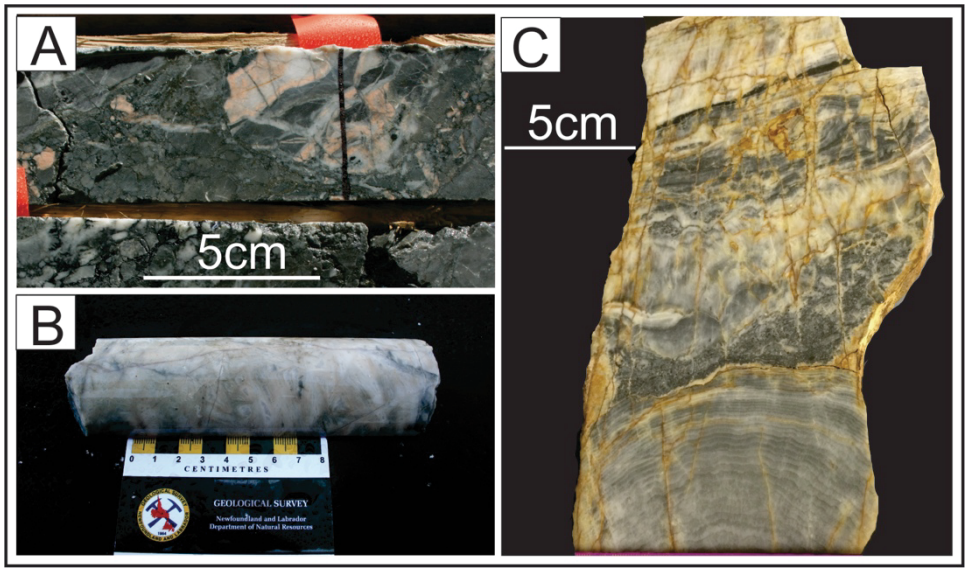

***Plate 6-3**: Representative photographs of alteration mineralogy and hydrothermal-related textures at the Big Easy prospect; A) Banded quartz-adularia (peach-pink) veins, brecciated (DDH: BE-11-03); B) Blading within quartz-adularia veining (DDH: BE-11-05); C) Sinter (fine grey banding at bottom) with successive interbedded silica and sediment layers (towards top) (Collected from: 710076E, 5347562N).*

6.4.2 Mineralization: Mineralogy and Associations

Pyrite is finely disseminated throughout the silicified host rocks (~10%), and locally associated with chalcopyrite, which occurs interstitially to the pyrite grains. Clarke (2013) also identified trace arsenopyrite and sphalerite locally. Precious metal mineralization occurs locally as inclusions of Ag-tellurides and selenides within pyrite, and as late fracture fill composed of electrum and acanthite cross cutting pyrite, both corresponding to hydrothermal brecciation (Clarke, 2013). The majority of precious metal mineralization however, is concentrated within fine dark serrate bands found within the crustiform quartz-silica-adularia banded veins, which are referred to as ginguro ("silver-black") bands, following a traditional Japanese miner's term (*Plate 6-4*). The ginguro banding assemblage is composed of native Ag and acanthite ± electrum, chalcopyrite, freibergite ($Ag_6Cu_4Fe_2Sb_4S_{13-x}$) and naumannite (Ag_2Se) (Layne et al., 2016).

***Plate 6-4**: Representative photo of precious metal mineralization within 'ginguro'-style banding at the Big Easy prospect (DDH: BE-12-08). The dark banding occurs within banded quartz veins and is composed of native Ag and acanthite ± electrum, chalcopyrite, freibergite ($Ag_6Cu_4Fe_2Sb_4S_{13-x}$) and naumannite (Ag_2Se) (Layne et al., 2016).*

6.5 Long Harbour

The Long Harbour prospect is located along the northern shore of Fortune Bay, opposite the northwest shore of the Burin Peninsula (*Figure 6-1*). The prospect is hosted in an extensively outcropping flow-banded rhyolite unit of the Belle Bay Formation of the Long Harbour Group. The epithermal system occurs as a network of steeply dipping, NNW-SSE striking banded veins and breccias containing anomalous Au values that are

continuous over a strike length of approximately 70 m (*Plate 6-5*). Some of the best values include 3.4 g/t Au over 0.9m from a channel sample through brecciated and bladed quartz-adularia veining, and 5.2 g/t Au from a grab sample (Crewe and Seymour, 2007).

Plate 6-5*: Photograph of southern portion of Long Harbour prospect, showing network of continuous banded veins. Photo is facing NNW. Geotool is ~60cm long.*

6.5.1 Alteration and Hydrothermal Textures

Unlike the Heritage and Big Easy prospects, where veining is contained within an envelope of pervasive silicification, the host rocks at Long Harbour do not appear to be pervasively silicified, perhaps due to their initial high-silica (rhyolite) host protolith. VIRS analysis of veined samples consistently identified dickite and kaolinite, with lesser muscovite and local magnesite ($MgCO_3$). Dickite, a high-temperature polymorph of kaolinite, is not typical of low-sulphidation systems and generally associated with their high-sulphidation counterparts. In thin section, the dickite appears to predominantly

occur as a replacement of adularia, which could be the result of overprinting by later higher temperature hydrothermal fluids, or possibly the result of regional greenschist metamorphism.

Veins are typically 20 to 30 cm wide, but vary in width from 1 cm up to 50 cm locally (e.g., *Plate 6-5*). They consistently display crustiform and colloform banding comprised of quartz, chalcedony and adularia (*Plate 6-6 A-B*). Quartz breccias are well-developed throughout the prospect including jigsaw- (*Plate 6-6 C*) and cockade-style breccias (*Plate 6-6 C-D*). Multiple episodes of hydrothermal activity are evidenced by the occurrence of angular fragments of both banded veins and earlier hydrothermal breccia(s) within subsequent hydrothermal breccias (*Plate 6-6 E-F)*. Bladed textures are well-developed and prevalent throughout the extent of the veining (*Plate 6-6 G-I*). Blades are typically composed of quartz and adularia, and are locally up to 5 cm in length. Analysis of bladed texture samples, using SEM-EDX, identified local isolated grains of scheelite ($CaWO_4$) occurring in association with the quartz-adularia. This is consistent with the slightly elevated tungsten values reported in sample assays from the prospect. Southwest of the main veining, a unique feature was identified locally in subcrop, where chalcedonic silica occurs very finely banded perpendicular to quartz-adularia colloform-crustiform banded vein walls (*Plate 6-6 J*). This is similar in appearance to sinter and may be indicative of near surface formation. In thin section the silica layers sometimes show sedimentary-like features, including what appear to be load structures (*Plate 6-6 K-L*).

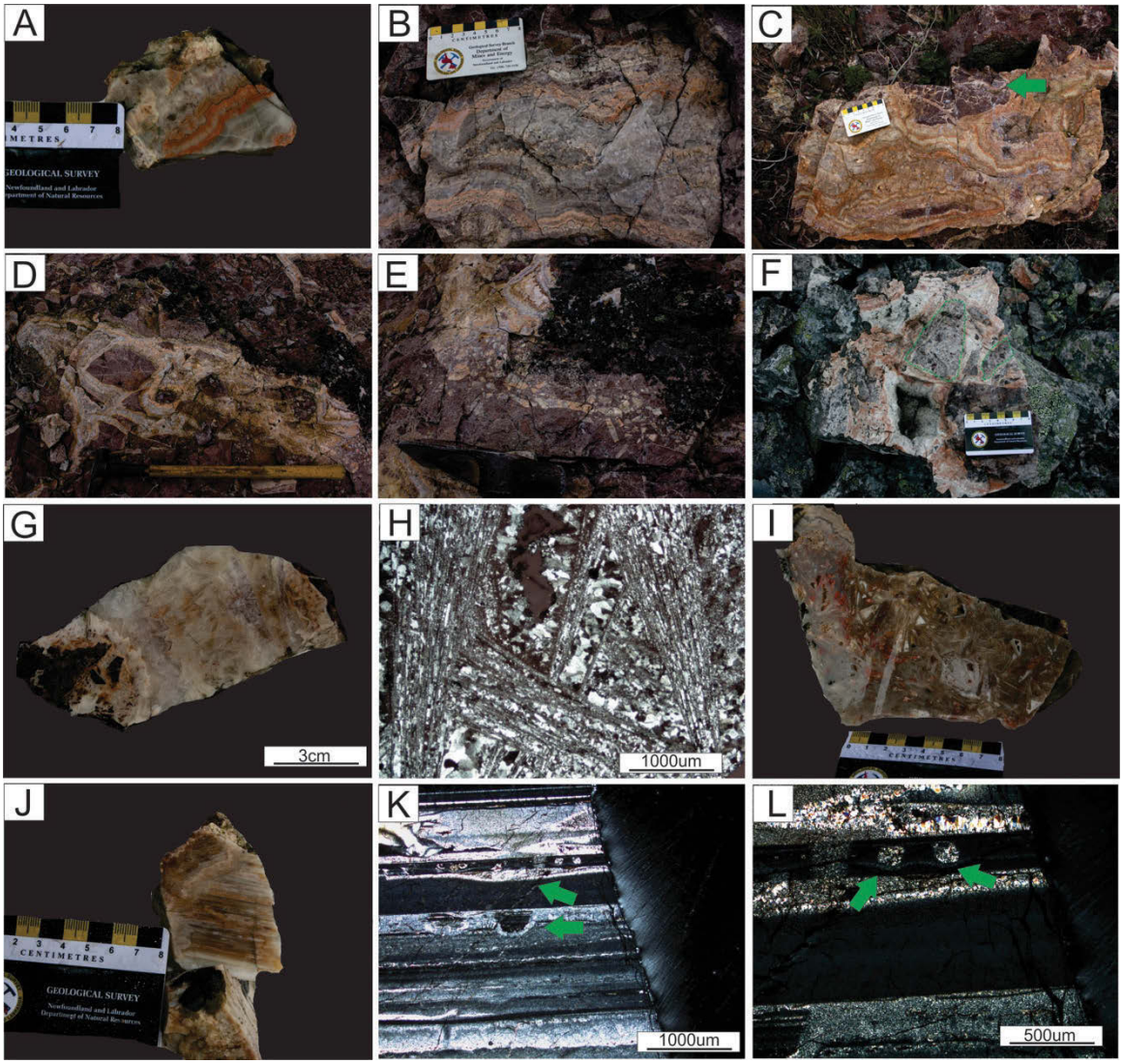

***Plate 6-6**: Representative photos and photomicrographs of the alteration and hydrothermal textures at the Long Harbour prospect; A) Crustiform-colloform banded veining composed of quartz, adularia (peach-pink) and chalcedonic silica (SF-12-52); B) 15cm wide vein displaying crustiform-colloform banding of quartz-adularia (STA-SF-12-115); C) Jigsaw-breccia through a rhyolite fragment (green arrow) contained within large banded vein with weakly developed cockade-breccia (STA-SF-12-115); D) Cockade-style breccia with bands of quartz-adularia radiating around breccia fragments (STA-SF-12-115); E) Quartz-adularia banded veins, brecciated by a secondary hydrothermal episode (STA-SF-12-115); F) Fragments of fine-grained hydrothermal breccia (highlighted by green dashed line) contained within secondary veining/cockade-style breccia (STA-SF-12-115); G) Blading developed within a banded quartz-silica vein (SF-12-58); H) Transmitted light (XPL; 2X) image of coarse blading, predominantly composed of quartz (SF-12-65); I) Distinct coarse bladed texture in hand sample (SF-12-60); J) Fine chalcedonic silica banding occurring adjacent to perpendicular crustiform quartz-adularia banding (left side of sample) indicative of shallow depth of formation (SF-12-57); K) Transmitted light (XPL; 2X) image of fine silica banding showing sedimentary-like load structures (green arrows) (SF-12-57); L) Close-up of previous (5X) showing finer-scale load structures resulting from two round quartz aggregates (SF-12-57).*

6.5.2 Mineralization: Mineralogy and Associations

All ore mineralization is sparse and very fine-grained, invisible to the unaided eye, and identified here using SEM BSE imaging combined with SEM-EDX. Sulphide and sulphosalt minerals were identified in a variety of samples, while precious metal mineralization and telluride minerals were found exclusively in quartz-adularia bladed horizons. A list of all minerals identified at the Long Harbour prospect, and their mode of occurrence is summarized in *Table 6-1*.

	Mineral Occurrence			
	Within or Closely Associated With Adularia-Quartz Blading (SF-12-52B, GS-12-325, SF-12-66, SF-12-60)	Within Chalcedonic Silica Banding (SF-12-57)	Within Quartz-Adularia Colloform-Crustiform Banding (GS-12-325)	Within Quartz Matrix of Breccia (SF-12-66)
AUMINERALIZATION				
Native Au	X			
Electrum (Au,Ag)	X			
SULPHIDES/SULPHOSALTS				
Arsenopyrite AsS	X			
Galena PbS	X	X	X	
Jamesonite $Pb_4FeSb_6S_{14}$	X	X		
Pyrrhotite $Fe_{1-x}S$	X			
Sphalerite ZnS	X			X
Boulangerite $Pb_5Sb_4S_{11}$		X		
Chalcopyrite $CuFeS_2$		X	X	
Acanthite Ag_2S			X	
TELLURIDES				
Chenguodaite $Ag_9FeTe_2S_4$	X			
Cervelleite Ag_4TeS	X			
Hessite Ag_2Te	X			
Altaite PbTe	X			
SELENIDES				
Naumannite Ag_2Se	X			
OTHER				
Native Bi	X			X
Native Sb			X	

***Table 6-1**: Summary of sulphide/ore mineralogy and occurrence at the Long Harbour prospect.*

Gold occurs within bladed textures as both native gold and electrum (65% Au, 35% Ag; *Plate 6-7 A-C*). Silver is deported within a number of other mineral phases associated with bladed textures including chenguodaite ($Ag_9FeTe_2S_4$; *Plate 6-7 D-E*), cervelleite (Ag_4TeS; *Plate 6-7 D-E*), Hessite (Ag_2Te) and occasionally naumannite

(Ag_2Se). Other minerals occurring within bladed textures include arsenopyrite (*Plate 6-7 F*), galena, jamesonite, pyrrhotite, sphalerite and native bismuth.

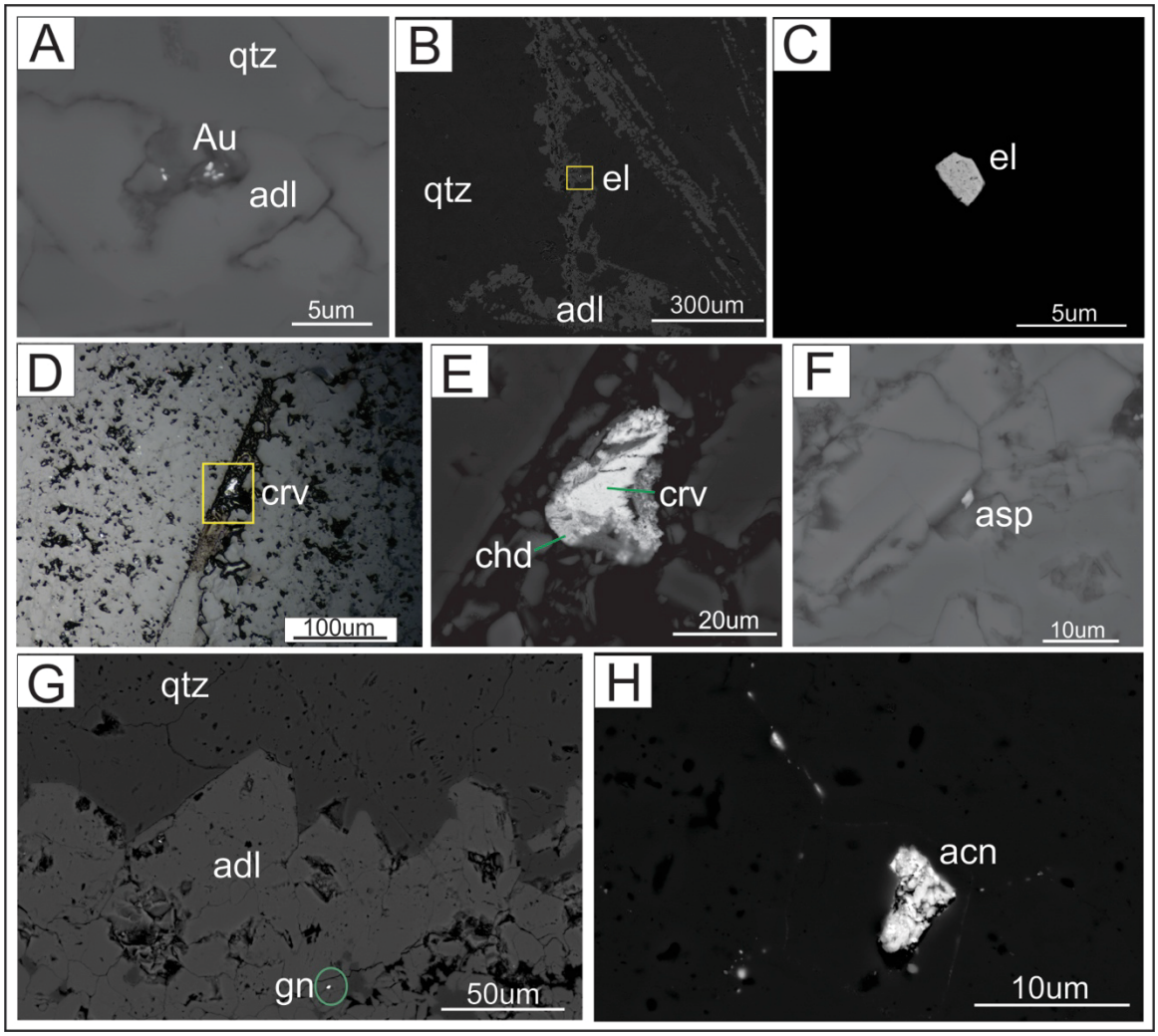

Plate 6-7*: Representative BSE-SEM and reflected light (D) images of mineralization at the Long Harbour prospect; A) Very fine-grained flecks of native gold (Au) within adularia (adl) blade (running horizontally) in quartz (qtz) matrix (SF-12-52b); B) Fine grain of electrum (el) contained within yellow box (close-up in C), occurring within adularia blading in quartz (GS-12-325); C) Closeup of electrum grain composed of ~65% Au:35% Ag (GS-12-325); D) Reflected light (20X) image of Ag-telluride, cervelleite (crv) within blading (SF-12-66); E) Close-up of previous, showing cervelleite rimmed by darker grey chenguodaite (chd) (SF-12-66); F) Arsenopyrite (asp) occurring adjacent to adularia blading (SF-12-52b); G) Fine grain of galena (gn) within crustiform banding of adularia-quartz (GS-12-325); H) Acanthite (acn) filling fine fractures in quartz banding (GS-12-325).*

Within the finely banded chalcedonic silica (*e.g., Plate 6-6 J*), four sulphide and sulpholsalt minerals were identified, two of which also occur within bladed textures. These minerals are galena, jamesonite ($Pb_4FeSb_6S_{14}$), boulangerite ($Pb_5Sb_4S_{11}$) and

chalcopyrite. Mineralization observed within quartz-adularia crustiform-colloform banding includes galena (*Plate 6-7 G*), chalcopyrite, acanthite (*Plate 6-7 H*), and native antimony. The more massive quartz comprising the matrix of the abundant hydrothermal breccias was found to host native bismuth and sphalerite.

6.6 Discussion

All three deposits (Heritage, Big Easy and Long Harbour) remain highly prospective for Au-Ag. The prospects all contain quartz-adularia, variably developed hydrothermal textures (e.g., crustiform-colloform banding, blading, brecciation), and sulphide minerals (e.g., arsenopyrite, galena, sphalerite) and precious metal minerals (e.g., electrum, native gold, acanthite) characteristic of low-sulphidation epithermal systems.

The presence of distinct bladed textures at each deposit is particularly important, as this is indicative of (shallow) boiling; an important process for the precipitation of gold in low-sulphidation epithermal systems. Bladed horizons are typically associated with the highest-grades of gold in these systems, however a vertical offset between the main gold ore zone and horizons of boiling-indicators has also been documented in some deposits (Simmons and Browne, 2000). A strong association between bladed textures and precious metal mineralization was found at Heritage and Long Harbour. At Big Easy however, precious metal mineralization is currently observed to have a strong affiliation with vein-banding and breccia-textures, without a direct affiliation with bladed textures.

The Big Easy prospect contains an unequivocal example of hotspring sinter, demonstrating preservation of the paleosurface (*see* Sinter Terrace in *Figure 6-4*). This is important because if the paleosurface is preserved, then the model prediction is that highest gold values would lie >150 m below this level (Hedenquist et al., 2000) (the stratigraphy at Big Easy does not appear overturned). A texture resembling sinter or, alternatively, shallow chalcedony blanket (*see* Chalcedony Blanket in *Figure 6-4*) was also identified locally at Long Harbour - where very fine silica banding was found to occur perpendicular to earlier crustiform banded vein walls, and showed sedimentary-

style load structures. In either case, this is interpreted to represent a very shallow depth of formation, and therefore is similarly significant for locating high-grade ore at Long Harbour as it is at Big Easy.

Another distinctive feature found at Long Harbour is the abundance of telluride minerals, which are not generally common in low-sulphidation epithermal deposits. However, this could be attributed to its association with alkaline magmatism (as discussed in *Chapter 3*), as opposed to Heritage and Big Easy, since other low-sulphidation deposits hosted in alkaline rocks have been documented as containing anomalous Au-telluride mineralization (Sillitoe and Hedenquist, 2003).

Unlike the high-sulphidation deposits discussed in *Chapter 5*, which are all hosted in similarly aged volcaniclastic rocks of the Marystown Group, associated with subduction-related magmatism, and interpreted to be the result of a single protracted hydrothermal event, the three low-sulphidation deposits discussed here formed in diverse host rocks and geological settings and are the result of at least two ages of parent plutonism (circa 566 Ma for Long Harbour; circa 575 Ma for Heritage and Big Easy; *Chapter 4*).

The ca. 575 Ma Marystown and Musgravetown groups, host to the Heritage and Big Easy prospects, respectively, show similar age and lithogeochemical affinities, both associated with subduction-related magmatism. The andesitic pyroclastic rocks at the Heritage prospect are characteristic of active continental arc volcanism, while the thick piles of epiclastic sediments present at the Big Easy prospect, are interpreted as late-subduction caldera fill- or volcanic-derived extension-related-sediments. Given the broadly similar ages and corresponding lithogeochemical signatures of the hosting lithological groups, mineralization at both Heritage and Big Easy logically represent epithermal mineralization related to the same protracted volcano-plutonic episode.

In contrast, the Long Harbour prospect is hosted in ca. 566 Ma alkaline flow banded rhyolite of the Long Harbour Group. These rocks are interpreted to be late- to post-subduction, extension-related volcanics, in an intra- or back-arc environment. The

distinct age and context of the Long Harbour Group rocks, and the unique abundance of telluride minerals at the prospect, suggest that a separate volcano-plutonic event was responsible for precious metal mineralization at the Long Harbour prospect. Furthermore, the maximum age for mineralization at the Long Harbour prospect corresponds with the absolute minimum age for mineralization at the Big Easy prospect, further distinguishing these two deposits temporally.

While the Heritage and Big Easy occurrences are hosted in contrasting lithologies (dominantly pyroclastic vs. coarse epiclastic), they are both fairly typical vein-bound low-sulphidation style deposits formed within intracaldera environments, and related to the same circa 575 Ma episode of parent plutonism within a calk-alkaline continental arc (*Chapters 3 & 4*). This same environment, tied to the Burin Knee – Swift Current Suite of granitoid plutons, thus becomes prospective throughout the greater Burin Peninsula region.

The Long Harbour occurrence is significant because it currently represents the only recognized example of a vein-bound low-sulphidation style deposit related to a discrete, definably younger (circa 566 Ma) episode of alkaline parent plutonism on the northwestern edge of the Burin Peninsula. This should provoke closer assessment of the volcano-plutonic rocks within the broader Long Harbour Group (*Figure 6-1*) as potential hosts to epithermal Au-Ag mineralization.

CHAPTER 7: CONCLUSIONS

1) Volcanic rocks of the Marystown Group (hosting the Stewart and other high-sulphidation (HS) deposits) and Musgravetown Group (proximal to the Big Easy low-sulphidation (LS) prospect) are of similar age, based on new U-Pb zircon dating (including a new age of 573.3 ± 2.7 Ma for rhyolite from the Musgravetown Group), and yield correlative geochemical signatures, representative of different facies within a single, contemporaneous volcanic arc environment, undergoing active subduction ca. 575 Ma. The volcaniclastic-dominated Marystown Group reflects an environment closely associated with active volcanic centres, while the marginally younger, epiclastic sediment-dominated Musgravetown Group reflects an intra-caldera setting, or alternatively, a more distal area of arc erosion. The Musgravetown Group has previously been interpreted as a distinctly younger lithological group.

2) Detailed geochronological and lithogeochemical investigations in conjunction with field observations at the Stewart prospect confirm a northwest younging direction within the local stratigraphy, which records a progression from more juvenile to more mature phases of arc volcanism. This work also provides further evidence linking the regional plutonism to the hosting volcaniclastic stratigraphy of the Marystown Group – since four volcanic lithologies (including a subvolcanic feeder dyke) overlap within error at 576 ± 1Ma and are contemporaneous with the 576 ±2.7Ma Bat Zone Granite (part of the Burin Knee Intrusive Suite) and other previously dated phases of the BKIS. The felsic volcaniclastic rocks and felsic intrusive units at Stewart also share similar geochemical signatures, characteristic of continental arc volcanism.

3) The Long Harbour Group is younger (a flow-banded rhyolite from the Belle Bay Formation yielding a new U-Pb age of 566.5 ± 1.9 Ma) and compositionally distinct from the Marystown and Musgravetown Groups. Geochemical signatures and lithologies at the Long Harbour prospect are indicative of alkaline volcano-

plutonism in an extensional environment during late-stages of arc volcanism. The Long Harbour Group was previously considered to be roughly contemporaneous with the Musgravetown Group.

4) A sample of epiclastic sediment from the Grandy's Pond Arenite Belt (GPAB) yielded a preliminary zircon U-Pb age of 566.2 ± 4.4 Ma - corresponding with the age of Long Harbour volcanism. The GPAB is predominantly derived from the erosion of volcanic rocks of the Marystown Group based on their similar geochemical signatures, but also contains additional detritus from the younger Long Harbour Group, possibly in the form of ash during active volcanism, yielding this ~566 Ma youngest zircon age.

5) The HS epithermal deposits are consistently hosted within calc-alkaline, felsic-intermediate volcaniclastic rocks of the Marystown Group, associated with active subduction in a volcanic arc environment. These attributes are consistent with typical high-sulphidation deposit models.

6) Timing of HS epithermal mineralization is constrained by volcanic host rock ages to a *maximum* of 584 ± 3 Ma at Hickey's Pond (or 585 ± 2 Ma when combined with the similar published age of 586 ± 3 Ma from the same unit; Sparkes et al., 2016) and 576.7 ± 2.5 Ma at Stewart. At Hickey's Pond, what is presumed to be hydrothermal zircon possibly yields a more explicit age of 572.5 ± 1.5 Ma for mineralization. The examples of HS mineralization studied thus appear coeval with the ca. 575 Ma regional plutonism represented by the Burin Knee-Swift Current Intrusive Suites (with a new age of 576 ± 2.7 Ma for the Bat Zone granite at the Stewart prospect).

7) Sulphur isotope microanalyses of pyrite, chalcopyrite and galena from the Hickey's Pond, Tower, and Stewart prospects, together yield a single population displaying a normal distribution, and $\delta^{34}S$ values ranging from -6.8 to +5.9‰ with an average of -0.6‰, consistent with a magmatic sulphur source for these deposits. On a deposit scale, more detailed trends are also evident. At Hickey's

Pond a transition from lighter isotopic values, measured from fine-grained vug-filling pyrite, to heavier isotopic values, measured from coarser-grained pyrite within cross-cutting quartz-sulphide veins, occurs. Similarly at Tower, two sub-populations occur, with more negative values associated with pyrite, chalcopyrite and pyrophyllite, and more positive values associated with pyrite with cores and rims occurring with alunite. In both cases, sulphur was derived from the same magmatic sulphur source, however the variance in the populations, defined by changing mineral assemblages or cross-cutting relationships, is interpreted as the presence of at least two generations of mineralization, precipitating under changing physiochemical conditions.

8) Given their spatial continuity, and similar deposit characteristics, host rock lithologies and $\delta^{34}S$ values, the HS deposits are considered to have formed as the result of a single protracted hydrothermal event ca. 575 Ma, but permissibly as early as ~585 Ma.

9) At Hickey's Pond, the most auriferous HS prospect in the study, gold occurs in the hypogene assemblage as native gold and calaverite ($AuTe_2$), and in the late supergene/weathering assemblage as fischesserite (Ag_3AuSe_2). This implies a hypogene fluid rich in selenium and tellurium (and gold), and subsequent conditions that produced supergene dissolution, mobilization and re-precipitation of Au-selenides, largely within the original porous HS vuggy silica zone, as potentially important factors for the enrichment of gold in HS epithermal systems in the region. While tellurides are described in the literature surrounding HS deposit models as a common occurrence, selenides are typically considered a more rare occurrence. Therefore, the abundance of fischesserite at Hickey's Pond is a rather unique feature.

10) The Ca- and Sr-phosphate minerals, woodhouseite and svanbergite, previously undocumented in the region, are abundant at all of the HS prospects, occurring as part of the advanced argillic alteration assemblage. Although these minerals are

not typically described as part of the HS deposit model, they have been documented at many well-known HS deposits around the world.

11) The link of the HS mineralization to an underlying porphyry system at the Stewart prospect remains inconclusive. The only new evidence to support the occurrence of a porphyry system, is the local presence of epidotized feldspars, associated with hydrothermal veining, which are clearly overprinted by subsequent HS-related pyrophyllite alteration.

12) A mineralogical investigation of the Forty Creek deposit suggests a possible intermediate-sulphidation (IS) epithermal origin, based on the abundance of precious metal-tellurides (e.g., petzite (Ag_3AuTe_2), sylvanite ($(Ag,Au)Te_2$)) and characteristic sulphide minerals. Sulphur isotope measurements at Forty Creek have an average $\delta^{34}S$ of -7.8‰, significantly lighter than the HS deposits, and indicative of a sulphur source perhaps influenced by biogenically derived sulphur from metasediments, and not purely the result of magmatic input.

13) The LS deposits are related to at least two discrete volcano-plutonic sequences; i) ca. 575 Ma mineralization at Heritage and Big Easy, both hosted in subduction-related stratigraphy of broadly similar age within the Marystown Group and Musgravetown Group, and ii) ca. 566 Ma mineralization at Long Harbour, containing an assemblage of precious metal-tellurides (e.g., cervelleite (Ag_4TeS), hessite (Ag_2Te)), and hosted in a distinctly younger and characteristically alkaline stratigraphy associated with late arc-extension. Both these sequences thus become highly prospective for epithermal Au-Ag deposits within the latest Neoproterozoic stratigraphy of the Western Avalon Zone in Newfoundland.

14) Further work on the Burin Peninsula, and broader Western Avalon Zone, should include; i) Additional, carefully selected geochronology targets to further constrain the age of mineralization at each of the deposits, particularly at the Heritage prospect, which is currently without any direct age constraints, ii) complementary LA-ICP-MS U-Pb zircon work, which would allow for the

analysis of distinct portions of individual grains, to provide more concrete answers for samples that yielded inconclusive results, and to further constrain known ages and relationships amongst the Marystown, Musgravetown and Long Harbour Groups, iii) More detailed sulphur isotope studies, including $\delta^{34}S$ measurements of the LS deposits to determine their regional signature and any variations amongst the deposits, and to compare with their HS counterparts, and iv) Fluid inclusion studies on the LS (and IS) deposits to provide informative temperature, depth and boiling level information for the hydrothermal systems. These studies would be particularly beneficial to continued exploration for Au-Ag at the Big Easy, Long Harbour and Heritage prospects.

REFERENCES

Andrews, R., 1997, First year assessment report on geological exploration for licences 4838-4840M, 4861M and 4863M on claims in the Paradise River, Sandy Harbour River and Monkstown Road areas on the Burin Peninsula, Newfoundland, Rockhopper Corporation: Newfoundland and Labrador Geological Survey, Assessment File 1M/0362, 14 pages.

Arribas, A., Jr., 1995, Characteristics of high-sulfidation epithermal deposits, and their relation to magmatic fluid: Mineralogical Association of Canada Short Course, v. 23, p. 419–454.

Arribas, A., Hedenquist, J.W., Itava, T., Okada, T., Concepcion, R.A. and Garcia, J.S., 1995, Contemporaneous formation of adjacent porphyry and epithermal Cu-Au deposits over 300 km in northern Luzon, Philippines: Geology, v. 23, no. 4, p. 337-340.

Ayuso, R.A., Seal, R., II, Foley, N., Offield, T.W. and Kunk, M., 1997, Genesis of gold deposits in the Carolina slate belt, USA: Regional constraints from trace element, Pb-Nd isotopic variations and $^{40}Ar/^{39}Ar$ geochronology: Geological Society of America Abstracts with Programs, v. 29, no. 6, p. A-60.

Ayuso, R.A., Wooden, J.L., Foley, N.K., Seal, II, R.R. and Sinha, A.K., 2005, U-Pb Zircon Ages and Pb Isotope Geochemistry of Gold Deposits in the Carolina Slate Belt of South Carolina: Society of Economic Geologists, Economic Geology, v. 100, p. 225-252.

Bainbridge, T., 1934, Memoranda relating to iron deposits at Placentia Bay, Newfoundland: Davenport and Company Aldwych, WC.2, London, England, Unpublished report, 11 pages.

Barrett, T.J., Dawson, G.L. and MacLean, W.H., 2008, Volcanic stratigraphy, alteration, and sea-floor setting of the Paleozoic Feitais massive sulphide deposit, Aljustrel, Portugal: Economic Geology, v. 103, p. 215-239.

Barton, P.B., Jr., 1970, Sulfide petrology: Mineralogical Society of America, Special Paper 3, p. 187–198.

Barton, P.B., Jr. and Skinner, B.J., 1967, Sulfide mineral stabilities, *in* Barnes, H. L., ed., Geochemistry of hydrothermal ore deposits: New York, Holt, Rinehart and Winston, p. 236–333.

Berger, B.R., Ayuso, R.A., Wynn, J.C. and Seal, R.R., 2008, Preliminary model of porphyry copper deposits: USGS, Open-File Report 2008-1321, 55 pages.

Bethke, P.M., Rye, R.O., Stoffregen, R.E. and Vikre, P.G., 2005, Evolution of the magmatic-hydrothermal acid-sulfate system at Summitville, Colorado: integration of geological, stable-isotope, and fluid-inclusion evidence: Chemical Geology, v. 215, p. 281-315.

Blackwood, R. F. and Kennedy, M. J., 1975, The Dover Fault: Western boundary of the Avalon Zone in northeastern Newfoundland: Canadian Journal of Earth Sciences, v. 12, p. 320–325.

Brueckner, S.M., Piercey, S.J., Layne, G.D., Piercey, G. and Sylvester, P.J., 2015, Variations of sulphur isotope signatures in sulphides from the metamorphosed Ming Cu(-Au) volcanogenic massive sulphide deposit, Newfoundland Appalachians, Canada: Mineralium Deposita, v. 50, no. 5, p. 619-640.

Cabanis, B. and Lecolle, M., 1989, Le diagramme La/10-Y/15-Nb/8: un outil pour la discrimination des series volcaniques et la mise en evidence des processus de mélange et/ou de contamination crustale: C.R. Acad. Sci. Ser. II, v. 309, p. 2023-2029.

Calon, T., 2001, Late Precambrian sedimentation and related orogenesis of the Avalon Peninsula, eastern Avalon Zone, Newfoundland: Geological Association of Canada, St. John's 2001 Field Trip Guidebook, Field Trip A9/B8, 32 pages.

Carmichael, I.S., 2002, The andesite aqueduct: perspectives on the evolution of intermediate magmatism in west-central (105-99°W) Mexico: Contributions to Mineralogy and Petrology, v. 143, p. 641-663.

Clarke, M., 2013, Host lithologies, breccia development, alteration and gold mineralization at the Big Easy prospect (Unpublished BSc. thesis): Memorial University of Newfoundland, St. John's, Newfoundland, 85 pages.

Condie, K.C., 1989, Geochemical changes in basalts and andesites across the Archean-Proterozoic boundary: identification and significance: Lithos, v. 23, p. 1-18.

Cooke, D.R. and Simmons, S.F., 2000, Characteristics and Genesis of Epithermal Gold Deposits: SEG Reviews, v. 13, p.221-244.

Crewe, T.M. and Seymour, C.R., 2007, Fifth year assessment report on geological, geochemical and trenching exploration for licence 10928M on claims in the Long Harbour area, Fortune Bay, Newfoundland, Cornerstone Resources Inc.: Newfoundland and Labrador Geological Survey, Assessment File 1M/11/0627, 53 pages.

Dahl, O.M., 1934, Third report on the iron deposits at Hickey's Pond, Placentia Bay, Newfoundland: Davenport and Company, Aldwych, W.C. 2, London, England, Unpublished report, 9 pages.

Dallmeyer, R. D., Hussey, E. M., O'Brien, S. J. and O'Driscoll, C. F., 1983, Chronology of tectonothermal activity in the western Avalon Zone of the Newfoundland Appalachians: Canadian Journal of Earth Sciences, v. 20, p. 355–363.

Dallmeyer, R.D. and Nance, R.D., 1994, $^{40}Ar/^{39}Ar$ whole-rock phyllite ages from late Precambrian rocks of the Avalon composite terrane, New Brunswick: evidence of Silurian-Devonian thermal rejuvenation: Canadian Journal of Earth Sciences, v. 31, p. 818–824.

Davenport, P.H., Nolan, L.W. and Hayes, J.P., 1988, Gold and associated elements in lake sediment from regional survey in the Gander Lake map area (NTS 2D), Newfoundland: Department of Mines, Newfoundland Geological Survey, Open File 2D/0175, 220 pages.

Dec, T., O'Brien, S. J. and Knight, I., 1992, Late Precambrian volcaniclastic deposits of the Avalonian Eastport Basin (Newfoundland Appalachians): Petrofacies, detrital clinopyroxene geochemistry and paleotectonic implications: Precambrian Research, v. 59, p. 243–262.

Degagne, P. and Robertson, D.J., 1985, Second year assessment report on geological and geochemical exploration for licence 2372 on claim block 1610 in the Monkstown Road area on the Burin Peninsula, southern Newfoundland, Kidd Creek Newfoundland Ltd. and Apex Geological Consultants Ltd.: Newfoundland and Labrador Geological Survey, Assessment File 1M/09/0233, 39 pages.

DeLazzer, A. and Dimmell, P., 2012, First, second and fifth year assessment report on geochemical and diamond drilling exploration for licences 13446M, 16633M, 17315M, 17342M and 19157M on claims in the Thorburn Lake area, eastern Newfoundland, Silver Spruce Resources Inc.: Newfoundland and Labrador Geological Survey, Assessment File 2D/0768, 181 pages.

Newfoundland and Labrador Department of Natural Resources, 2016, Exploration and Development Highlights 2015: Newfoundland and Labrador Department of Natural Resources, Mines Branch, p. 1-14.

Dill, H.G., 2001, The geology of aluminium phosphates and sulphates of the alunite group minerals: a review: Earth-Science Reviews, v. 53, p. 35-93.

Dimmell, P.M., 1998, Ninth year assessment report on compilation for licence 3497 on claim block 6284 in the Hickeys Pond area, on the Burin Peninsula, Newfoundland, Krinor Resources Inc.: Newfoundland and Labrador Geological Survey, Assessment File 1M/16/0373, 23 pages.

Dimmell, P.M., 2003, First year assessment report on prospecting and geochemical and trenching exploration for licences 8377M and 9190M on claims on the Monkstown Road area, on the Burin Peninsula, Newfoundland, KriPen Syndicate, Dimmell, P. and Turpin A.: Newfoundland and Labrador Geological Survey, Assessment File 1M/09/0477, 25 pages.

Dimmell, P., Harris, J. and Rompel, A., 2015, Fifth, sixth and eighth year assessment report on prospecting and geochemical and diamond drilling exploration for licences 13446M 16633M, and 23023M on claims in the Thorburn Lake area, eastern Newfoundland, Silver Spruce Resources Inc.: Newfoundland and Labrador Geological Survey, Assessment File 2D/0838, 154 pages.

Dimmell, P.M. and MacGillivray, G., 1989, First year assessment report on geological and geochemical exploration for licence 3433 on claim block 6099 in the Paradise River and Nine Island Pond areas on the Burin Peninsula, eastern Newfoundland, Corona Corporation: Newfoundland and Labrador Geological Survey, Assessment File 1M/09/0303, 42 pages.

Dimmell, P.M. and MacGillivray, G., 1990a, Fifth year assessment report on trenching and geochemical exploration for licence 2941 on the Stewart option property on claims 4132-4134, Burin Peninsula, Eastern Newfoundland, Corona Corporation: Newfoundland and Labrador Geological Survey, Assessment File 1M/0317, 17 pages.

Dimmell, P.M. and MacGillivray, G., 1990b, Sixth year assessment report on diamond drilling for licence 2941 on the Stewart option property on claims 5289 and 5290, Burin Peninsula, Eastern Newfoundland, Corona Corporation: Newfoundland and Labrador Geological Survey, Assessment File 1M/0242, 8 pages.

Dimmell, P.M. and MacGillivray, G., 1992, Second year assessment report on geochemical and diamond drilling exploration for licence 3497 on claim block 6284, Hickey's Pond property, Burin Peninsula area, Newfoundland, International Corona Corp.: Newfoundland and Labrador Geological Survey, Assessment File 1M/16/0326, 139 pages.

Dimmell P.M., MacGillivray, G. and Hoffman S.J., 1991, First year assessment report on geological and geochemical exploration for licence 3961 on claim blocks 5297-5301 in the Heffern Pond, Paradise River and Monkstown Road areas on the Burin Peninsula, eastern Newfoundland, International Corona Corporation: Newfoundland and Labrador Geological Survey, Assessment File 1M/0324, 158 pages.

Dimmell, P.M., MacGillivray, G. and Pickett, J.W., 1990, First year assessment report on geological and geochemical exploration and re-examination of drill core for licence 3497 on claim block 6284 in the Hickey's Pond area on the Burin Peninsula, southeastern Newfoundland, 2 reports, International Corona Corporation: Newfoundland and Labrador Geological Survey, Assessment File 1M/16/0313, 90 pages.

Dimmell, P., Wetherup, S. and Barrie, C., 2012, Second year, second year supplementary, third year and sixth year assessment report on prospecting and geochemical, geophysical and diamond drilling exploration for licences 13446M, 16633M, 17315M, 17342M and 19157M on claims in the Thorburn Lake area, eastern Newfoundland, Silver Spruce Resources Inc.: Newfoundland and Labrador Geological Survey, Assessment File 2D/0839, 258 pages.

Diner, Y., 1986, Report on the NewGold Joint Venture, Stewart Option, for licences 2619 and 2707, Westley Mines Ltd.: Newfoundland and Labrador Geological Survey, Assessment File 1M/0242, 9 pages.

Dorsch, J., Bambach, R.K. and Driese, S.G., 1994, Basin-rebound origin for the 'Tuscarora Unconformity' in southwestern Virginia and its bearing on the nature of the Taconic orogeny: American Journal of Science, v. 294, p. 237–255.

Dubé, B., Dunning, G.R. and Lauziere, K., 1995, Geology of the Hope Brook Mine, Newfoundland, Canada: A preserved late Proterozoic high-sulfidation epithermal gold deposit and its implications for exploration: Economic Geology, v. 93, p. 405-436.

Dunning, G.R., Barr, S.M., Raeside, R.P. and Jamieson, R.A., 1990, U-Pb zircon, titanite, and monazite ages in the Bras d'Or and Aspy terranes of Cape Breton Island, Nova Scotia: Implications for new evidence for Avalonian underthrusting: Canadian Journal of Earth Sciences, v. 36, p. 15-22.

Dunning, G. R. and O'Brien, S. J., 1989, Late Proterozoic-early Paleozoic crust in the Hermitage Flexure, Newfoundland Appalachians; U/Pb ages and tectonic significance: Geology, v. 17, no. 6, p. 548-551.

Dyke, B., 2007, First, second, fourth and fifth year assessment report on satellite imagery, prospecting, rock sampling, lake sediment sampling and stream sediment sampling for licences 9038M, 10975M, 11092M, 12650M and 12639M-12640M on claims in the Hickeys Pond and Powderhorn Hill areas, on the Burin Peninsula, Newfoundland, Cornerstone Resources Inc.: Newfoundland and Labrador Geological Survey, Assessment File 1M/0637, 25 pages.

Dyke, B., 2009a, Second, third, fourth, and seventh year assessment report of compilation on licences 12650M, 13637M, 13640M, 15461M-15464M, and 15969M-15972M on claims in the Hickey's Pond area, on the Burin Peninsula, Newfoundland, Cornerstone Resources Inc.: Newfoundland and Labrador Geological Survey, Assessment File 1M/0687, 37 pages.

Dyke, B., 2009b, First year assessment report on prospecting and geochemical exploration for licence 13446M on claims in the Thorburn Lake area, eastern Newfoundland, Cornerstone Resources Inc.: Newfoundland and Labrador Geological Survey, Assessment File 2D/0719, 37 pages.

Dyke, B, and Pratt, W., 2008, First, second, third, fifth, and sixth year assessment report of satellite imagery, property tour, prospecting, rock sampling, lake sediment sampling, stream sediment sampling, soil sediment sampling, mapping, terraspec and trenching on licences 8405M, 8406M, 8509M, 9038M, 10975M, 11092M, 12650M, 13189M, 13633M, 13637M-13640M, 14825M, 14827M and 14833M on claims in the Hickeys Pond and Powderhorn Hill areas, on the Burin Peninsula, Newfoundland, Cornerstone Resources Inc.: Newfoundland and Labrador Geological Survey, Assessment File 1M/0698, 317 pages.

Eichelberger, J.C., 1975, Origin of of andesite and dacite; evidence of mixing in Glass Mountain in California and at other circum-Pacific volcanoes: Geological Society of America Bulletin, v. 86, p. 1381-1391.

Einaudi, M.T., Hedenquist, J.W. and Inan, E.E., 2003, Sulfidation state of fluids in active and extinct hydrothermal systems: Transitions from porphyry to epithermal environments: Society of Economic Geologists, Special Publication 10, p. 285-313.

Feiss, P. G., Vance, K. R. and Wesolowski, D. J., 1993, Volcanic rock-hosted gold and base metal mineralization associated with Neoproterozoic-Early Paleozoic back-arc extension in the Carolina terrane, southern Appalachian Piedmont: Geology, v. 21, p. 439-442.

Fifarek, R.H. and Rye, R.O., 2005, Stable-isotope geochemistry of the Pierina high-sulphidation Au-Ag deposit, Peru: influence of hydrodynamics on SO_4^{2-}-H_2S sulphur isotopic exchange in magmatic-steam and steam-heated environments: Chemical Geology, v. 215, p. 253-279.

Finch, C.J., 1998, Inductively coupled plasma emission spectrometry (ICP-ES) at the geochemical laboratory, *in* Current Research, Newfoundland Department of Mines and Energy, Geological Survey, Report 98-1, p. 179-193.

Foley, N.K. and Ayuso, R.A., 2012, Gold deposits of the Carolina Slate Belt, southeastern United States: Age and origin of the major gold producers: U.S. Geological Survey, Open-File Report 2012:1179, 29 pages.

Foley, N.K., Ayuso, R.A., Seal, R.R., II, Offield, T.W., Wooden, J.N. and Sinha, A.K., 2000, Mineralogical evidence for the age and origin of disseminated gold-iron-sulfide deposits of the Carolina slate belt, USA [abs.]: Geological Society of America Abstracts with Programs, v. 32, p. A– 17.

Fortey, R.A. and Cocks, L.R.M., 2003, Palaeontological evidence bearing on global Ordovician-Silurian continental reconstructions: Earth-Science Reviews, v. 61, p. 245–307.

Froude, T., Way, R. and Wilton, D.H.C., 2002, Second and third year assessment report on prospecting and geochemical, geophysical and diamond drilling exploration for licences 7183M, 7366M and 7845M on claims in the Port Blandford area, eastern Newfoundland, Cornerstone Resources Inc.: Newfoundland and Labrador Geological Survey, Assessment File 2D/0412, 128 pages.

Giggenbach, W.F., 1992, Magma degassing and mineral deposition in hydrothermal systems along convergent plate boundaries: Economic Geology, v. 87, p. 1927-1944.

Gill, J.B., 1981, Orogenic Andesites and Plate Tectonics: Berlin, Springer Verlag, 390 p.

Gillon, K.A., Spence, W.H., Duckett, R.P. and Benson, C.J., 1995, Geology of the Ridgeway gold deposits, Ridgeway, South Carolina, *In* D.E. Crowe, ed., Selected Mineral Deposits of the Gulf Coast and Southeastern United States; Part 2; Gold Deposits of the Carolina Slate Belt: Society of Economic Geologists, Guidebook Series, v. 24, p. 53-87.

Hallberg, A., 1994, The Enasen gold deposit, central Sweden 1. A palaeoproterozoic high-sulphidation epithermal gold mineralization: Mineralium Deposita, v. 29, p. 150-162.

Hamilton, M.A. and Murphy, J.B., 2004, Tectonic significance of a Llanvirn age for the Dunn Point volcanic rocks, Avalon terrane, Nova Scotia, Canada: implications for the evolution of the Iapetus and Rheic Oceans: Tectonophysics, v. 379, p. 199–209.

Harris, J.L., 1981, Assessment report on prospecting and geochemical exploration for lot 2 in the Long Harbour area, Fortune Bay, Newfoundland, Riocanex Inc.: Newfoundland and Labrador Geological Survey, Assessment File 1M/11/0200, 12 pages.

Harris, J., 1996, First and second year assessment report on geological and geochemical exploration for licences 4554M and 4679M on claims in the Henry's Pond area, eastern Newfoundland, GT Exploration Ltd.: Newfoundland and Labrador Geological Survey, Assessment File 2D/0312, 29 pages.

Hatcher, R.D. Jr., Osberg, P.H., Drake, A.A., Jr., Robinson, P. and Thomas, W.A., 1990, Tectonic map of the U.S. Appalachians, *In* Hatcher, R.D. Jr., Thomas, W.A., and Viele, G.W., eds., The Appalachian-Ouachita orogen in the United States: Boulder, Colorado, Geological Society of America, The Geology of North America, v. F-2, Plate 1, scale 1:2,500,000.

Hayes, J.P. and O'Driscoll, C.F., 1989, Gold potential of the eastern Avalon high-alumina belt, Avalon Metallogeny Project-1989, *In* Report of Activities, Newfoundland Department of Mines and Energy, Mineral Development Division.

Hayes, J. P. and O'Driscoll, C. F., 1990, Regional setting and alteration within the eastern Avalon high-alumina belt, Avalon Peninsula, Newfoundland, *In* Current research, Newfoundland Department of Mines and Energy, Geological Survey Branch, Report 90-1, p. 145–155.

Hayes, J.P., 2000, First year assessment report on compilation prospecting and geophysical exploration for licences 6420M-6421M, 6476M-6468M and 6623M on claims in the Monkstown Road area, on the Burin Peninsula, Newfounland: Newfoundland and Labrador Geological Survey, Assessment File 1M/0537, 17 pages.

Heald, P., Foley, N.K. and Hayba, D.O., 1987, Comparative anatomy of volcanic-hosted epithermal deposits: Acid-sulfate and adularia-sericite types: Economic Geology, v. 82, p. 1-26.

Hedenquist, J.W., 1987, Mineralization associated with volcanic-related hydrothermal systems in the Circum-Pacific Basin, *In* Horn, M.K., ed., Circum Pacific Energy and Mineral Resources Conference, 4th, Singapore, l986, Transactions: American Association of Petroleum Geologists, p. 5l3–524.

Hedenquist, J.W., 2007, Prospectivity of epithermal and porphyry Au-(Cu) prospects, Burin Peninsula, Newfoundland: Internal report for Cornerstone Resources Inc., 27 pages.

Hedenquist, J.W. and Lowenstern, J.B., 1994, The role of magmas in the formation of hydrothermal ore deposits: Nature, v. 370, p. 519–527.

Hedenquist, J.W., Arribas, A.R. and Gonzalez-Urien, E., 2000, Exploration for epithermal gold deposits: SEG Reviews, v. 13, p. 245-277.

Hibbard, J., Stoddard, E., Secor, D. and Dennis, A., 2002, The Carolina zone: Overview of Neoproterozoic to early Paleozoic peri-Gondwanan terranes along the eastern flank of the southern Appalachians: Earth Science Reviews, v. 57, p. 299–339.

Hibbard, J.P., van Staal, C.R., Rankin, D. and Williams, H., 2006, Lithotectonic map of the Appalachian Orogen, Canada-United States of America: Geological Survey of Canada, Map 2096A, scale 1:1 500 000.

Hibbard, J.P., van Staal, C.R. and Miller, B.V., 2007a, Links among Carolina, Avalonia, and Ganderia in the Appalachian peri-Gondwanan realm: The Geological Society of America, Special Paper 433, p. 291-311.

Hibbard, J.P., van Staal, C.R. and Rankin, D.W., 2007b, A comparative analysis of pre-Silurian building blocks of the northern and southern Appalachians: American Journal of Science, v. 307, p. 23-45.

Hibbard, J.P., van Staal, C.R. and Rankin, D.W., 2010, Comparative analysis of the geological evolution of the northern and southern Appalachian orogen: Late Ordocivian-Permian, *In* From Rodinia to Pangea: The Lithotectonic Record of the Appalachian Region. Edited by R.P. Tollo M.J. Batholomew J.P. Hibbard. P.M. Karabinos, Geological Society of America, Memoir 206, p. 51-70.

Hikov, A., Velinova, N., Georgieva, S. and Kunov, A., 2004, Aluminum-phosphate-sulphate (APS) minerals in Bulgaria: characteristics and possibility for preservation, *In* International Symposium "Mineral Diversity Research and Preservation", 9-15 October, 2009, Sofia, Working papers, p. 37-48.

Hoskin, P.W.O., 1999, SIMS determination of ug g^{-1}-level fluorine in geological samples and its concentration in NIST SRM 610: Geostandards Newsletter, Journal of Geostandards and Geoanalysis, v. 23, p. 69-76.

Hoskin, P.W.O, Kinny, P.D. and Wyborn, D., 1998, Chemistry of hydrothermal zircon: Investigating timing and nature of water-rock interaction, *In* Water-rock Interaction. Arehart G.B., Hulston, J.R. (eds) Balkema, Rotterdam, The Netherlands, p. 545-548.

Howland, A.L., 1938, Precambrian iron bearing deposits of southeastern Newfoundland: Geological Survey of Newfoundland, Unpublished report, 43 pages.

Howland, A.L., 1940, Specularite-alunite mineralization at Hickey's Pond, Newfoundland: American Mineralogist, v. 25, p. 34-45.

Huard, A., 1989, Epithermal alteration and gold mineralization in late Precambrian volcanic rocks on the northern Burin Peninsula, southeastern Newfoundland (Unpublished Msc thesis), Memorial University of Newfoundland, St. John's. Newfoundland, 286 pages.

Huard, A. and O'Driscoll, C.F., 1985, Auriferous specularite-alunite-pyrophyllite deposits of the Hickey's Pond area, northern Burin Peninsula, Newfoundland, *In* Current Research, Newfoundland Department of Mines and Energy, Mineral Development Division, Report 85-1, p. 182-189.

Huard, A. and O'Driscoll, C.F., 1986, Epithermal gold mineralization in late Precambrian volcanic rocks on the Burin Peninsula, *In* Current Research. Newfoundland Department of Mines and Energy, Mineral Development Division, Report 86-1, p. 65-78.

Hughes, C.J., 1972, Late Precambrian volcanic rocks of Avalon, Newfoundland – a spilite/keratophyre province: recognition and implications: Canadian Journal of Earth Science, v. 10, p. 272-282.

Hussey, E.M., 1978, Geology of the Sound Island map area, (west half), Newfoundland, *In* Report of Activities. Newfoundland Department of Mines and Energy, Mineral Development Division, Report 78-1, p. 110-115.

Hussey, E. M., 1979, Geology of the Clode Sound area, Newfoundland, unpublished M.Sc. thesis, St. John's, Newfoundland, Memorial University of Newfoundland, 312 pages.

Israel, S., 1998, Geochronological, structural and stratigraphic investigation of a Precambrian unconformity between the Harbour Main Group and Conception Group, east coast Holyrood Bay, Avalon Peninsula, Newfoundland, Unpublished B.Sc. (Honors) thesis, Memorial University of Newfoundland, St. John's, Newfoundland, 78 pages.

Jensen, L.S., 1976, A new cation plot for classifying subalkalic volcanic rocks: Ontario Division of Mines, Misc. Paper 66.

Juliani, C., Rye, R.O., Nunes, C.M.D., Snee, L.W., Correa Silva, R.H., Monteiro, L.V.S., Bettencourt, J.S., Neumann, R. and Neto, A.A., 2005, Paleoproterozoic high-sulphidation mineralization in the Tapajos gold province, Amazonian craton, Brazil: geology, mineralogy, alunite argon age, and stable isotope constraints: Chemical Geology, v. 215, p.95-125.

Kellett, D.A., 2014, New age data refine extent and duration of Paleozoic and Neoproterozoic plutonism at Ganderia-Avlaonia boundary, Newfoundland: Canadian Journal of Earth Sciences, v. 51, no. 10, p. 943-972.

Kennedy, M. J., Blackwood, R. F., Colman-Sadd, S. P., O'Driscoll, C. F. and Dickson, W. L., 1982, The Dover-Hermitage Bay Fault: Boundary between the Gander and Avalon Zones, eastern Newfoundland, *In* St. Julien, P., and Beland. J., eds., Major structural zones and faults of the northern Appalachians: Waterloo, Ontario, Geological Association of Canada, Special Publication 24, p. 231–248

Kerr, A., Rafuse, H., Sparkes, G., Hinchey, J. and Sandeman, H.A., 2011, Visible/infrared spectroscopy (VIRS) as a research tool in economic geology: background and pilot studies from Newfoundland and Labrador, *In* Current Research, Government of Newfoundland and Labrador, Department of Natural Resources, Geological Survey, Report 11-1, p. 145-166.

King, A. F. (compiler), 1988a, Late Precambrian sedimentation and related orogenesis of the Avalon Peninsula, Eastern Avalon Zone, *In* Geological Association of Canada–Mineralogical Association of Canada–Canadian Society of Petroleum Geologists, Annual Meeting, Field Trip A-4, Guidebook, St. John's, Newfoundland, 84 pages.

King, A.F. (compiler), 1988b, Geology of the Avalon Penninsula, Newfoundland (parts of 1K, 1L, 1M, 1N and 2C): Government of Newfoundland and Labrador, Department of Mines and Energy, Mineral Development Division, Map 88-001 (coloured).

King, A. F., 1990, Geology of the St. John's area: Newfoundland Department of Mines and Energy, Geological Survey Branch Report 90-2, 88 pages.

Krogh, T.E., Strong D.F., O'Briend, S.J. and Papezik V.S., 1988, Precise U-Pb zircon dates from the Avalon Terrane in Newfoundland: Canadian Journal of Earth Sciences, v. 25, p. 442-453.

Labonte, J., 2010, Fourth, fifth seventh, eight year assessment report on prospecting, reclaimation and geochemical exploration for licences 12650M, 13637M, 15460M-15462M on claims in the Hickey's Pond and Powderhorn Hill areas, on the Burin Peninsula, Newfoundland, Cornerstone Resources Inc.: Newfoundland and Labrador Geological Survey, Assessment File 1M/0758, 87 pages.

Layne, G.D., Dimmell, P.M., Sparkes, G.W., Ferguson, S.A. and Dunning, G.R., 2016, The Big Easy Prospect: A Well-Preserved Late Neoproterozoic Low-Sulfidation Ag-Au Deposit in the Avalonian Terrance of Newfoundland, Canada [abs]: Geological Society of America, Abstracts with programs, 48(3), T1:16-2.

Le Maitre, R.W., Bateman, P., Dudek, A., Keller, J., Lameyre Le Bas, M.J., Sabine, P.A., Schmid, R., Sorensen, H., Streckeisen, A., Woolley, A.R. and Zanettin, B., 1989, A classification of igneous rocks and glossary of terms: Blackwell, Oxford.

Lorand, J.P., 1990, Are spinel lherzolite xenoliths representative of the abundance of sulfur in the upper mantle?: Geochimica et Cosmochimica Acta. v. 54, no. 5, p. 1487-1492

MacGillivray, G., Delazzer, A., Dimmell, P., Lambert, G. and Arehart, G.B., 2011, First year, first year supplementary and fourth year assessment report on geological, geochemical, geophysical and trenching exploration for licences 13446M, 16633M, 17315M and 17342M on claims in the Thorburn Lake area, eastern Newfoundland, Silver Spruce Resources Inc.: Newfoundland and Labrador Geological Survey, Assessment File 2D/0837, 130 pages.

Maddry, J.W. and Kilbey, T.R., 1995, Geology of the Haile gold mine, *In* D.E. Crowe, ed., Selected Mineral Deposits of the Gulf Coast and Southeastern United States; Part 2; Gold Deposits of the Carolina Slate Belt, Society of Economic Geologists, Guidebook Series, v. 24, p. 147-172

Mattinson, J.M., 2005, Zircon U-Pb chemical abrasion (CA-TIMS) method; combined annealing and multi-step partial dissolution analysis for improved precision and accuracy of zircon ages: Chemical Geology, v. 220, p. 47-66.

McBride, D., 1987, Second year assessment report on geological and geochemical exploration for licence 2571 on claim block 3965 in the Sandy Harbour River area on the Burin Peninsula, eastern Newfoundland, Cuvier Mines Inc.: Newfoundland and Labrador Geological Survey, Assessment File 1M/09/0266, 18 pages.

McCartney, W. D., 1967, Whitborne map-area, Newfoundland: Ottawa, Geological Survey of Canada Memoir 341,133 pages.

McKenzie, C.B., 1986, Geology and mineralization of the Chetwynd deposit, southwestern Newfoundland, Canada [abs]: *In* A.J. MacDonald, ed., Proceedings of Gold '86, an international symposium on the geology of gold. Gold '86, Toronto, p. 137-148.

McKenzie, C.B. and Gubins, A., 1983, First year assessment report on diamond drilling and geophysical exploration for licence 2268 on claim block 3317 in the Hickeys Pond area, Newfoundland, BP Selco, 2 reports: Newfoundland and Labrador Geological Survey, Assessment File 1M/16/0209, 46 pages.

McNamara, A.K., Niocaill, C.M., Van der Pluijm, B.A. and Van der Voo, R., 2001, West African proximity of the Avalon terrane in the latest Precambrian: GSA Bulletin, v. 113, no. 9, p. 1161-1170.

Milu, V., Milesi, J. and Leroy, J., 2004, Rosia Poieni copper deposit, Apuseni Mountains, Romania: advanced argillic overprint of a porphyry system: Mineralium Deposita, v. 39, no. 2, p. 173-188.

Miyashiro, A., 1974, Volcanic rock series in island arcs and active continental margins: American Journal of Science, v. 274, p. 321-355.

Murphy, J.B., 2007, Igneous Rock Associations 8. Arc Magmatism II: Geo-chemical and Isotopic Characteristics: Journal of the Geological Association of Canada, v. 34, no. 1, p. 7-35.

Murphy, J.B., Gutierrez-Alonso, G., Nance, R.D., Fernandez-Suarez, J., Keppie, J.D., Quesada, C., Strachan, R.A. and Dostal, J., 2006, Origin of the Rheic Ocean: Rifting along a Neoproterozoic suture?: Geology, v. 34, p. 325-328.

Murphy, J.B., Gutierrez-Alonso, G., Nance, D., Fernandez-Suarez, J., Keppie, J.D., Quesada, C., Strachan, R.A. and Dostal, J., 2008a, Tectonic Plates Come Apart at the Seams: American Scientist,v. 96, p.129-137.

Murphy, J.B., Keppie, D., Dostal, J. and Nance, D., 1999, Neoproterozoic–early Paleozoic evolution of Avalonia, *In* Ramos, V., and Keppie, D., eds., Laurentia-Gondwana Connections before Pangea: Geological Society of America, Special Paper 336, p. 253–266.

Murphy, J.B., McCausland P.J.A, O'Brien, S.J., Pisarevsky, S. and Hamilton, M.A., 2008b, Age, geochemistry and Sm-Nd isotopic signature of the 0.76 Ga Burin Group: Compositional equivalent of Avalonian basement?: Precambrian Research, v. 165, p. 37-48.

Murphy, J.B. and Nance, R.D., 2002, Sm-Nd isotopic systematics as tectonic tracers: An example from West Avalonia in the Canadian Appalachians: Earth-Science Reviews, v. 59, p. 77-100.

Murphy, J.B., Strachan, R.A., Nance, R.D., Parker, K.D. and Fowler, M.B., 2000, Proto-Avalonia: A 1.2–1.0 Ga tectonothermal event and constraints for the evolution of Rodinia: Geology, v. 28, p. 1071–1074.

Nance, R.D., Gutierrez-Alonso, G., Keppie, J.D., Linnemann, U., Murphy, J.B., Quesada, C., Strachan, R.A. and Woodcock, N.H., 2010, Evolution of the Rheic Ocean: Gondwana Research, v. 17, p. 194-222.

Nance, R.D. and Murphy, J.B., 1996, Basement isotopic signatures and Neoproterozoic paleogeography of Avalonian – Cadomian and related terranes in the circum-North Atlantic, *In* Nance, D., and Thompson, M., eds., Avalonian and Related Peri-Gondwanan Terranes of the Circum-North Atlantic: Geological Society of America, Special Paper, v. 304, p. 333–346.

Nance, R.D., Murphy, J.B. and Keppie, J.D., 2002, A Cordilleran model for the evolution of Avalonia: Tectonophysics, v. 352, p. 11-31.

Nance, R.D., Murphy, J.B., Strachan, R.A., D'Lemos, R.S. and Taylor, G.K., 1991, Late Proterozoic tectonostratigraphic evolution of the Avalonian and Cadomian terranes: Precambrian Research, v. 53, p. 41-78.

Noel, N., 2006a, First year assessment report on prospecting and trenching for licences 11096M, 11103M and 11691M in the Tower showing area on the Burin Peninsula, eastern Newfoundland: Newfoundland and Labrador Geological Survey, Assessment File 1M/09/0624, 17 pages.

Noel, N., 2006b, Third year assessment report on prospecting for licence 9570M, Central Burin area, eastern Newfoundland: Newfoundland and Labrador Geological Survey, Assessment File 1M/0590, 11 pages.

Normore, L.S., 2012, Geology of the Random Island map area (NTS 2C/04), Newfoundland, *In* Current Research, Newfoundland and Labrador Department of Natural Resources, Geological Survey, Report 12-1, p. 121-145.

O'Brien, S.J., Dubé, B. and O'Driscoll, C.F., 1999, High-sulfidation, epithermal-style hydrothermal systems in late Neoproterozoic Avalonian rocks on the Burin Peninsula, Newfoundland: implications for gold exploration, *In* Current Research, Newfoundland Department of Mines and Energy, Geological Survey, Report 99-1, p. 275-296.

O'Brien, S.J., Dubé, B., O'Driscoll, C.F. and Mills, J., 1998, Geological setting of gold mineralization and related hydrothermal alteration in late Neoproterozoic (post-640 Ma) Avalonian rocks of Newfoundland, with a review of coeval gold deposits elsewhere in the Appalachian Avalonian belt, *In* Current Research, Newfoundland Department of Mines and Energy, Geological Survey, Report 98-1, p. 93-124.

O'Brien, S. J., Dunning, G. R., Knight, I. and Dec, T., 1989, Late Precambrian geology of the north shore of Bonavista Bay (Clode Sound to Lockers Bay), *In* Report of activities, Newfoundland Department of Mines and Energy, Geological Survey Branch, p. 49–50.

O'Brien, S. J., Dunning, G. R., Dubé, B., O'Driscoll, C. F., Sparkes, B., Israel, S. and Ketchum, J., 2001, New insights into the Neoproterozoic geology of the central Avalon Peninsula (parts of NTS map areas 1N/6, 1N/7 and 1N/3), eastern Newfoundland, *In* Current Research, Newfoundland and Labrador Department of Natural Resources, Geological Survey, Report 01-1, p. 169-189.

O'Brien, S,J. and King, A.F., 2004, Neoproterozoic stratigraphy of the Bonavista Peninsula: Preliminary results, regional correlations and implications for sediment-hosted stratiform copper exploration in the Newfoundland Avalon Zone, *In* Current Research, Newfoundland and Labrador Department of Mines and Energy, Geological Survey, Report 02-1, p. 229-244.

O'Brien, S.J., King, A.F and O'Driscoll, C.F., 1997, Late Neoproterozoic geology of the central Avalon Peninsula, Newfoundland, with an overview of mineralization and hydrothermal alteration, *In* Current Research, Newfoundland Department of Mines and Energy, Geological Survey, Report 97-1, p. 257-282.

O'Brien, S. J. and Knight, I., 1988, Avalonian geology of southwest Bonavista Bay: Parts of the St. Brendans's (2C/13) and Eastport (2C/13) map areas, *In* Current Research, Newfoundland Department of Mines, Mineral Development Division, Report 88-1, p. 193–205.

O'Brien, S.J., Nunn, G.A.G., Dickson, W.L. and Tuach, J., 1984, Geology of the Terrenceville (1M/10) and Gisborne Lake (1M/15) map areas, southeast Newfoundland: Newfoundland Department of Mines and Energy, Mineral Development Division, Report 84-4, 54 pages.

O'Brien, S.J. and Nunn, G.A.G., 1980, Terrenceville (1M/10) and Gisborne Lake (1M/15) Map Areas, Newfoundland: Newfoundland Department of Mines and Energy, Mineral Development Division, Report 80-1, p. 120-133.

O'Brien, S.J., O'Brien, B.H., Dunning, G.R. and Tucker, R.D., 1996, Late Neoproterozoic Avalonian and related peri-Gondwanan rocks of the Newfoundland Appalachians: Geological Society of American, Special Paper 304, p. 9-28.

O'Brien, S.J. and O'Driscoll, C.F., 1996, Preliminary investigation of Neoproterozoic (Avalonian) rocks, northeastern Holyrood (NTS 1N/6) map area: notes on geology, mineralization and mineral exploration potential, *In* Current Research, Newfoundland Department of Mines and Energy, Geological Survey, p. 19-23.

O'Brien, S. J., O'Driscoll, C. F., Greene, B. A. and Tucker, R. D., 1995, Pre-Carboniferous geology of the Connaigre Peninsula and the adjacent coast of Fortune Bay, Southern Newfoundland, *In* Current research, Newfoundland Department of Natural Resources, Geological Survey Branch, Report 95-1, p. 267–297.

O'Brien, S. J., O'Driscoll, C. F. and Tucker, R. D., 1992, A reinterpretation of the geology of parts of the Hermitage Peninsula, southwestern Avalon Zone, Newfoundland, *In* Current research, Newfoundland Department of Mines and Energy, Geological Survey Branch, Report 92-1, p. 185–194.

O'Brien, S.J., Strong, P.G. and Evans, J.L., 1977, The geology of the Grand Bank (1M/4) and Lamaline (1L/3) map areas, Burin Peninsula, Newfoundland: Newfoundland Department of Mines and Energy, Mineral Development Division, Report 77-7, 16 pages.

O'Brien, S. J., Strong, D. F. and King, A. F., 1990, The Avalon Zone type area: Southeastern Newfoundland Appalachians, *In* Strachan, R. A., and Taylor, G. K., eds.., Avalonian and Cadomian geology of the North Atlantic: Glasgow, Blackies and Son, p. 166–193.

O'Brien, S.J. and Taylor, S.W., 1983, Geology of the Baine Harbour (1M/7) and Point Enragee (1M/6) map areas, southeastern Newfoundland: Newfoundland Department of Mines and Energy, Mineral Development Division, Report 83-5, 70 pages.

O'Brien, S. J., Tucker, R. D. and O'Driscoll, C. F., 1994, Neoproterozoic basement-cover relationships and the tectono-magmatic record of the Avalon Zone on the Hermitage Peninsula and environs, Newfoundland: New perspectives in the Appalachian-Caledonian Orogen: Geological Association of Canada Nuna Conference, Program and Abstracts, p. 21-22.

O'Brien, S.J., Wardle, R.J. and King, A.F., 1983, The Avalon Zone: A Pan-African terrane in the Appalachian Orogen of Canada: Geology Journal, v. 18, p. 195-222.

O'Driscoll, C.F., 1984, The Hickey's Pond belt: auriferous specularite-alunite-pyrophyllite-sericite mineralization near Placentia Bay, Newfoundland: Newfoundland Department of Mines and Energy, Mineral Development Division, Open File Report 1M/16(221), 12 pages.

O'Driscoll, C. F. and Strong, D. F., 1979, Geology and geochemistry of the Late Precambrian volcanic and intrusive rocks of the southwestern Avalon Zone in Newfoundland: Precambrian Research, v. 8, p. 19–48.

Ohmoto, H., 1972, Systematics of sulfur and carbon isotopes in hydrothermal ore deposits: Economic Geology, v. 67, p. 551-578.

Pearce, J.A., 1996, A user's guide to basalt discrimination diagrams, *In* Wyman, D.A. (ed.) Trace Element Geochemistry of Volcanic Rocks: Applications for Massive Sulphide Exploration: Geological Association of Canada, Short Course Notes 12, p. 79-113.

Pearce, J.A., 1983, Role of the sub-continental lithosphere in magma genesis at active continental margins, *In* Hawkesworth, C.J. and Norry, M.J. (eds.), Continental basalts and mantle xenoliths: Shiva, Nantwich, p. 230-249.

Pisarevsky, S.A., Wingate, T.D., Powell, C.MCA, Johnson, S. and Evans, D.A.A., 2003, Models of Rodinia assembly and fragmentation, *In* Yoshida, M., Windley, B.F., and Dasgupta, S., eds., Proterozoic East Gondwana: Supercontinent Assembly and Breakup: Geological Society, London, Special Publications, 206, p. 35-55.

Pollock, J.C. and Hibbard, J.P., 2010, Geochemistry and tectonic significance of the Stony Mountain gabbro, North Carolina: Implications for the Early Paleozoic evolution of Carolinia: Gondwana Research, v. 17, p. 500-515.

Pollock, J.C., Hibbard, J.P. and Sylvester, P.J., 2009), Early Ordovician rifting of Avalonia and birth of the Rheic Ocean: U–Pb detrital zircon constraints from Newfoundland: Journal of the Geological Society, v. 166, p. 501–515.

Pollock, J.C., Hibbard, J.P. and Sylvester, P.J., 2010, Depositional and tectonic setting of the Neoproterozoic-early Paleozoic rocks of the Virgilina sequence and Albemarle Group, North Carolina, *In* R.P. Tollo, M.J. Bartholomew, J.P. Hibbard, and P.M. Karabinos, eds., From Rodinia to Pangea: The Lithotectonic Record of the Appalachian Region: Geological Society of America, Memoir 206, p. 739-772.

Pollock, J.C., Hibbard, J.P. and vanStaal, C.R., 2012, A paleogeographical review of the peri-Gondwanan realm of the Appalachian orogeny: Canadian Journal of Earth Sciences, v. 49, p. 259-288.

Ralph, J.M., 1996, First year assessment report on prospecting and geochemical exploration for licence 4864M on claims in the Monkstown Road area, Newfoundland: Newfoundland and Labrador Geological Survey, Assessment File 1M/09/0377, 13 pages.

Reusch, D., 1985, First year assessment report on geological and geochemical exploration for licene 2571 on claim block 3965 in the Sandy Harbour River area on the Burin Peninsula, Newfoundland, Golden Hind Ventures Ltd.: Newfoundland and Labrador Geological Survey, Assessment File 1M/09/0243, 29 pages.

Reyes, A.G., 1990, Petrology of Philippine geothermal systems and application of alteration mineralogy to their assessment: Journal of Volcanology and Geothermal Research, v. 43, p. 279-309.

Roley, R.W., 1953, Diamond drilling report of Baldy fluorite prospect in the Fortune Bay area, Newfoundland, Reynolds Mining Corp. and Newfoundland and Labrador Corp. Ltd.: Newfoundland and Labrador Geological Survey, Assessment File 1M/11/0083, 4 pages.

Samson, S., Hibbard, J. and Wortman, G., 1995, Nd isotopic evidence for juvenile crust in the Carolina terrane, southern Appalachians: Contributions to Mineralogy and Petrology, v. 121, p. 171 – 184.

Saunders, P., 1996, First year assessment report on prospecting and geochemical exploration for licence 4554 on claim block 17112 in the Henrys Pond and Thorburn Lake areas, eastern Newfoundland, GT Exploration Ltd.: Newfoundland and Labrador Geological Survey, Assessment File 2D/0305, 19 pages.

Saunders, P. and Reusch, D., 1984, First year assessment report on geochemical exploration for licence 2372M on claim block 1610 in the Paradise River and Monkstown Road areas on the Burin Peninsula, Newfoundland, Apex Geological Consultants Ltd.: Newfoundland and Labrador Geological Survey, Assessment File 1M/09/0225, 43 pages.

Seal, R.R., 2006, Sulfur isotope geochemistry of sulphide minerals: Mineralogical Society of America, Reviews in Mineralogy and Geochemistry, v. 61, p. 633-677.

Sears, W. A., 1990, A geochemical, petrographic and metallogenic analysis of volcanogenic sulphide deposition within the Connaigre Bay Group, Hermitage Peninsula, Southern Newfoundland, unpublished M.Sc. thesis, St. John's, Memorial University of Newfoundland, 282 pages.

Setterfield, T., 2011, Third and eighth year assessment report of geological reconnaissance, prospecting, rock sampling, soil sediment sampling, stream sediment sampling and Terraspec mineral identification on licences 0131189M and 015460M on claims in the Camp Pond area, Stewart Property, on the Burin Peninsula, Newfoundland, TerraX Minerals Inc.: Newfoundland and Labrador Geological Survey, Assessment file 1M/0846, 94 pages.

Setterfield, T. and St-Hilaire, C., 2012, First, fifth, and ninth year assessment report of airborne magnetic surveying on licences 018389M, 018406M, 013189M, and 015460M on claims in the Camp Pond area, Stewart property, on the Burin Peninsula, Newfoundland, TerraX Minerals Inc., 2 reports: Newfoundland and Labrador Geological Survey, Assessment file 1M/0780, 72 pages.

Sexton, A., 2002, Fourteenth year assessment report on geological and geochemical exploration for licence 3497 on claim block 6944M in the Hickeys Pond area, on the Burin Peninsula, Newfoundland, GeoVector Management Inc and Western Keltic Mines Inc.: Newfoundland and Labrador Geological Survey, Assessment File 1M/16/0464, 68 pages.

Sexton, A., 2003, First year assessment report on geological and geochemical exploration for licenes 8406M and 8978M on claims in the Hickeys Pond area, on the Burin Peninsula, Newfoundland, GeoVector Management Inc and Western Keltic Mines Inc.: Newfoundland and Labrador Geological Survey, Assessment file 1M/0469, 69 pages.

Seymour, C.R., 2004a, First and second year assessment report on prospecting and geochemical exploration for licences 8671M, 8672M and 8675M on claims in the Long Harbour area, Fortune Bay, Newfoundland, Cornerstone Resources Inc.: Newfoundland and Labrador Geological Survey, Assessment File 1M/11/0513, 37 pages.

Seymour, C.R., 2004b, First year assessment report on prospecting and geochemical exploration for licences 9636M-9640M and 10148M on claims in the Long Harbour area, Fortune Bay, Newfoundland, Cornerstone Resources Inc.: Newfoundland and Labrador Geological Survey, Assessment File 1M/11/0515, 53 pages.

Seymour, C.R., 2006, Second and third year assessment report on prospecting and geochemical exploration for licences 10148M and 10928M on claims in the Long Harbour area, southern Newfoundland, Cornerstone Resources Inc.: Newfoundland and Labrador Geological Survey, Assessment File 1M/11/0585, 41 pages.

Sillitoe, R.H. and Hedenquist, J.W., 2003, Chapter 18: Linkages Between Volcanotectonic Settings, Ore-Fluid Compositions, and Epithermal Precious Metal Deposits: Society of Economic Geologists, Special Publication 10, 29 pages.

Sillitoe, R.H., 1999, Styles of high-sulphidation gold, silver and copper mineralization in the porphyry and epithermal environments, *In* Weber, G., ed., Pacrim '99 Congress, Bali, Indonesia, 1999, Proceedings: Parkville, Australasian Institute of Mining and Metallurgy, p. 29–44.

Smith, B.L., 1953, Fluorite deposits of Long Harbour, Fortune Bay: Newfoundland Department of Mines and Resources, Geological Survey Report no. 2, 22 pages.

Smith, S.A. and Hiscott, R.N., 1984, Latest Precambrian to Early Cambrian basin evolution, Fortune Bay, Newfoundland: Fault-bounded basin to platform: Canadian Journal of Earth Sciences, v. 21, p. 1379–1392.

Sparkes, G.W., 2012, New developments concerning epithermal alteration and related mineralization along the western margin of the Avalon zone, Newfoundland, *In* Current Research, Newfoundland and Labrador Department of Natural Resources, Geological Survey, Report 12-1, p. 103-120.

Sparkes, G.W. and Dunning, G.R., 2014, Late Neoproterozoic epithermal alteration and mineralization in the western Avalon zone: a summary of mineralogical investigations and new U/Pb geochronological results, *In* Current Research, Newfoundland and Labrador Department of Natural Resources, Geological Survey, Report 14-1, p.99-128.

Sparkes, G.W., Ferguson, S. and Sandeman, H.A.I., 2015, Visible/infrared spectroscopy data from Neoproterozoic epithermal systems of the western Avalon Zone (NTS map areas 2C/12, 13; 2D/1,8,9; 1L/13; 1M/3, 6, 7, 9, 10, 11, 15, 16) Newfoundland: Government of Newfoundland and Labrador, Department of Natural Resources, Geological Survey, Open File NFLD/3266, 90 pages.

Sparkes, G.W., Ferguson, S.A., Layne, G.D., Dunning, G.R., O'Brien, S.J. and Langille, A., 2016, The nature and timing of Neoproterozoic high-sulphidation gold mineralization from the Newfoundland Avalon Zone: Insights from new U-Pb ages, ore petrography and spectral data from the Hickey's Pond prospect, *In* Current Research, Newfoundland and Labrador Department of Natural Resources, Geological Survey, Report 16-1, p.91-116.

Sparkes, G.W., O'Brien, S.J., Dunning, G.R. and Dubé, B., 2005, U-Pb geochronological constraints on the timing of magmatism, epithermal alteration and low-sulfidation gold mineralization, eastern Avalon Zone, Newfoundland, *In* Current Research, Newfoundland Department of Mines and Energy, Geological Survey, Report 05-1, p. 115-130.

Sparkes, G.W. and Sandeman, H.A.I., 2015, Geochemical data from the western Avalon Zone (NTS map areas 2D/1, 2, 7, 9, 10, 15, 16; 1L/13, 14; 1M/3, 4, 6, 7, 9, 10, 11, 15, 16), Newfoundland: Newfoundland and Labrador Department of Natural Resources, Open File NFLD/3265, 167 pages.

Spence, W.N., Worthington, J.E., Jones, E. M. and Kin, I.T., 1980, Origin of the gold mineralization at the Haile mine, Lancaster County, South Carolina: Mining Engineering, v. 32, p. 70-73.

Stacey, J.S. and Kramers, J.D., 1975, Approximation of terrestrial lead isotope evolution by a two stage model: Earth and Planetary Science Letters, v. 26, p. 207-221.

Stein, H.J., Markey, B.J., Morgan, J.W., Zak, K., Zacharias, J. and Sundblad, K., 1996, Re-Os dating of Au deposits in shear zones using accessory molybdenite—Bohemian Massif, Carolina slate belt, and Fennoscandian shield examples: Geological Society of America Abstracts with Programs, v. 28, no. 7, p. A–474.

Stewart, R.V., 1986, First year assessment report on a gold sampling program-Newfoundland on claim blocks 4132-4134: Newfoundland and Labrador Geological Survey, Assessment File 1M/0237, 2 pages.

Stoffregen, R.E. and Alpers, C.N., 1987, Woodhouseite and svanbergite in hydrothermal ore deposits: products of apatite destruction during advanced argillic alteration: Canadian Mineralogist, v. 25, p. 201-211.

Stoffregen, R.E. and Cygan, G.L., 1990, An experimental study of Na-K exchange between alunite and aqueous sulfate solutions: American Mineralogist, v. 75, p. 209-220.

Strong, D. F., 1979, Proterozoic tectonics of Northwestern Gondwanaland: New evidence from eastern Newfoundland: Tectonophysics, v. 54, p. 81–101.

Strong, D. F. and Dostal, J., 1980, Dynamic partial melting of Proterozoic upper mantle: Evidence from rare earth elements in oceanic crust of eastern Newfoundland: Contributions to Mineralogy and Petrology, v. 72, p. 165–173.

Strong, D. F., O'Brien, S. J., Strong, P. G., Taylor, S. W. and Wilton, D. H. C., 1978a, Aborted Proterozoic rifting in Newfoundland: Canadian Journal of Earth Sciences, v. 15, p. 117–131.

Strong, D. F., O'Brien, S. J., Strong, P. G., Taylor, S. W. and Wilton, D. H., 1978b, Geology of the Marystown (1M/13) and St. Lawrence (1L/14) map areas, Newfoundland: Newfoundland Department of Mines and Energy, Mineral Development Division, Report 78-7, 81 pages.

Sun, S.S. and McDonough, W.F., 1989, Chemical and isotopic systematics of oceanic basalts: implications for mantle composition and processes, *In* Saunders, A.D. and Norry, M.J. (eds.), Magmatism in ocean basins: Geological Society of London, Special Publication 42, p. 313-345.

Swinden, H. S. and Hunt,P. A., 1991, A U-Pb zircon age from the Connaigre Bay Group, southwestern Avalon Zone, Newfoundland; implications for regional correlations and metallogenesis, *In* Radiogenic age and isotopic studies, Report 4, Geological Survey of Canada, Paper 90-2, 3-10.

Taylor, S. W., 1978, Geology of the Marystown map sheet (E/2), Burin Peninsula, southeastern Newfoundland, unpublished M.Sc. thesis, St. John's, Newfoundland, Memorial University of Newfoundland, 164 pages.

Taylor, B.E., 2007, Epithermal Gold Deposits, *In* Goodfellow, W.D., ed., Mineral Deposits of Canada: A Synthesis of Major Deposit-Types, District Metallogeny, the Evolution of Geological Provinces, and Exploration Methods: Geological Association of Canada, Mineral Deposits Division, Special Publication no. 5, p. 113-139.

Tuach, J., 1984, Metallogenic studies of granite associated mineralization in the Ackley Granite and the Cross Hills Plutonic Complex, Fortune Bay, Newfoundland, *In* Current Research, Newfoundland Department of Mines and Energy, Mineral Development Division, Report 84-1, p. 245-253.

Tuach, J., 1991, The geology and geochemistry of the Cross Hills Plutonic Suite, Fortune Bay, Newfoundland [NTS 1M/10], an Eocambrian to Cambrian alkaline gabbro-granodiorite-granite-peralkaline granite-syenite suite containing minor Zr-Y-Nb-REE mineralization: Government of Newfoundland and Labrador Department of Mines and Energy, Geological Survey Branch, Report 91-2, 86 pages.

Tucker, R. D. and McKerrow, W. S., 1995, Early Paleozoic chronology: A review in light of new U-Pb zircon ages from Newfoundland and Britain: Canadian Journal of Earth Sciences, v. 32, p. 368–379.

Turpin, A., 2010, First and third year assessment report on prospecting and geochemical exploration for licences 13446M and 16633M on claims in the Thorburn Lake area, eastern Newfoundland: Newfoundland and Labrador Geological Survey, Assessment File 2D/0805, 41 pages.

van Staal, C., Dewey, J., MacNiocaill, C. and McKerrow, W., 1998, The Cambrian-Silurian tectonic evolution of the northern Appalachians and British Caledonides: History of a complex, west and southwest Pacific-type segment of Iapetus, *In* Blundell, D., and Scott, A., eds., Lyell: The Past is the Key to the Present: Geological Society [London], Special Publication 143, p. 199–242.

van Staal, C. and Barr, S., 2012, Lithospheric architecture and tectonic evolution of the Canadian Appalachians and associated Atlantic margin, Chapter 2, *In* J.A. Percival, F.A. Cook and R.M. Clowes, eds., Tectonic Styles in Canada: the LITHOPROBE Perspective: Geological Association of Canada, Special Paper 49, p. 41-95.

van Staal, C.R., Whalen, J.B., Valverde-Vaquero, P., Zagorevski, A. and Rogers, N., 2009), Pre-Carboniferous, episodic accretion-related, orogenesis along the Laurentian margin of the northern Appalachians: Geological Society, London, Special Publications, v. 327, p. 271-316.

van Staal, C.R., 2007, Pre-Carboniferous tectonic evolution and metallogeny of the Canadian Appalachians, *In* Goodfellow, W.D. (ed.) Mineral Deposits of Canada: A Synthesis of Major Deposit Types, District Metallogeny, the Evolution of Geological Provinces & Exploration Methods: Geological Association of Canada, Mineral Deposits Division, Special Publication 5, p. 793 – 817.

Watson, E.B., Cherniak, D.J., Hanchar, J.M., Harrison, T.M. and Wark, D.A., 1997, The incorporation of Pb into zircon: Chemical Geology, v. 141, p. 19-31.

White, N.C., 1991, High sulfidation epithermal gold deposits: Characteristics and a model for their origin: Geological Survey of Japan, Report 277, p. 9-20

White, N.C. and Hedenquist, J.W., 1995, Epithermal gold deposits: styles, characteristics and exploration: Society of Economic Geologists Newsletter, no. 23, p. 1,9-13.

Williams, H., 1971, Geology of the Belleoram map area, Newfoundland: Ottawa, Geological Survey of Canada, Paper 70-65, 39 pages.

Williams, H., 1979, Appalachian Orogen in Canada: Canadian Journal of Earth Science, v. 16, p. 792-807.

Williams, H. and Hatcher, R.D., 1983, Appalachian suspect terranes, *In* Hatcher, R.D., Jr., Williams, H., and Zietz, I., eds., Contributions to the Tectonics and Geophysics of Mountain Chains: Geological Society of America, Memoir 158, p. 33-54.

Williams, H. and King, A. F., 1979, Trepassey map area, Newfoundland: Ottawa, Geological Survey of Canada, Memoir 389, 24 pages.

Winchester, J.A. and Floyd, P.A., 1977, Geochemical discrimination of different magma series and their differentiation products using immobile elements: Chemical Geology, v. 20, p. 325-343.

Wortman, G., Samson, S. and Hibbard, J., 2000, Precise U–Pb zircon constraints on the earliest magmatic history of the Carolina terrane: Journal of Geology, v. 108, p. 321–338.

Zagorevski, A., McNicoll, V. and van Staal, C.R., 2007, Distinct Taconic, Salinic and Acadian deformation along the Iapetus suture zone, Newfoundland Appalachians: Canadian Journal of Earth Sciences, v. 44, p. 1567-1585.

Zalnieriunas, R.V., 1987), Report on the 1986 Diamond Drilling Results of the New Gold Property (Stewart Option) for licence 2941, Burin Peninsula, Newfoundland, Novamin Resources Inc.: Newfoundland and Labrador Geological Survey, Assessment File 1M/061, 6 pages.

Zwaschka, M. and Scheetz, J.W., 1995, Detailed mine geology of the Brewer gold mine, Jefferson, South Carolina, *In* D.E. Crowe, ed., Selected Mineral Deposits of the Gulf Coast and Southeastern United States; Part 2; Gold Deposits of the Carolina Slate Belt: Society of Economic Geologists, Guidebook Series, v. 24, p. 95-146.

APPENDIX A: SAMPLE COLLECTION AND SAMPLE DESCRIPTIONS

Samples for this study were primary collected during the summer of 2012, while assisting Greg Sparkes, of the Newfoundland Geological Survey, during his three year project on the Burin Peninsula, assessing the mineral potential, and extent of the epithermal mineralization. The Heritage prospect was revisited in the fall of 2013 and spring of 2015, with some additional samples collected during the 2013 visit. Additional samples were also collected in the winter of 2015 from drill core of the Hickey's Pond prospect.

Samples were obtained from both surficial outcrop and drill core. Representative mineralized and altered samples were selected from all of the different prospects to assess the variations in characteristics and mineral associations of the precious metal mineralizaiton. Fresher, less altered samples were also collected for the purpose of U-Pb TIMS dating, focussing on host lithologies, distinct marker horizons, and cross cutting dykes to attempt to constrain the timing of mineralization, but also to refine the age brackets of some of the regional stratigraphy. Samples were also collected for whole rock lithogeochemistry, including those used for geochronology.

Table A-1 summarizes all of the samples collected for this study, including representative hand samples, and samples intended for other purposes including petrography, SIMS sulphur isotope and trace element analysis, U-Pb geochronology, Au+34 geochemistry, and major and trace element lithogeochemistry. The table includes sample names, locations in UTM coordinates (for outcrop samples only), names of hosting prospects, field station numbers/drill hole numbers/trench names from which samples were collected, a list of analyses conducted for this study, field-written sample descriptions, rock unit classifications (based on geochemistry and petrography), and alteration minerals identified with visible infra-red reflectance spectroscopy (VIRS).

Most samples are labeled with the prefix 'SF' and were collected specifically for this study by the author. Additional samples collected by other geologists that were used during this study for either petrography or geochronology, or referenced in *Chapter 2*, are

also included at the end of the list. Most of these additional samples were collected by Greg Sparkes (Newfoundland Geological Survey), either in 2011, or 2012 during fieldwork related to this project, and are prefixed with 'GS'. Two samples are included, prefixed with 'MC,' which were acquired from the B.Sc. thesis collection of Matt Clarke. The naming convention used for all of these sample subsets is the same, with the first set of digits denoting the year the sample was collected, and the second set of digits indicating the individual sample number. Any samples included, not adhering to these labeling conventions, were collected by Graham Layne, of Memorial University, in relation to this project.

Table A-2 summarizes all of the stations recorded during fieldwork and is included as a reference to some of the photos presented in *Chapters 2, 5 & 6*. The table includes field station numbers, locations in UTM coordinates, dates that locations were visited, lithological groupings, names of hosting prospect, and a list of samples collected.

Table A-1

Sample #	Year	UTM E	UTM N	Group	Prospect	Station/DDH/ Trench Name	Description	Alteration 1	Alteration 2	Lithology	Lab #	Analyses	Thin Section
SF-12-001	2012	692347	5286171	Marystown	Tower	STA-SF-12-009	Sil+Py alt, highly sheared at top of trench,	Pyrophyllite		Hydrothermal Alteration	7740822	Au+34; ICP majors & traces; SEM; SIMS (sulfur isotopes)	1x2
SF-12-002	2012	692360	5286188	Marystown	Tower	STA-SF-12-009	Sil+Py alt., as less sheared pod within the specularite alteration	Na Alunite		Hydrothermal Alteration	7740864	Au+34	1x2
SF-12-003	2012	692349	5286182	Marystown	Tower	STA-SF-12-009	wide zone of spectral hematite alt	Na Alunite		Hydrothermal Alteration	7740823	Au+34; ICP majors & traces	1x2
SF-12-004	2012	692363	5286188	Marystown	Tower	STA-SF-12-009	Specular hematite pod, 50 cm wide within sil+py alt.	Na Alunite		Hydrothermal Alteration	7740865	Au+34	1x2
SF-12-005	2012	692369	5286194	Marystown	Tower	STA-SF-12-009	Specular hematite BX up to 10 cm wide, hematite rich bands with 4-8mm small fragments of more alunite altered material.	Na Alunite		Hydrothermal Alteration	7740824	Au+34; ICP majors & traces; SEM	1x2
SF-12-006	2012	692358	5286191	Marystown	Tower	STA-SF-12-009	Folded bull quartz vein with coarse grained specularite.	Na Alunite		Hydrothermal Alteration	7740866	Au+34	1x2
SF-12-007	2012	692350	5286174	Marystown	Tower	STA-SF-12-009	Silica-quartz pod, fine-grained grey silica, boudinaged parallel with shear; Cornerstone channel sample 21221=1.5ppb Au over 0.5m	Pyrophyllite	Topaz	Hydrothermal Alteration			1x2
SF-12-008	2012	692346	5286174	Marystown	Tower	STA-SF-12-009	Dark grey silica veining, boudinaged, with fine grained intergrown specularite-silica and local coarse-grained pyrite	Na Alunite	Nacrite	Hydrothermal Alteration	7740867	Au+34	1x2
SF-12-009	2012	692434	5286148	Marystown	Tower	STA-SF-12-010	Grey silica pod, silica-pyrite alt., alunite altered fractures	Na Alunite		Hydrothermal Alteration	7740868	Au+34; SEM; SIMS (sulfur isotopes)	1x2
SF-12-010	2012	692432	5286149	Marystown	Tower	STA-SF-12-010	Silica-pyrite alteration	Na Alunite		Hydrothermal Alteration		SEM	1x2
SF-12-011	2012	692421	5286140	Marystown	Tower	STA-SF-12-010	White quartz with brown margins and coarse-grained pyrite; minor green silica	Na Alunite		Hydrothermal Alteration			1x2
SF-12-012	2012	692417	5286130	Marystown	Tower	STA-SF-12-010	Grey 1 m wide silica pod	Muscovite	Topaz	Hydrothermal Alteration	7740869	Au+34; SEM	1x2
SF-12-013	2012	692401	5286136	Marystown	Tower	STA-SF-12-010	Vuggy silica pod; light grey, fine-grained	Na Alunite	Pyrophyllite	Hydrothermal Alteration	7740871	Au+34	1x2
SF-12-014	2012	692400	5286136	Marystown	Tower	STA-SF-12-010	Silica-pyrite altered wallrock	Na Alunite		Hydrothermal Alteration			1x2
SF-12-015	2012	692507	5286210	Marystown	Tower	STA-SF-12-015	Silica-pyrite-alunite altered, foliated, oxidized; from subcrop	Na Alunite	Topaz	Hydrothermal Alteration	7740825	Au+34; ICP majors & traces; SEM	1x2
SF-12-016	2012	692492	5286215	Marystown	Tower	STA-SF-12-015	Grey-beige silica with darker brown silica sometimes as fine grained breccia matrix; +late bull quartz			Hydrothermal Alteration	7740872	Au+34	1x2
SF-12-017	2012	692508	5286235	Marystown	Tower	STA-SF-12-016	Silica-alunite; Alteration along contact margin	Na Alunite	Topaz	Hydrothermal Alteration			1x2
SF-12-018	2012	692523	5286232	Marystown	Tower	STA-SF-12-016	Grey-beige silica with pinkish silica fragment (an old primary volcanic feature?); +brown-beige silica	Muscovite	Pyrophyllite	Hydrothermal Alteration			1x2
SF-12-019a	2012	692593	5286283	Marystown	Tower	STA-SF-12-017	Possible topaz from subcrop, boulders, and outcrop; a) small sample with opaque brown chunks	Topaz	Paragonite	Hydrothermal Alteration		SEM	1x2
SF-12-019b	2012	692593	5286283	Marystown	Tower	STA-SF-12-017	b) grey sillica, bull qtz and brown silica along fractures	Topaz		Hydrothermal Alteration			1x2
SF-12-019c	2012	692593	5286283	Marystown	Tower	STA-SF-12-017	c) patchy grey and brown silica + minor late bull qtz,	Topaz		Hydrothermal Alteration			1x2
SF-12-019d	2012	692593	5286283	Marystown	Tower	STA-SF-12-017	d) grey silica with distinct opaque brown patches and brown silica bx	Topaz		Hydrothermal Alteration		SEM	1x2
SF-12-020	2012	692587	5286285	Marystown	Tower	STA-SF-12-017	Quartz-alunite-pyrite altered rep. from foliated material to the south	Na Alunite	Pyrophyllite	Hydrothermal Alteration			1x2
SF-12-021	2012	692582	5286287	Marystown	Tower	STA-SF-12-017	From other side of massive silica pods; quartz-alunite alteration	Na Alunite		Hydrothermal Alteration			1x2
SF-12-022	2012	692562	5286313	Marystown	Tower	STA-SF-12-018	Banded alunite-specularite-silica altered wallrock.	Na Alunite	Topaz	Hydrothermal Alteration	7740873	Au+34; U-Pb geochronology (rutile)	1x2
SF-12-023	2012	692529	5286336	Marystown	Tower	STA-SF-12-019	Weakly altered intermediate xstyl tuff	Muscovite	FeMgChlorite	Intermediate Crystal Tuff			1x2
SF-12-024	2012	692683	5286356	Marystown	Tower	STA-SF-12-20	Possible pyrophyllite with silica-py oxidized zone.	Pyrophyllite	Topaz	Hydrothermal Alteration			1x2
SF-12-025	2012	692683	5286356	Marystown	Tower	STA-SF-12-20	Specular hematite locally within silica-pyrite-pyrophyllite; adjacent to previous sample	Pyrophyllite		Hydrothermal Alteration			1x2
SF-12-026	2012	692638	5286385	Marystown	Tower	STA-SF-12-20	Specular hematite-alunite banding	Na Alunite		Hydrothermal Alteration	7740826	Au+34; ICP majors & traces; SEM	1x2
SF-12-027	2012	655388	5256169	Marystown	Stewart	STA-SF-12-27	Dark purple 20 cm wide intermediate tuff bed, fine-grained with large pits (weathered out fragments)	Muscovite	MgChlorite	Basaltic-Andesitic Lapilli Tuff	7740827	ICP majors & traces; U-Pb geochronology; SEM	1x2
SF-12-028	2012	649649	5253011	Marystown	Stewart	STA-SF-12-028	1 cm wide quartz vein cross cutting advanced argillic alt. with coarse-grained specularite (or covellite?)	FeChlorite	Muscovite	Hydrothermal Alteration	7740874	Au+34; SEM; SIMS (sulfur isotopes)	2x3
SF-12-029	2012	649654	5253009	Marystown	Stewart	STA-SF-12-028	Quartz Vein	Pyrophyllite	Muscovite	Hydrothermal Alteration			1x2
SF-12-030	2012	649653	5253012	Marystown	Stewart	STA-SF-12-028	Adjacent wallrock (vs vein) with primary igneous texture	Muscovite	Pyrophyllite	Tonalite	7740875	Au+34	1x2

SF-12-031	2012	649657	5253024	Marystown	Stewart	STA-SF-12-028	3-4 cm wide quartz vein (x2 reps) with black mineral?	Muscovite	Pyrophyllite	Hydrothermal Alteration	7740876	Au+34; SEM	1x2
SF-12-032	2012	649657	5253043	Marystown	Stewart	STA-SF-12-028	5 cm wide quartz vein, grey with pyrite	Siderite	Muscovite	Hydrothermal Alteration	7740877	Au+34; SEM	1x2
SF-12-32A	2012	649657	5253043	Marystown	Stewart	STA-SF-12-028	Same as above but larger with vein within silicified wallrock.	Muscovite	Pyrophyllite	Hydrothermal Alteration		SIMS (sulfur isotopes)	1x2
SF-12-033	2012	649683	5252996	Marystown	Stewart	STA-SF-12-028	Wallrock; silica-pyrite-chlorite altered	Muscovite	Pyrophyllite	Hydrothermal Alteration			1x2
SF-12-034	2012	649673	5253022	Marystown	Stewart	STA-SF-12-028	Quartz vein with blue mineral, probably specularite	FeChlorite	Dickite	Hydrothermal Alteration			1x2
SF-12-035	2012	650139	5253608	Marystown	Stewart	STA-SF-12-029	2-5 cm wide quartz vein from 'stockwork zone'; Silica-pyrite-chlorite altered wallrock			Hydrothermal Alteration	7740878	Au+34	1x2
SF-12-036	2012	650122	5253624	Marystown	Stewart	STA-SF-12-029	Silica-pyrite alteration of wallrock, oxidized weathered surface	Pyrophyllite		Hydrothermal Alteration			1x2
SF-12-037	2012	650120	5253627	Marystown	Stewart	STA-SF-12-029	Adjacent to a massive silica pod; boudinaged vein?	Muscovite	Pyrophyllite	Hydrothermal Alteration			1x2
SF-12-038	2012	650093	5253655	Marystown	Stewart	STA-SF-12-029	Stockwork quartz veining	FeChlorite		Hydrothermal Alteration			1x2
SF-12-039	2012	650094	5253657	Marystown	Stewart	STA-SF-12-029	Stockwork quartz veining	FeChlorite	Muscovite	Hydrothermal Alteration			1x2
SF-12-040	2012	650056	525651	Marystown	Stewart	STA-SF-12-029	Quartz vein with pyrite			Hydrothermal Alteration			1x2
SF-12-041	2012	650144	5253611	Marystown	Stewart	STA-SF-12-029	Mafic dyke cutting alteration and foliation	FeMgChlorite	Muscovite	Mafic Dyke	7740828	ICP majors & traces; U-Pb geochronology; SEM	2x3
SF-12-042	2012	650159	5253780	Marystown	Stewart	STA-SF-12-030	Wormy qtz vein; ptygmatically folded	Pyrophyllite	Dickite	Hydrothermal Alteration	7740879	Au+34	2x3
SF-12-043	2012	650857	5254413	Marystown	Stewart	STA-SF-12-032	Pink, felsic quartz crystal tuff (Stewart Tuff)	Phengite	Epidote	Dacitic Quartz-Feldspar Crystal Tuff (ST)	7740829	ICP majors & traces; U-Pb geochronology; SEM	1x2
SF-12-044	2012	651939	5254494	Burin Knee Intrusive Suite	Stewart	STA-SF-12-033	Coarse-grained acicular amphibole crystals in diorite	FeMgChlorite	Phengite	Diorite			1x2
SF-12-045	2012	651930	5254397	Burin Knee Intrusive Suite	Stewart	STA-SF-12-033	Altered granite-granodiorite	Phengite	Epidote	Granodiorite			1x2
SF-12-046	2012	652055	5254398	Burin Knee Intrusive Suite	Stewart	STA-SF-12-034	Medium-grained, pink granite-granodiorite	Phengite		Granite	7740831	ICP majors & traces; U-Pb geochronology; SEM	1x2
SF-12-047	2012	652071	5254390	Burin Knee Intrusive Suite	Stewart	STA-SF-12-034	Green altered granite-granodiorite	Phengite	Ankerite	Granite-Granodiorite			1x2
SF-12-048	2012	652071	5254390	Marystown	Stewart	STA-SF-12-034	Adjacent to above, altered volcanics, felsic crystal tuff	Phengite		Felsic Quartz-Feldspar Crystal Tuff			1x2
SF-12-049	2012	654969	5255825	Marystown	Forty Creek	STA-SF-12-114	Speck of chalcopyrite in boudinaged quartz vein from North end of 40 Creek trench; vein runs parallel to a mafic dyke	Muscovite		Hydrothermal Alteration			1x2
SF-12-050a	2012	654909	5255826	Marystown	Forty Creek	STA-SF-12-114	Mineralized quartz vein with chlorite from float	Muscovite		Hydrothermal Alteration		SEM; SIMS (sulfur isotopes)	2x3
SF-12-050b	2012	654909	5255826	Marystown	Forty Creek	STA-SF-12-114	Mineralized quartz vein with chlorite from float			Hydrothermal Alteration			1x2
SF-12-050c	2012	654909	5255826	Marystown	Forty Creek	STA-SF-12-114	Mineralized quartz vein with chlorite from float	FeMgChlorite	Muscovite	Hydrothermal Alteration		SEM; SIMS (sulfur isotopes)	1x2
SF-12-050d	2012	654909	5255826	Marystown	Forty Creek	STA-SF-12-114	Mineralized quartz vein with chlorite from float			Hydrothermal Alteration			
SF-12-050e	2012	654909	5255826	Marystown	Forty Creek	STA-SF-12-114	Mineralized quartz vein with chlorite from float	Muscovite		Hydrothermal Alteration		SEM; SIMS (sulfur isotopes)	1x2 (2)
SF-12-050f	2012	654909	5255826	Marystown	Forty Creek	STA-SF-12-114	Mineralized quartz vein with chlorite from float			Hydrothermal Alteration			1x2
SF-12-050g	2012	654909	5255826	Marystown	Forty Creek	STA-SF-12-114	Mineralized quartz vein with chlorite from float			Hydrothermal Alteration			
SF-12-050h	2012	654909	5255826	Marystown	Forty Creek	STA-SF-12-114	Mineralized quartz vein with chlorite from float			Hydrothermal Alteration		SEM	1x2
SF-12-051	2012	654323	5272240	Long Harbour	Long Harbour	STA-SF-12-115	Silica vein with colloform banding, adularia, coarse blading (2-3 cm) and green silica. Float spalled from outcrop.			Hydrothermal Alteration	7740881	Au+34	
SF-12-052	2012	645313	5272263	Long Harbour	Long Harbour	STA-SF-12-115	Adularia, colloform banding with finer blading (most around 1 cm) at southern end of trench from subcrop.			Hydrothermal Alteration	7740882	Au+34	2x3
SF-12-052b	2012	645313	5272263	Long Harbour	Long Harbour	STA-SF-12-115	Same subcrop with well-defined blading	Dickite		Hydrothermal Alteration		SEM	1x2
SF-12-053	2012	645295	5272278	Long Harbour	Long Harbour	STA-SF-12-115	Pink (possible) opal with fine banding in vein midway through trench	Muscovite		Hydrothermal Alteration			-

SF-12-054	2012	645292	5272284	Long Harbour	Long Harbour	STA-SF-12-115	7-10mm blading between 2-10 cm in quartz veining with brecciated rhyolite fragments Banded veins croscut. Adjacent to Cornerstone sample 15027 (2.9 g/t Au)			Hydrothermal Alteration			-
SF-12-055	2012	645289	5272287	Long Harbour	Long Harbour	STA-SF-12-115	Side of channel sample 15032 (3.4 g/t Au), cockade breccia with abundant blading mostly 1 cm, with adularia.	Dickite		Hydrothermal Alteration			1x2
SF-12-056	2012	645256	5272243	Long Harbour	Long Harbour	STA-SF-12-116	Flow banded rhyolite host rock, red in colour.			Flow Banded Rhyolite	7740832	ICP majors & traces; U-Pb geochronology; SEM	1x2
SF-12-057	2012	645279	5272198	Long Harbour	Long Harbour	STA-SF-12-116	Finely laminated white to beige opaline? silica sitting perpendicular to vein walls=very shallow settling out silica. From subcrop-outcrop. Measured at surface with orientation dipping 20 deg to 126 deg. (SE)			Hydrothermal Alteration		SEM	2x3
SF-12-058	2012	645272	5272146	Long Harbour	Long Harbour	STA-SF-12-116	Blading from SW of trench, subcrop	Dickite		Hydrothermal Alteration			-
SF-12-058a	2012	645272	5272146	Long Harbour	Long Harbour	STA-SF-12-116	Blading from SW of trench, subcrop			Hydrothermal Alteration			-
SF-12-058b	2012	645272	5272146	Long Harbour	Long Harbour	STA-SF-12-116	Colloform banding			Hydrothermal Alteration			-
SF-12-059	2012	645264	5272333	Long Harbour	Long Harbour	STA-SF-12-116	Blades and druzy quartz from NW of trench. Subcrop.	Muscovite	Dickite	Hydrothermal Alteration			2x3
SF-12-060	2012	645313	5272258	Long Harbour	Long Harbour	STA-SF-12-116	Coarse blading, subcrop, '3D' weathered blades.	Magnesite	Gypsum	Hydrothermal Alteration		SEM	1x2
SF-12-061	2012	645287	5272290	Long Harbour	Long Harbour	STA-SF-12-116	Weathered blades from north end of trench.	Dickite	Muscovite	Hydrothermal Alteration			-
SF-12-062	2012	645323	5272240	Long Harbour	Long Harbour	STA-SF-12-116	Float splayed from side of trench, with blading, pink silica banding	Magnesite	Gypsum	Hydrothermal Alteration			-
SF-12-063	2012	645323	5272240	Long Harbour	Long Harbour	STA-SF-12-116	Same location as above with good banding			Hydrothermal Alteration			-
SF-12-064	2012	645313	5272268	Long Harbour	Long Harbour	STA-SF-12-116	Banding from south end of trench.	Kaolinite PX		Hydrothermal Alteration			-
SF-12-065	2012	645310	5272369	Long Harbour	Long Harbour	STA-SF-12-118	Coarse blading in vein @ 180 deg, 20-50 cm wide, weak banding, mostly massive silca and coarse blades. 20 m north good crustiform banding develops	Dickite		Hydrothermal Alteration			2x3
SF-12-066	2012	645356	5272668	Long Harbour	Long Harbour	STA-SF-12-119	Coarse blading, strong cockade breccia	Muscovite		Hydrothermal Alteration		SEM	2x3
SF-12-067	2012	585728	5196993	Marystown	Heritage	Whaleback Trench	Green (chalcedonic) silica in brecciated silica veins	Phengite	Magnesite	Hydrothermal Alteration			-
SF-12-068	2012	585208	5195835	Marystown	Heritage	P1C Trench	White quartz breccia, subcrop, weak blading?	FeChlorite	Siderite	Hydrothermal Alteration			-
SF-12-068A	2012	585208	5195835	Marystown	Heritage	P1C Trench	In place vein with "3-D" blading	Phengite	FeMgChlorite	Hydrothermal Alteration			-
SF-12-069	2012	584744	5195041	Marystown	Heritage	P2 Trench	Coarse bladed textures in rusty siliceous rock, weak banding and adularia present	Muscovite		Hydrothermal Alteration		SEM	1x2
SF-12-070	2012	654422	5254712	Marystown	Stewart	STA-SF-12-135	Angular mafic fragments in red silt stone, plagioclase phyric	Phengite	Epidote	Andesitic Lapilli Tuff/Tuff Breccia			1x2
SF-12-071	2012	-	-	Marystown	Stewart	ST-11-01	16.9-17m pyrophyllite veinlets, 1% disseminated and fracture controlled pyrite in tonalite	Pyrophyllite	Muscovite	Hydrothermal Alteration		SEM	1x2
SF-12-072	2012	-	-	Marystown	Stewart	ST-11-01	36.8-36.9m pyrophyllite along fine fractures, semi-pervasive through matrix and possibly as larger (5mm) veinlets, tr-1% disseminated pyrite in tonalite	Pyrophyllite	Dickite	Hydrothermal Alteration			1x2
SF-12-073	2012	-	-	Marystown	Stewart	ST-11-01	48.5-49m (TerraX sample 1040534) Tonalite with weak pyrophyllite along microfractures and semi-pervasive through core	Pyrophyllite		Hydrothermal Alteration	7740833	Au+34; ICP majors & traces	1x2
SF-12-074	2012	-	-	Marystown	Stewart	ST-11-01	66.9m 1.5cm wide vein of pyrophyllite and more opaque cream mineral distinctive from pyrophyllite, cross cutting earlier fine pyrophyllite fractures in tonalite	Pyrophyllite	Dickite	Hydrothermal Alteration			1x2
SF-12-075	2012	-	-	Marystown	Stewart	ST-11-01	66m 1.5cm wide quartz vein in tonalite with pyrophyllite and dark blue-grey mineral (specular hematite?)	Pyrophyllite	Dickite	Hydrothermal Alteration			1x2
SF-12-076	2012	-	-	Marystown	Stewart	ST-11-01	83.64-84.45m (TerraX sample 1040562 - 666ppm Cu) Thin intermittent quartz stringers, strong foliation, 1% disseminated pyrite concentrated along fractures	Muscovite	Pyrophyllite	Hydrothermal Alteration			1x2
SF-12-077	2012	-	-	Marystown	Stewart	ST-11-01	89-89.5m (TerraX sample 1040566 - 506ppm Cu) Un-veined material of interval, silica-pyrite-pyrophyllite altered tonalite	Muscovite		Hydrothermal Alteration	7740834	Au+34; ICP majors & traces	1x2
SF-12-078	2012	-	-	Marystown	Stewart	ST-11-01	89.5-90.2m (TerraX sample 1040566 - 506ppm Cu) Veined portion of same sample; 25-30% grey quartz veining parallel to foliation and sometimes perpendicular, up to 10% pyrite locally	Muscovite		Hydrothermal Alteration		SEM	1x2
SF-12-079	2012	-	-	Marystown	Stewart	ST-11-01	98.86-98.92m Grey-white 10 cm wide quartz vein with 5% pyrite along fractures	Pyrophyllite	Muscovite	Hydrothermal Alteration			1x2
SF-12-080	2012	-	-	Marystown	Stewart	ST-11-01	100.5-100.6m White 3cm wide quartz vein with 1% clots of pyrite, sometimes oxidized and greenish.	Paragonite	Pyrophyllite	Hydrothermal Alteration			1x2
SF-12-081	2012	-	-	Marystown	Stewart	ST-11-01	104.1m Yellow pyrophyllite vein, 4 cm wide, foliation parallel	Pyrophyllite	Dickite	Hydrothermal Alteration			1x2
SF-12-082	2012	-	-	Marystown	Stewart	ST-11-01	105.6-106.1m (TerraX sample 1040578, 608ppm Cu) silica-pyrite altered with pyrophyllite along fractures and occassional specular hematite?	Paragonite		Hydrothermal Alteration			-

SF-12-083	2012	-	-	Marystown	Stewart	ST-11-01	116.55-116.6m 'wormy' quartz vein with 2cm wide band of pyrite through core	Pyrophyllite	Dickite	Hydrothermal Alteration		SEM; SIMS (sulfur isotopes)	1x2
SF-12-084	2012	-	-	Marystown	Stewart	ST-11-01	140.7-141.2m (TerraX sample 1040605, 674ppm Cu) less altered tonalite, primary igneous textures, chloritic	FeChlorite	Paragonitic Illite	Tonalite	7740835	Au+34; ICP majors & traces	1x2
SF-12-085	2012	-	-	Marystown	Stewart	ST-11-01	130.5-131.2m (TerraX sample 1040596 162ppm Cu) Proximal to above, semi-pervasive pyrophyllite and along fractures; Silica-pyrite alteraiton, foliated	Pyrophyllite		Hydrothermal Alteration	7740836	Au+34; ICP majors & traces	-
SF-12-086	2012	-	-	Marystown	Stewart	ST-11-01	144.58-144.6m; 2cm wide quartz vein enveloped in white mica, with purple-grey sulphide-galena?	Paragonitic Illite	Montmorillonite	Hydrothermal Alteration		SEM; SIMS (sulfur isotopes)	1x2
SF-12-087	2012	-	-	Marystown	Stewart	ST-11-01	149.5-150.38m (TerraX sample 1040611 300ppm Cu) Less altered tonalite; chloritic, occassional quartz stringers.	FeChlorite	Paragonite	Tonalite	7740837	Au+34; ICP majors & traces	-
SF-12-088	2012	-	-	Marystown	Stewart	ST-11-01	150.8-151.4m (TerraX sample 1040612 649ppm Cu) Silica-pyrite-pyrophyllite altered	Muscovite	Pyrophyllite	Hydrothermal Alteration	7740838	Au+34; ICP majors & traces	-
SF-12-089	2012	-	-	Marystown	Stewart	ST-11-01	150.38-150.45m Vein cross cutting less altered tonalite (taken from within sample SF-12-87)	Dickite	Kaolinite WX	Hydrothermal Alteration			1x2
SF-12-090	2012	-	-	Marystown	Stewart	ST-11-01	152.65-152.78m Grey quartz vein with vugs, trace pyrite, one dark grey fracture (hematite?)	Pyrophyllite	Dickite	Hydrothermal Alteration			-
SF-12-091	2012	-	-	Marystown	Stewart	ST-11-01	160.8-161m Fracture controlled chlorite and later fracture controlled pyrophyllite	Pyrophyllite		Hydrothermal Alteration			1x2
SF-12-092	2012	-	-	Marystown	Stewart	ST-11-01	171.55-171.63m Wormy grey quartz vein, 1 cm wide, with purple-grey soft metallic mineral	Pyrophyllite	Muscovite	Hydrothermal Alteration		SEM	1x2
SF-12-093	2012	-	-	Marystown	Stewart	ST-11-01	178.3-178.37m Pinkish hue in quartz veining/qtz flooding-alunite?	Muscovite	Pyrophyllite	Hydrothermal Alteration			-
SF-12-094	2012	-	-	Marystown	Stewart	ST-11-01	189-189.8m (118ppb Au, 359ppm Cu) Stockwork zone	Muscovite	Pyrophyllite	Hydrothermal Alteration	7740883	Au+34	-
SF-12-095	2012	-	-	Marystown	Stewart	ST-11-01	193.05-193.8m (86ppb Au, 1010ppm Cu) Stockwork zone, with pyrophyllite along fractures	Muscovite	Pyrophyllite	Hydrothermal Alteration	7740884	Au+34; SEM; SIMS (sulfur isotopes)	1x2
SF-12-096	2012	-	-	Marystown	Stewart	ST-11-01	202.1-202.8m (278ppb Au, 885ppm Cu) Stockwork zone, with pyrophyllite fractures up to 6mm wide and local pervasive pink alteration (alunite?)	Dickite	Paragonite	Hydrothermal Alteration	7740885	Au+34	-
SF-12-097	2012	-	-	Marystown	Stewart	ST-11-01	@209.2m white soft mineral in vein/filling fracture 6mm wide (ph 1018)	Muscovite	Pyrophyllite	Hydrothermal Alteration			-
SF-12-098	2012	-	-	Marystown	Stewart	ST-11-01	215.5-216.2m (847ppm Cu) Quartz stockwork	Muscovite	Pyrophyllite	Hydrothermal Alteration	7740886	Au+34	-
SF-12-099	2012	-	-	Marystown	Stewart	ST-11-01	234.6-235.4m (TerraX sample 1040674; 841ppb Au, 1050ppm Cu) Chlorite, tr-1% pyrite, occassional white 3-4mm qtz stringers slightly oblique to foliation	Muscovite	FeMgChlorite	Crystal-Lapilli Tuff	7740887	Au+34; SEM	1x2
SF-12-100A	2012	-	-	Marystown	Stewart	ST-11-01	240.8-241.5m (TerraX sample 1040679; 225ppb Au, 384ppm Cu) (A)same rock type as above with grey quartz veining (~25%) and sericite-specular hematite-chlorite filling fractures	FeChlorite	Muscovite	Hydrothermal Alteration	7740888	Au+34	-
SF-12-100B	2012	-	-	Marystown	Stewart	ST-11-01	240.8-241.5m (TerraX sample 1040679; 225ppb Au, 384ppm Cu) (B) Local pink patches nearing end of interval (alunite?)	Muscovite	Pyrophyllite	Hydrothermal Alteration			-
SF-12-101	2012	-	-	Marystown	Stewart	ST-11-01	243.7-244.2m (TerraX sample 1040682; 241 Au, 566ppmCu) Same rock as above, with dark grey fractures of specular hematite and chlorite	Muscovite		Hydrothermal Alteration	7740889	Au+34	-
SF-12-102	2012	-	-	Marystown	Stewart	ST-11-02	49-49.6m (TerraX sample 1040851; 118ppb Au) First half of terraX sample within mafic dyke, with opaque white-beige quartz veining (10%); dyke is fine-grained, chloritic, massive, with 2% disseminated pyrite	FeMgChlorite		Mafic Dyke	7740891	Au+34; ICP majors & traces	-
SF-12-103	2012	-	-	Marystown	Stewart	ST-11-02	49.6-50.2m (TerraX sample 1040851; 118ppb Au) Second half of TerraX sample within felsic volcanic, with illite alteration, ~5% rounded quartz eyes, 2% disseminated pyrite, trace opaque white-beige quartz in fractures cross cutting foliation	Muscovite		Felsic Crystal Tuff	7740839	Au+34; ICP majors & traces	-
SF-12-104	2012	691610	5286788	Marystown	Tower	STA-SF-12-136	Felsic-intermediate volcanic, initially interpreted as granitic dyke. 3m wide striking NE, in contact with fragmental mafic volcanic. Chloritic, green-grey colour, coarse-grained feldspar phenocrysts.	Muscovite	Epidote	Felsic-Intermediate Volcaniclastic	7740841	ICP majors & traces; U-Pb geochronology	1x2
SF-12-105	2012	-	-	Marystown	Stewart	ST-11-02	70.4-70.5m Quartz veining in fine-grained, massive chloritic mafic dyke; quartz veins are white with beige mineral along extensional fractures; 1-2% fracture controlled and disseminated pyrite	Epidote		Mafic Dyke			1x2
SF-12-106	2012	-	-	Marystown	Stewart	ST-11-01	433.84-433.94m Primary igneous textures with 10% coarse grained round quartz eyes, 5% medium-grained feldspars and occassional fragments in sericite, chlorite, silica altered matrix. Appears more like Caribou Tuff	Muscovite	FeMgChlorite	Dacitic Quartz-Crystal Tuff (CT)			1x2
SF-12-107	2012	-	-	Marystown	Stewart	ST-11-01	433.55-433.65m Foliated, chlorite-sericite altered, 2% pyrite along shear planes	Muscovite		Hydrothermal Alteration			1x2
SF-12-108	2012	-	-	Marystown	Stewart	ST-11-01	435.1-435.5m 'Stewart Tuff' with primary igneous textures, coarse-grained quartz-feldspar phenocrysts and occassional 1-3 cm mafic fragments, green-grey silceous matrix.	Phengite	Epidote	Dacitic Quartz-Feldspar-Crystal Tuff (ST)	7740842	ICP majors & traces	1x2
SF-12-109	2012	-	-	Marystown	Stewart	ST-11-01	430.5-431.2m 'Caribou tuff', stongly foliated, pyrite-pyrophyllite alteration	Muscovite		Dacitic Quartz-Crystal Tuff (CT)	7740843	Au+34; ICP majors & traces	-
SF-12-110	2012	-	-	Marystown	Stewart	ST-11-02	80.5-80.6m Soft, green pervasive alteration (illite?) occurring from 79.94-83m	Paragonite	Montmorillonite	Hydrothermal Alteration			-
SF-12-111	2012	-	-	Marystown	Stewart	ST-11-02	90.4-91.15m 'Caribou Tuff' with primary igneous textures; 10-13% rounded Medium-coarse-grained quartz eyes; occassional fiamme, 3% pyrite	Muscovite		Dacitic Quartz-Crystal Tuff (CT)	7740844	Au+34; ICP majors & traces	1x2

SF-12-112	2012	-	-	Marystown	Stewart	ST-11-02	174.2-174.3m Shear zone, folded, strongly altered	Paragonite	Gypsum	Hydrothermal Alteration			-
SF-12-113	2012	-	-	Marystown	Stewart	ST-11-02	175.75-175.85m White quartz vein,with coarse-grained clots of pyrite (~5%) and purple fluorite along fractures	Gypsum		Hydrothermal Alteration			-
SF-12-114	2012	-	-	Marystown	Stewart	ST-11-02	223.5-223.58m Start of TerraX sample 1040955, vuggy silica	Paragonite	Pyrophyllite	Hydrothermal Alteration			-
SF-12-115	2012	-	-	Marystown	Stewart	ST-11-02	233.2-234m Pink-orange alteration along shear planes and fractures - pyrophyllite? pyrite filling vugs	Paragonite	Pyrophyllite	Hydrothermal Alteration	7740845	Au+34; ICP majors & traces	-
SF-12-116	2012	-	-	Marystown	Stewart	ST-11-02	264.7-264.8m Quartz-alunite veining with 3% pyrite and locally vuggy; within felsic volcanic	Na Alunite	Pyrophyllite	Hydrothermal Alteration			-
SF-12-117	2012	-	-	Marystown	Stewart	ST-11-02	268.3-268.9m 4 cm wide pink alunite vein, locally vuggy with 3% pyrite in vugs; within a felsic volcanic	Na Alunite		Hydrothermal Alteration	7740892	Au+34	-
SF-12-118	2012	-	-	Marystown	Stewart	ST-11-02	275.65-275.72m Sulphide vein with chalcopyrite	Pyrophyllite		Hydrothermal Alteration		SEM	1x2
SF-12-119	2012	-	-	Marystown	Stewart	ST-11-02	280.5-280.55, start of TerraX sample 1040996; quartz-alunite vein, vuggy with 1-2% pyrite	Na Alunite		Hydrothermal Alteration			-
SF-12-120	2012	-	-	Marystown	Stewart	ST-11-02	291.5-291.6m Vuggy, sheared, quartz veinlets with 2% pyrite filling vugs	Dickite	Pyrophyllite	Hydrothermal Alteration			-
SF-12-121	2012	-	-	Marystown	Stewart	ST-11-02	299.8-299.9m Felsic volcaniclastic	Pyrophyllite	Dickite	Felsic Volcaniclastic			-
SF-12-122	2012	-	-	Marystown	Stewart	ST-11-02	306.1-306.2m 1 cm wide vuggy alunite veinlet	Na Alunite	Dickite	Hydrothermal Alteration			-
SF-12-123	2012	-	-	Marystown	Stewart	ST-11-02	316.17-316.22m Beige illite? vein	Na Alunite	Pyrophyllite	Hydrothermal Alteration			-
SF-12-124	2012	-	-	Marystown	Stewart	ST-11-02	325-325.08m Vuggy quartz-alunite, 1 cm wide vein with 5% pyrite	Na Alunite		Hydrothermal Alteration			-
SF-12-125	2012	-	-	Marystown	Stewart	ST-11-02	329.3-329.4m Vuggy with 5% pyrite and whisps of pyrophyllite	Pyrophyllite	Paragonite	Hydrothermal Alteration			-
SF-12-126	2012	-	-	Marystown	Stewart	ST-11-02	334.5-334.6m Pink-beige 3 cm wide vein parallel to core axis	Na Alunite		Hydrothermal Alteration			-
SF-12-127	2012	-	-	Marystown	Stewart	ST-11-02	339.4-339.65m Stockwork zone, 7% clots of pyrite and alunite?; >50% quartz/quartz flooding	Paragonite	Na Alunite	Hydrothermal Alteration			-
SF-12-128	2012	-	-	Marystown	Stewart	ST-11-02	378.3-378.35m 73 cm wide intensely silicified interval within intermediate intrusive	Na Alunite	Paragonite	Hydrothermal Alteration			-
SF-12-129	2012	-	-	Marystown	Stewart	ST-11-02	416.5-416.6m Hydrothermal breccia, 5-7% pyrite	Paragonite	Pyrophyllite	Hydrothermal Alteration			-
SF-12-130	2012	-	-	Marystown	Stewart	ST-11-02	444.5-444.6m (TerraX sample 1042615) Thin translucent grey quartz veinlets	Pyrophyllite	Gypsum	Hydrothermal Alteration			-
SF-12-131	2012	-	-	Marystown	Stewart	ST-11-02	485.7-485.8m Silica flooding with 3% pyrite	Paragonite	Pyrophyllite	Hydrothermal Alteration			-
SF-12-132	2012	-	-	Marystown	Stewart	ST-11-02	511-511.1m Pyrophyllite veining and other white mica	Pyrophyllite	Dickite	Hydrothermal Alteration			-
SF-12-133	2012	-	-	Marystown	Stewart	ST-11-02	504.35-504.4m Quartz-pyrophyllite vein with metallic grey mineral + pyrite	Paragonite	Pyrophyllite	Hydrothermal Alteration			-
SF-12-134	2012	-	-	Marystown	Stewart	ST-11-02	528.5-528.6m Pyrophyllite alteration	Paragonite	Gypsum	Hydrothermal Alteration			-
SF-12-135	2012	-	-	Marystown	Stewart	ST-11-02	532.4-532.45m Quartz vein with pyrite, fluorite and chlorite, 10 cm wide	FeMgChlorite		Hydrothermal Alteration			-
SF-12-136	2012	-	-	Marystown	Stewart	ST-11-02	569.2-569.3m Quartz vein with coarse-grained pyrite cubes and pyrophyllite	Pyrophyllite	Dickite	Hydrothermal Alteration			-
SF-12-137	2012	-	-	Marystown	Stewart	ST-11-02	584.4-584.5m EOH alteration	Paragonite		Hydrothermal Alteration			-
SF-12-138	2012	-	-	Marystown	Stewart	ST-11-03	64-64.5m Feldspar phenocrysts 2-4mm in dark green-grey fine-grained matrix; magnetic; silica altered?	MgChlorite	Epidote	Porphyritic Andesitic Basalt		U-Pb geochronology	1x2
SF-12-139	2012	-	-	Marystown	Stewart	ST-11-03	137.9-138.5m Massive mafic volcanic; 2% coarse-grained phenocrysts and fractures of magnetite	MgChlorite	Epidote	Massive Magnetite-Phyric Basalt	7740846	Au+34; ICP majors & traces	1x2
SF-12-140	2012	-	-	Marystown	Stewart	ST-11-03	189.8-189.9m Massive mafic volcanic, with magnetite stringer, circular alteration texture	FeMgChlorite	Epidote	Massive Magnetite-Phyric Basalt			1x2
SF-12-141	2012	-	-	Marystown	Stewart	ST-11-03	273-273.1m (TerraX sample 1042788) Fine-grained, massive, chloritic with disseminated and fracture controlled magnetite intergrown with pyrrhotite? Ilmenite?	MgChlorite		Massive Magnetite-Phyric Basalt			1x2
SF-12-142	2012	-	-	Marystown	Stewart	ST-11-03	376.6-377.4m Light grey, strongly silicified matrix, 3% porphyritic feldspar, 3% very fine-grained pyrite as blebs and along fractures	Phengite		Porphyritic Dacite Dyke	7740847	Au+34; ICP majors & traces	1x2
SF-12-143	2012	-	-	Marystown	Stewart	ST-11-03	377.6-377.7m (TerraX sample 1042830) same as above with white mica alteration	Phengite	Ankerite	Porphyritic Dacite Dyke			-
SF-12-144	2012	-	-	Marystown	Stewart	ST-11-03	385.3-386.65m Pink with 6-8% subhedral coarse-grained feldspar phenocrysts, 3% pyrite; silicified	MgChlorite	Epidote	Porphyritic Dacite Dyke		U-Pb geochronology; SEM	1x2
SF-12-145	2012	-	-	Marystown	Stewart	ST-11-03	389.1-389.25m Pink, siliceous, 5% medium-coarse-grained feldspar phenocrysts, local subangular xenoliths	MgChlorite	Epidote	Porphyritic Dacite Dyke			1x2

SF-12-146	2012	-	-	Marystown	Stewart	ST-11-03	389.65-389.75m Siliceous, feldspar-phyric, green, additional quartz phenocrysts, 5% pyrite.	MgChlorite	Phengite	Porphyritic Dacite Dyke			1x2
SF-12-147	2012	-	-	Marystown	Stewart	ST-11-03	57.3m Feldspar-phyric, massive	Epidote	Hornblende	Porphyritic Andesitic Basalt			-
SF-12-148	2012	686115	5289941	Grandy's Pond Arenite Belt	Monkstown Rd	STA-SF-12-137	Layers with fine-grained euhedral feldspar crystals, well bedded with finer more silty layers, and coarser lithic-rich layers; epiclastic	-	-	Feldspathic-Lithic-Arenite	7740848	ICP majors & traces; U-Pb geochronology; SEM	1x2
SF-12-149	2012	688151	5288458	Grandy's Pond Arenite Belt	Monkstown Rd	STA-SF-12-138	Well bedded, with evident cross bedding, rich in lithic clasts, bedded with finer layers of sandstone; fine-medium-grained euhedral feldspar crystals throughout; epiclastic	-	-	Feldspathic-Lithic-Arenite	7740849	ICP majors & traces; U-Pb geochronology	-
SF-12-150	2012	699314	5295023	Marystown	Hickey's Pond	STA-SF-12-139	Vuggy silica, Druzy quartz, oxidized, contains alunite; Western margin of vuggy silica zone	Na Alunite		Hydrothermal Alteration	7740893	Au+34; SEM	1x2
SF-12-151	2012	699317	5295024	Marystown	Hickey's Pond	STA-SF-12-139	Central portion of vuggy silica zone; Coarse vugs, oxidized	Na Alunite		Hydrothermal Alteration	7740894	Au+34; U-Pb geochronology (zircon-rutile); SEM; SIMS (trace element-Au)	1x2
SF-12-152	2012	699319	5295026	Marystown	Hickey's Pond	STA-SF-12-139	Eastern extent of vuggy silica zone; very oxidized; sulphide-rich with pyrite and grey metallic (tennantite)	Na Alunite		Hydrothermal Alteration	7740895	Au+34; SEM; SIMS (sulfur isotopes)	1x2
SF-12-153	2012	688801	5287550	Marystown	Monkstown Rd	STA-SF-12-140	Lazulite-alunite-specular hematite in fractures			Hydrothermal Alteration		SEM	1x2
SF-12-154	2012	688801	5287550	Marystown	Mokstown Rd	STA-SF-12-140	Quartz-specular hematite along fractures and local alunite?	Pyrophyllite		Hydrothermal Alteration			1x2
SF-13-155	2013	584723	5195026	Marystown	Heritage	P4 Trench	Coarse blading, primary carbonate? Sucrop	Muscovite		Hydrothermal Alteration			1x2 (2)
SF-13-155b	2013	584723	5195026	Marystown	Heritage	P4 Trench	Distinct bladed texture			Hydrothermal Alteration		SEM	1x2
SF-13-156	2013	584732	5195021	Marystown	Heritage	P4 Trench	Cherty pale brown silica from just south of Puddle Pond channel sample P4-02-12 (7 g/t Au)	Phengite		Hydrothermal Alteration		SEM	1x2
SF-13-157	2013	584725	5195025	Marystown	Heritage	P4 Trench	Blading in quartz vein			Hydrothermal Alteration			1x2
SF-13-158	2013	584732	5195023	Marystown	Heritage	P4 trench	Alligned column texture (Islickenlines?); Columns in SE direction parallel to qtz veining.			Hydrothermal Alteration		SEM	1x2
SF-13-159	2013	584755	5195056	Marystown	Heritage	P2 Trench	Amythest?	Muscovite		Hydrothermal Alteration			1x2
SF-13-160	2013	584850	5195300	Marystown	Heritage	L1 Trench/ "lunchspot"	Blading in outcrop, 2 m west of dyke			Hydrothermal Alteration		SEM	1x2
SF-13-161	2013	584850	5195300	Marystown	Heritage	L1 Trench/ "lunchspot"	Mafic dyke cross cutting veining, 1.5m wide, striking 170deg. Green, chloritic, amygdules filled with chlorite + open vesicles	FeMgChlorite	Phengitic Illite	Mafic Dyke	7740896	ICP majors & traces; U-Pb geochronology	1x2
SF-13-162	2013	-	-	Marystown	Heritage	HD-05-13	22.8-23m Massive andesite with strong silica-hematite alteration	FeChlorite	Siderite	Porphyritic Andesitic-Dacite			1x2 (2)
SF-13-163	2013	-	-	Marystown	Heritage	HD-05-13	49.85-49.95m Pink rhyolite with quartz phenocrysts.	Phengitic Illite		Rhyolitic Crystal Tuff			1x2
SF-13-164	2013	-	-	Marystown	Heritage	HD-05-13	69.1-69.3m Massive mafic dyke	FeMgChlorite	Muscovite	Mafic Dyke	7740897	ICP majors & traces	1x2
SF-13-165	2013	-	-	Marystown	Heritage	HD-05-13	94-94.15m Andesitic lapilli tuff - possibly epiclastic?; with heterolithic fragments, feldspar-phyric	Phengitic Illite	FeChlorite	Andesitic Lapilli Tuff			1x2
SF-13-166	2013	-	-	Marystown	Heritage	HD-04-13	58.6-58.75m Last 15 cm of Puddle Pond sample HD4-015-13 - hydrothermal breccia	Phengite	Siderite	Hydrothermal Alteration		SEM	1x2
SF-13-167	2013	-	-	Marystown	Heritage	HD-04-13	62.4-62.55m First 15 cm of Puddle Pond sample HD4-020-13; hydrothermal breccia/veining	Phengite		Hydrothermal Alteration			1x2
SF-13-168	2013	-	-	Marystown	Heritage	HD-04-13	131.5-131.7m Middle of Puddle Pond sample HD4-079-13; hydrothermal breccia with sphalerite 'blobs'	Muscovite	Ankerite	Hydrothermal Alteration		SEM	1x2
SF-13-169	2013	-	-	Marystown	Heritage	HD-04-13	140.1-140.3m Middle of Puddle Pond sample HD4-087-13 with 'intestinal' veining			Hydrothermal Alteration			1x2
SF-13-170	2013	-	-	Marystown	Heritage	HD-04-13	107.2-107.35m Middle of Puddle Pond sample HD4-053-13; blading and yellow micaceous mineral	Phengitic Illite		Hydrothermal Alteration			1x2 (2)
SF-13-171	2013	-	-	Marystown	Heritage	HD-01-13	18.2-18.3m Spherical blobby texture - hydrothermal? Igneous?	FeMgChlorite	Phengite	Hydrothermal Alteration			1x2
SF-13-172	2013	-	-	Marystown	Heritage	HD-01-13	31.9-32m Massive porphyritic andesite, tuff	FeMgChlorite	Phengitic Illite	Porphyritic Andesitic-Dacite			1x2
SF-13-173	2013	-	-	Marystown	Heritage	HD-01-13	58.5-58.7m Blading (Part of Puddle Pond sample HD1-040-13 with 8 g/t Au)	Muscovite	Ankerite	Hydrothermal Alteration		SEM	1x2
SF-13-174	2013	-	-	Marystown	Heritage	HD-02-13	18.9-18.95m Blades overprinted by grey silica	FeChlorite	Calcite	Hydrothermal Alteration			1x2
SF-13-175	2013	-	-	Marystown	Heritage	HD-02-13	31-31.2 m Blading in both vein and host rock? 20cm seciton of Puddle Pond sample HD2-024-13	Phengite	Ankerite	Hydrothermal Alteration			1x2 (2)
SF-13-176	2013	-	-	Marystown	Heritage	HD-02-13	47.2-47.5m Strange pervasive network-like volcanic texture - hydrothermal?			Hydrothermal Alteration			1x2 (2)
SF-13-177	2013	-	-	Marystown	Heritage	HD-03-13	21.5-21.55m Middle ofPuddle Pond sample HD3-016-13; Grey metallic mineral - galena?	Muscovite		Hydrothermal Alteration		SEM	1x2

SF-13-178	2013	585730	5196203	Marystown	Heritage	Ridge Trench	Mafic dyke from the Ridge trench; A)amygdaloidal, B) crystalline			Mafic (-Intermediate) Dyke	7740898	ICP majors & traces	1x2
SF-13-179	2013	585728	5196993	Marystown	Heritage	Whaleback Trench	Mafic dyke from the Whaleback trench			Mafic Dyke			1x2
SF-13-180	2013	585186	5196930	Marystown	Heritage	Zaxis Trench	Fairly homogeneous andesite; a lapilli tuff-tuff breccia, but with predominantly monolithic fragments similar in composition to the matrix.			Andesitic Lapilli Tuff	7740899	ICP majors & traces; U-Pb geochronology; SEM	1x2
SF-13-181	2013	-	-	Musgravetown	Big Easy	BE-12-8	67.75-72m Accretionary lapilli tuff, interbedded with pebble conglomerates and sandstones	Phengite	FeMgChlorite	Andesitic Accretionary Lapilli Tuff	7740901	ICP majors & traces; U-Pb geochronology; SEM	1x2
SF-15-182	2015	721878	5339899	Musgravetown	Big Easy	quarry	Green, bedded, coarse-grained sandstone; epiclastic			Sandstone			-
SF-15-183	2015	699417	5295054	Marystown	Hickeys Pond	-	Specularite breccia with silica-alunite fragments in 90% specularite-silica matrix, with cross cutting coarse quartz-specularite veins (sample from Sean O'Brien, 5 g/t Au)	-	-	Hydrothermal Alteration		SEM	1x2 (2)
SF-15-184	2015	699417	5295054	Marystown	Hickeys Pond	-	Huard thesis sample AH-85-345, Specularite breccia alternating w/ oxidized, fine-grained, red hematite breccia (sample cut from AH-85-345, from MSc thesis by Huard)	-	-	Hydrothermal Alteration		SEM	1x2 (2)
SF-13-185	2013	584820	5193308	Marystown	Heritage	quarry	(Graham Layne sample HBQ1) Amygdaloidal basalt from quarry - aka 'High Beach Basalt'	-	-	Amygdaloidal Basalt	7740902	ICP majors & traces	1x2
SF-15-186	2015	-	-	Marystown	Hickey's Pond	HP-90-02	~115.3m (Corona sample 21194, 1.96 g/t Au; NLGS sample 135101) specularite-alunite alteration, deformed, banded	Paragonite	Smectite	Hydrothermal Alteration		SEM	1x2
SF-15-187	2015	-	-	Marystown	Hickey's Pond	HP-90-02	~115.4m (Corona sample 21194, 1.96 g/t Au; NLGS sample 135102) Alunite-specularite alteration, deformed, banded	Muscovite	Kaolinite	Hydrothermal Alteration			-
SF-15-188	2015	-	-	Marystown	Hickey's Pond	HP-90-02	~115.9m (Corona sample 21194, 1.96 g/t Au; NLGS sample 135103) Alunite-specular hematite alteration, deformed, banded	Muscovite	Kaolinite	Hydrothermal Alteration			-
SF-15-189	2015	-	-	Marystown	Hickey's Pond	HP-90-02	~117m (Corona sample 21194,1.96 g/t Au; NLGS sample 135104) Quartz-specular hematite alteration, massive.	Muscovite	Kaolinite	Hydrothermal Alteration		SEM	1x2
SF-15-190	2015	-	-	Marystown	Hickey's Pond	HP-90-02	~117.2m (Corona sample 21194, 1.96 g/t Au; NLGS sample 135105) Quartz-specular hematite alteration, fairly massive	Paragonite	Kaolinite	Hydrothermal Alteration		SEM	1x2
SF-15-191	2015	-	-	Marystown	Hickey's Pond	HP-90-03	~61.75m (Corona sample 21154, 0.362 g/t Au; NLGS sample 135106) 10% pyrite, dickite/kaolinite along fractures, quartz and locally a brown alteration?	Na Alunite		Hydrothermal Alteration		SEM	1x2
SF-15-192	2015	-	-	Marystown	Hickey's Pond	HP-90-03	~63.1m (Corona sample 21156, 0.383 g/t Au; NLGS sample 135107) Grey quartz, alunite, pyrite	Na Alunite		Hydrothermal Alteration		SEM	1x2
SF-15-193	2015	-	-	Marystown	Hickey's Pond	HP-90-03	~64.1m (Corona sample 21157, 0.383 g/t Au; NLGS sample 135108) Grey quartz with abundant fine grained pyrite, and brecciated white quartz with oxidized/hematite fractures (x2 A&B)	Na Alunite	Kaolinite	Hydrothermal Alteration		SEM	1x2 (2)
SF-15-194	2015	-	-	Marystown	Hickey's Pond	HP-90-03	~64.3m (Corona sample 21157, 0.383 g/t Au; NLGS sample 135109) Grey silica with thin white silica veining, 1% fine-grained pyrite, cm-scale faulting	Na Alunite		Hydrothermal Alteration		SEM	1x2
SF-15-195	2015	-	-	Marystown	Hickey's Pond	HP-90-03	63.7-63.8m (Corona sample 21156, 0.383 g/t Au; NLGS sample 135110) Grey silica and brecciated white quartz veining with hematite/oxidized fractures, 1% fine-grained pyrite	Na Alunite	Kaolinite	Hydrothermal Alteration		SEM	1x2
GS-11-02	2011	688612	5287616	Marystown	Monkstown Rd	-	"strongly foliated quartz-white mica schist"	Muscovite		Hydrothermal Alteration			1x2
GS-11-10	2011	688906	5287746	Marystown	Monkstown Rd	-	"silica-pyrite alteration"	Na-Alunite		Hydrothermal Alteration			1x2
GS-11-11	2011	688906	5287746	Marystown	Monkstown Rd	-	"silica-hematite-alunite alteration"	Na-Alunite		Hydrothermal Alteration			1x2
GS-11-33	2011	650144	5253611	Marystown	Stewart	-	"Fine-grained mafic dyke"	FeMgChlorite	Muscovite	Mafic Dyke			-
GS-11-47	2011	649728	5253944	Marystown	Stewart	-	"White mica-pyrite altered crystal tuff"	Paragonite		Crystal Tuff			-
GS-11-52	2011	649633	5253923	Burin Knee Intrusive Suite	Stewart	-	"Fine-grained granodiorite"	FeMgChlorite	Phengitic Illite	Granodiorite			1x2
GS-11-75	2011	649455	5252679	Marystown	Stewart	-	"White mica-pyrite altered crystal tuff"	Pyrophyllite	Muscovite	Hydrothermal Alteration			-
GS-11-85	2011	689585	5288488	Marystown	Monkstown Rd	-	"white mica-pyrite alteration"	Pyrophyllite		Hydrothermal Alteration			1x2
GS-11-86	2011	689577	5288500	Marystown	Monkstown Rd	-	"silica-alunite alteration"	Na-Alunite		Hydrothermal Alteration			1x2
GS-11-94	2011	649270	5253527	Burin Knee Intrusive Suite	Stewart	-	"Fine-grained K-spar-rich granite"	Phengite	Epidote	Granite			-
GS-11-95	2011	649817	5252873	Marystown	Stewart	-	"Fine-grained, plagioclase-phyric, mafic volcanic"	Epidote	Actinolite	Mafic Volcanic			-
GS-11-97	2011	650217	5252286	Marystown	Stewart	-	"Pale purple lapilli tuff"	Epidote	Muscovite	Lapilli Tuff			-
GS-11-99	2011	650658	5254028	Marystown	Stewart	-	"Plagioclase-phyric mafic volcanic"	Phengite	Epidote	Mafic Volcanic			-
GS-11-124A	2011	688544	5287325	Marystown	Monkstown Rd	-	"folded white mica-pyrite alteration"	Pyrophyllite	Muscovite	Hydrothermal Alteration			1x2

GS-11-125	2011	688309	5286941	Marystown	Monkstown Rd	-	"silica-pyrite alteration"	FeMgChlorite	Muscovite	Hydrothermal Alteration			1x2
GS-11-126	2011	688283	5286937	Marystown	Monkstown Rd	-	"purplish silica alteration"	K-Alunite		Hydrothermal Alteration			1x2
GS-11-127	2011	688134	5286601	Marystown	Monkstown Rd	-	"alunite-specularite alteration"	K-Alunite		Hydrothermal Alteration			1x2
GS-11-167	2011	649789	5253902	Marystown	Stewart	STA-SF-12-029	Caribou Tuff	Paragonite	FeChlorite	Dacitic Quartz Crystal Tuff (CT)	7740821	ICP majors & traces; U-Pb geochronology; SEM	1x2
GS-11-455	2011	699307	5295047	Marystown	Hickey's Pond	-	"Qtz-alunite alt; no pyrite"; Zone C style alteration	Na-Alunite		Hydrothermal Alteration			1x2
GS-11-456	2011	699320	5295031	Marystown	Hickey's Pond	-	"Quartz-alunite alteration; no pyrite"; Transition Zone	Na-Alunite		Hydrothermal Alteration			1x2
GS-11-457	2011	699316	5295025	Marystown	Hickey's Pond	-	"Vuggy silica zone; sample is highly oxidized"			Hydrothermal Alteration		SEM	1x2
GS-11-458	2011	699316	5295025	Marystown	Hickey's Pond	-	"Possible vuggy silica texture"	Na-Alunite		Hydrothermal Alteration			1x2
GS-11-459	2011	699328	5295010	Marystown	Hickey's Pond	-	"Massive specular hematite in quartz vein"			Hydrothermal Alteration		SEM	1x2
GS-11-460	2011	699326	5295013	Marystown	Hickey's Pond	-	"Silica-specularite alteration"	Na-Alunite		Hydrothermal Alteration			1x2
GS-11-461	2011	699428	5294996	Marystown	Hickey's Pond	-	"Qtz-alunite alt; no pyrite"; Zone C style alteration	K-Alunite		Hydrothermal Alteration			1x2
GS-12-219	2012	692539	5286044	Marystown	Tower	STA-SF-12-012	"lapilli tuff"	Phengite	Epidote	Lapilli Tuff			-
GS-12-252	2012	652632	5253911	Marystown	Stewart	STA-SF-12-038	"fine-grained dark green, non-magnetic mafic volcanic	FeMgChlorite	Epidote	Mafic Volcanic			-
GS-12-254	2012	651311	5253887	Marystown	Stewart	STA-SF-12-040	"fine-grained, pale green intermediate volcanic	MgChlorite	Epidote	Intermediate Volcanic			-
GS-12-255	2012	651341	5253898	Marystown	Stewart	STA-SF-12-041	"fine-grained pink felsic dyke"	Phengite	Epidote	Felsic Dyke			1x2
GS-12-266	2012	649152	5252317	Burin Knee Intrusive Suite	Stewart	STA-SF-12-053	"Medium-grained, pink, K-feldspar-rich granite	Phengite	FeMgChlorite	Granite			1x2
GS-12-272	2012	652653	5254451	Marystown	Stewart	STA-SF-12-059	"lapilli tuff"	FeMgChlorite	Epidote	Lapilli Tuff			-
GS-12-288	2012	652601	5255888	Marystown	Stewart	STA-SF-12-083	"Chlorite-pyrite altered mafic tuff"	FeMgChlorite	Phengite	Mafic Tuff			-
GS-12-301	2012	653209	5255842	Marystown	Stewart	STA-SF-12-098	"Siliceous lapilli tuff"	Epidote	FeMgChlorite	Lapilli Tuff			-
GS-12-303	2012	654576	5255205	Marystown	Stewart	STA-SF-12-102	"Feldspar-phyric crystal tuff"	Phengite	Epidote	Crystal Tuff			-
GS-12-311	2012	654321	5255950	Marystown	Stewart	STA-SF-12-107	"Chlorite-pyrite altered mafic tuff"	FeMgChlorite	Phengite	Mafic Tuff			-
GS-12-325	2012	645289	5272287	Long Harbour	Long Harbour	-	"Colloform-crustiform banded chalcedonic silica vein; cockade style brecciation with up to 3.4 g/t Au"	Muscovite		Hydrothermal Alteration		SEM	1x2
GS-12-331	2012	655266	5255943	Marystown	Stewart	STA-SF-12-127	"Feldspar-phyric intermediate tuff"	Phengite	Epidote	Intermediate Tuff			-
GDL-40Ck	2012	654909	5255826	Marystown	40 Creek	STA-SF-12-114	telluride rich assemblage from 40 creek	-	-	Hydrothermal Alteration		SEM	1x2
SWC-2	2015	710696	5306734	Swift Current Intrusive Suite	-	-		-	-	Granite			1x2
HBQ2	2015	584820	5193308	Marystown	Heritage	quarry	Amygdaloidal basalt with large jasper clast from quarry	-	-	Basalt			1x2
HBQ3B	2015	584820	5193308	Marystown	Heritage	quarry	Amygdaloidal basalt from quarry	-	-	Basalt			1x2
WPR	2015	710285	5355024	Musgravetown	West Princess	WP-01-003	Flow Banded Rhyolite from drill core from West Princess prospect, ~5km north of Big Easy	-	-	Flow Banded Rhyolite			1x2
MC-12-01	2012	-	-	Musgravetown	Big Easy	BE-11-03	x-cutting fine-grained mafic dyke; 10.15-10.6m	-	-	Mafic Dyke			1x2
MC-12-06	2012	-	-	Musgravetown	Big Easy	BE-11-03	pebble conglomerate interbedded with sandstone; 207.66-207-76m	-	-	Pebble Conglomerate-Sandstone			2x3

Table A-2

Station #	UTM E	UTM N	Date	Group	Prospect	Samples Collected
STA-SF-12-001	659962	5255783	2012-07-26	Marystown	Stewart	
STA-SF-12-002	659501	5255848	2012-07-26	Marystown	Stewart	
STA-SF-12-003	659246	5255982	2012-07-26	Marystown	Stewart	
STA-SF-12-004	658280	5256213	2012-07-26	Marystown	Stewart	
STA-SF-12-005	658034	5256249	2012-07-26	Marystown	Stewart	
STA-SF-12-006	657827	5256272	2012-07-26	Marystown	Stewart	
STA-SF-12-007	657596	5256255	2012-07-26	Marystown	Stewart	
STA-SF-12-008	657212	5256247	2012-07-26	Marystown	Stewart	
STA-SF-12-009	692350	5286185	2012-08-01	Marystown	Tower	SF-12-01 to 08
STA-SF-12-010	692420	5286140	2012-08-01	Marystown	Tower	SF-12-09 to 14
STA-SF-12-011	692497	5285960	2012-08-02	Marystown	Tower	
STA-SF-12-012	692533	5286052	2012-08-02	Marystown	Tower	*GS-12-219*
STA-SF-12-013	692498	5286068	2012-08-02	Marystown	Tower	
STA-SF-12-014	692503	5286134	2012-08-02	Marystown	Tower	*GS-12-221*
STA-SF-12-015	692507	5286210	2012-08-02	Marystown	Tower	SF-12-15, 16
STA-SF-12-016	692508	5286235	2012-08-02	Marystown	Tower	SF-12-17, 18
STA-SF-12-017	692593	5286283	2012-08-02	Marystown	Tower	SF-12-19 a-d to 21
STA-SF-12-018	692562	5286313	2012-08-02	Marystown	Tower	SF-12-22
STA-SF-12-019	692529	5286336	2012-08-02	Marystown	Tower	SF-12-23
STA-SF-12-020	692686	5286356	2012-08-02	Marystown	Tower	SF-12-24 to -26
STA-SF-12-021	692733	5286314	2012-08-02	Marystown	Tower	*GS-12-223*
STA-SF-12-022	658065	5256256	2012-08-03	Marystown	Stewart	*GS-12-225*
STA-SF-12-023	657418	5256210	2012-08-03	Marystown	Stewart	*GS-12-226, 227*
STA-SF-12-024	657294	5256199	2012-08-03	Marystown	Stewart	*GS-12-228*
STA-SF-12-025	657245	5256235	2012-08-03	Marystown	Stewart	
STA-SF-12-026	657121	5256226	2012-08-03	Marystown	Stewart	*GS-12-229, GS-11-209*
STA-SF-12-027	655388	5256169	2012-08-03	Marystown	Stewart	SF-12-27
STA-SF-12-028	649649	5253011	2012-08-03	Marystown	Stewart	SF-12-28 to 34
STA-SF-12-029	650139	5253608	2012-08-03	Marystown	Stewart	SF-12-35 to 41; *GS-11-33, 167*
STA-SF-12-030	650159	5253780	2012-08-03	Marystown	Stewart	SF-12-42
STA-SF-12-031	650682	5254244	2012-08-03	Marystown	Stewart	
STA-SF-12-032	650857	5254413	2012-08-03	Marystown	Stewart	SF-12-43; *GS-11-107*
STA-SF-12-033	651930	5254497	2012-08-03	Marystown	Stewart	SF-12-44, 45; *GS-11-195*
STA-SF-12-034	652055	5254398	2012-08-03	Marystown	Stewart	SF-12-46 to 48; *GS-11-197, 198*
STA-SF-12-035	653014	5254044	2012-08-07	Marystown	Stewart	
STA-SF-12-036	653125	5254029	2012-08-07	Marystown	Stewart	
STA-SF-12-037	652716	5253858	2012-08-07	Marystown	Stewart	
STA-SF-12-038	652632	5253911	2012-08-07	Marystown	Stewart	*GS-12-252*
STA-SF-12-039	651191	5254184	2012-08-07	Marystown	Stewart	*GS-12-253*
STA-SF-12-040	651311	5253887	2012-08-07	Marystown	Stewart	*GS-12-254*
STA-SF-12-041	651341	5253898	2012-08-07	Marystown	Stewart	*GS-12-255*
STA-SF-12-042	651620	5253601	2012-08-07	Marystown	Stewart	*GS-12-256*
STA-SF-12-043	651359	5253487	2012-08-07	Marystown	Stewart	
STA-SF-12-044	651197	5253697	2012-08-07	Marystown	Stewart	*GS-12-257*
STA-SF-12-045	649092	5253122	2012-08-08	Marystown	Stewart	*GS-12-258*
STA-SF-12-046	649059	5252788	2012-08-08	Marystown	Stewart	*GS-12-259*
STA-SF-12-047	649064	5252710	2012-08-08	Marystown	Stewart	*GS-12-260, 261*
STA-SF-12-048	649051	5252669	2012-08-08	Marystown	Stewart	*GS-12-262*
STA-SF-12-049	649063	5252620	2012-08-08	Marystown	Stewart	*GS-12-263*
STA-SF-12-050	649057	5252565	2012-08-08	Marystown	Stewart	
STA-SF-12-051	649044	5252580	2012-08-08	Marystown	Stewart	
STA-SF-12-052	649092	5252671	2012-08-08	Marystown	Stewart	
STA-SF-12-053	649152	5252317	2012-08-08	Marystown	Stewart	*GS-12-266*
STA-SF-12-054	649110	5251749	2012-08-08	Marystown	Stewart	
STA-SF-12-055	649133	5251369	2012-08-08	Marystown	Stewart	

STA-SF-12-056	649322	5251945	2012-08-08	Marystown	Stewart	
STA-SF-12-057	649257	5252079	2012-08-08	Marystown	Stewart	
STA-SF-12-058	649370	5252121	2012-08-08	Marystown	Stewart	*GS-12-270*
STA-SF-12-059	652653	5254451	2012-08-09	Marystown	Stewart	*GS-12-272*
STA-SF-12-060	652856	5254748	2012-08-09	Marystown	Stewart	
STA-SF-12-061	653225	5254749	2012-08-09	Marystown	Stewart	
STA-SF-12-062	653774	5254994	2012-08-09	Marystown	Stewart	
STA-SF-12-063	653723	5254995	2012-08-09	Marystown	Stewart	
STA-SF-12-064	653632	5255020	2012-08-09	Marystown	Stewart	*GS-12-280*
STA-SF-12-065	653569	5255053	2012-08-09	Marystown	Stewart	
STA-SF-12-066	653466	5255059	2012-08-09	Marystown	Stewart	
STA-SF-12-067	653410	5255057	2012-08-09	Marystown	Stewart	
STA-SF-12-068	653362	5255006	2012-08-09	Marystown	Stewart	
STA-SF-12-069	653299	5254910	2012-08-09	Marystown	Stewart	
STA-SF-12-070	653213	5255069	2012-08-09	Marystown	Stewart	
STA-SF-12-071	653177	5255039	2012-08-09	Marystown	Stewart	
STA-SF-12-072	653049	5255038	2012-08-09	Marystown	Stewart	
STA-SF-12-073	652861	5255633	2012-08-09	Marystown	Stewart	
STA-SF-12-074	652854	5255145	2012-08-09	Marystown	Stewart	
STA-SF-12-075	652821	5255166	2012-08-09	Marystown	Stewart	
STA-SF-12-076	652762	5255259	2012-08-09	Marystown	Stewart	
STA-SF-12-077	652700	5255297	2012-08-09	Marystown	Stewart	
STA-SF-12-078	652693	5255440	2012-08-09	Marystown	Stewart	
STA-SF-12-079	652679	5255565	2012-08-09	Marystown	Stewart	
STA-SF-12-080	652723	5255655	2012-08-09	Marystown	Stewart	
STA-SF-12-081	652643	5255709	2012-08-09	Marystown	Stewart	
STA-SF-12-082	652656	5255767	2012-08-09	Marystown	Stewart	
STA-SF-12-083	652601	5255888	2012-08-09	Marystown	Stewart	*GS-12-288*
STA-SF-12-084	652384	5255935	2012-08-09	Marystown	Stewart	
STA-SF-12-085	653479	5255197	2012-08-14	Marystown	Stewart	
STA-SF-12-086	653758	5255180	2012-08-14	Marystown	Stewart	
STA-SF-12-087	653780	5255157	2012-08-14	Marystown	Stewart	
STA-SF-12-088	653859	5255124	2012-08-14	Marystown	Stewart	
STA-SF-12-089	654119	5255216	2012-08-14	Marystown	Stewart	
STA-SF-12-090	654090	5255275	2012-08-14	Marystown	Stewart	
STA-SF-12-091	654088	5255656	2012-08-14	Marystown	Stewart	
STA-SF-12-092	654033	5255771	2012-08-14	Marystown	Stewart	
STA-SF-12-093	653884	5256014	2012-08-14	Marystown	Stewart	
STA-SF-12-094	653705	5256307	2012-08-14	Marystown	Stewart	
STA-SF-12-095	653546	5256285	2012-08-14	Marystown	Stewart	
STA-SF-12-096	653378	5256205	2012-08-14	Marystown	Stewart	
STA-SF-12-097	653300	5256025	2012-08-14	Marystown	Stewart	*GS-12-300*
STA-SF-12-098	653209	5255842	2012-08-14	Marystown	Stewart	*GS-12-301*
STA-SF-12-099	653195	5255618	2012-08-14	Marystown	Stewart	*GS-12-302*
STA-SF-12-100	653243	5255530	2012-08-14	Marystown	Stewart	
STA-SF-12-101	653258	5255488	2012-08-14	Marystown	Stewart	
STA-SF-12-102	654576	5255205	2012-08-15	Marystown	Stewart	*GS-12-303*
STA-SF-12-103	654494	5255286	2012-08-15	Marystown	Stewart	*GS-12-304*
STA-SF-12-104	654297	5255723	2012-08-15	Marystown	Stewart	*GS-12-305*
STA-SF-12-105	654279	5255735	2012-08-15	Marystown	Stewart	*GS-12-306*
STA-SF-12-106	654328	5255897	2012-08-15	Marystown	Stewart	*GS-12-308 to 310*
STA-SF-12-107	654321	5255950	2012-08-15	Marystown	Stewart	*GS-12-311*
STA-SF-12-108	654326	5256059	2012-08-15	Marystown	Stewart	*GS-12-312*
STA-SF-12-109	654208	5256116	2012-08-15	Marystown	Stewart	*GS-12-313*
STA-SF-12-110	654475	5256173	2012-08-15	Marystown	Forty Creek	
STA-SF-12-111	654594	5256173	2012-08-15	Marystown	Forty Creek	
STA-SF-12-112	654680	5256097	2012-08-15	Marystown	Forty Creek	

STA-SF-12-113	654772	5255892	2012-08-15	Marystown	Forty Creek	
STA-SF-12-114	654969	5255825	2012-08-15	Marystown	Forty Creek	SF-12-49, 50 a-h
STA-SF-12-115	645305	5272260	2012-08-16	Long Harbour	Long Harbour	SF-12-51 to 55; *GS-12-325*
STA-SF-12-116	645280	5272200	2012-08-16	Long Harbour	Long Harbour	SF-12-56 to 64
STA-SF-12-117	645374	5272371	2012-08-16	Long Harbour	Long Harbour	
STA-SF-12-118	645310	5272369	2012-08-16	Long Harbour	Long Harbour	SF-12-65
STA-SF-12-119	645356	5272668	2012-08-16	Long Harbour	Long Harbour	SF-12-66
STA-SF-12-120	655266	5256094	2012-08-17	Marystown	Stewart	*GS-12-327*
STA-SF-12-121	655263	5256140	2012-08-17	Marystown	Stewart	
STA-SF-12-122	655195	5256189	2012-08-17	Marystown	Stewart	
STA-SF-12-123	655199	5256235	2012-08-17	Marystown	Stewart	
STA-SF-12-124	655208	5256289	2012-08-17	Marystown	Stewart	
STA-SF-12-125	655169	5255924	2012-08-17	Marystown	Stewart	*GS-12-330*
STA-SF-12-126	655227	5255936	2012-08-17	Marystown	Stewart	
STA-SF-12-127	655266	5255943	2012-08-17	Marystown	Stewart	*GS-12-331*
STA-SF-12-128	655014	5255799	2012-08-17	Marystown	Stewart	*GS-12-332*
STA-SF-12-129	654929	5255615	2012-08-17	Marystown	Stewart	*GS-12-333*
STA-SF-12-130	654833	5255449	2012-08-17	Marystown	Stewart	
STA-SF-12-131	654509	5255009	2012-08-17	Marystown	Stewart	
STA-SF-12-132	654501	5255000	2012-08-17	Marystown	Stewart	
STA-SF-12-133	654323	5254857	2012-08-17	Marystown	Stewart	
STA-SF-12-134	654359	5254814	2012-08-17	Marystown	Stewart	*GS-12-334*
STA-SF-12-135	654422	5254712	2012-08-17	Marystown	Stewart	SF-12-70
STA-SF-12-136	691610	5286788	2012-08-20	Marystown	Tower	SF-12-104
STA-SF-12-137	686115	5289941	2012-08-22	Grandy's Pond Arenite Belt	-	SF-12-148
STA-SF-12-138	688151	5288458	2012-08-22	Grandy's Pond Arenite Belt	-	SF-12-149
STA-SF-12-139	699315	5295024	2012-08-23	Marystown	Hickey's Pond	SF-12-150 to 152
STA-SF-12-140	688801	5287550	2012-06-20	Marystown	Monkstown Rd	SF-12-153, 154
STA-SF-12-141 /Whaleback	585728	5196993	2012-07-09	Marystown	Heritage	SF-12-67
STA-SF-12-142 /P1C	585208	5195835	2012-07-09	Marystown	Heritage	SF-12-68, 68a
STA-SF-12-143 /P2	584744	5195041	2012-07-09	Marystown	Heritage	SF-12-69
STA-SF-13-144 /P4	584723	5195026	2013-05-09	Marystown	Heritage	SF-13-155 to 158
STA-SF-13-145 /P2	584755	5195056	2013-05-09	Marystown	Heritage	SF-13-159
STA-SF-13-146 /L1	584850	5195300	2013-05-09	Marystown	Heritage	SF-13-160, 161
STA-SF-13-147 /Ridge	585730	5196203	2013-05-10	Marystown	Heritage	SF-13-178
STA-SF-13-148 /Whaleback	585728	5196993	2013-05-10	Marystown	Heritage	SF-13-179
STA-SF-13-149 /Zaxis	585186	5196930	2013-05-10	Marystown	Heritage	SF-13-180

APPENDIX B: LITHOGEOCHEMICAL SAMPLE PREPARATION AND METHODS OF ANALYSIS

Seventy-one samples were prepared for geochemical analysis at the rock preparation facilities at Memorial University. Samples were broken using a titanium carbide splitter, or rock-sawed to remove weathering and reduce the sample into smaller fragments. The fragments were then pulverized into a powder using a tungsten carbide disk-mill. Thirty-five samples were sent to the Department of Natural Resouces GSNL Laboratory for major and trace element analysis, fourty-six were sent to Becquerel Laboratories for INAA using the Au+43 package, and eight samples were sent to Activation Laboratories for major and trace element analysis using the 4litho research package.

Department of Natural Resources GSNL Laboratory

Inductively coupled plasma emission spectrometry (ICP-OES) was used for the elements: Ag, Be, Cu, Li, Mn, Ni, Pb, Rb, Sc, Ti, and Zn, using analytical methods after Finch (1998), but using a 4-acid digestion of HF-$HClO_4$-HCl plus HNO_3 instead of the 3-acid digestion.

Major elements, and the trace elements Ba and Zr were analyzed using inductively coupled plasma optical emission spectrometry following lithium borate fusion (FUS-ICP). Fusion occurred at 1000^{O} C for 30 minutes in a graphite crucible using a blend of different lithium borates. The molten sample was mixed with a 10% solution of nitric acid and stirred until dissolved. The solution was then measured by a Thermo Instruments iCap 6500 Inductively Coupled Plasma Optical Emission Spectrometer.

The remaining trace and rare-earth elements were analyzed using inductively coupled plasma mass spectrometry with fusion (ICP-MS-FUS). The same procedure was followed as described for FUS-ICP above, however, before being measured, the solution was further diluted 20 times and mixed with a 2% solution of nitric acid and then

measured by a Thermo Instruments X-Series II Inductively Coupled Plasma Mass Spectrometer.

Volatiles were determined using the gravimetric methods, and reported as loss on ignition (LOI).

Activation Laboratories (4litho research package)

Samples were mixed with lithium metaborate and lithium tetraborate and fused in an induction furnace. The molten sample was combined with a solution of 5% HNO_3 and mixed until dissolved. Major elements and the trace elements Ba, Be, Sc, Sr, V, and Zr were then analyzed using inductively coupled plasma optical emission spectrometry (FUS-ICP). The remaining trace and rare-earth elements were analyzed using inductively couple plasma mass spectrometry (FUS-MS).

Becquerel Laboratories (Au+34 package)

Altered and mineralized samples were analyzed for Au and other trace elements using instrumental neutron activation analysis (INAA). Samples were transferred to watertight vials containing a flux monitor and exposed to a flux of neutrons at the McMaster Nuclear Reactor, with a flux of $8X10^{12}$ neutrons/cm^2/sec. Samples were irradiated for twenty minutes while being rotated. The samples were left for a standard decay period of six days and then measured using a gamma-ray spectrometer containing a high resolution, coaxial germanium detector.

Further details on the analytical procedures for Activation Laboratories and Becquerel Laboratories can be found on their respective websites (http://www.actlabs.com; http://maxxam.ca/services/radiochemistry-neutron-activation-analysis).

APPENDIX C: GEOCHEMICAL DATA

Three tables are included in this appendix:

Table C-1 contains major and trace element data for samples collected for this project analyzed at the Department of Natural Resources GSNL laboratory. Additional data are incorporated for samples that were also analyzed using INAA at Becquerel Laboratories (Au+34). One sample is included from an Honours BSc thesis done on the Big Easy prospect (Clarke, 2013; Memorial University).

Table C-2 contains major and trace element data for samples analyzed at Activation Laboratories using the 4litho research package. Included is one sample collected specifically for this project, as well as seven other samples collected at a later date by Graham Layne in affiliation with this project.

Table C-3 contains trace element data for altered and mineralized samples collected for this project, analyzed at Becquerel Laboratories using the INAA Au+34 package, except Ag, which was measured at the GSNL laboratory.

Negative values, or values containing 'less than' symbols, indicate that the concentration of the specific element was below the detection limit. Where no value has been entered, it is because that element was not analyzed for in the sample using that particular method of analysis. Iron was converted to total iron as FeO, denoted FeO*, where *FeO*=Fe2O3Totalx0.8998.* The major element oxides and trace elements presented in the tables have **not** been recalculated for volatiles to a total of 100%. However, both major element oxides and trace elements were recalculated for volatiles to a total of 100% for interpretation. The Mg# was used as a fractionation index for mafic rocks in *Chapter 3*, where *Mg#=(MgO/(MgO+FeO*))x100.*

Trace elements that were consistently at or below the detection limit include Cd, In, and Tl. These elements were kept in the dataset, but not used for any geochemical interpretation. The Ti data used for interpretation was calculated from the corresponding major element oxide.

Other geochemical data used in this thesis was supplied by Greg Sparkes and Hamish Sandeman of the Geological Survey of Newfoundland and Labrador, and can be referenced in the open file report NFLD/3265 (Sparkes and Sandeman, 2015). The specific samples used are listed below.

BE10-008	HS12-214	GS-11-27	GS-11-29	GS-11-30	GS-11-31
GS-11-32	GS-11-47	GS-11-52	GS-11-59	GS-11-65	GS-11-66
GS-11-74	GS-11-75	GS-11-76	GS-11-78	GS-11-79	GS-11-88
GS-11-89	GS-11-91	GS-11-94	GS-11-95	GS-11-96	GS-11-99
GS-11-100	GS-11-101	GS-11-105	GS-11-107	GS-11-154	GS-11-173
GS-11-175	GS-11-180	GS-11-181	GS-11-195	GS-11-210	GS-11-212
GS-11-213	GS-11-329	GS-11-358	GS-11-362	GS-11-379	GS-11-380
GS-11-381	GS-11-383	GS-11-385	GS-11-388	GS-11-433	GS-11-434
GS-11-455	GS-11-456	GS-11-457	GS-11-460	GS-11-461	GS-12-255
GS-12-262	GS-13-08	GS-13-021			

Table C-1

Sample	UTM E	UTM N	Lab #	Prospect/Location	Description	SiO2	Al2O3	Fe2O3Total	FeO*	Fe2O3	FeO	MnO	MgO	CaO	Na2O	K2O	TiO2	P2O5	LOI	Total
Unit						%	%	%	%	%	%	%	%	%	%	%	%	%	%	%
Analysis						FUS-ICP	FUS-ICP	FUS-ICP	FUS-ICP	FUS-ICP	FUS-ICP	FUS-ICP	FUS-ICP	FUS-ICP	FUS-ICP	FUS-ICP	FUS-ICP	FUS-ICP	Grav	
LOD						0.01	0.01	0.01	0.01	0.01	0.01	0.001	0.01	0.01	0.01	0.01	0.001	0.001	0.01	
GS-11-167	649789	5253902	7740821	Stewart	Caribou Tuff (dacite)	72.61	14.78	2.25	2.03	0.14	1.90	0.047	2.42	0.03	0.11	2.59	0.372	0.038	4.13	99.38
MC-BE12-2	-	-	7740851	Big Easy	mafic dyke, DDH BE-12-12 216m	51.89	14.99	10.68	9.61	1.69	8.09	0.217	4.64	4.40	2.97	4.09	1.842	0.402	3.39	99.52
SF-12-001	692347	5286171	7740822	Tower	hydrothermal alteration	71.69	16.11	4.63	4.16	2.08	2.29	0.003	0.05	0.04	0.08	1.91	0.539	0.089	5.33	100.48
SF-12-003	692349	5286182	7740823	Tower	hydrothermal alteration	54.02	16.81	2.23	2.00	1.98	0.22	0.002	0.04	0.07	1.88	2.29	0.648	0.139	19.93	98.05
SF-12-005	692369	5286194	7740824	Tower	hydrothermal alteration	47.26	18.13	16.27	14.64	16.01	0.23	0.011	-0.01	0.13	1.27	0.98	0.366	0.326	15.27	100.01
SF-12-015	692507	5286210	7740825	Tower	hydrothermal alteration	63.50	12.41	5.10	4.59	1.65	3.10	0.005	0.03	0.10	0.87	1.42	0.547	0.185	16.00	100.15
SF-12-026	692638	5286385	7740826	Tower	hydrothermal alteration	62.82	13.27	2.62	2.36	2.41	0.19	0.001	0.02	0.07	1.44	1.52	0.619	0.125	16.26	98.76
SF-12-027	655388	5256169	7740827	Stewart	basaltic andesite tuff	52.51	20.40	10.43	9.39	6.92	3.16	0.159	3.87	1.67	2.11	3.57	1.339	0.120	3.83	100.01
SF-12-041	650144	5253611	7740828	Stewart	mafic dyke	52.32	18.09	14.13	12.71	1.36	11.49	0.115	5.92	0.24	0.22	1.61	1.113	0.219	5.37	99.34
SF-12-043	650857	5254413	7740829	Stewart	Stewart Tuff (dacite)	76.73	13.14	1.36	1.23	0.22	1.03	0.074	0.43	0.99	4.31	2.93	0.185	0.036	0.75	100.95
SF-12-046	652055	5254398	7740831	Stewart	granite	74.26	13.62	1.93	1.74	1.21	0.65	0.045	0.43	0.88	3.46	2.96	0.302	0.049	1.39	99.31
SF-12-056	645256	5272243	7740832	Long Harbour	banded rhyolite	77.42	10.65	2.07	1.87	1.70	0.34	0.017	-0.01	0.02	2.20	4.93	0.153	0.019	0.73	98.17
SF-12-073	-	-	7740833	Stewart	tonalite, DDH ST-11-01 49m	73.83	16.57	3.17	2.85	1.47	1.53	0.003	0.04	0.10	0.18	0.57	0.524	0.122	4.86	99.97
SF-12-077	-	-	7740834	Stewart	hydrothermal alteration, DDH ST-11-01 89m	75.10	12.22	4.75	4.28	1.93	2.54	0.004	0.35	0.02	0.07	3.07	0.376	0.008	4.17	100.13
SF-12-084	-	-	7740835	Stewart	tonalite, DDH ST-11-01 141m	72.19	14.46	4.10	3.69	0.64	3.11	0.108	2.25	0.32	0.20	2.46	0.396	0.087	3.40	99.96
SF-12-085	-	-	7740836	Stewart	hydrothermal alteration, DDH ST-11-01 131m	77.01	15.29	1.76	1.59	0.40	1.23	0.001	0.03	0.14	0.12	0.27	0.420	0.109	3.79	98.94
SF-12-087	-	-	7740837	Stewart	tonalite, DDH ST-11-01 150m	72.56	14.64	4.17	3.75	0.36	3.43	0.106	1.16	0.25	0.18	2.73	0.381	0.092	2.90	99.16
SF-12-088	-	-	7740838	Stewart	tonalite, DDH ST-11-01 151m	73.92	12.61	6.10	5.49	3.07	2.73	0.021	0.27	0.07	0.13	2.70	0.316	0.040	4.76	100.93
SF-12-102	-	-	7740891	Stewart	mafic dyke, DDH ST-11-02 49m	50.38	17.16	10.71	9.64	2.06	7.79	0.320	7.23	3.22	3.65	0.12	1.217	0.368	4.97	99.33
SF-12-103	-	-	7740839	Stewart	Caribou Tuff (dacite), DDH ST-11-02 50m	73.03	14.97	2.99	2.69	0.60	2.15	0.022	0.89	0.47	0.07	4.14	0.415	0.061	3.23	100.29
SF-12-104	691610	5286788	7740841	Tower	intermediate tuff	75.19	12.90	2.40	2.16	1.41	0.89	0.070	0.46	3.05	3.05	0.87	0.340	0.035	1.28	99.63
SF-12-108	-	-	7740842	Stewart	Stewart Tuff (dacite), DDH ST-11-01 435m	74.43	12.98	1.66	1.49	0.69	0.87	0.078	0.52	3.12	3.12	1.32	0.233	0.056	1.35	98.87
SF-12-109	-	-	7740843	Stewart	Caribou Tuff (dacite), DDH ST-11-01 431m	75.28	15.20	2.14	1.93	0.24	1.71	0.019	0.68	0.07	0.26	3.83	0.344	0.040	2.87	100.73
SF-12-111	-	-	7740844	Stewart	Caribou Tuff (dacite), DDH ST-11-02 91m	72.10	14.58	2.74	2.46	1.08	1.49	0.017	0.92	0.22	0.42	3.85	0.388	0.075	3.47	98.78
SF-12-115	-	-	7740845	Stewart	hydrothermal alteration, DDH ST-11-02 234m	61.43	17.36	7.32	6.58	4.93	2.15	0.004	-0.01	0.21	0.41	1.01	0.805	0.377	10.90	99.83
SF-12-139	-	-	7740846	Stewart	basalt, DDH ST-11-03 138m	44.36	16.84	10.90	9.81	4.80	5.49	0.181	10.68	10.13	1.72	0.26	0.821	0.127	4.27	100.29
SF-12-142	-	-	7740847	Stewart	dacite dyke, DDH ST-11-03 377m	75.62	13.17	1.31	1.18	0.00	0.00	0.028	0.39	0.43	3.64	4.04	0.252	0.039	1.58	100.50
SF-12-148	686115	5289941	7740848	Monkstown Rd	Grandy's Pond Arenite	61.39	16.31	6.42	5.77	3.31	2.80	0.159	3.04	2.20	6.45	1.40	0.756	0.150	1.97	100.23
SF-12-149	688151	5288458	7740849	Monkstown Rd	Grandy's Pond Arenite	60.17	17.57	5.88	5.29	4.47	1.27	0.173	1.22	2.26	6.72	2.13	0.872	0.081	1.83	98.90
SF-13-161	584488	5195247	7740896	Heritage	mafic dyke, Trench L1	42.15	15.81	10.14	9.13	1.90	7.42	0.346	4.50	10.48	0.13	3.17	1.214	0.340	11.66	99.94
SF-13-164	-	-	7740897	Heritage	mafic dyke, DDH HD-05-13 69m	46.07	17.55	11.21	10.08	3.46	6.97	0.313	6.35	5.42	2.97	2.14	1.014	0.217	6.77	100.02
SF-13-178	585730	5196203	7740898	Heritage	mafic dyke, Ridge Trench	52.42	17.33	9.40	8.46	2.26	6.43	0.336	2.94	3.93	5.01	2.44	1.249	0.287	4.04	99.38
SF-13-180	585186	5196930	7740899	Heritage	andesite tuff, Zaxis Trench (aka T(1)-13-12)	65.57	14.18	5.16	4.64	1.24	3.53	0.205	2.07	2.17	2.67	2.72	0.627	0.149	3.73	99.27
SF-13-181	-	-	7740901	Big Easy	andesite tuff, DDH BE-12-8 68m)	69.03	10.15	7.03	6.32	1.32	5.14	0.159	3.20	1.15	0.05	2.10	0.970	0.256	4.20	98.31
SF-13-185	584820	5193308	7740902	Heritage	basalt (aka HBQ1)	51.67	18.56	8.30	7.47	5.51	2.51	0.133	1.60	8.46	3.30	1.11	1.034	0.222	4.32	98.70

Au	Ag	Ag	As	As	Ba	Ba	Be	Bi	Bi	Cd	Ce	Co	Cr	Cr	Cs	Cs	Cu	Dy	Er	Eu
ppb	ppm	ppm	ppm	ppm	ppm	ppm	ppm	ppm	ppm	ppm	ppm	ppm	ppm	ppm	ppm	ppm	ppm	ppm	ppm	ppm
INAA	ICP-OES	ICP-OES	ICP-MS-FUS	ICP-MS-FUS	FUS-ICP	ICP-MS-FUS	ICP-OES	ICP-MS-FUS	ICP-MS-FUS	ICP-MS-FUS	ICP-MS-FUS	ICP-MS-FUS	ICP-MS-FUS	FUS-ICP	ICP-MS-FUS	ICP-MS-FUS	ICP-OES	ICP-MS-FUS	ICP-MS-FUS	ICP-MS-FUS
1	0.05	0.1	0.50	5.00	1.00	1.00	0.10	0.10	0.40	0.20	0.10	1.00	1.00	1.00	0.10	0.50	1.00	0.10	0.10	0.05
-	-	0.1	3.58	-	1143.33	1070.00	2.68	-0.10	-	-0.20	59.60	63.78	1.00	-	1.80	-	8	2.85	1.77	0.937
-	-	-0.1	8.87	-	525.81	467.80	3.14	0.90	-	-0.20	51.41	27.63	104.30	-	1.66	-	46	8.22	4.82	2.266
11	-	-0.1	3.34	-	521.11	464.30	0.48	0.28	-	-0.20	49.13	56.28	3.90	-	0.63	-	43	0.69	0.61	0.511
-1	-	-0.1	2.82	-	894.49	837.80	0.16	0.46	-	-0.20	55.35	44.40	4.98	-	-0.10	-	4	0.71	0.79	0.920
2	-	-0.1	1.93	-	1466.50	1362.00	0.13	0.64	-	-0.20	57.80	50.32	3.41	-	-0.10	-	3	0.97	0.58	1.544
117	-	0.1	5.44	-	1098.06	1028.00	0.11	1.08	-	0.29	50.97	118.10	2.11	-	-0.10	-	36	0.61	0.40	0.815
21	-	-0.1	3.10	-	554.01	534.60	0.13	-0.10	-	-0.20	20.04	84.72	-1.00	-	0.14	-	5	0.91	0.75	0.275
-	-	-0.1	5.45	-	826.86	751.70	1.38	0.12	-	-0.20	66.20	49.42	28.79	-	4.67	-	14	4.54	2.48	1.812
-	-	-0.1	2.69	-	431.06	400.50	0.84	0.20	-	-0.20	27.72	53.37	25.52	-	0.79	-	16	3.51	2.10	1.111
-	-	-0.1	0.78	-	971.30	902.20	1.30	0.13	-	-0.20	43.53	136.10	1.58	-	0.95	-	2	2.43	1.61	0.534
-	-	-0.1	0.74	-	805.99	753.00	1.68	0.12	-	-0.20	61.51	63.96	-1.00	-	1.98	-	5	4.06	2.74	1.029
-	-	-0.1	3.67	-	49.81	51.83	2.33	0.11	-	-0.20	87.06	160.00	2.01	-	1.38	-	2	14.67	11.67	0.515
12	-	0.1	7.55	-	644.42	600.70	0.43	0.19	-	0.22	48.81	40.49	2.91	-	0.29	-	215	3.16	2.35	0.870
20	-	0.1	1.66	-	769.03	721.70	0.64	0.16	-	-0.20	24.42	108.00	5.25	-	0.95	-	503	1.10	0.90	0.281
21	-	0.2	2.76	-	778.77	713.10	2.43	-0.10	-	-0.20	36.51	76.42	2.32	-	1.38	-	713	2.05	1.22	0.740
12	-	-0.1	3.38	-	70.52	63.25	0.31	0.15	-	-0.20	39.18	45.98	2.86	-	0.26	-	22	0.71	0.37	0.443
20	-	-0.1	3.12	-	897.98	796.20	2.28	-0.10	-	-0.20	47.96	86.72	-1.00	-	1.48	-	315	2.08	1.30	0.945
128	-	0.2	6.46	-	871.49	792.80	0.85	0.34	-	-0.20	38.63	105.70	1.45	-	1.21	-	725	2.11	1.37	0.649
7	0.36	-	-	5.06	29.79	-	1.19	-	0.49	-0.20	65.46	42.69	-	136.28	-	-0.50	81	4.37	2.31	3.010
2	-	-0.1	3.75	-	830.33	755.50	1.60	-0.10	-	-0.20	52.27	43.81	3.48	-	2.98	-	7	2.98	2.00	0.777
-	-	-0.1	6.05	-	251.62	232.10	1.30	0.11	-	-0.20	62.59	69.93	0.76	-	2.50	-	6	5.68	3.65	0.971
-	-	-0.1	4.15	-	597.01	558.50	1.44	-0.10	-	-0.20	46.75	88.56	1.86	-	1.27	-	16	2.67	1.63	0.686
5	-	0.1	60.50	-	709.31	648.80	0.70	-0.10	-	-0.20	41.38	78.65	0.83	-	3.00	-	68	3.26	2.33	0.777
3	-	0.2	3.09	-	847.44	767.90	1.03	-0.10	-	-0.20	64.63	51.40	3.53	-	2.27	-	9	3.12	1.96	0.721
4	-	-0.1	2.34	-	845.76	750.60	0.26	0.11	-	-0.20	70.13	44.83	7.62	-	0.18	-	29	1.48	0.66	1.316
2	-	-0.1	1.81	-	65.01	58.56	0.33	0.20	-	-0.20	13.97	59.89	520.10	-	0.49	-	18	2.73	1.61	1.007
-1	-	-0.1	4.01	-	1023.75	920.10	1.82	0.31	-	0.21	63.48	135.10	1.65	-	0.37	-	42	2.74	1.67	0.731
-	-	-0.1	4.02	-	327.18	290.60	1.16	-0.10	-	-0.20	36.85	65.97	22.55	-	0.80	-	3	4.02	2.51	1.498
-	-	-0.1	3.46	-	959.74	904.30	1.72	0.12	-	-0.20	54.18	66.65	16.99	-	0.74	-	26	4.63	2.65	3.314
-	0.21	-	-	7.54	190.68	-	1.54	-	-0.40	-0.20	34.10	123.00	-	79.82	-	3.02	58	4.29	2.14	1.471
-	0.39	-	-	-5.00	425.42	-	0.96	-	0.48	0.26	34.85	51.90	-	7.81	-	3.89	64	3.30	1.88	1.353
-	0.37	-	-	-5.00	566.36	-	1.38	-	-0.40	-0.20	57.43	47.55	-	7.03	-	1.02	81	5.55	3.35	1.664
-	-0.05	-	-	-5.00	206.49	-	1.42	-	0.43	-0.20	41.62	111.20	-	3.19	-	1.79	11	5.14	2.96	1.060
-	0.53	-	-	85.23	81.64	-	1.80	-	-0.40	-0.20	45.78	40.12	-	14.08	-	1.76	19	6.33	3.64	2.507
-	0.16	-	-	52.89	376.45	-	0.84	-	0.71	0.23	39.93	61.69	-	6.24	-	2.49	63	3.37	2.04	1.309

Ga	Ge	Gd	Hf	Ho	In	In	La	Li	Lu	Mn	Mo	Mo	Nb	Nd	Ni	Pb	Pb	Pr	Rb
ppm	ppm	ppm	ppm	ppm	ppm	ppm	ppm	ppm	ppm	ppm	ppm	ppm	ppm	ppm	ppm	ppm	ppm	ppm	ppm
ICP-MS-FUS	ICP-MS-FUS	ICP-MS-FUS	ICP-MS-FUS	ICP-MS-FUS	ICP-MS-FUS	ICP-MS-FUS	ICP-MS-FUS	ICP-OES	ICP-MS-FUS	ICP-OES	ICP-MS-FUS	ICP-MS-FUS	ICP-MS-FUS	ICP-MS-FUS	ICP-OES	ICP-MS-FUS	ICP-OES	ICP-MS-FUS	ICP-MS-FUS
1.00	0.01	0.10	0.20	0.10	0.10	0.20	0.50	0.10	0.05	1.00	1.00	2.00	1.00	0.10	1.00	5.00	1.00	0.05	2.00
16.05	2.082	4.13	5.32	0.56	-0.10	-	31.03	16.52	0.346	381.87	4.29	-	9.14	23.62	1.91	60.70	123.41	6.476	68.04
19.47	3.241	8.46	6.89	1.63	0.16	-	21.68	23.88	0.672	1542.40	1.20	-	12.14	32.43	34.82	26.22	-1.00	6.934	94.91
22.38	1.333	1.36	4.81	0.15	-0.10	-	29.57	0.56	0.207	32.43	10.74	-	9.37	14.90	4.75	20.08	39.67	4.788	22.73
16.65	2.533	1.67	4.19	0.27	-0.10	-	29.80	-0.10	0.211	14.37	1.07	-	7.78	22.16	-1.00	23.19	24.22	6.046	3.52
11.94	12.270	2.92	3.66	0.17	-0.10	-	28.93	-0.10	0.150	49.01	40.37	-	5.41	25.48	4.60	292.00	353.94	6.820	2.13
8.94	2.751	1.44	3.37	0.13	-0.10	-	27.03	0.40	0.126	34.79	56.63	-	5.76	19.18	5.03	199.80	281.81	5.543	2.88
11.87	1.656	0.95	3.29	0.24	-0.10	-	11.32	-0.10	0.136	19.81	3.24	-	6.77	7.85	-1.00	18.13	13.99	2.058	4.25
25.64	5.616	5.23	4.45	0.86	-0.10	-	34.85	49.28	0.379	1148.32	1.41	-	10.48	30.53	19.49	13.87	-1.00	0.000	115.90
20.21	3.624	4.03	2.55	0.69	-0.10	-	12.00	163.92	0.315	830.88	-1.00	-	5.49	15.71	25.30	23.18	4.45	3.578	38.45
10.25	0.938	2.82	3.02	0.43	-0.10	-	24.41	4.59	0.273	579.09	-1.00	-	12.85	16.65	4.87	6.24	3.06	4.799	56.43
13.91	2.244	4.50	4.86	0.86	-0.10	-	30.59	6.97	0.430	340.40	-1.00	-	10.02	26.46	1.10	8.02	12.58	7.180	76.60
22.33	2.464	8.18	17.07	3.53	0.11	-	35.84	8.00	1.608	145.15	1.38	-	29.41	33.27	-1.00	15.35	16.17	8.239	143.80
21.08	1.954	3.46	5.08	0.73	-0.10	-	26.98	3.29	0.461	26.16	9.18	-	9.95	18.59	2.19	46.67	89.31	5.170	13.45
14.12	2.877	1.26	4.30	0.25	0.38	-	14.22	3.50	0.163	42.65	34.60	-	7.98	7.80	4.16	16.51	24.76	2.404	64.44
15.34	2.979	2.46	4.15	0.39	-0.10	-	17.75	48.55	0.210	813.28	26.50	-	8.84	14.45	3.64	41.50	66.20	4.213	54.19
5.32	2.778	1.43	4.36	0.13	-0.10	-	21.56	3.12	0.111	16.69	9.44	-	7.32	13.35	-1.00	18.13	18.19	4.110	6.74
11.70	3.916	2.87	4.13	0.38	0.20	-	23.48	29.44	0.233	840.97	14.33	-	10.49	18.60	3.88	24.81	36.56	5.104	64.23
11.85	1.598	2.44	3.08	0.48	1.24	-	21.85	6.71	0.213	176.68	13.61	-	7.96	13.40	5.63	25.54	49.48	3.971	61.65
17.93	3.310	5.81	2.63	0.78	-	-0.20	32.74	88.87	0.249	2217.58	-	-2.00	5.95	33.95	63.53	-	12.48	8.279	-
17.04	1.376	2.93	4.55	0.59	-0.10	-	24.51	9.35	0.313	182.57	2.67	-	9.83	20.63	3.12	11.40	15.86	5.591	98.27
13.59	3.138	6.03	6.75	1.25	-0.10	-	28.59	3.92	0.597	536.03	-1.00	-	14.03	27.18	1.68	9.89	9.98	7.125	25.63
10.36	1.926	2.87	2.72	0.53	-0.10	-	25.21	3.21	0.276	598.88	0.70	-	9.11	16.50	2.20	18.02	20.85	4.786	46.75
12.85	2.654	3.48	4.62	0.66	0.10	-	20.30	3.94	0.383	157.58	4.09	-	8.93	18.34	2.55	15.04	10.52	4.806	100.90
14.79	2.563	3.55	4.85	0.62	-0.10	-	35.25	10.12	0.323	136.27	2.39	-	8.33	24.81	2.32	22.30	141.84	6.969	93.01
21.08	2.428	4.49	4.50	0.20	0.10	-	33.60	0.46	0.149	40.63	5.43	-	10.14	29.64	9.22	81.26	208.29	7.857	14.39
15.13	2.547	2.58	1.33	0.54	-0.10	-	6.09	16.11	0.235	1179.13	-1.00	-	1.88	9.25	126.23	17.98	-1.00	1.928	5.47
13.52	1.901	3.65	4.17	0.58	-0.10	-	32.41	2.90	0.329	240.64	2.58	-	17.25	22.91	1.23	5.76	20.18	6.797	71.09
17.43	2.079	4.39	2.87	0.82	-0.10	-	18.53	14.61	0.359	1152.63	0.92	-	6.70	18.85	11.99	19.99	3.80	4.539	29.46
20.32	3.855	5.57	6.60	0.90	-0.10	-	28.87	12.79	0.422	1245.90	0.55	-	10.83	28.03	8.53	27.68	2.89	6.759	42.73
18.04	3.236	4.56	2.52	0.77	-	-0.20	15.47	86.64	0.303	2441.92	-	-2.00	6.04	20.10	50.09	-	-1.00	4.388	-
17.17	2.667	4.14	1.93	0.63	-	-0.20	16.51	98.13	0.230	2193.94	-	-2.00	3.09	20.08	22.67	-	-1.00	4.539	-
20.07	3.396	6.11	4.67	1.11	-	-0.20	27.69	41.28	0.445	2384.16	-	2.23	10.24	30.28	15.34	-	-1.00	7.396	-
19.11	2.245	4.75	3.91	1.04	-	-0.20	20.97	32.14	0.466	1557.57	-	-2.00	9.32	20.60	6.85	-	-1.00	5.030	-
21.61	2.529	6.38	4.64	1.16	-	-0.20	17.45	41.86	0.537	1252.83	-	1.86	7.08	28.00	16.79	-	-1.00	6.232	-
17.88	3.278	4.06	2.47	0.65	-	-0.20	20.14	35.21	0.255	959.34	-	-2.00	5.30	20.82	12.25	-	1.40	4.897	-

Rb	Sb	Sc	Se	Sm	Sn	Sr	Ta	Tb	Te	Ti	Th	Tl	Tm	U	V	W	Y	Yb	Zn	Zr
ppm	ppm	ppm	ppm	ppm	ppm	ppm	ppm	ppm	ppm	ppm	ppm	ppm	ppm	ppm	ppm	ppm	ppm	ppm	ppm	ppm
ICP-OES	INAA	ICP-OES	INAA	ICP-MS-FUS	ICP-MS-FUS	ICP-MS-FUS	ICP-MS-FUS	ICP-MS-FUS	INAA	ICP-OES	ICP-MS-FUS	ICP-MS-FUS	ICP-MS-FUS	ICP-MS-FUS	ICP-MS-FUS	ICP-MS-FUS	ICP-MS-FUS	ICP-MS-FUS	ICP-OES	FUS-ICP
1.00	0.10	0.10	1	0.10	1.00	2.00	0.50	0.10	20	1.00	0.10	0.10	0.05	0.10	5.00	1.00	1.00	0.10	1.00	1.00
-	-	5.46	-	4.00	3.08	45.44	1.28	0.50	-	577.06	10.45	-0.10	0.27	2.03	29.71	243.20	15.25	1.97	180.51	204.15
-	-	34.21	-	8.31	2.32	185.30	0.94	1.29	-	12206.08	4.09	-0.10	0.65	1.02	212.40	2.23	41.35	4.43	100.31	298.71
-	0.30	7.55	-1	1.99	2.79	147.70	1.11	0.15	-20	220.31	11.20	-0.10	0.11	1.21	74.14	219.00	4.17	1.13	20.81	198.02
-	1.00	7.38	-1	3.52	2.78	311.10	0.81	0.16	-20	305.31	9.40	-0.10	0.15	1.12	88.15	189.50	4.78	1.16	4.25	176.36
-	-0.10	4.16	-1	3.78	7.04	759.90	1.39	0.20	-20	471.73	9.03	-0.10	0.09	1.60	153.60	223.70	4.00	0.96	6.02	140.15
-	-0.10	6.02	-2	2.68	10.99	225.00	2.01	0.15	-20	478.67	7.52	-0.10	0.08	1.03	76.00	404.60	3.40	0.69	9.10	134.16
-	0.10	5.40	-1	0.97	2.67	278.70	1.16	0.13	-20	439.03	4.22	-0.10	0.10	0.64	108.30	343.30	6.02	0.81	4.08	123.35
-	-	34.30	-	5.53	1.20	197.20	1.58	0.81	-	8049.42	4.71	-0.10	0.35	1.14	153.60	62.00	22.95	2.47	102.15	180.53
-	-	35.97	-	4.11	1.39	55.59	1.11	0.56	-	5141.28	3.93	-0.10	0.33	0.86	304.00	65.34	17.08	1.85	260.70	91.35
-	-	4.06	-	2.84	0.81	127.40	4.18	0.35	-	1266.33	10.39	-0.10	0.24	2.37	11.75	492.90	13.48	1.88	28.62	92.59
-	-	5.01	-	5.03	5.13	91.90	2.39	0.55	-	1870.98	8.87	-0.10	0.35	1.80	15.22	237.30	20.03	2.99	38.10	169.12
-	-	1.77	-	6.44	7.38	16.21	5.31	1.85	-	1025.84	18.26	-0.10	1.75	1.78	0.86	572.10	88.58	10.95	54.81	613.03
-	0.70	7.21	-1	3.49	4.76	267.80	1.43	0.49	-20	533.19	11.06	-0.10	0.38	4.47	48.16	150.00	20.22	2.93	56.76	201.06
-	-0.10	7.70	-1	1.12	4.86	38.62	3.18	0.14	-20	467.11	11.25	-0.10	0.11	2.15	39.20	428.40	6.59	1.12	45.49	165.80
-	-0.10	6.18	-1	3.27	3.98	135.70	2.23	0.28	-20	1081.59	9.78	-0.10	0.18	1.77	37.75	292.10	9.30	1.19	382.27	159.90
-	-0.10	3.01	-1	2.20	7.00	21.65	2.41	0.16	-20	645.49	10.29	-0.10	0.07	1.33	37.03	180.50	3.19	0.66	15.45	175.36
-	-0.10	6.75	-1	3.19	4.10	112.70	2.49	0.35	-20	1845.43	9.85	-0.10	0.17	1.27	42.19	301.10	11.34	1.44	362.91	173.82
-	-0.10	6.07	-1	2.44	3.92	98.74	2.58	0.32	-20	1096.92	7.26	-0.10	0.19	1.63	32.99	373.00	11.24	1.35	98.18	137.56
5.35	0.80	35.57	2	6.99	0.83	211.60	0.63	0.77	-20	7715.55	3.26	-0.10	0.24	0.65	260.70	37.16	22.98	2.08	133.35	108.84
-	-0.10	7.36	-1	3.61	2.45	20.25	1.08	0.45	-20	2541.09	9.79	-0.10	0.28	2.11	36.57	145.60	15.91	1.95	36.19	187.15
-	-	12.04	-	5.61	2.85	343.60	2.46	0.94	-	2283.27	14.09	-0.10	0.54	3.15	9.64	243.40	31.78	3.53	56.82	252.98
-	-	4.90	-	2.90	1.49	307.80	2.07	0.40	-	1400.62	9.62	-0.10	0.23	2.24	15.29	318.20	13.78	1.54	52.84	96.78
-	-0.10	11.57	-1	3.53	9.98	28.01	1.78	0.50	-20	756.41	9.31	-0.10	0.36	2.13	31.96	288.90	19.35	2.62	58.00	167.92
-	-0.10	7.01	-1	4.32	2.30	22.46	1.83	0.51	-20	1315.84	9.99	-0.10	0.28	2.30	31.27	193.30	16.40	2.13	526.91	193.68
-	0.20	7.66	15	5.67	5.23	750.10	0.90	0.46	-20	1161.38	5.67	-0.10	0.10	1.49	104.80	131.10	4.62	0.80	19.61	176.03
-	-0.10	30.18	-1	2.23	-1.00	359.40	-0.50	0.44	-20	4946.31	0.71	-0.10	0.24	0.17	214.50	61.41	13.90	1.59	75.12	47.28
-	-0.10	3.90	-1	4.37	0.85	122.60	4.91	0.46	-20	1542.31	12.19	-0.10	0.27	2.73	14.23	485.20	17.28	2.01	32.43	148.99
-	-	19.78	-	4.22	1.08	177.70	2.88	0.67	-	4588.60	3.63	-0.10	0.33	0.84	83.22	181.60	21.29	2.26	96.13	111.60
-	-	9.48	-	6.16	2.03	244.90	2.40	0.73	-	5666.36	4.22	-0.10	0.36	1.24	48.72	203.30	24.17	2.63	91.75	315.40
276.50	-	28.61	-	4.56	0.79	122.10	0.65	0.69	-	7504.00	2.03	-0.10	0.29	0.44	256.20	19.56	20.78	2.10	100.29	95.88
109.71	-	34.04	-	4.93	0.73	458.60	0.73	0.58	-	6334.30	3.12	-0.10	0.25	0.67	298.30	59.03	16.76	1.75	113.92	70.82
103.24	-	27.14	-	6.71	1.62	363.60	1.82	0.99	-	7907.97	5.37	-0.10	0.46	1.25	265.10	87.90	28.61	2.96	86.89	164.12
184.90	-	18.48	-	4.55	1.80	101.60	1.87	0.80	-	3728.99	5.20	-0.10	0.48	1.00	74.36	147.70	27.72	3.31	71.57	133.82
138.15	-	20.02	-	6.29	1.67	7.82	1.45	1.02	-	6652.61	2.41	-0.10	0.52	0.68	72.92	91.43	33.81	3.68	84.46	179.30
47.78	-	26.68	-	4.55	0.91	702.00	1.87	0.60	-	6711.42	4.66	-0.10	0.29	0.77	240.60	151.70	18.46	1.75	67.70	88.08

Table C-2

Sample				*SF-12-138*	*HBQ-3B*	*SCB-2*	*SCB-3A*	*SWC-2*	*GDL15-01*	*GS-WPR-GREY*	*GS-WPR-RED*
Prospect/Location				Stewart	Heritage	Seal Cove	Seal Cove	Swift Current	Big Easy	West Princess	West Princess
UTM E				-	584820	619407	619407	710696	710440	-	-
UTM N				-	5193308	5228793	5228793	5306734	5351242	-	-
Rock Type				basalt	basalt	granodiorite	diorite	granite	mafic dyke	rhyolite	rhyolite
	Unit	Analysis	LOD								
SiO2	%	FUS-ICP	0.01	50.70	50.77	71.56	58.02	72.82	42.44	77.39	71.65
Al2O3	%	FUS-ICP	0.01	17.60	18.19	14.05	16.05	13.85	17.38	11.68	14.85
Fe2O3Total	%	FUS-ICP	0.01	10.72	10.19	3.64	8.26	2.23	12.52	1.69	2.01
FeO*	%	FUS-ICP		9.65	9.17	3.28	7.43	2.01	11.27	1.52	1.81
MnO	%	FUS-ICP	0.001	0.135	0.151	0.058	0.143	0.061	0.370	0.033	0.033
MgO	%	FUS-ICP	0.01	4.99	3.35	0.63	3.00	0.58	7.97	0.13	0.41
CaO	%	FUS-ICP	0.01	8.00	8.14	2.14	6.56	1.58	5.54	0.45	0.83
Na2O	%	FUS-ICP	0.01	3.64	3.12	3.67	3.03	3.36	2.96	4.03	4.84
K2O	%	FUS-ICP	0.01	0.58	0.48	3.30	2.22	4.34	2.55	3.59	3.82
TiO2	%	FUS-ICP	0.001	1.053	1.148	0.383	1.433	0.316	1.866	0.187	0.287
P2O5	%	FUS-ICP	0.01	0.130	0.240	0.080	0.260	0.090	0.320	0.040	0.050
LOI	%			2.16	4.12	0.99	0.96	0.77	6.45	0.35	0.69
Total	%		0.01	99.71	99.90	100.50	99.95	100.00	100.40	99.57	99.47
Ag	ppm	FUS-MS	0.5	< 0.5	< 0.5	< 0.5	< 0.5	< 0.5	< 0.5	< 0.5	< 0.5
As	ppm	FUS-MS	5	< 5	< 5	< 5	< 5	< 5	< 5	< 5	< 5
Ba	ppm	FUS-ICP	3	164	189	604	542	837	1846	778	859
Be	ppm	FUS-ICP	1	< 1	1	3	2	2	2	2	2
Bi	ppm	FUS-MS	0.1	< 0.1	< 0.1	< 0.1	< 0.1	< 0.1	< 0.1	< 0.1	< 0.1
Ce	ppm	FUS-MS	0.05	20	43.1	76	63.8	69.6	33.4	56.9	87.9
Co	ppm	FUS-MS	1	132	54	128	98	117	50	150	85
Cr	ppm	FUS-MS	20	< 20	30	50	20	60	170	< 20	30
Cs	ppm	FUS-MS	0.1	0.8	3	2.4	3.3	1.1	2.8	0.6	1.6
Cu	ppm	FUS-MS	10	< 10	40	< 10	30	< 10	120	< 10	< 10
Dy	ppm	FUS-MS	0.01	2.75	3.55	6.75	5.33	3.88	5.74	3.53	4.77
Er	ppm	FUS-MS	0.01	1.5	2.03	4.09	3.02	2.31	3.33	2.25	3.09
Eu	ppm	FUS-MS	0.005	1.03	1.27	1.35	1.61	1.09	1.84	0.794	1.2
Ga	ppm	FUS-MS	1	16	17	17	17	14	17	9	15
Gd	ppm	FUS-MS	0.01	2.96	4.13	6.67	5.76	4.09	5.81	3.14	4.62
Ge	ppm	FUS-MS	0.5	0.8	1.4	1.2	1	1	0.8	0.5	0.7
Hf	ppm	FUS-MS	0.1	1.5	2.4	5.6	5.2	4.4	3.1	3.4	4.9
Ho	ppm	FUS-MS	0.01	0.54	0.7	1.37	1.05	0.78	1.14	0.73	1.01
In	ppm	FUS-MS	0.1	< 0.1	< 0.1	< 0.1	< 0.1	< 0.1	< 0.1	< 0.1	< 0.1
La	ppm	FUS-MS	0.05	8.83	20.7	36.3	30.1	33.4	13.5	27	46.5
Lu	ppm	FUS-MS	0.002	0.203	0.299	0.616	0.481	0.404	0.47	0.44	0.521
Mo	ppm	FUS-MS	2	< 2	< 2	< 2	< 2	< 2	< 2	< 2	< 2
Nb	ppm	FUS-MS	0.2	2.5	4.5	9.5	17.2	7.2	6.5	8.2	12.1
Nd	ppm	FUS-MS	0.05	12.7	21	33.5	31.2	26.7	20.8	20.4	31.1
Ni	ppm	FUS-MS	20	< 20	< 20	< 20	< 20	< 20	60	< 20	< 20
Pb	ppm	FUS-MS	5	< 5	9	14	12	12	< 5	7	15
Pr	ppm	FUS-MS	0.01	2.59	5.1	8.68	7.42	7.24	4.5	5.82	8.89
Rb	ppm	FUS-MS	1	11	13	126	74	144	63	63	88
Sb	ppm	FUS-MS	0.2	< 0.2	< 0.2	< 0.2	< 0.2	< 0.2	< 0.2	< 0.2	< 0.2
Sc	ppm	FUS-ICP	1	25	28	11	23	4	39	3	4
Sm	ppm	FUS-MS	0.01	3.01	4.63	7.34	6.38	4.97	5.68	3.85	5.95
Sn	ppm	FUS-MS	1	2	2	3	3	2	3	3	4
Sr	ppm	FUS-ICP	2	594	473	147	390	235	345	60	95
Ta	ppm	FUS-MS	0.01	2.01	0.85	5.64	3.27	3.07	0.55	4.84	2.83
Tb	ppm	FUS-MS	0.01	0.46	0.62	1.09	0.91	0.66	0.96	0.56	0.78
Th	ppm	FUS-MS	0.05	0.61	5.11	10.7	7.55	15.9	0.93	11.1	13.6
Tl	ppm	FUS-MS	0.05	< 0.05	< 0.05	0.43	0.29	0.51	0.24	0.24	0.28
Tm	ppm	FUS-MS	0.005	0.215	0.305	0.628	0.447	0.359	0.489	0.381	0.478
U	ppm	FUS-MS	0.01	0.2	1.06	2.43	1.75	2.61	0.35	1.54	8.36
V	ppm	FUS-ICP	5	259	286	25	151	26	359	9	21
W	ppm	FUS-MS	0.5	380	99.3	548	331	499	31.1	592	323
Y	ppm	FUS-MS	0.5	14.1	19.3	37.4	29.1	22.2	30.6	21.5	29.6
Yb	ppm	FUS-MS	0.01	1.42	1.91	3.99	2.98	2.54	3.08	2.72	3.34
Zn	ppm	FUS-MS	30	90	80	50	90	40	110	30	50
Zr	ppm	FUS-ICP	1	59	98	241	206	189	139	129	201

Table C-3

Sample				*SF-12-001*	*SF-12-002*	*SF-12-003*	*SF-12-004*	*SF-12-005*	*SF-12-006*	*SF-12-008*	*SF-12-009*	*SF-12-012*	*SF-12-013*	*SF-12-015*	*SF-12-016*	*SF-12-022*	*SF-12-026*
Lab #				7740822	7740864	7740823	7740865	7740824	7740866	7740867	7740868	7740869	7740871	7740825	7740872	7740873	7740826
Prospect/Location				Tower	Tower	Tower	Tower	Tower	Tower	Tower	Tower	Tower	Tower	Tower	Tower	Tower	Tower
UTM E				692347	692360	692349	692363	692369	692358	692346	692434	692417	692401	692507	692492	692562	692638
UTM N				5286171	5286188	5286182	5286188	5286194	5286191	5286174	5286148	5286130	5286136	5286210	5286215	5286313	5286385
	Unit	*Analysis*	*LOD*														
Au	ppb	INAA	1	11	16	-1	-1	2	3	-1	35	56	8	117	30	5	21
Ag	ppm	ICP-OES	0.1	-0.1	0.14	-0.1	0.07	-0.1	-0.05	-0.05	0.09	0.18	0.07	0.1	0.05	-0.05	-0.1
As	ppm	INAA	0.5	-0.5	7.2	-0.5	2.0	-0.5	2.9	2.2	5.0	6.4	3.1	-0.5	3.0	2.2	-0.5
Ba	ppm	INAA	50	490	550	840	780	1400	500	990	440	130	330	990	-50	680	520
Br	ppm	INAA	1	-1	-1	-1	-1	-1	-1	-1	-1	-1	-1	-1	-1	-1	-1
Ce	ppm	INAA	3	42	47	56	50	43	28	25	9	-3	21	44	-3	32	13
Co	ppm	INAA	5	55	64	49	42	55	110	130	140	275	120	120	251	45	84
Cr	ppm	INAA	10	13	-10	-10	-10	10	-10	-10	-10	-10	-10	-10	-10	-10	11
Cs	ppm	INAA	0.5	0.9	-0.5	-0.5	-0.5	-0.5	-0.5	-0.5	-0.5	-0.5	-0.5	-0.5	-0.5	-0.5	-0.5
Eu	ppm	INAA	0.5	-0.5	0.6	0.8	1.2	1.5	-0.5	0.9	-0.5	-0.5	-0.5	0.6	-0.5	-0.5	-0.5
Fe	%	INAA	0.1	2.7	1.8	1.5	1.9	10.9	2.4	2.5	0.6	0.3	0.3	3.1	0.2	1.0	1.7
Hf	ppm	INAA	1	10	4	3	4	3	-1	2	2	4	4	5	4	4	5
La	ppm	INAA	1	26	24	30	28	30	17	15	4	1	13	26	2	17	11
Lu	ppm	INAA	0.05	0.19	0.17	0.23	0.26	0.17	0.15	0.13	0.17	0.19	0.22	0.28	0.17	0.15	0.17
Mo	ppm	INAA	1	13	20	-1	-1	46	9	4	54	19	23	61	67	3	1
Na	%	INAA	0.05	0.15	1.00	1.50	1.30	1.00	0.71	0.45	0.42	-0.05	0.41	0.66	-0.05	1.20	1.10
Rb	ppm	INAA	5	25	-5	-5	-5	-5	-5	5	-5	-5	-5	-5	-5	-5	-5
Sb	ppm	INAA	0.1	0.3	0.9	1.0	1.0	-0.1	0.5	0.8	0.4	0.4	0.3	-0.1	0.6	0.9	0.1
Sc	ppm	INAA	0.1	5.6	3.8	7.1	6.1	4.1	2.9	2.8	4.1	4.0	4.2	5.6	3.7	4.9	6.1
Se	ppm	INAA	1	-1	9	-1	-1	-1	7	-3	-3	-4	-3	-2	-4	-2	-1
Sm	ppm	INAA	0.8	2.0	2.8	3.1	3.8	3.7	1.9	1.8	0.3	0.2	0.9	2.3	0.2	1.4	0.9
Ta	ppm	INAA	0.5	1.9	1.6	1.6	1.1	1.8	2.0	2.0	3.8	6.2	4.3	2.9	4.5	1.0	2.2
Tb	ppm	INAA	0.5	-0.5	-0.5	-0.5	-0.5	-0.5	-0.5	-0.5	-0.5	-0.5	-0.5	-0.5	-0.5	-0.5	-0.5
Te	ppm	INAA	20	-20	-20	-20	-20	-20	-20	-20	-20	-20	-20	-20	-20	-20	-20
Th	ppm	INAA	0.5	11.2	8.3	9.5	9.1	8.9	5.3	4.5	2.5	2.4	3.9	7.0	3.0	4.7	4.1
W	ppm	INAA	1	216	253	184	171	217	440	480	510	963	457	374	898	169	313
U	ppm	INAA	0.5	1.6	1.7	1.8	1.9	2.0	0.9	1.3	1.1	1.6	1.5	1.3	1.5	0.9	0.9
Yb	ppm	INAA	0.5	-0.5	-0.5	1.0	1.4	0.7	-0.5	-0.5	-0.5	-0.5	-0.5	-0.5	0.9	-0.5	0.9
Zr	ppm	INAA	100	200	-100	190	190	150	130	-100	-100	220	-100	140	-100	-100	110

SF-12-028	*SF-12-030*	*SF-12-031*	*SF-12-032*	*SF-12-035*	*SF-12-042*	*SF-12-051*	*SF-12-052*	*SF-12-073*	*SF-12-077*	*SF-12-084*	*SF-12-085*	*SF-12-087*	*SF-12-088*	*SF-12-094*	*SF-12-095*	*SF-12-096*
7740874	7740875	7740876	7740877	7740878	7740879	7740881	7740882	7740833	7740834	7740835	7740836	7740837	7740838	7740883	7740884	7740885
Stewart	Stewart	Stewart	Stewart	Stewart	Stewart	L. Harbour	L. Harbour	Stewart	Stewart	Stewart	Stewart	Stewart	Stewart	Stewart	Stewart	Stewart
649649	649653	649657	649657	650139	650159	654323	645313	-	-	-	-	-	-	-	-	-
5253011	5253012	5253024	5253043	5253608	5253780	5272240	5272263	-	-	-	-	-	-	-	-	-
236	609	644	984	410	19	29	97	12	20	21	12	20	128	137	75	132
0.57	0.11	0.93	0.58	0.44	0.07	0.22	1.36	0.1	0.1	0.2	-0.1	-0.1	0.2	0.31	0.38	0.20
4.1	3.8	5.7	3.9	17.0	2.8	9.2	7.1	6.4	-0.5	-0.5	-0.5	-0.5	1.8	4.9	4.3	5.1
260	720	140	310	190	70	-50	-50	590	660	700	75	790	740	340	590	520
-1	-1	-1	-1	-1	-1	-1	-1	-1	-1	-1	-1	-1	-1	-1	-1	-1
39	40	19	8	38	32	-7	-7	40	11	31	41	46	28	47	21	26
190	53	170	150	130	130	315	367	39	100	69	44	83	95	110	76	110
-10	-10	-10	-10	-10	-10	-24	-24	-10	-10	-10	-10	-10	-10	-10	-10	-10
0.6	1.4	0.5	0.8	-0.5	-0.5	3.9	5.1	-0.5	1.4	1.9	-0.5	1.7	1.6	1.0	1.8	1.5
-0.5	1.0	-0.5	-0.5	0.9	-0.5	-0.5	-0.5	0.9	-0.5	0.5	0.5	0.9	-0.5	-0.5	1.3	-0.5
3.6	2.9	5.1	3.0	6.1	2.1	-0.1	-0.1	1.9	2.8	2.3	1.1	2.4	3.4	5.4	4.1	2.9
-1	4	-1	-1	1	1	-1	-1	8	12	9	8	10	10	3	4	3
15	20	10	4	24	20	-1	3	24	13	17	20	23	18	23	13	12
0.32	0.42	0.20	0.20	0.31	0.08	-0.05	-0.05	0.41	0.20	0.17	0.13	0.29	0.22	0.25	0.12	0.26
51	17	107	350	14	41	-1	-1	10	38	30	11	17	15	28	27	12
0.08	0.17	0.05	0.13	0.05	-0.05	-0.05	-0.05	0.10	0.14	0.22	0.07	0.20	0.17	0.13	0.19	0.15
21	60	12	25	16	-5	140	260	14	71	56	6	70	60	45	69	79
0.4	0.5	0.5	0.3	0.4	0.3	136.0	100.0	0.7	-0.1	-0.1	-0.1	-0.1	-0.1	0.2	0.2	0.1
4.3	10.0	3.7	2.4	5.4	1.2	-0.1	-0.1	7.8	5.7	4.9	3.3	4.9	4.1	3.9	5.8	5.1
-4	-2	6	-3	13	-3	-7	-8	-1	-1	-1	-1	-1	-1	-4	-3	-3
4.0	5.7	2.5	0.8	3.7	1.2	0.2	0.6	2.8	1.0	2.6	1.9	3.2	1.7	2.7	2.0	3.2
4.5	2.1	3.3	3.3	4.1	2.9	8.3	12.0	1.5	3.4	2.4	1.8	2.5	2.8	3.5	2.3	3.4
0.5	1.1	-0.5	-0.5	0.7	-0.5	-0.5	-0.5	-0.5	-0.5	-0.5	-0.5	-0.5	-0.5	-0.5	-0.5	-0.5
-20	-20	-20	-20	-20	-20	-20	-20	-20	-20	-20	-20	-20	-20	-20	-20	-20
5.9	8.2	2.1	2.8	6.9	6.2	-0.5	-0.3	10.3	10.2	9.2	10.0	10.0	6.7	9.3	8.6	10.3
710	247	607	559	495	483	1160	1350	142	380	261	167	291	336	383	262	450
1.1	2.7	1.2	0.6	1.5	1.0	-0.5	-0.5	4.6	2.0	1.7	1.2	1.3	1.5	1.0	1.4	1.4
2.0	2.3	1.1	1.1	1.6	-0.5	-1.1	-1.1	2.4	-0.5	0.9	-0.5	1.0	1.1	1.2	-0.5	1.0
-100	210	-100	-100	-100	-100	-100	-100	180	150	170	170	150	160	-100	-100	200

SF-12-098	*SF-12-099*	*SF-12-100A*	*SF-12-101*	*SF-12-102*	*SF-12-103*	*SF-12-109*	*SF-12-111*	*SF-12-115*	*SF-12-117*	*SF-12-139*	*SF-12-142*	*SF-12-150*	*SF-12-151*	*SF-12-152*
7740886	7740887	7740888	7740889	7740891	7740839	7740843	7740844	7740845	7740892	7740846	7740847	7740893	7740894	7740895
Stewart	Stewart	Stewart	Stewart	Stewart	Stewart	Stewart	Stewart	Stewart	Stewart	Stewart	Stewart	H. Pond	H. Pond	H. Pond
-	-	-	-	-	-	-	-	-	-	-	-	699314	699317	699319
-	-	-	-	-	-	-	-	-	-	-	-	5295023	5295024	5295026
123	1560	169	118	7	2	5	3	4	-1	2	-1	10500	3830	60400
0.31	0.48	0.11	0.10	0.36	-0.1	0.1	0.2	-0.1	0.07	-0.1	-0.1	9.98	8.58	43.99
3.3	5.2	1.8	5.3	3.4	-0.5	-0.5	-0.5	-0.5	1.3	-0.5	-0.5	259.0	202.0	1310.0
630	680	450	480	-50	820	650	780	770	2300	73	970	180	200	-145
-1	-1	-1	-1	-1	-1	-1	-1	-1	-1	-1	-1	-1	-1	-78
41	49	38	39	71	43	41	54	68	120	7	57	-12	-3	-370
79	71	100	85	46	41	79	55	47	25	69	140	140	120	88
-10	-10	-10	-10	170	-10	-10	-10	-10	-10	560	-10	-38	-66	-36
1.5	1.8	1.9	1.9	-0.5	4.6	4.3	3.1	-0.5	-0.5	-0.5	0.8	-0.5	-0.5	-9.7
0.8	1.0	0.7	0.7	3.9	0.6	0.6	0.7	1.1	2.2	1.0	-0.5	-1.5	-1.6	-0.5
3.9	4.1	2.2	3.5	8.1	1.8	1.4	1.7	4.3	2.0	7.5	0.9	1.2	0.6	6.4
4	4	3	4	3	8	10	8	7	4	2	3	-2	-1	-1
21	28	20	24	37	20	21	28	34	71	7	31	6	3	-19
0.22	0.50	0.20	0.25	0.31	0.28	0.42	0.32	0.18	0.19	0.24	0.35	0.30	0.38	-1.90
7	13	32	29	-1	2	5	2	5	3	-1	-1	5	7	-46
0.15	0.16	0.15	0.15	2.90	0.18	0.27	0.27	0.30	1.90	1.20	2.50	0.13	0.41	-2.60
79	95	82	90	-5	120	130	110	18	28	-5	77	-5	-5	-14
-0.1	0.1	0.1	0.1	0.8	-0.1	-0.1	-0.1	0.2	0.2	-0.1	-0.1	364.0	411.0	1400.0
5.3	7.7	5.0	5.9	36.6	5.4	8.9	5.6	8.7	10.0	34.2	3.2	5.6	4.7	4.0
-3	-3	-2	-2	2	-1	-1	-1	15	-1	-1	-1	12	15	66
3.4	4.8	3.0	2.9	7.5	3.2	3.5	3.5	5.2	5.4	2.6	3.7	1.1	0.3	-0.8
3.0	2.1	2.5	1.8	0.7	1.6	2.3	2.0	1.3	0.6	0.6	4.8	3.9	2.3	1.8
-0.5	1.0	-0.5	-0.5	0.9	-0.5	-0.5	0.5	-0.5	-0.5	0.5	-0.5	-0.5	-0.5	-0.5
-20	-20	-20	-20	-20	-20	-20	-20	-20	-20	-20	-20	130	59	850
9.1	11.0	8.7	8.6	3.2	10.4	8.9	10.0	5.8	7.2	0.7	12.9	4.0	1.1	1.6
290	258	407	273	38	151	277	194	133	75	65	497	548	460	260
1.1	2.6	1.4	1.7	0.8	2.4	2.3	2.3	1.6	1.4	0.1	2.9	1.0	0.9	-12.3
0.9	3.5	0.9	1.6	2.3	1.3	2.2	1.8	-0.5	0.7	1.5	1.5	-1.9	-1.9	-64.8
-100	-100	170	150	230	180	160	190	170	-100	-100	140	-100	-360	-100

APPENDIX D: GEOCHEMICAL STANDARDS AND DUPLICATES

Five tables are included in this appendix:

Table D-1 contains standard and duplicate data measured during major element analysis using inductively coupled plasma emission spectrometry with fusion (FUS-ICP) at the Department of Natural Resources GSNL laboratory.

Table D-2 contains standard and duplicate data measured during trace element analysis using inductively coupled plasma optical emission spectrometry (ICP-OES) at the Department of Natural Resources GSNL laboratory.

Table D-3 contains standard and duplicate data measured during trace element analysis using inductively coupled plasma mass spectrometry with fusion (MS-FUS) at the Department of Natural Resources GSNL laboratory.

Table D-4 contains standard and duplicate data measured during trace element analysis using instrumental neutron activation analysis (INAA) at Becquerel Laboratories.

Table D-5 contains standard and duplicate data measured during major and trace element analysis using inductively coupled plasma optical emission spectrometry and mass spectrometry, both with fusion (FUS-ICP; MS-FUS), at Activation Laboratories.

Negative values, or values containing 'less than' symbols, indicate that the concentration of the specific element was below the detection limit. Where no value has been entered, it is because that element was not analyzed for in the sample using that particular method of analysis. The major element oxide and trace element data presented here have **not** been recalculated for volatiles to a total of 100%.

Table D-1

Lab #	Sample #		SiO2	Al2O3	Fe2O3Total	Fe2O3	FeO	MnO	MgO	CaO	Na2O	K2O	TiO2	P2O5	LOI	Total	Cr	Zr	Ba
	Unit		%	%	%	%	%	%	%	%	%	%	%	%	%	%	ppm	ppm	ppm
	Analysis		FUS-ICP	FUS-ICP	FUS-ICP	FUS-ICP	FUS-ICP	FUS-ICP	FUS-ICP	FUS-ICP	FUS-ICP	FUS-ICP	FUS-ICP	FUS-ICP	Grav		FUS-ICP	FUS-ICP	FUS-ICP
	LOD		0.01	0.01	0.01	0.01	0.01	0.001	0.01	0.01	0.01	0.01	0.001	0.001	0.01		1.00	1.00	1.00
Standards																			
7740840	*W-2*	measured	51.21	15.49	10.92	-	-	0.170	6.42	10.53	2.42	0.64	1.056	0.120			86	83	170
	W-2	reference	52.68	15.45	10.83	1.53	8.34	0.167	6.37	10.86	2.20	0.63	1.060	0.140			92	100	170
7740900	*DR-N*	measured	51.52	17.36	9.51	-	-	0.219	4.22	6.84	2.82	1.47	1.049	0.223			30	123	385
	DR-N	reference	52.85	17.52	9.70	3.70	5.40	0.220	4.40	7.05	2.99	1.70	1.090	0.250			40	125	385
Duplicates																			
7740823	*SF-12-003*		54.02	16.81	2.23	1.98	0.22	0.002	0.04	0.07	1.88	2.29	0.648	0.139	19.93	98.05	6	176	894
7740830	*7740823*	duplicate	54.55	16.94	2.19	1.97	0.20	0.003	0.03	0.07	1.91	2.21	0.661	0.135	19.56	98.25	5	197	913
7740835	*SF-12-084*		72.19	14.46	4.10	0.64	3.11	0.108	2.25	0.32	0.20	2.46	0.396	0.087	3.40	99.96	-1	160	779
7740850	*7740835*	duplicate	72.26	14.39	3.94	0.64	2.97	0.108	2.24	0.33	0.06	2.44	0.391	0.089	3.60	99.84	-1	183	773

Table D-2

Lab #	Sample #		Be	Cu	Li	Mn	Ni	Pb	Rb	Sc	Ti	Zn
	Unit		ppm	ppm	ppm	ppm	ppm	ppm	ppm	ppm	ppm	ppm
	Analysis		ICP-OES	ICP-OES	ICP-OES	ICP-OES	ICP-OES	ICP-OES	ICP-OES	ICP-OES	ICP-OES	ICP-OES
	LOD		0.10	1.00	0.10	1.00	1.00	1.00	1.00	0.10	1.00	1.00
Standards												
7740840	*SY-4*	measured	2.7	6	37.7	776	10	5	-	1.0	1750	96
7740900	*SY-4*	measured	2.6	6	36.7	805	11	4	55	1.0	1728	92
	SY-4	reference	2.6	7	37.0	819	9	10	55	1.1	1500	93
Duplicates												
7740823	*SF-12-003*		0.2	4	-0.1	14	-1	24	-	7.4	305	4
7740830	*7740823*	duplicate	0.2	4	-0.1	12	1	23	-	7.4	242	4
7740835	*SF-12-084*		2.4	713	48.6	813	4	66	-	6.2	1082	382
7740850	*7740835*	duplicate	2.5	730	50.0	834	4	66	-	6.3	1043	394

Table D-3

Lab #	Sample #		V	Cr	Co	Ga	Ge	As	As	Rb	Sr	Y	Nb	Mo
	Unit		ppm	ppm	ppm	ppm	ppm	ppm	ppm	ppm	ppm	ppm	ppm	ppm
	Analysis		ICP-MS-FUS	ICP-MS-FUS	ICP-MS-FUS	ICP-MS-FUS	ICP-MS-FUS	ICP-MS-FUS	ICP-MS-FUS	ICP-MS-FUS	ICP-MS-FUS	ICP-MS-FUS	ICP-MS-FUS	ICP-MS-FUS
	LOD		5	1	1	1	0.01	0.5	5.0	2	2	1	1	1
Standards														
7740840	*W-2*	measured	261	88	44	18	2.79	2.4	-	18	191	19	7	-1
	W-2	reference	260	92	43	17	-	1.2	1	21	190	23	8	-
7740900	*DR-N*	measured	231	-	41	21	4	-	-5	-	403	25	8	2
	DR-N	reference	220	40	35	22	2	3	3	73	400	26	7	1
Duplicates														
7740823	*SF-12-003*		88	5	44	17	2.5	3	-	4	311	5	7.8	1
7740830	*7740823*	duplicate	91	7	45	16	1.9	3	-	3	296	5	9.6	1
7740835	*SF-12-084*		38	2	76	15	3.0	3	-	54	136	9	8.8	27
7740850	*7740835*	duplicate	35	1	74	15	1.9	4	-	51	128	10	9.9	24

Cd	In	In	Sn	Cs	Ba	La	Ce	Pr	Nd	Sm	Eu	Gd	Tb	Dy
ppm	ppm	ppm	ppm	ppm	ppm	ppm	ppm	ppm	ppm	ppm	ppm	ppm	ppm	ppm
ICP-MS-FUS	ICP-MS-FUS	ICP-MS-FUS	ICP-MS-FUS	ICP-MS-FUS	ICP-MS-FUS	ICP-MS-FUS	ICP-MS-FUS	ICP-MS-FUS	ICP-MS-FUS	ICP-MS-FUS	ICP-MS-FUS	ICP-MS-FUS	ICP-MS-FUS	ICP-MS-FUS
0.2	0.1	0.2	1	0.1	1	0.5	0.1	0.05	0.1	0.1	0.05	0.1	0.1	0.1
-0.2	-0.1	-	2	0.7	160	10.1	21.9	2.77	12.1	3.3	1.06	3.7	0.6	3.6
-	-	-	-	1.0	170	10.0	23.0	-	13.0	3.3	1.00	-	0.6	3.6
0.2	-	-0.2	2	2.0	-	22.0	45.4	5.62	23.5	4.9	1.43	5.5	0.8	5.0
0.9	0.08	0.08	2	6.3	385	21.5	46.0	5.70	23.5	5.4	1.45	4.7	0.8	4.6
-0.2	-0.1	-	3	-0.1	838	29.8	55.4	6.05	22.2	3.5	0.92	1.7	0.16	0.7
0.3	-0.1	-	3	-0.1	805	29.1	54.3	6.07	21.0	3.6	1.01	1.9	0.12	0.8
-0.2	-0.1	-	4	1.4	713	17.8	36.5	4.21	14.5	3.3	0.74	2.5	0.28	2.0
-0.2	-0.1	-	3	1.4	707	17.4	35.8	4.12	15.2	2.9	0.77	2.4	0.31	2.0

Ho	Er	Tm	Yb	Lu	Hf	Ta	W	Tl	Pb	Bi	Bi	Th	U
ppm	ppm	ppm	ppm	ppm	ppm	ppm	ppm	ppm	ppm	ppm	ppm	ppm	ppm
ICP-MS-FUS	ICP-MS-FUS	ICP-MS-FUS	ICP-MS-FUS	ICP-MS-FUS	ICP-MS-FUS	ICP-MS-FUS	ICP-MS-FUS	ICP-MS-FUS	ICP-MS-FUS	ICP-MS-FUS	ICP-MS-FUS	ICP-MS-FUS	ICP-MS-FUS
0.1	0.1	0.05	0.1	0.05	0.2	0.5	1	0.1	5	0.1	0.4	0.1	0.1
0.7	2.2	0.32	2.0	0.30	2.4	-0.5	-1	-0.1	11	-0.1	-	2.1	0.5
0.8	2.5	0.38	2.1	0.33	2.6	0.5	-	-	9	-	-	2.4	0.5
0.9	2.9	0.37	2.4	0.38	3.4	1.0	151	-0.1	-	-	-0.4	4.6	1.4
1.0	2.5	0.39	2.5	0.40	3.5	0.6	130	0.7	55.0	0.5	0.5	5.0	1.5
0.27	0.79	0.15	1.16	0.21	4.2	0.8	190	-0.1	23	0.5	-	9.40	1.12
0.19	0.75	0.15	1.11	0.20	4.1	2.1	184	-0.1	21	0.9	-	9.20	1.38
0.39	1.22	0.18	1.19	0.21	4.2	2.2	292	-0.1	42	-0.1	-	9.78	1.77
0.33	1.26	0.18	1.26	0.21	4.6	2.4	284	-0.1	41	0.1	-	9.96	1.74

Table D-4

Lab #	Sample #		Au	As	Ba	Br	Ce	Co	Cr	Cs	Eu	Fe	Hf	La	Lu	Mo	Na	Rb	Sb	Sc	Se	Sm	Ta	Tb	Th	U	W	Yb	Zr	Wt
	Unit		ppb	ppm	ppm	ppm	ppm	ppm	ppm	ppm	ppm	%	ppm	ppm	ppm	ppm	%	ppm	ppm	ppm	ppm	ppm	ppm	ppm	ppm	ppm	ppm	ppm	ppm	g
	Analysis		INAA	INAA	INAA	INAA	INAA	INAA	INAA	INAA	INAA	INAA	INAA	INAA	INAA	INAA	INAA	INAA	INAA	INAA	INAA	INAA	INAA	INAA	INAA	INAA	INAA	INAA	INAA	
	LOD		1	1	50	1	3	5	10	0.5	0.5	0.1	1	1	0.05	1	0.05	5	0.1	0.1	1	0.8	0.5	0.5	0.5	0.5	1	0.5	100	
Standards																														
7740840	*WGB-1*	measured	2	2.1	810	-1	7	26	280	-0.5	1.2	4.3	2	7	0.17	-1	1.50	16	2.1	37.2	-1	2.4	0.3	-0.5	0.9	0.8	-1	1.3	-100	26.70
	WGB-1	reference	3	1.5-5	851	-	14-20	30	291	0.5	1.3	4.7	2	9	0.2-0.3	1	1.59	20	2.0	44.0	0.1-0.8	2.8	0.3-1	0.5	1.0	0.8	1-3.5	1.4	44	
7740880	*SY-4*	measured	-2	1.2	300	218	120	-2	16	1.7	2.3	4.4	12	56	2.00	-1	4.90	51	-0.1	1.3	-1	12.6	0.6	2.7	1.2	0.7	-1	16.0	480	19.47
	SY-4	reference	-	0.1-2	340	217	122	3	12	1.5	2.0	4.3	11	58	2.10	0.2-3	5.25	55	0.01-0.3	1.1	0.01-4	12.7	0.9	2.6	1.4	0.8	0.2-15	14.8	517	
Duplicates																														
7740864	*SF-12-02*		16	7.2	550	-1	47	64	-10	-0.5	0.6	1.8	4	24	0.17	20	1.00	-5	0.9	3.8	9	2.8	1.6	-0.5	8.3	1.7	253	-0.5	-100	29.81
7740870	*7740864*	duplicate	14	6.7	500	-1	48	66	-10	-0.5	0.6	1.8	4	25	0.19	18	1.10	-5	0.8	4.1	7	2.7	1.5	-0.5	7.7	1.5	241	-0.5	170	24.07
7740882	*SF-12-52*		97	7.1	-50	-1	-7	367	-24	5.1	-0.5	-0.1	-1	3	-0.05	-1	-0.05	260	100.0	-0.1	-8	0.6	12.0	-0.5	-0.3	-0.5	1350	-1.1	-100	21.63
7740890	*7740882*	duplicate	95	6.0	-50	-1	-7	384	-21	5.9	-0.5	-0.1	-1	2	-0.05	2	0.07	280	104.0	-0.1	-8	0.6	13.0	-0.5	-0.4	-0.6	1410	-1.0	-100	18.67

Table D-5

Sample #		SiO2	Al2O3	Fe2O3Total	MnO	MgO	CaO	Na2O	K2O	TiO2	P2O5	LOI	Total	Sc	Be	V	Cr
Unit		%	%	%	%	%	%	%	%	%	%	%	%	ppm	ppm	ppm	ppm
Analysis		FUS-ICP	FUS-ICP	FUS-ICP	FUS-ICP	FUS-ICP	FUS-ICP	FUS-ICP	FUS-ICP	FUS-ICP	FUS-ICP	FUS-ICP	FUS-ICP	FUS-ICP	FUS-ICP	FUS-ICP	FUS-MS
LOD		0.01	0.01	0.01	0.001	0.01	0.01	0.01	0.01	0.001	0.01			1	1	5	20
Standards																	
NIST 694	measured	11.32	1.89	0.74	0.013	0.35	43.1	0.89	0.54	0.118	30.16			-	-	1613	-
NIST 694	reference	11.2	1.8	0.79	0.0116	0.33	43.6	0.86	0.51	0.11	30.2			-	-	1740	-
DNC-1	measured	46.9	18.12	10.18	0.147	10.05	11.42	1.93	0.22	0.48	0.08			31	-	157	280
DNC-1	reference	47.15	18.34	9.97	0.15	10.13	11.49	1.89	0.234	0.48	0.07			31	-	148	270
GBW 07113	measured	73.84	13.21	3.23	0.141	0.14	0.57	2.55	5.47	0.289	0.05			6	4	< 5	-
GBW 07113	reference	72.8	13	3.21	0.14	0.16	0.59	2.57	5.43	0.3	0.05			5	4	5	-
W-2a	measured	52.21	15.19	11.02	0.166	6.32	11	2.13	0.6	1.066	0.13			35	< 1	272	100
W-2a	reference	52.4	15.4	10.7	0.163	6.37	10.9	2.14	0.626	1.06	0.13			36	1.3	262	92
SY-4	measured	49.78	20.8	6.11	0.107	0.51	8.02	6.98	1.63	0.284	0.14			< 1	3	9	-
SY-4	reference	49.9	20.69	6.21	0.108	0.54	8.05	7.1	1.66	0.287	0.131			1.1	2.6	8	-
BIR-1a	measured	47.68	15.58	11.71	0.172	9.64	13.53	1.81	0.02	0.976	0.03			43	< 1	330	370
BIR-1a	reference	47.96	15.5	11.3	0.175	9.7	13.3	1.82	0.03	0.96	0.021			44	0.58	310	370
LKSD-3	measured	-	-	-	-	-	-	-	-	-	-			-	-	-	90
LKSD-3	reference	-	-	-	-	-	-	-	-	-	-			-	-	-	87
TDB-1	measured	-	-	-	-	-	-	-	-	-	-			-	-	470	250
TDB-1	reference	-	-	-	-	-	-	-	-	-	-			-	-	471	251
DTS-2b	measured	-	-	-	-	-	-	-	-	-	-			-	-	-	> 10000
DTS-2b	reference	-	-	-	-	-	-	-	-	-	-			-	-	-	15500
CTA-AC-1	measured	-	-	-	-	-	-	-	-	-	-			-	-	-	-
CTA-AC-1	reference	-	-	-	-	-	-	-	-	-	-			-	-	-	-
NCS DC86312	measured	-	-	-	-	-	-	-	-	-	-			-	-	-	-
NCS DC86312	reference	-	-	-	-	-	-	-	-	-	-			-	-	-	-
ZW-C	measured	-	-	-	-	-	-	-	-	-	-			-	-	-	-
ZW-C	reference	-	-	-	-	-	-	-	-	-	-			-	-	-	-
Duplicates																	
SF-12-27		52.25	19.7	10.79	0.155	3.63	1.74	2.07	3.38	1.351	0.13	3.78	98.98	32	2	162	40
SF-12-27	duplicate	53.06	20.18	10.68	0.155	3.66	1.74	2.15	3.51	1.378	0.11	3.78	100.4	33	2	165	40

Co	Ni	Cu	Zn	Ga	Ge	As	Rb	Sr	Y	Zr	Nb	Mo	Ag	In	Sn	Sb	Cs	Ba	La	Ce
ppm	ppm	ppm	ppm	ppm	ppm	ppm	ppm	ppm	ppm	ppm	ppm	ppm	ppm	ppm	ppm	ppm	ppm	ppm	ppm	ppm
FUS-MS	FUS-MS	FUS-MS	FUS-MS	FUS-MS	FUS-MS	FUS-MS	FUS-MS	FUS-ICP	FUS-MS	FUS-ICP	FUS-MS	FUS-MS	FUS-MS	FUS-MS	FUS-MS	FUS-MS	FUS-MS	FUS-ICP	FUS-MS	FUS-MS
1	20	10	30	1	0.5	5	1	2	0.5	1	0.2	2	0.5	0.1	1	0.2	0.1	3	0.05	0.05
-	-	-	-	-	-	-	-	-	-	-	-	-	-	-	-	-	-	-	-	-
-	-	-	-	-	-	-	-	-	-	-	-	-	-	-	-	-	-	-	-	-
53	250	90	60	-	-	-	3	143		35	-	-	-	-	-	1	-	103	3.9	-
57	247	100	70	-	-	-	5	144		38	-	-	-	-	-	0.96	-	118	3.6	-
-	-	-	-	-	-	-	-	43		418	-	-	-	-	-	-	-	511	-	-
-	-	-	-	-	-	-	-	43		403	-	-	-	-	-	-	-	506	-	-
43	80	110	80	17	1.3	-	20	193	20.9	88	8.3	< 2	< 0.5	-	-	-	-	168	-	24.5
43	70	110	80	17	1	-	21	190	24	94	7.9	0.6	0.046	-	-	-	-	182	-	23
-	-	-	-	-	-	-	-	1190	-	531	-	-	-	-	-	-	-	339	-	-
-	-	-	-	-	-	-	-	1191	-	517	-	-	-	-	-	-	-	340	-	-
47	160	-	70	-	-	-	-	109	15.5	15	-	-	-	-	-	-	-	6	-	2
52	170	-	70	-	-	-	-	110	16	18	-	-	-	-	-	-	-	6		1.9
30	-	-	-	-	-	25	73	-	27	-	-	2	2.5	-	3	1	2.2	-	48.3	91
30	-	-	-	-	-	27	78	-	30	-	-	2	2.7	-	3	1.3	2.3	-	52	90
-	90	340	150	-	-	-	-	-	34.4	159	-	-	-	-	-	-	-	-	17.1	40.2
-	92	323	155	-	-	-	-	-	36	156	-	-	-	-	-	-	-	-	17	41
124	3760	-	-	-	-	-	-	-	-	-	-	-	-	-	-	-	-	-	-	-
120	3780	-	-	-	-	-	-	-	-	-	-	-	-	-	-	-	-	-	-	-
-	-	50	40	-	-	-	-	-	294	-	-	-	-	-	-	-	-	-	> 2000	> 3000
-	-	54	38	-	-	-	-	-	272	-	-	-	-	-	-	-	-	-	2176	3326
-	-	-	-	-	-	-	-	-	941	-	-	-	-	-	-	-	-	-	> 2000	170
-	-	-	-	-	-	-	-	-	976	-	-	-	-	-	-	-	-	-	2360	190
-	-	-	940	102	-	-	> 1000	-	-	-	193	-	-	-	-	-	249	-	-	-
-	-	-	1050	99	-	-	8500	-	-	-	198	-	-	-	-	-	260	-	-	-
50	< 20	20	110	23	0.7	< 5	136	205	26.9	194	6.2	< 2	< 0.5	< 0.1	3	< 0.2	6.2	795	39.4	79
49	< 20	20	110	22	0.7	< 5	134	211	26.4	200	6.3	< 2	< 0.5	< 0.1	3	< 0.2	6.1	816	39	78.5

Pr	Nd	Sm	Eu	Gd	Tb	Dy	Ho	Er	Tm	Yb	Lu	Hf	Ta	W	Tl	Pb	Bi	Th	U
ppm	ppm	ppm	ppm	ppm	ppm	ppm	ppm	ppm	ppm	ppm	ppm	ppm	ppm	ppm	ppm	ppm	ppm	ppm	ppm
FUS-MS	FUS-MS	FUS-MS	FUS-MS	FUS-MS	FUS-MS	FUS-MS	FUS-MS	FUS-MS	FUS-MS	FUS-MS	FUS-MS	FUS-MS	FUS-MS	FUS-MS	FUS-MS	FUS-MS	FUS-MS	FUS-MS	FUS-MS
0.01	0.05	0.01	0.005	0.01	0.01	0.01	0.01	0.01	0.005	0.01	0.002	0.1	0.01	0.5	0.05	5	0.1	0.05	0.01
-	-	-	-	-	-	-	-	-	-	-	-	-	-	-	-	-	-	-	-
-	-	-	-	-	-	-	-	-	-	-	-	-	-	-	-	-	-	-	-
-	5.1	-	-	-	-	-	-	-	-	-	-	-	-	-	-	-	-	-	-
-	5.2	-	-	-	-	-	-	-	-	-	-	-	-	-	-	-	-	-	-
-	-	-	-	-	-	-	-	-	-	-	-	-	-	-	-	-	-	-	-
-	-	-	-	-	-	-	-	-	-	-	-	-	-	-	-	-	-	-	-
-	13.1	3.4	-	-	0.63	3.9	0.78	-	-	2.1	0.3	2.4	-	0.7	0.09	-	< 0.1	2.3	0.49
-	13	3.3	-	-	0.63	3.6	0.76	-	-	2.1	0.33	2.6	-	0.3	0.2	-	0.03	2.4	0.53
-	-	-	-	-	-	-	-	-	-	-	-	-	-	-	-	-	-	-	-
-	-	-	-	-	-	-	-	-	-	-	-	-	-	-	-	-	-	-	-
-	-	1	-	-	-	-	-	-	-	-	-	-	-	-	-	-	-	-	-
-	-	1.1	-	-	-	-	-	-	-	-	-	-	-	-	-	-	-	-	-
-	43.6	7.8	1.4	-	-	5	-	-	-	2.8	0.41		-	-	-	-	-	10.5	4.7
-	44	8	1.5	-	-	4.9	-	-	-	2.7	0.4		-	-	-	-	-	11.4	4.6
-	24.1	-	2	-	-	-	-	-	-	3.3	-	-	-	-	-	-	-	2.8	-
-	23	-	2.1	-	-	-	-	-	-	3.4	-	-	-	-	-	-	-	2.7	-
-	-	-	-	-	-	-	-	-	-	-	-	-	-	-	-	-	-	-	-
-	-	-	-	-	-	-	-	-	-	-	-	-	-	-	-	-	-	-	-
-	1110	160	44.3	127	14	-	-	-	-	10.4	1.08	-	2.72	-	-	-	-	22.3	4
-	1087	162	46.7	124	13.9	-	-	-	-	11.4	1.08	-	2.65	-	-	-	-	21.8	4.4
-	1550	-	-	235	31.6	180	33.5	97.9	13.3	85.1	12	-	-	-	-	-	-	24.1	-
-	1600	-	-	225	34.6	183	36	96.2	15.1	87.79	11.96	-	-	-	-	-	-	23.6	-
-	-	-	-	-	-	-	-	-	-	-	-	-	79.2	327	33.4	-	-	-	-
-	-	-	-	-	-	-	-	-	-	-	-	-	82	320	34	-	-	-	-
8.63	33.5	6.62	1.9	5.89	0.86	5	0.96	2.83	0.421	2.69	0.393	4.5	0.73	77.9	0.71	8	< 0.1	4.8	1.18
8.81	34.9	6.45	2.02	5.96	0.88	5.06	0.96	2.8	0.428	2.65	0.414	4.7	0.81	76.8	0.79	8	< 0.1	4.8	1.18

APPENDIX E: CHARACTERISTICS OF HIGH- AND LOW-SULPHIDATION EPITHERMAL-STYLE AU MINERALIZATION OF THE BURIN PENINSULA

Table E-1: Summary of the results presented in *Chapters 5* and *6* for the Hickey's Pond, Tower, Stewart, Forty Creek, Heritage, Big Easy, and Long Harbour prospects, highlighting the main characteristics of epithermal-style mineralization found in the Burin Peninsula region. The general characteristics of typical high-, intermediate- and low-sulphidation epithermal, and porphyry deposits are also presented for comparison, with data compiled from White and Hedenquist (1995), Hedenquist et al. (2000), Cooke and Simmons (2000), Sillitoe and Hedenquist (2003), Einaudi et al. (2003), and Berger et al. (2008). Additional data for Big Easy compiled from Clarke (2013) and Layne et al. (2016). APS=aluminum phosphate-sulphate minerals, including woodhouseite and svanbergite, P=porphyry, HS=high-sulphidation, IS=intermediate sulphidation, LS=low-sulphidation. Ore minerals listed in italics are late-stage and not part of the hypogene assemblage.

Table E-1

Prospect	Classification	Host Rocks	Hydrothermal Alteration	Weathering/Supergene Alteration	Ore Style	Ore Related Textures	Enriched Metals	Tellurides/ Selenides	Precious Metal Ore	Other Sulphides/Ore
Typical P Deposit	**P**	**felsic-intermediate porphyritic intrusives and lesser volcaniclastics**	**quartz-K-feldspar-biotite-muscovite, quartz-muscovite, quartz-kaolinite, epidote-chlorite**	**Goethite, jarosite, hematite, gypsum, kaolinite**	**vein and fracture fill, vein stockwork, disseminated**	**veining, stockwork veining, alteration zoning**	**Cu, Au, Mo, Ag, Zn, Pb, As, Sb, Sn, Te**	**Te**	**native Au, Au tellurides**	**chalcopyrite, pyrite, bornite, enargite, chalcocite, molybdenite, sphalerite, galena, tetrahedrite**
Typial HS Deposit	**HS**	**Subaerial, intermediate volcanics/volcaniclastics**	**vuggy silica, quartz-alunite, dickite/kaolinite-pyrophyllite-muscovite, smectite-illite, +/- phosphates/sulfates, barite**	**Fe-oxides and oxyhydroxides, sulfates (alunite, jarosite, barite), kaolinite/clays**	**primarily disseminated and replacement ore, also breccia and vein fill**	**vuggy silica, veining, breccias, alteration zoning**	**Au, Ag, Cu, Bi, As, Sb, Te, Sn, Mo, Pb**	**Te, rare Se**	**Electrum, native Au, acanthite, Au-tellurides**	**pyrite, specularite, enargite, luzonite-famatinite, tetrahedrite-tennantite, covellite, bornite, chalcocite, diginite, chalcopyrite**
Stewart	HS/P?	Dacitic quartz crystal tuff and tonalite	pyrophyllite, dickite, muscovite, Fe-chlorite, local quartz-alunite, smectite, woodhouseite, svanbergite, xenotime, barite	hematite	replacement, disseminated, vein and fracture fill	veining, stockwork veining, local vuggy silica	Cu, Au, Ag, Pb, Mo, Zn, Se	none found	none found	pyrite, chalcopyrite,specularite, galena, molybdenite
Hickey's Pond	HS	Intermediate volcaniclastics	vuggy silica, quartz-alunite,woodhouseite-svanbergite, pyrophyllite, dickite, paragonite, barite	kaolinite, angelellite, hematite, scorodite, goethite, jarosite	replacement/disseminated, vein, and breccia	vuggy silica, quartz-sulphide veining, local brecciation, strong alteration zoning	Cu, Au, Ag, As, Sb, Se, Bi, Te	Se>>Te	native Au, calaverite (Au-telluride), hessite (Ag-telluride), *fischesserite (Au-Ag-selenide), acanthite, naumannite (Ag-selenide), electrum*	pyrite, specularite, tennantite, enargite, bornite, tsumoite (BiTe), klockmannite (CuSe), galena, *chalcopyrite, covellite, cinnabar, tiemannite (HgSe)*
Tower	HS	Intermediate volcaniclastics	silica, quartz-alunite, pyrophyllite, topaz, rutile, barite	kaolinite, hematite, muscovite	replacement/disseminated, veining	silica pods, veining, local brecciation	minor Cu, Au, Mo, Te, Se	minor Te	none found	pyrite, specularite, chalcopyrite, tennantite, tsumoite (BiTe),
Monkstown Rd	HS	Intermediate volcaniclastics	quartz, lazulite, pyrophyllite, alunite, woodhouseite-svanbergite, rutile, barite		diseminated, veins	veining	minor Au	none found	none found	specularite, pyrite

Typical IS Deposit	**IS**	**Andesite-rhyolite**	**quartz, muscovite, illite, Mn-carbonates**	**Fe-oxides and oxyhydroxides, sulfates, clays**	**vein fill, breccias and stockworks**	**crustiform and comb quartz**	**Ag, Au, Zn, Pb, Cu**	**Te, rare Se**	**Ag-sulfosalts, acanthite**	**chalcopyrite, sphalerite, tennantite, tetrahedrite, pyrite, galena**
40 Creek	IS?	Intermediate volcaniclastics	quartz, Fe-Mg-chlorite, muscovite, epidote	anglesite, hematite	vein fill	veining	Ag, Au, Te, Pb, Hg, Cu, Zn, Sb, Se	Te>>Se	Tellurides [hessite(Ag), petzite(Ag,Au), sylvanite(Au,Ag)], *acanthite, naumannite (Ag-selenide)*	pyrite, chalcopyrite, sphalerite, galena, altaite (PbTe), *covellite, native Te*
Typical LS Deposit	**LS**	**bimodal basalt-rhyolite, volcanics, volcaniclastics, and sedimentary rocks**	**quartz, chalcedony, adularia, calcite, illite-smectite**	**Fe-oxides and oxyhydroxides, kaolinite/clays, barite**	**primarily filling veins with sharp boundaries or as stockworks and breccias**	**blading, crustiform and colloform banding, breccia, comb texture, sillica sinter**	**Ag, Au, As, Sb, Se, Zn, Hg, Pb**	**Se>Te**	**Electrum, native Au, Au-Ag-selenides, acanthite**	**pyrite, arsenopyrite, chalcopyrite, pyrrhotite, sphalerite, galena**
Long Harbour	LS	Flow banded rhyolite	quartz, chalcedony, adularia, kaolinite, magnesite, scheelite, barite, muscovite	kaolinite, hematite, anglesite	veins and breccias	colloform-crustiform banding, blading, breccia, comb texture, possible sinter	Au, Ag, W, As, Sb, Te	Te>>Se	native Au, electrum, naumannite(Ag-selenide), hessite (Ag-telluride), Ag-sulfosalts/tellurides (chenguodaite, cervelleite), acanthite	arsenopyrite, altaite, galena, jamesonite, pyrrhotite, sphalerite, native Bi, chalcopyrite, native Sb
Heritage	LS	Pyroclastic andesite	quartz, chalcedony, adularia, calcite, phengite	hematite, muscovite, barite	veins and breccias	blading, breccia, colloform-crustiform banding	Au, Ag, Zn, Pb, As, Sb, minor Te, Se	Se=Te	Hessite (Ag-telluride), Naumannite (Ag-selenide), acanthite w/ native Ag	Pyrite, sphalerite, galena, chalcopyrite, minor stibnite, native Bi, arsenopyrite
Big Easy	LS	Epiclastic pebble conglomerate	quartz, chalcedony, adularia, carbonate, muscovite, illite-smectite		veins and breccias	colloform-crustiform banding, silica sinter, minor blading	Au, Ag, Cu, Hg, As, Sb, Se	Se>Te	Native Ag, Electrum, acanthite, Freibergite (Ag-sulfosalt), Naumannite (Ag-selenide), Ag-tellurides	pyrite, chalcopyrite, sphalerite, arsenopyrite

APPENDIX F: SULPHUR ISOTOPE DATA

Table F-1: Sulphur isotope measurements from individual grains of pyrite, chalcopyrite and galena from high-sulphidation epithermal-related deposits on the Burin Peninsula.

Table F-2: Standards measured during analysis.

Table F-1

Sample	Mineral	$^{34}S/^{32}S$ per mil	SEM	$^{34}S/^{32}S$ ratio	2SD	SEM %	Poisson %	N	Description
Hickey's Pond									
SF-12-152-04-PY1	Pyrite	**-1.8**	0.3	0.04371358	0.00021567	0.0281126	0.02333246	77	fg aggregate of pyrite in quartz-alunite groundmass
SF-12-152-06-PY2	Pyrite	**-3.7**	0.2	0.04363046	0.00014028	0.01856248	0.02337195	75	fg aggregate of pyrite in vug w/ tennantite
SF-12-152-02-PY3	Pyrite	**1.4**	0.4	0.04385028	0.00029331	0.03786804	0.0265251	78	mg pyrite in quartz-alunite-sulphide veining w/ tennantite
SF-12-152-09-PY4	Pyrite	**-0.3**	0.3	0.04377555	0.00023141	0.03072596	0.02450127	74	cg pyrite in quartz-alunite-sulphide veining w/ tennantite
SF-12-152-03-PY5	Pyrite	**0.4**	0.5	0.04380839	0.00034976	0.04579007	0.02427566	76	mg pyrite in vug w/ bornite-chalcopyrite-covellite
SF-12-152-07-PY6	Pyrite	**0.9**	0.5	0.0438301	0.00040207	0.05296232	0.02430114	75	mg euhedral pyrite in quartz-alunite sulphide veining w/ tennantite
SF-12-152-08-PY7	Pyrite	**0.1**	0.5	0.04379439	0.00039899	0.05191234	0.0239734	77	mg euhedral pyrite in quartz-alunite sulphide veining w/ tennantite
SF-12-152-10-PY8	Pyrite	**0.1**	0.4	0.04379448	0.00029841	0.03907971	0.02406128	76	cg pyrite in quartz-alunite-sulphide veining w/ tennantite
SF-12-152-01-PY9	Pyrite	**-3.0**	0.3	0.04366096	0.00021577	0.02834445	0.02437069	76	fg pyrite in vug w/ bornite-chalcopyrite-covellite
Tower									
SF-12-01-01-PY1	Pyrite	**-3.4**	0.5	0.043541	0.000384	0.050548	0.025254	76	mg pyrite subhedral w/ pyrophyllite-quartz and chalcopyrite
SF-12-01-04-PY2	Pyrite	**-4.6**	0.4	0.043489	0.000273	0.035773	0.023665	77	mg subhedral-euhedral pyrite w/ pyrophyllite-quartz
SF-12-01-02-PY3	Pyrite	**-3.4**	0.4	0.043542	0.000323	0.042824	0.024012	75	cg subhedral pyrite w/ pyrophyllite-quartz
SF-12-01-03-PY4	Pyrite	**-3.4**	0.4	0.043543	0.000293	0.038111	0.023849	78	mg elongate pyrite w/ pyrophyllite-quartz
SF-12-09-01-PY1	Pyrite	**1.7**	0.7	0.043767	0.000526	0.068051	0.023756	78	fg euhedral pyrite w/ core and rim + chalcopyrite in alunite-quartz
SF-12-09-03-PY2	Pyrite	**3.0**	0.4	0.043820	0.000272	0.035838	0.024144	75	chalcopyrite-rich core of fg subhedral pyrite in alunite-quartz
SF-12-09-03-PY3	Pyrite	**0.8**	0.3	0.04363193	0.00018742	0.02479986	0.02668301	75	rim of fg subhedral pyrite in alunite-quartz
SF-12-09-06-PY4	Pyrite	**2.3**	0.3	0.04369777	0.00023166	0.0308139	0.02993001	74	fg anhedral inclusion rich pyrite in alunite-quartz
SF-12-09-05-PY5	Pyrite	**1.9**	0.5	0.04367874	0.00036572	0.04770982	0.02600992	77	anhedral elongate fg pyrite w/ core-rim in alunite-quartz
SF-12-01-01-CPY1	Chalcopyrite	**-6.8**	0.6	0.04325505	0.00043647	0.05749652	0.02387568	77	interstitial chalcopyrite w/ pyrite in pyrophyllite-quartz
Stewart									
SF-12-28-03-Py1	Pyrite	**-1.3**	0.1	0.04366276	0.00010653	0.01418093	0.02372088	74	inclusion-rich core of cg anhedral pyrite w/ white mica
SF-12-28-03-Py2	Pyrite	**-2.0**	0.2	0.04363037	0.00012895	0.01706385	0.02380645	75	rim of cg anhedral pyrite w/ white mica
SF-12-28-02-Py3	Pyrite	**-2.8**	0.2	0.04359442	0.00012907	0.0168702	0.02390495	77	fg sub-euhedral pyrite intergrown w/ specularite-chalcopyrite-chlorite
SF-12-28-04-Py4	Pyrite	**-2.6**	0.2	0.04360416	0.00012708	0.01671579	0.02434378	76	fg euhedral pyrite intergrown with chalcopyrite-chlorite
SF-12-28-01-Py5	Pyrite	**-1.0**	0.4	0.04367261	0.0003143	0.04127551	0.02608926	76	inclusion-rich core of cg anhedral pyrite w/ white mica
SF-12-28-01-Py6	Pyrite	**-2.0**	0.6	0.04363209	0.00041293	0.05392565	0.02459699	77	rim of cg anhedral pyrite w/ white mica
SF-12-32a-01-Py1	Pyrite	**-4.4**	0.4	0.043498	0.000260	0.035505	0.024068	71	inclusion-rich core of mg anhedral pyrite w/ pyrophyllite
SF-12-32a-01-Py2	Pyrite	**-2.4**	0.3	0.043586	0.000203	0.026755	0.022976	76	rim of mg anhedral pyrite w/ pyrophyllite
SF-12-32a-02-Py3	Pyrite	**-1.0**	0.6	0.043648	0.000437	0.058176	0.024224	74	fg euhedral pyrite intergrown with chalcopyritealong fine fractures
SF-12-83-01-Py1	Pyrite	**4.8**	0.4	0.043902	0.000301	0.039355	0.023576	76	pyrite w/ interstitial chalcopyrite in quartz-sulphide vein
SF-12-86-02-Py1	Pyrite	**3.2**	0.4	0.043829	0.000304	0.039745	0.022372	76	mg-cg disseminated pyrite in white mica alteration
SF-12-95-02-Py1	Pyrite	**3.7**	0.4	0.0438817	0.00026497	0.03486211	0.025112	75	fg pyrite with cores and rims in aggregate, associated with pyrophyllite
SF-12-95-03-Py2	Pyrite	**5.9**	0.5	0.043979	0.00034681	0.04464518	0.02395038	78	inclusion-rich core of cg subhedral pyrite w/ pyrophyllite-muscovite
SF-12-95-03-Py3	Pyrite	**3.9**	0.3	0.04388687	0.00022163	0.02877565	0.02403748	77	rim of cg subhedral pyrite w/ pyrophyllite-muscovite
SF-12-95-01-Py4	Pyrite	**1.6**	0.3	0.043759	0.000208	0.027291	0.022598	76	fg pyrite intergrown w/ chalcopyrite associated w/ pyrophyllite-muscovite
SF-12-28-02-Cpy1	Chalcopyrite	**-2.8**	0.6	0.04343141	0.00047602	0.06327907	0.02512253	75	fg chalcopyrite intergrown with pyrite-specularite-chlorite
SF-12-28-05-Cpy2	Chalcopyrite	**-4.6**	0.8	0.04335093	0.00056277	0.07545439	0.02466911	74	fg chalcopyrite intergrown with specularite and chlorite
SF-12-28-04-Cpy3	Chalcopyrite	**-2.5**	0.5	0.04344236	0.00037928	0.05040669	0.02404907	75	fg chalcopyrite intergrown with euhedral pyrite and chlorite
SF-12-32a-02-Cpy1	Chalcopyrite	**-3.5**	0.4	0.04348496	0.00033566	0.04427175	0.02653897	76	fg chalcopyrite intergrown w/ fg pyrite along fine fractures

SF-12-83-01-Cpy1	Chalcopyrite	**2.3**	0.9	0.04365174	0.00063997	0.08579603	0.02460856	73	interstitial chalcopyrite to pyrite in quartz-sulphide vein
SF-12-86-01-Cpy1	Chalcopyrite	**-0.9**	0.5	0.04360028	0.00039779	0.05232698	0.02478888	76	mg chalcopyrite intergrown with galena and chlorite in quartz vein
SF-12-86-04-Cpy2	Chalcopyrite	**-1.5**	0.5	0.04357258	0.00036172	0.04730278	0.02742342	77	cg chalcopyrite intergrown with chlorite in quartz vein, associated w/ galena
SF-12-95-01-Cpy1	Chalcopyrite	**2.0**	0.6	0.04363698	0.000474	0.06313623	0.02345153	74	fg chalcopyrite intergrown w/ pyrite, associated w/ pyrophyllite-muscovite
SF-12-86-01-Gn1	Galena	**1.2**	0.7	0.04293365	0.00046752	0.06372471	0.03237186	73	mg galena intergrown with chalcopyrite and chlorite in quartz vein
SF-12-86-03-Gn2	Galena	**-2.3**	0.5	0.04278259	0.00039866	0.05379959	0.02940627	75	cg galena intergrown with chlorite in quartz vein, associated with cpy
Forty Creek									
SF-12-50a-02-Py1	Pyrite	**-5.3**	0.4	0.04355932	0.00032465	0.04274623	0.0242517	76	fg disseminated pyrite
SF-12-50c-04-Py1	Pyrite	**-6.3**	0.5	0.04351595	0.00033747	0.04447814	0.02453441	76	early fg disseminated pyrite
SF-12-50a-01-Cpy1	Chalcopyrite	**-6.2**	0.3	0.04337112	0.00023841	0.03195042	0.02239743	74	Chalcopyrite intergrown with galena
SF-12-50c-02-Cpy1	Chalcopyrite	**-7.2**	0.3	0.04332676	0.00022344	0.0297749	0.02247572	75	Chalcopyrite associated with hessite
SF-12-50c-05-Cpy2	Chalcopyrite	**-8.5**	0.5	0.04326813	0.00035948	0.0479677	0.02697396	75	Chalcopyrite intergrown with hessite-sphalerite
SF-12-50c-04-Cpy3	Chalcopyrite	**-9.8**	0.5	0.04321573	0.00040976	0.05367912	0.02760386	78	Chalcopyrite intergrown with hessite-sphalerite
SF-12-50e-01-Cpy1	Chalcopyrite	**-8.7**	0.4	0.04326263	0.00032176	0.04237878	0.02643427	77	Chalcopyrite intergrown with hessite
SF-12-50a-01-Gn1	Galena	**-10.5**	0.6	0.04266656	0.000425	0.05869552	0.03089608	72	Galena intergrown with chalcopyrite

Table F-2

Standard	Mineral	$^{34}S/^{32}S$ per mil	SEM	$^{34}S/^{32}S$ ratio	2SD	SEM %	Poisson %	N
UL9 2 Oct 22 2015	Pyrite	15.7	0.2	0.04448223	0.00014825	0.01924224	0.02258691	75
UL9 3 Oct 22 2015	Pyrite	15.7	0.2	0.04448499	0.00014471	0.01865675	0.02257868	76
UL9 4 Oct 30 2015	Pyrite	15.7	0.3	0.04428619	0.00024552	0.03118756	0.02524881	79
UL9 1 Oct 23 2015	Pyrite	15.5	0.2	0.04440286	0.00014464	0.01856053	0.02528396	77
UL9 2 Oct 23 2015	Pyrite	16.0	0.2	0.04442384	0.00015454	0.02008491	0.02475818	75
UL9 3 Oct 23 2015	Pyrite	15.5	0.2	0.04439932	0.00016394	0.02117773	0.0254435	76
UL9 1 Oct 27 2015	Pyrite	15.9	0.3	0.044391	0.000249	0.034052	0.025611	68
UL9 2 Oct 27 2015	Pyrite	15.9	0.3	0.044392	0.000269	0.034276	0.024567	78
UL9 3 Oct 27 2015	Pyrite	15.8	0.4	0.044385	0.000313	0.041823	0.024772	71
UL9 4 Oct 30 2015	Pyrite	15.7	0.3	0.04428619	0.00024552	0.03118756	0.02524881	79
Nor 2 Oct 29 2015	Chalcopyrite	8.0	0.8	0.04398821	0.00057464	0.07644888	0.02357838	73
Nor 3 Oct 29 2015	Chalcopyrite	8.2	0.6	0.04400062	0.00045133	0.05882973	0.02675782	76
Nor 4 Oct 29 2015	Chalcopyrite	8.5	0.5	0.04401366	0.00034808	0.04535786	0.02554409	76
Nor 1 Nov 3 2015	Chalcopyrite	8.3	0.6	0.04391509	0.00045236	0.05947221	0.02471582	75
Nor 2 Nov 3 2015	Chalcopyrite	8.3	0.6	0.04391412	0.00043899	0.05771468	0.02442222	75
Nor 3 Nov 3 2015	Chalcopyrite	8.1	0.6	0.04390613	0.00043339	0.0577652	0.02433621	73
HT10 1 Oct 30 2015	Galena	14.1	0.6	0.04372874	0.00043506	0.05669038	0.03057859	77
HT10 2 Oct 30 2015	Galena	14.0	0.4	0.04372495	0.00032326	0.04240131	0.02845971	76
HT10 1 Nov 6 2015	Galena	13.8	0.5	0.04347894	0.00039457	0.05204908	0.03173893	76
HT10 2 Nov 6 2015	Galena	13.8	0.5	0.0434796	0.00035225	0.04646505	0.03198444	76
HT10 4 Nov 6 2015	Galena	14.6	0.4	0.04351522	0.00030895	0.0409914	0.03046265	75

APPENDIX G: SEM-EDX SPECTRA

Hickey's Pond

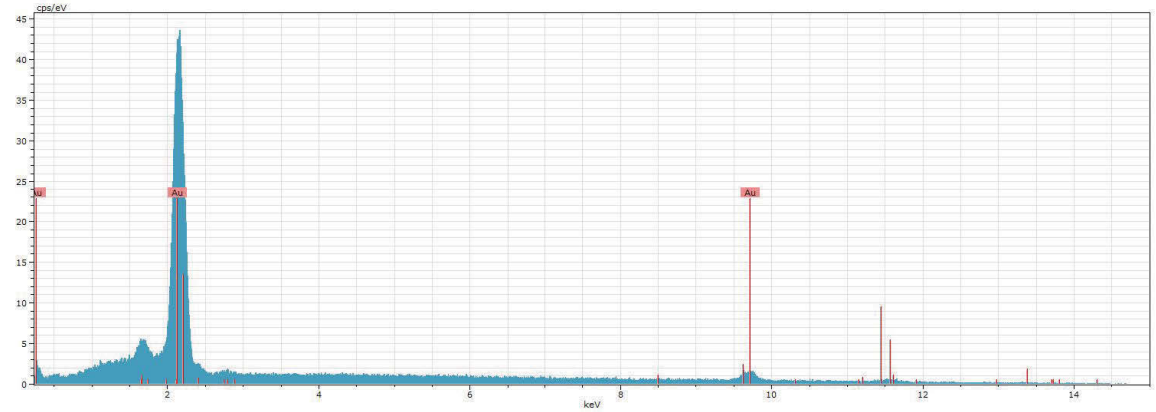

Native gold

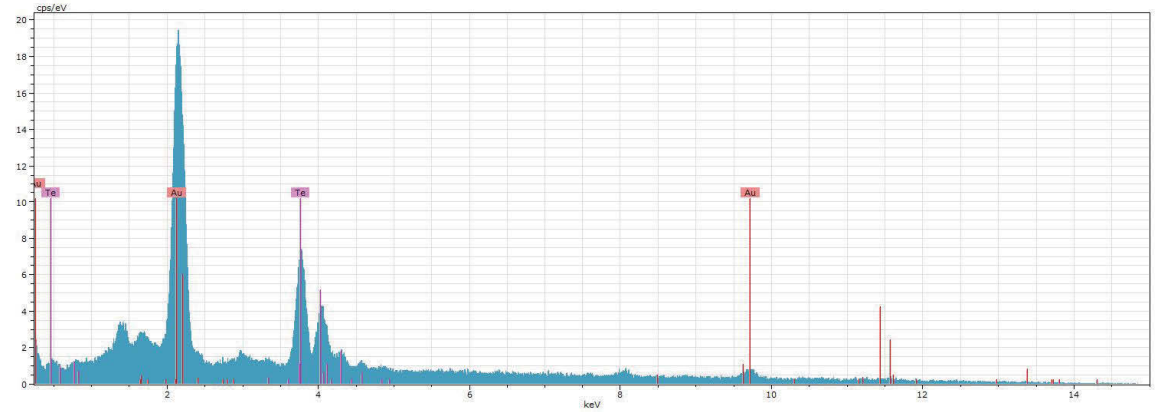

Calaverite $AuTe_2$

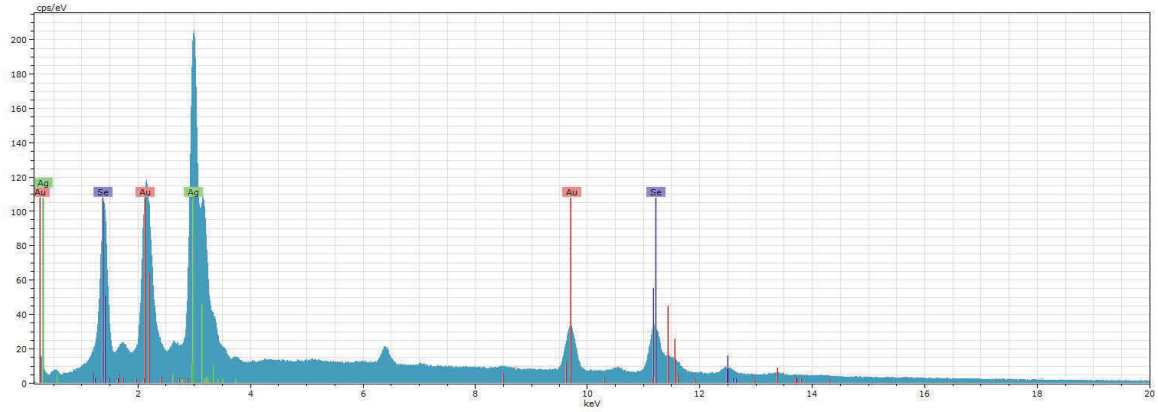

Fischesserite Ag_3AuSe_2

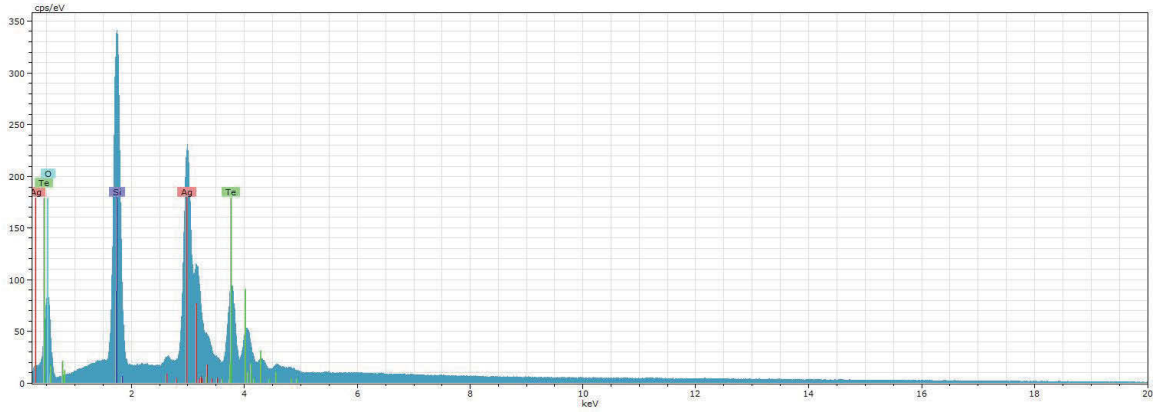

Hessite Ag_2Te (in quartz)

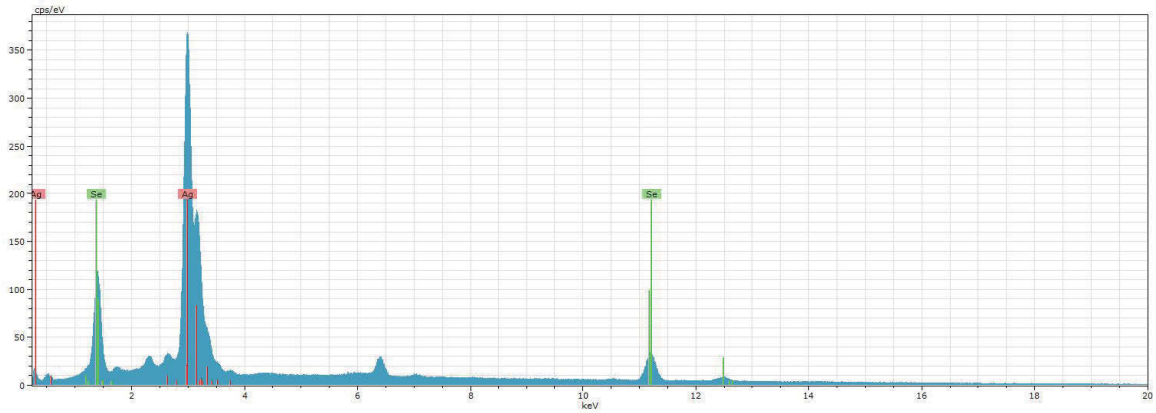

Naumannite Ag_2Se

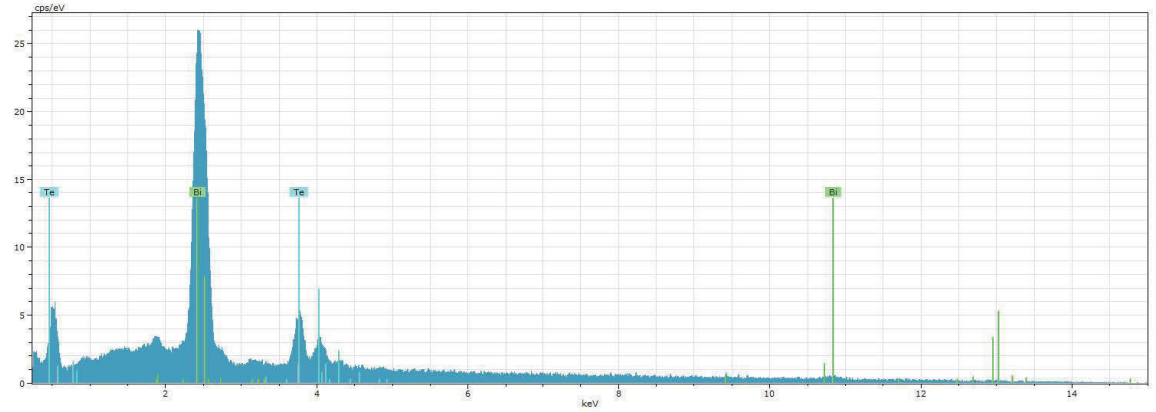

Tsumoite BiTe

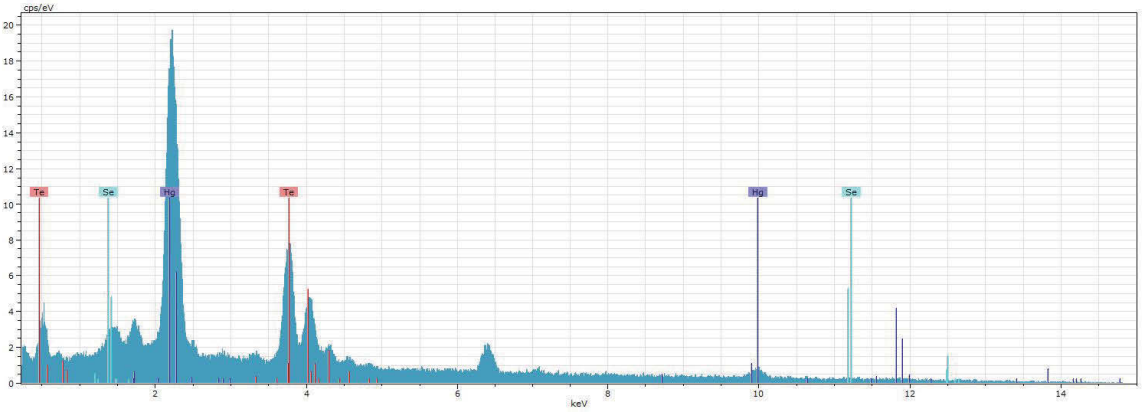

Coloradoite HgTe

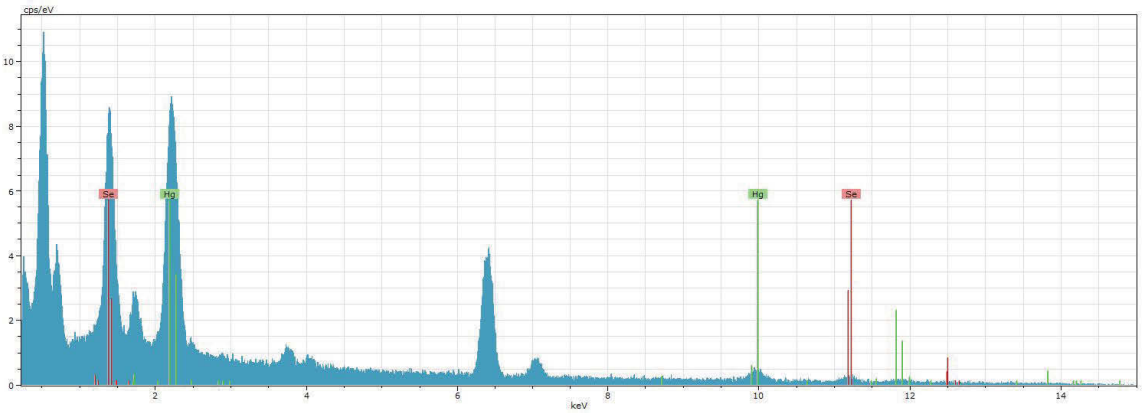

Tiemannite HgSe (with iron-oxide and quartz)

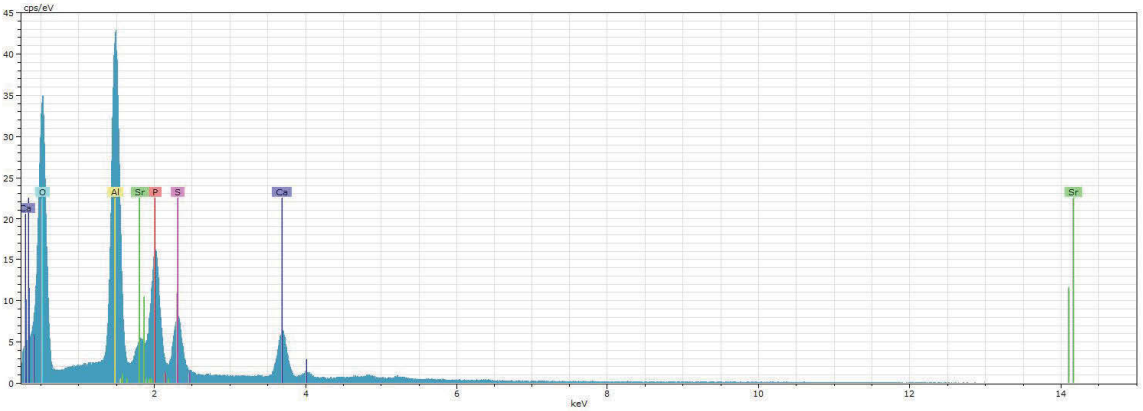

Woodhouseite $CaAl_3(SO_4)(PO_4)(OH)_6$

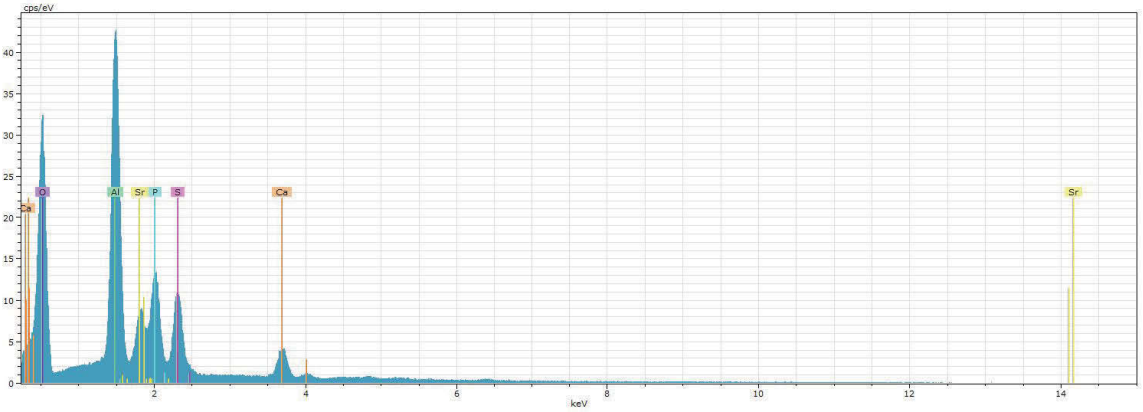

Woodhouseite ($CaAl_3(SO_4)(PO_4)(OH)_6$) – Svanbergite ($SrAl_3(SO_4)(PO_4)(OH)_6$)

Tower

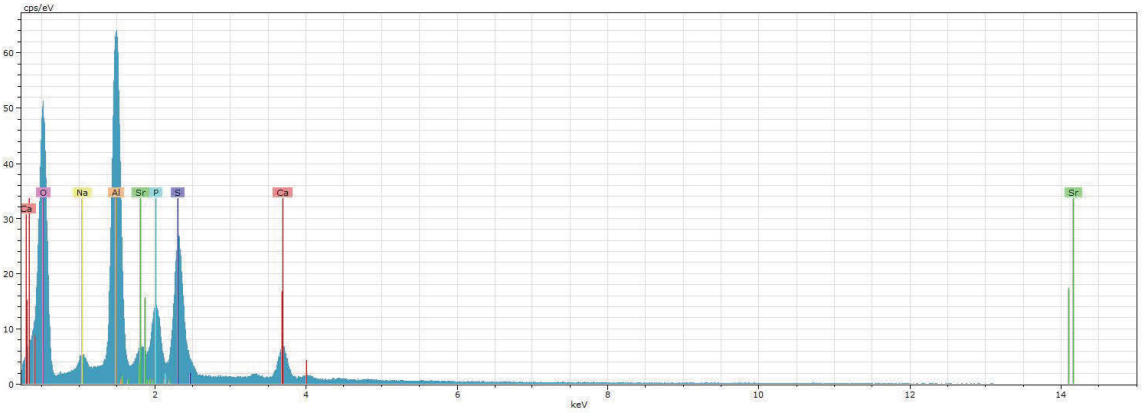

Woodhouseite ($CaAl_3(SO_4)(PO_4)(OH)_6$)

Monkstown Road

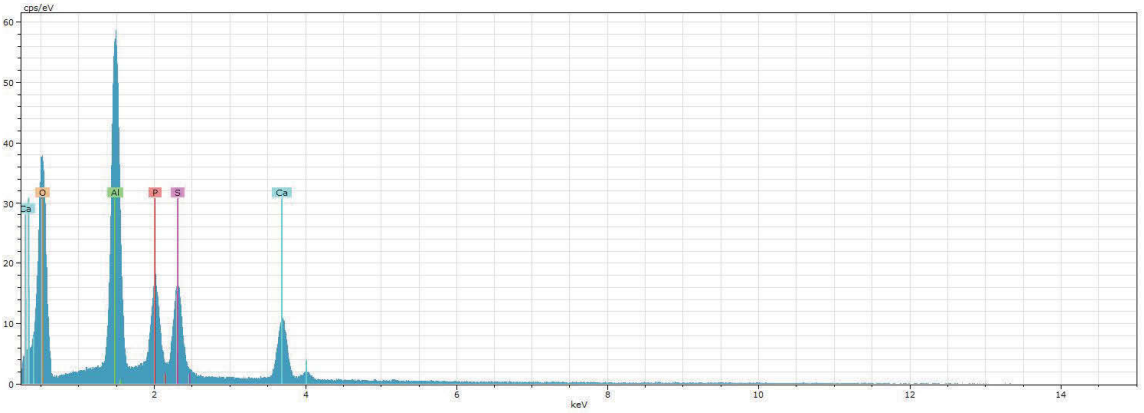

Woodhouseite ($CaAl_3(SO_4)(PO_4)(OH)_6$)

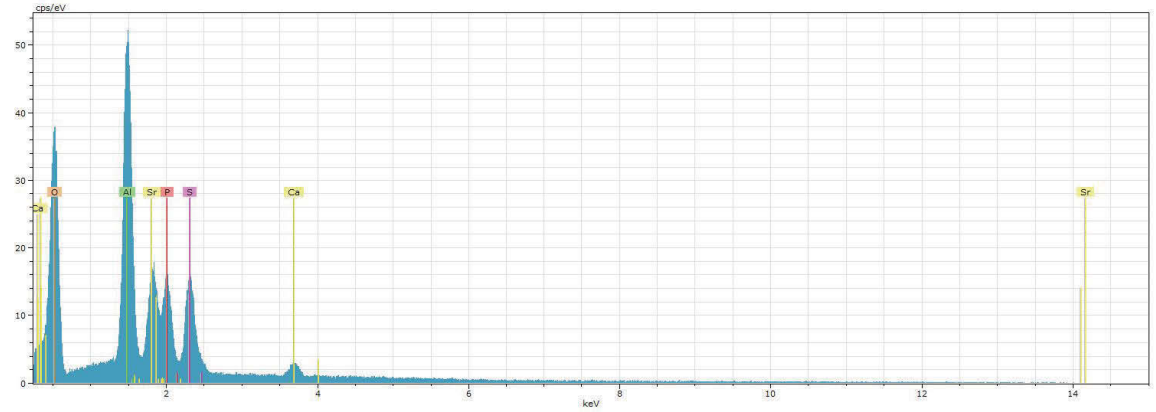

Svanbergite ($SrAl_3(SO_4)(PO_4)(OH)_6$)

Forty Creek

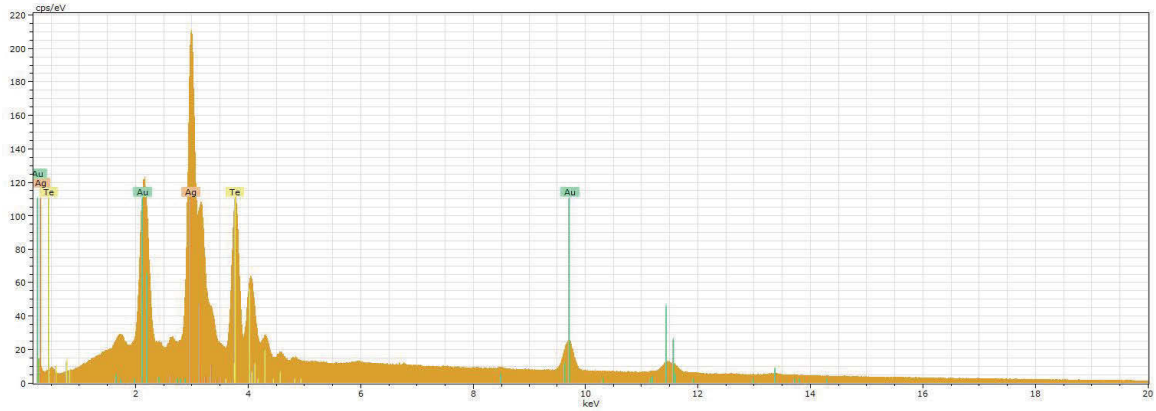

Petzite Ag_3AuTe_2

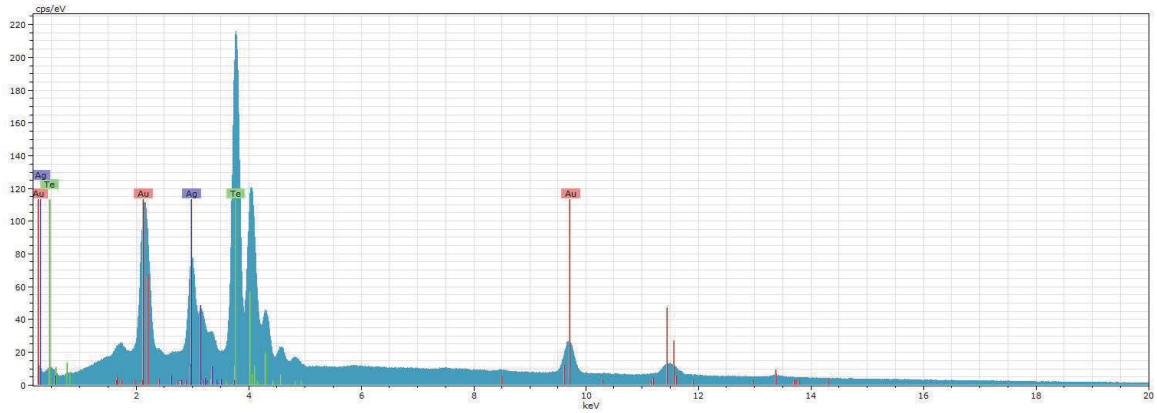

Sylvanite $AgAuTe_4$

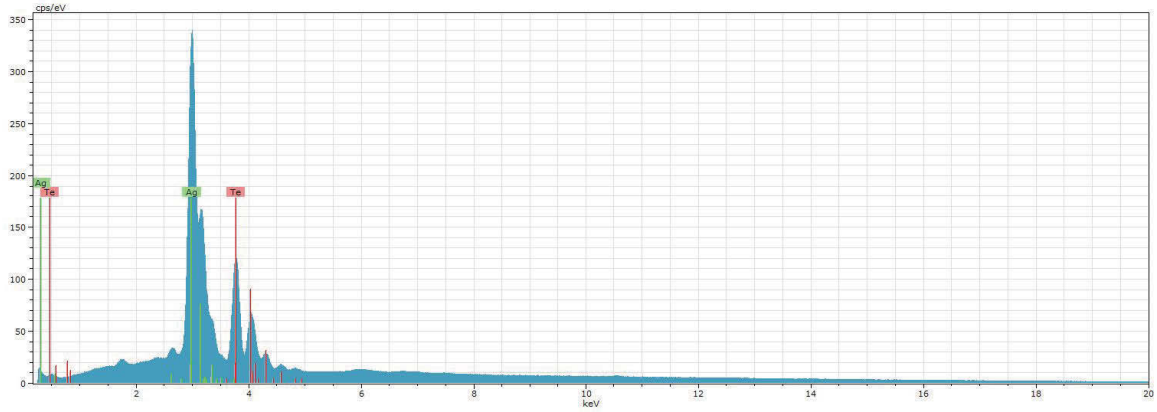

Hessite Ag_2Te

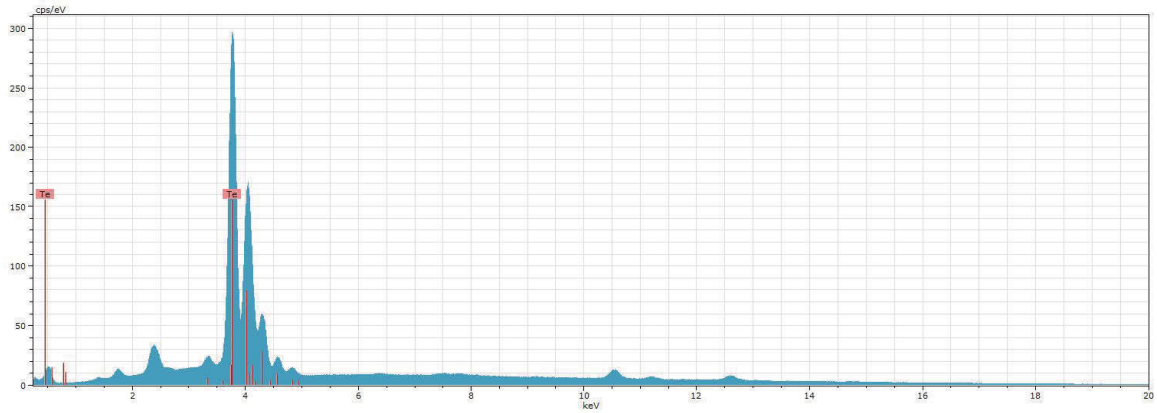

Native tellurium

Long Harbour

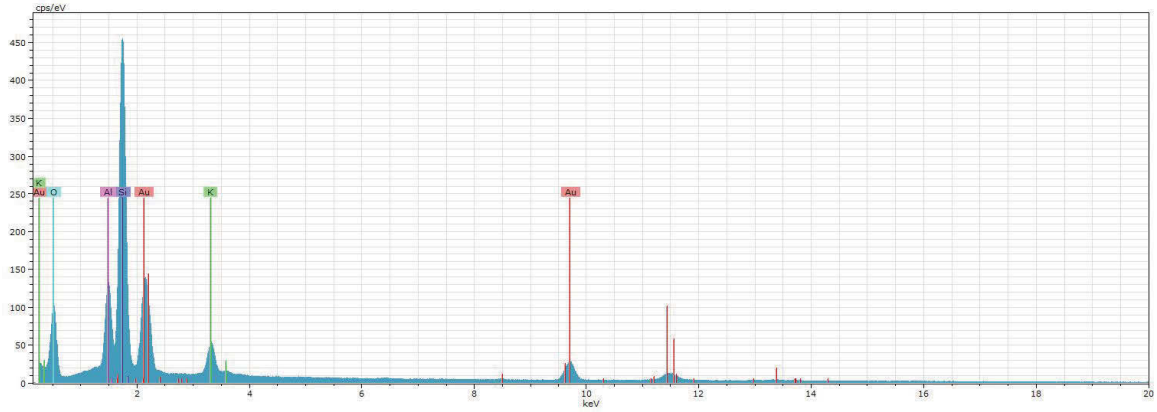

Native gold (with adularia)

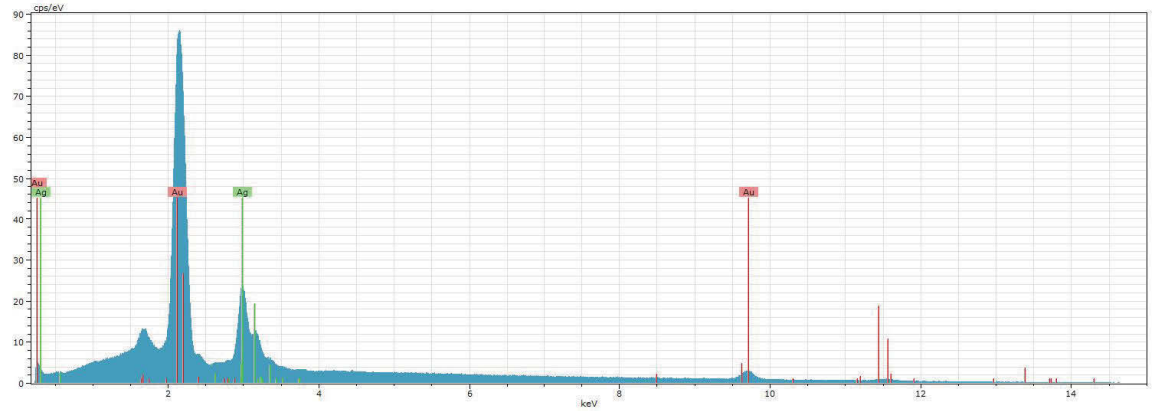

Electrum (65% Au, 35% Ag)

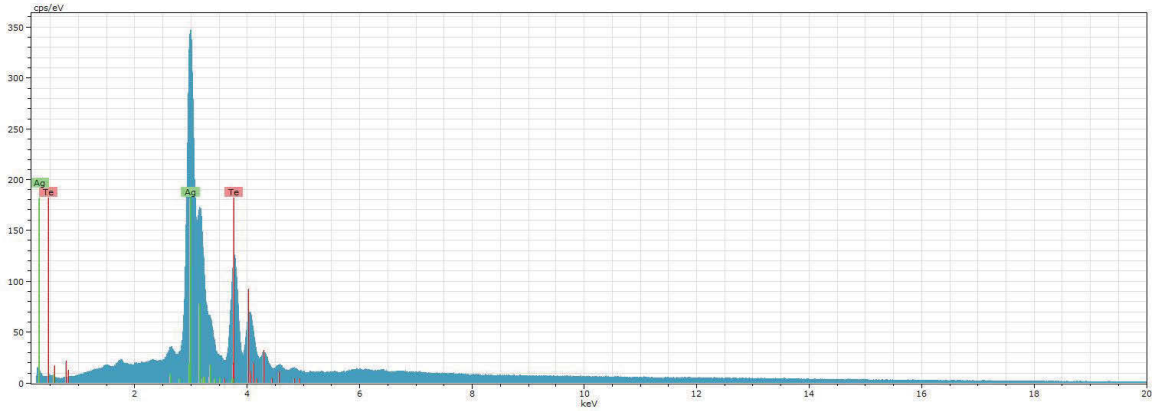

Hessite Ag_2Te

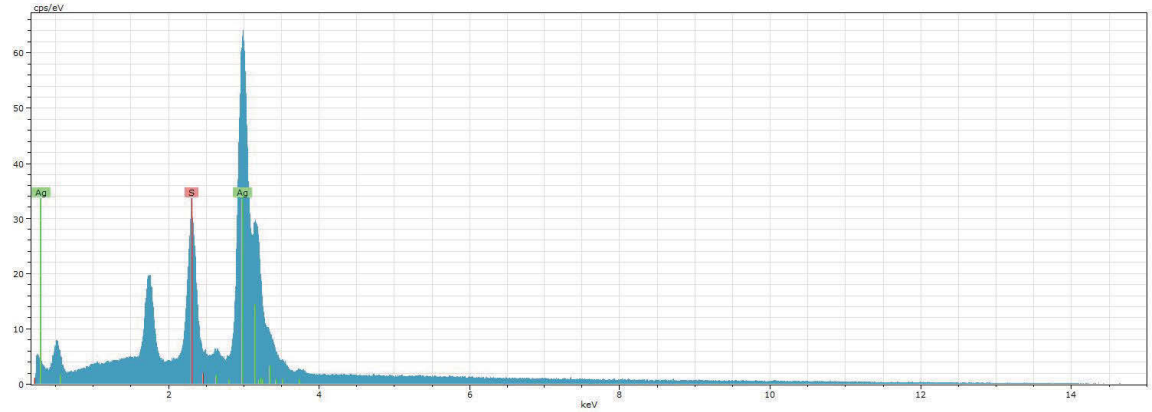

Acanthite Ag_2S (with quartz)

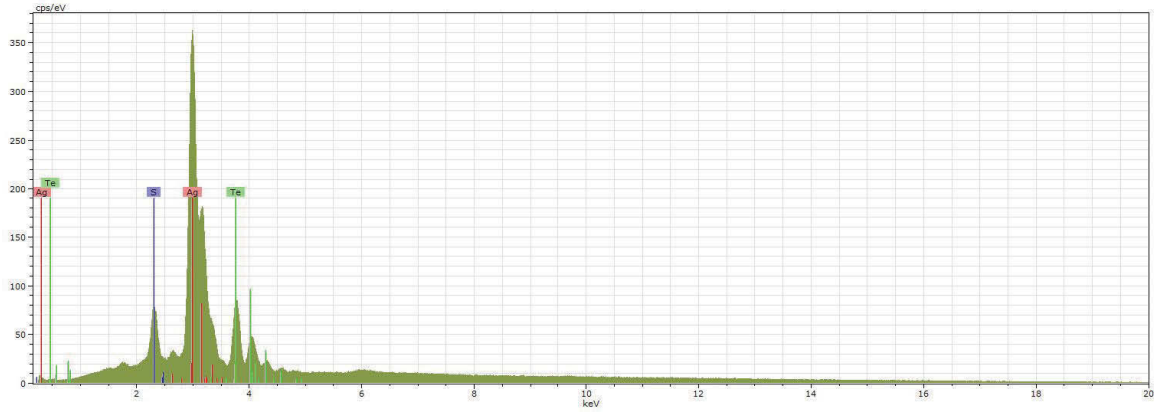

Cervelleite Ag_4TeS

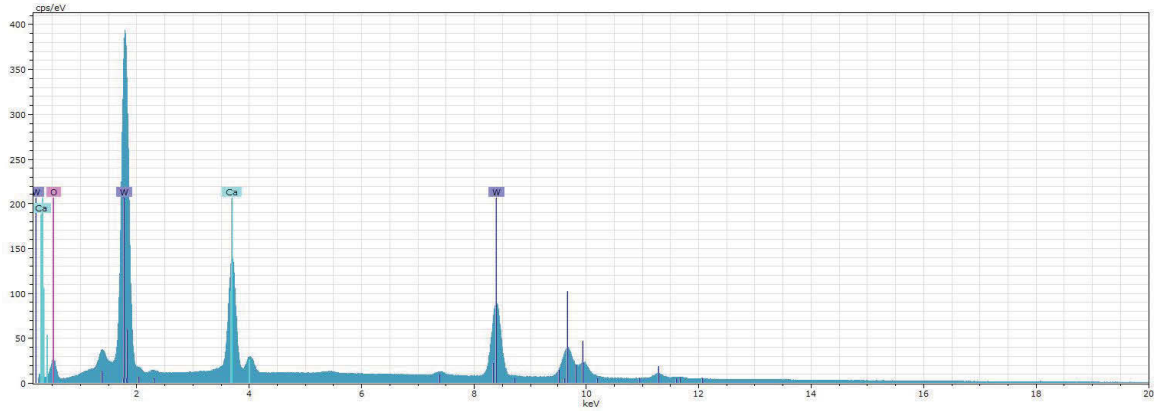

Scheelite $CaWO_4$